Current Natural Sciences

Zi-Cai LI, Hung-Tsai HUANG,
Yimin WEI and Liping ZHANG

The Method of Fundamental Solutions: Theory and Applications

SCIENCE PRESS

edp sciences

Printed in France

EDP Sciences – ISBN(print): 978-2-7598-3171-5 – ISBN(ebook): 978-2-7598-3172-2
DOI: 10.1051/978-2-7598-3171-5

All rights relative to translation, adaptation and reproduction by any means whatsoever are reserved, worldwide. In accordance with the terms of paragraphs 2 and 3 of Article 41 of the French Act dated March 11, 1957, “copies or reproductions reserved strictly for private use and not intended for collective use” and, on the other hand, analyses and short quotations for example or illustrative purposes, are allowed. Otherwise, “any representation or reproduction – whether in full or in part – without the consent of the author or of his successors or assigns, is unlawful” (Article 40, paragraph 1). Any representation or reproduction, by any means whatsoever, will therefore be deemed an infringement of copyright punishable under Articles 425 and following of the French Penal Code.

The printed edition is not for sale in Chinese mainland. Customers in Chinese mainland please order the print book from Science Press. ISBN of the China edition: Science Press 978-7-03-074916-1

© Science Press, EDP Sciences, 2023

This book is dedicated to our families.

Contents

Preface . . . XI
Acknowledgements . . . XV

CHAPTER 1
Introduction . . . 1

1.1 Historic Review . . . 1
1.2 Basic Algorithms . . . 3
1.3 Numerical Experiments . . . 5
1.4 Characteristics of the MFS . . . 11

Part I. Laplace's Equation . . . 15

CHAPTER 2
Dirichlet Problems . . . 19

2.1 Basic Algorithms of MFS . . . 19
2.2 Preliminary Lemmas . . . 21
2.3 Main Theorems . . . 27
2.4 Stability Analysis for Disk Domains . . . 32
2.5 Proof Methodology . . . 39

CHAPTER 3
Neumann Problems . . . 41

3.1 Introduction . . . 41
3.2 Method of Fundamental Solutions . . . 42
    3.2.1 Description of Algorithms . . . 42
    3.2.2 Main Results of Analysis and Their Applications . . . 44
3.3 Stability Analysis of Disk Domains . . . 45
3.4 Stability Analysis for Bounded Simply-Connected Domains . . . 49
    3.4.1 Trefftz Methods . . . 50
    3.4.2 Collocation Trefftz Methods . . . 52
3.5 Error Estimates . . . 54
3.6 Concluding Remarks . . . 58

CHAPTER 4

Other Boundary Problems 61
4.1 Mixed Boundary Condition Problems 61
4.2 Interior Boundary Conditions 66
4.3 Annular Domains 70

CHAPTER 5

Combined Methods 77
5.1 Combined Methods 77
5.2 Variant Combinations of FS and PS 79
  5.2.1 Simplified Hybrid Combination 79
  5.2.2 Hybrid Plus Penalty Combination 81
  5.2.3 Indirect Combination 84
5.3 Combinations of MFS with Other Domain Methods 86
  5.3.1 Combined with FEM 86
  5.3.2 Combined with FDM 87
  5.3.3 Combined with Radial Basis Functions 90
5.4 Singularity Problems by Combination of MFS and MPS 91

CHAPTER 6

Source Nodes on Elliptic Pseudo-Boundaries 99
6.1 Introduction 99
6.2 Algorithms of MFS 101
6.3 Error Analysis 103
  6.3.1 Preliminary Lemmas 103
  6.3.2 Error Bounds 107
6.4 Stability Analysis 113
6.5 Selection of Pseudo-Boundaries 119
6.6 Numerical Experiments 121
6.7 Concluding Remarks 124

Part II. Helmholtz's Equations and Other Equations 125

CHAPTER 7

Helmholtz Equations in Simply-Connected Domains 127
7.1 Introduction 127
7.2 Algorithms 128
7.3 Error Analysis for Bessel Functions 131
  7.3.1 Preliminary Lemmas 131
  7.3.2 Error Bounds with Small k 134
  7.3.3 Exploration of Bounded k 140
7.4 Stability Analysis for Disk Domains 146
7.5 Application to BKM 149

CHAPTER 8

Exterior Problems of Helmholtz Equation . . . 155

8.1 Introduction . . . 155
8.2 Standard MFS . . . 157
  8.2.1 Basic Algorithms . . . 157
  8.2.2 Brief Error Analysis . . . 159
8.3 Numerical Characteristics of Spurious Eigenvalues by MFS . . . 161
8.4 Modified MFS . . . 165
8.5 Error Analysis for Modified MFS . . . 166
  8.5.1 Preliminary Lemmas . . . 167
  8.5.2 Error Bounds . . . 175
8.6 Stability Analysis for Modified MFS . . . 179
8.7 Numerical Experiments . . . 181
  8.7.1 Circular Pseudo-Boundaries by Two MFS . . . 181
  8.7.2 Non-Circular Pseudo-Boundaries by Modified MFS . . . 186
8.8 Concluding Remarks . . . 188

CHAPTER 9

Helmholtz Equations in Bounded Multiply-Connected Domains . . . 191

9.1 Introduction . . . 191
9.2 Bounded Simply-Connected Domains . . . 192
  9.2.1 Algorithms . . . 192
  9.2.2 Brief Error Analysis . . . 193
9.3 Bounded Multiply-Connected Domains . . . 197
  9.3.1 Algorithms . . . 197
  9.3.2 Error Analysis . . . 198
9.4 Stability Analysis for Ring Domains . . . 201
9.5 Numerical Experiments . . . 210
9.6 Concluding Remarks . . . 214

CHAPTER 10

Biharmonic Equations . . . 215

10.1 Introduction . . . 215
10.2 Preliminary Lemmas . . . 217
10.3 Error Bounds . . . 224
10.4 Stability Analysis for Circular Domains . . . 228
  10.4.1 Approaches for Seeking Eigenvalues . . . 228
  10.4.2 Eigenvalues $\lambda_k(\Phi)$ and $\lambda_k(D\Phi)$ . . . 231
  10.4.3 Bounds of Condition Number . . . 236
10.5 Numerical Experiments . . . 242

CHAPTER 11

Elastic Problems . . . 247

11.1 Introduction . . . 247
11.2 Linear Elastostatics Problems in 2D . . . 247
  11.2.1 Basic Theory . . . 247
  11.2.2 Traction Boundary Conditions . . . 249
  11.2.3 Fundamental Solutions . . . 250
  11.2.4 Particular Solutions . . . 251
11.3 HTM, MFS and MPS . . . 252
  11.3.1 Algorithms of HTM . . . 252
  11.3.2 Algorithms of MFS and MPS . . . 252
11.4 Errors Between FS and PS . . . 254
  11.4.1 Preliminary Lemmas . . . 254
  11.4.2 Polynomials ∇P_n Approximated by $\left(\frac{x-\xi}{r^2}\right)$ and $\left(\frac{y-\eta}{r^2}\right)$ . . . 257
  11.4.3 Other Proof for Theorem 11.4.1 . . . 258
  11.4.4 The Polynomials $\mathcal{L}P_n$ Approximated by Principal FS . . . 261
11.5 Error Bounds for MFS and HTM . . . 264
  11.5.1 The MFS . . . 264
  11.5.2 The HTM Using FS . . . 266
11.6 Numerical Experiments . . . 268
11.7 Appendix: Addition Theorems of FS in Linear Elastostatics . . . 271
  11.7.1 Preliminary Lemmas . . . 271
  11.7.2 Addition Theorems . . . 277

CHAPTER 12

Cauchy Problems . . . 281

12.1 Introduction . . . 281
12.2 Algorithms of Collocation Trefftz Methods . . . 281
12.3 Characteristics . . . 284
  12.3.1 Existence and Uniqueness . . . 284
  12.3.2 Ill-Posedness of Inverse Problems . . . 287
12.4 Error and Stability Analysis . . . 290
  12.4.1 Error Analysis . . . 290
  12.4.2 Stability Analysis . . . 291
12.5 Applications to Cauchy Data . . . 295
  12.5.1 Errors on Cauchy Boundary . . . 295
  12.5.2 Sensitivity of Solutions on Cauchy Data . . . 296
12.6 Numerical Experiments and Concluding Remarks . . . 297

CHAPTER 13

3D Problems . . . 301

13.1 Introduction . . . 301
13.2 Method of Particular Solutions . . . 302
13.3 Method of Fundamental Solutions . . . 309

13.3.1 Algorithms 309
13.3.2 Link to MPS 310
13.4 Error Analysis for MFS 313
13.4.1 Preliminary Lemmas 314
13.4.2 Error Bounds 321
13.5 Numerical Experiments 324
13.5.1 Collocation Equations on Γ 324
13.5.2 By MFS 325
13.5.3 By MPS 330
13.6 Concluding Remarks 331
13.7 Appendix: 3D Problems of Helmholtz Equations 332
13.7.1 Interior Dirichlet Problems 332
13.7.2 Exterior Dirichlet Problems 333

Part III. Selection of Source Nodes and Related Topics 335

CHAPTER 14
Comparisons of MFS and MPS 339

14.1 Introduction 339
14.2 Two Basis Boundary Methods 340
14.2.1 Method of Particular Solutions 340
14.2.2 Method of Fundamental Solutions 342
14.3 The MFS-QR 346
14.3.1 Algorithms in Elliptic Coordinates 346
14.3.2 Characteristics of MFS-QR 349
14.4 Numerical Experiments and Comparisons 354
14.4.1 Highly Smooth Boundary Data 355
14.4.2 Boundary Data with Strong Singularity 356
14.4.3 Better Pseudo-Boundaries 358
14.5 Concluding Remarks 360

CHAPTER 15
Stability Analysis for Smooth Closed Pseudo-Boundaries 361

15.1 Introduction 361
15.2 Relations Between FS and PS 362
15.3 Bounds of Cond for Non-Elliptic Pseudo-Boundaries 365

CHAPTER 16
Singularity Problems from Source Functions; Removal Techniques 375

16.1 Introduction 376
16.2 Analytical Framework for CTM in [169] 378
16.3 Error Bounds for Singular Solutions from (16.1.3) 380
16.4 Singularity for Polygonal Domains and Arbitrary Domains 383

16.5 Removal Techniques for Laplace's Equation 384
16.5.1 For the Case of Q^* Outside Γ 384
16.5.2 For the Case of Q^* Inside Γ under the Image Node Existing . 386
16.6 Numerical Experiments 388
16.7 Applications to Amoeba-Like Domains 390
16.7.1 Numerical Results 390
16.7.2 Removal Techniques Linked to Source Identification Problems 394
16.8 Concluding Remarks 399

CHAPTER 17
Source Nodes on Pseudo Radial-Lines 401

17.1 Introduction 401
17.2 Pseudo Radial-Lines 404
17.2.1 One Pseudo Radial-Line 404
17.2.2 Two Pseudo Radial-Lines 408
17.3 Stability Analysis 409
17.3.1 Lower Bound Estimates of Cond for Basic Case 409
17.3.2 Upper Bound Estimates of Cond for Variant Case by Case II. 412
17.4 Numerical Experiments 415
17.4.1 Disk Domains 415
17.4.2 Non-Disk Domains 420
17.5 Concluding Remarks 424

Epilogue 427

References 431

Glossary of Symbols 443

Index 449

Preface

The fundamental solutions (FS) satisfy the governing equations in a solution domain S, and they are the functions of the distance $|\overline{PQ}|$, where $P \in \bar{S}$ and Q are the source nodes. For Laplace's equation, the FS is known as $\ln|\overline{PQ}|$ in 2D and $\frac{1}{|\overline{PQ}|}$ in 3D. When the source nodes Q_i are located outside S with $|\overline{PQ_i}| > 0$, no singularity exists for the FS. Their linear combinations, such as $\sum_i c_i \ln|\overline{PQ_i}|$ or $\sum_i c_i \frac{1}{|\overline{PQ_i}|}$, are chosen, and the unknown coefficients c_i can be found from the exterior and the interior boundary conditions. This method is called the method of fundamental solutions (MFS). The MFS was first used in Kupradze [131] in 1963; numerous reports of computation by the MFS have appeared since then. So far there exist only a few papers for analysis. It is now an urgent time to fill up the gap between theory and computation. This is the motivation for our research and this book. In this book, various numerical algorithms are introduced and their characteristics are addressed. The main efforts are paid to establish the theoretical analysis in errors and stability.

For wide applications of the MFS, readers may refer to the monographs by Chen *et al.* [39] in 2008 and Kolodziej and Zielinski [128] in 2009. A recent overview of the MFS for solvability, uniqueness, convergence and stability is given by Cheng and Hong [58] in 2020. In the monograph by Cheng, Chen, and Karageorghis [57], wide applications of the MFS are introduced systematically for solving various partial differential equations (PDE). More applications of the MFS are reported in International Workshops on the Method of Fundamental Solutions in Ayia Napa, Cyprus, June 11–13, 2007; National Sun Yat-sen University, Taiwan, March 15–18, 2011; Zhejiang University, China, October 11–13, 2015; Technical University of Poznan, Poland, July 4–9, 2017; and the University of Lisbon, Portugal, July 29–31, 2019. Since 2011, they have held and joined together with International Workshops on Trefftz Methods.

DOI: 10.1051/978-2-7598-3171-5.c901
© Science Press, EDP Sciences, 2023

The source nodes Q_i are located outside Γ. There are various choices: scatter, random, an outside closed contour Γ_R or radial lines. The contour Γ_R and the radial lines are employed to control the source nodes for improving numerical performance. Since the contour Γ_R is not the physical boundary Γ, the pseudo-boundary (*i.e.*, the superfluous, fictitious boundary) is called. In this book, various kinds of closed pseudo-boundaries Γ_R are chosen except the pseudo radial-lines in the last chapter. In computation, the following questions are encountered immediately: how should the pseudo-boundary Γ_R be chosen, and how should the source nodes be located on Γ_R? The circular pseudo-boundary Γ_R (or the spherical pseudo-boundary surface S_R in 3D) is simple and efficient. The pseudo-boundary Γ_R near boundary Γ with an almost equal distance/ratio is beneficial for better stability. The abscissas of quadrature rules on Γ_R are good locations for the source nodes. Careful choices of source nodes are an important issue in both computation and analysis. Smooth solutions are discussed in Parts I and II, and the circular pseudo-boundaries are chosen except in Chapter 6, where the elliptic pseudo-boundaries are studied. Singular solutions are discussed in Part III, and pseudo-boundaries near the boundary are chosen. The pseudo radial-lines are particularly studied in Chapter 17.

Once the pseudo-boundaries (or the pseudo radial-lines) are chosen, more theoretical questions arise. What are the convergence rates and the growth rates of condition numbers (Cond)? How can the MFS be combined with other methods to handle corner singularity and the singularity from the source functions? How can the spurious eigenvalues be removed for the Helmholtz equation by the MFS? The error and stability analysis is explored systematically in this book to answer these important questions. The objective of the theoretical analysis is not only to support the computations in existing literature but also to find discoveries and to provide some useful guidance for users. Many new findings were found and published in our research papers; this book is a summary of them. A systematic analysis of the MFS has been established in this book, which is also related to our previous monographs [146, 162, 169].

This book includes seventeen chapters with a preface, outlines of three parts, an epilogue, and references. In the introductory chapter, a brief history of the MFS is reviewed. The algorithms of the MFS are described, and numerical examples of Motz's problem are reported. Moreover, the numerical characteristics of the MFS are addressed.

Part I is for Laplace's equation and includes five chapters. Chapter 2 studies Dirichlet problems, where the basic error and stability analysis is explored with the important proof techniques. Optimal convergence rates are obtained, and bounds of Cond are derived to show the exponential growth. Chapter 3 discusses Neumann problems and Chapter 4 other problems. Chapter 5 introduces the combined methods of the MFS with other methods, such as the method of particular solutions (MPS), the finite element method (FEM), the finite difference method (FDM), and the radial basis function method (RBFM). In Chapters 2–5, the error analysis is made for the simple circular pseudo-boundaries, while in Chapter 6, the elliptic pseudo-boundaries are chosen to reduce ill-conditioning for long-narrow domains.

Part II is for Helmholtz equations and other equations, and includes seven chapters. Since the solutions of Helmholtz equations have greatly distinct characteristics, the MFS solving Helmholtz equations is studied in Chapters 7–9. Chapter 7 discusses the real solutions in a bounded simply-connected domain S, while Chapter 8 discusses the complex solutions in exterior problems, where the newly modified MFS is proposed to eliminate all spurious eigenvalues. In Chapter 9, the complex MFS is used for the bounded multiply-connected domains, where the error and stability analyses are made. Moreover, other classic equations by MFS are also studied in Chapters 10–13. Chapter 10 discusses biharmonic equations in 2D. Chapter 11 discusses elastic problems in 2D, and Chapter 12 discusses Cauchy problems. Chapter 13 studies Laplace's equation in 3D by the MFS and establishes error analysis.

Part III is for the selection of source nodes and includes four chapters. An essential issue of the MFS is how to properly select the source nodes outside S. For highly smooth solutions, the circular/elliptic pseudo-boundaries in Parts I and II are often optimal. Otherwise, better source nodes should be sought by trial computations. Since high accuracy and ill-conditioning are coexistent in computation (see "*the trade-off principle*" in Wendland [243]), we propose the sensitivity index as a criterion to select better source nodes. In Chapter 14, based on the sensitivity index, comparisons are made for the MFS and the MPS, as well as for different locations of source nodes. In Chapter 15, the stability analysis is made for the smooth closed pseudo-boundaries. Chapter 16 studies the singularity problems caused by the source functions as the source nodes are located near the boundary Γ. Reduced convergence rates are derived for the MPS and the MFS, and new removal techniques are proposed to recover the optimal convergence rates. In the last chapter, new source nodes on two pseudo radial lines are proposed, and the lower and upper bounds of Cond are provided. The new algorithms using the pseudo radial-lines may become a new competent algorithm in the MFS family.

Since the materials in this book are adapted from our own research papers, novelty is the first characteristic of this book. There are many books on error analysis, but there are few for both errors and stability analyses. The analysis of both errors and stability together is the second characteristic of this book. In Part III, better source nodes can be found by the sensitivity index. Numerical examples are reported in most chapters, and important computational issues are also discussed. Hence, the combination of both theory and computation is the third characteristic of this book.

This book is written for researchers, graduate students, university students, mathematicians, and engineers. The first introductory chapter is easy to follow. Since each chapter is an independent research topic, the readers may directly jump to the chapter that interests them. This book can also be used as an advanced textbook for researchers and graduate students. Since the algorithms of the MFS are straightforward and simple to carry out, one may understand and use them easily. Users may find this book helpful because it covers clear descriptions of algorithms, numerical characteristics, theoretical conclusions, discoveries, shortcuts and pitfalls, and numerical examples. Hence, this book can offer a wide range of readers to understand the use of MFS and various applications in scientific/engineering computing.

Zi-Cai LI, Hung-Tsai HUANG,
Yimin WEI, Liping ZHANG
June 2022

Acknowledgements

We sincerely appreciate Drs. C.S. Chen, A. Karageorghis, and A.H.-D. Cheng for their encouragement and support during our study of the MFS. We are indebted to Drs. M.G. Lee, C.S. Chen, A.H.-D. Cheng, J.T. Chen, J. Huang, T.T. Lu, Z. Tian, F. Dou, and Y. Chen for their collaboration on the publications related to this book. We also express our thanks to Jeffrey Luther and Shih-Che Fu for their helpful suggestions for this book. We are also grateful to X. Li and the editorial staff at Academic Science Press, Beijing for their support and assistance in publishing this book.

This book is a summary of the international collaborated research between the National Sun Yat-sen University and I-Shou University, Taiwan, and Fudan University and the Zhejiang University of Technology, China. This book and the related works were supported in part by the Ministry of Science and Technology of Taiwan, and by the National Natural Science Foundation of China under grant 12271108, Innovation Program of Shanghai Municipal Education Commission and Shanghai Municipal Science and Technology Commission under grant 23WZ2501400, Key Laboratory of Mathematics for Nonlinear Sciences and Fudan University and the Ministry of Science and Technology of China under grant G2023132005L.

Chapter 1

Introduction

> *Everything is simpler than you think*
> *and at the same time more complex than you imagine.*
> Johann Wolfgang von Goethe, 1749–1832.

This introductory chapter is organized as follows. First, the history of the method of fundamental solutions (MFS) is briefly reviewed. In Section 1.2, the algorithms of the MFS are described. In Section 1.3, numerical experiments are carried out for Motz's problem by the MFS, and in the last section, the characteristics of the MFS are addressed. The simplicity and high efficiency of numerical algorithms are displayed in this chapter. The theoretical foundation behind them will be explored in Part I. Partial materials of this chapter are adapted from [150].

1.1 Historic Review

The MFS was first used in Kupradze [131] in 1963. Since then, numerous reports of MFS for computations have appeared. See some excellent reviews of MFS in Fairweather and Karageorghis [80], Cho *et al.* [63], Golberg and Chen [87], and a systematic introduction to the MFS in Chen *et al.* [37]. In Cheng *et al.* [57], a pre-history of numerical methods by using the fundamental solutions (FS) before Kupradze [131] is reviewed, and wide applications of the MFS are introduced systematically for solving various partial differential equations (PDE). To celebrate the progress of MFS, the First International Workshop on the Method of Fundamental Solutions (MFS 2007) was held in Ayia Napa, Cyprus, June 11–13, 2007. However, there exist only a dozen articles for analysis [26, 64, 120–123, 140, 141, 189, 212, 215, 216, 218]. Let us mention some important works here. In Mathon and Johnston [189], the source nodes of the MFS are sought by nonlinear equations. Nonlinear solvers confine applications though. When the outside source nodes Q_i are given in advance, the linear algebraic equations are obtained in Section 1.2. Since no mesh partition is needed, the MFS is of meshless algorithms. The progress of the MFS has been made for the potential problems in Mey [191] and Katsurada and Okamoto [123], harmonic and biharmonic problems with singularities in Karageorghis [114],

DOI: 10.1051/978-2-7598-3171-5.c001
© Science Press, EDP Sciences, 2023

and eigenvalues of the Helmholtz equation in Karageorghis [115]. Besides, the MFS using the singular value decomposition (SVD) is developed in Ramachandran [205], and the truncated SVD (TSVD) in Chen *et al.* [36] to improve numerical stability. For a bounded simply-connected domain S, when the source nodes of FS are located uniformly on an outside circle of S, the polynomial convergence rates are proved in Bogomolny [26], and the exponential convergence rates are provided in Katsurada and Okamoto [123].

Note that the MFS works only for the homogenous PDE. To extend MFS to the nonhomogeneous PDE, the related work is given by Alves and Chen [4]. Analysis for the Poisson and the modified Helmholtz equation in disks is given in Li [140, 141]. On the other hand, ill-conditioning (*i.e.*, instability) is the most severe issue of MFS. For Dirichlet problems, the exponential growth of the traditional condition number (Cond) is provided in Kitagawa [125, 126] and Christiansen [64, 66] for the simple case that both the source and the collocation nodes are located uniformly on circles. The least-squares algorithms have been studied in Smyrlis [215] and Smyrlis and Karageorghis [217], but the analysis is confined to disk domains. The MFS is also reviewed in Chen *et al.* [52, Section 4.1.2]. The MFS in solid mechanics is introduced by Wang and Qin [237] in 2019. Two governing equations are the biharmonic equation and the Cauchy–Navier equation, which are discussed in Chapters 10 and 11, respectively. A recent overview of the MFS for solvability, uniqueness, convergence, and stability is given in Cheng and Hong [58] in 2020 with an extensive list of 363 references. Wide applications of the MFS are introduced systematically in the monograph [57] by Cheng *et al.* For the MFS, the theory is much behind the success of computation. To seek a solid theoretical basis has been the focus of our study in the past fifteen years. Progress has been reported in various journals, and this book provides a systematic introduction.

Besides the MFS, there are other terminologies in literature [128, p.5]: the fundamental solution method, the fundamental collocation method, the source function method, the charge simulation method, the discrete singularity method, the boundary point method, and the superposition method.

In this chapter, the algorithms of MFS are described for Laplace's equation with the mixed boundary conditions. Numerical experiments are carried out for Motz's problem, by adding the singular solutions or by using the local refinements of collocation nodes. The condition number (Cond) is large, but the effective condition number (Cond_eff) may not be. Moreover, the expansion coefficients from the MFS may be large in magnitude with different signs, causing another kind of instability: catastrophic cancelation in the final harmonic solutions. Hence for practical applications, the accuracy and the ill-conditioning must be balanced against each other. To mitigate the ill-conditioning, we may solicit regularization, such as the TSVD and the Tikhonov regularization (TR) in Li *et al.* [161] and Zhang *et al.* [259]. More explorations on a balance between accuracy and ill-conditioning are given in Chapter 6 and Part III.

1.2 Basic Algorithms

Consider Laplace's equation with the mixed type of the Dirichlet and the Robin boundary conditions in 2D,

$$\Delta u = \frac{\partial^2 u}{\partial x^2} + \frac{\partial^2 u}{\partial y^2} = 0 \text{ in } S, \tag{1.2.1}$$

$$u = f \text{ on } \Gamma_D, \tag{1.2.2}$$

$$\frac{\partial u}{\partial \nu} + \alpha u = g \text{ on } \Gamma_R, \tag{1.2.3}$$

where α is a nonnegative constant, S a bounded simply-connected domain with the smooth boundary $\partial S = \Gamma_D \cup \Gamma_R \, (= \Gamma)$, and ν the exterior normal of Γ. Denote

$$r_{\max} = \max_{S} r, \quad r_{\min} = \max_{S_{\text{in}}(S_{\text{in}} \subseteq S)} r, \tag{1.2.4}$$

where S_{in} is a disk inside S (see Figure 1.1). A circle surrounding S is given by

$$\ell_R = \{(r,\theta) | r = R, 0 \le \theta \le 2\pi\}, \quad R > r_{\max}. \tag{1.2.5}$$

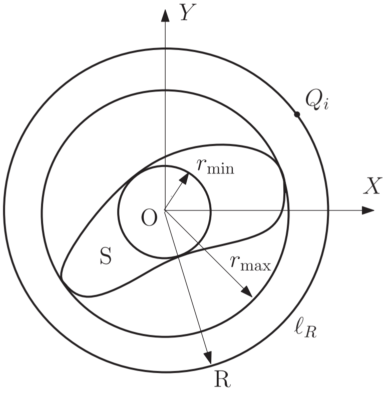

FIG. 1.1 – The solution domain S with three circles.

Let the source (charge) nodes Q be located outside S, then the fundamental solutions (FS)

$$\phi(r,\theta) = \ln|\overline{PQ}|, \quad P \in S \cup \partial S, \tag{1.2.6}$$

are harmonic, where $P = \{(x,y) \,|\, x = r\cos\theta, y = r\sin\theta\}$. Based on Bogomolny [26], the source nodes Q_i may be located uniformly on ℓ_R,

$$Q_i = \{(x,y) \,|\, x = R\cos(ih),\ y = R\sin(ih)\},$$

where $R > r_{\max}$ and $h = \frac{2\pi}{N}$. We obtain the FS

$$\phi_i(P) = \ln|\overline{PQ_i}|, \quad i = 1, 2, ..., N. \tag{1.2.7}$$

The numerical solution can be found by a linear combination,

$$u_N = \sum_{i=1}^{N} c_i \phi_i(P), \tag{1.2.8}$$

where c_i are the unknown coefficients to be determined. Since u_N satisfies Laplace's equation in S already, the coefficients c_i can be sought by enforcing the boundary conditions (1.2.2) and (1.2.3) only. We will follow the Trefftz method (TM) in [146, 170, 185] to seek u_N (*i.e.*, c_i). Denote the energy by

$$I(v) = \int_{\Gamma_D} (v - f)^2 + w^2 \int_{\Gamma_R} \left(\frac{\partial v}{\partial \nu} + \alpha v - g \right)^2, \tag{1.2.9}$$

where w is a positive weight. We choose $w = \frac{1}{N}$ in our computations (see [185]). Also denote by V_N the set of (1.2.8). Then the numerical solution u_N can be obtained by

$$I(u_N) = \min_{v \in V_N} I(v). \tag{1.2.10}$$

When the integrals in (1.2.9) involve an approximation, we have

$$\widehat{I}(v) = \widehat{\int_{\Gamma_D}} (v - f)^2 + w^2 \widehat{\int_{\Gamma_R}} \left(\frac{\partial v}{\partial \nu} + \alpha v - g \right)^2, \tag{1.2.11}$$

where $\widehat{\int}_{\Gamma_D}$ and $\widehat{\int}_{\Gamma_R}$ are the numerical approximations of $\int_{\Gamma_D}$ and $\int_{\Gamma_R}$ by some quadrature rules, such as the central, the trapezoidal, and the Gaussian rules. Hence, the numerical solution $\tilde{u}_N \in V_N$ is obtained by

$$\widehat{I}(\tilde{u}_N) = \min_{v \in V_N} \widehat{I}(v). \tag{1.2.12}$$

We may establish the collocation equations directly from (1.2.2) and (1.2.3) to yield

$$\sum_{i=1}^{N} c_i \phi_i(P_j) = f(P_j), \quad P_j \in \Gamma_D, \tag{1.2.13}$$

$$\sum_{i=1}^{N} c_i \left[\frac{\partial}{\partial \nu} \phi_i(P_j) + \alpha \phi_i(P_j) \right] = g(P_j), \quad P_j \in \Gamma_R. \tag{1.2.14}$$

Let Γ_D and Γ_R be divided into small subsections Γ_D^j and Γ_R^j with the meshspacings $\triangle h_j$, *i.e.*, $\Gamma_D = \bigcup_{j=1}^{M_1} \Gamma_D^j$ and $\Gamma_R = \bigcup_{j=1}^{M_2} \Gamma_R^j$. We obtain from (1.2.13) and (1.2.14)

$$\sqrt{\triangle h_j} \sum_{i=1}^{N} c_i \phi_i(P_j) = \sqrt{\triangle h_j}\, f(P_j), \quad P_j \in \Gamma_D, \quad j = 1, 2, ..., M_1, \tag{1.2.15}$$

$$w\sqrt{\triangle h_j}\sum_{i=1}^{N} c_i\left\{\frac{\partial}{\partial \nu}\phi_i(P_j)+\alpha\phi_i(P_j)\right\} = w\sqrt{\triangle h_j}\ g(P_j), \tag{1.2.16}$$

$$P_j \in \Gamma_R, \quad j = M_1+1, ..., M_1+M_2,$$

where P_j are the midpoints of Γ_D^j and Γ_R^j. The equations (1.2.15) and (1.2.16) are equivalent to (1.2.12), where the central rule is chosen for $\widehat{\int}_{\Gamma_D}$ and $\widehat{\int}_{\Gamma_R}$. In computation, we may choose the number of collocation nodes to be larger than (or equal to) the number of source nodes, *i.e.*, $M = M_1 + M_2 \geq N$. When the Gaussian rule is chosen, the following collocation equations are obtained,

$$\sqrt{\beta_j}\sum_{i=1}^{N} c_i\phi_i(P_j) = \sqrt{\beta_j}\ f(P_j), \quad P_j \in \Gamma_D, \tag{1.2.17}$$

$$w\sqrt{\beta_j}\sum_{i=1}^{N} c_i\left\{\frac{\partial}{\partial \nu}\phi_i(P_j)+\alpha\phi_i(P_j)\right\} = w\sqrt{\beta_j}\ g(P_j), \quad P_j \in \Gamma_R, \tag{1.2.18}$$

where P_j are the Gaussian nodes and β_j are the weights. The equations, (1.2.15), (1.2.16) and (1.2.17), (1.2.18), are also called the collocation Trefftz method (CTM) in [146, 169]. Similar approaches as in (1.2.17) and (1.2.18) are studied in [215, 217], where the least-squares MFS is used, and the analysis is confined to disk domains.

1.3 Numerical Experiments

Choose the rectangle domain $S = \{(x, y)| -1 < x < 1, 0 < y < 1\}$. Consider Motz's problem in S (see Figure 1.2):

$$\Delta u = 0, \quad (x, y) \text{ in } S, \tag{1.3.1}$$

$$u = 500 \text{ on } \overline{AB}, \quad u = 0 \text{ on } \overline{DO}, \tag{1.3.2}$$

$$\frac{\partial u}{\partial \nu} = 0 \text{ on } \overline{BC} \cup \overline{CD} \cup \overline{OA}. \tag{1.3.3}$$

There exists a singularity at O due to the intersection of Dirichlet and Neumann boundary conditions. Motz's problem is a benchmark of singularity problems discussed in [146, 169]. Since the FS (1.2.7) is smooth on ∂S, we should add singular functions into the FS. The singular particular solutions (SPS) are given in Li [146] as

$$\sum_{i=0}^{L} D_i r^{i+\frac{1}{2}} \cos\left(i+\frac{1}{2}\right)\theta. \tag{1.3.4}$$

By adding (1.3.4) into (1.2.8), we choose the following admissible functions,

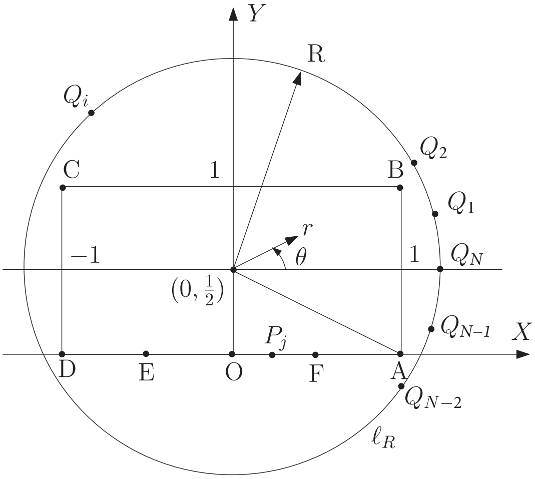

Fig. 1.2 – Location of source nodes for Motz's problem.

$$u_{L,N} = \sum_{i=0}^{L} D_i r^{i+\frac{1}{2}} \cos\left(i+\frac{1}{2}\right)\theta + \sum_{i=1}^{N} c_i \phi_i(P). \tag{1.3.5}$$

The admissible functions as in (1.3.5) are also given in Alves and Leitao [5] for an enriched MFS domain decomposition technique. Let M denote the number of collocation nodes along $\overline{AB}$. Then the total number of collocation nodes on ∂S in Figure 1.2 is $m = 6M$. The number of unknown coefficients in (1.3.5) is $L + N + 1$. In computation, choose $m = 6M \geq L + N + 1 = n$. From [185], using the Gaussian rule is beneficial to better accuracy for the leading singular coefficients D_i in (1.3.4). We choose the Gaussian rule of six nodes, where M is multiples of 6.

Define the boundary errors by

$$\|\epsilon\|_B = \left\{ \widehat{\int}_{\overline{AB}\cup\overline{DO}} \epsilon^2 + w^2 \widehat{\int}_{\overline{BC}\cup\overline{CD}\cup\overline{OA}} \left(\frac{\partial \epsilon}{\partial v}\right)^2 \right\}^{\frac{1}{2}},$$

where $\epsilon = u - \tilde{u}_{L,N}$. We use the SVD to solve (1.2.15) and (1.2.16). Choose $R = \sqrt{3}$ and $L = 3$. Errors and condition numbers are listed in Table 1.1. Table 1.2 shows that integer $L = 3$ is for better accuracy. From Table 1.1, we can find the following numerical rates,

$$\|\epsilon\|_B = O(0.8^N), \qquad \left|\frac{\triangle D_0}{D_0}\right| = O(0.8^N), \tag{1.3.6}$$

and

$$\text{Cond} = O(1.8^N), \quad \text{Cond\_eff} = O(1.2^N). \tag{1.3.7}$$

From (1.3.6) and (1.3.7), both errors and condition numbers are exponential *via* N. Note that the growth rate of Cond_eff is much lower than that of Cond, so that Cond_eff is a better estimate for the true stability of rounding errors (also see [162]).

From Table 1.1 we can see that norm $\|\mathbf{x}\|$ is large. Moreover, the coefficients c_i of $\mathbf{x}$ are large with different signs (see Table 1.4). After the coefficients D_i and c_i have been obtained, the final harmonic solutions are computed by (1.3.5). Since the gap $(R - r_{\max}) \geq c_0 > 0$, the FS as $\ln|\overline{PQ_i}|$ are bounded, and the harmonic solutions of (1.3.1)–(1.3.3) satisfy $\max_S |u_N| = 500$, then there must occur a severe catastrophic cancelation in (1.3.5), which is another kind of instability. On the other hand, the Cond and the Cond_eff are used for the stability of coefficients D_i and c_i from the MFS. Hence the final solutions (1.3.5) suffer severe instability from both rounding errors and catastrophic cancelation.

To deal with the singularity at O in Figure 1.2, the second technique is to adopt the local refinements of P_j near O as in the finite element method (FEM),

$$|\overline{OP_j}| = (jh)^q, \quad j = 1, 2, ..., \quad q \geq 1. \tag{1.3.8}$$

Choose (1.2.8) with the FS only, where the coefficients are obtained from the MFS. Afterwards, the leading coefficients in (1.3.4) can be evaluated by

$$D_\ell = \frac{2}{\pi r^{\ell + \frac{1}{2}}} \int_0^\pi u_N(r, \theta) \cos\left(\ell + \frac{1}{2}\right)\theta d\theta, \quad \ell = 0, 1, 2, 3. \tag{1.3.9}$$

The leading coefficient D_0 indicates the intensity factor, which is important in both theory and application.

The radius $R = \sqrt{3}$ in (1.2.5) is chosen in computation, based on numerical tests. For Motz's problem, errors and condition numbers are listed in Table 1.3, and some coefficients c_i and D_i in Table 1.4. The uniform collocation nodes with $h = \frac{1}{M}$ are used on ∂S, except those on $\overline{OE} \cup \overline{OF}$ in Figure 1.2, where the collocation nodes P_j are given by (1.3.8). In computation, we choose $|\overline{OF}| = |\overline{OE}| = \frac{1}{8}$ and retain the invariant M of collocation nodes on $\overline{OA}$ and $\overline{OD}$.

Errors and condition numbers are provided in Table 1.3 with $R = \sqrt{3}$ and $q = 4$, and the following numerical rates can be observed:

$$\|\epsilon\|_B = O(0.74^N), \quad \left|\frac{\triangle D_0}{D_0}\right| = O(0.97^N), \tag{1.3.10}$$

$$\sigma_{\max} = O(1), \quad \sigma_{\min} = O(0.487^N), \tag{1.3.11}$$

$$\text{Cond} = O(2.05^N), \quad \text{Cond\_eff} = O(1.37^N), \tag{1.3.12}$$

$$\|\mathbf{x}\| = O(1.47^N). \tag{1.3.13}$$

Tab. 1.1 – The errors and the condition numbers for Motz's problem by the MFS with (1.3.5) for $R = \sqrt{3}$ and $L = 3$, where M is the number of Gaussian nodes on $\overline{AB}$.

N	28	56	70	84	112
M	20	40	50	60	80
$\Vert\epsilon\Vert_B$	5.364(−5)	5.811(−8)	1.982(−8)	6.371(−9)	1.319(−9)
D_0	401.15985538326	401.16241731078	401.16243448162	401.16244628868	401.16245133388
$\left\vert\frac{\triangle D_0}{D_0}\right\vert$	6.477(−6)	9.082(−8)	4.802(−8)	1.864(−8)	6.011(−9)
D_1	87.567762254026	87.655630978127	87.655463873408	87.655806577205	87.655865753394
$\left\vert\frac{\triangle D_1}{D_1}\right\vert$	1.006(−3)	3.299(−6)	5.206(−6)	1.296(−6)	6.211(−7)
D_2	16.923603267895	17.195543463056	17.208492441230	17.218929768087	17.227194606456
$\left\vert\frac{\triangle D_2}{D_2}\right\vert$	1.823(−2)	2.458(−3)	1.707(−3)	1.101(−3)	6.219(−4)
D_3	−10.31963392978	−8.066136032966	−8.116802472857	−8.072012037121	−8.073689995482
$\left\vert\frac{\triangle D_3}{D_3}\right\vert$	2.786(−1)	6.293(−4)	5.648(−3)	9.872(−5)	3.066(−4)
β_n	1.572(−5)	7.370(−8)	−9.758(−9)	−4.665(−9)	−4.640(−10)
$\Vert\mathbf{x}\Vert$	4.346(2)	1.297(4)	7.901(5)	1.660(8)	4.445(12)
$\Vert\mathbf{b}\Vert$	1.118(2)	7.906(1)	7.071(1)	6.455(1)	5.590(1)
$\sigma_{\max}$	9.967(−1)	9.787(−1)	9.752(−1)	9.729(−1)	9.700(−1)
$\sigma_{\min}$	6.106(−7)	5.851(−12)	1.308(−14)	3.727(−17)	2.381(−22)
Cond	1.632(6)	1.672(11)	7.458(13)	2.610(16)	4.074(21)
Cond_eff	4.213(5)	1.042(9)	6.844(9)	1.043(10)	5.282(10)

The Cond_eff is much smaller than the Cond because norm $\|\mathbf{x}\|$ is large. Note that some coefficients c_i in Table 1.4 are also large with different signs, to cause the catastrophic cancelation in the final harmonic solution (1.3.5). However, there exists the empirical relation from (1.3.12) and (1.3.13),

$$\text{Cond} \approx \text{Cond\_eff} \times \|\mathbf{x}\|. \tag{1.3.14}$$

Motz's problem is a benchmark of singularity problems (see [146, 169]), and the algorithms are also simple compared with the boundary element method (BEM). In general, the errors with $O(10^{-5})$ are satisfactory for engineering problems. From Table 1.1, the errors with $\|\epsilon\|_B = 5.364(-5)$ are obtained by $N = 28$ and $L = 3$, while $\text{Cond} = 1.632(6)$ from Table 1.1. Note that only 32 unknown coefficients are needed to reach the relative error $\frac{\|\epsilon\|_B}{\|u\|_B} = 1.073(-7)$, where $\|u\|_B = 500$. Simple algorithms and high accuracy make the MFS very attractive in scientific/engineering computing.

Tab. 1.2 – The errors and the condition numbers for Motz's problem by the MFS with (1.3.5) for $R = \sqrt{3}$, $M = 50$ and $N = 70$.

L	1	2	3	4
$\|\epsilon\|_B$	4.310(−5)	1.185(−6)	1.982(−8)	4.0714(−10)
D_0	401.13173081557	401.16280525410	401.16243448162	401.16245348347
$\left\|\frac{\triangle D_0}{D_0}\right\|$	7.658(−5)	8.762(−7)	4.802(−8)	6.525(−10)
D_1	87.626121504438	87.713968940637	87.655463873408	87.655882773581
$\left\|\frac{\triangle D_1}{D_1}\right\|$	3.400(−4)	6.622(−4)	5.206(−6)	4.269(−7)
D_2	–	17.171202178929	17.208492441230	17.237739905330
$\left\|\frac{\triangle D_2}{D_2}\right\|$	–	3.870(−3)	1.707(−3)	1.016(−5)
D_3	–	–	−8.116802472857	−8.084520000876
$\left\|\frac{\triangle D_3}{D_3}\right\|$	–	–	5.648(−3)	1.648(−3)
D_4	–	–	–	1.4267531744418
$\left\|\frac{\triangle D_4}{D_4}\right\|$	–	–	–	9.387(−3)
β_n	3.267(−6)	−3.703(−7)	−9.758(−9)	−5.634(−10)
$\|\mathbf{x}\|$	6.618(8)	6.259(7)	7.901(5)	4.945(4)
$\|\mathbf{b}\|$	7.071(1)	7.071(1)	7.071(1)	7.071(1)
$\sigma_{\max}$	9.733(−1)	9.743(−1)	9.752(−1)	9.837(−1)
$\sigma_{\min}$	1.612(−14)	1.608(−14)	1.308(−14)	1.155(−14)
Cond	6.037(13)	6.059(13)	7.458(13)	8.519(13)
Cond_eff	6.627(6)	7.025(7)	6.844(9)	1.238(11)

TAB. 1.3 – The errors and the condition numbers for Motz's problem by the MFS with local refinements for $R = \sqrt{3}$ and $q = 4$.

N	28	42	56	70	84
M	20	30	40	50	60
$\|\epsilon\|_B$	0.877(−2)	0.214(−3)	0.864(−5)	0.274(−6)	0.130(−7)
D_0	402.09184254292	405.63488484792	401.64565381496	403.901058544929	401.504514344611
$\left\|\frac{\triangle D_0}{D_0}\right\|$	0.232(−2)	0.112(−1)	0.120(−2)	0.683(−2)	0.853(−3)
D_1	85.486201212337	83.156628936543	86.5255205015507	84.918939324102	86.8840334693767
$\left\|\frac{\triangle D_1}{D_1}\right\|$	0.248(−1)	0.513(−1)	0.129(−1)	0.312(−1)	0.881(−2)
D_2	17.204611447517	16.345251566472	16.7878829220685	16.318930673832	16.6395941822623
$\left\|\frac{\triangle D_2}{D_2}\right\|$	0.193(−2)	0.518(−1)	0.261(−1)	0.533(−1)	0.347(−1)
D_3	−7.710600862676	−8.140490333528	−7.8077693048529	−8.052717961510	−7.8482111479329
$\left\|\frac{\triangle D_3}{D_3}\right\|$	0.447(−1)	0.858(−2)	0.326(−1)	0.229(−2)	0.276(−1)
β_n	−0.141(−1)	−0.535(−3)	0.139(−4)	0.698(−6)	−0.213(−7)
$\|\mathbf{x}\|$	0.502(5)	0.214(7)	0.935(8)	0.471(10)	0.220(12)
$\|\mathbf{b}\|$	112	91.3	79.1	70.7	64.5
$\sigma_{\max}$	0.865	0.865	0.865	0.865	0.865
$\sigma_{\min}$	0.293(−6)	0.257(−9)	0.153(−11)	0.150(−15)	0.983(−19)
Cond	0.295(7)	0.337(10)	0.566(13)	0.576(16)	0.880(19)
Cond_eff	0.758(4)	0.166(6)	0.553(7)	0.999(8)	0.298(10)

TAB. 1.4 – Some coefficients for Motz's problem by the MFS with local refinements for $R = \sqrt{3}$, $q = 4$, $M = 60$ and $N = 84$, where the order of coefficients c_i is shown in Figure 1.2.

D_0	401.504514344611	D_1	86.8840334693767
D_2	16.6395941822623	D_3	−7.8482111479329
c_1	0.491387321370(3)	c_{43}	−0.51752378965(2)
c_2	−0.48322716360(3)	c_{44}	0.632198747372(2)
c_3	0.498631040500(3)	c_{45}	−0.80643532201(2)
c_4	−0.62046428611(3)	c_{46}	0.114822228337(3)
c_5	0.852602439285(3)	c_{47}	−0.87211046751(2)
	...		...
c_{22}	−0.86704303039(7)	c_{64}	−0.10599564313(12)
c_{23}	0.677226463301(7)	c_{65}	0.841202271679(11)
c_{24}	−0.46990352789(7)	c_{66}	−0.54819461868(11)
c_{25}	0.289846804493(7)	c_{67}	0.294891303375(11)
c_{26}	−0.15916310560(7)	c_{68}	−0.13193813281(11)
	...		...
c_{39}	−0.25060228690(2)	c_{81}	0.1723748649982(4)
c_{40}	0.239726174582(2)	c_{82}	−0.107905955330(4)
c_{41}	−0.35894541412(2)	c_{83}	0.7343071927688(3)
c_{42}	0.366354824136(2)	c_{84}	−0.589529464196(3)

1.4 Characteristics of the MFS

For PDE, new numerical algorithms may be proposed from some preliminary computation. Then the following three important issues of analysis need to be studied: (1) convergence with the error bounds, (2) stability with the bounds of the Cond and the Cond_eff, and (3) the combined algorithms with other numerical methods *because no method is perfect.* A numerical method, such as the FEM or the BEM, can stand as a competitive and popular method if its efficiency has been proven numerically and if the theoretical analysis of the above three issues has been established. The book from Li [146] focused on the third issue: combinations of different methods, accompanied by error and stability analysis. One important method in [146] is called the CTM, which was discussed systematically in the book [169] by Li *et al.*

For the MFS, since there have appeared numerous reports on computations (see Section 1.1), it is now imperative to respond to the following theoretical and computational issues.

I. Error analysis. Since MFS is a special method of TM using the FS, the analytical framework of TM in [145, 146, 176] and the book [169] is also valid for the MFS. The error bounds of TM are studied in [171]. Since the extra errors between the FS and the harmonic polynomials may be found from addition theorems, the error bounds of the solutions by the MFS can be derived. The optimal polynomial convergence rates can be achieved as the MPS in [169]. Such a conclusion is supported throughout the entire book. This is the main theoretical goal of this book.

For Laplace's equation, the error bounds are derived in Chapters 2–6. Exponential convergence rates can be achieved for analytic solutions. When the functions (1.3.5) are chosen, the singularity of Motz's problem is removed so that the numerical solutions converge fast. This explains the high accuracy in (1.3.6) and (1.3.10).

II. Stability analysis. For the MFS, instability is the most severe issue. From (1.3.7) and (1.3.12), we can see that both Cond and Cond_eff grow exponentially as the number of FS increases, but Cond_eff may be much smaller than Cond (see [162]). The bounds of the Cond are derived in Chapters 2, 3, and 6. In some cases, the Cond and the Cond_eff are so huge thus to damage the numerical solutions in double precision. Of course, we may employ Mathematica using unlimited working digits, to produce useful numerical solutions. However, the more working digits are used, the more CPU time and computer storage are needed. Besides, the TSVD and the TR may be employed to reduce severe ill-conditioning (see Li *et al.* [161]). Moreover, preconditioning may also be applied. Note that the MFS-QR in Antunes [8] is not a variant of the MFS but a variant of the method of particular solutions (MPS) (see Chapter 14). For the MFS, high accuracy and ill-conditioning coexist in computation. Stability analysis is the second theoretical goal of this book.

III. Combined methods of MFS. Since source nodes Q are located outside the solution domain S, the FS, $\ln|\overline{PQ}|$ with $P \in \bar{S}$, is highly smooth. Hence, the standard MFS is poor for singularity problems. The standard MFS is invalid for corner singularity, except by some techniques, such as adding singular functions and using the local refinements in Section 1.3. The combined methods are studied in [146], where the MPS, the FEM, the finite difference method (FDM), the finite volume method (FVM), and the radial basis functions method (RBFM), are combined together for complicated problems, and different coupling techniques are explored. The combinations of the MPS with other methods are provided in the book [169], while the combinations of the MFS with other methods are explored in Chapter 5. In Chapter 16, we discuss the singularity caused by the source functions, when the source nodes are located near the boundary Γ. Removal techniques using combined methods are also solicited.

The following four characteristics are also relevant to the analysis and applications.

IV. Link to the MPS. Both the MFS and the MPS are classified into the Trefftz family in [169]. Both FS and PS satisfy the homogeneous governing equations already; only the boundary conditions are dealt with. The relations between FS and PS may be found by addition theorems, and the error bounds of the MFS can be derived. Hence, the linkage between MFS and MPS is essential. Comprehensive comparisons among the MFS, the MPS, and the MFS-QR are explored in Chapter 14. New techniques of stability analysis are explored for the non-circulant matrices in Chapter 6, and they also involve the stability analysis of the MPS. The analysis of the MFS cannot be fulfilled without the MPS. Some deep developments for the MPS are also included in this book, such as the CTM involving numerical integrations in Chapter 16 and the new analysis of the MPS in Chapters 11–16. The same optimal convergence rates are obtained for both the MFS and the MPS. The MPS may offer better numerical performance in accuracy and stability, provided that suitable particular functions can be found. Take Laplace's equation as an example. The harmonic polynomials vary for different shapes of domains and different boundary conditions. For the domains S near a disk with radius a, the harmonic functions are given by

$$u_n(\rho, \theta) = a_0 + \sum_{i=1}^{n} \left(\frac{\rho}{a}\right)^i \{a_i \cos(i\theta) + b_i \sin(i\theta)\}, \tag{1.4.1}$$

where a_i and b_i are unknown coefficients to be sought. For the domains near ellipses, other harmonic functions are given in Chapter 6. Moreover, different harmonic functions are given in [193, 223]. For the polygons with different boundary conditions, numerous local harmonic functions are explored in [169, Chapter 11]. By contrast, the uniform and simple FS as in (1.2.8) are chosen in the MFS. The algorithms of the MFS are much simpler than those of the MPS.

V. Link to the BIE. Both the MFS and the boundary integral equation (BIE) stem from the FS. For Helmholtz equations, both the MFS and the boundary integral equation method (BIEM) suffer from spurious eigenvalues, so correct solutions cannot be found. Removals of spurious eigenvalues are imperative in the application, and the exterior problems are studied by using the modified MFS in Chapter 8. When Dirichlet problems of the Laplace and biharmonic equations in 2D are solved by the MFS and the BEM, there may be multiple solutions caused by some special shapes of boundary Γ, called degenerate scales. The algorithms of the MFS without degenerate scales are also addressed clearly in this book.

VI. Locations of source nodes. How to choose the source nodes is an important issue in computation. For smooth solutions, the source nodes are located uniformly on circles outside the solution domain. They are simple and effective since the optimal polynomial convergence rates can be achieved. For peanut-like domains and long-narrow domains, the source nodes on pseudo-ellipses are beneficial and studied in Chapter 6 and Part III. The 3D Laplace equation by the MFS is studied in Chapter 13, and the error analysis is made, which may be applied to other kinds of 3D problems. The source nodes are located based on the abscissas of quadrature rules on the pseudo-surfaces; they are "*grid-like*", simple and efficient. For singular solutions, some pseudo-boundaries near the boundary Γ are recommended. Moreover, two pseudo radial-lines are proposed in Chapter 17. Better selections for source nodes are explored in Part III based on the sensitivity index.

VII. Simplicity of algorithms. The MFS is one kind of boundary methods. Boundary methods are much simpler than domain methods, such as the FEM and the FDM, because the problems of PDE are reduced by one dimension. The BEM in [104, 210] is a well-known boundary method, where the same FS is chosen. Since $Q_i \in \Gamma$ and the zero-distance $|\overline{PQ_i}| = 0$ occurs at $P = Q_i$, the algorithms of the BEM are more complicated than those of the MFS. The MPS in [169] is another boundary method, where various harmonic functions are chosen. The simple and uniform collocation equations (1.2.15) and (1.2.16) are a remarkable advantage over the MPS and the BEM. It is due to the modest human effort needed that the MFS has become an attractive and competitive method for scientific/engineering computing.

Part I

Laplace's Equation

> "*Without an acquaintance with the rules of propriety,*
> *it is impossible for the character to be established.*"
> Confucius, 551–479 B.C.

The theory of the method of fundamental solutions (MFS) is explored in Part I. Part I consists of five chapters. Chapter 2 is for Dirichlet problems, where the basic error and stability analysis is explored with some important proof techniques. Based on Bogomolny [26], the error bounds are derived for the bounded simply-connected domains to give the optimal polynomial convergence rates. Based on the circulant matrices in Davis [71], the bounds of condition numbers (Cond) are derived for disk domains to display the exponential growth rates. The proof techniques in Chapter 2 are essential to the MFS, and they can be applied to other chapters.

Chapter 3 is for Neumann problems, where the optimal convergence rates in $\mathbf{L}^2$ and $\mathbf{H}^1$ norms in S can be achieved. The singularity of the operators is dealt with by the truncated singular value decomposition (TSVD) to reduce the Cond significantly. Moreover, the bounds of condition numbers are derived for the bounded simply-connected domains. Chapter 4 discusses other problems, such as mixed boundary problem, interface problem, and annular domain problems. Error analysis is made.

Since the fundamental solutions (FS) are highly smooth, combining the MFS with other numerical methods is necessary for the solutions from corner singularity. Algorithms and analysis are explored in Chapter 5. Most of the analysis in this book is for circular pseudo-boundaries. Elliptic pseudo-boundaries are solicited in Chapter 6 for better stability, and the bounds of errors and condition numbers are derived. Since the discrete matrices obtained are non-circulant matrices, new stability analysis is explored in Chapter 6 to derive the bounds of Cond. Elliptic pseudo-boundaries are often employed for selecting better source nodes in Part III.

We cite three lemmas from Chapter 2, which will be often used in this book.

Lemma I.1 (Basic Lemma A). *For the 2π-periodic function $g = g(x)$, denote the error*

$$\triangle_N(g) = T_N(g) - \int_0^{2\pi} g(x)\,dx, \tag{I.1}$$

where the trapezoidal rule, $T_N(g) = h\sum_{k=0}^{N-1} g(kh)$ with $h = \frac{2\pi}{N}$, is used. Then we have

$$\triangle_N(\sin mx) = 0, m = 1, 2, \ldots, \tag{I.2}$$

$$\triangle_N(\cos mx) = \begin{cases} 2\pi, & \text{if } m = vN, v = 1, 2, \ldots, \\ 0, & \text{otherwise.} \end{cases} \tag{I.3}$$

Lemma I.2 (Basic Lemma B). *Let function $g(x) \in C^\infty[0,\, 2\pi]$ satisfy the periodic boundary conditions $g^{(\ell)}(0) = g^{(\ell)}(2\pi)$ with $\ell = 0,\, 1, \ldots$. Then we have the errors,*

$$\begin{aligned} &T_N(g(x)\cos(kx)) - \int_0^{2\pi} g(x)\cos(kx)\,dx \\ &= \pi \sum_{v=1}^{\infty} \{\alpha_{vN-k} + \alpha_{vN+k}\}, \quad k = 0,\, 1, \ldots, N-1, \end{aligned} \tag{I.4}$$

where coefficients $\alpha_\ell = \frac{1}{\pi}\int_0^{2\pi} g(x)\cos(\ell x)\,dx$ with $\ell = 0,\, 1, \ldots$.

Series expansions of the fundamental solutions (called addition theorems) are essential to algorithms and analysis of the MFS.

Lemma I.3 (Addition Theorem). *There exist the series expansions for the FS in polar coordinates,*

$$\begin{aligned} \ln|\overline{PQ}| &= \ln|P(\mathbf{y}) - Q(\mathbf{x})| = \ln|P(r,\phi) - Q(\rho,\theta)| \\ &= \begin{cases} \ln r - \sum_{n=1}^{\infty} \frac{1}{n}\left(\frac{\rho}{r}\right)^n \cos n(\theta - \phi), & \rho < r, \\ \ln\rho - \sum_{n=1}^{\infty} \frac{1}{n}\left(\frac{r}{\rho}\right)^n \cos n(\theta - \phi), & \rho > r, \end{cases} \end{aligned} \tag{I.5}$$

where $\mathbf{x} = (\rho, \theta)$ and $\mathbf{y} = (r, \phi)$.

The following circulant lemma, the condition number, and the effective condition number are often used for stability analysis. Denote the circulant matrix $\mathbf{A} \in \mathbf{R}^{N\times N}$ by

$$\mathbf{A} = \text{circulant}(a_0, a_1, \ldots, a_{N-1}) = \begin{pmatrix} a_0 & a_1 & \cdots & a_{N-1} \\ a_{N-1} & a_0 & \cdots & a_{N-2} \\ \vdots & \vdots & \cdots & \vdots \\ a_1 & a_2 & \cdots & a_0 \end{pmatrix}, \tag{I.6}$$

where $a_i = \frac{1}{2}\ln|R^2 + \rho^2 - 2R\rho\,\cos(ih)|$ with $i = 0,\, 1, \ldots, N-1$. We cite a lemma from Davis [71].

Lemma I.4 (Circulant Lemma). *For the symmetric matrix $\mathbf{A} = \text{circulant}(a_0, a_1, \ldots, a_{N-1})$ with real entries a_i, the eigenvalues of $\mathbf{A}$ are real and given by*

$$\lambda_k = \sum_{j=0}^{N-1} a_j \cos(kjh), \quad k = 0, 1, \ldots, N-1, \tag{I.7}$$

where $h = \frac{2\pi}{N}$. *Also, the vector* $\mathbf{y}_0 = \frac{1}{\sqrt{N}}(1, 1, \ldots, 1)^T \in \mathbf{R}^N$ *is the eigenvector corresponding to the leading eigenvalue* λ_0.

Consider an overdetermined system $\mathbf{Fx} = \mathbf{b}$, where $\mathbf{F} \in \mathbf{R}^{M\times N}(M \geq N)$, $\mathbf{x} \in \mathbf{R}^N$ and $\mathbf{b} \in \mathbf{R}^M$. For the nonsingular matrix $\mathbf{F}$, the condition number (Cond) and the effective condition number (Cond_eff) are given in [162] by

$$\text{Cond} = \frac{\sigma_{\max}}{\sigma_{\min}}, \quad \text{Cond\_eff} = \frac{\|\mathbf{b}\|}{\sigma_{\min}\|\mathbf{x}\|}, \tag{I.8}$$

where $\|\mathbf{x}\|$ is the Euclidean norm, and $\sigma_{\max}$ and $\sigma_{\min}$ are the maximal and the minimal singular values of $\mathbf{F}$, respectively. For the nonsingular symmetric (or circulant) matrix $\mathbf{F} \in \mathbf{R}^{N\times N}$, the eigenvalues λ_i of $\mathbf{F}$ are real. The condition number and the effective condition number are simplified in [162] by

$$\text{Cond} = \frac{\max_i|\lambda_i|}{\min_i|\lambda_i|}, \quad \text{Cond\_eff} = \frac{\|\mathbf{b}\|}{\min_i|\lambda_i|\|\mathbf{x}\|}. \tag{I.9}$$

Let us cite the key results in Chapter 2. The source nodes Q_i are located uniformly on an outside circle with radius $R > r_{\max} = \max_S r$. Let $u \in \mathbf{H}^p(S)$ $(p > 1)$ and $R \neq 1$ be given. When the N of the FS is chosen moderately large, we derive the following error bounds,

$$\|u - u_N\|_{0,\Gamma} \leq C\frac{1}{N^{p-\frac{1}{2}}}\|u\|_{p,S}, \quad \|u - u_N\|_{0,S} \leq C\frac{1}{N^p}\|u\|_{p,S}, \tag{I.10}$$

where C is a bounded constant independent of N. For the analytic solution u, the equation (I.10) indicates the exponential convergence. For the disk domain S with radius ρ, when $R > \rho$ and $R \neq 1$, we have the following bound,

$$\text{Cond} \leq \frac{N|\ln R|}{2}\left(\frac{R}{\rho}\right)^{\frac{N}{2}}. \tag{I.11}$$

For the non-circular domain S, we have

$$\text{Cond} \leq \frac{N^{\left(1+\frac{\mu}{2}\right)}|\ln R|}{2}\left(\frac{R}{r_{\min}}\right)^{\frac{N}{2}}, \tag{I.12}$$

where $r_{\min} = \min_S r$, and $\mu \in [0, 2]$ is a constant independent of N. Note that the basic proof techniques in Chapter 2 are valid for other equations and problems, and similar results as (I.10)–(I.12) can also be obtained. See Parts I and II. Hence, a uniformly theoretical scheme has been established, to greatly enhance the MFS in a wide range of applications.

Chapter 2

Dirichlet Problems

This chapter consists of the basic error and stability analysis. Based on Bogomolny [26], the error bounds are derived for the bounded simply-connected domains, to give the optimal polynomial convergence rates. Based on circulant matrices in Davis [71], the bounds of condition numbers are derived only for disk domains, to display the exponential growth. The basic proof techniques are explored, to lay a theoretical basis for the method of fundamental solution (MFS) in 2D, which can be developed for other problems and various differential equations in other chapters.

This chapter is organized as follows. In the first section, the basic algorithms of the MFS are described. In Section 2.2, some preliminary lemmas are given, and in Section 2.3, the main theorems of error bounds are proved. In Section 2.4, stability analysis is made for disk domains. In the last section, the proof methodology used in this chapter is addressed. The materials of this chapter are adapted from [151, 163].

2.1 Basic Algorithms of MFS

Consider Laplace's equation with the Dirichlet boundary condition,

$$\Delta u = \frac{\partial^2 u}{\partial x^2} + \frac{\partial^2 u}{\partial y^2} = 0 \text{ in } S, \tag{2.1.1}$$

$$u = f \text{ on } \Gamma, \tag{2.1.2}$$

where S is a bounded simply-connected domain with a smooth boundary Γ $(= \partial S)$. Denote

$$r_{\max} = \max_{S} r, \quad r_{\min} = \max_{S_{\text{in}}(S_{\text{in}} \subseteq S)} r, \tag{2.1.3}$$

where S_{in} is a disk inside S (see Figure 1.1). A circle surrounding S is given by

$$\ell_R = \{(r, \theta) | r = R,\ 0 \le \theta \le 2\pi\}, \quad R > r_{\max}. \tag{2.1.4}$$

DOI: 10.1051/978-2-7598-3171-5.c002
© Science Press, EDP Sciences, 2023

Let the source (charge) nodes Q be located outside S, then the fundamental solutions (FS)

$$\phi(r,\theta) = \ln|\overline{PQ}|, \quad P \in S \cup \partial S, \tag{2.1.5}$$

are harmonic, where $P = \{(x,y)|x = r\ \cos\theta, y = r\ \sin\theta\}$. Based on Bogomolny [26], the source nodes $Q_i = \{(x,y)|x = R\ \cos(ih), y = R\ \sin(ih)\}$ may be simply located uniformly on ℓ_R, where $R > r_{\max}$ and $h = \frac{2\pi}{N}$. We obtain the FS, $\phi_i(P) = \ln|\overline{PQ_i}|$, $i = 1, 2, \ldots, N$, and the numerical solution is given by a linear combination,

$$u_N = \sum_{i=1}^{N} c_i \phi_i(P), \tag{2.1.6}$$

where c_i are the unknown coefficients to be sought. Since u_N satisfies Laplace's equation in S already, the coefficients c_i can be sought by enforcing the boundary condition (2.1.2) only. We will follow the Trefftz method (TM) in [146, 169] to seek u_N (*i.e.*, c_i). Denote the energy

$$I(v) = \int_\Gamma (v - f)^2. \tag{2.1.7}$$

Also denote by V_N the set of (2.1.6). Then the numerical solution u_N can be obtained by

$$I(u_N) = \min_{v \in V_N} I(v). \tag{2.1.8}$$

The TM solution u_N also satisfies

$$\|u - u_N\|_{0,\Gamma} = \min_{v \in V_N} \|u - v\|_{0,\Gamma}, \tag{2.1.9}$$

and

$$[u - u_N, v] = 0, \quad \forall v \in V_N, \tag{2.1.10}$$

where $[u,v] = \int_\Gamma uv$.

When the integrals in (2.1.7) involve approximation, denote

$$\widehat{I}(v) = \widehat{\int_\Gamma} (v - f)^2, \tag{2.1.11}$$

where $\widehat{\int}_\Gamma$ is a numerical approximation of $\int_\Gamma$ by some quadrature rules, such as the central, the trapezoidal or the Gaussian rule. Hence, the numerical solution $\tilde{u}_N \in V_N$ is obtained by

$$\widehat{I}(\tilde{u}_N) = \min_{v \in V_N} \widehat{I}(v). \tag{2.1.12}$$

We may establish the collocation equations directly from (2.1.2) to yield

$$\sum_{i=1}^{N} c_i \phi_i(P_j) = f(P_j), \quad P_j \in \mathbf{\Gamma}. \tag{2.1.13}$$

Let $\mathbf{\Gamma}$ be divided into small $\mathbf{\Gamma}_j$ with the meshspacings $\triangle h_j$, *i.e.*, $\mathbf{\Gamma} = \bigcup_{j=1}^{M} \mathbf{\Gamma}_j$. We obtain from (2.1.13)

$$\sqrt{\triangle h_j} \sum_{i=1}^{N} c_i \phi_i(P_j) = \sqrt{\triangle h_j}\, f(P_j), \quad P_j \in \mathbf{\Gamma},\ j = 1, 2, \ldots, M, \tag{2.1.14}$$

where P_j are the midpoints of $\mathbf{\Gamma}_j$. The equation (2.1.14) are just equivalent to (2.1.12), where the central rule is chosen for $\widehat{\int}_{\mathbf{\Gamma}}$. In computation, we may choose the number of collocation nodes to be equal to (or larger than) that of source nodes, *i.e.*, $M \geq N$. When the Gaussian rule is chosen, the following collocation equations are obtained,

$$\sqrt{\beta_j} \sum_{i=1}^{N} c_i \phi_i(P_j) = \sqrt{\beta_j}\, f(P_j), \quad P_j \in \mathbf{\Gamma}, \tag{2.1.15}$$

where P_j are the Gaussian nodes, weights $\beta_j = O(\triangle h)$, and $\triangle h = \max_j \triangle h_j$. The equations (2.1.15) are called the collocation Trefftz method (CTM) in [169].

2.2 Preliminary Lemmas

We prove the following lemma given in [26, 72].

Lemma 2.2.1 (Basic Lemma A). *For the 2π-periodic function $g = g(x)$, denote the error*

$$\triangle_N(g) = T_N(g) - \int_0^{2\pi} g(x)dx, \tag{2.2.1}$$

where the trapezoidal rule, $T_N(g) = h\sum_{k=0}^{N-1} g(kh) := \Sigma_N(g)$ with $h = \frac{2\pi}{N}$. Then there exist the equalities,

$$\triangle_N(\sin mx) = 0, m = 1, 2, \ldots, \tag{2.2.2}$$

$$\triangle_N(\cos mx) = \begin{cases} 2\pi, & \text{if } m = vN, v = 1, 2, \ldots, \\ 0, & \textit{otherwise.} \end{cases} \tag{2.2.3}$$

Proof. Denote the imaginary $\mathbf{i} = \sqrt{-1}$. We have for $\theta \in [0,\, 2\pi]$

$$T_N(\exp(\mathbf{i}n\theta)) = h \sum_{k=0}^{N-1} \exp(\mathbf{i}nkh). \tag{2.2.4}$$

When n is multiples of N, *i.e.*, $n = vN$ with $v = 0,\, 1, 2, \ldots$, we have

$$nkh = (vN)k\frac{2\pi}{N} = 2\pi v k, \tag{2.2.5}$$

to give

$$T_N(\exp(\mathbf{i}n\theta)) = h\sum_{k=0}^{N-1}\exp(\mathbf{i}2\pi vk) = hN = 2\pi. \tag{2.2.6}$$

Otherwise (*i.e.*, $n \neq vN$ with $v = 0, 1, 2, \ldots$), we have from the sum of the geometric series with ratio $\exp(nh\mathbf{i})$

$$T_N(\exp(\mathbf{i}n\theta)) = h\sum_{k=0}^{N-1}\exp(\mathbf{i}nkh) = h\frac{1-\exp(\mathbf{i}nNh)}{1-\exp(\mathbf{i}nh)} = h\frac{1-\exp(\mathbf{i}n2\pi)}{1-\exp(\mathbf{i}nh)} = 0. \tag{2.2.7}$$

On the other hand, since $\exp(\mathbf{i}n\theta) = \cos(n\theta) + \mathbf{i}\,\sin(n\theta)$, we have

$$T_N(\exp(\mathbf{i}n\theta)) = T_N(\cos(n\theta)) + \mathbf{i}T_N(\sin(n\theta)). \tag{2.2.8}$$

By comparing (2.2.6) and (2.2.7) with the following exact values,

$$\int_0^{2\pi} d\theta = 2\pi, \int_0^{2\pi}\cos(n\theta)\,d\theta = \int_0^{2\pi}\sin(n\theta)\,d\theta = 0, \quad n = 1, 2, \ldots, \tag{2.2.9}$$

we obtain the desired results (2.2.2) and (2.2.3). ■

Denote nodes $\mathbf{x} = Q = (x, y) = (\rho, \theta)$ and $\mathbf{y} = P = (\xi, \eta) = (r, \phi)$, where $x = \rho\cos\theta$, $y = \rho\sin\theta$, $\xi = r\cos\phi$, $\eta = r\sin\phi$. Then $\rho = \sqrt{x^2 + y^2}$ and $r = \sqrt{\xi^2 + \eta^2}$. The FS of Laplace's equation is given by $\ln|\overline{PQ}| = \ln\sqrt{\rho^2 - 2\rho r\cos(\theta - \phi) + r^2}$. The series expansions of fundamental solutions (called addition theorems) are essential to algorithms and analysis of the MFS. We have the following addition theorem.

Lemma 2.2.2 (Addition Theorem). *There exist the series expansions for the FS in polar coordinates,*

$$\begin{aligned}\ln|\overline{PQ}| &= \ln|P(\mathbf{y}) - Q(\mathbf{x})| = \ln|P(r,\phi) - Q(\rho,\theta)| \\ &= \begin{cases} \ln r - \sum_{n=1}^{\infty}\frac{1}{n}\left(\frac{\rho}{r}\right)^n \cos n(\theta - \phi), & \rho < r, \\ \ln\rho - \sum_{n=1}^{\infty}\frac{1}{n}\left(\frac{r}{\rho}\right)^n \cos n(\theta - \phi), & \rho > r, \end{cases}\end{aligned} \tag{2.2.10}$$

where $\mathbf{x} = (\rho, \theta)$ *and* $\mathbf{y} = (r, \phi)$.

Proof. In [90, 1.514], there exists an equality,

$$\ln(1 - 2x\,\cos\phi + x^2) = -2\sum_{n=1}^{\infty}\frac{\cos(n\phi)}{n}x^n,\ x^2 \leq 1,\ x\,\cos\phi \neq 1. \tag{2.2.11}$$

For $\rho < r$, denote $x = \frac{\rho}{r} < 1$. We have

$$\begin{aligned}\ln|\overline{PQ}| &= \ln\sqrt{r^2 - 2\rho r\,\cos(\theta - \phi) + \rho^2} = \frac{1}{2}\ln(r^2 - 2\rho r\,\cos(\theta - \phi) + \rho^2) \\ &= \frac{1}{2}\{\ln(r^2) + \ln(1 - 2x\,\cos(\theta - \phi) + x^2)\}.\end{aligned} \tag{2.2.12}$$

Since $x < 1$, we have $x\cos(\theta-\phi) \neq 1$. From (2.2.11), the equation (2.2.12) leads to

$$\ln|\overline{PQ}| = \ln r - \sum_{n=1}^{\infty}\frac{\cos n(\theta-\phi)}{n}x^n = \ln r - \sum_{n=1}^{\infty}\frac{1}{n}\left(\frac{\rho}{r}\right)^n \cos n(\theta-\phi).$$

This is the first equation in (2.2.10), and the second equation in (2.2.10) follows by switching ρ and r. ■

Denote nodes $P(\rho,\theta)\in\bar{S}$, and the source nodes $Q(R,\psi)$ outside S with $R>\rho$. From the first equality in (2.2.10), we have

$$\ln|\overline{PQ}| = \ln\sqrt{\rho^2-2\rho R\cos(\theta-\psi)+R^2} = \ln R - \sum_{n=1}^{\infty}\frac{1}{n}\left(\frac{\rho}{R}\right)^n \cos n(\theta-\psi), \quad \rho<R.$$

Then we obtain the following lemma from the orthogonality of trigonometric functions.

Lemma 2.2.3. *For $R>\rho$ and $R\neq 1$, there exist the equalities,*

$$\int_0^{2\pi}\ln\left(\sqrt{\rho^2-2\rho R\cos(\theta-\psi)+R^2}\right)d\psi = 2\pi\ln R,$$

$$\int_0^{2\pi}\ln\left(\sqrt{\rho^2-2\rho R\cos(\theta-\psi)+R^2}\right)\cos(m\psi)\,d\psi = -\frac{\pi}{mR^m}\rho^m\cos(m\theta), \quad m=1,2,\ldots,$$

$$\int_0^{2\pi}\ln\left(\sqrt{\rho^2-2\rho R\cos(\theta-\psi)+R^2}\right)\sin(m\psi)\,d\psi = -\frac{\pi}{mR^m}\rho^m\sin(m\theta), \quad m=1,2,\ldots.$$

From Lemma 2.2.3, there exist the equalities for $R>\rho$,

$$1 = \frac{1}{2\pi\ln R}\int_0^{2\pi}\ln\left(\sqrt{\rho^2-2\rho R\cos(\theta-\psi)+R^2}\right)d\psi, \quad R\neq 1, \tag{2.2.13}$$

$$\begin{aligned} C_m(\rho,\theta) &= \rho^m\cos(m\theta) \qquad (2.2.14)\\ &= -\frac{mR^m}{\pi}\int_0^{2\pi}\ln\left(\sqrt{\rho^2-2\rho R\cos(\theta-\psi)+R^2}\right)\cos(m\psi)\,d\psi, \quad m=1,2,\ldots,\\ S_m(\rho,\theta) &= \rho^m\sin(m\theta) \qquad (2.2.15)\\ &= -\frac{mR^m}{\pi}\int_0^{2\pi}\ln\left(\sqrt{\rho^2-2\rho R\cos(\theta-\psi)+R^2}\right)\sin(m\psi)\,d\psi, \quad m=1,2,\ldots. \end{aligned}$$

Denote the norm

$$\|v\|_{0,\Gamma} = \left\{\int_\Gamma v^2\right\}^{\frac{1}{2}}. \tag{2.2.16}$$

The solution u_N of the MFS by (2.1.8) also satisfies

$$\|u - u_N\|_{0,\Gamma} = \min_{v \in V_N} \|u - v\|_{0,\Gamma}. \tag{2.2.17}$$

Denote the harmonic polynomials of order n by

$$\begin{aligned} P_n(\rho, \theta) &= \frac{a_0}{2} + \sum_{m=1}^{n} \rho^m \{a_m \cos(m\theta) + b_m \sin(m\theta)\} \\ &= \frac{a_0}{2} + \sum_{m=1}^{n} \{a_m C_m(\rho, \theta) + b_m S_m(\rho, \theta)\}, \end{aligned} \tag{2.2.18}$$

where $C_m(\rho, \theta) = \rho^m \cos(m\theta)$ and $S_m(\rho, \theta) = \rho^m \sin(m\theta)$. Then we have the following approximations,

$$1 \approx \sum_{k=1}^{N} \alpha_{k,0} \phi_k(\rho, \theta), \tag{2.2.19}$$

$$C_m(\rho, \theta) = \rho^m \cos(m\theta) \approx \sum_{k=1}^{N} \alpha_{k,m} \phi_k(\rho, \theta), \quad m = 1, 2, \ldots, \tag{2.2.20}$$

$$S_m(\rho, \theta) = \rho^m \sin(m\theta) \approx \sum_{k=1}^{N} \beta_{k,m} \phi_k(\rho, \theta), \quad m = 1, 2, \ldots. \tag{2.2.21}$$

From (2.2.18)–(2.2.21), we have

$$P_n(\rho, \theta) \approx \sum_{k=1}^{N} c_k \phi_k(\rho, \theta) := \Sigma_N(P_n; \rho, \theta), \tag{2.2.22}$$

where the coefficients

$$c_k = \frac{\alpha_{k,0} a_0}{2} + \sum_{m=1}^{n} (\alpha_{k,m} a_m + \beta_{k,m} b_m). \tag{2.2.23}$$

Below, we will derive bounds of the errors

$$\|P_n(\rho, \theta) - \Sigma_N(P_n; \rho, \theta)\|_{q,\Gamma_\rho}, \tag{2.2.24}$$

where $\Gamma_\rho = \{(r, \theta) | 0 \le r \le \rho, 0 \le \theta \le 2\pi\}$ and $\|v\|_{q,\Gamma_\rho}$ are the Sobolev norms.

Denote

$$\Sigma_N(P_n; \rho, \theta) = h \sum_{k=1}^{N} d_k \phi_k(\rho, \theta), \tag{2.2.25}$$

where d_k are the coefficients and $\phi_k(\rho, \theta) = \ln \sqrt{\rho^2 - 2\rho R \cos(\theta - \psi_k) + R^2}$ with $\psi_k = kh$ and $h = \frac{2\pi}{N}$. The coefficients $\alpha_{k,m}$ and $\beta_{k,m}$ can be found from (2.2.13)–(2.2.15),

$$\Sigma_N(1;\rho,\theta)=\sum_{k=1}^{N}\alpha_{k,0}\phi_k(\rho,\theta),\quad \alpha_{k,0}=\frac{h}{2\pi\,\ln R},\quad R\neq 1,$$

$$\Sigma_N(C_m;\rho,\theta)=\sum_{k=1}^{N}\alpha_{k,m}\phi_k(\rho,\theta),\quad \alpha_{k,m}=-h\left(\frac{mR^m}{\pi}\right)\cos(mkh),\quad m=1,2,\ldots,$$

$$\Sigma_N(S_m;\rho,\theta)=\sum_{k=1}^{N}\beta_{k,m}\phi_k(\rho,\theta),\quad \beta_{k,m}=-h\left(\frac{mR^m}{\pi}\right)\sin(mkh),\quad m=1,2,\ldots.$$

We only derive in detail the errors in (2.2.20)

$$EC_m(\rho,\theta)=\rho^m\cos(m\theta)-\sum_{k=1}^{N}\alpha_{k,m}\phi_k(\rho,\theta), \tag{2.2.26}$$

since the errors for (2.2.19) and (2.2.21) can be derived similarly. To this end, we expand (2.2.26) as a Fourier series,

$$EC_m(\rho,\theta)=\frac{a_{0,m}}{2}+\sum_{k=1}^{\infty}\{a_{k,m}\,\cos(k\theta)+b_{k,m}\,\sin(k\theta)\}, \tag{2.2.27}$$

where the Fourier coefficients are given by

$$a_{k,m}=\frac{1}{\pi}\int_0^{2\pi}EC_m(\rho,\theta)\cos(k\theta)\,d\theta,\quad k=0,\,1,2,\ldots, \tag{2.2.28}$$

$$b_{k,m}=\frac{1}{\pi}\int_0^{2\pi}EC_m(\rho,\theta)\sin(k\theta)\,d\theta,\quad k=1,2,\ldots. \tag{2.2.29}$$

Lemma 2.2.4. *For the Fourier expansions in (2.2.27), the Fourier coefficients are given by*

$$a_{k,m}=\begin{cases}\frac{m}{k}R^{m-k}\rho^k, & \text{if } k=\pm m+\nu N,\ \nu=1,2,\ldots,\\ 0, & \textit{otherwise},\end{cases} \tag{2.2.30}$$

$$b_{k,m}=0,\quad \forall k,m. \tag{2.2.31}$$

Proof. We have

$$\begin{aligned} a_{k,m} &= T_1-T_2 \qquad (2.2.32)\\ &:=\frac{1}{\pi}\int_0^{2\pi}C_m(\rho,\theta)\cos(k\theta)\,d\theta-\frac{1}{\pi}\left\{\left(-h\frac{mR^m}{\pi}\right)\int_0^{2\pi}\sum_{j=1}^{N}\phi_j(\rho,\theta)\cos(mjh)\cos(k\theta)\,d\theta\right\}.\end{aligned}$$

From (2.2.14),

$$\begin{aligned}
T_1 &= \frac{1}{\pi}\int_0^{2\pi}\left(-\frac{mR^m}{\pi}\right)\left\{\int_0^{2\pi}\ln\left(\sqrt{\rho^2-2\rho R\,\cos(\theta-\psi)+R^2}\right)\cos(m\psi)\,d\psi\right\}\cos(k\theta)\,d\theta \\
&= \frac{1}{\pi}\left(-\frac{mR^m}{\pi}\right)\int_0^{2\pi}\left\{\int_0^{2\pi}\ln\left(\sqrt{\rho^2-2\rho R\,\cos(\theta-\psi)+R^2}\right)\cos(k\theta)\,d\theta\right\}\cos(m\psi)\,d\psi \\
&= \frac{1}{\pi}\left(-\frac{mR^m}{\pi}\right)\int_0^{2\pi}\frac{-\pi}{kR^k}\,C_k(\rho,\psi)\cos(m\psi)\,d\psi \\
&= \frac{1}{\pi}\left(\frac{m}{k}R^{m-k}\rho^k\right)\int_0^{2\pi}\cos(k\psi)\cos(m\psi)\,d\psi. \qquad (2.2.33)
\end{aligned}$$

Similarly, we obtain

$$\begin{aligned}
T_2 &= \frac{1}{\pi}\left(-\frac{mR^m}{\pi}\right)\int_0^{2\pi}h\sum_{j=1}^{N}\left(\ln\sqrt{\rho^2-2\rho R\,\cos(\theta-\psi_j)+R^2}\right)\cos(mjh)\cos(k\theta)\,d\theta \\
&= \frac{1}{\pi}\left(-\frac{mR^m}{\pi}\right)h\sum_{j=1}^{N}\cos(mjh)\left\{\int_0^{2\pi}\left(\ln\sqrt{\rho^2-2\rho R\,\cos(t)+R^2}\right)\cos k(t-\psi_j)\,dt\right\} \\
&= \frac{1}{\pi}\left(-\frac{mR^m}{\pi}\right)\left(-\frac{kR^k}{\pi}\right)^{-1}h\sum_{j=1}^{N}C_k(\rho,\psi_j)\cos(mjh) \\
&= \frac{1}{\pi}\left(\frac{m}{k}R^{m-k}\rho^k\right)h\sum_{j=1}^{N}\cos(kjh)\cos(mjh). \qquad (2.2.34)
\end{aligned}$$

Hence the coefficients $a_{k,m}$ are found by

$$a_{k,m} = T_1 - T_2 = \frac{1}{\pi}\left(\frac{m}{k}R^{m-k}\rho^k\right)\triangle_N(\cos(k\psi)\cos(m\psi)). \qquad (2.2.35)$$

Since $\cos(k\psi)\cos(m\psi) = \frac{1}{2}\{\cos(k+m)\psi + \cos(k-m)\psi\}$, from Lemma 2.2.1 we have $a_{0,m} = 0$ and

$$\begin{aligned}
a_{k,m} &= T_1 - T_2 = \frac{1}{2\pi}\left(\frac{m}{k}R^{m-k}\rho^k\right)\{\triangle_N(\cos(k+m)\psi) + \triangle_N(\cos(k-m)\psi)\} \\
&= \frac{m}{k}R^{m-k}\rho^k, \quad \text{if } k = \pm m + vN,\ v = 1, 2, \ldots.
\end{aligned}$$

This is the first desired result (2.2.30).

Similarly, we have from Lemma 2.2.1 again

$$\begin{aligned}
b_{k,m} &= \frac{1}{\pi}\left(\frac{m}{k}R^{m-k}\rho^k\right)\triangle_N(\cos(m\psi)\sin(k\psi)) \\
&= \frac{1}{2\pi}\left(\frac{m}{k}R^{m-k}\rho^k\right)\{\triangle_N(\sin(k+m)\psi) + \triangle_N(\sin(k-m)\psi)\} = 0.
\end{aligned}$$

This gives the second result (2.2.31) and completes the proof of Lemma 2.2.4. ■

2.3 Main Theorems

Denote two circles $\Gamma_{\max} = \{(r,\theta) | r = r_{\max}, 0 \le \theta \le 2\pi\}$ and $\Gamma_{\min} = \{(r,\theta) | r = r_{\min}, 0 \le \theta \le 2\pi\}$, where $r_{\max}$ and $r_{\min}$ are given in (2.1.3).

Theorem 2.3.1. *Let $u \in \mathbf{H}^p(S)$ $(p > 1)$ and $R \neq 1$ be given, and suppose that the following bound holds,*

$$2^{2q+1}\left(\frac{R}{\rho}\right)^{-2N} \le 1, \quad q \ge 0. \tag{2.3.1}$$

Then there exists the bound for $q \ge 0$,

$$\|P_n(r,\theta) - \Sigma_N(P_n; r,\theta)\|_{q,\Gamma} \le CN^q \left(\frac{R}{r_{\max}}\right)^{2n-N} \left(\frac{r_{\max}}{r_{\min}}\right)^n \|P_n(r,\theta)\|_{0,\Gamma}, \tag{2.3.2}$$

where C is a bounded constant independent of n and N.

Proof. The basic proof approaches follow Bogomolny [26]. Denote the circle $\Gamma_\rho = \{(r,\theta) | r = \rho, 0 \le \theta \le 2\pi\}$. We have from (2.2.26)

$$\begin{aligned}
\|EC_m(\rho,\theta)\|^2_{q,\Gamma_\rho} &= \sum_{\ell=0}^{q} \int_{\Gamma_\rho} \{D^\ell(EC_m(\rho,\theta))\}^2 \rho\, d\theta \le C \sum_{k=1}^{\infty} a^2_{k,m} k^{2q} \\
&= C \sum_{k=\pm m+\nu N}^{\infty} k^{2q} \left(\frac{m}{k} R^{m-k} \rho^k\right)^2 = C \sum_{k=\pm m+\nu N}^{\infty} \frac{m^2}{k^2} k^{2q} \rho^{2k} R^{2(m-k)} \\
&= C\left\{ \sum_{k=-m+\nu N}^{\infty} \frac{m^2}{k^2} k^{2q} \rho^{2k} R^{2(m-k)} + \sum_{k=m+\nu N}^{\infty} \frac{m^2}{k^2} k^{2q} \rho^{2k} R^{2(m-k)} \right\} \\
&:= D_1 + D_2.
\end{aligned} \tag{2.3.3}$$

First, we have

$$\begin{aligned}
D_1 &= \sum_{k=-m+\nu N}^{\infty} \frac{m^2}{k^2} k^{2q} \rho^{2k} R^{2(m-k)} \\
&= \sum_{\nu=1}^{\infty} \frac{m^2}{(-m+\nu N)^2} R^{2(m-(-m+\nu N))} \rho^{2(-m+\nu N)} (-m+\nu N)^{2q} \\
&\le \frac{m^2}{(-m+N)^2} N^{2q} \left(\frac{R}{\rho}\right)^{2m} R^{2m} \times \sum_{\nu=1}^{\infty} \left(\frac{R}{\rho}\right)^{-2\nu N} \nu^{2q}.
\end{aligned} \tag{2.3.4}$$

Since $N > 2n \ge 2m$, we have $\frac{m}{N-m} \le 1$. When the condition (2.3.1) holds, there exists the bound from Bogomolny [26, p.665]

$$\sum_{\ell=1}^{\infty} \left(\frac{R}{\rho}\right)^{-2N\ell} \ell^{2q} \le 2\left(\frac{R}{\rho}\right)^{-2N}, \quad R > \rho. \tag{2.3.5}$$

Hence, we have from (2.3.4) and (2.3.5)

$$D_1 \le 2N^{2q}\left(\frac{R}{\rho}\right)^{2m}\left(\frac{R}{\rho}\right)^{-2N}R^{2m} = 2N^{2q}\left(\frac{R}{\rho}\right)^{2(m-N)}R^{2m}. \tag{2.3.6}$$

Obviously, there exists the bound,

$$D_2 = \sum_{k=m+vN}^{\infty}\frac{m^2}{k^2}k^{2q}\rho^{2k}R^{2(m-k)} \le CD_1. \tag{2.3.7}$$

Then we have from (2.3.3)–(2.3.7)

$$\|EC_m(\rho,\theta)\|^2_{q,\Gamma_\rho} \le CN^{2q}\left(\frac{R}{\rho}\right)^{2(m-N)}R^{2m}. \tag{2.3.8}$$

Similarly we have

$$\|EC_0(\rho,\theta)\|^2_{q,\Gamma_\rho} \le C\left(\frac{1}{\ln R}\right)^2 N^{2q}\left(\frac{R}{\rho}\right)^{-2N}, \quad R \ne 1, \tag{2.3.9}$$

$$\|ES_m(\rho,\theta)\|^2_{q,\Gamma_\rho} \le CN^{2q}\left(\frac{R}{\rho}\right)^{2(m-N)}R^{2m}. \tag{2.3.10}$$

From (2.3.8)–(2.3.10) and the Schwarz inequality, we have for $0<\tilde{\rho}\le\rho$

$$\begin{aligned}
&\|P_n(r,\theta) - \Sigma_N(P_n;r,\theta)\|_{q,\Gamma_\rho} \\
&\le \frac{|a_0|}{2}\|EC_0(\rho,\theta)\|_{q,\Gamma_\rho} + \sum_{m=1}^{n}|a_m|\|EC_m(\rho,\theta)\|_{q,\Gamma_\rho} + \sum_{m=1}^{n}|b_m|\|ES_m(\rho,\theta)\|_{q,\Gamma_\rho} \\
&\le \left\{\left(\left(\frac{a_0}{2}\right)^2 + \sum_{m=1}^{n}\tilde{\rho}^{2m}(a_m^2+b_m^2)\right)\left(\sum_{m=0}^{n}\frac{1}{\tilde{\rho}^{2m}}\|EC_m(\rho,\theta)\|^2_{q,\Gamma_\rho}\right)\right\}^{\frac{1}{2}}.
\end{aligned} \tag{2.3.11}$$

Moreover, we have the bound from (2.3.8),

$$\begin{aligned}
&\sum_{m=0}^{n}\frac{1}{\tilde{\rho}^{2m}}\|EC_m(\rho,\theta)\|^2_{q,\Gamma_\rho} \le C\sum_{m=0}^{n}\frac{1}{\tilde{\rho}^{2m}}N^{2q}\left(\frac{R}{\rho}\right)^{2(m-N)}R^{2m} \\
&= CN^{2q}\left(\frac{R}{\rho}\right)^{-2N}\sum_{m=0}^{n}\frac{1}{\tilde{\rho}^{2m}}R^{2m}\left(\frac{R}{\rho}\right)^{2m} = CN^{2q}\left(\frac{R}{\rho}\right)^{-2N}\sum_{m=0}^{n}\left(\frac{R}{\rho}\right)^{4m}\left(\frac{\rho}{\tilde{\rho}}\right)^{2m} \\
&\le CN^{2q}\left(\frac{R}{\rho}\right)^{-2N}\left(\frac{R}{\rho}\right)^{4n}\left(\frac{\rho}{\tilde{\rho}}\right)^{2n} \le CN^{2q}\left(\frac{R}{\rho}\right)^{4n-2N}\left(\frac{\rho}{\tilde{\rho}}\right)^{2n}.
\end{aligned} \tag{2.3.12}$$

On the other hand, there exists the bound,

$$\left(\frac{a_0}{2}\right)^2 + \sum_{m=1}^{n} \tilde{\rho}^{2m}(a_m^2 + b_m^2) \le \|P_n(\tilde{\rho}, \theta)\|_{0,\Gamma_{\tilde{\rho}}}^2. \tag{2.3.13}$$

Hence, we have from (2.3.11)–(2.3.13)

$$\begin{aligned}
&\|P_n(r,\theta) - \Sigma_N(P_n; r, \theta)\|_{q,\Gamma_\rho}^2 \\
&\le CN^{2q}\left(\frac{R}{\rho}\right)^{4n-2N}\left(\frac{\rho}{\tilde{\rho}}\right)^{2n}\left\{\left(\frac{a_0}{2}\right)^2 + \sum_{m=1}^{n} \tilde{\rho}^{2m}(a_m^2 + b_m^2)\right\} \\
&\le CN^{2q}\left(\frac{R}{\rho}\right)^{4n-2N}\left(\frac{\rho}{\tilde{\rho}}\right)^{2n}\|P_n(\tilde{\rho}, \theta)\|_{0,\Gamma_{\tilde{\rho}}}.
\end{aligned} \tag{2.3.14}$$

Also since $\Delta v = 0$, there exist the bounds in [15, 195],

$$\|v\|_{k,\Gamma} \le C\|v\|_{k+\frac{1}{2},S}, \quad \|v\|_{k+\frac{1}{2},S} \le C\|v\|_{k,\Gamma}. \tag{2.3.15}$$

Then we have from (2.3.14) and (2.3.15)

$$\begin{aligned}
\|P_n(r,\theta) - \Sigma_N(P_n; r, \theta)\|_{q,\Gamma}^2 &\le C\|P_n(r,\theta) - \Sigma_N(P_n; r,\theta)\|_{q+\frac{1}{2},S}^2 \\
&\le C\|P_n(r,\theta) - \Sigma_N(P_n; r,\theta)\|_{q+\frac{1}{2},S_{\max}}^2 \\
&\le C\|P_n(r_{\max},\theta) - \Sigma_N(P_n; r_{\max},\theta)\|_{q,\Gamma_{\max}}^2 \\
&\le CN^{2q}\left(\frac{R}{r_{\max}}\right)^{4n-2N}\left(\frac{r_{\max}}{r_{\min}}\right)^{2n}\|P_n(r,\theta)\|_{0,\Gamma_{\max}}^2 \\
&\le CN^{2q}\left(\frac{R}{r_{\max}}\right)^{4n-2N}\left(\frac{r_{\max}}{r_{\min}}\right)^{2n}\|P_n(r,\theta)\|_{0,\Gamma}^2.
\end{aligned} \tag{2.3.16}$$

In the last bound in (2.3.16), we have used the continuity extension. See Remark 2.3.1 below. From the smooth boundary $\mathbf{\Gamma}$, under the assumption $u \in \mathbf{H}^p(S)$ $(p > 1)$, the solution in S can be extended continuously to the boundary $\mathbf{\Gamma}_{\max}$. We then have $\|P_n(r,\theta)\|_{0,\Gamma_{\max}} \le C\|P_n(r,\theta)\|_{0,\Gamma}$. This completes the proof of Theorem 2.3.1. ■

Remark 2.3.1 (Continuity Extension). *From Adams [2, Chapter IV], for the bounded domain* S *with the* C^1 *boundary* $\mathbf{\Gamma}$*, the solution* $u \in \mathbf{H}^k(S)$ *with* $k \ge 0$ *can be extended continuously to the entire 2D plane. Denote by* $S_{r_{\max}}$ *a disk with radius* $r_{\max}$*. The solution under the assumption* $u \in \mathbf{H}^p(S)$ $(p > 1)$ *can be extended to* $u \in \mathbf{H}^p(S_{r_{\max}})$ $(p > 1)$*. Based on the Sobolev imbedded theorem in Adams [2, Chapter V], the* u *is continuous in* $S_{r_{\max}}$*; called the continuity extension in this book. We then have the bounds,*

$$\|u\|_{\infty,S_{r_{\max}}} \le C, \tag{2.3.17}$$

$$\|P_n(r,\theta)\|_{0,\Gamma_{\max}} \approx \|u\|_{0,\Gamma_{\max}} \asymp O(1), \tag{2.3.18}$$

$$\|P_n(r,\theta)\|_{0,\Gamma_{\max}} \le C\|P_n(r,\theta)\|_{0,\Gamma} \le C\|u\|_{0,\Gamma} \asymp O(1), \tag{2.3.19}$$

where the notation $a \asymp O(b)$ *means that there exist two positives bounded constant* c_0 *and* C *independent of* n *such that* $c_0 b \le a \le Cb$*. The continuity extension also means that the harmonic polynomials (2.2.18) are valid for* $\rho \le r_{\max}$*. The continuity extension holds for the Lipschitz boundary* Γ *(see Brenner and Scott [28, p.31]). Since the polygonal domains* S *have the Lipschitz boundary* Γ*, the continuity extension is also valid. We may simply assume the continuous solutions* $u \in C(S)$ *instead.*

Theorem 2.3.2. *Let the conditions in Theorem 2.3.1 hold. Suppose that* N *satisfies*

$$\left(\frac{R}{r_{\max}}\right)^{2n-N}\left(\frac{r_{\max}}{r_{\min}}\right)^{n} \le \frac{1}{n^{p-\frac{1}{2}}}. \tag{2.3.20}$$

For the Dirichlet problem, there exists the error bound,

$$\|u-u_N\|_{0,\Gamma} \le C\frac{1}{N^{p-\frac{1}{2}}}\|u\|_{p,S}, \tag{2.3.21}$$

where C *is a bounded constant independent of* N*.*

Proof. Choose $v = u_N^* = \Sigma_N(P_n)$, and denote $u = P_n(r,\theta) + R_n(r,\theta)$. From (2.2.17) we have

$$\|u-u_N\|_{0,\Gamma} \le \|u-u_N^*\|_{0,\Gamma} \le \|P_n(r,\theta)-u_N^*\|_{0,\Gamma} + \|R_n(r,\theta)\|_{0,\Gamma}. \tag{2.3.22}$$

For $u \in \mathbf{H}^p(S)$, there exist the bounds

$$\|R_n(r,\theta)\|_{k,S} \le C\frac{1}{n^{p-k}}\|u\|_{p,S}. \tag{2.3.23}$$

Then we have from the embedding theorem [15]

$$\begin{aligned}\|R_n(r,\theta)\|_{0,\Gamma} &\le C\|R_n(r,\theta)\|_{\frac{1}{2},S}\\ &\le C\Big\{\|R_n(r,\theta)\|_{0,S}\|R_n(r,\theta)\|_{1,S}\Big\}^{\frac{1}{2}} \le C\frac{1}{n^{p-\frac{1}{2}}}\|u\|_{p,S}.\end{aligned} \tag{2.3.24}$$

On the other hand, when (2.3.20) is satisfied, we may choose

$$N \approx 2n + \frac{n\ln\left(\frac{r_{\max}}{r_{\min}}\right) + \left(p-\frac{1}{2}\right)\ln n}{\ln\left(\frac{R}{r_{\max}}\right)} \le Cn. \tag{2.3.25}$$

Hence we obtain from Theorem 2.3.1 at $q=0$

$$\|P_n(r,\theta)-u_N^*\|_{0,\Gamma} = O\left(\frac{1}{n^{p-\frac{1}{2}}}\|P_n\|_{0,\Gamma_{\max}}\right) = O\left(\frac{1}{n^{p-\frac{1}{2}}}\|P_n\|_{0,\Gamma}\right). \tag{2.3.26}$$

Moreover, since $u \approx P_n$, there exists the bound,

$$\|P_n\|_{0,\Gamma} \le C\|u\|_{0,\Gamma} \le C\|u\|_{\frac{1}{2},S} \le C\|u\|_{p,S}, \tag{2.3.27}$$

to give

$$\|P_n(r,\theta) - u_N^*\|_{0,\Gamma} = O\left(\frac{1}{n^{p-\frac{1}{2}}}\|u\|_{p,S}\right). \tag{2.3.28}$$

Combining (2.3.22), (2.3.24) and (2.3.28) gives

$$\|u - u_N\|_{0,\Gamma} \le C\frac{1}{n^{p-\frac{1}{2}}}\|u\|_{p,S}, \tag{2.3.29}$$

and the desired result (2.3.21) follows from $\frac{1}{n} \le \frac{C}{N}$. Compared with [26, (4.3)], the bound in (2.3.2) is sharper without a fact of $\sqrt{n}$. This completes the proof of Theorem 2.3.2. ■

Remark 2.3.2. *Let us examine the conditions in Theorem 2.3.1. The relaxed regularity $u \in \mathbf{H}^p(S)$ $(p > 1)$ of the solution is valid for the singularity problems caused by corners in Chapter 1 and the source functions in Chapter 17. The radius $R \ne 1$ of the pseudo-circular boundary of source nodes is needed to guarantee the uniqueness of Laplace's solution. Otherwise, the unit pseudo-circle with radius $R = 1$ is called the degenerate scale, which is avoided except when specified. See Remark 2.4.1 below. Finally, let us examine (2.3.1) and (2.3.5). Assumption (2.3.1) holds for large N since $N \ge \left(q + \frac{1}{2}\right)\ln 2/\ln\left(\frac{R}{\rho}\right)$. The large N is of our application; see the large $N = O(n)$ from (2.3.25). Then both (2.3.1) and (2.3.5) hold naturally. Hence, we will not provide the assumption (2.3.1) explicitly in the following chapters.*

Lemma 2.3.1. *Let the conditions in Theorem 2.3.1 hold. Then there exists the error bound,*

$$\|u - u_N\|_{-\frac{1}{2},\Gamma} = C\frac{1}{N^p}\|u\|_{p,S}, \tag{2.3.30}$$

where C is a bounded constant independent of N.

Proof. Define the negative norm

$$\|w\|_{-\frac{1}{2},\Gamma} = \sup_{v \in \mathbf{H}^{\frac{1}{2}}(\Gamma)} \frac{1}{\|v\|_{\frac{1}{2},\Gamma}} \int_\Gamma w \cdot v. \tag{2.3.31}$$

Let $t \in \mathbf{H}^{\frac{1}{2}}(\Gamma)$ and $\eta \in \mathbf{H}^1(S)$ satisfy the following auxiliary problem,

$$\Delta\eta = 0 \text{ in } S, \quad \eta = t \text{ on } \Gamma.$$

There exists the bound from (2.1.10) and Theorem 2.3.2,

$$\begin{aligned}\int_\Gamma (u-u_N)\cdot t &= [u-u_N, t] = [u-u_N,\eta] = [u-u_N,\eta-\eta_N]\\ &\leq \|u-u_N\|_{0,\Gamma}\times\|\eta-\eta_N\|_{0,\Gamma} \leq C\frac{1}{N^{p-\frac{1}{2}}}\|u\|_{p,S}\times\frac{1}{N^{\frac{1}{2}}}\|\eta\|_{1,S} \qquad (2.3.32)\\ &\leq C\frac{1}{N^p}\|u\|_{p,S}\|t\|_{\frac{1}{2},\Gamma},\end{aligned}$$

where we have used the bound $\|\eta\|_{1,S} \leq C\|\eta\|_{\frac{1}{2},\Gamma} = C\|t\|_{\frac{1}{2},\Gamma}$. From (2.3.32), we get

$$\frac{1}{\|t\|_{\frac{1}{2},\Gamma}}\int_\Gamma (u-u_N)\cdot t \leq C\frac{1}{N^p}\|u\|_{p,S}. \tag{2.3.33}$$

The desired result (2.3.30) follows from (2.3.33) and (2.3.31) with $w = u - u_N$. ■

Based on $\|v\|_{0,S} \leq C\|v\|_{-\frac{1}{2},\Gamma}$, from $\Delta v = 0$ and Lemma 2.3.1, we have the following corollary.

Corollary 2.3.1. *Let the conditions in Theorem 2.3.1 hold. Then for the Dirichlet problem, the numerical solutions by the MFS have the optimal error bound in* $\mathbf{L}^2$ *norm,*

$$\|u-u_N\|_{0,S} = O\left(\frac{1}{N^p}\right)\|u\|_{p,S}. \tag{2.3.34}$$

Remark 2.3.3. *The MFS is the Trefftz method using the FS as the admissible functions. The error bounds between harmonic polynomials and FS are given in Theorem 2.3.1. Theorem 2.3.2 displays that the MFS and the MPS have the same optimal polynomial convergence rates.*

2.4 Stability Analysis for Disk Domains

Denote a disk domain S by $S = \{(r,\theta)|r<\rho, 0\leq\theta<2\pi\}$ and its circular boundary by $\ell_\rho = \{(r,\theta)|r=\rho, 0\leq\theta\leq 2\pi\}$. The source and the collocation nodes are uniformly located on ℓ_R and ℓ_ρ as

$$Q_i = \{R\cos(ih), R\sin(ih)\}, P_i = \{\rho\cos(ih), \rho\sin(ih)\}, \quad i = 1, 2, \ldots, N,$$

where $\rho < R$ and $h = \frac{2\pi}{N}$ (see Figure 2.1). Consider

$$\Delta u = 0 \text{ in } S, \quad u = f \text{ on } \Gamma = \ell_R.$$

From (2.1.6) the collocation equations are given as

$$\sum_{i=1}^N c_i\phi_i(P_j) = f(P_j), \quad P_j\in\ell_\rho, \tag{2.4.1}$$

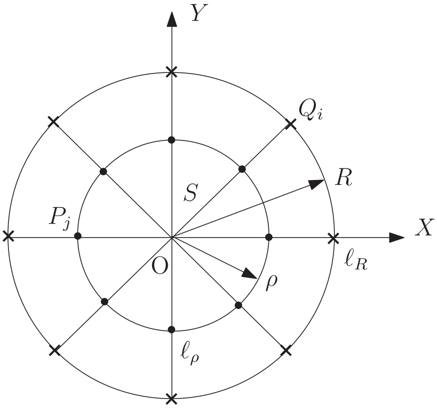

FIG. 2.1 – The locations of source nodes Q_i and collocation nodes P_j.

where $\phi_i(P_j) = \ln|\overline{P_jQ_i}|$. From $|\overline{P_jQ_i}|^2 = R^2 + \rho^2 - 2R\rho\cos((i-j)h)$, we obtain

$$\phi_i(P_j) = \ln|\overline{P_jQ_i}| = \frac{1}{2}\ln|R^2 + \rho^2 - 2R\rho\cos((i-j)h)|.$$

We may rewrite (2.4.1) as the matrix form $\mathbf{Ax} = \mathbf{b}$, where $\mathbf{x} = (c_1, c_2, \ldots, c_N)^T$, $\mathbf{b} = (f(P_1), f(P_2), \ldots, f(P_N))^T$, and $\mathbf{A} \in \mathbf{R}^{N\times N}$. The matrix $\mathbf{A}$ is the symmetric circulant matrix, denoted by

$$\mathbf{A} = \text{circulant}(a_0, a_1, \ldots, a_{N-1}) = \begin{pmatrix} a_0 & a_1 & \cdots & a_{N-1} \\ a_{N-1} & a_0 & \cdots & a_{N-2} \\ \vdots & \vdots & \cdots & \vdots \\ a_1 & a_2 & \cdots & a_0 \end{pmatrix}, \tag{2.4.2}$$

where the entries

$$a_i = \frac{1}{2}\ln|R^2 + \rho^2 - 2R\rho\cos ih|, \quad i = 0, 1, \ldots, N-1. \tag{2.4.3}$$

We have a lemma by Davis [71].

Lemma 2.4.1 (Circulant Lemma). *Let matrix* $\mathbf{A} = \text{circulant}(a_0, a_1, \ldots, a_{N-1})$ *with real entries* a_i. *Then the eigenvalues of* $\mathbf{A}$ *are real and given by*

$$\lambda_k = \sum_{j=0}^{N-1} a_j \cos(kjh), \quad k = 0, 1, \ldots, N-1,$$

where $h = \frac{2\pi}{N}$. *Also, the vector* $\mathbf{y}_0 = \frac{1}{\sqrt{N}}(1, 1, \ldots, 1)^T$ *is the eigenvector corresponding to the leading eigenvalue* λ_0.

Lemma 2.4.2 (Basic Lemma B). *Let* $g(x) \in C^\infty[0, 2\pi]$ *satisfy the periodical boundary conditions,*

$$g^{(\ell)}(0) = g^{(\ell)}(2\pi), \quad \ell = 0, 1, \ldots. \tag{2.4.4}$$

There exist the errors

$$\begin{aligned} &T_N(g(x)\cos(kx)) - \int_0^{2\pi} g(x)\cos(kx)\,dx \\ &\quad = \pi \sum_{v=1}^{\infty} \{\alpha_{vN-k} + \alpha_{vN+k}\}, \quad k = 0, 1, \ldots, N-1, \end{aligned} \tag{2.4.5}$$

where

$$\alpha_\ell = \frac{1}{\pi} \int_0^{2\pi} g(x)\cos(\ell x)\,dx, \quad \ell = 0, 1, \ldots. \tag{2.4.6}$$

Proof. Since $g(x)$ satisfies (2.4.4), it can be expanded as trigonometric functions

$$g(x) = \frac{\alpha_0}{2} + \sum_{\ell=1}^{\infty} \{\alpha_\ell \cos(\ell x) + \beta_\ell \sin(\ell x)\}, \quad x \in [0, 2\pi], \tag{2.4.7}$$

where the coefficients α_ℓ are given in (2.4.6) and

$$\beta_\ell = \frac{1}{\pi} \int_0^{2\pi} g(x)\sin(\ell x)\,dx, \quad \ell = 1, 2, \ldots. \tag{2.4.8}$$

We have the integrand

$$g(x)\cos(kx) = \frac{\alpha_0}{2}\cos(kx) + \sum_{\ell=1}^{\infty} \{\alpha_\ell \cos(\ell x)\cos(kx) + \beta_\ell \sin(\ell x)\cos(kx)\}. \tag{2.4.9}$$

Since

$$\begin{aligned} \cos(\ell x)\cos(kx) &= \frac{1}{2}\{\cos(\ell + k)x + \cos(\ell - k)x\}, \\ \sin(\ell x)\cos(kx) &= \frac{1}{2}\{\sin(\ell + k)x + \sin(\ell - k)x\}, \end{aligned} \tag{2.4.10}$$

we have from Lemma 2.2.1 (Basic Lemma A) and (2.4.9)

$$\begin{aligned} &T_N(g(x)\cos(kx)) - \int_0^{2\pi} g(x)\cos(kx)\,dx \\ &= \frac{1}{2}\sum_{\ell=1}^{\infty} \{\alpha_\ell \triangle_N(\cos(\ell + k)x) + \alpha_\ell \triangle_N(\cos(\ell - k)x)\} \\ &= \pi \left\{ \sum_{\ell + k = vN} \alpha_\ell + \sum_{\ell - k = vN} \alpha_\ell \right\} = \pi \sum_{v=1}^{\infty} \{\alpha_{vN-k} + \alpha_{vN+k}\}, \quad k = 0, 1, \ldots, N-1. \end{aligned} \tag{2.4.11}$$

This is the desired result (2.4.5), and completes the proof of Lemma 2.4.2. ■

Theorem 2.4.1 *For $\rho < R$ (i.e., $a = \frac{R}{\rho} > 1$), the eigenvalues of matrix* $\mathbf{A}$ *in (2.4.2) are given by*

$$\lambda_0 = N\,\ln R + \varepsilon, \quad \varepsilon \approx -\frac{1}{a^N}, \tag{2.4.12}$$

$$\lambda_k = -\frac{N}{2k}\frac{1}{a^k} - \frac{N}{2}\sum_{v=1}^{\infty}\left\{\frac{1}{(vN-k)\,a^{vN-k}} + \frac{1}{(vN+k)\,a^{vN+k}}\right\}, \tag{2.4.13}$$

where $h = \frac{2\pi}{N}$ and $k = 1, 2, \ldots, N-1$.

Proof. From Lemma 2.4.1 (Circulant Lemma) we have the eigenvalues of $\mathbf{A}$,

$$\lambda_k = \sum_{j=0}^{N-1} a_j\,\cos(kjh). \tag{2.4.14}$$

From (2.4.14) and (2.4.3),

$$\begin{aligned}\lambda_0 &= \sum_{j=0}^{N-1} a_j = \frac{1}{2}\sum_{j=0}^{N-1}\ln|R^2 + \rho^2 - 2R\rho\,\cos(jh)| \\ &= N\,\ln\rho + \frac{1}{2h}\sum_{j=0}^{N-1} h\,\ln(1 + a^2 - 2a\,\cos(jh)).\end{aligned} \tag{2.4.15}$$

Denote function $g(x) = \ln(1 + a^2 - 2a\,\cos x)$. Then $g(x) \in C^{\infty}[0,\, 2\pi]$ is a periodical function satisfying (2.4.4). From Gradshteyn and Ryzhik [90, 4.224(15), 4.397(6)], there exist the integral formulas,

$$\int_0^{2\pi}\ln(1 + a^2 - 2a\,\cos x)\,dx = \begin{cases} 0, & \text{if } a^2 \le 1, \\ 2\pi\,\ln a^2, & \text{if } a^2 > 1, \end{cases} \tag{2.4.16}$$

and

$$\int_0^{2\pi}\ln(1 + a^2 - 2a\,\cos x)\cos(kx)\,dx = \begin{cases} -\dfrac{2\pi}{k}\,a^k, & \text{if } a^2 < 1, \\ -\dfrac{2\pi}{ka^k}, & \text{if } a^2 > 1. \end{cases} \tag{2.4.17}$$

Hence we have the expansions

$$g(x) = \ln(1 + a^2 - 2a\,\cos x) = \frac{\alpha_0}{2} + \sum_{\ell=1}^{\infty}\{\alpha_\ell\,\cos(\ell x) + \beta_\ell\,\sin(\ell x)\}, \tag{2.4.18}$$

where $a = \frac{R}{\rho} > 1$, and

$$\alpha_0 = 4\,\ln a, \;\; \alpha_\ell = -\frac{2}{\ell a^\ell}, \quad \ell = 1, 2, \ldots. \tag{2.4.19}$$

Moreover, from Lemma 2.4.2 (Basic Lemma B) we have for $k = 0$

$$\sum_{j=0}^{N-1} h \ln(1 + a^2 - 2a \cos(jh)) = \int_0^{2\pi} \ln(1 + a^2 - 2a \cos x)\, dx + 2\pi \sum_{\nu=1}^{\infty} \alpha_{\nu N}, \quad (2.4.20)$$

where α_ℓ are given in (2.4.19). From (2.4.16) and (2.4.19), the equation (2.4.20) yields

$$\sum_{j=0}^{N-1} h \ln(1 + a^2 - 2a \cos(jh)) = 4\pi \ln a - 4\pi \sum_{\nu=1}^{\infty} \frac{1}{(\nu N) a^{\nu N}}. \quad (2.4.21)$$

Hence we obtain from $h = \frac{2\pi}{N}$, (2.4.15) and (2.4.21)

$$\lambda_0 = N \ln\rho + \frac{1}{2h} 4\pi \left\{ \ln a - \sum_{\nu=1}^{\infty} \frac{1}{\nu N a^{\nu N}} \right\} = N \ln R + \varepsilon, \quad (2.4.22)$$

where $\varepsilon = -\sum_{\nu=1}^{\infty} \frac{1}{\nu a^{\nu N}}$. Since

$$\frac{1}{a^N} < |\varepsilon| < \frac{1}{(1 - a^N) a^N}, \quad (2.4.23)$$

the equation (2.4.22) gives the first result (2.4.12).

Next for λ_k in (2.4.14) we have from (2.4.3)

$$\begin{aligned} \lambda_k &= \frac{1}{2} \sum_{j=0}^{N-1} \ln(R^2 + \rho^2 - 2R\rho \cos(jh)) \cos(kjh) \\ &= \frac{\ln\rho}{h} \sum_{j=0}^{N-1} h \cos(kjh) + \frac{1}{2h} \sum_{j=0}^{N-1} h \ln(1 + a^2 - 2a \cos(jh)) \cos(kjh). \end{aligned} \quad (2.4.24)$$

From Lemma 2.2.1 there exists the equality,

$$\sum_{j=0}^{N-1} h \cos(kjh) = \int_0^{2\pi} \cos(kx)\, dx = 0, \quad k < N. \quad (2.4.25)$$

Also from Lemma 2.4.2, (2.4.17) and (2.4.18),

$$\begin{aligned} &\sum_{j=0}^{N-1} h \ln(1 + a^2 - 2a \cos(jh)) \cos(kjh) \\ &= \int_0^{2\pi} \ln(1 + a^2 - 2a \cos x) \cos(kx)\, dx + \pi \sum_{\nu=1}^{\infty} \{\alpha_{\nu N - k} + \alpha_{\nu N + k}\}, \end{aligned} \quad (2.4.26)$$

where $\alpha_\ell = -\frac{2}{\ell a^\ell}$. From (2.4.17) and (2.4.19), the equation (2.4.26) yields

$$\sum_{j=0}^{N-1} h \ln(1+a^2-2a\cos(jh))\cos(kjh)$$
$$= -\frac{2\pi}{ka^k} - 2\pi\sum_{v=1}^{\infty}\left\{\frac{1}{(vN-k)\,a^{vN-k}} + \frac{1}{(vN+k)\,a^{vN+k}}\right\}. \tag{2.4.27}$$

Hence, we obtain from (2.4.24), (2.4.25) and (2.4.27)

$$\lambda_k = -\frac{1}{2h}\left[\frac{2\pi}{ka^k} + 2\pi\sum_{v=1}^{\infty}\left\{\frac{1}{(vN-k)\,a^{vN-k}} + \frac{1}{(vN+k)\,a^{vN+k}}\right\}\right] \tag{2.4.28}$$
$$= -\frac{N}{2k}\frac{1}{a^k} - \frac{N}{2}\sum_{v=1}^{\infty}\left\{\frac{1}{(vN-k)\,a^{vN-k}} + \frac{1}{(vN+k)\,a^{vN+k}}\right\}, \quad k = 1, 2, \ldots, N-1.$$

This is the second result (2.4.13) and completes the proof of Theorem 2.4.1. ■

The traditional condition number of $\mathbf{A}$ in (2.4.2) with full rank is defined by

$$\text{Cond} = \frac{\max_i|\lambda_i|}{\min_i|\lambda_i|}, \tag{2.4.29}$$

where λ_i are the eigenvalues of $\mathbf{A}$. From (2.4.13) we have for $k \geq 1$

$$|\lambda_k| \geq \frac{N}{2k}\frac{1}{a^k} + \frac{N}{2}\frac{1}{(N-k)\,a^{N-k}} = \frac{N}{2}q(k), \tag{2.4.30}$$

where the function $q(k) = \frac{1}{ka^k} + \frac{1}{(N-k)a^{N-k}}$. To reach the minimum of $q(x)$, we may seek $q'(x) = 0$, where

$$q'(x) = \frac{1}{a^{N-x}}\left[\frac{1}{(N-x)^2} + \frac{\ln a}{N-x}\right] - \frac{1}{a^x}\left(\frac{1}{x^2} + \frac{\ln a}{x}\right), \quad a > 1. \tag{2.4.31}$$

Without loss of generality, assume that N is even. When $\bar{k} = \frac{N}{2}$, we have $q'\left(\frac{N}{2}\right) = 0$ and $q\left(\frac{N}{2}\right) = \frac{4}{Na^{\frac{N}{2}}}$. Hence we obtain from (2.4.30)

$$\min_{k\geq 1}|\lambda_k| \geq \frac{N}{2}q\left(\frac{N}{2}\right) = \frac{2}{a^{\frac{N}{2}}}. \tag{2.4.32}$$

From (2.4.12) and (2.4.32), we have the following corollary.

Corollary 2.4.1. *Let $\rho < R$ and $R \neq 1$, then there exists the bound,*

$$\text{Cond} = \frac{\lambda_0}{\min_{k\geq 1}|\lambda_k|} \leq \frac{N|\ln R|}{2}\left(\frac{R}{\rho}\right)^{\frac{N}{2}}. \tag{2.4.33}$$

From (2.4.12), we have $|\lambda_0| = \max_k|\lambda_k|$ if $R \neq 1$, but $|\lambda_0| = \min_k|\lambda_k|$ if $R = 1$. The equation (2.4.33) is exactly for $R > 1$. For $R < 1$, the bound (2.4.33) is slightly modified as $\text{Cond} \le \frac{N(|\ln R| + |\varepsilon|)}{2}\left(\frac{R}{\rho}\right)^{\frac{N}{2}}$, where ε is given in (2.4.12). The Cond in (2.4.33) also coincides with Kitagawa [126].

When radius $R = 1$, we have $|\lambda_0| = |\varepsilon| = O\left(\frac{1}{a^N}\right)$ from (2.4.12). Also from (2.4.13) we have for $k \ge 1$

$$\begin{aligned} |\lambda_k| &\le \frac{N}{2k}\frac{1}{a^k} + 2\frac{N}{2}\sum_{v=1}^{\infty}\frac{1}{(vN-k)\,a^{vN-k}} \\ &\le \frac{N}{2a} + N\sum_{v=1}^{\infty}\frac{1}{(N-k)\,a^{vN-k}} \le \frac{N}{2a} + \frac{N}{(1-a^{-N})}\frac{1}{(N-k)\,a^{N-k}} \le CN. \end{aligned} \tag{2.4.34}$$

Then for the case at $R = 1$, we give the following corollary.

Corollary 2.4.2. *Let $\rho < R = 1$ in degenerate scales, there exists the bound*

$$\text{Cond} = \frac{\max_{k \ge 1}|\lambda_k|}{|\lambda_0|} \le CN\left(\frac{R}{\rho}\right)^N,$$

where C is a bounded constant independent of N.

Remark 2.4.1. *Note that for $R = 1$ of degenerate scales, the matrix $\mathbf{A}$ is nonsingular but very singular. Here let us consider the solutions by the MFS for $\rho < R = 1$. When $\rho < R = 1$, the solution in (1.2.8) is reduced to*

$$u_N = \sum_{i=1}^{N} c_i \psi_i(\theta), \tag{2.4.35}$$

where $\psi_i(\theta) = \frac{1}{2}\ln(1 + \rho^2 - 2\rho\cos(\theta - ih))$ and $h = \frac{2\pi}{N}$. Since the circulant $\mathbf{A}$ at $R = 1$ is very singular due to λ_0 in (2.4.12), we may seek the numerical solution from the truncated singular value decomposition (TSVD),

$$\mathbf{x}_{\text{LSM}} = \sum_{i=1}^{N-1}\frac{\mathbf{u}_i^T\mathbf{b}}{\sigma_i}\mathbf{v}_i, \tag{2.4.36}$$

where $\sigma_i = |\lambda_i|$ and $\mathbf{x}_{\text{LSM}} = (\bar{c}_1, \bar{c}_2, \ldots, \bar{c}_N)^T$. From Lemma 2.4.1, $(1, 1, \ldots, 1)^T$ is the eigenvector corresponding to $\lambda_0 = 0$. Then the general solution of $\mathbf{x}$ is given by

$$u_N = \sum_{i=1}^{N} c_i \psi_i(\theta) + c, \tag{2.4.37}$$

where c is an arbitrary constant. Based on the analysis for $R = 1$ above, the difficulty of $R = 1$ can be bypassed by using the TSVD. In fact, the non-unique solutions may also be removed for the boundary integral equation (BIE). See Christiansen [65]. Such a technique is also used for the Neumann problem of Laplace's equation in the next chapter.

2.5 Proof Methodology

In this section, let us address the proof methodology for the analysis in the entire book. The proof methodology of error analysis was developed by Bogomolny [26] in 1985, as well as [169, 176]. For smooth solutions, the fundamental solutions can be split into the particular solutions (PS) plus some extra errors. The extra errors should be further estimated carefully; they are reported in this and the following chapters. Under certain conditions, the bounds of such extra errors may not exceed those of the PS, so that the polynomial convergence rates can be achieved. In theory, the convergence rates of the MFS are the same as those of the MPS. In fact, the numerous reports by the MFS provide satisfactory solutions (see [39, 128]), which have been supported by the theoretical analysis in this book. The other methodology is based on the Galerkin approaches; details appear elsewhere.

The ill-conditioning is very severe for the MFS. The proof methodology of stability analysis is developed by Davis [71] in 1979 for circulant matrices, as well as [158, 162]. In [162, Chapter 6], the stability of the MFS is for the effective condition number; in this book, the stability is devoted to a systematic and theoretical foundation of the MFS itself. We will explore the stability of the MFS for Laplace's equation, Helmholtz's equation, and biharmonic equations. The condition numbers grow exponentially as the number of source nodes increases. For the boundary knot method (BKM) in Section 7.5, a super-exponential growth of Cond occurs. Therefore, large condition numbers are always obtained. A balance must be taken carefully between accuracy and stability so that the ill-conditioning will not deteriorate the accuracy of the final numerical solutions.

Locating the source nodes is an important issue in computation (see Chen *et al.* [38]). For 2D problems, the simple circular pseudo-boundary has been widely used in applications. The main analysis of this book is devoted to circular pseudo-boundaries. The optimal convergence rates can also be achieved. However, for the long-narrow domains, the Cond will be too large, thus damaging the accuracy of numerical solutions. Elliptic pseudo-boundaries are explored in Chapter 6 to reduce the Cond. Since the discrete matrices obtained are not circulant matrices, the new proof techniques are explored in Chapter 6 to derive the bounds of Cond. Elliptic pseudo-boundaries are more often employed for selecting better source nodes in Part III.

For the MFS, the Japanese scholars, Katsurada M., Kitagawa T., Okamoto H., etc., established a theory for the simple case that both the solution domains and the pseudo-boundaries are circular [120, 123, 125, 126]. For Jordan domains with an analytic boundary, conformal mapping is employed to transform both the solution domains and the pseudo-boundaries to concircular [121, 122]. For general non-disk solution domains, the basic analysis was first published in Bogomolny [26] in 1985 and by Li *et al.* [150, 151, 163] in 2008. Since then, such a basic analysis has been proven to be effective for differential equations and problems in bounded simply-connected domains, multiply-connected domains, and unbounded domains. New theoretical results of the MFS are summarized in this book.

Chapter 3

Neumann Problems

3.1 Introduction

Since Neumann problems satisfying the consistent conditions have multiple solutions, the stability analysis of the MFS is particularly interesting. Hence this chapter is devoted to Neumann problems in non-disk domains to provide new error and stability analyses. The bounds of both errors and condition numbers are derived in detail. The optimal convergence rates in $\mathbf{L}^2$ and $\mathbf{H}^1$ norms in S can be achieved, but the condition number grows exponentially as the number of fundamental solutions (FS) increases.

By circulant matrices in Davis [71], the eigenvalues of the stiffness matrix from the MFS can be derived exactly for Neumann boundary conditions, under the simple case that the source and the collocation nodes are uniformly located on concentric circles. When the stiffness matrix is singular or near singular, the numerical solutions can be found by the truncated singular value decomposition (TSVD). See Hansen [96] and Li *et al.* [161]. In fact, the TSVD was used in Ramachandran [205] to lessen the ill-conditioning of the MFS. In this chapter, we adopt the TSVD to reduce huge condition numbers (Cond) of the MFS down to $O(\sqrt{\text{Cond}})$. See Corollaries 3.3.1 and 3.4.2. For Neumann problems in the bounded simply-connected domains, we also derive the bounds of Cond. Moreover, the error bounds are derived to achieve optimal convergence rates.

This chapter is organized as follows. In the next section, algorithms of the MFS are described, the main results in this chapter are briefly addressed and some guidance is provided for applications. For Neumann problems, the bounds of Cond are derived for disk domains in Section 3.3, and for the bounded simply-connected domains in Section 3.4. In Section 3.5, an error analysis is made. In the last section, some concluding remarks are made. The MFS for Neumann problems in this chapter is intriguing due to its distinct features. The materials of this chapter are adapted from [167].

DOI: 10.1051/978-2-7598-3171-5.c003
© Science Press, EDP Sciences, 2023

3.2 Method of Fundamental Solutions

3.2.1 Description of Algorithms

Consider Laplace's equation with the Neumann boundary condition in 2D,

$$\Delta u = \frac{\partial^2 u}{\partial x^2} + \frac{\partial^2 u}{\partial y^2} = 0 \text{ in } S, \tag{3.2.1}$$

$$\frac{\partial u}{\partial \nu} = g \text{ on } \Gamma, \tag{3.2.2}$$

where S is a bounded simply-connected domain with a smooth boundary $\Gamma = \partial S$, and ν the exterior normal of Γ. For the solution existence of (3.2.1) and (3.2.2), we need the consistent condition$\int_\Gamma g = 0$, so that the solution plus any constant is also a solution. Let the boundary Γ be smooth without corners (see Figure 1.1). The assumption of g is described in Section 3.2.2 as $g \in \mathbf{H}^q(\Gamma)$ with $q \geq \frac{1}{2}$. Denote in Figure 1.1,

$$r_{\max} = \max_S r, \quad r_{\min} = \max_{S_{\text{in}}(S_{\text{in}} \subseteq S)} r, \tag{3.2.3}$$

where S_{in} is an inscribed disk of S. Denote nodes $P \in S \cup \partial S$ with $P = \{(x, y)|x = r\ \cos\theta, y = r\ \sin\theta\}$, and the source (*i.e.*, charge) nodes Q outside S. A pseudo-circle surrounding S is given by $\ell_R = \{(r, \theta)|r = R, 0 \leq \theta \leq 2\pi\}$ with $R > r_{\max}$. The source nodes Q_i may be simply located uniformly on ℓ_R (see Chapter 2),

$$Q_i = \{(x, y)|x = R\cos(ih),\ y = R\sin(ih)\}, \tag{3.2.4}$$

where $R > r_{\max}$ and $h = \frac{2\pi}{N}$. We obtain the FS,

$$\phi_i(P) = \ln|\overline{PQ_i}|, \ \ i = 1, 2, ..., N, \tag{3.2.5}$$

and denote the numerical solutions of (3.2.1) and (3.2.2) as a linear combination,

$$u_N = c + \sum_{i=1}^{N} c_i \phi_i(P), \tag{3.2.6}$$

where c_i are the unknown coefficients to be sought, and c is an arbitrary constant. Since u_N satisfies Laplace's equation in S already, the coefficients c_i can be sought by satisfying the boundary condition (3.2.2) only. Denote the energy

$$I(v) = \int_\Gamma \left(\frac{\partial v}{\partial \nu} - g\right)^2. \tag{3.2.7}$$

Also denote by V_N the set of (3.2.6). Then the numerical solution u_N can be sought by

$$I(u_N) = \min_{v \in V_N} I(v). \tag{3.2.8}$$

When the integral in (3.2.7) involves approximation, denote

$$\widehat{I}(v) = \widehat{\int_\Gamma} \left(\frac{\partial v}{\partial \nu} - g\right)^2, \tag{3.2.9}$$

where $\widehat{\int_\Gamma}$ is the numerical approximation of $\int_\Gamma$ by some quadrature rules, such as the Gaussian rule. Hence, the numerical solution $\tilde{u}_N \in V_N$ is obtained by

$$\widehat{I}(\tilde{u}_N) = \min_{v \in V_N} \widehat{I}(v). \tag{3.2.10}$$

We may establish the collocation equations directly from (3.2.2), to yield

$$\sum_{i=1}^{N} c_i \left\{ \frac{\partial}{\partial \nu} \phi_i(P_j) \right\} = g(P_j), \quad P_j \in \mathbf{\Gamma}. \tag{3.2.11}$$

On the other hand, let $\mathbf{\Gamma}$ be divided into small $\mathbf{\Gamma}^j$ with the meshspacings $\triangle h_j$, *i.e.*, $\mathbf{\Gamma} = \bigcup_{j=1}^{M} \mathbf{\Gamma}^j$. We obtain from (3.2.11)

$$\sqrt{\beta_j} \sum_{i=1}^{N} c_i \left\{ \frac{\partial}{\partial \nu} \phi_i(P_j) \right\} = \sqrt{\beta_j}\ g(P_j), \quad P_j \in \mathbf{\Gamma}, \tag{3.2.12}$$

where P_j are the Gaussian nodes, the weights $\beta_j = O(\triangle h)$, and $\triangle h = \max_j \triangle h_j$. In computation, we may choose the number of collocation nodes to be equal to (or larger than) that of source nodes. The equations (3.2.12) are called the collocation Trefftz method (CTM) in [169]. The equations (3.2.12) are equivalent to (3.2.10), where the Gaussian rule (or the trapezoidal rule) is chosen for $\widehat{\int_\Gamma}$. This displays that the CTM is the TM involving quadrature approximation. Hence the MFS is just the Trefftz methods in [169] by using FS.

The overdetermined system is obtained from (3.2.12),

$$\mathbf{F}\mathbf{x} = \mathbf{b}, \tag{3.2.13}$$

where $\mathbf{F} \in \mathbf{R}^{M \times N}$ $(M \geq N)$, $\mathbf{x} \in \mathbf{R}^N$ and $\mathbf{b} \in \mathbf{R}^M$. In this chapter, consider the rank deficient with $\text{rank}(\mathbf{F}) = t \leq N$. The singular value decomposition (SVD) of $\mathbf{F}$ is given by $\mathbf{F} = \mathbf{U}\mathbf{\Sigma}\mathbf{V}^T$, where the matrices $\mathbf{U} \in \mathbf{R}^{M \times M}$ and $\mathbf{V} \in \mathbf{R}^{N \times N}$ are orthogonal, and matrix $\mathbf{\Sigma} \in \mathbf{R}^{M \times N}$ is diagonal. The non-zero diagonal entries of $\mathbf{\Sigma}$ are given by t positive singular values: $\sigma_1 \geq \cdots \geq \sigma_t > 0$ with $t \leq N$. Denote $\mathbf{U} = (\mathbf{u}_1, \mathbf{u}_2, ..., \mathbf{u}_M)$ and $\mathbf{V} = (\mathbf{v}_1, \mathbf{v}_2, ..., \mathbf{v}_N)$, where $\mathbf{u}_i \in \mathbf{R}^M$ and $\mathbf{v}_i \in \mathbf{R}^N$ are vectors. The solution of (3.2.13) is obtained by

$$\mathbf{x} = \sum_{i=1}^{t} \frac{\mathbf{u}_i^T \mathbf{b}}{\sigma_i} \mathbf{v}_i. \tag{3.2.14}$$

The modified condition number for (3.2.14) is defined in van Loan [182] by

$$\widehat{\text{Cond}} = \frac{\sigma_1}{\sigma_t}. \tag{3.2.15}$$

When $t < N$, the solution from (3.2.14) is called the TSVD solution. To distinguish the condition number with rank deficient from the traditional condition number $\text{Cond} = \frac{\sigma_1}{\sigma_N}$ with $\sigma_N > 0$, we use the notation $\widehat{\text{Cond}}$ in (3.2.15) with a hat. Even for $\text{rank}(\mathbf{F}) = N$, when $\sigma_{t+1}, ..., \sigma_N$ are infinitesimal, the TSVD solution (3.2.14) is solicited for better stability; see Hansen [96], Ramachandran [205], and Li *et al.* [161].

3.2.2 Main Results of Analysis and Their Applications

Since the FS in (3.2.5) with Q_i located outside S are highly smooth, the functions as (3.2.6) are not suitable to approximate the singular solutions, where their derivatives are unbounded. The combined method may be solicited and introduced in Chapter 5. From the error analysis in Section 3.5, we confine the smooth problems for a smooth boundary Γ without corners and assume that the solutions of (3.2.1) and (3.2.2) satisfy

$$u \in \mathbf{H}^p(S)/\mathbf{P}_0(S), \quad p \geq 2, \tag{3.2.16}$$

where $\mathbf{H}^p(S)/\mathbf{P}_0(S)$ is a quotient space, $\mathbf{H}^p(S)$ are the Sobolev spaces, and $\mathbf{P}_0(S)$ is the constant space. The equation (3.2.16) implies

$$g \in \mathbf{H}^q(\Gamma), \quad q \geq \frac{1}{2}. \tag{3.2.17}$$

The condition (3.2.17) may be relaxed to $g \in \mathbf{H}^q(\Gamma)$ with $q > 0$ for the solutions involving singularity by the MFS. Note that for the interior Neumann problems, the solutions must satisfy $u \in \mathbf{H}^1(S)/\mathbf{P}_0(S)$ and $g \in \mathbf{H}^{-\frac{1}{2}}(\Gamma)$ from Babuska and Aziz [15]. Under (3.2.16), the optimal convergence in $\mathbf{L}^2$ and $\mathbf{H}^1$ norms in S can be achieved, and given in Theorem 3.5.1 as

$$\|u - u_N\|_{k,S} = O\left(\frac{1}{N^{p-k}}\right)\|u\|_{p,S}, \quad k = 0, 1. \tag{3.2.18}$$

The above errors in the quotient space $\mathbf{H}^k(S)/\mathbf{P}_0(S)$ mean that the differences of a constant solution are not included in (3.2.18). The stability is severer for the MFS. Under the source nodes given in (3.2.4), the following bounds of Cond are given in Corollary 3.4.2 as

$$\text{Cond}(\mathbf{F}) = \frac{\sigma_{\max}(\mathbf{F})}{\sigma_{\min}(\mathbf{F})} \leq C\left(\frac{R}{r_{\min}}\right)^N, \tag{3.2.19}$$

$$\widehat{\text{Cond}}(\mathbf{F}) = \frac{\sigma_{\max}(\mathbf{F})}{\sigma_{\min-\text{next}}(\mathbf{F})} \leq C\left(\frac{R}{r_{\min}}\right)^{\frac{N}{2}}, \tag{3.2.20}$$

where $r_{\min}$ is given in (3.2.3), and C is a bounded constant independent of N. From (3.2.18), the higher degree of smoothness the solution u has (*i.e.*, the higher p is), the faster the convergence is reached. For the infinitely smooth solution with $p = \infty$, the equations (3.2.18) indicate the exponential convergence.

Here, let us outline the key ideas of analysis to help readers to follow the proof easily. Under (3.2.4), the eigenvalues of circulant matrices are known from the Davis theory [72] in Circulant Lemma, and the errors of the trapezoidal rule can be found from Basic Lemmas A and B in Part I. Hence, the eigenvalues of matrix **A** in (3.3.3) can be derived for disk domains in Section 3.3. Based on the matrix and numerical analysis, the eigenvalues of matrix **F** in (3.2.13) can also be derived for the bounded simply-connected domains in Section 3.4. Note that the bounds in (3.2.19) and (3.2.20) have exponential rates *via* N.

Since the MFS can be classified into the Trefftz method, we may derive the error bounds by following Chapter 2. From (3.5.16) and (3.5.18), the errors of the MFS can be split into two parts: (a) the remainder R_n of the harmonic polynomials P_n, and (b) the differences between P_n and a special solution u_N^* of the MFS. The bounds of (b) can also be derived by Basic Lemmas A and B in Part I, where the source nodes on circles in (3.2.4) play a key role in [151]. The optimal convergence means that the error orders of the MFS solutions are the same as those of the best harmonic polynomials in [169, 171]. However, since the exponential Cond may damage the accuracy of the numerical solutions, reducing the Cond is significant for the MFS in applications.

3.3 Stability Analysis of Disk Domains

Consider the Neumann problem (3.2.1) and (3.2.2) on disk domains with radius ρ. For the uniformly distributed collocation nodes, the equations (3.2.11) lead to

$$\sum_{i=1}^{N} c_i \frac{\partial}{\partial r}\phi_i(P_j) = g(P_j), \quad j = 1, 2, ..., N, \tag{3.3.1}$$

where $\phi_i(P_j) = \ln|\overline{Q_iP_j}|$, the source nodes Q_i are given in (3.2.4), and the collocation nodes

$$P_j = (\rho\, \cos(jh), \rho\, \sin(jh)), \quad j = 1, 2, ..., N, \tag{3.3.2}$$

with $R > \rho$. The equations (3.3.1) are denoted by

$$\mathbf{Ax} = \mathbf{b}, \tag{3.3.3}$$

where $\mathbf{x} = (c_1, c_2, ..., c_n)^T$, $\mathbf{b} = (g(P_1), g(P_2), ..., g(P_N))^T$, and $\mathbf{A} \in \mathbf{R}^{N\times N}$. Below, we give the explicit entries of matrix **A**. We have

$$\frac{\partial}{\partial r}\phi_i(P_j) = \frac{\partial}{\partial r}\ln|\overline{Q_iP_j}| = \frac{1}{|\overline{Q_iP_j}|}\cos(\vec{r}, \overrightarrow{Q_iP_j}), \tag{3.3.4}$$

where $\vec{r} = \overrightarrow{OP_j} = \rho\, \cos(jh)\, \vec{\ell} + \rho\, \sin(jh)\vec{m}$,

$$\overrightarrow{Q_iP_j} = (\rho\, \cos(jh) - R\, \cos(ih))\, \vec{\ell} + (\rho\, \sin(jh) - R\, \sin(ih))\vec{m},$$

$h = \frac{2\pi}{N}$, and $\vec{\ell}$ and $\vec{m}$ are the unit vectors along x and y directions, respectively. Moreover, the following equalities exist:

$$\begin{aligned}\cos(\vec{r}, \overrightarrow{Q_iP_j}) &= \frac{(\vec{r}, \overrightarrow{Q_iP_j})}{|\vec{r}||\overrightarrow{Q_iP_j}|}\\ &= \frac{1}{\rho|\overline{Q_iP_j}|}\{\rho\cos(jh)[\rho\cos(jh) - R\cos(ih)] + \rho\sin(jh)[\rho\sin(jh) - R\sin(ih)]\}\\ &= \frac{1}{\rho|\overline{Q_iP_j}|}\{\rho^2 - \rho R\cos(j-i)h\}.\end{aligned}$$

Then we have the derivatives from (3.3.4),

$$\frac{\partial}{\partial r}\phi_i(P_j) = -\frac{\rho R\cos(j-i)h - \rho^2}{\rho\{R^2+\rho^2-2R\rho\cos(j-i)h\}} = -\frac{a\cos(j-i)h - 1}{\rho\{a^2+1-2a\cos(j-i)h\}},$$

where $a = \frac{R}{\rho} > 1$. Hence, $\mathbf{A}$ is also a circulant matrix,

$$\mathbf{A} = \text{circulant}(a_0, a_1, ..., a_{N-1}), \tag{3.3.5}$$

where the entries

$$a_0 = \frac{1}{\rho(1-a)}, \tag{3.3.6}$$

$$a_k = -\frac{a\cos kh - 1}{\rho(1+a^2-2a\cos kh)}, \quad k = 1, 2, ..., N-1. \tag{3.3.7}$$

Since $a_i = a_{N-i}$, the matrix $\mathbf{A}$ is symmetric. We have the following theorem.

Theorem 3.3.1. *For the Neumann problem (3.2.1) and (3.2.2) on disk domain S, the eigenvalues of matrix $\mathbf{A}$ from the MFS in (3.3.1) are given by*

$$\lambda_0 = \frac{-N}{\rho(1-a^{-N})} \times \frac{1}{a^N} = \frac{-N}{\rho(a^N-1)}, \tag{3.3.8}$$

$$\begin{aligned}\lambda_k &= -\frac{N}{2\rho}\left\{\frac{1}{a^k} + \frac{1}{1-a^{-N}}\left(\frac{1}{a^{N-k}} + \frac{1}{a^{N+k}}\right)\right\}\\ &= -\frac{N}{2\rho}\left\{a^{-k} + \frac{a^k + a^{-k}}{a^N - 1}\right\}, \quad k = 1, 2, ..., N-1,\end{aligned} \tag{3.3.9}$$

where $a = \frac{R}{\rho} > 1$.

Proof. Form Circulant Lemma in Part I, the eigenvalues of the circulant matrix $\mathbf{A}$ are given by

$$\lambda_k = \sum_{j=0}^{N-1} a_j\cos(kjh), \quad k = 0, 1, ..., N-1, \tag{3.3.10}$$

where a_j are given in (3.3.6) and (3.3.7). First, we have from Basic Lemma B in Part I

$$\begin{aligned}\lambda_0 &= \sum_{j=0}^{N-1} a_j = -\sum_{j=0}^{N-1} \frac{a\,\cos(jh) - 1}{\rho(1 + a^2 - 2a\,\cos(jh))} \\ &= -\frac{1}{\rho h}\left\{\int_0^{2\pi} \frac{a\,\cos x - 1}{1 + a^2 - 2a\,\cos x}\,dx\right\} + \triangle\lambda_0,\end{aligned} \tag{3.3.11}$$

where the explicit $\triangle\lambda_0$ is given in (3.3.16) below. Since

$$\frac{a\,\cos x - 1}{1 + a^2 - 2a\,\cos x} = -\frac{1}{2} + \frac{a^2 - 1}{2}\frac{1}{1 + a^2 - 2a\,\cos x},$$

the equation (3.3.11) leads to

$$\lambda_0 = \frac{1}{\rho h}\left\{\pi - \frac{a^2 - 1}{2}\int_0^{2\pi} \frac{1}{1 + a^2 - 2a\,\cos x}\,dx\right\} + \triangle\lambda_0. \tag{3.3.12}$$

There exists the integration formula in [90, 3.613(2)],

$$\int_0^{2\pi} \frac{\cos(kx)}{1 + a^2 - 2a\,\cos x}\,dx = \begin{cases} \dfrac{2\pi a^k}{1 - a^2}, & \text{if } a^2 < 1, \\ \dfrac{2\pi}{(a^2 - 1)}\dfrac{1}{a^k}, & \text{if } a^2 > 1. \end{cases} \tag{3.3.13}$$

Hence we have from (3.3.12) and (3.3.13)

$$\lambda_0 = \frac{1}{\rho h}\left\{\pi - \frac{a^2 - 1}{2} \times \frac{2\pi}{a^2 - 1}\right\} + \triangle\lambda_0 = \triangle\lambda_0. \tag{3.3.14}$$

Now, we show $\triangle\lambda_0$. From (3.3.13) we have the expansion,

$$\frac{1}{1 + a^2 - 2a\,\cos x} = \frac{\bar{\alpha}_0}{2} + \sum_{\ell=1}^{\infty}\{\bar{\alpha}_\ell\,\cos(\ell x) + \bar{\beta}_\ell\,\sin(\ell x)\}, \tag{3.3.15}$$

where $a^2 > 1$ and $\bar{\alpha}_\ell = \frac{2}{a^2-1}\frac{1}{a^\ell}$ $(\ell \geq 1)$. Also from Basic Lemma B and (3.3.12), we obtain

$$\triangle\lambda_0 = -\frac{1}{\rho h}\frac{a^2 - 1}{2} \times 2\pi \sum_{v=1}^{\infty} \bar{\alpha}_{vN} = -\frac{N}{\rho}\sum_{v=1}^{\infty}\frac{1}{a^{vN}} = \frac{-N}{\rho(1 - a^{-N})} \times \frac{1}{a^N}. \tag{3.3.16}$$

Combining (3.3.14) and (3.3.16) gives the first desired result (3.3.8).

Next, we have from (3.3.10) and Basic Lemma B

$$\begin{aligned}\lambda_k &= -\sum_{j=0}^{N-1} \frac{\cos(kjh)(a\,\cos(jh) - 1)}{\rho(1 + a^2 - 2a\,\cos(jh))} \\ &= -\frac{1}{\rho h}\int_0^{2\pi} \frac{\cos(kx)(a\,\cos x - 1)}{1 + a^2 - 2a\,\cos x}\,dx + \triangle\lambda_k, \quad k = 1, 2, ..., N - 1,\end{aligned} \tag{3.3.17}$$

where the explicit $\triangle\lambda_k$ is given in (3.3.19) below. Since

$$\cos(kx)\,\cos x = \frac{1}{2}\{\cos(k+1)x + \cos(k-1)x\},$$

we have from (3.3.17) and (3.3.13)

$$\begin{aligned}
\lambda_k &= \frac{1}{\rho h}\left\{-\frac{a}{2}\int_0^{2\pi}\frac{\cos(k+1)x+\cos(k-1)x}{1+a^2-2a\,\cos x}\,dx + \int_0^{2\pi}\frac{\cos kx}{1+a^2-2\,\cos x}\,dx\right\} + \triangle\lambda_k \\
&= \frac{1}{\rho h}\left\{-\frac{a}{2}\frac{2\pi}{a^2-1}\left(\frac{1}{a^{k+1}}+\frac{1}{a^{k-1}}\right) + \frac{2\pi}{a^2-1}\frac{1}{a^k}\right\} + \triangle\lambda_k \\
&= -\frac{1}{\rho h}\frac{\pi}{a^k} + \triangle\lambda_k = -\frac{N}{2\rho a^k} + \triangle\lambda_k. \qquad (3.3.18)
\end{aligned}$$

From Basic Lemma B, we obtain from (3.3.15) and (3.3.18)

$$\begin{aligned}
\triangle\lambda_k &= \frac{1}{\rho h}\left\{-\frac{a\pi}{2}\sum_{\nu=1}^{\infty}(\bar{\alpha}_{\nu N-(k+1)}+\bar{\alpha}_{\nu N+(k+1)}+\bar{\alpha}_{\nu N-(k-1)}+\bar{\alpha}_{\nu N+(k-1)})\right. \\
&\qquad \left. + \pi\sum_{\nu=1}^{\infty}(\bar{\alpha}_{\nu N-k}+\bar{\alpha}_{\nu N+k})\right\} \\
&= \frac{2\pi}{\rho h}\frac{1}{a^2-1}\left\{-\frac{a}{2}\sum_{\nu=1}^{\infty}\left(\frac{1}{a^{\nu N-(k+1)}}+\frac{1}{a^{\nu N+(k+1)}}+\frac{1}{a^{\nu N-(k-1)}}+\frac{1}{a^{\nu N+(k-1)}}\right)\right. \\
&\qquad \left. + \sum_{\nu=1}^{\infty}\left(\frac{1}{a^{\nu N-k}}+\frac{1}{a^{\nu N+k}}\right)\right\} \\
&= -\frac{\pi}{\rho h}\sum_{\nu=1}^{\infty}\left\{\frac{1}{a^{\nu N-k}}+\frac{1}{a^{\nu N+k}}\right\} = -\frac{N}{2\rho(1-a^{-N})}\left\{\frac{1}{a^{N-k}}+\frac{1}{a^{N+k}}\right\}.
\end{aligned}$$

(3.3.19)

Combining (3.3.18) and (3.3.19) gives the desired result (3.3.9), and this completes the proof of Theorem 3.3.1. ■

In fact, we have used Mathematica to compute λ_k for three different cases: (1) the eigenvalues of matrix **A** in (3.3.5), (2) the equation (3.3.10), and (3) the equations (3.3.8) and (3.3.9). The computed eigenvalues for the three cases are perfectly matched with each other.

From (3.3.9) we have for $k \ge 1$

$$|\lambda_k| = \frac{N}{2\rho}\left\{\frac{1}{a^k}+\frac{1}{1-a^{-N}}\left(\frac{1}{a^{N-k}}+\frac{1}{a^{N+k}}\right)\right\} \le |\lambda_1| \le CN. \qquad (3.3.20)$$

Let N be even without loss of generality, we have

$$|\lambda_k| \ge |\lambda_{\frac{N}{2}}| \ge c_0 N a^{-\frac{N}{2}}, \quad k = 1, 2, ..., N-1, \qquad (3.3.21)$$

where C and c_0 (> 0) are two constants independent of N. In the following, C and c_0 (> 0) are always the constants independent of N, but their values may be different in different contexts.

Note that from (3.3.8) and (3.3.9) we have $\min_k|\lambda_k| = |\lambda_0| > 0$, to indicate the non-singularity of matrix $\mathbf{A}$ in (3.3.3) from the MFS. This result is interesting for Neumann's problems. However, since

$$|\lambda_0| \approx \frac{N}{\rho}\frac{1}{a^N} = \frac{N}{\rho}\left(\frac{\rho}{R}\right)^N \tag{3.3.22}$$

is much smaller than others in (3.3.21) (*i.e.*, $|\lambda_0| \ll |\lambda_k|\,(k \geq 1)$), for better stability we should employ the TSVD solution from (3.2.14). By ignoring the components with respect to $\mathbf{v}_N$ $(= \mathbf{y}_0)$, we have

$$\mathbf{x} = \sum_{i=1}^{N-1} \frac{\mathbf{u}_i^T \mathbf{b}}{\sigma_i} \mathbf{v}_i, \tag{3.3.23}$$

where $t = N - 1$ in (3.2.14). In this case, the modified condition number,

$$\widehat{\text{C}}\text{ond} = \frac{\max|\lambda_i|}{\text{min–next}|\lambda_i|}, \tag{3.3.24}$$

is given from (3.2.15), where $\text{min–next}|\lambda_i| > 0$ and $\min|\lambda_i| \approx 0$. Then we have the following corollary from (3.3.20)–(3.3.22).

Corollary 3.3.1. *Let the conditions in Theorem 3.3.1 hold. Then the bound exists,*

$$\text{Cond} = \frac{|\lambda_1|}{|\lambda_0|} \leq C\left(\frac{R}{\rho}\right)^N. \tag{3.3.25}$$

Also by the TSVD in (3.3.23),

$$\widehat{\text{C}}\text{ond} = \frac{|\lambda_1|}{\left|\lambda_{\frac{N}{2}}\right|} \leq C\left(\frac{R}{\rho}\right)^{\frac{N}{2}}. \tag{3.3.26}$$

3.4 Stability Analysis for Bounded Simply-Connected Domains

From Section 3.2, the MFS is classified to the Trefftz method by choosing the FS as admissible functions. Hence, we may study the MFS as the TM in [224], and the TM involving an integration approximation (*i.e.*, the CTM) in [169].

3.4.1 Trefftz Methods

Consider the Neumann problem (3.2.1) and (3.2.2), where S is a bounded simply-connected domain. First, we study the stability of the TM (3.2.8) without integration approximation, and obtain the normal equation $\mathbf{Bx} = \mathbf{d}$, where $\mathbf{x} = (c_1, c_2, ..., c_N)^T$, $\mathbf{d} \in \mathbf{R}^N$ is the known vector, and $\mathbf{B} \in \mathbf{R}^{N\times N}$. The matrix $\mathbf{B}$ is symmetric and positive definite. Let $I_0(v) = \mathbf{x}^T\mathbf{Bx}$, where $v \in V_N$ and

$$I_0(v) = \int_\Gamma \left(\frac{\partial v}{\partial \nu}\right)^2. \tag{3.4.1}$$

Hence, the maximal and the minimal eigenvalues of B can be obtained by

$$\lambda_{\max}(\mathbf{B}) = \max_{\mathbf{x}\neq 0} \frac{\mathbf{x}^T\mathbf{Bx}}{\mathbf{x}^T\mathbf{x}} = \max_{\substack{\mathbf{x}\neq 0\\ v\in V_N}} \frac{I_0(v)}{\|\mathbf{x}\|^2}, \tag{3.4.2}$$

$$\lambda_{\min}(\mathbf{B}) = \min_{\mathbf{x}\neq 0} \frac{\mathbf{x}^T\mathbf{Bx}}{\mathbf{x}^T\mathbf{x}} = \min_{\substack{\mathbf{x}\neq 0\\ v\in V_N}} \frac{I_0(v)}{\|\mathbf{x}\|^2}. \tag{3.4.3}$$

When $R > r_{\max}$, since the derivatives $\frac{\partial\phi_i}{\partial\nu}(P)$ are bounded on $\mathbf{\Gamma}$, we have from the Schwarz inequality

$$\begin{aligned}\int_\Gamma \left(\frac{\partial v}{\partial \nu}\right)^2 ds &= \int_\Gamma \left\{\sum_{i=1}^N c_i \frac{\partial\phi_i}{\partial\nu}(s)\right\}^2 ds \le \sum_{i=1}^N c_i^2 \left\{\int_\Gamma \sum_{i=1}^N \left|\frac{\partial\phi_i}{\partial\nu}(s)\right|^2 ds\right\} \\ &\le CN \sum_{i=1}^N c_i^2 \le CN\|\mathbf{x}\|^2.\end{aligned} \tag{3.4.4}$$

From (3.4.1) and (3.4.2), we obtain

$$\lambda_{\max}(\mathbf{B}) = \max_{\substack{\mathbf{x}\neq 0\\ v\in V_N}} \frac{1}{\|\mathbf{x}\|^2} \int_\Gamma \left(\frac{\partial v}{\partial \nu}\right)^2 \le CN. \tag{3.4.5}$$

The challenging work is to estimate the lower bound of $\lambda_{\min}(\mathbf{B})$ in (3.4.3).

Since the matrix $\mathbf{B}$ is nonsingular from Theorem 3.3.1, we have $\lambda_{\min}(\mathbf{B}) > 0$. Denote the inscribed disk by S_0 ($\subseteq S$) and its circular boundary $\mathbf{\Gamma}_0$ by

$$S_0 = \{(r,\theta) | r \le r_{\min}, 0 \le \theta \le 2\pi\}, \quad \mathbf{\Gamma}_0 = \{(r,\theta) | r = r_{\min}, 0 \le \theta \le 2\pi\},$$

where $r_{\min}$ is given in (3.2.3).

Lemma 3.4.1. *Let* $v \in \mathbf{H}^p(S)$ $\left(p > \frac{3}{2}\right)$, *then the bound exists,*

$$I_0(v) \ge c_0 \min_{v\in V_N} \|v_r\|^2_{0,\Gamma_0}, \tag{3.4.6}$$

where $v_r = \frac{\partial v}{\partial r}$, *and* $c_0\,(> 0)$ *is a constant independent of* N.

Proof. For the harmonic functions $v \in V_N$ in S, we have from Oden and Reddy [195]

$$\|v\|_{\frac{3}{2},S} \le C\|v_\nu\|_{0,\Gamma},$$

where $v_\nu = \frac{\partial v}{\partial \nu}$. Then it follows from (3.4.1) that

$$I_0(v) \ge c_0\|v\|^2_{\frac{3}{2},S}. \tag{3.4.7}$$

Moreover, since $\Delta v = 0$ and $S_0 \subseteq S$, we have from [195]

$$\|v\|_{\frac{3}{2},S} \ge \|v\|_{\frac{3}{2},S_0} \ge c_0\|v_r\|_{0,\Gamma_0}. \tag{3.4.8}$$

Hence, we obtain from (3.4.7) and (3.4.8)

$$I_0(v) \ge c_0\|v_r\|^2_{0,\Gamma_0}.$$

This is the desired result (3.4.6). ■

It is shown in [169] that even by the rough central rule, the integrals $\int_{\Gamma_0} v_r^2$ and $\widehat{\int}_{\Gamma_0} v_r^2$ are equivalent to each other,

$$\overline{\|v_r\|}_{0,\Gamma_0} \asymp \|v_r\|_{0,\Gamma_0}, \quad v \in V_N, \tag{3.4.9}$$

where $\overline{\|v_r\|}_{0,\Gamma_0} = \sqrt{\widehat{\int}_{\Gamma_0} v_r^2}$. The equation (3.4.9) means that there exist two positive constants C_1 and C_2 such that

$$C_1\int_{\Gamma_0} v_r^2 \le \widehat{\int}_{\Gamma_0} v_r^2 \le C_2\int_{\Gamma_0} v_r^2. \tag{3.4.10}$$

Theorem 3.4.1. *Let (3.4.9) hold. Then the bounds exist,*

$$\lambda_{\min}(\mathbf{B}) \ge c_0 N\left(\frac{r_{\min}}{R}\right)^{2N}, \tag{3.4.11}$$

$$\lambda_{\min-\text{next}}(\mathbf{B}) \ge c_0 N\left(\frac{r_{\min}}{R}\right)^{N}. \tag{3.4.12}$$

Proof. We have

$$\begin{aligned} \|v_r\|^2_{0,\Gamma_0} &= \int_{\Gamma_0} v_r^2 = \int_{\Gamma_0}\left(\frac{\partial}{\partial r}\sum_{i=1}^N c_i\phi_i(P)\right)^2 \\ &= \sum_{i,j=1}^N c_i c_j \int_{\Gamma_0} \frac{\partial\phi_i(P)}{\partial r}\frac{\partial\phi_j(P)}{\partial r}, \quad P \in \mathbf{\Gamma}_0. \end{aligned} \tag{3.4.13}$$

Denote $P_\ell^* = (r_{\min}\cos(\ell h), r_{\min}\sin(\ell h))$, $\ell = 1, 2, ..., N$ with $h = \frac{2\pi}{N}$. We have from (3.4.13) and (3.4.9)

$$\begin{aligned} \|v_r\|^2_{0,\Gamma_0} \geq c_0 \overline{\|v_r\|}^2_{0,\Gamma_0} &= c_0 h\ r_{\min} \sum_{i,j=1}^{N} c_i c_j \sum_{\ell=1}^{N} \frac{\partial \phi_i(P_\ell^*)}{\partial r} \frac{\partial \phi_j(P_\ell^*)}{\partial r} \\ &= c_0 h\ r_{\min} \sum_{\ell=1}^{N} \sum_{i,j=1}^{N} c_i c_j \frac{\partial \phi_i(P_\ell^*)}{\partial r} \frac{\partial \phi_j(P_\ell^*)}{\partial r} = c_0 h\ r_{\min} \mathbf{x}^T \mathbf{A}^T \mathbf{A} \mathbf{x}, \end{aligned} \tag{3.4.14}$$

where $\mathbf{A}$ is the symmetric and circulant matrix (3.3.5) with $\rho = r_{\min}$. From (3.3.8) the bound exists,

$$\frac{\mathbf{x}^T \mathbf{A}^T \mathbf{A} \mathbf{x}}{\mathbf{x}^T \mathbf{x}} \geq \min_k (\lambda_k^2(\mathbf{A})) \geq \lambda_0^2(\mathbf{A}) = c_0 N^2 \left(\frac{r_{\min}}{R}\right)^{2N}. \tag{3.4.15}$$

Since $v \in V_N$ and $v \in \mathbf{H}^p(S)\big(p > \frac{3}{2}\big)$, Lemma 3.4.1 holds. Hence, from Lemma 3.4.1, (3.4.3), (3.4.14) and (3.4.15), we obtain

$$\lambda_{\min}(\mathbf{B}) \geq c_0 \frac{\|v_r\|^2_{0,\Gamma_0}}{\|\mathbf{x}\|^2} \geq c_0 h r_{\min} \frac{\mathbf{x}^T \mathbf{A}^T \mathbf{A} \mathbf{x}}{\|\mathbf{x}\|^2} \geq \bar{c}_0 N \left(\frac{r_{\min}}{R}\right)^{2N},$$

where $\bar{c}_0\ (> 0)$ is also a constant independent of N. This is the first desired result (3.4.11). We have from (3.3.21)

$$\lambda_{\min-\text{next}}(\mathbf{B}) = \min_{k \geq 1} (\lambda_k^2(\mathbf{A})) \geq \lambda_{\frac{N}{2}}^2(\mathbf{A}) = c_0 N^2 \left(\frac{r_{\min}}{R}\right)^{N}.$$

This completes the proof of Theorem 3.4.1. ■

From Theorem 3.4.1 and (3.4.5), we obtain the following corollary.

Corollary 3.4.1. *Let (3.4.9) hold, then the bounds exist,*

$$\text{Cond}(\mathbf{B}) \leq C \left(\frac{R}{r_{\min}}\right)^{2N}, \quad \widehat{\text{C}}\text{ond}(\mathbf{B}) \leq C \left(\frac{R}{r_{\min}}\right)^{N}.$$

3.4.2 Collocation Trefftz Methods

In computation, we use (3.2.12) with $M \geq N$, and obtain an overdetermined system,

$$\mathbf{F}\mathbf{x} = \mathbf{d}, \tag{3.4.16}$$

where $\mathbf{x} = (c_1, c_2, ..., c_N)^T$, $\mathbf{d} \in \mathbf{R}^M$, and $\mathbf{F} \in \mathbf{R}^{M \times N}$. We have $\widehat{I}_0(v) = \mathbf{x}^T \mathbf{F}^T \mathbf{F} \mathbf{x}$, where

$$\widehat{I}_0(v) = \widehat{\int_\Gamma} \left(\frac{\partial v}{\partial \nu}\right)^2. \tag{3.4.17}$$

Denote the discrete norms $\overline{\|v_v\|_{0,\Gamma}} = \sqrt{\widehat{\int_\Gamma} v_v^2}$, where $\widehat{\int_\Gamma}$ is the numerical approximation of $\int_\Gamma$ by the Gaussian rule (or the trapezoidal rule). From [169], assume that the following equivalence exists:

$$\overline{\|v_v\|_{0,\Gamma}} \asymp \|v_v\|_{0,\Gamma}, \quad v \in V_N. \tag{3.4.18}$$

Denote the singular values σ_i of $\mathbf{F}$ in (3.4.16), and

$$\sigma_{\max} = \max_i \sigma_i, \quad \sigma_{\min-\text{next}} > \sigma_{\min} = \min_i \sigma_i > 0.$$

We have the following theorem.

Theorem 3.4.2. *Let (3.4.9) and (3.4.18) hold. For the MFS in (3.2.12) with* $M \geq N$, *the following bounds exist*

$$\sigma_{\max}(\mathbf{F}) = \sigma_1(\mathbf{F}) \leq C\sqrt{N}, \tag{3.4.19}$$

$$\sigma_{\min}(\mathbf{F}) = \sigma_N(\mathbf{F}) \geq c_0\sqrt{N}\left(\frac{r_{\min}}{R}\right)^N, \tag{3.4.20}$$

$$\sigma_{\min-\text{next}}(\mathbf{F}) \geq c_0\sqrt{N}\left(\frac{r_{\min}}{R}\right)^{\frac{N}{2}}. \tag{3.4.21}$$

Proof. From (3.4.18) we have

$$\widehat{I}_0(v) \asymp I_0(v), \quad v \in V_N, \tag{3.4.22}$$

where $\widehat{I}_0(v)$ and $I_0(v)$ are given in (3.4.17) and (3.4.1), respectively. From (3.4.22) and (3.4.5), we get

$$\begin{aligned} \lambda_{\max}(\mathbf{F}^T\mathbf{F}) &= \max_{\mathbf{x}\neq 0} \frac{\mathbf{x}^T\mathbf{F}^T\mathbf{F}\mathbf{x}}{\mathbf{x}^T\mathbf{x}} = \max_{\substack{\mathbf{x}\neq 0 \\ v\in V_N}} \frac{\widehat{I}_0(v)}{\|\mathbf{x}\|^2} \\ &\leq C \max_{\substack{\mathbf{x}\neq 0 \\ v\in V_N}} \frac{I_0(v)}{\|\mathbf{x}\|^2} = C\lambda_{\max}(\mathbf{B}) \leq \bar{C}N, \end{aligned} \tag{3.4.23}$$

where $\bar{C}$ is a bounded constant independent of N. Next, from (3.4.22) and (3.4.11) we have

$$\begin{aligned} \lambda_{\min}(\mathbf{F}^T\mathbf{F}) &= \min_{\mathbf{x}\neq 0} \frac{\mathbf{x}^T\mathbf{F}^T\mathbf{F}\mathbf{x}}{\mathbf{x}^T\mathbf{x}} = \min_{\substack{\mathbf{x}\neq 0 \\ v\in V_N}} \frac{\widehat{I}_0(v)}{\|\mathbf{x}\|^2} \\ &\geq c_0 \min_{\substack{\mathbf{x}\neq 0 \\ v\in V_N}} \frac{I_0(v)}{\|\mathbf{x}\|^2} = c_0\lambda_{\min}(\mathbf{B}) \geq \bar{c}_0 N\left(\frac{r_{\min}}{R}\right)^{2N}, \end{aligned} \tag{3.4.24}$$

where $\bar{c}_0$ (> 0) is also a constant independent of N. The desired results (3.4.19) and (3.4.20) follow from (3.4.23), (3.4.24) and the following equalities,

$$\sigma_{\max}(\mathbf{F}) = \{\lambda_{\max}(\mathbf{F}^T\mathbf{F})\}^{\frac{1}{2}}, \quad \sigma_{\min}(\mathbf{F}) = \{\lambda_{\min}(\mathbf{F}^T\mathbf{F})\}^{\frac{1}{2}}.$$

Similarly, the equation (3.4.21) follows from (3.4.12). This completes the proof of Theorem 3.4.2. ■

We have the following corollary from Theorem 3.4.2.

Corollary 3.4.2. *Let the conditions in Theorem 3.4.2 hold. Then the bounds exist,*

$$\text{Cond}(\mathbf{F}) = \frac{\sigma_{\max}(\mathbf{F})}{\sigma_{\min}(\mathbf{F})} \le C\left(\frac{R}{r_{\min}}\right)^N, \tag{3.4.25}$$

$$\widehat{\text{Cond}}(\mathbf{F}) = \frac{\sigma_{\max}(\mathbf{F})}{\sigma_{\min-\text{next}}(\mathbf{F})} \le C\left(\frac{R}{r_{\min}}\right)^{\frac{N}{2}}. \tag{3.4.26}$$

Corollary 3.4.2 indicates that the TSVD may greatly improve the stability of Neumann problems by the MFS.

3.5 Error Estimates

Since the MFS can be regarded as the TM using the FS, we may follow the analysis of TM in [146, 169], and pay attention to the errors between the harmonic polynomials and the fundamental solutions as in Chapter 2. To avoid multiple solutions, we may follow [105] by adding a constraint as

$$u|_D = d_0, \tag{3.5.1}$$

where the given point $D \in \Gamma$, and d_0 is a constant (*i.e.*, $d_0 = 1$). Then the solution of (3.2.1) and (3.2.2) is unique since $\int_\Gamma g = 0$ and (3.5.1). Note that for $v \in \mathbf{H}^1(S)$ satisfying (3.5.1), the norms $\|v\|_{1,S}$ and $|v|_{1,S}$ are equivalent to each other: $\|v\|_{1,S} \asymp |v|_{1,S}$. In fact, the equation (3.5.1) may not be used in computation; see the numerical results in [167].

Choose

$$u_N = \sum_{i=1}^{N} c_i \phi_i(r,\theta), \quad (r,\theta) \in S, \tag{3.5.2}$$

where $\phi_i(r,\theta) = \ln\sqrt{R^2 + r^2 - 2Rr\cos(\theta - ih)}$ and $h = \frac{2\pi}{N}$. Let $\bar{V}_N$ denote the set of the functions in (3.5.2) satisfying (3.5.1). Also denote

$$I(v) = \int_\Gamma \left(\frac{\partial v}{\partial \nu} - g\right)^2, \quad \widehat{I}(v) = \widehat{\int_\Gamma} \left(\frac{\partial v}{\partial \nu} - g\right)^2. \tag{3.5.3}$$

Then for the Neumann problem, the solutions of the TM and the CTM using FS are given by, respectively,

$$I(u_N) = \min_{v \in \bar{V}_N} I(v), \tag{3.5.4}$$

and

$$\widehat{I}(\tilde{u}_N) = \min_{v \in \bar{V}_N} \widehat{I}(v). \tag{3.5.5}$$

Below, we only derive the error bounds of u_N by the TM (3.5.4), since the error bounds for (3.5.5) can be obtained similarly (see [169]). Denote the inner product

$$[u, v]_{B^*} = \int_\Gamma \frac{\partial u}{\partial \nu}\frac{\partial v}{\partial \nu}, \tag{3.5.6}$$

and the boundary norm

$$\|v\|_{B^*} = \sqrt{[v, v]_{B^*}} = \left\|\frac{\partial v}{\partial \nu}\right\|_{0,\Gamma}. \tag{3.5.7}$$

By following [146], the solution of u_N also satisfies the minimum property,

$$\|u - u_N\|_{B^*} = \min_{v \in \bar{V}_N} \|u - v\|_{B^*}, \tag{3.5.8}$$

and the orthogonality property,

$$[u - u_N, v]_{B^*} = 0, \quad \forall\, v \in \bar{V}_N. \tag{3.5.9}$$

In Figure 1.1, denote two disks $S_{\min}$ and $S_{\max}$ by

$$S_{\min} \subset S \subset S_{\max}, \tag{3.5.10}$$

where $S_{\min} = \{(r, \theta) | 0 \le r < r_{\min}, 0 \le \theta < 2\pi\}$, $S_{\max} = \{(r, \theta) | 0 \le r < r_{\max}, 0 \le \theta < 2\pi\}$, and $r_{\max}$ and $r_{\min}$ are given in (3.2.3). Denote the harmonic polynomial functions of order n by

$$P_n = P_n(r, \theta) = \frac{\alpha_0}{2} + \sum_{i=1}^{n} r^i (\alpha_i \cos i\theta + \beta_i \sin i\theta), \tag{3.5.11}$$

where α_i and β_i are coefficients. Also denote the FS by

$$u_N = \sum_{i=1}^{N} c_i \ln|\overline{PQ_i}|, \tag{3.5.12}$$

where $P \in (S \cup \partial S)$, and Q_i are given in (3.2.4). We cite a lemma from Section 11.4.1.

Lemma 3.5.1. *Let $u \in C(S)$ hold. Then there exists a special FS denoted by u_N^* $(\in V_N)$ such that for large $N > 2n$,*

$$\left\|\frac{\partial}{\partial \nu}(P_n(r, \theta) - u_N^*)\right\|_{q,\Gamma} \le CN^{q+1}\left(\frac{R}{r_{\max}}\right)^{2n-N}\left(\frac{r_{\max}}{r_{\min}}\right)^n \|P_n(r, \theta)\|_{0,\Gamma}, \tag{3.5.13}$$

where ν is the exterior normal to Γ, $\|v\|_{q,\Gamma}$ is the Sobolev norm, and $P_n(r, \theta)$ is given in (3.5.11).

Lemma 3.5.2. *Let* Γ *be a smooth boundary, condition (3.2.16) hold, and* N *satisfy*

$$\left(\frac{R}{r_{\max}}\right)^{2n-N}\left(\frac{r_{\max}}{r_{\min}}\right)^{n} \le \frac{1}{n^{p-\frac{1}{2}}}. \tag{3.5.14}$$

Then for the Neumann problem, the solution u_N *by the MFS has the error bound,*

$$\|u-u_N\|_{B^*} = O\left(\frac{1}{N^{p-\frac{3}{2}}}\right)\|u\|_{p,S}. \tag{3.5.15}$$

Proof. Let the exact solution as

$$u = u(r,\theta) = P_n(r,\theta) + R_n(r,\theta), \tag{3.5.16}$$

where $P_n(r,\theta)$ is given in (3.5.11), and the residuals

$$R_n = R_n(r,\theta) = \sum_{i=n+1}^{\infty} r^i(\alpha_i \cos(i\theta) + \beta_i \sin(i\theta)), \tag{3.5.17}$$

and α_i and β_i are the exact coefficients. We have from (3.5.8)

$$\|u-u_N\|_{B^*} \le \|u-u_N^*\|_{B^*} \le \left\|\frac{\partial}{\partial v}(P_n - u_N^*)\right\|_{0,\Gamma} + \left\|\frac{\partial}{\partial v}R_n\right\|_{0,\Gamma}. \tag{3.5.18}$$

When $u \in \mathbf{H}^p(S)$ $(p \ge 2)$ from (3.2.16), the following bound exists from [15],

$$\left\|\frac{\partial}{\partial v}R_n\right\|_{0,\Gamma} \le C\|R_n\|_{\frac{3}{2},S} = O\left(\frac{1}{n^{p-\frac{3}{2}}}\|u\|_{p,S}\right). \tag{3.5.19}$$

When $u \in \mathbf{H}^p(S)$ $\left(p > \frac{3}{2}\right)$ for the singularity problems with corners, all error estimates of MFS in this chapter hold; details are omitted. When N is chosen to satisfy (3.5.14), we have $N \asymp n$. Then we obtain from (3.5.13)

$$\left\|\frac{\partial}{\partial v}(P_N(r,\theta) - u_N^*)\right\|_{0,\Gamma} = O\left(\frac{1}{n^{p-\frac{3}{2}}}\|P_n(r,\theta)\|_{0,\Gamma}\right). \tag{3.5.20}$$

Since $P_n(r,\theta) \approx u$, we have $\|P_n(r,\theta)\|_{0,\Gamma} \le C\|u\|_{0,\Gamma} \le C\|u\|_{\frac{1}{2},S} \le C\|u\|_{p,S}$. Hence, the equation (3.5.20) leads to

$$\left\|\frac{\partial}{\partial v}(P_n(r,\theta) - u_N^*)\right\|_{0,\Gamma} = O\left(\frac{1}{n^{p-\frac{3}{2}}}\right)\|u\|_{p,S}. \tag{3.5.21}$$

Combining (3.5.18), (3.5.19) and (3.5.21) and noting $n \asymp N$ yield the desired result (3.5.15), and this completes the proof of Lemma 3.5.2. ■

To obtain domain errors, we need to estimate the bounds of negative norms on $\mathbf{\Gamma}$. Define the negative norms,

$$\left\|\frac{\partial w}{\partial \nu}\right\|_{-\ell,\Gamma} = \sup_{v\in\mathbf{H}^{\ell}(\Gamma)} \frac{1}{\|v\|_{\ell,\Gamma}} \int_{\Gamma} \frac{\partial w}{\partial \nu}\cdot v. \tag{3.5.22}$$

Lemma 3.5.3. *Let the conditions in Lemma 3.5.2 hold. Then the error bounds exist,*

$$\left\|\frac{\partial}{\partial \nu}(u-u_N)\right\|_{-\frac{1}{2},\Gamma} \le C\frac{1}{N^{p-1}}\|u\|_{p,S}, \tag{3.5.23}$$

$$\left\|\frac{\partial}{\partial \nu}(u-u_N)\right\|_{-\frac{3}{2},\Gamma} \le C\frac{1}{N^{p}}\|u\|_{p,S}. \tag{3.5.24}$$

Proof. Let $t\in\mathbf{H}^{\frac{3}{2}}(\mathbf{\Gamma})$ and $\eta\in\mathbf{H}^{3}(S)$ satisfy the following auxiliary problem,

$$\Delta\eta = 0 \text{ in } S, \tag{3.5.25}$$

$$\frac{\partial\eta}{\partial\nu} = t \text{ on } \mathbf{\Gamma}, \tag{3.5.26}$$

$$\eta|_D = 1, \quad D\in\mathbf{\Gamma}. \tag{3.5.27}$$

Then we have from (3.5.22) and (3.5.26)

$$\left\|\frac{\partial(u-u_N)}{\partial\nu}\right\|_{-\frac{3}{2},\Gamma} \le \frac{1}{\|t\|_{\frac{3}{2},\Gamma}}\int_{\Gamma}\frac{\partial(u-u_N)}{\partial\nu}\cdot t = \frac{1}{\|t\|_{\frac{3}{2},\Gamma}}\int_{\Gamma}\frac{\partial(u-u_N)}{\partial\nu}\cdot\frac{\partial\eta}{\partial\nu}. \tag{3.5.28}$$

Hence from (3.5.28), (3.5.6), (3.5.9) and Lemma 3.5.2,

$$\begin{aligned}\int_{\Gamma}\frac{\partial(u-u_N)}{\partial\nu}\cdot\frac{\partial\eta}{\partial\nu} &= [u-u_N,\eta]_{B^*} \qquad\qquad (3.5.29)\\ &= [u-u_N,\eta-\eta_N]_{B^*} \le \|u-u_N\|_{B^*}\|\eta-\eta_N\|_{B^*}\\ &\le C\left(\frac{1}{N^{p-\frac{3}{2}}}\|u\|_{p,S}\right)\times\left(\frac{1}{N^{\frac{3}{2}}}\|\eta\|_{3,S}\right) = \frac{C}{N^p}\|u\|_{p,S}\times\|\eta\|_{3,S}.\end{aligned}$$

However, from the auxiliary problem (3.5.25)–(3.5.27), we have

$$\|\eta\|_{3,S} \le C\|t\|_{\frac{3}{2},\Gamma}. \tag{3.5.30}$$

The second desired result (3.5.24) follows from (3.5.28)–(3.5.30) and (3.5.22).

Next, we prove the first result (3.5.23). From the Sobolev interpolation theory in [15], the bound exists,

$$\|v\|_{-\frac{1}{2},\Gamma} \leq C\Big\{\|v\|_{0,\Gamma}\Big\}^{\frac{2}{3}} \times \Big\{\|v\|_{-\frac{3}{2},\Gamma}\Big\}^{\frac{1}{3}}. \tag{3.5.31}$$

Hence, we have from (3.5.24), (3.5.31) and Lemma 3.5.2,

$$\begin{aligned}\left\|\frac{\partial}{\partial v}(u-u_N)\right\|_{-\frac{1}{2},\Gamma} &\leq C\left\{\left\|\frac{\partial}{\partial v}(u-u_N)\right\|_{0,\Gamma}\right\}^{\frac{2}{3}} \times \left\{\left\|\frac{\partial}{\partial v}(u-u_N)\right\|_{-\frac{3}{2},\Gamma}\right\}^{\frac{1}{3}} \\ &\leq C\left\{\frac{1}{N^{p-\frac{3}{2}}}\right\}^{\frac{2}{3}} \times \left\{\frac{1}{N^{p}}\right\}^{\frac{1}{3}} \|u\|_{p,S} = C\frac{1}{N^{p-1}}\|u\|_{p,S}.\end{aligned}$$

This is the first desired result (3.5.23), and completes the proof of Lemma 3.5.3. ■

Theorem 3.5.1. *Let the conditions in Lemma 3.5.2 hold. Then for the Neumann problem, the numerical solutions by the MFS have the optimal error bounds in both* $\mathbf{L}^2$ *and* $\mathbf{H}^1$ *norms in* S*,*

$$\|u-u_N\|_{k,S} = O\left(\frac{1}{N^{p-k}}\right)\|u\|_{p,S}, \quad k=0,1. \tag{3.5.32}$$

Proof. Since for the harmonic function $(u-u_N)$, the bound exists,

$$\|u-u_N\|_{k,S} \leq C\left\|\frac{\partial}{\partial v}(u-u_N)\right\|_{k-\frac{3}{2},\Gamma}. \tag{3.5.33}$$

Then the desired results (3.5.32) follow from Lemma 3.5.3. ■

For the quotient space $\mathbf{H}^k(S)/\mathbf{P}_0(S)$, the differences of a constant solution are not included in (3.5.33). For the pure Neumann problem, the optimal rates in both $\mathbf{L}^2$ and $\mathbf{H}^1$ norms in S are derived in this section. Under (3.2.16), the polynomial convergence rates are obtained. When Laplace's solutions are infinitely smooth, the exponential convergence rates can also be achieved, as those by the method of particular solutions (MPS) in [169]. Note that the proof here does not need the assumption of inverse inequalities in [146, 169]. However, for the mixed boundary problems in Chapter 4, the analytical approaches as in [146, 150, 163] should be solicited based on the assumption of inverse inequalities. This is a distinct feature in the error analysis for Neumann problems.

3.6 Concluding Remarks

To close this chapter, let us address a few remarks.

1. For disk domains, the eigenvalues of the stiffness matrix from the MFS are expressed in Theorem 3.3.1 in terms of N^v and a^k, which may easily lead to the sharp bounds of Cond in Corollary 3.3.1. The exponential growth rates of

condition numbers are obtained. Note that the discrete matrix from the MFS is not singular for Neumann problems. For the bounded simply-connected domains, the new and sharp bounds of Cond by the MFS are derived in Section 3.4, and the exponential growth rates are obtained.

2. To reduce condition numbers significantly, the TSVD in (3.3.23) is used by removing the component of $\mathbf{y}_0$ corresponding to λ_0. This is a distinct feature of Neumann problems by the MFS. In contrast, for Dirichlet problems and mixed boundary problems, the improvement of stability using (3.3.23) is not so significant. See [161]. Of course, we may use $t < N-1$ in (3.2.14) to reduce the Cond significantly, while the errors will increase. To balance the ill-conditioning and accuracy, we may solicit the sensitivity index in Chapter 14 for seeking a better t as in Zhang *et al.* [259]. On the other hand, the Tikhonov regularization (TR) may be employed also to reduce the Cond significantly. To balance the ill-conditioning and accuracy, the sensitivity index is also applied to seek the regularization parameter. See Part III and [259].

3. Let us compare the results in this chapter with those of other boundary conditions of Laplace's equation in Chapters 2 and 4. The optimal convergence in $\mathbf{L}^2$ norms in S is derived in [151] for Dirichlet problems in both the bounded simply-connected domains and the annular domains. In this chapter, the error bounds in $\mathbf{L}^2$ and $\mathbf{H}^1$ norms in S are derived for Neumann problems without using the inverse inequalities in [146, 150, 163] to give the optimal polynomial convergence rates.

4. For the Dirichlet problems in disk domains with radius ρ, there exist the sharp bounds in Chapter 2,

$$\text{Cond} \le \frac{N|\ln R|}{2}\left(\frac{R}{\rho}\right)^{\frac{N}{2}}, \quad \rho < R \ne 1, \tag{3.6.1}$$

$$\text{Cond} \le CN\left(\frac{R}{\rho}\right)^{N}, \quad \rho < R = 1. \tag{3.6.2}$$

For the mixed boundary problems in the bounded simply-connected domains, the following bounds are derived in [163],

$$\text{Cond}(\mathbf{F}) \le CN^2\left(\frac{R}{r_{\min}}\right)^{\frac{N}{2}}. \tag{3.6.3}$$

The bounds of (3.6.1) and (3.6.3) are slightly larger than those of (3.3.26) and (3.4.26) of $\widehat{\text{Cond}}(\mathbf{F})$, respectively. Note that the MFS for the Neumann problem in this chapter is more interesting and intriguing due to its distinct features, and the new analysis and the new numerical techniques may enhance the wide application of the MFS. Numerical experiments are reported in [167].

Chapter 4

Other Boundary Problems

This chapter considers other boundary problems of Laplace's equation, such as the mixed boundary problems of Dirichlet and Robin conditions, the interface problems, and the annular domain problems. The error analysis is made for the non-circular boundary to give the polynomial convergence rates. The materials of this chapter are adapted from [149–151].

4.1 Mixed Boundary Condition Problems

Consider Laplace's equation with the mixed type of Dirichlet and Robin boundary conditions,

$$\Delta u = \frac{\partial^2 u}{\partial x^2} + \frac{\partial^2 u}{\partial y^2} = 0 \text{ in } S, \tag{4.1.1}$$

$$u = f \text{ on } \Gamma_D, \tag{4.1.2}$$

$$\frac{\partial u}{\partial \nu} + \alpha u = g \text{ on } \Gamma_R, \tag{4.1.3}$$

where α is a non-negative constant, S a bounded simply-connected domain with the smooth boundary $\Gamma = \Gamma_D \cup \Gamma_R$, and ν the exterior normal of Γ. Choose the source nodes $Q_i = \{(x, y) | x = R\cos(ih), y = R\sin(ih)\}$, $i = 1, 2, \ldots, N$, with $h = \frac{2\pi}{N}$ and $R > r_{\max} = \max_S r$. We obtain the fundamental solutions (FS), $\phi_i(P) = \ln|\overline{PQ_i}|$, $i = 1, 2, \ldots, N$, and the numerical solution of (4.1.1)–(4.1.3) is given by a linear combination,

$$u_N = \sum_{i=1}^{N} c_i \ln|\overline{PQ_i}|, \tag{4.1.4}$$

where c_i are the unknown coefficients to be sought. Denote the energy

DOI: 10.1051/978-2-7598-3171-5.c004
© Science Press, EDP Sciences, 2023

$$I(v) = \int_{\Gamma_D} (v-f)^2 + w^2 \int_{\Gamma_R} \left(\frac{\partial v}{\partial \nu} + \alpha v - g \right)^2, \tag{4.1.5}$$

where the weight $w = \frac{1}{N}$ in [185]. Also, denote by V_N the set of (4.1.4). Then the numerical solution u_N can be obtained by

$$I(u_N) = \min_{v \in V_N} I(v). \tag{4.1.6}$$

When the integrals in (4.1.5) involve approximation, denote

$$\widehat{I}(v) = \widehat{\int}_{\Gamma_D} (v-f)^2 + w^2 \widehat{\int}_{\Gamma_R} \left(\frac{\partial v}{\partial \nu} + \alpha v - g \right)^2, \tag{4.1.7}$$

where $\widehat{\int}_{\Gamma_D}$ and $\widehat{\int}_{\Gamma_R}$ are the numerical approximations of $\int_{\Gamma_D}$ and $\int_{\Gamma_R}$ by some quadrature rules, such as the central or the Gaussian rule. Hence, the numerical solution $\tilde{u}_N \in V_N$ is obtained by

$$\widehat{I}(\tilde{u}_N) = \min_{v \in V_N} \widehat{I}(v). \tag{4.1.8}$$

The collocation equations are given in Section 1.2.

Denote the numerical solution in (4.1.4) by

$$u_N = \sum_{i=1}^{N} c_i \phi_i(r, \theta), \quad (r, \theta) \in S, \tag{4.1.9}$$

where

$$\phi_i(r, \theta) = \ln|\overline{PQ_i}| = \ln\sqrt{R^2 + r^2 - 2Rr\cos(\theta - \xi_i)}, \tag{4.1.10}$$

with $\xi_i = ih$ and $h = \frac{2\pi}{N}$. Let $a = \frac{R}{r} > 1$. There exist the derivatives,

$$\frac{\partial \phi_i(r,\theta)}{\partial r} = -\frac{a\cos(\theta - \xi_i) - 1}{r(a^2 + 1 - 2a\cos(\theta - \xi_i))}, \tag{4.1.11}$$

$$\frac{\partial \phi_i(r,\theta)}{\partial \theta} = \frac{a\sin(\theta - \xi_i)}{(a^2 + 1 - 2a\cos(\theta - \xi_i))}. \tag{4.1.12}$$

Denote by η the angle of the normal $\vec{\nu}$ from the radial direction $\vec{r}$ at the node $P(r, \theta) \in \Gamma$. From (4.1.11) and (4.1.12), we have

$$\begin{aligned} \frac{\partial \phi_i(r,\theta)}{\partial \nu} &= \frac{\partial \phi_i(r,\theta)}{\partial r}\cos\eta + \frac{\partial \phi_i(r,\theta)}{r\partial \theta}\sin\eta \\ &= -\frac{a\cos(\theta - \xi_i + \eta) - \cos\eta}{r(a^2 + 1 - 2a\cos(\theta - \xi_i))}. \end{aligned} \tag{4.1.13}$$

Let V_N denote the set of the admissible functions in (4.1.9). Denote the boundary norm

$$\|v\|_B = \left\{ \|v\|^2_{0,\Gamma_D} + w^2 \left\| \frac{\partial v}{\partial \nu} + \alpha v \right\|^2_{0,\Gamma_R} \right\}^{\frac{1}{2}}. \tag{4.1.14}$$

From (4.1.6) we have

$$\|u - u_N\|_B = \min_{v \in V_N} \|u - v\|_B. \tag{4.1.15}$$

Denote in Figure 1.1,

$$r_{\max} = \max_S r, \quad r_{\min} = \max_{S_{\text{in}}(S_{\text{in}} \subseteq S)} r, \tag{4.1.16}$$

where S_{in} is a disk inside S.

Lemma 4.1.1. *Let* $S_{\min} \subseteq S \subseteq S_{\max}$ *and* $u \in \mathbf{H}^p(S)$ $\left(p > \frac{3}{2}\right)$ *hold. Suppose that the large* N *satisfies*

$$\left(\frac{R}{r_{\max}}\right)^{2n-N} \left(\frac{r_{\max}}{r_{\min}}\right)^n \le n^{-p+\frac{1}{2}}. \tag{4.1.17}$$

Then when $w = \frac{1}{N}$, *the solution* u_N *by the Trefftz method (TM) has the error bound,*

$$\|u - u_N\|_B = O\left(\frac{1}{N^{p-\frac{1}{2}}}\right). \tag{4.1.18}$$

Proof. We have

$$u(r,\theta) = P_n(r,\theta) + R_n(r,\theta), \tag{4.1.19}$$

where $P_n(r,\theta)$ is the harmonic polynomials of order n,

$$P_n(r,\theta) = \frac{\alpha_0}{2} + \sum_{i=1}^{n} r^i \{\alpha_i \cos(i\theta) + \beta_i \sin(i\theta)\}, \tag{4.1.20}$$

α_i and β_i are the Fourier coefficients, and $R_n = R_n(r,\theta)$ is the residual. From $u \in \mathbf{H}^p(S)$, there exists the bound,

$$\|R_n(r,\theta)\|_{k,S} = \|u(r,\theta) - P_n(r,\theta)\|_{k,S} = O\left(\frac{1}{n^{p-k}} \|u\|_{p,S}\right), \quad p > k. \tag{4.1.21}$$

For the given $P_n(r,\theta)$, we find $u_N^* = \Sigma_N(P_n) \in V_N$ in Chapter 2. Then we have from (4.1.15)

$$\|u - u_N\|_B \le \|u - u_N^*\|_B. \tag{4.1.22}$$

Also from the embedding theorem, there exist the bounds,

$$\|v\|_{0,\Gamma} \leq C\|v\|_{\frac{1}{2},S}, \quad \left\|\frac{\partial v}{\partial \nu}\right\|_{0,\Gamma} \leq C\|v\|_{\frac{3}{2},S}. \tag{4.1.23}$$

Then we have from (4.1.14) and (4.1.23)

$$\begin{aligned}\|v\|_B &\leq \|v\|_{0,\Gamma_D} + w\left\|\frac{\partial v}{\partial \nu}\right\|_{0,\Gamma_R} + w\alpha\|v\|_{0,\Gamma_R} \\ &\leq (1+w\alpha)\|v\|_{\frac{1}{2},S} + w\|v\|_{\frac{3}{2},S} \leq C\Big\{\|v\|_{\frac{1}{2},S} + w\|v\|_{\frac{3}{2},S}\Big\}.\end{aligned} \tag{4.1.24}$$

Hence, we obtain from (4.1.22), (4.1.19) and the triangle inequality

$$\begin{aligned}\|u - u_N\|_B &\leq C\Big\{\|u - u_N^*\|_{\frac{1}{2},S} + w\|u - u_N^*\|_{\frac{3}{2},S}\Big\} \\ &\leq C\Big\{\|R_n(r,\theta)\|_{\frac{1}{2},S} + w\|R_n(r,\theta)\|_{\frac{3}{2},S} \\ &\quad + \|P_n(r,\theta) - u_N^*\|_{\frac{1}{2},S} + w\|P_n(r,\theta) - u_N^*\|_{\frac{3}{2},S}\Big\} \\ &:= C(T_1 + T_2).\end{aligned} \tag{4.1.25}$$

Since there exist the bounds,

$$\|R_n\|_{k,S} = O\left(\frac{1}{n^{p-k}}\|u\|_{p,S}\right), \quad k = \frac{1}{2}, \frac{3}{2}, \tag{4.1.26}$$

we have from $w = \frac{1}{N}$

$$T_1 = \|R_n\|_{\frac{1}{2},S} + w\|R_n\|_{\frac{3}{2},S} = O\left(\frac{1}{n^{p-\frac{1}{2}}}\right). \tag{4.1.27}$$

Next, denote the disks $S_{\max}$ and $S_{\min}$ such that $S_{\min} \subseteq S \subseteq S_{\max}$, where

$$S_{\max} = \{(r,\theta) | r < r_{\max}, 0 \leq \theta < 2\pi\}, \quad S_{\min} = \{(r,\theta) | r < r_{\min}, 0 \leq \theta < 2\pi\},$$

and $r_{\max}$ and $r_{\min}$ are given in (4.1.16). For $\Delta v = 0$, we have $\|v\|_{k,S} \leq C\|v\|_{k-\frac{1}{2},\partial S}$ from Oden and Reddy [195, p.195]. Then

$$\begin{aligned}T_2 &= \|P_n(r,\theta) - u_N^*\|_{\frac{1}{2},S} + w\|P_n(r,\theta) - u_N^*\|_{\frac{3}{2},S} \\ &\leq \|P_n(r,\theta) - u_N^*\|_{\frac{1}{2},S_{\max}} + w\|P_n(r,\theta) - u_N^*\|_{\frac{3}{2},S_{\max}} \\ &\leq C\Big\{\|P_n(r,\theta) - u_N^*\|_{0,\partial S_{\max}} + w\|P_n(r,\theta) - u_N^*\|_{1,\partial S_{\max}}\Big\}.\end{aligned} \tag{4.1.28}$$

Similarly to Theorem 2.3.1, we can obtain

$$T_2 \leq C\left(\frac{R}{r_{\max}}\right)^{2n-N}\left(\frac{r_{\max}}{r_{\min}}\right)^n \|P_n(r,\theta)\|_{0,\Gamma}. \tag{4.1.29}$$

From $u \in \mathbf{H}^p(S)$ $\left(p > \frac{3}{2}\right)$, we conclude that $u \in C(S)$ and $P_n(r,\theta) \approx u$ such that $\|P_n(r,\theta)\|_{0,\Gamma} = O(1)$. The equation (4.1.29) leads to

$$T_2 \leq C\left(\frac{R}{r_{\max}}\right)^{2n-N}\left(\frac{r_{\max}}{r_{\min}}\right)^{n}, \tag{4.1.30}$$

where C is a constant independent of N. Moreover, when the equation (4.1.17) holds, *i.e.*,

$$N \approx 2n + \frac{n\,\ln\left(\frac{r_{\max}}{r_{\min}}\right) + \left(p-\frac{1}{2}\right)\ln n}{\ln\left(\frac{R}{r_{\max}}\right)} \leq Cn, \tag{4.1.31}$$

we have

$$T_2 = O\left(\frac{1}{n^{p-\frac{1}{2}}}\right). \tag{4.1.32}$$

Combining (4.1.25), (4.1.27) and (4.1.32) gives the desired result (4.1.18) by noting $\frac{1}{n} \leq C\frac{1}{N}$. This completes the proof of Lemma 4.1.1. ■

Lemma 4.1.2. *Suppose that there exists a positive constant* μ *independent of* N *such that*

$$\|v\|_{1,\Gamma_D} \leq CN^{\mu}\|v\|_{0,\Gamma_D}, \quad v \in V_N, \tag{4.1.33}$$

where V_N *is the set of (4.1.9)*, and C *is a constant independent of* N. *For* $\Delta v = 0$, *there exists the bound,*

$$\|v\|_{1,S} \leq C\left(N^{\frac{\mu}{2}} + \frac{1}{w}\right)\|v\|_B. \tag{4.1.34}$$

Proof. For the harmonic function $v \in V_N$ in S, we have from Oden and Reddy [195]

$$\|v\|_{1,S} \leq C\left\{\|v\|_{\frac{1}{2},\Gamma_D} + \left\|\frac{\partial v}{\partial \nu} + \alpha v\right\|_{-\frac{1}{2},\Gamma_R}\right\}. \tag{4.1.35}$$

Since (4.1.33) we have

$$\|v\|_{\frac{1}{2},\Gamma_D} \leq C\left\{\|v\|_{1,\Gamma_D}\|v\|_{0,\Gamma_D}\right\}^{\frac{1}{2}} \leq CN^{\frac{\mu}{2}}\|v\|_{0,\Gamma_D}, \tag{4.1.36}$$

and

$$\left\|\frac{\partial v}{\partial \nu} + \alpha v\right\|_{-\frac{1}{2},\Gamma_R} \leq C\left\|\frac{\partial v}{\partial \nu} + \alpha v\right\|_{0,\Gamma_R}. \tag{4.1.37}$$

We have from (4.1.35)–(4.1.37) for $\Delta v = 0$

$$\|v\|_{1,S} \leq C\left\{N^{\frac{\mu}{2}}\|v\|_{0,\Gamma_D} + \left\|\frac{\partial v}{\partial \nu} + \alpha v\right\|_{0,\Gamma_R}\right\} \leq C\left(N^{\frac{\mu}{2}} + \frac{1}{w}\right)\|v\|_B. \tag{4.1.38}$$

This completes the proof of Lemma 4.1.2. ■

From Lemmas 4.1.1 and 4.1.2, we have the following theorem.

Theorem 4.1.1. *Let the conditions in Lemmas 4.1.1 and 4.1.2 hold. Then the numerical solutions by the TM using FS have the error bound,*

$$\|u - u_N\|_{1,S} = O\left(\frac{1}{N^{p-\eta}}\right), \tag{4.1.39}$$

where $\eta = \frac{1}{2} + \max\{1, \frac{\mu}{2}\}$.

The stability analysis for the mixed boundary problems (4.1.1)–(4.1.3) are given in [162, p.155, Section 6.5], and the numerical experiments are reported in Chapter 1.

4.2 Interior Boundary Conditions

For simplicity, we split S into two disjoint subdomains S^+ and S^- with a smooth common interior boundary Γ_0. Consider the interior boundary condition on Γ_0,

$$\Delta u = 0 \text{ in } S, \tag{4.2.1}$$

$$u = f \text{ on } \Gamma_D, \quad \frac{\partial u}{\partial \nu} = g \text{ on } \Gamma_N, \tag{4.2.2}$$

$$u^+ = u^-, \quad \frac{\partial u^+}{\partial \nu} = \frac{\partial u^-}{\partial \nu} \text{ on } \Gamma_0, \tag{4.2.3}$$

where $u^\pm = u$ on $S^\pm$, ν is the exterior normal of $\Gamma \cup \Gamma_0$, and $\Gamma = \Gamma_D \cup \Gamma_N$. Denote

$$r_{\max} = \max_{S} r, \quad r_{\min} = \max_{S_{\text{in}}(S_{\text{in}} \subseteq S)} r, \tag{4.2.4}$$

$$r^\pm_{\max} = \max_{S^\pm} r, \quad r^\pm_{\min} = \max_{S^\pm_{\text{in}}(S^\pm_{\text{in}} \subseteq S^\pm)} r. \tag{4.2.5}$$

In both error and stability analyses, the ratio $r_{\max}/r_{\min}$ is crucial. The smaller ratio has better accuracy and stability of the solutions by the MFS. Hence, for some complicated solution domains S, there may exist a division with an interface Γ_0 such that

$$\max\left\{\frac{r^+_{\max}}{r^+_{\min}}, \frac{r^-_{\max}}{r^-_{\min}}\right\} \leq \frac{r_{\max}}{r_{\min}}. \tag{4.2.6}$$

Besides, when there exist different singularities in S^+ and S^-, different local singular functions are added into different FS in S^+ and S^-. Hence, the interior boundary conditions (4.2.3) are important to theory and computation of the MFS. Numerical results for Motz's problem are reported in Chapter 1, and the error analysis is given below.

A new space $\mathbf{H}$ is defined by

$$\mathbf{H} = \{v | v \in \mathbf{L}_2(S), v \in \mathbf{H}^1(S^{\pm}), \Delta v = 0 \text{ in } S^{\pm}\}, \tag{4.2.7}$$

and the norms are defined by

$$\|v\|_1 = \left\{ \|v\|^2_{1,S^+} + \|v\|^2_{1,S^-} \right\}^{\frac{1}{2}}, \quad |v|_1 = \left\{ |v|^2_{1,S^+} + |v|^2_{1,S^-} \right\}^{\frac{1}{2}}. \tag{4.2.8}$$

The circles surrounding $S^{\pm}$ are given by

$$\ell_{R^{\pm}} = \{(r^{\pm}, \theta^{\pm}) | r^{\pm} = R^{\pm}, 0 \leq \theta^{\pm} \leq 2\pi\}, \quad R^{\pm} > r^{\pm}_{\max}, \tag{4.2.9}$$

where $(r^{\pm}, \theta^{\pm})$ are two polar coordinates with centers $O^{\pm}$ in $S^{\pm}$. Hence, we may choose two kinds of the FS such that $\phi^{\pm}(r^{\pm}, \theta^{\pm}) = \ln|\overline{P^{\pm} Q^{\pm}}|$ with $P^{\pm} \in (S^{\pm} \cup \partial S^{\pm})$ to approximate the solutions $u^{\pm}$ in $S^{\pm}$. The source nodes on $\ell_{\mathrm{R}^{\pm}}$ are given by

$$Q^{\pm}_i = \{(x, y) | x = R^{\pm} \cos(ih^{\pm}),\ y = R^{\pm} \sin(ih^{\pm})\},$$

where $R^{\pm} > r^{\pm}_{\max}$, $h^+ = 2\pi/N$ and $h^- = 2\pi/M$. Here we may choose different N and M. The FS in $S^{\pm}$ are given by $\phi^{\pm}_i(P^{\pm}) = \ln|\overline{P^{\pm} Q^{\pm}_i}|$ to yield the piecewise FS,

$$u_{N,M} = \begin{cases} u^+_N = \sum\limits_{i=1}^{N} c_i \phi^+_i(P^+), \\ u^-_M = \sum\limits_{i=1}^{M} d_i \phi^-_i(P^-), \end{cases} \tag{4.2.10}$$

where c_i and d_i are the unknown coefficients to be sought.

Let $V_{N,M}$ denote the set of (4.2.10). Also denote the energy

$$I(v) = \int_{\Gamma_D} (v - f)^2 + w^2 \int_{\Gamma_N} (v_\nu - g)^2 + \int_{\Gamma_0} (v^+ - v^-)^2 + w^2 \int_{\Gamma_0} (v^+_\nu - v^-_\nu)^2,$$

where $v_\nu = \frac{\partial v}{\partial \nu}$, and the weight $w = \max\{\frac{1}{N}, \frac{1}{M}\}$. The TM reads: to seek $u_{N,M}$ such that

$$I(u_{N,M}) = \min_{v \in V_{N,M}} I(v). \tag{4.2.11}$$

Denote the boundary norm

$$\|v\|_B = \left\{ \|v\|^2_{0,\Gamma_D} + w^2 \|v_\nu\|^2_{0,\Gamma_N} + \|v^+ - v^-\|^2_{0,\Gamma_0} + w^2 \|v^+_\nu - v^-_\nu\|^2_{0,\Gamma_0} \right\}^{\frac{1}{2}}. \tag{4.2.12}$$

The solution $u_{N,M}$ satisfies

$$\|u - u_{N,M}\|_B = \min_{v \in V_{N,M}} \|u - v\|_B. \tag{4.2.13}$$

To follow [146, pp.103–137], we assume that the following inverse inequalities hold,

$$\|v_\nu\|_{0,\Gamma_D} \le K_{N,M}\|v\|_1, \quad \|v_\nu\|_{0,\Gamma_0} \le K_{N,M}\|v\|_1, \tag{4.2.14}$$

$$\|v\|_{0,\Gamma_D} \le q_{N,M}\|v\|_1, \quad \|v\|_{0,\Gamma_0} \le q_{N,M}\|v\|_1, \tag{4.2.15}$$

where $q_{N,M}$ is a small constant, but $K_{N,M}$ is unbounded when $M, N \to \infty$. We cite the following lemma from [146, p.107].

Lemma 4.2.1. *For* $v \in V_{N,M}$*, let the inverse inequalities (4.2.14) and (4.2.15) hold. Choose* $M \asymp N$ *and* $w = O\big(\frac{1}{N}\big)$*. Then there exists the error bound,*

$$\|v\|_1 \le C\Big(K_{N,M} + \frac{q_{N,M}}{w}\Big)\|v\|_B, \tag{4.2.16}$$

where C *is a constant independent of* N *and* M*.*

Lemma 4.2.2. *Let* $u \in \mathbf{H}^p(S^+)$ *and* $u \in \mathbf{H}^\sigma(S^-)$ $\big(p, \sigma \ge \frac{3}{2}\big)$ *hold. Suppose that the large* N *and* M *satisfy*

$$\left(\frac{R^+}{r^+_{\max}}\right)^{2n-N}\left(\frac{r^+_{\max}}{r^+_{\min}}\right)^n \le n^{-p+\frac{1}{2}}, \quad \left(\frac{R^-}{r^-_{\max}}\right)^{2n-M}\left(\frac{r^-_{\max}}{r^-_{\min}}\right)^n \le n^{-\sigma+\frac{1}{2}}. \tag{4.2.17}$$

Then there exists the error bound,

$$\|u - u_{N,M}\|_B = C\left\{\frac{1}{N^{p-\frac{1}{2}}}\|u\|_{p,S^+} + \frac{1}{M^{\sigma-\frac{1}{2}}}\|u\|_{\sigma,S^-}\right\}, \tag{4.2.18}$$

where C *is a constant independent of* N *and* M*.*

Proof. We have

$$\|v\|_B \le \|v\|_{0,\Gamma_D} + w\|v_\nu\|_{0,\Gamma_N} + \|v^+ - v^-\|_{0,\Gamma_0} + w\|v^+_\nu - v^-_\nu\|_{0,\Gamma_0}. \tag{4.2.19}$$

From the triangle inequality and the embedding theorem, we have

$$\begin{aligned} \|v\|_B &\le \|v\|_{0,\partial S^+} + \|v\|_{0,\partial S^-} + w(\|v_\nu\|_{0,\partial S^+} + \|v_\nu\|_{0,\partial S^-}) \\ &\le C\Big\{\|v^+\|_{\frac{1}{2},S^+} + \|v^-\|_{\frac{1}{2},S^-} + w\Big(\|v^+\|_{\frac{3}{2},S^+} + \|v^-\|_{\frac{3}{2},S^-}\Big)\Big\}. \end{aligned} \tag{4.2.20}$$

When $u \in \mathbf{H}^p(S^+)$ and $u \in \mathbf{H}^\sigma(S^-)$, there exist the piecewise harmonic polynomials of order n,

$$u^*_n = \begin{cases} u^+_n = P^+_n = \sum\limits_{i=1}^n (r^+)^i\big(a^+_i \cos\big(i\theta^+\big) + b^+_i \sin\big(i\theta^+\big)\big) & \text{in } S^+, \\ u^-_n = P^-_n = \sum\limits_{i=1}^n (r^-)^i\big(a^-_i \cos(i\theta^-) + b^-_i \sin(i\theta^-)\big) & \text{in } S^-. \end{cases} \tag{4.2.21}$$

Denote

$$u = u^\pm_n + R^\pm_n \quad \text{in } S^\pm. \tag{4.2.22}$$

There exist the bounds,

$$\|R_n^+\|_{k,S^+} = O\left(\frac{1}{n^{p-k}}\right)\|u\|_{p,S^+}, \quad \|R_n^-\|_{k,S^-} = O\left(\frac{1}{n^{\sigma-k}}\right)\|u\|_{\sigma,S^-}. \tag{4.2.23}$$

Hence, letting $v = \Sigma_{N,M}(u_n^*)$ we have

$$\|u - u_{N,M}\|_B \le C\|u - \Sigma_{N,M}(u_n^*)\|_B := C(T_1 + T_2), \tag{4.2.24}$$

where

$$\begin{aligned} T_1 &= \|P_n^+ - \Sigma_N(P_n^+)\|_{\frac{1}{2},S^+} + \|P_n^- - \Sigma_M(P_n^-)\|_{\frac{1}{2},S^-} \\ &\quad + w\Big(\|P_n^+ - \Sigma_N(P_n^+)\|_{\frac{3}{2},S^+} + \|P_n^- - \Sigma_M(P_n^-)\|_{\frac{3}{2},S^-}\Big), \end{aligned} \tag{4.2.25}$$

and

$$T_2 = \|R_n^+\|_{\frac{1}{2},S^+} + w\|R_n^+\|_{\frac{3}{2},S^+} + \|R_n^-\|_{\frac{1}{2},S^-} + w\|R_n^-\|_{\frac{3}{2},S^-}. \tag{4.2.26}$$

Moreover, there exist following bounds for $w = O(\frac{1}{N}) = O(\frac{1}{M})$,

$$\|R_n^+\|_{\frac{1}{2},S^+} + w\|R_n^+\|_{\frac{3}{2},S^+} = O\left(\frac{1}{n^{p-\frac{1}{2}}}\|u\|_{p,S^+}\right), \tag{4.2.27}$$

$$\|R_n^-\|_{\frac{1}{2},S^-} + w\|R_n^-\|_{\frac{3}{2},S^-} = O\left(\frac{1}{n^{\sigma-\frac{1}{2}}}\|u\|_{\sigma,S^-}\right). \tag{4.2.28}$$

When the conditions (4.2.17) are satisfied, we have

$$\|P_n^+ - \Sigma_N(P_n^+)\|_{\frac{1}{2},S^+} + w\|P_n^+ - \Sigma_N(P_n^+)\|_{\frac{3}{2},S^+} = O\left(\frac{1}{n^{p-\frac{1}{2}}}\right)\|u\|_{p,S^+}, \tag{4.2.29}$$

$$\|P_n^- - \Sigma_M(P_n^-)\|_{\frac{1}{2},S^-} + w\|P_n^- - \Sigma_M(P_n^-)\|_{\frac{3}{2},S^-} = O\left(\frac{1}{n^{\sigma-\frac{1}{2}}}\right)\|u\|_{\sigma,S^-}. \tag{4.2.30}$$

Combining (4.2.25)–(4.2.30) gives

$$T_1 + T_2 \le C\left\{\frac{1}{N^{p-\frac{1}{2}}}\|u\|_{p,S^+} + \frac{1}{M^{\sigma-\frac{1}{2}}}\|u\|_{\sigma,S^-}\right\}. \tag{4.2.31}$$

The desired result (4.2.18) follows from (4.2.24) and (4.2.31). ■

Based on Lemmas 4.2.1 and 4.2.2, we have the following theorem.

Theorem 4.2.1. *Let the conditions in Lemmas 4.2.1 and 4.2.2 hold. Then for Laplace's equation involving the interior boundary conditions (4.2.3), the numerical solutions by the TM using FS have the error bound,*

$$\|u - u_{N,M}\|_1 \le C\left(K_{N,M} + \frac{q_{N,M}}{w}\right)\left\{\frac{1}{N^{p-\frac{1}{2}}}\|u\|_{p,S^+} + \frac{1}{M^{\sigma-\frac{1}{2}}}\|u\|_{\sigma,S^-}\right\}. \tag{4.2.32}$$

Moreover, if $K_{N,M} = O(\sqrt{N})$ *and* $q_{N,M} = O\left(\frac{1}{\sqrt{N}}\right)$, *then there exists the optimal convergence rate in* $\mathbf{H}^1$ *norm,*

$$\|u - u_{N,M}\|_1 \leq C\left\{\frac{1}{N^{p-1}}\|u\|_{p,S^+} + \frac{1}{M^{\sigma-1}}\|u\|_{\sigma,S^-}\right\}. \tag{4.2.33}$$

4.3 Annular Domains

Let $S_2 \subset S_1$ and an annular domain $S_a = S_1 \backslash S_2$. Consider the Dirichlet problem in the annular domain S_a,

$$\Delta u = 0,\ (x,y) \in S_a, \tag{4.3.1}$$

$$u = g_1, (x,y) \in \Gamma_{\text{out}}, \quad u = g_2,\ (x,y) \in \Gamma_{\text{in}}, \tag{4.3.2}$$

where both Γ_{out} and Γ_{in} are smooth without any overlaps: $\Gamma_{\text{out}} \cap \Gamma_{\text{in}} = \emptyset$. The particular solutions in S_a are given by

$$\begin{aligned} u &= u(\rho,\theta;\bar{\rho},\bar{\theta}) = u_1(\rho,\theta) + u_2(\bar{\rho},\bar{\theta}), \\ u_1(\rho,\theta) &= \frac{a_0}{2} + \sum_{n=1}^{\infty} \rho^n\{a_n \cos(n\theta) + b_n \sin(n\theta)\}, \\ u_2(\bar{\rho},\bar{\theta}) &= \bar{a}_0 \ln\bar{\rho} + \sum_{n=1}^{\infty} \bar{\rho}^n\{\bar{a}_n \cos(n\bar{\theta}) + \bar{b}_n \sin(n\bar{\theta})\}, \end{aligned} \tag{4.3.3}$$

where a_n, b_n, $\bar{a}_n$ and $\bar{b}_n$ are the exact coefficients. Two systems of polar coordinates are denoted by (ρ,θ) and $(\bar{\rho},\bar{\theta})$; they may have different origins.

Denote nodes $P(\rho,\theta) \in \bar{S}_a$. For the source nodes $Q(R,\theta)$ outside S_1 with $R > r_{\max} = \max \rho|_{\rho\in\Gamma_{\text{out}}}$, choose the FS,

$$\Phi_i(P) = \ln|\overline{PQ_i}|, \quad Q_i = (R, ih), \quad i = 1,\ 2, \ldots, M,$$

where $h = 2\pi/M$. Similarly, for the source nodes $\bar{Q}(\bar{R},\bar{\theta})$ inside S_2 with $\bar{R} < \bar{r}_{\min} = \min \bar{\rho}|_{\bar{\rho}\in\Gamma_{\text{in}}}$, choose the other FS

$$\bar{\Phi}_i(P) = \ln|\overline{P\bar{Q}_i}|, \quad \bar{Q}_i(P) = (\bar{R}, i\bar{h}), \quad i = 1,\ 2, \ldots, \bar{M},$$

where $\bar{h} = 2\pi/\bar{M}$. We obtain the linear combination,

$$u_{M-\bar{M}} = \sum_{i=1}^{M} c_i\Phi_i(P) + \sum_{i=1}^{\bar{M}} \bar{c}_i\bar{\Phi}_i(P), \tag{4.3.4}$$

where c_i and $\bar{c}_i$ are unknown coefficients. Numerical experiments for annular domains are reported in [178], and the error analysis is given below.

Define the boundary norm

$$\|v\|_{0,\partial S_a} = \|v\|_{0,\Gamma_{\text{out}}\cup\Gamma_{\text{in}}} = \left\{\|v\|^2_{0,\Gamma_{\text{out}}} + \|v\|^2_{0,\Gamma_{\text{in}}}\right\}^{\frac{1}{2}}.$$

Denote by $V_{M-\bar{M}}$ the set of (4.3.4). Both coefficients c_i and $\bar{c}_i$ can be sought by

$$\begin{aligned}\|u_{M-\bar{M}} - u\|_{0,\Gamma_{\text{out}} \cup \Gamma_{\text{in}}} &= \left\{ \|u_{M-\bar{M}} - g_{\text{out}}\|^2_{0,\Gamma_{\text{out}}} + \|u_{M-\bar{M}} - g_{\text{in}}\|^2_{0,\Gamma_{\text{in}}} \right\}^{\frac{1}{2}} \\ &= \inf_{v \in V_{M-\bar{M}}} \left\{ \left(\|v - g_{\text{out}}\|^2_{0,\Gamma_{\text{out}}} + \|v - g_{\text{in}}\|^2_{0,\Gamma_{\text{in}}} \right)^{\frac{1}{2}} \right\}.\end{aligned} \tag{4.3.5}$$

We may also employ the collocation equations directly to satisfy the Dirichlet conditions (4.3.2),

$$\sqrt{\omega_j}\ u_{M-\bar{M}}(P_j) = \sqrt{\omega_j}\ g_{\text{out}}(P_j), \quad P_j \in \Gamma_{\text{out}}, \tag{4.3.6}$$

$$\sqrt{\bar{\omega}_j}\ u_{M-\bar{M}}(\bar{P}_j) = \sqrt{\bar{\omega}_j}\ g_{\text{in}}(\bar{P}_j), \quad \bar{P}_j \in \Gamma_{\text{in}}, \tag{4.3.7}$$

where $P_j = (\rho_j, \theta_j)$, $\bar{P}_j = (\bar{\rho}_j, \bar{\theta}_i)$, $\omega_j\,(>0)$ and $\bar{\omega}_j\,(>0)$ are suitable weights. The equation (4.3.4) with (4.3.5) (or (4.3.6) and (4.3.7)) are the MFS for (4.3.1) and (4.3.2). The annular problems by the MFS are discussed in Tsangaris *et al.* [228], where the interior and the exterior boundaries are confined to concentric circles only.

Denote the finite terms of PS in S_1 by

$$P_N(\rho, \theta) = \frac{a_0}{2} + \sum_{n=1}^{N} \rho^n \{a_n \cos(n\theta) + b_n \sin(n\theta)\}, \tag{4.3.8}$$

where a_n and b_n are the exact coefficients. By the trapezoidal rule, the PS in (4.3.8) may be approximated by the FS from Chapter 2

$$P_N(\rho, \theta) \approx \sum_{i=1}^{M} c_i^* \Phi_i(P) := v_M^*, \tag{4.3.9}$$

with the coefficients,

$$c_i^* = \frac{1}{M} \left\{ \frac{1}{4} \frac{a_0}{\ln R} + \sum_{n=1}^{N} nR^n (a_n \cos(nih) + b_n \sin(nih)) \right\}, \tag{4.3.10}$$

where $h = \frac{\pi}{M}$. The denominator in (4.3.10) is assumed to be nonzero (*i.e.*, $R \neq 1$). We cite Theorem 2.3.1 in Chapter 2.

Theorem 4.3.1. *Suppose that Laplace's solutions* $u_1 \in C(S_a)$. *For* P_N *in (4.3.8) and* v_M^* *in (4.3.9), when* M *is large, there exists the error bound between the FS and the PS,*

$$\|P_N - v_M^*\|_{0,\Gamma_{\text{out}}} \leq C \left(\frac{r_{\max}}{R} \right)^{M-2N} \left(\frac{r_{\max}}{r_{\min}} \right)^{N} \|u_1\|_{0,\Gamma_{\text{out}}}, \tag{4.3.11}$$

where $r_{\max}$ *and* $r_{\min}$ *are the maximal and the minimal radii of* Γ_{out}, *respectively.*

Next, denote the finite terms of other PS inside S_2 by

$$\bar{P}_{\bar{N}}(\bar{\rho}, \bar{\theta}) = \bar{a}_0 \ln\bar{\rho} + \sum_{n=1}^{\bar{N}} \bar{\rho}^n \{\bar{a}_n \cos(n\bar{\theta}) + \bar{b}_n \sin(n\bar{\theta})\}, \tag{4.3.12}$$

where $\bar{a}_n$ and $\bar{b}_n$ are the exact coefficients. Denote nodes $\bar{P}(\bar{\rho}, \bar{\theta}) \in \bar{S}$, and the source nodes $\bar{Q}(\bar{R}, \bar{\phi})$ inside S_2 with $\bar{R} < \bar{r}_{\min}$. From addition theorem in Lemma I.3 in Part I, we have the series expansion for $\bar{R} < \bar{\rho}$,

$$\ln|\overline{\bar{P}\bar{Q}}| = \ln\sqrt{\bar{\rho}^2 - 2\bar{\rho}\bar{R}\cos(\bar{\theta} - \bar{\phi}) + \bar{R}^2} = \ln\bar{\rho} - \sum_{n=1}^{\infty} \frac{1}{n}\left(\frac{\bar{R}}{\bar{\rho}}\right)^n \cos n(\bar{\theta} - \bar{\phi}).$$

Then we have the following lemma.

Lemma 4.3.1. *For $\bar{R} < \bar{\rho}$, there exist the equalities,*

$$\int_0^{2\pi} \ln\left(\sqrt{\bar{\rho}^2 - 2\bar{\rho}\bar{R}\cos(\bar{\theta} - \bar{\psi}) + \bar{R}^2}\right) d\bar{\psi} = 2\pi \ln\bar{\rho},$$
$$\int_0^{2\pi} \ln\left(\sqrt{\bar{\rho}^2 - 2\bar{\rho}\bar{R}\cos(\bar{\theta} - \bar{\psi}) + \bar{R}^2}\right) \cos(m\bar{\psi})\, d\bar{\psi} = -\frac{\pi}{m}\left(\frac{\bar{R}}{\bar{\rho}}\right)^m \cos(m\bar{\theta}),\ m = 1, 2, \ldots,$$
$$\int_0^{2\pi} \ln\left(\sqrt{\bar{\rho}^2 - 2\bar{\rho}\bar{R}\cos(\bar{\theta} - \bar{\psi}) + \bar{R}^2}\right) \sin(m\bar{\psi})\, d\bar{\psi} = -\frac{\pi}{m}\left(\frac{\bar{R}}{\bar{\rho}}\right)^m \sin(m\bar{\theta}),\ m = 1, 2, \ldots.$$

By the trapezoidal rule, the solutions in (4.3.12) may be approximated by the following FS, similarly,

$$\bar{P}_{\bar{N}}(\bar{\rho}, \bar{\theta}) \approx \sum_{i=1}^{\bar{M}} \bar{c}_i \bar{\Phi}_i(P) := \bar{v}^*_{\bar{M}}, \tag{4.3.13}$$

where the coefficients,

$$\bar{c}^*_i = \frac{1}{\bar{M}}\left\{\frac{1}{2}\bar{a}_0 + \sum_{n=1}^{\bar{N}} \frac{n}{\bar{R}^n}\left(\bar{a}_n \cos(ni\bar{h}) + b_n \sin(ni\bar{h})\right)\right\}, \tag{4.3.14}$$

and $\bar{h} = 2\pi/\bar{M}$. Similarly, by following the proof of Theorem 2.3.1 in Chapter 2, we have the following theorem (details are given in [151]).

Theorem 4.3.2. *Suppose that Laplace's solutions $u_2 \in C(S_a)$. For $\bar{P}_{\bar{N}}$ in (4.3.12) and $\bar{v}^*_{\bar{M}}$ in (4.3.13), when $\bar{M}$ is large, there exists the error bound,*

$$\|\bar{P}_{\bar{N}} - \bar{v}^*_{\bar{M}}\|_{0,\Gamma_{\text{in}}} \le C\left(\frac{\bar{R}}{\bar{r}_{\min}}\right)^{(\bar{M}-2\bar{N})}\left(\frac{\bar{r}_{\max}}{\bar{r}_{\min}}\right)^{\bar{N}} \|u_2\|_{0,\Gamma_{\text{in}}}, \tag{4.3.15}$$

where $\bar{r}_{\max}$ and $\bar{r}_{\min}$ are the maximal and the minimal radii of Γ_{in}, respectively.

The error bounds for annular domains can be easily obtained by the decomposition techniques below. Denote the error functions,

$$\delta = P_N + \bar{P}_{\bar{N}} - (v^*_M + \bar{v}^*_{\bar{M}}) := \delta_1 + \delta_2,$$

where

$$\delta_1 = P_N(\rho,\theta) - \sum_{i=1}^{M} c_i \Phi_i(P) := P_N - v_M^*,$$
$$\delta_2 = \bar{P}_{\bar{N}}(\bar{\rho},\bar{\theta}) - \sum_{i=1}^{\bar{M}} \bar{c}_{ij} \bar{\Phi}_i(\bar{P}) := \bar{P}_{\bar{N}} - \bar{v}_{\bar{M}}^*.$$

Theorem 4.3.3. *Suppose that Laplace's solutions satisfy* $u \in C(S_a)$. *When* M *and* $\bar{M}$ *are large, there exist the error bounds between the FS and the PS,*

$$\begin{aligned} &\|P_N + \bar{P}_{\bar{N}} - (v_M^* + \bar{v}_{\bar{M}}^*)\|_{0,\Gamma_{\text{out}} \cup \Gamma_{\text{in}}} \\ &\quad \le C\left\{ \left(\frac{r_{\max}}{R}\right)^{M-2N} \left(\frac{r_{\max}}{r_{\min}}\right)^{N} \|u_1\|_{0,\Gamma_{\text{out}}} + \left(\frac{\bar{R}}{\bar{r}_{\min}}\right)^{\bar{M}-2\bar{N}} \left(\frac{\bar{r}_{\max}}{\bar{r}_{\min}}\right)^{\bar{N}} \|u_2\|_{0,\Gamma_{\text{in}}} \right\}, \end{aligned} \tag{4.3.16}$$

where P_N *is given in (4.3.8),* $\bar{P}_{\bar{N}}$ *in (4.3.12),* v_M^* *in (4.3.9), and* $\bar{v}_{\bar{M}}^*$ *in (4.3.13).*

Proof. We have

$$\begin{aligned} &\|P_N + \bar{P}_{\bar{N}} - (v_M^* + \bar{v}_{\bar{M}}^*)\|_{0,\Gamma_{\text{out}} \cup \Gamma_{\text{in}}} \\ &\quad \le \|P_N - v_M^*\|_{0,\Gamma_{\text{out}} \cup \Gamma_{\text{in}}} + \|\bar{P}_{\bar{N}} - \bar{v}_{\bar{M}}^*\|_{0,\Gamma_{\text{out}} \cup \Gamma_{\text{in}}}. \end{aligned} \tag{4.3.17}$$

The distance from the inside source nodes $\bar{Q}_i$ to the interior boundary Γ_{in} is closer than that to the exterior boundary Γ_{out}. From (4.3.15) in Theorem 4.3.2, the errors $(\bar{P}_{\bar{N}} - \bar{v}_{\bar{M}}^*)$ on Γ_{in} are dominant,

$$\|\bar{P}_{\bar{N}} - \bar{v}_{\bar{M}}^*\|_{0,\Gamma_{\text{out}} \cup \Gamma_{\text{in}}} \le C\|\bar{P}_{\bar{N}} - \bar{v}_{\bar{M}}^*\|_{0,\Gamma_{\text{in}}}. \tag{4.3.18}$$

Similarly, the distance from the outside source nodes Q_i to Γ_{out} is closer than that to Γ_{in}. From (4.3.11) in Theorem 4.3.1, the errors $(P_N - v_M^*)$ on Γ_{out} are dominant,

$$\|P_N - v_M^*\|_{0,\Gamma_{\text{out}} \cup \Gamma_{\text{in}}} \le C\|P_N - v_M^*\|_{0,\Gamma_{\text{out}}}. \tag{4.3.19}$$

Then we have from (4.3.17)–(4.3.19)

$$\|P_N + \bar{P}_{\bar{N}} - (v_M^* + \bar{v}_{\bar{M}}^*)\|_{0,\Gamma_{\text{out}} \cup \Gamma_{in}} \le C\left\{\|P_N - v_M^*\|_{0,\Gamma_{\text{out}}} + \|\bar{P}_{\bar{N}} - \bar{v}_{\bar{M}}^*\|_{0,\Gamma_{\text{in}}}\right\}.$$

The desired result (4.3.16) follows from Theorems 4.3.1 and 4.3.2. ■

Theorem 4.3.4. *Let* $R \neq 1$ *and the conditions in Theorem 4.3.3 hold. Suppose that the solutions* $u_1 \in \mathbf{H}^p(\Gamma_{\text{out}})$ $(p \ge 1)$ *and* $u_2 \in \mathbf{H}^{\bar{p}}(\Gamma_{\text{in}})$ $(\bar{p} \ge 1)$. *When* $M\,(> N)$ *and* $\bar{M}\,(> \bar{N})$ *are large enough to satisfy (4.3.23) below, there exists the error bound of the MFS,*

$$\|u - u_{M-\bar{M}}\|_{0,\Gamma_{\text{out}} \cup \Gamma_{\text{in}}} = O(M^{-p})\|u_1\|_{p,\Gamma_{\text{out}}} + O(\bar{M}^{-\bar{p}})\|u_2\|_{\bar{p},\Gamma_{\text{in}}}. \tag{4.3.20}$$

Proof. Denote $R_{N-\bar N} = u - P_{N-\bar N}$, $P_{N-\bar N} = P_N + \bar P_{\bar N}$ and $R_{N-\bar N} = R_N + \bar R_{\bar N}$, where

$$R_N = R_N(\rho,\theta) = \sum_{n=N+1}^{\infty} \rho^n\{a_n \cos(n\theta) + b_n \sin(n\theta)\},$$
$$\bar R_{\bar N} = \bar R_{\bar N}(\rho,\theta) = \sum_{n=\bar N+1}^{\infty} \bar\rho^n\{\bar a_n \cos(n\bar\theta) + \bar b_n \sin(n\bar\theta)\}.$$

The residuals R_N and $\bar R_{\bar N}$ have the bounds,

$$\|R_N\|_{0,\Gamma_{\text{out}}} \le C\frac{1}{N^p}\|u_1\|_{p,\Gamma_{\text{out}}}, \quad \|\bar R_{\bar N}\|_{0,\Gamma_{\text{in}}} \le C\frac{1}{\bar N^{\bar p}}\|u_2\|_{\bar p,\Gamma_{\text{in}}}. \tag{4.3.21}$$

Then we have from (4.3.21)

$$\begin{aligned}\|R_{N-\bar N}\|_{0,\Gamma_{\text{out}}\cup\Gamma_{\text{in}}} &\le \|R_N\|_{0,\Gamma_{\text{out}}\cup\Gamma_{\text{in}}} + \|R_{\bar N}\|_{0,\Gamma_{\text{out}}\cup\Gamma_{\text{in}}}\\ &\le C\Big\{\|R_N\|_{0,\Gamma_{\text{out}}} + \|R_{\bar N}\|_{0,\Gamma_{\text{in}}}\Big\} \le C\Big\{\frac{1}{N^p}\|u_1\|_{p,\Gamma_{\text{out}}} + \frac{1}{\bar N^{\bar p}}\|u_2\|_{\bar p,\Gamma_{\text{in}}}\Big\}.\end{aligned} \tag{4.3.22}$$

Choose the special v^*_M with coefficients c^*_i in (4.3.10) to approximate u_N, and $\bar v^*_{\bar M}$ with coefficients $\bar c^*_i$ in (4.3.14) to approximate $\bar u_{\bar N}$. From (4.3.5), (4.3.22) and Theorem 4.3.3, we have

$$\begin{aligned}&\|u - u_{M-\bar M}\|_{0,\Gamma_{\text{out}}\cup\Gamma_{\text{in}}} \le \|u - v^*_{M-\bar M}\|_{0,\Gamma_{\text{out}}\cup\Gamma_{\text{in}}}\\ &\le \|R_{N-\bar N}\|_{0,\Gamma_{\text{out}}\cup\Gamma_{\text{in}}} + \|P_{N-\bar N} - v^*_{M-\bar M}\|_{0,\Gamma_{\text{out}}\cup\Gamma_{\text{in}}}\\ &\le C\Big\{\frac{1}{N^p}\|u_1\|_{p,\Gamma_{\text{out}}} + \frac{1}{\bar N^{\bar p}}\|u_2\|_{\bar p,\Gamma_{\text{in}}} + \Big(\frac{r_{\max}}{R}\Big)^{M-2N}\Big(\frac{r_{\max}}{r_{\min}}\Big)^{N}\|u_1\|_{0,\Gamma_{\text{out}}}\\ &\quad + \Big(\frac{\bar R}{\bar r_{\min}}\Big)^{\bar M-2\bar N}\Big(\frac{\bar r_{\max}}{\bar r_{\min}}\Big)^{\bar N}\|u_2\|_{0,\Gamma_{\text{in}}}\Big\}.\end{aligned}$$

To reach the optimal convergence rates in (4.3.20), choose M and $\bar M$ large enough such that

$$M \ge 2N + \frac{p\ \ln N + N\ \ln\Big(\frac{r_{\max}}{r_{\min}}\Big)}{\ln\Big(\frac{R}{r_{\max}}\Big)}, \quad \bar M \ge 2\bar N + \frac{\bar p\ \ln \bar N + \bar N\ \ln\Big(\frac{\bar r_{\max}}{\bar r_{\min}}\Big)}{\ln\Big(\frac{\bar r_{\min}}{\bar R}\Big)}. \tag{4.3.23}$$

Then we have

$$\|u - u_{M-\bar M}\|_{0,S_{\text{out}}\cup\Gamma_{\text{in}}} = O\Big(\frac{1}{N^p}\Big)\|u_1\|_{p,\Gamma_{\text{out}}} + O\Big(\frac{1}{\bar N^{\bar p}}\Big)\|u_2\|_{\bar p,\Gamma_{\text{in}}}. \tag{4.3.24}$$

From (4.3.23), we may choose $M \le CN$ and $\bar M \le C\bar N$, and the desired result (4.3.20) follows from (4.3.24). ■

Remark 4.3.1. *Suppose that* $u \in \mathbf{H}^{p+\frac{1}{2}}(S_a)$. *Since* $u = u_1 + u_2$, *we have* $u_1, u_2 \in \mathbf{H}^{p+\frac{1}{2}}(S_a)$, $u_1 \in \mathbf{H}^p(\Gamma_{\text{out}})$ *and* $u_2 \in \mathbf{H}^p(\Gamma_{\text{in}})$. *Then we have* $\bar p = p$ *for Theorem 4.3.4. Moreover, suppose that the solution has different types of regularity in* S_a *as follows.*

There exist two sub-annular domains: $V_1 \subset S_a$ *with* $\Gamma_{\rm out} \subset \partial V_1$*, and* $V_2 \subset S_a$ *with* $\Gamma_{\rm in} \subset \partial V_2$*, to have* $u \in \mathbf{H}^{p+\frac{1}{2}}(V_1)$ *and* $u \in \mathbf{H}^{\bar{p}+\frac{1}{2}}(V_2)$*. Since* $u = u_1 + u_2$*, we have* $u_1 \in \mathbf{H}^{p+\frac{1}{2}}(V_1)$ *and then* $u_1 \in \mathbf{H}^{p}(\Gamma_{\rm out})$*. Similarly,* $u_2 \in \mathbf{H}^{\bar{p}}(\Gamma_{\rm in})$*. Hence the different assumption of solution regularity in Theorem 4.3.4 is valid.*

Chapter 5

Combined Methods

To deal with singularity problems, some renovations in [147] should be developed for the method of fundamental solutions (MFS). The solution singularity caused by corners of the solution domain is studied in this chapter. First, the local refinements of the source nodes near corners are adopted. Next, a few leading singular particular solutions (SPS) in [169] may be added into fundamental solutions (FS), as done in Chapter 1. Such an adding technique is also employed in [138] for the corner and crack singularity of linear elastostatics. In this chapter, we may employ the combined techniques of [147], where the SPS are chosen in the subdomains of S involving singularity, and the FS in the rest of S. Different efficient coupling techniques are explored, and variant kinds of combined methods of the MFS are discussed with other methods, such as the finite element method (FEM), the finite difference method (FDM), and the radial basis functions (RBF). Numerical experiments are reported for the unbounded domain problems to display the efficiency of the combined algorithms for the singularity problems with corners and infinity. The materials of this chapter are adapted from [149, 174].

5.1 Combined Methods

For corner singularity problems, the local SPS near singular points is well known, and the Trefftz method (TM) using the SPS has been fully developed in the monograph [169]. Since the FS in the solution domain S are continuous, the numerical solutions of the MFS are poor in accuracy near the singularity points, except where some renovations in [146] are adopted. A natural combination is that the SPS and the FS are used simultaneously for the subdomains of singular and smooth solutions, respectively. For unbounded problems, we may choose the SPS and the FS for unbounded and bounded subdomains, respectively. In this section, we take bounded domains for analysis but provide some numerical examples for unbounded domains with singularity in the last section.

DOI: 10.1051/978-2-7598-3171-5.c005
© Science Press, EDP Sciences, 2023

Consider the equations (4.2.1)–(4.2.3) in the previous chapter. Let $S = S^+ \cup S^-$, $\Gamma_0 = \overline{S}^+ \cap \overline{S}^-$, and choose the FS and the SPS in S^+ and S^-, respectively. The piecewise admissible functions (4.2.10) are modified as

$$u_{N,M} = \begin{cases} u_N^+ = \sum_{i=1}^{N} c_i \phi_i^+(P^+) \text{ in } S^+, \\ u_M^- = \sum_{i=1}^{M} d_i \phi_i^-(P^-) \text{ in } S^-, \end{cases} \tag{5.1.1}$$

where c_i and d_i are the unknown coefficients to be sought. The functions ϕ_i^+ are still the FS, but ϕ_i^- are the local SPS satisfying $\Delta\phi_i^- = 0$ in S^-. We may choose the harmonic polynomials u_M^- of order M in S^-. Then the functions (5.1.1) lead to

$$u_{N,M} = \begin{cases} u_N^+ = \sum_{i=1}^{N} c_i \phi_i^+(P^+) \text{ in } S^+, \\ u_M^- = \dfrac{a_0}{2} + \displaystyle\sum_{i=1}^{M} d_i (r^-)^i \{a_i \cos(i\theta^-) + b_i \sin(i\theta^-)\} \text{ in } S^-. \end{cases} \tag{5.1.2}$$

Suppose that the inverse inequalities (4.2.14) and (4.2.15) hold. Then Lemma 4.2.2 and Theorem 4.2.1 hold, and the optimal convergence rates can be achieved.

Next, consider the corner singularity problems with $u \in \mathbf{H}^{\sigma}(S)\,(1 < \sigma < 2)$, and employ the SPS. Take Motz's problem in Chapter 1 for example. The solution $u \in \mathbf{H}^{\frac{3}{2}-\delta}(S)$ $(0 < \delta \ll 1)$ with crack singularity. There exists the SPS in [146],

$$u_M^- = \sum_{i=0}^{\infty} \bar{d}_i r^{i+\frac{1}{2}} \cos\left(i + \frac{1}{2}\right)\theta, \tag{5.1.3}$$

where $\bar{d}_i$ are the exact coefficients. Choose the semi-disk,

$$S^- = \{(r,\theta) | 0 \le r \le r_{\max}^- < 1, 0 \le \theta \le \pi\},$$

and S^+ is the rest of S. Hence the solution $u = \bar{u}_M^- + R_M^-$, where

$$u_M^- = \sum_{i=0}^{M} \bar{d}_i r^{i+\frac{1}{2}} \cos\left(i + \frac{1}{2}\right)\theta, \tag{5.1.4}$$

and the residual R_M^- has the bound

$$\|R_M^-\|_{1,S^-} = O((r_{\max}^-)^M). \tag{5.1.5}$$

The admissible functions for Motz's problem are given by

$$u_{N,M} = \begin{cases} u_N^+ = \sum_{i=1}^{N} c_i \phi_i^+(P^+) \text{ in } S^+, \\ u_M^- = \sum_{i=1}^{M} d_i r^{i+\frac{1}{2}} \cos(i + \frac{1}{2})\theta \text{ in } S^-. \end{cases} \tag{5.1.6}$$

We have the following theorem, similarly.

Theorem 5.1.1. *Let the conditions in Lemma 4.2.1 hold. Suppose that the large* N *satisfies*

$$\left(\frac{R^+}{r^+_{\max}}\right)^{2n-N}\left(\frac{r^+_{\max}}{r^+_{\min}}\right)^n \le n^{-p+\frac{1}{2}}. \tag{5.1.7}$$

Then for Motz's problem, the numerical solutions by the TM using both FS and PS have the error bound,

$$\|u-u_{N,M}\|_1 \le C\Big(K_{N,M}+\frac{q_{N,M}}{w}\Big)\Big\{\frac{1}{N^{p-\frac{1}{2}}}+(r^-_{\max})^M\Big\}. \tag{5.1.8}$$

In computation, for Motz's problem we may divide S into three subdomains, S^-_0, S^+_1 and S^+_2. Then $S=S^-_0\cup S^+_1\cup S^+_2$. In S^+_1 and S^+_2 we may choose two different FS. The numerical solutions can be easily obtained from the TM using FS in $S^+_1\cup S^+_2$ and PS in S^-_0. Numerical examples are reported in [149].

5.2 Variant Combinations of FS and PS

Choose the piecewise admissible functions (5.1.1), but apply different coupling techniques on their common boundary Γ_0 to lead to different TM combinations. In this section, we briefly provide algorithms and error bounds because the detailed proof may follow the arguments in [146, 169].

5.2.1 Simplified Hybrid Combination

Define the energy

$$a_H(u,v)=\iint_{S^+}\nabla u\nabla v+\iint_{S^-}\nabla u\nabla v+\int_{\Gamma_0}\Big(\frac{\partial u^+}{\partial \nu}v^- - \frac{\partial v^+}{\partial \nu}u^-\Big)+\int_{\Gamma_D}\frac{\partial u}{\partial \nu}v, \tag{5.2.1}$$

where ν is the exterior normal of ∂S^+. Denote by $V_{N,M}$ the set of (5.1.1). The hybrid combination of the Trefftz method (simply denoted by H-TM) using FS and PS reads: to seek $u^H_{N,M}\in V_{N,M}$ such that

$$a_H(u^H_{N,M},v)=t(v), \quad v\in V_{N,M}, \tag{5.2.2}$$

where

$$t(v)=\int_{\Gamma_N} gv+\int_{\Gamma_D}\frac{\partial v}{\partial \nu}f. \tag{5.2.3}$$

Note that the bias normal derivatives on Γ_0 are needed in (5.2.1), where only the normal derivatives of FS are used. If we wish to use only the normal derivatives of PS, the H-TM reads: to seek $u^H_{N,M}\in V_{N,M}$ such that

$$a^*_H(u^H_{N,M},v)=t(v), \quad v\in V_{N,M}, \tag{5.2.4}$$

where

$$a_H^*(u,v)=\iint_{S^+}\nabla u\nabla v+\iint_{S^-}\nabla u\nabla v+\int_{\Gamma_0}\left(\frac{\partial u^-}{\partial v}v^+-\frac{\partial v^-}{\partial v}u^+\right)+\int_{\Gamma_D}\frac{\partial u}{\partial v}v, \quad (5.2.5)$$

where v is the exterior normal of ∂S^-. By using the Green formula,

$$\iint_{S^\pm}\nabla u\nabla v=\int_{\partial S^\pm}\frac{\partial u^\pm}{\partial v}v^\pm, \quad (5.2.6)$$

the algorithms in (5.2.2) and (5.2.4) are carried out on boundary $\Gamma\cup\Gamma_0$ only. From [146, 169], we have the following theorem.

Theorem 5.2.1. *There exists the bound,*

$$\|u-u_{N,M}^H\|_1\le C\inf_{v\in v_{N,M}}\|u-v\|_1, \quad (5.2.7)$$

where C is a constant independent of N and M. Moreover, let $u\in\mathbf{H}^p(S^+)$ and $u\in\mathbf{H}^\sigma(S^-)$ $\left(p,\sigma\ge\frac{3}{2}\right)$. Suppose that the large N satisfies

$$\left(\frac{R^+}{r_{\max}^+}\right)^{2n-N}\left(\frac{r_{\max}^+}{r_{\min}^+}\right)^n\le\frac{1}{n^{p-\frac{1}{2}}}. \quad (5.2.8)$$

Then there exists the bound of $u_{N,M}^H$ by the H-TM,

$$\|u-u_{N,M}^H\|_1\le C\left(\frac{1}{N^{p-1}}\|u\|_{p,S^+}+\frac{1}{M^{\sigma-1}}\|u\|_{\sigma,S^-}\right). \quad (5.2.9)$$

Proof. Denote the auxiliary solution

$$u_{N,M}^*=\begin{cases}u_N^+=\Sigma_N\left(P_n^+;r^+,\theta^+\right)\text{ in }S^+,\\ u_M^-=P_n^-(r^-,\theta^-)\text{ in }S^-,\end{cases} \quad (5.2.10)$$

where

$$P_n^\pm=P_n^\pm(r^\pm,\theta^\pm)=\frac{a_0^\pm}{2}+\sum_{i=1}^{n^\pm}(r^\pm)^i\left\{a_i^\pm\cos\left(i\theta^\pm\right)+b_i^\pm\sin\left(i\theta^\pm\right)\right\}\text{ in }S^\pm. \quad (5.2.11)$$

In (5.2.11), $n^+=N$ and $n^-=M$, and $a_i^\pm$ and $b_i^\pm$ are the exact expansion coefficients of the solution u in $S^\pm$. Hence we have

$$\begin{aligned}\|u-u_{N,M}^H\|_1&\le C\|u-u_{N,M}^*\|_1\\&\le\|P_n^+-\Sigma_N(P_n^+;r^+,\theta^+)\|_{1,S^+}+\|R_n^+\|_{1,S^+}+\|R_M^-\|_{1,S^-}.\end{aligned} \quad (5.2.12)$$

There exist the bounds,

$$\|R_n^+\|_{1,S^+}\le C\frac{1}{n^{p-1}}\|u\|_{p,S^+},\quad \|R_M^-\|_{1,S^-}\le C\frac{1}{M^{\sigma-1}}\|u\|_{\sigma,S^-}. \quad (5.2.13)$$

For the harmonic functions v satisfying $\Delta v = 0$, we have from Oden and Reddy [195]

$$\|v\|_{1,S^+} \le C\|v\|_{\frac{1}{2},\partial S^+} \le C\sqrt{\|v\|_{0,\partial S^+}\,\|v\|_{1,\partial S^+}}\,. \tag{5.2.14}$$

When the conditions (5.2.8) are satisfied to give $N \le Cn$, we have from Theorem 2.3.1 and (5.2.14)

$$\begin{aligned}\|P_n^+ - \Sigma_N(P_n^+; r^+, \theta^+)\|_{1,S^+} &\le C\sqrt{\frac{1}{n^{p-\frac{1}{2}}} \times \frac{1}{n^{p-\frac{3}{2}}}}\,\|P_n^+(r^+, \theta^+)\|_{0,\partial S^+} \\ &\le C\frac{1}{N^{p-1}}\,\|u\|_{0,\partial S^+} \le C\frac{1}{N^{p-1}}\,\|u\|_{p,S^+}\,.\end{aligned} \tag{5.2.15}$$

Combining (5.2.12)–(5.2.15) gives the desired result (5.2.9). ■

When there exists an integration approximation in (5.2.2), we seek $\hat{u}^H_{N,M} \in V_{N,M}$ such that $\hat{a}_H(\hat{u}^H_{N,M}, v) = \hat{t}(v)$ for all $v \in V_{N,M}$, where

$$\hat{a}_H(u, v) = \widehat{\int_{\partial S^+}} \frac{\partial u}{\partial v} v + \widehat{\int_{\partial S^-}} \frac{\partial u}{\partial v} v + \widehat{\int_{\Gamma_0}} \left(\frac{\partial u^+}{\partial v} v^- - \frac{\partial v^+}{\partial v} u^-\right) + \widehat{\int_{\Gamma_D}} \frac{\partial u}{\partial v} v, \tag{5.2.16}$$

$$\hat{t}(v) = \widehat{\int_{\Gamma_N}} gv + \widehat{\int_{\Gamma_D}} \frac{\partial v}{\partial v} f. \tag{5.2.17}$$

We have the following theorem from [149].

Theorem 5.2.2. *There exists the bound,*

$$\begin{aligned}\|u - \hat{u}^H_{N,M}\|_1 \le C \inf_{v \in V_{N,M}} \|u - v\|_1 + C \sup_{w \in V_{N,M}} \frac{1}{\|w\|_1} \Bigg\{ &\left|\left(\int_{\partial S^+} - \widehat{\int_{\partial S^+}}\right) \frac{\partial u}{\partial v} w\right| \\ &+ \left|\left(\int_{\partial S^-} - \widehat{\int_{\partial S^-}}\right) \frac{\partial u}{\partial v} w\right| + \left|\left(\int_{\Gamma_0} - \widehat{\int_{\Gamma_0}}\right) \frac{\partial u}{\partial v} w^-\right| + \left|\left(\int_{\Gamma_0} - \widehat{\int_{\Gamma_0}}\right) \frac{\partial w^+}{\partial v} u\right| \\ &+ \left|\left(\int_{\Gamma_D} - \widehat{\int_{\Gamma_D}}\right) \frac{\partial u}{\partial v} w\right| + \left|\left(\int_{\Gamma_D} - \widehat{\int_{\Gamma_D}}\right) \frac{\partial w}{\partial v} f\right| + \left|\left(\int_{\Gamma_N} - \widehat{\int_{\Gamma_N}}\right) gw\right| \Bigg\}.\end{aligned} \tag{5.2.18}$$

The polynomial convergence rates can also be achieved.

5.2.2 Hybrid Plus Penalty Combination

The hybrid combination has a drawback in that the constant is excluded in the admissible functions in S^+ in (5.2.2) (or S^- in (5.2.4)). To overcome such a drawback, we solicit the hybrid plus penalty TM in [146, 169]. For simplicity, consider the Robin problem,

$$\Delta u = 0 \text{ in } S, \tag{5.2.19}$$

$$\frac{\partial u}{\partial \nu} + \alpha u = g \text{ on } \partial S, \tag{5.2.20}$$

where $\alpha > 0$. The solution $u \in \mathbf{H}^1(S)$ satisfies

$$a(u, v) = f(v), \quad v \in \mathbf{H}^1(S), \tag{5.2.21}$$

where

$$a(u, v) = \iint_S \nabla u \nabla v + \int_{\partial S} \alpha uv, \quad f(v) = \int_{\partial S} gv. \tag{5.2.22}$$

Let S be divided by $\mathbf{\Gamma}_0$ into S^+ and S^-, and also choose the admissible functions (5.1.1). This set is also denoted by $v \in V_{N,M}$. The hybrid plus penalty coupling along the interior boundary $\mathbf{\Gamma}_0$ between FS and PS is given by

$$\begin{aligned} D(u, v) = {} & P_c N^{\zeta} \int_{\Gamma_0} (u^+ - u^-)(v^+ - v^-) \\ & - \int_{\Gamma_0} \left(\alpha \frac{\partial u^+}{\partial \nu} + \beta \frac{\partial u^-}{\partial \nu} \right)(v^+ - v^-) - \int_{\Gamma_0} \left(\alpha \frac{\partial v^+}{\partial \nu} + \beta \frac{\partial v^-}{\partial \nu} \right)(u^+ - u^-), \end{aligned} \tag{5.2.23}$$

where $\alpha + \beta = 1$ and $N \asymp M$. In (5.2.23), ζ is a positive power, and P_c is a large constant but still independent of N and M. The hybrid plus penalty TM (denoted by HP-TM) reads: to seek $u_{N,M}^{HP} \in V_{N,M}$ such that

$$a_h^{HP}(u_{N,M}^{HP}, v) = f(v), \quad v \in V_{N,M}, \tag{5.2.24}$$

where

$$a_h^{HP}(u, v) = \iint_{S^+} \nabla u \nabla v + \iint_{S^-} \nabla u \nabla v + D(u, v) + \int_{\partial S} \alpha uv. \tag{5.2.25}$$

Denote the norm

$$\|v\|_h = \left\{ \|v\|_{1,S^+}^2 + \|v\|_{1,S^-}^2 + P_c N^{\zeta} \|v^+ - v^-\|_{0,\Gamma}^2 + \|v\|_{0,\partial S}^2 \right\}^{\frac{1}{2}}. \tag{5.2.26}$$

We have the following lemma.

Lemma 5.2.1. *Suppose that there exists a constant* $\mu\,(> 0)$ *independent of* N *and* M *such that*

$$\left\| \frac{\partial v^+}{\partial \nu} \right\|_{0,\Gamma_0} \leq C N^{\mu} \|v\|_{1,S^+}. \tag{5.2.27}$$

Then there exist the bounds,

$$|a_h^{HP}(u,v)| \le C\|u\|_h\|v\|_h, \quad v \in V_{N,M}, \tag{5.2.28}$$

$$c_0\|v\|_H^2 \le a_h^{HP}(v,v), \quad v \in V_{N,M}, \tag{5.2.29}$$

where $c_0\,(>0)$ *and* C *are two constants independent of* N *and* M*.*

Based on Lemma 5.2.1, we have the following lemma.

Lemma 5.2.2. *Let (5.2.27) hold. Then there exists the bound,*

$$\|u - u_{N,M}^{HP}\|_h \le C \inf_{v \in V_{N,M}} \|u - v\|_h, \quad v \in V_{N,M}. \tag{5.2.30}$$

Theorem 5.2.3. *Let (5.2.27),* $u \in \mathbf{H}^p(S^+)$ $(p \ge 2)$ *and* $u \in \mathbf{H}^\sigma(S^-)$ $(\sigma \ge 2)$ *hold. Suppose that* N *satisfies (5.2.8). Then there exists the bound,*

$$\|u - u_{N,M}^{HP}\|_h \le C\left\{\frac{1}{N^{p-1-\delta}} + \frac{1}{M^{\sigma-1-\delta}}\right\}, \tag{5.2.31}$$

where $\delta = \max\{0, \frac{\zeta-1}{2}\}$.

Proof. We have

$$\|v\|_h = \{\|v\|_1^2 + P_c N^\zeta \|v^+ - v^-\|_{0,\Gamma_0}^2 + \alpha\|v\|_{0,\partial S}^2\}^{\frac{1}{2}}. \tag{5.2.32}$$

Since the bound of $\|u - u_{N,M}^{HP}\|_1$ has been obtained in Section 5.2.1 already, we only derive the bounds of the rest terms in (5.2.32). There exists the bound,

$$\begin{aligned} &\|(u - u_{N,M}^*)^+ - (u - \bar{u}_{N,M}^*)^-\|_{0,\Gamma_0} \\ &= \|(u - u_N^*) - (u - \bar{u}_M)\|_{0,\Gamma_0} \le \|u - u_N^*\|_{0,\Gamma_0} + \|u - \bar{u}_M\|_{0,\Gamma_0} \\ &\le \|P_n^+ - \mathbf{\Sigma}_N(P_n^+; r, \theta)\|_{0,\Gamma_0} + \|R_N^+\|_{0,\Gamma_0} + \|R_M^-\|_{0,\Gamma_0} \le C\left\{\frac{1}{N^{p-\frac{1}{2}}} + \frac{1}{M^{\sigma-\frac{1}{2}}}\right\}, \end{aligned} \tag{5.2.33}$$

provided that the N satisfies (5.2.8). Hence we have

$$N^{\zeta/2}\|(u - u_N^*) - (u - \bar{u}_M)\|_{0,\Gamma_0} \le C\left\{\frac{1}{N^{p-1-\delta}} + \frac{1}{M^{\sigma-1-\delta}}\right\}. \tag{5.2.34}$$

Similarly,

$$\|(u - u_{N,M}^*)\|_{0,\partial S} \le \|(u - u_N^*)\|_{0,\partial S} + \|(u - \bar{u}_M)\|_{0,\partial S} \le C\left\{\frac{1}{N^{p-\frac{1}{2}}} + \frac{1}{M^{\sigma-\frac{1}{2}}}\right\}. \tag{5.2.35}$$

Based on Lemma 5.2.2, the desired result (5.2.31) is obtained from Section 5.2.1 and (5.2.33)–(5.2.35). ■

From Theorem 5.2.3 we may choose $\zeta = 1$ in (5.2.23). When the integration involves approximation by some quadrature rules, the error bounds can be obtained similarly.

5.2.3 Indirect Combination

On the interior boundary Γ_0, the continuity condition $u^+ = u^-$ may be fulfilled by using the Lagrange multiplier $\lambda \left(= \frac{\partial u}{\partial \nu}\right)$ on Γ_0. Denote

$$\lambda_L = \sum_{i=1}^{L} a_i t_i(s), \tag{5.2.36}$$

where a_i are the unknown coefficients, and $t_i(s)$ are the piecewise polynomials of order i. We may choose the Chebyshev polynomials,

$$t_i(s) = T_i(s) = \cos(i \arccos s), \;\; s \in [0,1]. \tag{5.2.37}$$

Denote by $V_{N,M} \times V_L$ the set of (5.1.1) and (5.2.37). Also denote

$$B(u, v; \lambda, \eta) = -\int_{\Gamma_0} \lambda(v^+ - v^-) - \int_{\Gamma_0} \eta(u^+ - u^-). \tag{5.2.38}$$

Consider the Robin problem (5.2.19) and (5.2.20). The coefficients c_i, d_i and a_i are sought by the Lagrange multiplier TM combination (or called the indirect TM combination): to seek $(u_{N,M} \times \lambda_L) \in V_{N,M} \times V_L$ such that

$$a_h^{\text{indir}}(u_{N,M}, v; \lambda_L, \eta) = f(v), \tag{5.2.39}$$

where

$$a_h^{\text{indir}}(u, v; \lambda, \eta) = \iint_{S^+} \nabla u \nabla v + \iint_{S^-} \nabla u \nabla v + B(u, v; \lambda, \eta). \tag{5.2.40}$$

Assume that for $\int_{\Gamma_0} \mu(v^+ - v^-)$, the following Ladyzhenskaya-Babuska-Brezzi (LBB) condition is satisfied: for $\mu_L \in V_L, \exists v_{N,M} \in V_{N,M}$ $(v_{N,M} \neq 0)$ such that

$$\left| \int_{\Gamma_0} \mu_L (v_N^+ - v_M^-) \right| \geq \beta \| v_{N,M} \|_1 \| \mu_L \|_{-\frac{1}{2},\Gamma_0}, \tag{5.2.41}$$

where $\beta \, (> 0)$ is a constant independent of N, M and L. The negative norm is defined by

$$\| \mu \|_{-\frac{1}{2},\Gamma_0} = \sup_v \frac{\left| \int_{\Gamma_0} \mu (v^+ - v^-) d\ell \right|}{\| v^+ \|_{\frac{1}{2},\Gamma_0} + \| v^- \|_{\frac{1}{2},\Gamma_0}},$$

$$\| v \|_{\frac{1}{2},\Gamma_0} = \left\{ \int_{\Gamma_0} \int_{\Gamma_0} \frac{(v(P) - v(Q))^2}{|\overline{PQ}|^2} d\ell(P) d\ell(Q) + \left(\frac{1}{d^+} + \frac{1}{d^-} \right) \| v \|_{0,\Gamma_0}^2 \right\}^{\frac{1}{2}},$$

where $d^{\pm}$ are roughly the diameters of $S^{\pm}$. We have the following lemma from [146, 169].

Lemma 5.2.3. *Let the LBB condition hold. For the solutions of the indirect TM combination, there exist error bounds,*

$$\|\lambda - \lambda_L\|_{-\frac{1}{2},\Gamma_0} \le C\left\{\inf_{v\in V_{N,M}} \|u-v\|_1 + \inf_{\eta\in V_L} \|\lambda-\eta\|_{-\frac{1}{2},\Gamma_0}\right\}, \tag{5.2.42}$$

$$\|u - u_{N,M}\|_{-\frac{1}{2},\Gamma_0} \le C\left\{\inf_{v\in V_{N,M}} \|u-v\|_1 + \inf_{\eta\in V_L} \|\lambda-\eta\|_{-\frac{1}{2},\Gamma_0}\right\}, \tag{5.2.43}$$

where C is a constant independent of N, M and L.

Theorem 5.2.4. *Let the LBB condition, $u \in \mathbf{H}^p(S^+)$ $(p \ge 2)$, $u \in \mathbf{H}^\sigma(S^-)$ $(\sigma \ge 2)$ and $\lambda \in \mathbf{H}^\mu(\Gamma_0)$ hold. Also, assume that the N satisfies (5.2.8). Then there exist the bounds,*

$$\|\lambda - \lambda_L\|_{-\frac{1}{2},\Gamma_0} \le C\left\{\frac{1}{N^{p-1}} + \frac{1}{M^{\sigma-1}} + \frac{1}{L^\mu}\right\}, \tag{5.2.44}$$

$$\|u - u_{N,M}\|_{-\frac{1}{2},\Gamma_0} \le C\left\{\frac{1}{N^{p-1}} + \frac{1}{M^{\sigma-1}} + \frac{1}{L^\mu}\right\}. \tag{5.2.45}$$

Proof. Choose

$$\lambda_L^* = \sum_{i=1}^{L} a_i^* t_i(s), \tag{5.2.46}$$

where a_i^* are the exact expansion coefficients of u. Hence, the residual R_L $(= u - u_L^*)$ has the bound,

$$\|R_L\|_{k,\Gamma_0} = O\left(\frac{1}{L^{\mu-k}}\right), \quad k < \mu. \tag{5.2.47}$$

Choose $u_{N,M}^* \times \lambda_L^* \in V_{N,M} \times V_L$. From Lemma 5.2.3, we have

$$\|\lambda - \lambda_L\|_{-\frac{1}{2},\Gamma_0} \le C\left\{\|u - u_{N,M}^*\|_1 + \|\lambda - \lambda_L^*\|_{-\frac{1}{2},\Gamma_0}\right\}, \tag{5.2.48}$$

$$\|u - u_{N,M}\|_{-\frac{1}{2},\Gamma_0} \le C\left\{\|u - u_{N,M}^*\|_1 + \|\lambda - \lambda_L^*\|_{-\frac{1}{2},\Gamma_0}\right\}. \tag{5.2.49}$$

The bound $\|u - u_{N,M}^*\|_1$ is given in Section 5.2.1 by

$$\|u - u_{N,M}^*\|_1 \le C\left\{\frac{1}{N^{p-1}} + \frac{1}{M^{p-1}}\right\}. \tag{5.2.50}$$

Also, we have from (5.2.47)

$$\|\lambda - \lambda_L^*\|_{-\frac{1}{2},\Gamma_0} = \|R_L\|_{-\frac{1}{2},\Gamma_0} \le C\|R_L\|_{0,\Gamma_0} \le C\frac{1}{L^\mu}. \tag{5.2.51}$$

Combining (5.2.48)–(5.2.51) gives the desired results (5.2.44) and (5.2.45). ■

5.3 Combinations of MFS with Other Domain Methods

5.3.1 Combined with FEM

The finite element method (FEM) is the popular numerical method for partial differential equations (PDE), due to great flexibility and deep analysis. Hence it is important to combine the MFS with the FEM. Consider the equations (5.2.19) and (5.2.20). Let S be divided by Γ_0 into S^+ and S^-, where S^- is a polygon. The subdomain S^- can be again split into the quasiuniform triangular elements $\triangle_{ij}$, *i.e.*, $S^- = \cup_{ij}\triangle_{ij}$. The FS and the k-order piecewise Lagrange polynomials v_k are chosen in S^+ and S^-, respectively. Then the admissible functions are given by

$$u_{N,h} = \begin{cases} u_N^+ = \sum\limits_{i=1}^{N} c_i \phi_i^+(P^+) \text{ in } S^+, \\ u_h^k \text{ in } S^-, \end{cases} \tag{5.3.1}$$

where ϕ_i^+ are the FS. From the previous section, we have different combined algorithms of FS. In this section, we choose one of them and provide the error bounds. Denote by $V_{N,h}$ the set of (5.3.1). The hybrid plus penalty coupling is given by

$$D(u,v) = \frac{P_c}{h^\tau}\int_{\Gamma_0}(u^+ - u^-)(v^+ - v^-) - \int_{\Gamma_0}\frac{\partial u^+}{\partial \nu}(v^+ - v^-) - \int_{\Gamma_0}\frac{\partial v^+}{\partial \nu}(u^+ - u^-), \tag{5.3.2}$$

where $\tau > 0$, ν is the exterior normal of ∂S^+, and h the maximal boundary of $\triangle_{ij}$. The constant P_c in (5.3.2) may be large, but still independent of N and h. For easy computation, the bias derivatives $\frac{\partial u^+}{\partial \nu}$ and $\frac{\partial v^+}{\partial \nu}$ are used. The hybrid plus penalty combination of MFS and FEM reads: to seek $u_{N,h} \in V_{N,h}$ such that

$$A_{N,h}(u_{N,h}, v) = f(v), \tag{5.3.3}$$

where

$$A_{N,h}(u,v) = \iint_{S^+} \nabla u \nabla v + \iint_{S^-} \nabla u \nabla v + D(u,v) + \int_{\partial S} \alpha u v, \tag{5.3.4}$$

$$f(v) = \int_{\partial S} g v. \tag{5.3.5}$$

Denote the norm

$$\|v\|_h = \left\{ \|v\|_{1,S^+}^2 + \|v\|_{1,S^-}^2 + \frac{P_c}{h^\tau}\|v^+ - v^-\|_{0,\Gamma_0}^2 + \|v\|_{0,\partial S}^2 \right\}^{\frac{1}{2}}. \tag{5.3.6}$$

From [146], we have the following lemma.

Lemma 5.3.1. *Suppose that there exists a constant* $\mu\,(>0)$ *independent of* N *and* h *such that*

$$\left\|\frac{\partial v^+}{\partial \nu}\right\|_{0,\Gamma_0} \le C N^{\mu} \|v\|_{1,S^+}. \tag{5.3.7}$$

When $\tau > 0$ *in (5.3.2), there exist the bounds,*

$$|a_{N,h}(u,v)| \le C\|u\|_h \|v\|_h, \quad v \in V_{N,h}, \tag{5.3.8}$$

$$c_0\|v\|_h^2 \le a_{N,h}(v,v), \quad v \in V_{N,h}, \tag{5.3.9}$$

where $c_0\,(>0)$ *and* C *are two constants independent of* N *and* h*. Moreover, the solutions of the hybrid plus penalty combination of MFS and FEM have the optimal convergence rates,*

$$\|u - u_{N,h}\|_h \le C \inf_{v \in V_{N,h}} \|u - v\|_h, \quad v \in V_{N,h}. \tag{5.3.10}$$

Theorem 5.3.1. *Let (5.3.7),* $u \in \mathbf{H}^p(S^+)$ $(p \ge 2)$ *and* $u \in \mathbf{H}^k(S^-)$ $(k \ge 2)$ *hold. Suppose that the* N *satisfies (5.2.8). Then there exists the bound,*

$$\|u - u_{N,h}\|_h \le C\left\{\frac{1}{N^{p-1-\delta}} + h^{k-1}\right\}, \tag{5.3.11}$$

where $\delta = \max\{0, \frac{\tau-1}{2}\}$.

As to the inequality (5.3.7), the analysis may follow [163].

5.3.2 Combined with FDM

In [146], the finite difference method (FDM) can be viewed as a special FEM using the piecewise bilinear and linear elements on $\triangle_{ij}$ and $\Box_{ij}$, respectively, by using some special quadrature rules. Divide S by Γ_0 into S^+ and S^-. The MFS and the FDM can be used in S^+ and S^-, respectively. Again, the polygon S^- is split by the coordinate lines into rectangles $\Box_{ij}$ and triangles $\triangle_{ij}$, *i.e.*, $S^- = \cup_{ij}(\Box_{ij} \cup \triangle_{ij})$. Note that the boundary nodes are located just on $\partial S^- \cup \Gamma_0$, and triangular elements $\triangle_{ij}$ occur only at $\partial S^- \cup \Gamma_0$. Hence, the rectangles $\Box_{ij}$ are dominant in S^-. We have

$$\widehat{\iint_{S^-}} \nabla u \nabla v = \sum_{ij}\left\{\widehat{\iint_{\Box_{ij}}} \nabla u \nabla v + \widehat{\iint_{\triangle_{ij}}} \nabla u \nabla v\right\}, \tag{5.3.12}$$

$$\widehat{\iint_{\Box_{ij}}} \nabla u \nabla v = \widehat{\iint_{\Box_{ij}}} u_x v_x + \widehat{\iint_{\Box_{ij}}} u_y v_y, \tag{5.3.13}$$

$$\widehat{\iint_{\triangle_{ij}}} \nabla u \nabla v = \widehat{\iint_{\triangle_{ij}}} u_x v_x + \widehat{\iint_{\triangle_{ij}}} u_y v_y. \tag{5.3.14}$$

Denote $\Box_{ij} = \{(x,y)|x_i < x < x_{i+1}, y_j < y < y_{j+1}\}$ with the boundary lengths $h_i = x_{i+1} - x_i$ and $k_j = y_{j+1} - y_j$. The piecewise bilinear functions $v \in \Box_{ij}$ are given by

$$\begin{aligned} v(x,y) = \frac{1}{h_i k_j}\{&(x_{i+1}-x)(y_{j+1}-y)v_{ij} + (x-x_i)(y_{j+1}-y)v_{i+1,j} \\ &+ (x_{i+1}-x)(y-y_j)v_{i,j+1} + (x-x_i)(y-y_j)v_{i+1,j+1}\}, \quad (x,y) \in \Box_{ij}. \end{aligned} \tag{5.3.15}$$

The approximate integrations are evaluated by different rules,

$$\widehat{\iint_{\Box_{ij}}} u_x v_x = \frac{h_i k_j}{2}\left\{u_x\left(i+\frac{1}{2},j\right)v_x\left(i+\frac{1}{2},j\right) + u_x\left(i+\frac{1}{2},j+1\right)v_x\left(i+\frac{1}{2},j+1\right)\right\},$$
$$\widehat{\iint_{\Box_{ij}}} u_y v_y = \frac{h_i k_j}{2}\left\{u_y\left(i,j+\frac{1}{2}\right)v_y\left(i,j+\frac{1}{2}\right) + u_y\left(i+1,j+\frac{1}{2}\right)v_y\left(i+1,j+\frac{1}{2}\right)\right\}.$$

For $\triangle_{ij}$, we only take the upper triangular elements for discussions,

$$\triangle_{ij} = \left\{(x,y)|x_i < x < x_{i+1}, y_j < y < y_j + \frac{k_j}{h_i}(x-x_i)\right\}.$$

The different rules are given by

$$\widehat{\iint_{\triangle_{ij}}} u_x v_x = \frac{h_i k_j}{2} u_x\left(i+\frac{1}{2},j\right)v_x\left(i+\frac{1}{2},j\right),$$
$$\widehat{\iint_{\triangle_{ij}}} u_y v_y = \frac{h_i k_j}{2}\left\{u_y\left(i,j+\frac{1}{2}\right)v_y\left(i,j+\frac{1}{2}\right)\right\}.$$

The piecewise admissible functions are chosen as

$$v = \begin{cases} u_N^+ = \sum_{i=1}^{N} c_i \phi_i^+(P^+) \text{ in } S^+, \\ u_h^1 \text{ in } S^-, \end{cases} \tag{5.3.16}$$

where ϕ_i^+ are the FS, and u_h^1 are the piecewise bilinear and liner functions on S^-. Denote by $V_{N,h}$ the set of (5.3.16). From [146], the penalty combination of MFS and FDM reads: to seek $u_{N,h} \in V_{N,h}$ such that

$$a_{N,h}(u_{N,h}, v) = f_h(v), \quad v \in V_{N,h}, \tag{5.3.17}$$

where

$$a_{N,h}(u,v) = \iint_{S^+} \nabla u \nabla v + \widehat{\iint_{S^-}} \nabla u \nabla v + \frac{P_c}{h^2}\widehat{\int_{\Gamma_0}}(u^+ - u^-)(v^+ - v^-) + \widehat{\int_{\partial S}} \alpha uv,$$
$$f_h(v) = \widehat{\int_{\partial S}} gv,$$

where $h = \max_{ij}\{h_i, k_j\}$, and P_c is a large constant, but still independent of N and h. Denote the norm

$$\overline{\|v\|}_h = \left\{ \|v\|^2_{1,S^+} + \overline{\|v\|}^2_{1,S^-} + \frac{P_c}{h^2}\overline{\|v^+ - v^-\|}^2_{0,\Gamma_0} + \overline{\|v\|}^2_{0,\partial S} \right\}^{\frac{1}{2}}, \tag{5.3.18}$$

where

$$\overline{\|v\|}^2_{1,S^-} = \overline{|v|}^2_{1,S^-} + \overline{|v|}^2_{0,S^-}, \tag{5.3.19}$$

$$\overline{|v|}^2_{1,S^-} = \sum_{ij} \widehat{\iint_{\square_{ij}}} \nabla v \nabla v + \sum_{ij} \widehat{\iint_{\triangle_{ij}}} \nabla v \nabla v, \tag{5.3.20}$$

$$\overline{|v|}^2_{0,S^-} = \sum_{ij} \widehat{\iint_{\square_{ij}}} v^2 + \sum_{ij} \widehat{\iint_{\triangle_{ij}}} v^2, \tag{5.3.21}$$

$$\overline{\|v^+ - v^-\|}^2_{0,\Gamma_0} = \widehat{\int_{\Gamma_0}} (v^+ - v^-)^2, \quad \overline{\|v\|}^2_{0,\partial S} = \widehat{\int_{\partial S}} v^2. \tag{5.3.22}$$

In (5.3.21), the quadrature rules are given by

$$\begin{aligned} \widehat{\iint_{\square_{ij}}} v^2 &= \frac{h_i k_j}{4}\left\{ v^2_{ij} + v^2_{i+1,j} + v^2_{i,j+1} + v^2_{i+1,j+1} \right\}, \\ \widehat{\iint_{\triangle_{ij}}} v^2 &= \frac{h_i k_j}{8}\left\{ v^2_{ij} + 2v^2_{i+1,j} + v^2_{i,j+1} \right\}. \end{aligned} \tag{5.3.23}$$

From [146], we have the following theorem.

Theorem 5.3.2. *There exist the bounds,*

$$|a_{N,h}(u,v)| \leq C\overline{\|u\|}_h \overline{\|v\|}_h, \quad v \in V_{N,h}, \tag{5.3.24}$$

$$c_0 \overline{\|v\|}^2_h \leq \hat{a}_{N,h}(v,v), \quad v \in V_{N,h}, \tag{5.3.25}$$

where $c_0\,(>0)$ *and* C *are two constants independent of* N *and* h. *Moreover, for the solutions of the penalty combination of MFS and FDM, there exists the bound,*

$$\begin{aligned} \overline{\|u - u_{N,h}\|}_h &\leq C \inf_{v \in V_{N,h}} \overline{\|u - v\|}_h \\ &\quad + C \sup_{w \in V_{N,h}} \frac{1}{\overline{\|w\|}_h} \left\{ \left| \left(\iint_{S^-} - \widehat{\iint_{S^-}} \right) \nabla u \nabla w \right| + \left| \left(\int_{\Gamma_0} - \widehat{\int_{\Gamma_0}} \right) \frac{\partial u}{\partial \nu}(w^+ - w^-) \right| \right. \\ &\quad \left. + \left| \widehat{\int_{\Gamma_0}} \left(\frac{\partial u}{\partial \nu} - \frac{\partial u^-}{\partial \nu} \right)(w^+ - w^-) \right| + \left| \left(\int_{\partial S} - \widehat{\int_{\partial S}} \right) g v \right| \right\}, \end{aligned} \tag{5.3.26}$$

where C *is a constant independent of* N *and* h.

Let $u \in \mathbf{H}^p(S^+)$ $\left(p \geq \frac{3}{2}\right)$ and $u \in \mathbf{H}^3(S^-)$ hold. Based on Theorem 5.3.2 and Lemma 5.3.1, we can obtain the error bound,

$$\overline{\|u - u_{N,h}\|_h} \leq C\left\{h^2 + h^2 N^{2\mu} + \frac{1}{N^{p-1}}\right\}, \tag{5.3.27}$$

by following the above arguments.

5.3.3 Combined with Radial Basis Functions

In [169], the error bounds of Kansa's method using the radial basis functions (RBF) are derived. Under the framework of combined methods in [146], we may combine the MFS with the RBF. In this subsection, we only take the following inverse multiquadric radial basis functions for discussions,

$$g_i(P^-) = \frac{1}{\sqrt{|\overline{P^-Q^-}|^2 + c^2}}. \tag{5.3.28}$$

The combinations of other kinds of RBF can be similarly developed. In (5.3.28), $P^- = P(x,y) \in (S^- \cup \partial S^-)$, but the source points Q^- are located in $S^- \cup \partial S^-$ as well, which is different from the FS, where the source points must be located outside $S^- \cup \partial S^-$. We may choose the piecewise admissible functions,

$$u_{N,M} = \begin{cases} u_N^+ = \sum\limits_{i=1}^{N} c_i \phi_i^+(P^+) \text{ in } S^+, \\ u_M^- = \sum\limits_{i=1}^{M} d_i g_i(P^-) \text{ in } S^-, \end{cases} \tag{5.3.29}$$

where the functions $\phi_i^+(P^+)$ and $g_i(P^-)$ are the FS and the RBF, respectively. Consider the Dirichlet problems,

$$\Delta u = \begin{cases} 0 \text{ in } S^+, \\ f(x,y) \text{ in } S^-, \end{cases} \tag{5.3.30}$$

$$u = 0 \text{ on } \partial S. \tag{5.3.31}$$

For simplicity, assume that the admissible functions in (5.3.29) satisfy the Dirichlet boundary condition (5.3.31). Otherwise, the corresponding collocation equations are needed. Denote by $V_{N,M}$ the set of (5.3.29) satisfying (5.3.31). The combination of FS and RBF reads: to seek $u_{N,M} \in V_{N,M}$ such that

$$\hat{B}_{N,M}(u_{N,M}, v) = \hat{f}(v), \quad v \in V_{N,M}, \tag{5.3.32}$$

where

$$\begin{aligned} \hat{B}_{N,M}(u,v) = & \iint_{S^+} \nabla u \nabla v + \int_{\Gamma_0} u_\nu^- v^- + P_c \widehat{\iint_{S^-}} \Delta u \Delta v \\ & + P_c M \widehat{\int_{\Gamma_0}} (u^+ - u^-)(v^+ - v^-) + P_c \widehat{\int_{\Gamma_0}} (u_\nu^+ - u_\nu^-)(v_\nu^+ - v_\nu^-), \end{aligned} \tag{5.3.33}$$

$$\hat{f}(v) = -P_c \widehat{\int_{\partial S^-}} f \Delta v. \tag{5.3.34}$$

Denote the norm

$$|||v||| = \left\{ \|v\|^2_{1,S^+} + P_c \|v\|^2_{1,S^-} + P_c \|\Delta v\|^2_{0,S^-} + P_c M \|v^+ - v^-\|^2_{0,\Gamma_0} + P_c \|v^+_\nu - v^-_\nu\|^2_{0,\Gamma_0} \right\}^{\frac{1}{2}}.$$

From [169], we have the following theorem.

Theorem 5.3.3. *Suppose that there exist the bounds,*

$$\left|\hat{B}_{N,M}(u,v)\right| \leq C|||u||| \times |||v|||, \quad v \in V_{N,M}, \tag{5.3.35}$$

$$c_0 |||v|||^2 \leq \hat{B}_{N,M}(v,v), \quad v \in V_{N,M}, \tag{5.3.36}$$

where c_0 (> 0) *and* C *are two constants independent of* N *and* M*. Moreover, the solutions of the combination of FS and RBF have the optimal convergence estimates,*

$$|||u - u_{N,M}||| \leq C \inf_{v \in V_{N,M}} |||u - v|||. \tag{5.3.37}$$

More detailed bounds can be obtained similarly, and two inequalities (5.3.35) and (5.3.36) are explored in [169, p.201]. The error bounds can be obtained from [169], by adding the error bounds of $\|P_n - \Sigma_N(P_n; r, \theta)\|_{1,S^+}$.

In summary, many combined algorithms in [146, 169] can be employed for combining FS. Hence the MFS can be integrated into the combined family, to enrich the combined methods and to extend the wide applications of MFS.

5.4 Singularity Problems by Combination of MFS and MPS

For the bounded simply-connected domains involving singularity, numerical experiments of combined algorithms of the MFS are reported in [178]. In this section, consider the exterior problems of Laplace's equation involving singularity. There exist two kinds of infinity conditions, (1) $|u| \leq C$ and (2) $u = O(\ln \rho)$. For the exterior problems of Helmholtz's equation, the Sommerfeld radiation conditions are satisfied at infinity, and the MFS is discussed in Chapter 8. Consider a crack singularity existing in exterior problems (*i.e.*, unbounded domains), and employ the combination of PS and FS. The numerical results coincide with the analysis made.

Consider the crack problem in the unbounded domain in [107] (see Figure 5.1),

$$\Delta u = 0 \text{ in } S_\infty, \tag{5.4.1}$$

$$u = 1 \text{ on } \Gamma_{\text{in}}, \tag{5.4.2}$$

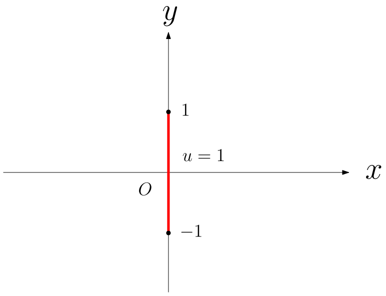

FIG. 5.1 – The exterior problem with an interior crack.

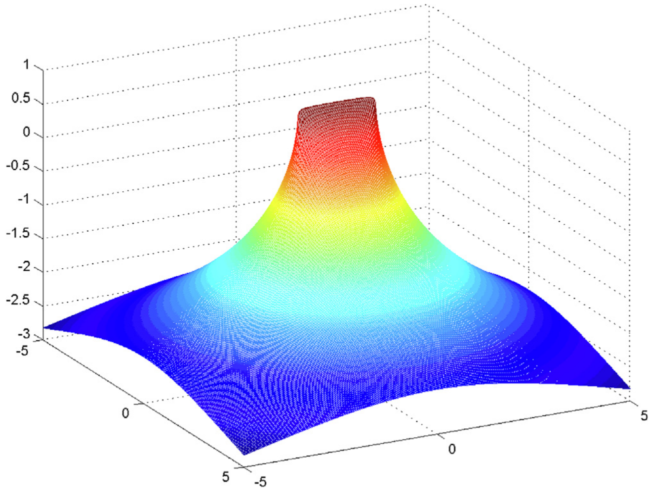

FIG. 5.2 – Shape of the exact solution (5.4.5).

$$u = O(\ln\rho) \text{ as } \rho \to \infty, \tag{5.4.3}$$

where $\Gamma_{\text{in}} = \{x = 0 \cap -1 < y < 1\}$. The exact solution of (5.4.1)–(5.4.3) is known in [107] as (see Figure 5.2)

$$u(P) = -\int_{\Gamma_{\text{in}}} \ln|\overline{PQ}|v(Q)\,d\ell_Q, \tag{5.4.4}$$

where $P(x,y) \in S_\infty \cup \Gamma_{\text{in}},\ Q = (\xi,\eta) \in \Gamma_{\text{in}}$, and the exact solution

$$v(Q) = \frac{1}{\pi\ \ln 2\sqrt{1 - \{y(Q)\}^2}}. \tag{5.4.5}$$

First, let us find the infinite condition (5.4.3). We have from (5.4.4) and (5.4.5)

$$u(x,y) = -\frac{1}{\pi\ \ln 2}\int_{-1}^{1}\frac{\ln\sqrt{x^2+(y-s)^2}}{\sqrt{1-s^2}}\,ds = u(\rho,\theta),$$

where $\rho = \sqrt{x^2+y^2}$. When $\rho \to \infty$ we have

$$\ln\sqrt{x^2+(y-s)^2} = \ln\sqrt{(x^2+y^2)+s^2-2ys} \approx \ln\rho.$$

Then we obtain

$$u(\rho,\theta) \approx -\frac{\ln\rho}{\pi\ \ln 2}\int_{-1}^{1}\frac{1}{\sqrt{1-s^2}}\,ds. \tag{5.4.6}$$

By using the integration formula

$$\int\frac{dx}{\sqrt{a^2-x^2}} = \arcsin\frac{x}{a} + c,$$

we have

$$\int_{-1}^{1}\frac{ds}{\sqrt{1-s^2}} = 2\int_{0}^{1}\frac{ds}{\sqrt{1-s^2}} = 2\ \arcsin\ x|_0^1 = 2(\arcsin\ 1 - \arcsin\ 0) = \pi. \tag{5.4.7}$$

Hence, from (5.4.6) and (5.4.7) we obtain that when $\rho \to \infty$, $u(\rho,\theta) \approx -\frac{\ln\rho}{\ln 2}$. This is a type of $O(\ln\rho)$ for the infinity condition.

We give a reason for physics to choose $u = O(\ln\rho)$ as $\rho \to \infty$. In fact, the models (5.4.1)–(5.4.3) are simplified from the 3D exterior problem, where there exists a crack wall with a height of 2 but an infinite length. Although such a case is unrealistic in real physics, the infinity condition $O(\ln\rho)$ is important and interesting from a mathematical point of view. In fact, for the boundary integral equation in [107, 190], the infinity condition $u = O(\ln\rho)$ as $\rho \to \infty$ is often discussed. We seek an effective TM in [169] for solving (5.4.1)–(5.4.3). When the combinations of FS and PS are chosen in the TM, both high accuracy and good stability can be achieved (also see [146]).

The algorithms of the TM and the CTM for (5.4.1) and (5.4.2) are similar to those in Section 5.1. To cope with the infinity boundary conditions, choose the particular solutions,

$$u_N = -\frac{\ln\rho}{\ln 2} + \sum_{i=1}^{N} d_i\rho^{-2i}\cos(2i\theta),\ \text{or}\ u_N = d_0\ \ln\rho + \sum_{i=1}^{N} d_i\rho^{-2i}\cos(2i\theta),$$

for the exterior domain, where d_0 is an unknown coefficient to be determined. Since there exist two corner singularities with $u = O\big(\sqrt{r_\pm}\big)$ at points $(0,\pm1)$, choose the singular solutions $u_L^\pm = 1 + \sum_{i=0}^{L} d_i^\pm r_\pm^{i+\frac{1}{2}}\sin\big(i+\frac{1}{2}\big)\theta_\pm$, where $(r_\pm,\theta_\pm)$ are the polar coordinates with origins $(0,\pm1)$. From the symmetry of this problem, we may simplify the problem (5.4.1)–(5.4.3) to one in the first quadrant $S_\infty^\pm$ (see Figure 5.3) as

$$\Delta u = 0 \text{ in } S_\infty^+, \tag{5.4.8}$$

$$\frac{\partial u}{\partial y} \text{ in } y = 0, \tag{5.4.9}$$

$$u = 1 \text{ on } (x=0) \cap (0<y<1), \tag{5.4.10}$$

$$\frac{\partial u}{\partial x} = 0 \text{ on } (x=0) \cap (y>1), \tag{5.4.11}$$

$$u = -\frac{1}{\ln 2} \ln\rho \text{ (or } u = d_0 \ln\rho) \text{ as } \rho \to \infty, \tag{5.4.12}$$

where $S_\infty^+ = \{(x,y) | x > 0 \,\text{and}\, y > 0\}$.

We divide S_∞^+ into three subdomains as shown in Figure 5.3, $S_\infty^+ = S_0^+ \cup S_1^+ \cup S_\infty^-$, where S_0^+, S_1^+ and the exterior domain S_∞^- are defined by

$$S_0^+ = \left\{(r,\theta) | 0 \le r < 1, 0 \le \theta \le \pi, \text{ satisfying } y > \frac{1}{2}\right\}, \tag{5.4.13}$$

$$S_1^+ = \left\{(\rho,\psi) | 0 \le \rho < 1, 0 \le \psi \le \frac{\pi}{2}, \text{ satisfying } y < \frac{1}{2}\right\}, \tag{5.4.14}$$

$$S_\infty^- = \{(\rho,\psi) | \rho > 1, 0 \le \psi \le \frac{\pi}{2}, \text{ excluding } S_0 \cup S_1\}, \tag{5.4.15}$$

where (ρ,ψ) and (r,θ) are the polar coordinates with origins (0, 0) and (0, 1), respectively (see Figure 5.3). We choose the following two kinds of admissible solutions.

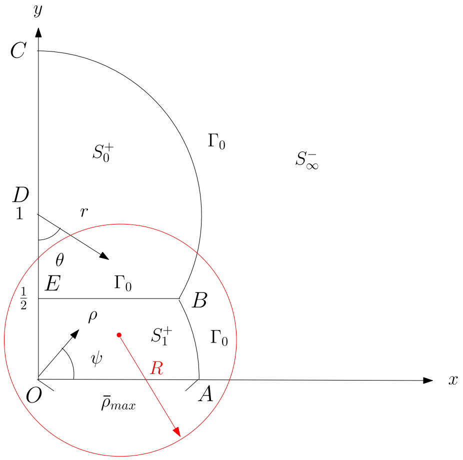

FIG. 5.3 – The partition for the crack singularity and exterior problem.

I. The piecewise particular solutions:

$$u_{N,L,M}=\begin{cases} u_N=1+\sum\limits_{i=0}^{N} c_i\rho^{2n+1}\cos(2n+1)\psi \ \text{ in } S_1^+, \\ u_L^+ \ =1+\sum\limits_{i=0}^{L} d_i r^{i+\frac{1}{2}}\sin\big(i+\frac{1}{2}\big)\theta \ \text{ in } S_0^+, \\ u_M^+ \ = a_0 \ \ln\rho+\sum\limits_{i=1}^{M} a_i\rho^{-2i}\cos(2i\psi) \ \text{ in } S_\infty^-, \end{cases} \tag{5.4.16}$$

where c_i, d_i and a_i are the unknown coefficients.

II. Combination of TM with PS and FS: To follow Li [146, 149], we solicit the combination of TM with PS and FS. Choose the fundamental solutions, to give

$$u_{N,L,M}=\begin{cases} \bar{u}_N^+ \ =\sum\limits_{i=1}^{N} c_i\phi_i \ \text{ in } S_1^+, \\ u_L^+ \ =1+\sum\limits_{i=0}^{L} d_i r^{i+\frac{1}{2}}\sin\big(i+\frac{1}{2}\big)\theta \ \text{ in } S_0^+, \\ u_M^+ \ = a_0 \ \ln\rho+\sum\limits_{i=1}^{M} a_i\rho^{-2i}\cos(2i\psi) \ \text{ in } S_\infty^-, \end{cases} \tag{5.4.17}$$

where $\phi_i=\ln\sqrt{R^2+\rho^2-2R\rho\,\cos\big(\psi-\frac{2\pi}{N}\,i\big)}$ are the traditional FS.
Since the subdomain S_1^+ is bounded, the radius of the source circle with origin $\big(\frac{1}{2},\frac{1}{4}\big)$ is given by

$$R>\bar{\rho}_{\max}=\max_{S_1}\,\bar{\rho}=\sqrt{\left(\frac{1}{2}\right)^2+\left(\frac{1}{4}\right)^2}=\sqrt{0.25+0.0625}=0.559. \tag{5.4.18}$$

Since the piecewise solutions (5.4.16) satisfy (5.4.8) and the boundary conditions (5.4.9)–(5.4.12) already, they should be forced to satisfy the interior boundary continuity conditions: $u^+=u^-$ and $u_\nu^+ + u_\nu^- = 0$ on Γ_0 only, where $u^\pm=u|_{S^\pm}$, and $u_\nu^\pm=\frac{\partial u^\pm}{\partial \nu}$ which are the exterior normal derivatives of $\Gamma_0\cap S^\pm$. Denote the energy

$$T(v)=\int_{\Gamma_0}(v^+-v^-)^2+w^2\int_{\Gamma_0}(v_\nu^+ + v_\nu^-)^2, \tag{5.4.19}$$

and denote by $V_{N,L,M}$ the set of (5.4.16) or (5.4.17). The TM using PS (*i.e.*, the MPS) reads: to seek $u_{N,L,M}\in V_{N,L,M}$ such that

$$T(u_{N,L,M})=\min_{v\in V_{N,L,M}} T(v),$$

where the weight $w=\frac{1}{\max\{N,L,M\}}$ (see [146, 169]). The collocation equations on Γ_0 can be formulated, similarly to those in Section 1.2.

Since the FS in S_1^+ for (5.4.17) do not satisfy the boundary conditions (5.4.9) and (5.4.10), the TM using (5.4.17) (*i.e.*, the combination of MFS and MPS) is modified as

$$T^*(v) = T(v) + \int_{\overline{OE}} (v-1)^2 + w^2 \int_{\overline{OA}} v_\nu^2, \tag{5.4.20}$$

where $T(v)$ is given by (5.4.19). Define the boundary errors for the MPS,

$$\|\varepsilon\|_B = \left\{ \int_{\Gamma_0} (v^+ - v^-)^2 + w^2 \int_{\Gamma_0} (v_\nu^+ + u_\nu^-)^2 \right\}^{\frac{1}{2}},$$

and for the combination of the MFS and the MPS,

$$\|\varepsilon\|_{B^*} = \left\{ \int_{\overline{OE}} (v-1)^2 + w^2 \int_{\overline{OA}} v_\nu^2 + \int_{\Gamma_0} (v^+ - v^-)^2 + w^2 \int_{\Gamma_0} (v_\nu^+ + u_\nu^-)^2 \right\}^{\frac{1}{2}}.$$

We choose $a_0 = -\frac{1}{\ln 2}$ (or a_0 as an unknown coefficient in computation), but only report the results of the unknown a_0. The integrals in $|\varepsilon|_{B^*}$ and $|\varepsilon|_B$ are evaluated by the central or the Gaussian rule. For the MPS, the errors, the condition numbers, and the coefficients are listed in Table 5.1. The exact solutions $u(1,0)$ and $u(0,1.2)$ are given in [107]:

$$u(1,0) = -\frac{1}{\ln 2} \ln\left(\frac{1+\sqrt{2}}{2}\right) = -0.271553303,$$

$$u(0,1.2) = -\frac{1}{\ln 2} \ln\left(\frac{1.2+\sqrt{1.2^2-1}}{2}\right) = 0.102120702.$$

In the tables, $\widehat{u}$ denotes the numerical solutions from the MPS or the combination of MFS and MPS. From Table 5.1, we find that the numerical results of the MPS and the combination of MFS and MPS are close to each other, but the solutions of the MPS are more accurate. We can see that by the MPS, the leading coefficient $d_0 = -2.040278893$ has ten significant digits. From Tables 5.1 and 5.2, we can also see the asymptotic rates for the MPS,

$$\|\varepsilon\|_B = O((0.44)^N), \quad \text{Cond} = O((2.17)^N), \tag{5.4.21}$$

and for the combination of MFS and MPS,

$$\|\varepsilon\|_{B^*} = O((0.68)^N), \quad \text{Cond} = O((1.87)^N). \tag{5.4.22}$$

The numerical results (5.4.21) and (5.4.22) coincide with the analysis of combined algorithms of the MFS made.

Tab. 5.1 – The errors and the condition numbers for the crack singularity problem (5.4.8)−(5.4.12) by the MPS.

(L, N, M)	(10, 10, 10)	(15, 15, 15)	(20, 20, 20)	(25, 25, 25)	(30, 30, 30)
$\|\varepsilon\|_B$	4.21(−6)	6.25(−8)	9.90(−10)	2.12(−11)	2.97(−13)
$\|u-\widehat{u}\|_{\infty,\Gamma_0}$	1.18(−5)	3.47(−7)	4.25(−9)	8.20(−10)	6.40(−11)
$\|u_n-\widehat{u}_n\|_{\infty,\Gamma_0}$	4.50(−4)	1.63(−5)	2.67(−7)	7.40(−8)	5.38(−9)
$\|u(1,0)-\widehat{u}(1,0)\|$	9.66(−7)	7.56(−10)	8.84(−11)	1.30(−11)	1.75(−12)
$\|u(0,1.2)-\widehat{u}(0,1.2)\|$	4.43(−7)	2.62(−8)	1.05(−9)	1.48(−10)	3.75(−12)
Cond	8.56(2)	3.72(4)	1.70(6)	8.16(7)	4.11(9)
Cond_eff	1.99(2)	6.83(3)	2.47(5)	9.60(6)	3.92(8)
a_0	−1.44269301442893	−1.44269494289677	−1.44269504480382	−1.44269504144279	−1.44269504090324
$\left\|\frac{\triangle a_0}{a_0}\right\|$	1.40(−6)	6.79(−8)	2.71(−9)	3.84(−10)	9.89(−12)
a_1	−0.360671125598704	−0.360673770823228	−0.360673759699562	−0.360673760145356	−0.360673760219852
d_0	−2.04027765688346	−2.04027883928822	−2.04027889533347	−2.04027889349253	−2.04027889320100
d_1	−0.170022161345209	−0.170023266835309	−0.170023239965007	−0.170023240927329	−0.170023241093981

TAB. 5.2 – The errors and the condition numbers for the crack singularity problem (5.4.8)–(5.4.12) by combination of MFS and MPS with $R = 1.2$.

(L, N, M)	(8, 10, 6)	(12, 15, 9)	(16, 20, 12)	(20, 25, 15)	(24, 30, 18)
$\\|\varepsilon\\|_{B^*}$	3.77(−4)	4.23(−5)	1.72(−6)	2.29(−7)	3.84(−8)
$\\|u - \widehat{u}\\|_{\infty,\Gamma_0 \cup \overline{OE}}$	1.48(−3)	2.23(−4)	1.09(−5)	1.58(−6)	3.46(−7)
$\\|u_n - \widehat{u}_n\\|_{\infty,\Gamma_0 \cup \overline{OA}}$	1.72(−2)	2.97(−3)	1.72(−4)	2.98(−5)	5.43(−6)
$\|u(1,0) - \widehat{u}(1,0)\|$	2.58(−4)	3.87(−5)	1.42(−6)	1.20(−7)	2.33(−8)
$\|u(0,1.2) - \widehat{u}(0,1.2)\|$	1.66(−5)	4.82(−6)	1.14(−7)	1.87(−8)	5.91(−9)
Cond	3.32(2)	5.71(3)	1.41(5)	2.60(6)	6.00(7)
Cond_eff	1.24(2)	1.72(3)	3.24(4)	5.01(5)	5.91(6)
a_0	−1.44260681893624	−1.44267784754449	−1.44269467722486	−1.44269497470446	−1.44269502111402
$\left\|\dfrac{\triangle a_0}{a_0}\right\|$	6.12(−5)	1.19(−5)	2.52(−7)	4.59(−8)	1.37(−8)
a_1	−0.360244052612593	−0.3606677425268	−0.360673760365405	−0.360673772519427	−0.36067376527848
d_0	−2.04019808712366	−2.04026726275563	−2.04027861986542	−2.04027885368193	−2.04027888047951
d_1	−0.169802255646863	−0.170018772480365	−0.170023177947295	−0.170023255143582	−0.170023243395147

Chapter 6

Source Nodes on Elliptic Pseudo-Boundaries

For the method of fundamental solutions (MFS), the source nodes on circles outside the solution domain S have been widely applied in numerical computation; see Chapters 1–5. In this chapter, the source nodes on an ellipse are proposed for solving Laplace's equation using the MFS, and a robust error and stability analysis is established. The bounds of errors and condition numbers are derived for the bounded simply-connected domains. Polynomial convergence rates can be achieved, but the exponential growth of the condition number (Cond) is also obtained. Note that for the stability analysis of the MFS in Chapters 2 and 3, the circulant matrices in Davis [7] are always employed. This is the first time that stability analysis to be explored for the non-circular pseudo-boundaries, based on the new techniques without using circulant matrices. Moreover, the criteria for evaluating numerical techniques are provided and some strategies for choosing the pseudo-boundaries are suggested. The materials of this chapter are adapted from [74].

6.1 Introduction

In this chapter, we study the case where the source nodes are located on ellipses outside S. First, let us state the characteristics of the MFS and the importance of choosing source nodes. From the boundary integral equations (BIE), the fundamental solutions (FS) satisfy the governing equations in S, and they are the functions of the distance $|\overline{PQ}|$, where $P \in \bar{S}$ and Q are source nodes. For Laplace's equation, the FS is known as $\ln|\overline{PQ}|$ in 2D and $\frac{1}{|\overline{PQ}|}$ in 3D. When the source nodes Q_i are located outside S with $|\overline{PQ_i}| > 0$, no singularity exists for the FS. To solve the boundary value problems of the homogeneous partial differential equations (PDE), their linear combinations, such as $\sum_i c_i \ln|\overline{PQ_i}|$ or $\sum_i c_i \frac{1}{|\overline{PQ_i}|}$, are chosen to satisfy the exterior and interior boundary conditions only. This method is called the method of fundamental solutions (MFS). When the source

DOI: 10.1051/978-2-7598-3171-5.c006
© Science Press, EDP Sciences, 2023

nodes are released from the boundary $\Gamma\,(=\partial S)$, where should they go? There are various choices: scatter, random, or an outside closed contour Γ_R. The last one is employed to control the source nodes in previous chapters. Since Γ_R is not the physical boundary Γ, the pseudo-boundary (*i.e.*, the superfluous, fictitious boundary) is called. In computation, the following questions are encountered immediately: how should the pseudo-boundary Γ_R be chosen, and how should the source nodes on Γ_R be located? Since some uniform distribution (*i.e.*, *via* angle or length) is often selected, the better choices of pseudo-boundaries are the theme of this chapter.

Let us address the motivation and the necessity of this study. For Laplace's equation in a bounded simply-connected domain S, the fundamental solutions are known as $\ln r = \ln|\overline{PQ}|$, where $P \in \bar{S}$ and the source nodes Q are located outside S. When the Q are located on circles in Chapter 2 (*i.e.*, the circular pseudo-boundaries), polynomial convergence rates are obtained, but condition numbers have exponential growth. For the long strip-shaped S, the Cond is so huge that it damages the accuracy of numerical solutions. In this case, it is natural to choose the source nodes located on an ellipse outside S (*i.e.*, elliptic pseudo-boundaries). The strict error and stability analysis is explored in this chapter. Polynomial convergence rates may also be achieved. Most importantly, the condition number can be reduced significantly, compared to circular pseudo-boundaries. Note that in previous chapters, for stability analysis of the MFS in 2D, the circulant matrices [71] are always employed. In this chapter, we explore new stability analysis for elliptic pseudo-boundaries in 2D, based on the new proof techniques.

Besides, the conformal transformation from a circle was suggested in [123] to yield a non-circular pseudo-boundary. The greedy adaptive techniques of Schaback [211] may select some good locations of source nodes, where no pseudo-boundaries exist.

There arises a question: how can better pseudo-boundaries be found? The criteria for evaluating numerical techniques are proposed, and the strategy for choosing source nodes is suggested as follows. The circular pseudo-boundaries are most important and efficient for the MFS in 2D; other kinds of non-circular pseudo-boundaries may also be considered when very severe instability occurs. For long strip-shaped domains, elliptic pseudo-boundaries are strongly recommended. When the solution domains are far different from circular/elliptic domains, pseudo-boundaries nearly to the domain boundary as given in Chen *et al.* [38, 139] may be employed. See Part III. Moreover, the new pseudo radial-lines are explored in the last chapter.

This chapter is organized as follows. In the next section, the algorithms of the MFS are described, where the elliptic source nodes are chosen. In Section 6.3, the error analysis is made, and the bounds of errors are derived. In Section 6.4, the bounds of Cond are derived based on new proof techniques. In Section 6.5, better choices of pseudo-boundaries are discussed. In Section 6.6, numerical experiments are carried out to verify the analysis and discussions made. In the last section, a few concluding remarks are made.

6.2 Algorithms of MFS

The elliptic coordinates (ρ,θ) are defined in [180] by (see Figure 6.1)

$$x = \sigma \cosh\rho \, \cos\theta, \quad y = \sigma \sinh\rho \, \sin\theta, \tag{6.2.1}$$

where $\sigma > 0$, $0 \le \rho < \infty$ and $0 \le \theta \le 2\pi$. When $\rho = \rho_0 \in (0,\infty)$, the equation (6.2.1) leads to an ellipse

$$\frac{x^2}{\sigma^2 \cosh^2(\rho_0)} + \frac{y^2}{\sigma^2 \sinh^2(\rho_0)} = 1,$$

with two semi-axes are $a = \sigma\cosh(\rho_0)$ and $b = \sigma\sinh(\rho_0)$. When the Cartesian coordinates (x,y) are known, the elliptic coordinates are defined from (6.2.1). The explicit formulas are derived in [180] as

$$\rho = \sinh^{-1}(F(x,y;\sigma)), \quad \theta = \arccos\left(\frac{x}{\sigma\cosh\rho}\right),$$

where

$$F(x,y;\sigma) = \frac{1}{\sqrt{2}\sigma}\sqrt{(x^2+y^2-\sigma^2) + \sqrt{(x^2+y^2-\sigma^2)^2 + 4\sigma^2 y^2}}.$$

In this chapter, consider Laplace's equation with the Dirichlet condition,

$$\Delta u = 0 \text{ in } \; S, \quad u = f \text{ on } \boldsymbol{\Gamma}, \tag{6.2.2}$$

where $f \in \mathbf{R}$ is a known function, and S a bounded simply-connected domain with a smooth boundary $\boldsymbol{\Gamma}\,(= \partial S)$. Denote two nodes $\mathbf{x} = P(\rho,\theta) = P(x,y)$ and

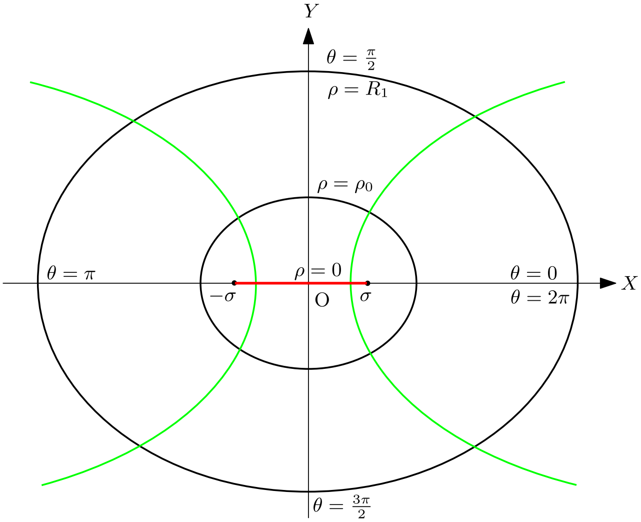

FIG. 6.1 – The elliptic coordinates with (ρ,θ), where $R_1 > \rho_0$.

$\mathbf{y} = Q(R, \phi) = Q(\xi, \eta)$, where (ρ, θ) and (R, ϕ) are the elliptic coordinates, but (x, y) and (ξ, η) are the Cartesian coordinates. Then we have the distance to the origin O,

$$\begin{aligned}|\overline{OP}|^2 &= x^2 + y^2 = \sigma^2 \cosh^2\rho \, \cos^2\theta + \sigma^2 \sinh^2\rho \, \sin^2\theta \\ &= \sigma^2\{(\sinh^2\rho + 1)\cos^2\theta + \sinh^2\rho \, \sin^2\theta\} = \sigma^2(\sinh^2\rho + \cos^2\theta).\end{aligned}$$

Similarly, for $Q_j = (R, \phi_j) = (\xi_j, \eta_j)$, the distance $|\overline{OQ_j}|^2 = \xi_j^2 + \eta_j^2 = \sigma^2(\sinh^2 R + \cos^2\phi_j)$. Then we find

$$|\overline{PQ_j}| = \sqrt{(x - \xi_j)^2 + (y - \eta_j)^2} = \sqrt{|\overline{OP}|^2 + |\overline{OQ_j}|^2 - 2\cos(\Theta_j)|\overline{OP}||\overline{OQ_j}|},$$

where $\Theta_j = \angle POQ_j$. The uniform nodes along angle as $\phi_j = \frac{2\pi}{N} j$ are also chosen. The source nodes $Q_j = (R, \phi_j)$ are chosen on an ellipse outside S with $R > \rho_{\max} = \max \rho|_\Gamma$. The FS are given by

$$\Phi_j(\rho, \theta) = \ln|\overline{PQ_j}|, \tag{6.2.3}$$

and the approximate solution can be written as a linear combination of FS

$$u_N = \sum_{j=1}^{N} c_j \Phi_j(\rho, \theta), \tag{6.2.4}$$

where c_j are the unknown coefficients to be sought by the Trefftz method (TM) in [169]. Since the functions (6.2.4) already satisfy Laplace's equation, we may establish the boundary collocation equations directly from the Dirichlet condition in (6.2.2).

Let Γ be divided into small Γ_ℓ with the meshspacing $\triangle h_\ell$, *i.e.*, $\Gamma = \bigcup_{\ell=1}^{M} \Gamma_\ell$. For simplicity, choose (ρ_ℓ, θ_ℓ) as the midpoints of Γ_ℓ. We obtain the collocation equations,

$$\sqrt{\triangle h_\ell} \sum_{j=1}^{N} c_j \Phi_j(\rho_\ell, \theta_\ell) = \sqrt{\triangle h_\ell} \, f(\rho_\ell, \theta_\ell), \;\; \ell = 1, 2, \ldots, M, \tag{6.2.5}$$

where $M \geq N$. The equations (6.2.5) lead to an overdetermined system $\mathbf{Fx} = \mathbf{b}$, where $\mathbf{F} \in \mathbf{R}^{M\times N} (M \geq N)$, $\mathbf{x} \in \mathbf{R}^N$ and $\mathbf{b} \in \mathbf{R}^M$. Let V_N be the set of FS in (6.2.4). The TM reads: to seek $u_N \in V_N$ such that

$$I(u_N) = \min_{v \in V_N} I(v), \quad I(v) = \int_\Gamma (v - f)^2. \tag{6.2.6}$$

When the integrals in (6.2.6) involve a numerical approximation, the TM reads: to seek $\tilde{u}_N \in V_N$ such that

$$\widehat{I}(\tilde{u}_N) = \min_{v \in V_N} \widehat{I}(v), \quad \widehat{I}(v) = \widehat{\int_\Gamma} (v - f)^2, \tag{6.2.7}$$

where $\widehat{\int_\Gamma}$ is a numerical approximation of $\int_\Gamma$. The equation (6.2.5) is equivalent to (6.2.7), where the central rule is chosen.

6.3 Error Analysis

6.3.1 Preliminary Lemmas

The addition theorem of FS is *essential* to analysis of the MFS. The elliptic coordinates (6.2.1) can be expressed by the complex,

$$z = x + \mathbf{i}y = \sigma \cosh w, \tag{6.3.1}$$

where $w = \rho + \mathbf{i}\theta$ and $\mathbf{i} = \sqrt{-1}$. Denote the other node in the same elliptic coordinate system (6.3.1) by

$$z_0 = x_0 + \mathbf{i}y_0 = \sigma \cosh w_0, \tag{6.3.2}$$

where $w_0 = r + \mathbf{i}\phi$. Denote $\mathbf{x} = (\rho, \theta)$ and $\mathbf{y} = (r, \phi)$. We have the addition theorem ($i.e.$, the series expansions).

Theorem 6.3.1 (Addition Theorem). *In the same elliptic coordinate system (6.2.1), let z and z_0 denote two nodes given in (6.3.1) and (6.3.2), respectively. There exist the series expansions for the FS,*

$$\begin{aligned}\ln|z - z_0| &= r + \ln\left(\frac{\sigma}{2}\right) \\ &\quad -2\sum_{n=1}^{\infty} \frac{1}{n} e^{-nr}\{\cosh(n\rho)\cos(n\theta)\cos(n\phi) + \sinh(n\rho)\sin(n\theta)\sin(n\phi)\}, \quad \rho < r,\end{aligned} \tag{6.3.3}$$

$$\begin{aligned}\ln|z - z_0| &= \rho + \ln\left(\frac{\sigma}{2}\right) \\ &\quad -2\sum_{n=1}^{\infty} \frac{1}{n} e^{-n\rho}\{\cosh(nr)\cos(n\theta)\cos(n\phi) + \sinh(nr)\sin(n\theta)\sin(n\phi)\}, \quad \rho > r.\end{aligned} \tag{6.3.4}$$

Proof. Although the basic ideas of the proof follow from Morse and Feshbach [193], the arguments below are more comprehensive and beneficial to real application. We have from (6.3.1) and (6.3.2)

$$\begin{aligned}\ln|z - z_0| &= \frac{1}{2}\ln(|z - z_0|^2) = \frac{1}{2}\ln\{\sigma^2|\cosh w - \cosh w_0|^2\} \\ &= \frac{1}{2}\ln\left\{\left(\frac{\sigma}{2}\right)^2 |e^{w} + e^{-w} - e^{w_0} - e^{-w_0}|^2\right\} \\ &= \ln\frac{\sigma}{2} + \ln\{|e^{w} + e^{-w} - e^{w_0} - e^{-w_0}|\}.\end{aligned} \tag{6.3.5}$$

There exists the equality

$$e^{w} + e^{-w} - e^{w_0} - e^{-w_0} = 4\sinh\left(\frac{w + w_0}{2}\right)\sinh\left(\frac{w - w_0}{2}\right). \tag{6.3.6}$$

Then we have from (6.3.5) and (6.3.6)

$$\ln|z-z_0| = \ln\frac{\sigma}{2} + \ln\left\{\left|2\sinh\left(\frac{w+w_0}{2}\right)\right|\right\} + \ln\left\{\left|2\sinh\left(\frac{w-w_0}{2}\right)\right|\right\}. \tag{6.3.7}$$

For $z = re^{\mathbf{i}\theta}$, we have $\ln z = \ln r + \mathbf{i}\theta$ and then

$$\ln|z| = \ln r = \Re(\ln z), \tag{6.3.8}$$

where $\Re(z)$ is the real part of complex z. From (6.3.8) we have

$$\begin{aligned}\ln\left\{\left|2\sinh\left(\frac{w+w_0}{2}\right)\right|\right\} &= \ln\left\{\left|e^{\frac{w+w_0}{2}}\left(1-e^{-(w+w_0)}\right)\right|\right\}\\ &= \Re\left(\frac{w+w_0}{2}\right) + \Re\left(\ln\left(1-e^{-(w+w_0)}\right)\right)\\ &= \Re\left(\frac{w+w_0}{2}\right) - \Re\left(\sum_{n=1}^{\infty}\frac{1}{n}e^{-n(w+w_0)}\right)\\ &= \Re\left(\frac{w+w_0}{2}\right) - \Re\left(\sum_{n=1}^{\infty}\frac{1}{n}e^{-n[\rho+r+\mathbf{i}(\theta+\phi)]}\right),\end{aligned} \tag{6.3.9}$$

where we have used the series,

$$\ln(1-z) = -\sum_{n=1}^{\infty}\frac{z^n}{n}, \quad |z|<1. \tag{6.3.10}$$

For the last term on the right hand side in (6.3.7), when $\rho < r$, we have similarly

$$\begin{aligned}\ln\left(\left|2\sinh\left(\frac{w_0-w}{2}\right)\right|\right) &= \ln\left(\left|e^{\frac{w_0-w}{2}}\left(1-e^{-(w_0-w)}\right)\right|\right)\\ &= \Re\left(\frac{w_0-w}{2}\right) + \Re(\ln(1-e^{-(w_0-w)}))\\ &= \Re\left(\frac{w_0-w}{2}\right) - \Re\left(\sum_{n=1}^{\infty}\frac{1}{n}e^{-n[r-\rho+\mathbf{i}(\phi-\theta)]}\right).\end{aligned} \tag{6.3.11}$$

Combining (6.3.9) and (6.3.11) gives

$$\begin{aligned}&\ln\left(\left|2\sinh\left(\frac{w+w_0}{2}\right)\right|\right) + \ln\left(\left|2\sinh\left(\frac{w_0-w}{2}\right)\right|\right)\\ &= \Re(w_0) - \Re\left(\sum_{n=1}^{\infty}\frac{1}{n}\left(e^{-n[\rho+r+\mathbf{i}(\theta+\phi)]} + e^{-n[r-\rho+\mathbf{i}(\phi-\theta)]}\right)\right)\\ &= r - \sum_{n=1}^{\infty}\frac{1}{n}\{e^{-n(\rho+r)}\cos n(\theta+\phi) + e^{-n(-\rho+r)}\cos n(-\theta+\phi)\}\\ &= r - 2\sum_{n=1}^{\infty}\frac{1}{n}e^{-nr}\{\cosh(n\rho)\cos(n\theta)\cos(n\phi) + \sinh(n\rho)\sin(n\theta)\sin(n\phi)\}, \text{ for } \rho < r.\end{aligned} \tag{6.3.12}$$

The first series expansion (6.3.3) follows from (6.3.7) and (6.3.12).

On the other hand, when $\rho > r$ we replace (6.3.11) by

$$\ln\left(\left|2\sinh\left(\frac{w-w_0}{2}\right)\right|\right) = \Re\left(\frac{w-w_0}{2}\right) - \Re\left(\sum_{n=1}^{\infty}\frac{1}{n}e^{-n[\rho-r+\mathbf{i}(\theta-\phi)]}\right), \tag{6.3.13}$$

and the proof for the second series expansion (6.3.4) is similar. This completes the proof of Theorem 6.3.1. ■

In elliptic coordinates, let $z = P(\rho,\theta) \in \bar{S}$ and the source nodes $z_0 = Q(R,\phi)$ with $R > \rho_{\max} = \max\ \rho|_\Gamma$. We have from (6.3.3)

$$\begin{aligned}\ln|z-z_0| = \ln|\overline{PQ}| &= R + \ln\left(\frac{\sigma}{2}\right) \\ &- 2\sum_{n=1}^{\infty}\frac{1}{n}e^{-nR}\{\cosh(n\rho)\cos(n\theta)\cos(n\phi) + \sinh(n\rho)\sin(n\theta)\sin(n\phi)\}, \quad \rho < R.\end{aligned} \tag{6.3.14}$$

The particular solutions (PS) in elliptic coordinates are given from [180],

$$u(\rho,\theta) = \alpha_0 + \sum_{k=1}^{\infty} e^{-kR}\{\alpha_k\cosh(k\rho)\cos(k\theta) + \beta_k\sinh(k\rho)\sin(k\theta)\} := P_n + R_n,$$

where the PS of degree n and their residuals are given by

$$P_n = P_n(\rho,\theta) = \alpha_0 + \sum_{k=1}^{n} e^{-kR}\{\alpha_k\cosh(k\rho)\cos(k\theta) + \beta_k\sinh(k\rho)\sin(k\theta)\}, \tag{6.3.15}$$

$$R_n = R_n(\rho,\theta) = \sum_{k=n+1}^{\infty} e^{-kR}\{\alpha_k\cosh(k\rho)\cos(k\theta) + \beta_k\sinh(k\rho)\sin(k\theta)\}, \tag{6.3.16}$$

where α_k and β_k in (6.3.15) and (6.3.16) are the exact coefficients. From [169], if the exact solution $u \in \mathbf{H}^p(S)$, then there exist the bounds,

$$\|R_n(\rho,\theta)\|_{q,\partial S} = O\left(\frac{1}{n^{p-q}}\|u\|_{p,\partial S}\right), \quad q < p, \tag{6.3.17}$$

$$\|R_n(\rho,\theta)\|_{q,\partial S} = O\left(\frac{1}{n^{p-q-\frac{1}{2}}}\|u\|_{p,S}\right), \quad q + \frac{1}{2} < p, \tag{6.3.18}$$

where $\|\cdot\|_{q,\partial S}$ and $\|\cdot\|_{q,S}$ are the Sobolev norms.

Based on (6.3.14), we obtain the following lemma from the orthogonality of trigonometric functions.

Lemma 6.3.1. *There exist the equalities,*

$$\int_0^{2\pi}\ln|\overline{PQ}|\,d\phi = 2\pi\left(R + \ln\left(\frac{\sigma}{2}\right)\right), \tag{6.3.19}$$

$$\int_0^{2\pi} \ln|\overline{PQ}|\,\cos(m\phi)\,d\phi = -\frac{2\pi}{m}\,e^{-mR}\cosh(m\rho)\cos(m\theta), \tag{6.3.20}$$

$$\int_0^{2\pi} \ln|\overline{PQ}|\,\sin(m\phi)\,d\phi = -\frac{2\pi}{m}\,e^{-mR}\sinh(m\rho)\sin(m\theta). \tag{6.3.21}$$

For $P_n(\rho,\theta)$, we may find an approximate solution $u_N^* \in V_N$. Below, we provide the explicit coefficients c_j^* in (6.2.4). By the trapezoidal rule, we obtain from Basic Lemma A in Part I

$$\begin{aligned}\int_0^{2\pi} \ln|\overline{PQ}|\,\cos(m\phi)\,d\phi &\approx h\sum_{j=1}^{N} \ln|\overline{PQ_j}|\,\cos(m\phi_j)\\ &= h\sum_{j=1}^{N} \Phi_j(\rho,\theta)\,\cos(mjh), \quad m = 0,\,1,\ldots,\end{aligned} \tag{6.3.22}$$

where $\phi_j = jh$, $h = \frac{2\pi}{N}$, and $\Phi_j(\rho,\theta)$ are given in (6.2.3). Similarly,

$$\int_0^{2\pi} \ln|\overline{PQ}|\,\sin(m\phi)\,d\phi \approx h\sum_{j=1}^{N} \Phi_j(\rho,\theta)\sin(mjh), \quad m = 1,\,2,\ldots. \tag{6.3.23}$$

From Lemma 6.3.1, (6.3.22) and (6.3.23), we find the approximation between FS and PS,

$$P_n(\rho,\theta) \approx \sum_{j=1}^{N} c_j^*\Phi_j(\rho,\theta) = u_N^* := \Sigma_N(P_n;\rho,\theta), \tag{6.3.24}$$

where the coefficients

$$c_j^* = \frac{1}{N}\left\{\frac{\alpha_0}{R+\ln\left(\frac{\sigma}{2}\right)} - \sum_{m=1}^{n} m(\alpha_m\cos(mjh) + \beta_m\sin(mjh))\right\}. \tag{6.3.25}$$

Note that the factor as $R+\ln\left(\frac{\sigma}{2}\right)$ appears in the denominator in (6.3.25), which must be nonzero. Denote by a_R and b_R two semi-axes of ellipse ℓ_R with $\rho = R$. From [180] we assume

$$R+\ln\left(\frac{\sigma}{2}\right) = \ln\left(\frac{a_R+b_R}{2}\right) \neq 0, \tag{6.3.26}$$

to give $a_R + b_R \neq 2$. We write this result as a lemma.

Lemma 6.3.2. *Suppose the exterior ellipse of source nodes satisfies* $a_R + b_R \neq 2$ *(Otherwise when* $a_R + b_R = 2$*, the degenerate scales are called). For* $P_n(\rho,\theta)$ *in*

(6.3.15), there always exists a special FS, denoted by $u_N^* = \Sigma_N(P_n;\rho,\theta)(\in V_N)$ *in (6.3.24) with the coefficients (6.3.25), such that the approximation (6.3.24) holds.*

6.3.2 Error Bounds

For $(P_n - u_N^*)$, first we evaluate the errors resulting from the approximation (6.3.22),

$$e^{-mR}\cosh(m\rho)\cos(m\theta) \approx \sum_{j=1}^{N} \alpha_{jm}\Phi_j(\rho,\theta), \quad m = 1,\, 2, \ldots,$$

where the coefficients $\alpha_{jm} = -\frac{1}{N} m \cos(mjh)$ are given from (6.3.25). Denote the errors

$$E_m(\rho,\theta) = e^{-mR}\cosh(m\rho)\cos(m\theta) - \sum_{j=1}^{N} \alpha_{jm}\Phi_j(\rho,\theta). \tag{6.3.27}$$

We expand (6.3.27) as the Fourier series,

$$E_m(\rho,\theta) = \frac{a_{0m}}{2} + \sum_{\ell=1}^{\infty}\{a_{\ell m}\,\cos(\ell\theta) + b_{\ell m}\,\sin(\ell\theta)\}, \tag{6.3.28}$$

where

$$\begin{aligned} a_{\ell m} &= \frac{1}{\pi}\int_0^{2\pi} E_m(\rho,\theta)\,\cos(\ell\theta)\,d\theta, \quad \ell = 0,\, 1, \ldots, \\ b_{\ell m} &= \frac{1}{\pi}\int_0^{2\pi} E_m(\rho,\theta)\,\sin(\ell\theta)\,d\theta, \quad \ell = 1,\, 2, \ldots. \end{aligned}$$

Lemma 6.3.3. *For the Fourier coefficients in (6.3.28), there exist the explicit Fourier coefficients:*

$$a_{\ell m} = \begin{cases} \frac{m}{\ell} e^{-R\ell}\cosh(\ell\rho), & \text{if } \ell = \pm m + \mu N,\ \mu = 1,\, 2, \ldots, \\ 0, & \text{otherwise}, \end{cases} \tag{6.3.29}$$

$$b_{\ell m} = 0, \quad \forall \ell, m. \tag{6.3.30}$$

Proof. We have from (6.3.27) and (6.3.28)

$$\begin{aligned} E_m(\rho,\theta) &= e^{-mR}\cosh(m\rho)\cos(m\theta) - \left\{-\frac{m}{N}\sum_{j=1}^{N} \ln|\overline{PQ_j}|\,\cos(mjh)\right\} \\ &= \frac{a_{0m}}{2} + \sum_{\ell=1}^{\infty}\{a_{\ell m}\,\cos(\ell\theta) + b_{\ell m}\,\sin(\ell\theta)\}, \end{aligned}$$

where

$$
\begin{aligned}
a_{\ell m} &= \frac{1}{\pi}\int_0^{2\pi}\{e^{-mR}\cosh(m\rho)\cos(m\theta)\}\cos(\ell\theta)\,d\theta \\
&\quad + \frac{m}{N\pi}\int_0^{2\pi}\left\{\sum_{j=1}^{N}\ln|\overline{PQ_j}|\right\}\cos(mjh)\cos(\ell\theta)\,d\theta := B_1 - B_2.
\end{aligned}
\tag{6.3.31}
$$

In fact, since B_2 is an approximation of B_1 by the trapezoidal rule, we have from Lemma 6.3.1

$$
\begin{aligned}
B_1 &= -\frac{1}{\pi}\int_0^{2\pi}\frac{m}{2\pi}\left\{\int_0^{2\pi}\ln|\overline{PQ}|\ \cos(m\phi)\,d\phi\right\}\cos(\ell\theta)\,d\theta \\
&= -\frac{m}{2\pi^2}\int_0^{2\pi}\left\{\int_0^{2\pi}\ln|\overline{PQ}|\ \cos(\ell\theta)\,d\theta\right\}\cos(m\phi)\,d\phi \\
&= \frac{1}{\pi}\frac{m}{\ell}\,e^{-R\ell}\cosh(\ell\rho)\int_0^{2\pi}\cos(\ell\phi)\cos(m\phi)\,d\phi.
\end{aligned}
$$

Based on Basic Lemmas A and B in Part I, we obtain from (6.3.31)

$$
\begin{aligned}
a_{\ell m} &= \frac{1}{\pi}\frac{m}{\ell}\,e^{-R\ell}\cosh(\ell\rho)\times\triangle_N(\cos(\ell\phi)\ \cos(m\phi)) \\
&= \frac{1}{\pi}\frac{m}{\ell}\,e^{-R\ell}\cosh(\ell\rho)\times\frac{1}{2}\{\triangle_N(\cos(\ell+m)\phi)+\triangle_N(\cos(\ell-m)\phi)\} \\
&= \frac{m}{\ell}\,e^{-R\ell}\cosh(\ell\rho), \quad \ell=\pm m+\mu N,\ \mu=1,\,2,\ldots,
\end{aligned}
$$

where

$$
\triangle_N(g(x)) = h\sum_{k=0}^{N-1}g(kh) - \int_0^{2\pi}g(x)\,dx.
$$

Otherwise $a_{\ell m}=0$. This is the desired result (6.3.29). Similarly, the equation (6.3.30) follows from (I.2) in Part I. This completes the proof of Lemma 6.3.3. ■

When $m=0$, we estimate the errors from (6.3.19)

$$
E_0(\rho,\theta) = 1 - \frac{1}{2\pi\left(R+\ln\left(\frac{\sigma}{2}\right)\right)}\widehat{\int_0^{2\pi}}\ln|\overline{PQ}|\,d\phi = 1 - \sum_{j=1}^{N}\alpha_{0m}\Phi_j(\rho,\theta),
$$

where $\alpha_{0m}=\frac{1}{N}\frac{1}{R+\ln(\sigma/2)}$. We have from (6.3.14)

$$\begin{aligned} E_0(\rho,\theta) &= \frac{1}{2\pi\big(R+\ln\big(\frac{\sigma}{2}\big)\big)}\left(\int_0^{2\pi} - \widehat{\int_0^{2\pi}}\right)\ln|\overline{PQ}|\,d\phi \\ &= -\frac{1}{R+\ln\big(\frac{\sigma}{2}\big)}\sum_{\mu=1}^{\infty}\frac{1}{\mu N}\,e^{-\mu NR}\cosh(\mu N\rho)\times\cos(\mu N\theta), \end{aligned}$$

to give

$$\begin{aligned} \int_0^{2\pi} E_0^2(\rho,\theta)\,d\theta &= \pi\left(\frac{1}{R+\ln\big(\frac{\sigma}{2}\big)}\right)^2\sum_{\mu=1}^{\infty}\left(\frac{1}{\mu N}\,e^{-\mu NR}\cosh(\mu N\rho)\right)^2 \\ &\le C\frac{1}{N^2}\,e^{-2NR}\big(\cosh(N\rho)\big)^2 \le C\frac{1}{N^2}\,e^{-2N(R-\rho)}, \end{aligned} \tag{6.3.32}$$

where we have used the condition (6.3.26).

Next, we evaluate the errors resulting from the approximation (6.3.23),

$$e^{-mR}\sinh(m\rho)\sin(m\theta) \approx \sum_{j=1}^{N}\beta_{jm}\Phi_j(\rho,\theta), \quad m=1,\,2,\ldots,$$

where the coefficients $\beta_{jm} = -\frac{m}{N}\sin(mjh)$ are also given from (6.3.25). Denote the errors

$$E_m^*(\rho,\theta) = e^{-mR}\sinh(m\rho)\sin(m\theta) - \sum_{j=1}^{N}\beta_{jm}\Phi_j(\rho,\theta). \tag{6.3.33}$$

We also expand (6.3.33) as the Fourier series,

$$E_m^*(\rho,\theta) = \frac{a_{0m}^*}{2} + \sum_{\ell=1}^{\infty}\{a_{\ell m}^*\cos(\ell\theta) + b_{\ell m}^*\sin(\ell\theta)\}, \tag{6.3.34}$$

$$\begin{aligned} a_{\ell m}^* &= \frac{1}{\pi}\int_0^{2\pi} E_m^*(\rho,\theta)\cos(\ell\theta)\,d\theta, \quad \ell=0,\,1,\ldots, \\ b_{\ell m}^* &= \frac{1}{\pi}\int_0^{2\pi} E_m^*(\rho,\theta)\sin(\ell\theta)\,d\theta, \quad \ell=1,\,2,\ldots. \end{aligned}$$

Similarly, we have the following lemma.

Lemma 6.3.4. *For the Fourier coefficients in (6.3.34), there exist the explicit Fourier coefficients:*

$$b_{\ell m}^* = \begin{cases} \mp\frac{m}{\ell}\,e^{-R\ell}\sinh(\ell\rho), & \text{if } \ell = \pm m + \mu N,\ \mu = 1,\,2,\ldots, \\ 0, & \text{otherwise}, \end{cases}$$

$$a_{\ell m}^* = 0, \quad \forall\,\ell, m.$$

Denote the ellipse $\Gamma_\rho = \{(r,\theta)|r=\rho, 0 \le \theta \le 2\pi\}$, $r_{\min} \le \rho \le r_{\max}$ on Γ, where (r,θ) are elliptic coordinates. We have the following theorem.

Theorem 6.3.2. *Suppose that* $u \in \mathbf{H}^p(S)$ $(p>1)$ *and the condition (6.3.26) hold. There exists the bound,*

$$\|P_n(\rho,\theta) - \Sigma_N(P_n;\rho,\theta)\|_{0,\Gamma_\rho} \le Ce^{-(R-r_{\max})(N-2n)} e^{n(r_{\max}-r_{\min})} \|P_n(\rho,\theta)\|_{0,\Gamma}, \tag{6.3.35}$$

where C *is a constant independent of* n *and* N.

Proof. Based on Lemma 6.3.3 and [180], we have

$$\begin{aligned} \|E_m(\rho,\theta)\|^2_{0,\Gamma_\rho} &= \int_0^{2\pi} E^2_m(\rho,\theta)\ \sigma\sqrt{\sinh^2\rho + \sin^2\theta}\ d\theta \\ &\le C\int_0^{2\pi} E^2_m(\rho,\theta)\,d\theta \le C\sum_{\ell=1}^{\infty} \alpha^2_{\ell m} = C \sum_{\ell=\pm m+\mu N} \left\{\frac{m}{\ell}\,e^{-R\ell}\cosh(\ell\rho)\right\}^2. \end{aligned} \tag{6.3.36}$$

Since $n\,(\ge m)$ and $N\,(>2n)$ are large, we have from $R>\rho$ and (6.3.36)

$$\begin{aligned} \|E_m(\rho,\theta)\|^2_{0,\Gamma_\rho} &\le Cm^2\left\{\sum_{\ell=-m+\mu N}\left(\frac{e^{-R\ell}}{\ell}\cosh(\ell\rho)\right)^2 + \sum_{\ell=m+\mu N}\left(\frac{e^{-R\ell}}{\ell}\cosh(\ell\rho)\right)^2\right\} \\ &\le Cm^2\left\{\frac{e^{-R(N-m)}}{N-m}\cosh((N-m)\rho)\right\}^2, \end{aligned}$$

to give

$$\begin{aligned} \|E_m(\rho,\theta)\|_{0,\Gamma_\rho} &\le Cm\frac{e^{-R(N-m)}}{N-m}\cosh((N-m)\rho) \\ &\le Ce^{-R(N-m)}\cosh((N-m)\rho) \le Ce^{-(R-\rho)(N-m)}. \end{aligned} \tag{6.3.37}$$

Note that from (6.3.32), the bound (6.3.37) is also valid for $m=0$ under the condition (6.3.26).

Similarly, from (6.3.33) and Lemma 6.3.4, we have

$$\begin{aligned} \|E^*_m(\rho,\theta)\|_{0,\Gamma_\rho} &\le Cm\frac{e^{-R(N-m)}}{N-m}\sinh((N-m)\rho) \\ &\le Ce^{-R(N-m)}\sinh((N-m)\rho) \le Ce^{-(R-\rho)(N-m)}. \end{aligned} \tag{6.3.38}$$

Hence for $\tilde{\rho} \in [r_{\min}, r_{\max}]$, we have from the Schwarz inequality

$$\begin{aligned}
&\|P_n(\rho,\theta)-\Sigma_N(P_n;\rho,\theta)\|^2_{0,\Gamma_\rho}\\
&\quad=\left\|\alpha_0E_0(\rho,\theta)+\sum_{m=1}^{n}(\alpha_mE_m(\rho,\theta)+\beta_mE^*_m(\rho,\theta))\right\|^2_{0,\Gamma_\rho}\\
&\quad\le\left\|\alpha_0E_0(\rho,\theta)+\sum_{m=1}^{n}(\alpha_me^{-mR}\cosh(m\tilde{\rho}))\frac{E_m(\rho,\theta)}{e^{-mR}\cosh(m\tilde{\rho})}\right\|^2_{0,\Gamma_\rho}\\
&\qquad+\left\|\sum_{m=1}^{n}(\beta_me^{-mR}\sin(m\tilde{\rho}))\frac{E^*_m(\rho,\theta)}{e^{-mR}\sinh(m\tilde{\rho})}\right\|^2_{0,\Gamma_\rho}\\
&\quad\le\left\{\alpha_0^2+\sum_{m=1}^{n}\alpha_m^2e^{-2mR}\cosh^2(m\tilde{\rho})\right\}\left\{\sum_{m=0}^{n}\left\{\frac{\|E_m(\rho,\theta)\|_{0,\Gamma_\rho}}{e^{-mR}\cosh(m\tilde{\rho})}\right\}^2\right\}\\
&\qquad+\left\{\sum_{m=1}^{n}\beta_m^2e^{-2mR}\sinh^2(m\tilde{\rho})\right\}\left\{\sum_{m=1}^{n}\left\{\frac{\|E^*_m(\rho,\theta)\|_{0,\Gamma_\rho}}{e^{-mR}\sinh(m\tilde{\rho})}\right\}^2\right\}.
\end{aligned}\tag{6.3.39}$$

From (6.3.37) we have

$$\begin{aligned}
\sum_{m=0}^{n}\left\{\frac{\|E_m(\rho,\theta)\|_{0,\Gamma_\rho}}{e^{-mR}\cosh(m\tilde{\rho})}\right\}^2&\le C\sum_{m=0}^{n}\Big(e^{m(R-\tilde{\rho})}e^{-(R-\rho)(N-m)}\Big)^2\\
&\le C\Big(e^{n(R-\tilde{\rho})}e^{-(R-\rho)(N-n)}\Big)^2.
\end{aligned}\tag{6.3.40}$$

When both n and $(N-n)$ are large, we have

$$e^{n(R-\tilde{\rho})}e^{-(R-\rho)(N-n)}=e^{-(R-\rho)(N-2n)}e^{n(\rho-\tilde{\rho})}\le e^{-(R-r_{\max})(N-2n)}e^{n(r_{\max}-r_{\min})}.\tag{6.3.41}$$

Combining (6.3.40) and (6.3.41) gives

$$\sum_{m=0}^{n}\left\{\frac{\|E_m(\rho,\theta)\|_{0,\Gamma_\rho}}{e^{-mR}\cosh(m\tilde{\rho})}\right\}^2\le C\Big\{e^{-(R-r_{\max})(N-2n)}e^{n(r_{\max}-r_{\min})}\Big\}^2.\tag{6.3.42}$$

Similarly, we have from (6.3.38)

$$\sum_{m=1}^{n}\left\{\frac{\|E^*_m(\rho,\theta)\|_{0,\Gamma_\rho}}{e^{-mR}\sinh(m\tilde{\rho})}\right\}^2\le C\Big\{e^{-(R-r_{\max})(N-2n)}e^{n(r_{\max}-r_{\min})}\Big\}^2.\tag{6.3.43}$$

On the other hand, there exists the bound,

$$\begin{aligned}
&\alpha_0^2 + \sum_{m=1}^{n} e^{-2mR}\{\alpha_m^2 \cosh^2(m\tilde{\rho}) + \beta_m^2 \sinh^2(m\tilde{\rho})\} \\
&\le C\int_0^{2\pi} P_n^2(\tilde{\rho},\theta)\,d\theta \le C\int_0^{2\pi}\left\{P_n^2(\tilde{\rho},\theta)\sigma\sqrt{\sinh^2\tilde{\rho}+\sin^2\theta}\right\}d\theta \\
&= C\|P_n\|_{0,\Gamma_{\tilde{\rho}}}^2 \le C\|P_n(\rho,\theta)\|_{0,\Gamma}^2.
\end{aligned} \tag{6.3.44}$$

Combining (6.3.39)–(6.3.44) gives

$$\begin{aligned}
&\|P_n(\rho,\theta) - \Sigma_N(P_n;\rho,\theta)\|_{0,\Gamma_\rho}^2 \\
&\le C\left\{\sum_{m=0}^{n}\frac{\|E_m^*(\rho,\theta)\|_{0,\Gamma_\rho}}{e^{-mR}\cosh(m\tilde{\rho})} + \sum_{m=1}^{n}\frac{\|E_m^*(\rho,\theta)\|_{0,\Gamma_\rho}}{e^{-mR}\sinh(m\tilde{\rho})}\right\} \\
&\quad\times\left\{\alpha_0^2 + \sum_{m=1}^{n} e^{-2mR}\{\alpha_m^2 \cosh^2(m\tilde{\rho}) + \beta_m^2 \sinh^2(m\tilde{\rho}\}\right\} \\
&\le C\Big\{e^{-(R-r_{\max})(N-2n)}\,e^{n(r_{\max}-r_{\min})}\|P_n(\rho,\theta)\|_{0,\Gamma_{\tilde{\rho}}}\Big\}^2 \\
&\le C\Big\{e^{-(R-r_{\max})(N-2n)}\,e^{n(r_{\max}-r_{\min})}\|P_n(\rho,\theta)\|_{0,\Gamma}\Big\}^2.
\end{aligned} \tag{6.3.45}$$

In the last bound in (6.3.45), we have used the continuity extension in Remark 2.3.1 of Chapter 2. From the smooth boundary Γ, under the assumption $u \in \mathbf{H}^p(S)$ $(p > 1)$, the solution in S can be extended continuously to the elliptic boundary $\Gamma_{r_{\max}}$. We then have $\|P_n(\rho,\theta)\|_{0,\Gamma_{\tilde{\rho}}} \le C\|P_n(\rho,\theta)\|_{0,\Gamma_{r_{\max}}} \le C\|P_n(\rho,\theta)\|_{0,\Gamma}$. This completes the proof of Theorem 6.3.2. ■

Theorem 6.3.3. *Suppose that* $u \in \mathbf{H}^p(S)$ $(p > 1)$ *and the condition (6.3.26) hold. When the large* $N\,(> 2n)$ *satisfies (6.3.51) below, the solution* u_N *from the MFS using an elliptic pseudo-boundary has the polynomial convergence rate,*

$$\|u - u_N\|_{0,\Gamma} = O\left(\frac{1}{N^{p-\frac{1}{2}}}\|u\|_{p,S}\right). \tag{6.3.46}$$

Proof. The errors for the solutions u_N from (6.2.6) are given by

$$\|u - u_N\|_{0,\Gamma} = \inf_{v\in V_N}\|u - v\|_{0,\Gamma} \le \|u - u_N^*\|_{0,\Gamma}, \tag{6.3.47}$$

where $u_N^*\,(= \Sigma_N(P_n;\rho,\theta))$ is given in (6.3.24). We have from (6.3.47) and (6.3.18)

$$\begin{aligned}
\|u - u_N\|_{0,\Gamma} &\le \|u - u_N^*\|_{0,\Gamma} \le \|P_n - u_N^*\|_{0,\Gamma} + \|R_n\|_{0,\Gamma} \\
&\le C\|P_n - u_N^*\|_{0,\Gamma_\rho} + O\left(\frac{1}{n^{p-\frac{1}{2}}}\|u\|_{p,S}\right),
\end{aligned} \tag{6.3.48}$$

where $\rho = r_{\max}$. Based on (6.3.48), the desired (6.3.46) follows provided that

$$\|P_n - u_N^*\|_{0,\Gamma_\rho} = \|P_n - \Sigma_N(P_n;\rho,\theta)\|_{0,\Gamma_\rho} = O\left(\frac{1}{n^{p-\frac{1}{2}}}\|u\|_{p,S}\right). \tag{6.3.49}$$

From Theorem 6.3.2 and (6.3.49), to satisfy (6.3.49), we may choose large N such that

$$e^{-(R-r_{\max})(N-2n)}e^{n(r_{\max}-r_{\min})} \le n^{-\left(p-\frac{1}{2}\right)}, \tag{6.3.50}$$

to give

$$N \ge 2n + \frac{n(r_{\max}-r_{\min}) + \left(p-\frac{1}{2}\right)\ln n}{R - r_{\max}}. \tag{6.3.51}$$

This completes the proof of Theorem 6.3.3. ■

Remark 6.3.1. *Based on Addition Theorem 6.3.1, the MFS can be developed for Laplace's equation in unbounded and annular domains [151], where the source nodes can be located on ellipses. The polynomial rates are also obtained by the error analysis in this section. For the ellipse ℓ_R with $\rho = R$, denote two semi-axes as $a_R = \sigma\cosh R$ and $b_R = \sigma\sinh R$; we have $e^R = \frac{a_R + b_R}{\sigma}$. Similarly, for the ellipse $\ell_{\max}$ with $\rho = r_{\max}$, denote two semi-axes as $a_{\max} = \sigma\cosh(r_{\max})$ and $b_{\max} = \sigma\sinh(r_{\max})$, and for $\ell_{\min}$ with $\rho = r_{\min}$, as $a_{\min} = \sigma\cosh(r_{\min})$ and $b_{min} = \sigma\sinh(r_{\min})$. Then the bounds (6.3.35) are rewritten as*

$$\begin{aligned} &\|P_n(\rho,\theta) - \Sigma_N(P_n;\rho,\theta)\|_{0,\Gamma_\rho} \\ &\le C\left\{\frac{a_{\max}+b_{\max}}{a_R+b_R}\right\}^{N-2n}\left\{\frac{a_{\max}+b_{\max}}{a_{\min}+b_{\min}}\right\}^{n}\|P_n(\rho,\theta)\|_{0,\Gamma}. \end{aligned} \tag{6.3.52}$$

The bounds (6.3.52) are analogous to those for the circular pseudo-boundary in Chapter 2 provided that the equivalent circles are formulated, where the radii are the mean of two-axes of ellipses. Note that the relax assumption $u \in \mathbf{H}^p(S)$ $(p > 1)$ in Theorem 6.3.3 is for strongly singular solutions. The relax assumption is applied in Chapter 16, where the strong singularity is caused by the source functions with the source nodes located near boundary Γ.

6.4 Stability Analysis

Consider the Dirichlet problem (6.2.2). We first explore the stability analysis for elliptic domains in detail. Then the stability analysis for non-elliptic domains is briefly provided. Denote an elliptic solution domain by $S_0 = \{(r,\theta)|0 \le r < \rho, 0 \le \theta < 2\pi\}$ with the elliptic boundary $\Gamma\,(= \partial S_0)$. Choose the source and the collocation nodes uniformly *via* angle θ as

$$Q_i = \{(x,y)|x = \sigma\cosh R\,\cos(ih),\ y = \sigma\sinh R\,\sin(ih)\}, \tag{6.4.1}$$

$$P_j = \{(x,y)|x = \sigma\cosh\rho\,\cos(jh),\ y = \sigma\sinh\rho\,\sin(jh)\}, \tag{6.4.2}$$

where $\rho < R$ and $h = \frac{2\pi}{N}$. The collocation equations (6.2.5) lead to

$$\sqrt{\triangle h_\ell}\sum_{j=1}^{N} c_j\Phi_j(P_\ell) = \sqrt{\triangle h_\ell}\, f(P_\ell),\ \ P_\ell \in \Gamma,\ \ \ell = 1, 2, \ldots, N, \tag{6.4.3}$$

where $\Gamma = \{(r,\theta)|r = \rho, 0 \le \theta \le 2\pi\}$, $P_\ell = (\rho, \theta_\ell)$, and c_j are unknown coefficients. The fundamental solutions $\Phi_j(P_\ell)$ are given in (6.2.3). For the ellipse Γ, there exists the equivalence for weights, $\triangle h_\ell \asymp h$, where the notation $a \asymp b$ (or $a \asymp O(b)$) with $b > 0$ means that there exist two constants $c_0\ (> 0)$ and C such that $c_0 b \le a \le Cb$. For stability, we may discuss the following simpler equations, equivalently

$$\sqrt{h}\sum_{j=1}^{N} c_j\Phi_j(P_\ell) = \sqrt{h}\, f(P_\ell),\ \ P_\ell \in \Gamma,\ \ \ell = 1, 2, \ldots, N. \tag{6.4.4}$$

Denote (6.4.4) by

$$\mathbf{Dx} = \mathbf{b}, \tag{6.4.5}$$

where $\mathbf{D} \in \mathbf{R}^{N\times N}$, $\mathbf{x} = (c_1, c_2, \ldots, c_N)^T$ and $\mathbf{b} = \sqrt{h}(f(P_1), f(P_2), \ldots, f(P_N))^T \in \mathbf{R}^N$. Note that the entries $D_{i,i\pm k}$ are various for i, so that the matrix $\mathbf{D}$ in (6.4.5) is not circulant as in Davis [71]. Stability analysis can't succeed as in Chapters 2 and 3. We have to solicit new proof approaches (called the matrix splitting techniques in this chapter). Similarly to error analysis, we will link the matrix $\mathbf{D}$ to the discrete matrix of the MPS, and use the relations (6.3.24) and (6.3.25) between FS and PS.

Let $N = 2n+1$, and consider the particular solutions (6.3.15) of order n. The simple collocation equations of the MPS on nodes (6.4.2) are given in

$$\begin{aligned}\sqrt{h}P_n(\rho,\theta_\ell) &= \sqrt{h}\left\{\alpha_0 + \sum_{k=1}^{n} e^{-kR}(\alpha_k\cosh(k\rho)\cos(k\theta_\ell) + \beta_k\sinh(k\rho)\sin(k\theta_\ell))\right\}\\ &= \sqrt{h}\, f(P_\ell),\ \ \ell = 1, 2, \ldots, N,\ \ P_\ell \in \Gamma.\end{aligned} \tag{6.4.6}$$

Denote (6.4.6) as

$$\mathbf{Gy} = \mathbf{b}, \tag{6.4.7}$$

where $\mathbf{G} \in \mathbf{R}^{N\times N}$, $\mathbf{y} = (\alpha_0, \alpha_1, \ldots, \alpha_n, \beta_1, \ldots, \beta_n)^T$ and $\mathbf{b} = \sqrt{h}(f(P_1), f(P_2), \ldots, f(P_N))^T$. From (6.4.5) and (6.4.7), we have

$$\mathbf{Dx} = \mathbf{Gy}. \tag{6.4.8}$$

The coefficient relations between $\mathbf{x}$ and $\mathbf{y}$ are found from (6.3.25) by

$$\mathbf{x} = \mathbf{Ey}, \quad \mathbf{y} = \mathbf{E}^{-1}\mathbf{x}, \tag{6.4.9}$$

where the nonsingular matrix $\mathbf{E} \in \mathbf{R}^{N\times N}$. From (6.4.8) and (6.4.9), we have $\mathbf{Dx} = \mathbf{GE}^{-1}\mathbf{x}$, and give the matrix identity,

$$\mathbf{D} = \mathbf{GE}^{-1}. \tag{6.4.10}$$

The maximal singular value $\sigma_{\max}(\mathbf{D}) = O(\sqrt{N})$ can be easily obtained, and it shall be given later. The main work is to derive the lower bound of $\sigma_{\min}(\mathbf{D})$.

Lemma 6.4.1. *For the nonsingular matrices* $\mathbf{G} \in \mathbf{R}^{N\times N}$ *and* $\mathbf{E} \in \mathbf{R}^{N\times N}$*, there exists the lower bound,*

$$\sigma_{\min}(\mathbf{D}) \geq \frac{\sigma_{\min}(\mathbf{G})}{\sigma_{\max}(\mathbf{E})}. \tag{6.4.11}$$

Proof. From (6.4.10), we have $\mathbf{D}^{-1} = \mathbf{E}\mathbf{G}^{-1}$ and give

$$\|\mathbf{D}^{-1}\| \leq \|\mathbf{E}\|\|\mathbf{G}^{-1}\|. \tag{6.4.12}$$

Since $\|\mathbf{D}^{-1}\| = \frac{1}{\sigma_{\min}(\mathbf{D})}$ and $\|\mathbf{E}\| = \sigma_{\max}(\mathbf{E})$, the equation (6.4.12) leads to

$$\frac{1}{\sigma_{\min}(\mathbf{D})} \leq \frac{\sigma_{\max}(\mathbf{E})}{\sigma_{\min}(\mathbf{G})}. \tag{6.4.13}$$

This gives the desired result (6.4.11). ■

Lemma 6.4.2. *For the MPS, there exists the bound,*

$$\sigma_{\min}(\mathbf{G}) \geq c_0 e^{-n(R-\rho)} \geq c_0 e^{-\frac{N}{2}(R-\rho)}, \tag{6.4.14}$$

where $c_0\,(>0)$ *is a constant independent of* $N\,(=2n+1)$*.*

Proof. We have from (6.4.6)

$$\mathbf{y}^T\mathbf{G}^T\mathbf{G}\mathbf{y} = \widehat{\int_0^{2\pi}} P_n^2(\rho,\theta)\,d\theta,$$

where $\widehat{\int}$ is the quadrature approximation by the trapezoidal rule. Based on Basic Lemma B in Part I, there exist no errors for $N = 2n+1$. Then we have from (6.3.15) and the orthogonality of trigonometric functions

$$\begin{aligned}
\mathbf{y}^T\mathbf{G}^T\mathbf{G}\mathbf{y} &= \widehat{\int_0^{2\pi}} P_n^2(\rho,\theta)\,d\theta = \int_0^{2\pi} P_n^2(\rho,\theta)\,d\theta \qquad (6.4.15)\\
&= \int_0^{2\pi}\left\{\alpha_0 + \sum_{k=1}^{n} e^{-kR}\{\alpha_k\cosh(k\rho)\cos(k\theta) + \beta_k\sinh(k\rho)\sin(k\theta)\}\right\}^2 d\theta\\
&= 2\pi\alpha_0^2 + \pi\sum_{k=1}^{n} e^{-2kR}\{\alpha_k^2\cosh^2(k\rho) + \beta_k^2\sinh^2(k\rho)\}\\
&\geq c_0 e^{-2nR}\sinh^2(n\rho)\times\left\{\alpha_0^2 + \sum_{k=1}^{n}(\alpha_k^2+\beta_k^2)\right\} \geq c_0 e^{-2n(R-\rho)}\times\mathbf{y}^T\mathbf{y},
\end{aligned}$$

by noting $0<\rho<R$. Then we have

$$\sigma_{\min}(\mathbf{G}) = \min_{\mathbf{y}\neq 0}\left\{\frac{\mathbf{y}^T\mathbf{G}^T\mathbf{G}\mathbf{y}}{\mathbf{y}^T\mathbf{y}}\right\}^{\frac{1}{2}} \geq c_0\, e^{-n(R-\rho)} \geq c_0\, e^{-\frac{N}{2}(R-\rho)},$$

where we have used $n=\frac{N-1}{2}$. This is the desired result (6.4.14). ■

From (6.3.25), denote matrix $\mathbf{E}\in\mathbf{R}^{N\times N}$ in (6.4.9) by

$$\begin{aligned}\mathbf{E} &= -\frac{1}{N}\begin{pmatrix} \frac{-1}{R+\ln(\sigma/2)} & \cos\phi_1 & \cdots & n\cos n\phi_1 & \sin\phi_1 & \cdots & n\sin n\phi_1 \\ \frac{-1}{R+\ln(\sigma/2)} & \cos\phi_2 & \cdots & n\cos n\phi_2 & \sin\phi_2 & \cdots & n\sin n\phi_2 \\ \vdots & \vdots & \vdots & \vdots & \vdots & \vdots & \vdots \\ \frac{-1}{R+\ln(\sigma/2)} & \cos\phi_N & \cdots & n\cos n\phi_N & \sin\phi_N & \cdots & n\sin n\phi_N \end{pmatrix} \qquad (6.4.16)\\ &= -\frac{1}{N}\mathbf{E}^*\mathrm{diag}\Big(\frac{-1}{R+\ln(\sigma/2)}, 1,\, 2, \ldots, n, 1,\, 2, \ldots, n\Big),\end{aligned}$$

where matrix $E^*\in\mathbf{R}^{N\times N}$ as

$$\mathbf{E}^* = \begin{pmatrix} 1 & \cos\phi_1 & \cdots & \cos n\phi_1 & \sin\phi_1 & \cdots & \sin n\phi_1 \\ 1 & \cos\phi_2 & \cdots & \cos n\phi_2 & \sin\phi_2 & \cdots & \sin n\phi_2 \\ \vdots & \vdots & \vdots & \vdots & \vdots & \vdots & \vdots \\ 1 & \cos\phi_N & \cdots & \cos n\phi_N & \sin\phi_N & \cdots & \sin n\phi_N \end{pmatrix}, \qquad (6.4.17)$$

where $N=2n+1$, $h=\frac{2\pi}{N}$ and $\phi_j = jh$.

Lemma 6.4.3. *For the matrix* $\mathbf{E}^*$ *in (6.4.17), there exists the bound* $\sigma_{\max}(\mathbf{E}^*)\leq\sqrt{N}$.

Proof. Denote the function $Q_n(\phi)=\alpha_0+\sum_{k=1}^n\{\alpha_k\cos k\phi+\beta_k\sin k\phi\}$, where α_k and β_k are coefficients. We have from Basic Lemma B

$$\begin{aligned}\mathbf{y}^T(\mathbf{E}^*)^T\mathbf{E}^*\mathbf{y} &= \frac{1}{h}\widehat{\int_0^{2\pi}} Q_n^2(\phi)\,d\phi = \frac{N}{2\pi}\int_0^{2\pi} Q_n^2(\phi)\,d\phi\\ &= \frac{N}{2\pi}\int_0^{2\pi}\left\{\alpha_0+\sum_{k=1}^n\{\alpha_k\cos(k\phi)+\beta_k\sin(k\phi)\}\right\}^2 d\phi \qquad (6.4.18)\\ &= N\left\{\alpha_0^2+\frac{1}{2}\sum_{k=1}^n\{\alpha_k^2+\beta_k^2\}\right\}\leq N\mathbf{y}^T\mathbf{y},\end{aligned}$$

which implies

$$\sigma_{\max}(\mathbf{E}^*) = \max_{\mathbf{y}\neq 0}\left\{\frac{\mathbf{y}^T(\mathbf{E}^*)^T\mathbf{E}^*\mathbf{y}}{\mathbf{y}^T\mathbf{y}}\right\}^{\frac{1}{2}}\leq\sqrt{N}.$$

■

For the ellipse Γ with $r=\rho$, two semi-axes are $a=\sigma\cosh\rho$ and $b=\sigma\sinh\rho$. For a larger ellipse Γ_R with $r=R>\rho$, two semi-axes are $a_R=\sigma\cosh R$ and $b_R=\sigma\sinh R$. We have the following theorem.

Theorem 6.4.1. *For the elliptic domain $S_0 = \{(r,\theta)|0 \le r < \rho, 0 \le \theta < 2\pi\}$, choose the source nodes (R,θ_j) on the ellipse Γ_R as in (6.4.1). When $R + \ln\frac{\sigma}{2} \ne 0$ (i.e., $a_R + b_R \ne 2$), there exists the bound of the condition number,*

$$\text{Cond} \le C \max\left\{\frac{1}{R+\ln\frac{\sigma}{2}}, N\right\} \times \left(\frac{e^R}{e^\rho}\right)^{\frac{N}{2}} = C \max\left\{\frac{1}{\ln\frac{a_R+b_R}{2}}, N\right\} \times \left(\frac{a_R+b_R}{a+b}\right)^{\frac{N}{2}}, \tag{6.4.19}$$

where $R > \rho$ in elliptic coordinates.

Proof. We have from (6.4.16) and Lemma 6.4.3

$$\sigma_{\max}(\mathbf{E}) \le \frac{1}{N}\max\left\{\frac{1}{R+\ln\left(\frac{\sigma}{2}\right)}, n\right\} \times \sqrt{N} \le C\frac{1}{\sqrt{N}}\max\left\{\frac{1}{R+\ln\left(\frac{\sigma}{2}\right)}, N\right\}. \tag{6.4.20}$$

Also from Lemmas 6.4.1 and 6.4.2 and (6.4.20),

$$\sigma_{\min}(\mathbf{D}) = \frac{\sigma_{\min}(\mathbf{G})}{\sigma_{\max}(\mathbf{E})} \ge c_0 e^{-\frac{N}{2}(R-\rho)} \times \sqrt{N}\max\left\{R + \ln\left(\frac{\sigma}{2}\right), \frac{1}{N}\right\}. \tag{6.4.21}$$

Next, we show

$$\sigma_{\max}(\mathbf{D}) = \sqrt{\lambda_{\max}(\mathbf{D}^T\mathbf{D})} \le C\sqrt{N}. \tag{6.4.22}$$

For $R > \rho$, the FS as $\Phi_j(\rho_\ell, \theta_\ell)$ in (6.2.3) are all bounded as $O(1)$. Then entries of the matrix $\mathbf{D}$ in (6.4.5) have $D_{ij} = O\left(\frac{1}{\sqrt{N}}\right)$. All entries of the matrix $\mathbf{D}^T\mathbf{D}$ have the bound $O(1)$, and the maximal eigenvalue $\lambda_{\max}(\boldsymbol{D}^T\mathbf{D}) \le CN$, to give the desired (6.4.22). Combining (6.4.21) and (6.4.22), we obtain the bound of the condition number

$$\begin{aligned}\text{Cond}(\mathbf{D}) = \frac{\sigma_{\max}(\mathbf{D})}{\sigma_{\min}(\mathbf{D})} \le C\frac{\sqrt{N}}{\sigma_{\min}(\mathbf{D})} &\le C \max\left\{\frac{1}{R+\ln\left(\frac{\sigma}{2}\right)}, N\right\} \times e^{\frac{N}{2}(R-\rho)} \qquad (6.4.23)\\ = C \max\left\{\frac{1}{R+\ln\left(\frac{\sigma}{2}\right)}, N\right\} \times \left(\frac{e^R}{e^\rho}\right)^{\frac{N}{2}} &= C \max\left\{\frac{1}{\ln\frac{a_R+b_R}{2}}, N\right\} \times \left(\frac{a_R+b_R}{a+b}\right)^{\frac{N}{2}},\end{aligned}$$

where we have used the equalities: $R + \ln\left(\frac{\sigma}{2}\right) = \ln\frac{a_R+b_R}{2}$ and $e^R = \frac{a_R+b_R}{\sigma}$. This is the desired bound (6.4.19), and completes the proof of Theorem 6.4.1. ∎

The above stability analysis is made for the elliptic domain S_0. For the non-elliptic domains S, we may follow [163, 222] to obtain the bounds of Cond. Suppose that there exists a positive constant $\mu\,(\ge 1)$ independent of N such that

$$\|v\|_{1,\Gamma} \le CN^\mu \|v\|_{0,\Gamma}, \quad v \in V_N, \tag{6.4.24}$$

where V_N is the set of (6.2.4), and C is a constant independent of N. Let $r_{\min} = \min\, \rho|_S$, and the ellipse $\ell_{\min}$ with $\rho = r_{\min}$. Denote its semi-axes as $a_{\min}$ and $b_{\min}$. Then we can prove the following theorem; details are omitted.

Theorem 6.4.2. *Let the condition (6.4.24) be given, and the conditions in Theorem 6.4.1 hold. For the non-elliptic domains* S*, choose the source nodes* (R, θ_j) *on ellipse* Γ_R *with* $R > \rho_{\max}$ *as in (6.4.1). Then there exists the bound,*

$$\begin{aligned}\mathrm{Cond}(\mathbf{F}) &\le CN^{\frac{\mu}{2}} \max\left\{\frac{1}{R+\ln\frac{\sigma}{2}}, N\right\} \times \left(\frac{e^R}{e^{r_{\min}}}\right)^{\frac{N}{2}}\\ &= CN^{\frac{\mu}{2}} \max\left\{\frac{1}{\ln\frac{a_R+b_R}{2}}, N\right\} \times \left(\frac{a_R+b_R}{a_{\min}+b_{\min}}\right)^{\frac{N}{2}}.\end{aligned}$$

Finally, let us compare the Cond above with that for the circular pseudo-boundaries. To avoid confusion, denote the polar coordinates by (r°, θ°) with the superscript "$\circ$" at the top in this section. Let us review the results of Li *et al.* [163]. When the source nodes are located uniformly on an exterior circle at radii $\bar{R}^\circ$ $(> \bar{r}^\circ_{\max} = \max\ r^\circ|_\Gamma)$, for the mixed type of Dirichlet and Neumann conditions on Γ in [163], we have

$$\mathrm{Cond}^\circ = O\left(N^2\left(\frac{\bar{R}^\circ}{\bar{r}^\circ_{\min}}\right)^{\frac{N}{2}}\right), \tag{6.4.25}$$

where $\bar{r}^\circ_{\min} = \min\ r^\circ|_\Gamma$. For simplicity, consider the elliptic domain S only, where the ellipse Γ has semi-axes a and b. First, choose the elliptic pseudo-boundary ℓ_R with two semi-axes a_R and b_R satisfying $a_R + b_R \neq 2$, to obtain from Theorem 6.4.1

$$\mathrm{Cond} = O\left(N\left(\frac{a_R+b_R}{a+b}\right)^{\frac{N}{2}}\right).$$

For comparison we also choose the circular pseudo-boundaries with radius $\bar{R}^\circ = a_R$. From (6.4.25) we obtain

$$\mathrm{Cond}^\circ = O\left(N^2\left(\frac{a_R}{b}\right)^{\frac{N}{2}}\right),$$

where $b = \bar{r}^\circ_{\min}$. Since $b < a$ and $b_R < a_R$, we have

$$\frac{a_R+b_R}{a+b} < \frac{a_R+a_R}{b+b} = \frac{a_R}{b},$$

which means $\mathrm{Cond} < \mathrm{Cond}^\circ$. When the ellipse Γ is long and narrow, we have $b \ll a$ and so $b_R \ll a_R$. Then we conclude

$$\frac{a_R+b_R}{a+b} \ll \frac{a_R}{b},$$

which implies $\mathrm{Cond} \ll \mathrm{Cond}^\circ$. The above conclusions also hold for the long strip-shaped domains. We state this result as a corollary.

Corollary 6.4.1. *For the long strip-shaped domains, using elliptic pseudo-boundaries in the MFS is remarkably advantageous in stability, compared with using circular pseudo-boundaries.*

Remark 6.4.1. *For Lemmas 6.4.2 and 6.4.3, we may prove them by using the discrete Fourier series in [179]. When the partition of source nodes is quasi-uniform on the angle variables, Lemmas 6.4.2 and 6.4.3 are also valid because similar proofs hold if the equalities in (6.4.15) and (6.4.18) are modified as*

$$\mathbf{y}^T\mathbf{G}^T\mathbf{G}\mathbf{y} \asymp \widehat{\int}_0^{2\pi} P_n^2(\rho,\theta)\,d\theta \asymp \int_0^{2\pi} P_n^2(\rho,\theta)\,d\theta,$$

$$\mathbf{y}^T(\mathbf{E}^*)^T\mathbf{E}^*\mathbf{y} \asymp \frac{1}{h}\widehat{\int}_0^{2\pi} Q_n^2(\phi)\,d\phi \asymp \frac{N}{2\pi}\int_0^{2\pi} Q_n^2(\phi)\,d\phi.$$

Remark 6.4.2. *Note that for the stability analysis of the MFS in Chapters 2 and 3, the circulant matrices in [71] are always employed. In this section, the discrete matrix may be split into two sub-matrices as* $\mathbf{D} = \mathbf{G}\mathbf{E}^{-1}$ *in (6.4.10) of Lemma 6.4.1, and then the estimates of Cond can be derived. Such treatment is called the matrix splitting technique. Similarly to error analysis, we first find the bounds of* Cond *for the MPS and then derive those for the MFS via their matrix relation. Moreover, by using the matrix splitting technique, it is easy to show that from* $\triangle h_\ell \asymp h$, *the discrete matrices from (6.4.3) and (6.4.4) have the same exponential growth rates in (6.4.19). Since stability analysis is a critical issue, the new proof techniques are significant and important to the MFS. The matrix splitting technique will be applied in Part III.*

6.5 Selection of Pseudo-Boundaries

First, we provide several criteria for evaluating the numerical methods (or numerical techniques): (1) accuracy, (2) stability, (3) bypassing the degenerate scales and the spurious eigenvalues, (4) wide applications, (5) complexity and CPU time, and (6) simple algorithms and easy programming. Accuracy, stability, and theoretical analysis are the most important criteria. However, high accuracy and good stability can't succeed for one method simultaneously, except in some special cases. The finite element method (FEM) owns low accuracy and good stability, but the spectral method (SM) owns high accuracy and severe instability. The null field method (NFM) and the interior field method (IFM) were proposed in [154, 180] for the circular/elliptic domains with circular/elliptic holes. High-order polynomial convergence rates are obtained, while excellent stability can also be achieved as Cond $= O(N)$, where N is the number of PS used. This is a special case because the solution domains are confined to be circular/elliptic only. The MFS and the MPS are like the SM.

Now, we discuss better locations of the source nodes for the MFS. The most important and popular location is on the circles outside S in 2D. From Chapters 2 and 3, the bounds of both errors and Cond can be derived for the bounded simply-connected domains. The optimal polynomial convergence rates are obtained.

Furthermore, exponential convergence rates can be achieved, if the solution is highly smooth. However, the Cond always grows exponentially *via* the number N of FS used. Hence, the ill-conditioning of discrete matrices from the MFS is very severe in numerical computation. If the unlimited working digits are used, no effects are caused by this ill-conditioning, and the circular pseudo-boundaries are the simplest and most efficient. See Tsai and Lin [225]. The circular pseudo-boundaries are optimal for the solution domains near disks for both accuracy and stability in real application. For arbitrary domains, the far source nodes will cause huge condition numbers, which is troublesome in real application. See Li [150]. The numerical errors of the solutions are reported in Katsurada and Okamoto [123]; the computation was terminated by huge Cond. The high accuracy and the worse instability really co-existed; it is called the trade-off principle in Wendland [243, p.208]. This is an intrinsic characteristic of highly accurate numerical algorithms, such as the SM, the MPS, and the MFS. For both analysis and computation, we conclude that the key issue for better pseudo-boundaries is stability, not accuracy.

Take the third criterion (3) for example. The degenerate scales may be easily bypassed if using circular/elliptic pseudo-boundaries; otherwise, they may occur. We give a remark.

Remark 6.5.1. *For the Dirichlet problem of Laplace's equation in 2D, there always exist unique solutions. For the boundary element method (BEM), however, there may exist multiple solutions at the logarithmic capacity* $C_\Gamma = 1$*, called the degenerate scales. For the Helmholtz equation, the MFS also suffers from spurious eigenvalues; see Chapters 7–9. For circular and elliptic pseudo-boundaries, the degenerate scales are known as* $R^\circ = 1$ *and* $a_R + b_R = 2$*, respectively. For a general pseudo-boundary* Γ_R*, the degenerate scales are unknown. When the pseudo-boundaries are neither circular nor elliptic,* Γ_R *must be chosen very carefully, so that the degenerate sales can be bypassed.*

One key concern is whether or not the severe instability will affect the accuracy. If yes, better locations of the pseudo-boundaries should be sought to reduce the severe instability significantly. In summary, we suggest the following strategies to choose the pseudo-boundaries.

I. Circular pseudo-boundaries should be considered first. If the solution domains are not far different from disks, the circular pseudo-boundaries are the best to use. For the circular pseudo-boundaries, the MFS ranks highly in all criteria except stability.
II. The elliptic pseudo-boundaries in this chapter are strongly recommended when the solution domain is long strip-shaped. See the numerical examples in the next section and [74].
III. For the singular solutions and more complicated solution domains, such as star-like and amoeba-like domains, neither circular nor elliptic pseudo-boundaries are effective. The source nodes may be located on a smooth closed contour Γ_R outside S with nearly a constant distance/ratio as shown in Chen *et al.* [38, 139]. Further study for selecting better source nodes is developed in Part III.

6.6 Numerical Experiments

Consider Motz's problem in Section 1.3, and choose

$$u_{L,N} = \sum_{j=0}^{L} D_j r^{j+\frac{1}{2}} \cos\left(j+\frac{1}{2}\right)\theta + \sum_{j=1}^{N} c_j \ln(r_j), \tag{6.6.1}$$

where D_j and c_j are unknown coefficients, and

$$r_j = |\overline{PQ_j}| = \sqrt{R^2+\rho^2-2R\rho\cos(\theta-\phi_j)}, \quad R > \rho,$$

where $P = \rho e^{\mathrm{i}\theta}$ and $Q_j = Re^{\mathrm{i}\phi_j}$. Let M denote the number of the collocation nodes along $\overline{AB}$. Then the total number of the collocation nodes on ∂S in Figure 1.2 is $m = 6M$. The number of the unknown coefficients in (6.6.1) is $(L+N+1)$. In computation we choose $m = 6M \geq L+N+1 = n$. Define the boundary errors

$$\|\epsilon\|_B = \left\{ \widehat{\int}_{\overline{AB}\cup\overline{DO}} \epsilon^2 + w^2 \widehat{\int}_{\overline{BC}\cup\overline{CD}\cup\overline{OA}} \left(\frac{\partial\epsilon}{\partial\nu}\right)^2 \right\}^{\frac{1}{2}},$$

where $\epsilon = u - u_{L,N}$ and the weight $w = \frac{1}{n}$. In this section, we choose three kinds of pseudo-boundaries: circular, elliptic, and rectangular. Choose $\left(0,\frac{1}{2}\right)$ as the origin, and $r_{\max} = \frac{\sqrt{5}}{2}$. For circular pseudo-boundaries, the numerical results are provided in Tables 1.1–1.4 of Chapter 1. In this section, choose an outside ellipse ℓ_{ell} defined by (see Figure 6.2),

$$\frac{x^2}{a_R^2} + \frac{\left(y-\frac{1}{2}\right)^2}{b_R^2} = 1, \tag{6.6.2}$$

where two semi-axes are $a_R = 2$ and $b_R = 1.5$. Moreover, choose a larger rectangle ℓ_{rect} given by (Figure 6.3)

$$\ell_{\text{rect}} = \{(x,y) | -(1+b) \leq x \leq 1+b, -b \leq y \leq 1+b\}, \tag{6.6.3}$$

with $b = 0.5$. The source nodes are located uniformly on ℓ_{ell} (or on four edges of ℓ_{rect}). Note that for ℓ_{ell}, we choose $\frac{a_R+b_R}{2} \approx R = \sqrt{3}$ for comparisons with Figure 6.2 in accuracy (see Remark 6.3.1). For ℓ_{rect}, choose the equal distance to Γ (as $b = 0.5$), which may illustrate some choices of the source nodes in Part III. The computed results are listed in Tables 6.1 and 6.2.

For Motz's problem, when the leading singular solutions in (6.6.1) with the exact coefficients D_i are removed, the rest solution $u^- = O\left(r^{L+\frac{3}{2}}\right)$ has $u^- \in \mathbf{H}^{L+\frac{5}{2}-\delta}(S)$ with $0<\delta \ll 1$ from Li *et al.* [171]. The adding singular solutions as in (6.6.1) will play a key role in high accuracy [169]. Based on Theorem 6.3.3, we obtain the theoretical estimates at $p = L+\frac{5}{2}$,

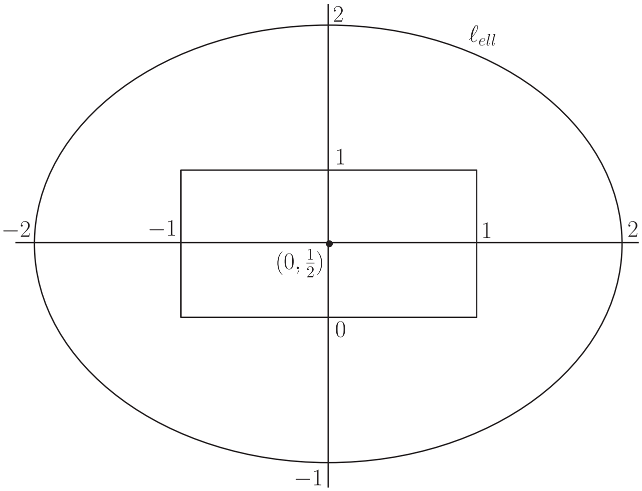

FIG. 6.2 – An outside elliptic pseudo-boundary ℓ_{ell} with $a_R = 2$ and $b_R = 1.5$.

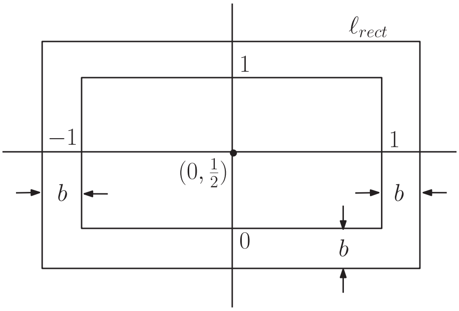

FIG. 6.3 – An outside rectangular pseudo-boundary ℓ_{rect} of S.

$$\|\epsilon\|_B = O\left(\frac{1}{N^{p-\frac{1}{2}-\delta}} \|u^-\|_{p,S}\right) = O\left(\frac{1}{N^{L+2-\delta}}\right), \quad L = 3,\ 4. \tag{6.6.4}$$

From Table 6.1, we have

$$\|\epsilon\|_B = O\left(\frac{1}{N^{10.8}}\right) = O((0.79)^N), \quad \text{Cond} = O(1.62^N). \tag{6.6.5}$$

The numerical errors (6.6.5) have higher convergence rates than (6.6.4), and the elliptic pseudo-boundaries offer better stability and accuracy.

Let us compare the numerical results between the elliptic and the rectangular pseudo-boundaries. For $N = 84, M = 60$ and $L = 4$, we cite some data from Tables 6.1 and 6.2, Tab. 6.1 – The errors and the condition numbers for Motz's problem by the MFS with (6.6.1) at $L = 4$ for the elliptic pseudo-boundary ℓ_{ell} with $a_R = 2$ and $b_R = 1.5$.

N	28	56	70	84	112
M	20	40	50	60	80
$\Vert\epsilon\Vert_B$	0.158(−2)	0.981(−6)	0.793(−7)	0.201(−7)	0.453(−8)
$\frac{\triangle D_0}{D_0}$	0.837(−4)	0.109(−6)	0.149(−6)	0.399(−7)	0.146(−7)
$\frac{\triangle D_1}{D_1}$	0.645(−2)	0.237(−4)	0.167(−4)	0.206(−5)	0.252(−6)
$\frac{\triangle D_2}{D_2}$	0.215	0.326(−2)	0.298(−2)	0.176(−2)	0.104(−2)
$\frac{\triangle D_3}{D_3}$	0.655(−1)	0.239(−1)	0.159(−1)	0.744(−2)	0.386(−2)
$\Vert\mathbf{x}\Vert$	0.113(4)	0.312(6)	0.250(8)	0.675(10)	0.116(16)
Cond	0.373(7)	0.709(13)	0.150(16)	0.268(19)	0.169(25)
Cond_eff	0.449(6)	0.227(10)	0.540(10)	0.328(11)	0.105(12)

Tab. 6.2 – The errors and the condition numbers for Motz's problem by the MFS with (6.6.1) at $L = 4$ for the rectangular pseudo-boundary ℓ_{rect} with $b = 0.5$.

N	24	60	72	84	108
M	20	40	50	60	80
$\Vert\epsilon\Vert_B$	0.224(−2)	0.831(−7)	0.144(−7)	0.621(−8)	0.158(−8)
$\frac{\triangle D_0}{D_0}$	0.652(−4)	0.665(−7)	0.299(−7)	0.169(−7)	0.647(−8)
$\frac{\triangle D_1}{D_1}$	0.544(−2)	0.542(−6)	0.304(−6)	0.411(−6)	0.373(−6)
$\frac{\triangle D_2}{D_2}$	0.306	0.214(−2)	0.143(−2)	0.107(−2)	0.659(−3)
$\frac{\triangle D_3}{D_3}$	0.444	0.402(−2)	0.336(−2)	0.235(−2)	0.111(−2)
$\Vert\mathbf{x}\Vert$	413.5	497.9	1081	8938	0.145(7)
Cond	0.189(5)	0.422(10)	0.351(12)	0.239(14)	0.227(17)
Cond_eff	0.695(4)	0.869(8)	0.306(11)	0.235(12)	0.123(13)

$$\Vert\epsilon\Vert_B = 0.201(-7), \quad \text{Cond} = 0.268(19), \quad \Vert\mathbf{x}\Vert = 0.675(10),$$

$$\Vert\epsilon\Vert_B = 0.621(-8), \quad \text{Cond} = 0.239(14), \quad \Vert\mathbf{x}\Vert = 8938.$$

The rectangular pseudo-boundaries have a better numerical performance. The improvement in accuracy is insignificant, while the improvement in stability is remarkable. The signs of coefficients c_i from the MFS change quickly (see Table 1.4 in Chapter 1). The amounts of $\Vert\mathbf{x}\Vert$ reflect one kind of stability from the subtraction cancelation. Note that $\Vert\mathbf{x}\Vert = 8938$ from Figure 6.3 is remarkably smaller than $\Vert\mathbf{x}\Vert = 0.675(10)$ from Figure 6.2. Hence, an outside pseudo-boundary $\mathbf{\Gamma}_R$ with nearly an equal distance to $\mathbf{\Gamma}$ (as in Chapter 16 and [38, 139]) may be significant to reduce the ill-conditioning. This conclusion supports the discussion on choosing the pseudo-boundaries in Section 6.5.

6.7 Concluding Remarks

To close this chapter, let us address the novelties.

1. This chapter is devoted to the MFS using non-circular pseudo-boundaries. For the elliptic pseudo-boundaries, the error bounds are given in Theorem 6.3.3 to provide the polynomial convergence rates, and the bounds of the Cond in Theorems 6.4.1 and 6.4.2 to display the exponential growth rates.
2. Compared with the stability analysis in the previous chapters, the discrete matrix is not circulant [71], and new techniques of matrix splitting are solicited. Since stability analysis is a critical issue, the new proof techniques in this chapter are important to the MFS. See Remark 6.4.2.
3. Based on the evaluation criteria for numerical techniques, the circular pseudo-boundaries should be first considered, and the elliptic pseudo-boundaries are strongly recommended for the long strip-shaped domains. The selection of better source nodes is the theme of Part III.
4. Numerical experiments are reported for Motz's problem in Section 6.6 and for the long-narrow elliptic domains in [74] to support the analysis made and the discussions in Section 6.6. More numerical examples are reported in Part III.

Part II

Helmholtz's Equations and Other Equations

Order and simplification are the first steps
toward the mastery of a subject –
the actual enemy is the unknown.
Thomas Mann, 1875–1955.

The theory of the method of fundamental solutions (MFS) has been established for Laplace's equations in Part I. It is important to extend the theory to other classic equations and problems. This is the goal of Part II, which consists of seven chapters. The MFS for Helmholtz equations has variant characteristics: the source nodes may be (or may not be) located on the domain boundary Γ, unique or multiple solutions (also called the spurious eigenvalues), and removals of spurious eigenvalues. Similarly to Part I, the error and stability analysis is made and the locations of source nodes are studied. The results are fruitful and summarized in Chapters 7–9. In Chapter 7, Bessel functions are chosen as the fundamental solutions (FS), and it is unnecessary to confine the source nodes outside the solution domain S. When the source nodes are just located on the boundary Γ, the MFS leads to the boundary knot method (BKM) in [53, 100]. Both the MFS and the boundary element method (BEM) stem from FS, and they suffer from annoying spurious eigenvalues. The new modified MFS is proposed in Chapter 8 to eliminate all spurious eigenvalues of exterior problems by the traditional MFS. In Chapter 9, the complex FS is used for the bounded multiply-connected domains, and the new modified MFS in Chapter 8 is employed for the interior source nodes. No spurious eigenvalues are confirmed and the stability analysis is made for the bounded multiply-connected domains. Chapters 7–9 provide a solid theoretical basis of the MFS for the Helmholtz equations in the exterior problems and the interior problems with simply-connected and multiply-connected domains. The MFS for modified Helmholtz equations is reported in [222]. Unique solutions always exist and the numerical characteristics are simpler than those of Helmholtz equations. Hence the theoretical results in [222] are not included in this book.

In Chapters 10–13, we study the MFS for other classic equations and problems. Chapter 10 is for biharmonic equations and error bounds are derived. Bounds of condition numbers are derived to show a high consistency between the theoretical estimates and the numerical computations. Chapter 11 is for the 2D elastic problems. The Cauchy–Navier equation of linear elastostatics is chosen, and the MFS and the hybrid Trefftz method (HTM) using FS are studied. Error analysis is made, and new addition theorems of FS in linear elastostatics are derived. Chapter 12 is for Cauchy problems of Laplace's equation. The basic analysis of classic equations in Chapters 2–11 may be extended to other kinds of complicated equations and problems; Cauchy problems are regarded as an example discussed in this book. In Chapter 13, the MFS is used for 3D Laplace's equation and basic error analysis is explored. The algorithms and analysis in Chapter 13 can also be extended to 3D Helmholtz equations.

Circular pseudo-boundaries are chosen for 2D equations in Chapters 7–12 and spherical pseudo-surfaces for 3D Laplace's equation in Chapter 13. The pseudo-boundaries and the pseudo-surfaces near the domain boundaries with an equal distance/ratio may reduce the ill-conditioning significantly; they are necessary for complicated shapes of boundary Γ and singularity problems. For non-circular pseudo-boundaries and non-spherical pseudo-surfaces, numerical tests are also provided in Chapters 8 and 13. Further analysis for Helmholtz and other equations may be developed by following the analysis in Chapters 14–16. However, once the singularity is removed, circular pseudo-boundaries and spherical pseudo-surfaces become optimal. See Chapters 1, 5 and 16. In summary, the strict analysis in Parts I and II has provided a solid theoretical basis for the MFS, to make it to become a competitive numerical method for partial differential equations (PDE).

Chapter 7

Helmholtz Equations in Simply-Connected Domains

7.1 Introduction

In this chapter, we use the method of fundamental solutions (MFS) to solve the Helmholtz equation $\Delta u + k^2 u = 0$ for a bounded simply-connected domain S, where k^2 is not exactly equal to any eigenvalue λ for the eigenvalue problem $\Delta u + \lambda u = 0$ in S with $u|_{\partial S} = 0$, but it may be close to λ. We choose the Bessel functions as admissible functions, but focus on the error and stability analysis. In the MFS, the well-known rule is that the source nodes (R, ϕ) are located outside S as $R > r_{\max}$, where $r_{\max}$ is the maximal radius of S. This rule is no longer necessary to obey for the MFS using Bessel functions. This chapter will provide a strict theoretical analysis, thus enhancing the MFS. Numerical experiments are given in [177] to support the analysis and conclusions made. This is the first novelty in this chapter.

The error analysis for the Helmholtz equation is more complicated than that for the modified Helmholtz equation in [222] since the Bessel functions $J_n(x)$ have infinite zeros. Consider the crucial and degenerate cases when $J_n(kR) \approx 0$ and $J_n(k\rho) \approx 0$. There exist few reports for the analysis of such a degeneracy. The method of particular solutions (MPS) was discussed in Li *et al.* [149] and [169, p.283] for the degeneracy case $k^2 \to \lambda_\ell$, where λ_ℓ is an eigenvalue of Laplace's operator and the bounds of errors are derived. In this chapter, the error bounds of the MFS for such a degeneracy are also explored for the bounded simply-connected domains. This is the second novelty of this chapter.

There exist spurious eigenvalues for the MFS using the Bessel and the Neumann functions. The spurious eigenvalues are called in this book for the case that the solution of the Helmholtz equation can not be found even for $k^2 \neq \{\lambda_\ell\}$, due to either the algorithm singularity or the divergence of numerical solutions. It is discovered that the MFS using Bessel and Neumann functions suffers from spurious eigenvalues. However, the MFS using Hankel functions may bypass all spurious eigenvalues; see Section 9.2. There exist many reports for the Helmholtz equation by the MFS using Hankel functions (*e.g.*, [25, 81, 194, 207, 226]), but only Barnett and Betcke

DOI: 10.1051/978-2-7598-3171-5.c007
© Science Press, EDP Sciences, 2023

[20] involved some analysis, where the errors and condition numbers are provided for disk domains by using Katsurada's approaches [120–123]. For the bounded simply-connected domains, only "*a conjecture*" is proposed in [20] that the behavior of accuracy and stability is analogous to that of disk domains.

This chapter is organized as follows. In the next section, the algorithms of the MFS using Bessel functions are described. In Section 7.3, we explore the error and stability analysis for the MFS using the Bessel functions for the Dirichlet problem. In particular, the source nodes are not necessarily located outside the solution domains, and the degeneracy is also considered. In Section 7.4, we explore the stability analysis for the MFS using Bessel functions. In the last section, we apply the analysis to the boundary knot method (BKM), where the source nodes are located just on the physical boundary Γ. For disk domains, the super-exponential growth rates of condition number (Cond) are obtained. Balancing stability and accuracy is imperative for the BKM. The materials of this chapter are adapted from [177, 250].

7.2 Algorithms

Consider the Helmholtz equation with the mixed type of Dirichlet and Neumann boundary conditions,

$$\begin{cases} \Delta u + k^2 u = 0 \text{ in } S, \\ u = f \text{ on } \Gamma_D, \\ \dfrac{\partial u}{\partial \nu} = g \text{ on } \Gamma_N, \end{cases} \tag{7.2.1}$$

where S is a bounded simply-connected domain, $\Gamma = (\Gamma_D \cup \Gamma_N)$ the smooth boundary, and ν the exterior normal of Γ_N. Denote two nodes: $\mathbf{x} = Q = (x, y) = (\rho, \theta)$ and $\mathbf{y} = P = (\xi, \eta) = (r, \phi)$ in polar coordinates. Then $x = \rho \cos\theta$, $y = \rho \sin\theta$, $\rho = \sqrt{x^2 + y^2}$, $\xi = r \cos\phi$, and $\eta = r \sin\phi$. The fundamental solutions (FS) for the Helmholtz equation are given by the Hankel function $H_0^{(1)}(kr)$ of the first kind of zero order,

$$r = |\overline{PQ}| = \sqrt{R^2 + \rho^2 - 2R\rho \cos(\theta - \phi)}, \quad R > \rho. \tag{7.2.2}$$

The Hankel functions of the first kind of order n are defined by Watson [239],

$$H_n^{(1)}(z) = J_n(z) + \mathbf{i} Y_n(z), \tag{7.2.3}$$

where $\mathbf{i} = \sqrt{-1}$, and $J_n(z)$ and $Y_n(z)$ are the Bessel and the Neumann functions of order n, respectively, defined by

$$J_\mu(z) = \sum_{i=0}^{\infty} \frac{(-1)^i}{\Gamma(i+1)\Gamma(i+\mu+1)} \left(\frac{z}{2}\right)^{2i+\mu}, \tag{7.2.4}$$

$$Y_\mu(z) = \frac{J_\mu(z)\cos(\mu\pi) - J_{-\mu}(z)}{\sin(\mu\pi)}. \tag{7.2.5}$$

For (7.2.5), when μ is an integer, the right-hand side is defined by its limit. In (7.2.4) $\Gamma(x)$ is the Gamma function defined in [1, p.255],

$$\Gamma(x) = \int_0^\infty t^{x-1} e^{-t}\, dt, \quad x > 0.$$

For integer $n \geq 0$, $\Gamma(n+1) = n!$. We also cite two useful formulas for $J_0(z)$ from [1, 90, 239],

$$J_0(z) = \frac{1}{\pi}\int_0^\pi \cos(z\, \sin\theta)\, d\theta = \frac{1}{\pi}\int_0^\pi \cos(z\, \cos\theta)\, d\theta, \tag{7.2.6}$$

$$J_0(z) = \frac{2}{\pi}\int_0^\infty \sin(z\, \cosh t)\, dt, \quad z > 0. \tag{7.2.7}$$

Since the boundary conditions in (7.2.1) are real, the solution is also real. We may choose the real Bessel functions as FS,

$$\Phi_j(\rho, \theta) = J_0(kr_j) = J_0\left(k\sqrt{R^2 + \rho^2 - 2R\rho\, \cos(\theta - \phi_j)}\right), \tag{7.2.8}$$

where $\phi_j = \frac{2\pi}{N} j$ and $Q_j = (R, \phi_j)$ are the source nodes. We formulate a linear combination,

$$u_N = \sum_{j=1}^N c_j \Phi_j(\rho, \theta), \tag{7.2.9}$$

where c_j are the real coefficients to be sought by the Trefftz method (TM) in [169]. In the traditional MFS, we have to choose the radius to satisfy (see Figure 7.1)

$$R > r_{\max}, \tag{7.2.10}$$

where $r_{\max} = \max\, r|_S$. After the analysis given later, we discover that the above condition is not necessary for the MFS using Bessel functions.

Denote by V_N the set of FS as (7.2.9). The TM reads: to seek $u_N \in V_N$ such that

$$I(u_N) = \min_{v \in V_N} I(v), \tag{7.2.11}$$

where

$$I(v) = \int_{\Gamma_D} (v - f)^2 + w^2 \int_{\Gamma_N} (v_\nu - g)^2, \tag{7.2.12}$$

where $v_\nu = \frac{\partial v}{\partial \nu}$ and $w = 1/N$ in computation. When the integrals in (7.2.12) involve a numerical approximation, the TM reads: to seek $\tilde{u}_N \in V_N$ such that

$$\widehat{I}(\tilde{u}_N) = \min_{v \in V_N} \widehat{I}(v), \tag{7.2.13}$$

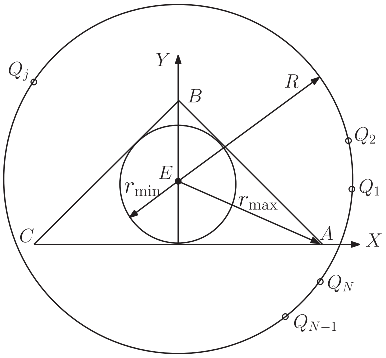

FIG. 7.1 – The source nodes Q_i for MFS.

where

$$\widehat{I}(v) = \widehat{\int}_{\Gamma_D} (v-f)^2 + w^2 \widehat{\int}_{\Gamma_N} (v_\nu - g)^2, \tag{7.2.14}$$

and $\widehat{\int}_{\Gamma_D}$ and $\widehat{\int}_{\Gamma_N}$ are the approximations of $\int_{\Gamma_D}$ and $\int_{\Gamma_N}$ by the trapezoidal rule (or the Gaussian rule), respectively.

Since v $(\in V_N)$ satisfies the Helmholtz equation already, we may establish the boundary collocation equations, directly from the Dirichlet and Neumann conditions in (7.2.1),

$$\sum_{j=1}^{N} c_j \Phi_j(\rho_\ell, \theta_\ell) = f(\rho_\ell, \theta_\ell), \quad (\rho_\ell, \theta_\ell) \in \Gamma_D, \tag{7.2.15}$$

$$\sum_{j=1}^{N} c_j \frac{\partial}{\partial \nu} \Phi_j(\rho_\ell, \theta_\ell) = g(\rho_\ell, \theta_\ell), \quad (\rho_\ell, \theta_\ell) \in \Gamma_N, \tag{7.2.16}$$

where

$$\frac{\partial}{\partial \nu} \Phi_j(\rho, \theta) = \frac{\partial}{\partial \nu} J_0(kr_j) = -kJ_1(kr_j) \frac{\partial r_j}{\partial \nu}, \tag{7.2.17}$$

where $\frac{d}{dz} J_0(z) = -J_1(z)$ and r_j are given in (7.2.8). Let Γ_D and Γ_N be divided into small Γ_D^ℓ and Γ_N^ℓ with the mesh spacing $\triangle h_\ell$: $\Gamma_D = \bigcup_{\ell=1}^{M_1} \Gamma_D^\ell$ and $\Gamma_N = \bigcup_{\ell=1}^{M_2} \Gamma_N^\ell$. We may assign some weights on both sides in (7.2.15) and (7.2.16) to give

$$\sqrt{\triangle h_\ell} \sum_{j=1}^{N} c_j \Phi_j(\rho_\ell, \theta_\ell) = \sqrt{\triangle h_\ell}\, f(\rho_\ell, \theta_\ell),\ \ell = 1, 2, ..., M_1,\ (\rho_\ell, \theta_\ell) \in \Gamma_D, \tag{7.2.18}$$

$$\begin{aligned} & w\sqrt{\triangle h_\ell}\sum_{j=1}^{N} c_j \frac{\partial}{\partial v}\Phi_j(\rho_\ell,\theta_\ell) = w\sqrt{\triangle h_\ell}\ g(\rho_\ell,\theta_\ell), \\ & \ell = M_1+1,...,M_1+M_2,\ (\rho_\ell,\theta_\ell)\in\Gamma_N. \end{aligned} \tag{7.2.19}$$

The total number of collocation equations is $M = M_1 + M_2$. The equations (7.2.18) and (7.2.19) are just equivalent to (7.2.13) and (7.2.14), where the trapezoidal (or the central) rule is chosen for $\widehat{\int}_{\Gamma_D}$ and $\widehat{\int}_{\Gamma_N}$. We may also assign other weights on both sides in (7.2.15) and (7.2.16) by the Gaussian rule [169]. For real solutions, we may also choose the MFS using the Neumann functions in (7.2.5), and the corresponding algorithms as well as a brief analysis are provided in [177]. Below, we only explore the analysis for the MFS using Bessel functions.

7.3 Error Analysis for Bessel Functions

The error analysis of the Helmholtz equation is more challenging than that for the modified Helmholtz equation in [222] since the Bessel functions $J_n(x)$ have infinite zeros. For an easy exploration of the analysis, in Section 7.3.2, we first discuss the simple case of small k (*i.e.*, low frequency of long-wavelength) such that $J_n(kR)$ and $J_n(k\rho)$ used are all positive. Then we discuss the bounded k in Section 7.3.3, and explore the crucial and degenerate cases when $J_n(kR) \approx 0$ and $J_n(k\rho) \approx 0$.

7.3.1 Preliminary Lemmas

From Watson [239, p.361], there exists the addition theorem for $R > \rho$,

$$H_0^{(1)}\left(k\sqrt{R^2+\rho^2-2R\rho\,\cos(\theta-\phi)}\right) = \sum_{m=-\infty}^{\infty} H_m^{(1)}(kR)J_m(k\rho)\cos m(\theta-\phi). \tag{7.3.1}$$

From (7.2.3), we obtain the addition theorem for real functions

$$J_0\left(k\sqrt{R^2+\rho^2-2R\rho\,\cos(\theta-\phi)}\right) = \sum_{m=-\infty}^{\infty} J_m(kR)J_m(k\rho)\cos m(\theta-\phi). \tag{7.3.2}$$

Since $J_{-m}(z) = (-1)^m J_m(z)$, we have

$$\begin{aligned} & J_0\left(k\sqrt{R^2+\rho^2-2R\rho\,\cos(\theta-\phi)}\right) \\ & = J_0(kR)J_0(k\rho) + 2\sum_{m=1}^{\infty} J_m(kR)J_m(k\rho)\cos m(\theta-\phi). \end{aligned} \tag{7.3.3}$$

Note that in [239, p.361], the condition $R > \rho$ is needed for (7.3.1) using Hankel functions, but not for (7.3.3) using Bessel functions.

Based on (7.3.3), we have the following lemma from the orthogonality of trigonometric functions.

Lemma 7.3.1. *There exist the equalities,*

$$\int_0^{2\pi} J_0\left(k\sqrt{R^2+\rho^2-2R\rho\,\cos(\theta-\phi)}\right)d\phi = 2\pi J_0(kR)J_0(k\rho), \tag{7.3.4}$$

$$\int_0^{2\pi} J_0\left(k\sqrt{R^2+\rho^2-2R\rho\,\cos(\theta-\phi)}\right)\cos(m\phi)\,d\phi = 2\pi J_m(kR)J_m(k\rho)\cos(m\theta), \tag{7.3.5}$$

$$\int_0^{2\pi} J_0\left(k\sqrt{R^2+\rho^2-2R\rho\,\cos(\theta-\phi)}\right)\sin(m\phi)\,d\phi = 2\pi J_m(kR)J_m(k\rho)\sin(m\theta). \tag{7.3.6}$$

The solutions of the Helmholtz equation can also be expressed by

$$u(\rho,\theta) = P_n(\rho,\theta) + R_n(\rho,\theta), \tag{7.3.7}$$

where the particular solutions (PS) of degree n are given by

$$P_n(\rho,\theta) = J_0(k\rho)a_0 + \sum_{m=1}^{n} J_m(k\rho)\{a_m\,\cos(m\theta) + b_m\,\sin(m\theta)\}, \tag{7.3.8}$$

and the residual

$$R_n(\rho,\theta) = \sum_{m=n+1}^{\infty} J_m(k\rho)\{a_m\,\cos(m\theta) + b_m\,\sin(m\theta)\}. \tag{7.3.9}$$

The coefficients a_m and b_m in (7.3.8) and (7.3.9) are the exact coefficients. From [169], if the solution satisfies $u \in \mathbf{H}^p(S)$, then there exist the bounds,

$$\|R_n(\rho,\theta)\|_{q,S} = O\left(\frac{1}{n^{p-q}}\|u\|_{p,S}\right), \quad q<p, \tag{7.3.10}$$

$$\|R_n(\rho,\theta)\|_{q,\partial S} = O\left(\frac{1}{n^{p-q-\frac{1}{2}}}\|u\|_{p,S}\right), \quad q<p. \tag{7.3.11}$$

For $P_n(\rho,\theta)$, we may find an approximate solution $u_N^* \in V_N$. Below we provide the explicit coefficients c_j in (7.2.9). By the trapezoidal rule, we obtain from Lemma 2.2.1

$$\begin{aligned}&\int_0^{2\pi} J_0\left(k\sqrt{R^2+\rho^2-2R\rho\,\cos(\theta-\phi)}\right)d\phi\\ &\approx h\sum_{j=1}^{N} J_0\left(k\sqrt{R^2+\rho^2-2R\rho\,\cos(\theta-\phi_j)}\right),\end{aligned} \tag{7.3.12}$$

where $h = \frac{2\pi}{N}$ and $\phi_j = jh$. Similarly, we have

$$\begin{aligned}&\int_0^{2\pi} J_0\Big(k\sqrt{R^2+\rho^2-2R\rho\,\cos(\theta-\phi)}\Big)\cos(m\phi)\,d\phi\\&\approx h\sum_{j=1}^{N} J_0\Big(k\sqrt{R^2+\rho^2-2R\rho\,\cos(\theta-\phi_j)}\Big)\cos(mjh),\end{aligned}\tag{7.3.13}$$

and

$$\begin{aligned}&\int_0^{2\pi} J_0\Big(k\sqrt{R^2+\rho^2-2R\rho\,\cos(\theta-\phi)}\Big)\sin(m\phi)\,d\phi\\&\approx h\sum_{j=1}^{N} J_0\Big(k\sqrt{R^2+\rho^2-2R\rho\,\cos(\theta-\phi_j)}\Big)\sin(mjh).\end{aligned}\tag{7.3.14}$$

From Lemma 7.3.1 and (7.3.12)–(7.3.14), we may approximate (7.3.8) by

$$P_n(\rho,\theta) \approx \sum_{j=1}^{N} c_j^*\Phi_j(\rho,\theta) = u_N^* := \Sigma_N(P_n;\rho,\theta),\tag{7.3.15}$$

where $\Phi_j(\rho,\theta)$ are given in (7.2.8), and the coefficients

$$\begin{aligned}c_j^* &= \frac{h}{2\pi}\left\{\frac{a_0}{J_0(kR)} + \sum_{m=1}^{n}\frac{1}{J_m(kR)}\{a_m\,\cos(mjh) + b_m\,\sin(mjh)\}\right\}\\&= \frac{1}{N}\left\{\frac{a_0}{J_0(kR)} + \sum_{m=1}^{n}\frac{1}{J_m(kR)}\{a_m\,\cos(mjh) + b_m\,\sin(mjh)\}\right\},\end{aligned}\tag{7.3.16}$$

provided that all $J_i(kR) \neq 0$. We write this result as a lemma.

Lemma 7.3.2. *Let all $J_i(kR) \neq 0$. Then for $P_n(\rho,\theta)$ there always exists a special FS, denoted as $u_N^* = \Sigma_N(P_n;\rho,\theta)$ ($\in V_N$) with the coefficients (7.3.16), such that the approximation (7.3.15) holds.*

Denote by $j_{n,k}$ the kth zero of $J_n(z)$. It is known that the minimal zero of $J_0(z)$ is given in [1] as $j_{0,1} = 2.4048255577$. When $0<z<j_{0,1}$, we have

$$J_i(z) > 0, \quad i = 0, 1, \ldots.\tag{7.3.17}$$

Hence, we may choose $kR<j_{0,1}$ such that all $J_i(kR) \neq 0$. For small z, there exists the formula in Watson [239, p.33],

$$J_n^2(z) = \frac{(\frac{1}{2}z)^{2n}}{(n!)^2}\left\{1 - \frac{T_2 z^2}{(2n+1)} + \frac{T_4 z^4}{1\cdot 2\cdot (2n+1)(2n+2)} - \cdots\right\},\tag{7.3.18}$$

where

$$T_2 = \frac{2n+1}{2n+2}, \quad T_4 = \frac{(2n+1)(2n+3)}{(2n+2)(2n+4)}, \ldots.\tag{7.3.19}$$

In fact, for $|z| < 2$ we have from (7.3.19)

$$|J_n(z)| \approx \frac{1}{n!}\left(\frac{z}{2}\right)^n. \tag{7.3.20}$$

The approximation (7.3.20) can also be obtained from (7.2.4). Hence we may require a small k such that $kR < 2$. Such a condition may guarantee (7.3.17) and (7.3.20). Below by the MFS in (7.2.13), we may seek the Helmholtz solutions first for the small k (*e.g.*, $k^2 < \lambda_{\min}$) of the sample in Section 7.3.2. Note that the small R is also assumed in [230].

The transverse vibration of a plane homogeneous membrane is described as the wave equation by (see [223])

$$\frac{\partial^2 w}{\partial t^2} = a^2 \Delta w, \tag{7.3.21}$$

where constant a^2 (> 0) is the membrane tension divided by the membrane density. Let $w = ue^{\mathrm{i}\omega t}$, the equation (7.3.21) leads to the Helmholtz equation (7.2.1), where $k = \frac{\omega}{a}$. Hence small k reflects a low frequency of long wavelength, and the error analysis in the next subsection also has some physical application.

7.3.2 Error Bounds with Small k

In this subsection, for small k, we provide the error analysis for the bounded simply-connected domain S. For simplicity, consider the Dirichlet problem,

$$\begin{cases} \Delta u + k^2 u = 0 \text{ in } S, \\ u = f \text{ on } \Gamma, \end{cases}$$

where $\Gamma = \partial S$ (*i.e.*, $\Gamma_N = \varnothing$ and $\Gamma_D = \Gamma$). From (7.2.11) we have

$$\|u - u_N\|_{0,\Gamma} = \inf_{v \in V_N} \|u - v\|_{0,\Gamma}. \tag{7.3.22}$$

Choose $v = u_N^*$, where u_N^* is given in (7.3.15). Then we have from (7.3.22)

$$\begin{aligned} \|u - u_N\|_{0,\Gamma} \le \|u - u_N^*\|_{0,\Gamma} &\le \|P_n - u_N^*\|_{0,\Gamma} + \|R_n\|_{0,\Gamma} \\ &= \|P_n - u_N^*\|_{0,\Gamma} + O\left(\frac{1}{n^{p-\frac{1}{2}}}\|u\|_{p,S}\right), \end{aligned} \tag{7.3.23}$$

where we have used (7.3.11). It is natural to request the errors

$$\|P_n - u_N^*\|_{0,\Gamma} = O\left(\frac{1}{n^{p-\frac{1}{2}}}\|u\|_{p,S}\right). \tag{7.3.24}$$

We only derive the errors from (7.3.12) and (7.3.13) because the errors from (7.3.14) are similar. We have

$$J_m(k\rho)\cos(m\theta) \approx \sum_{j=1}^{N} \alpha_{jm}\Phi_j(\rho,\theta), \quad m = 0,1,2,..., \tag{7.3.25}$$

where the coefficients in (7.3.25) are given from (7.3.16)

$$\alpha_{jm} = \frac{1}{N}\frac{\cos(mjh)}{J_m(kR)}, \quad J_m(kR) \neq 0. \tag{7.3.26}$$

Denote the errors

$$E_m(\rho,\theta) = J_m(k\rho)\cos(m\theta) - \sum_{j=1}^{N} \alpha_{jm}\Phi_j(\rho,\theta). \tag{7.3.27}$$

To derive the errors (7.3.27), we may expand (7.3.27) as the Fourier series,

$$E_m(\rho,\theta) = \frac{a_{0m}}{2} + \sum_{\ell=1}^{\infty}\{a_{\ell m}\cos(\ell\theta) + b_{\ell m}\sin(\ell\theta)\}, \tag{7.3.28}$$

where

$$a_{\ell m} = \frac{1}{\pi}\int_0^{2\pi} E_m(\rho,\theta)\cos(\ell\theta)\,d\theta, \quad \ell = 0,1,...,$$

$$b_{\ell m} = \frac{1}{\pi}\int_0^{2\pi} E_m(\rho,\theta)\sin(\ell\theta)\,d\theta, \quad \ell = 1,2,....$$

Lemma 7.3.3. *Suppose that* $k^2 \neq \lambda_j$, *where* λ_j *is an eigenvalue of*

$$-\Delta u = \lambda u \text{ in } S, \quad u = 0 \text{ on } \Gamma.$$

When kR *is small such that all* $J_m(kR) \neq 0$, *for the Fourier coefficients in (7.3.28), there exist the explicit Fourier coefficients,*

$$a_{\ell m} = \begin{cases} \pi\frac{J_\ell(kR)J_\ell(k\rho)}{J_m(kR)}, & \text{if } \ell = \pm m + \mu N, \quad \mu = 1,2,..., \\ 0, & \textit{otherwise}, \end{cases} \tag{7.3.29}$$

$$b_{\ell m} = 0, \quad \forall \ell, m. \tag{7.3.30}$$

Proof. We have from (7.3.27) and (7.3.28)

$$\begin{aligned} E_m(\rho,\theta) &= J_m(k\rho)\cos(m\theta) \\ &\quad - \frac{1}{N}\frac{1}{J_m(kR)}\sum_{j=1}^{N} J_0\left(k\sqrt{R^2+\rho^2-2R\rho\cos(\theta-jh)}\right)\cos(mjh) \\ &= \frac{a_{0m}}{2} + \sum_{\ell=1}^{\infty}\{a_{\ell m}\cos(\ell\theta) + b_{\ell m}\sin(\ell\theta)\}, \end{aligned}$$

where

$$
\begin{aligned}
a_{\ell m} &= \int_0^{2\pi} J_m(k\rho)\cos(m\theta)\cos(\ell\theta)\,d\theta \qquad (7.3.31)\\
&\quad - \frac{1}{N}\frac{1}{J_m(kR)}\int_0^{2\pi}\left\{\sum_{j=1}^{N} J_0\left(k\sqrt{R^2+\rho^2-2R\rho\,\cos(\theta-jh)}\right)\cos(mjh)\cos(\ell\theta)\right\}d\theta\\
&:= B_1 - B_2.
\end{aligned}
$$

In fact, since B_2 is the approximation of B_1 by the trapezoidal rule, we have from Lemma 7.3.1

$$
\begin{aligned}
B_1 &= \int_0^{2\pi}\frac{1}{2\pi J_m(kR)}\left\{\int_0^{2\pi} J_0\left(k\sqrt{R^2+\rho^2-2R\rho\,\cos(\theta-\phi)}\right)\cos(m\phi)\,d\phi\right\}\cos(\ell\theta)\,d\theta\\
&= \frac{1}{2\pi J_m(kR)}\int_0^{2\pi}\left\{\int_0^{2\pi} J_0\left(k\sqrt{R^2+\rho^2-2R\rho\,\cos(\theta-\phi)}\right)\cos(\ell\theta)\,d\theta\right\}\cos(m\phi)\,d\phi\\
&= \frac{J_\ell(kR)J_\ell(k\rho)}{J_m(kR)}\int_0^{2\pi}\cos(\ell\phi)\cos(m\phi)\,d\phi.
\end{aligned}
$$

Also based on Basic Lemmas A and B in Part I, we obtain from (7.3.31)

$$
\begin{aligned}
a_{\ell m} &= \frac{J_\ell(kR)J_\ell(k\rho)}{J_m(kR)}\triangle_N(\cos(\ell\phi)\cos(m\phi))\\
&= \frac{J_\ell(kR)J_\ell(k\rho)}{2J_m(kR)}\{\triangle_N(\cos(\ell+m)\phi)+\triangle_N(\cos(\ell-m)\phi)\}\\
&= \pi\frac{J_\ell(kR)J_\ell(k\rho)}{J_m(kR)}, \quad \ell=\pm m+\mu N, \quad \mu=1,2,...,
\end{aligned}
$$

where

$$
\triangle_N(g(x)) = h\sum_{k=0}^{N-1} g(kh) - \int_0^{2\pi} g(x)\,dx.
$$

Otherwise we have $a_{\ell m}=0$. This is the desired result (7.3.29). Similarly, the equation (7.3.30) follows from (I.2) in Part I. ■

Denote the circle $\Gamma_\rho = \{(r,\theta)|r=\rho, 0\le\theta\le 2\pi\}$ with $r_{\min}\le\rho\le r_{\max}$, where $r_{\min}=\min\,\rho|_\Gamma$ and $r_{\max}=\max\,\rho|_\Gamma$. We have the following theorem.

Theorem 7.3.1. *Let k be small and $k^2\neq\{\lambda_j\}$ such that for $m=0,1,2,...,$*

$$
J_m(kR)\neq 0, \qquad (7.3.32)
$$

$$
J_m(k\rho)\neq 0, \quad r_{\min}\le\rho\le r_{\max}. \qquad (7.3.33)
$$

For $u\in\mathbf{H}^p(S)$ $(p>1)$, there exists the bound,

$$\|P_n(\rho,\theta)-\Sigma_N(P_n;\rho,\theta)\|_{q,\Gamma}\le C\sqrt{n}N^q\,\frac{|J_{N-n}(kr_{\max})J_{N-n}(kR)|}{\mathcal{T}_n}\,\|P_n(\rho,\theta)\|_{0,\Gamma}, \tag{7.3.34}$$

where C is a constant independent of n, N and λ (>0), and

$$\mathcal{T}_n=\frac{1}{n!}\left(\frac{kR}{2}\right)^n\times\frac{1}{n!}\left(\frac{kr_{\min}}{2}\right)^n. \tag{7.3.35}$$

Proof. Based on (7.3.27) and (7.3.29), we have

$$\|E_{jm}(\rho,\theta)\|^2_{q,\Gamma}\le C\sum_{\ell=1}^{\infty}\ell^{2q}\alpha^2_{\ell m}=C\pi^2\sum_{\ell=\pm m+\mu N}\ell^{2q}\left\{\frac{J_\ell(kR)J_\ell(k\rho)}{J_m(kR)}\right\}^2. \tag{7.3.36}$$

From [1, pp.360,365], when n is large and kr is bounded, there exist the approximations,

$$J_n(kr)\approx\frac{1}{\sqrt{2\pi n}}\left(\frac{ekr}{2n}\right)^n\approx\frac{1}{n!}\left(\frac{kr}{2}\right)^n. \tag{7.3.37}$$

Since both n $(\ge m)$ and N $(>2n)$ are large, we have from (7.3.36) and (7.3.37)

$$\begin{aligned}\|E_m(\rho,\theta)\|^2_{q,\Gamma}&\le C\frac{\pi^2}{J^2_m(kR)}\left\{\sum_{\ell=-m+\mu N}\ell^{2q}J^2_\ell(kR)J^2_\ell(k\rho)+\sum_{\ell=m+\mu N}\ell^{2q}J^2_\ell(kR)J^2_\ell(k\rho)\right\}\\&\le C\frac{N^{2q}}{J^2_m(kR)}J^2_{N-m}(kR)J^2_{N-m}(k\rho),\end{aligned}$$

to give

$$\|E_m(\rho,\theta)\|_{q,\Gamma}\le C\frac{N^q}{J_m(kR)}J_{N-m}(kR)J_{N-m}(k\rho). \tag{7.3.38}$$

Also for $\widetilde{\rho}\in[r_{\min},r_{\max}]$, we have from the Schwarz inequality

$$\begin{aligned}&\|P_n(\rho,\theta)-\Sigma_N(P_n;\rho,\theta)\|^2_{q,\Gamma_\rho}\\&\le\left\{a_0^2J_0^2(k\tilde{\rho})+\sum_{m=1}^{n}(a_m^2+b_m^2)J^2_m(k\tilde{\rho})\right\}\left\{\sum_{m=0}^{n}\frac{\|E_m(\rho,\theta)\|^2_{q,\Gamma_\rho}}{J^2_m(k\tilde{\rho})}\right\}.\end{aligned} \tag{7.3.39}$$

From (7.3.38),

$$\sum_{m=0}^{n}\frac{1}{J^2_m(k\tilde{\rho})}\|E_m(\rho,\theta)\|^2_{q,\Gamma_\rho}\le CN^{2q}\sum_{m=0}^{n}\left(\frac{J_{N-m}(k\rho)J_{N-m}(kR)}{J_m(kR)J_m(k\tilde{\rho})}\right)^2. \tag{7.3.40}$$

When both n and $(N-n)$ are large, the nominator in (7.3.40) has the bounds,

$$J_{N-m}(k\rho)J_{N-m}(kR) \le J_{N-n}(k\rho)J_{N-n}(kR) \le J_{N-n}(kr_{\max})J_{N-n}(kR). \qquad (7.3.41)$$

For small x (< 2) we may use the approximation (7.3.20) of Bessel functions. Since the functions $|J_m(kR)J_m(kr)|$ are decreasing *via* m but increasing *via* r, from (7.3.37) we have for $m \le n$

$$\begin{aligned} |J_m(kR)J_m(kr)| &\ge |J_n(kR)J_n(kr)| \ge |J_n(kR)J_n(kr_{\min})| \\ &\approx \frac{1}{2\pi n}\left(\frac{e^2k^2Rr_{\min}}{2^2n^2}\right)^n \approx \frac{1}{n!}\left(\frac{kR}{2}\right)^n \times \frac{1}{n!}\left(\frac{kr_{\min}}{2}\right)^n = \mathcal{T}_n. \end{aligned} \qquad (7.3.42)$$

Then from (7.3.40)–(7.3.42),

$$\sum_{m=0}^{n} \frac{1}{J_m^2(k\tilde{\rho})}\|E_m(\rho,\theta)\|^2_{q,\Gamma_\rho} \le CnN^{2q}\left(\frac{J_{N-n}(kr_{\max})J_{N-n}(kR)}{\mathcal{T}_n}\right)^2. \qquad (7.3.43)$$

On the other hand, there also exists the bound from the continuity extension in Remark 2.3.1 in Chapter 2,

$$J_0^2(k\tilde{\rho})a_0^2 + \sum_{m=1}^{n}(a_m^2+b_m^2)J_m^2(k\tilde{\rho}) \le C\|P_n(\tilde{\rho},\theta)\|^2_{0,\Gamma_{\tilde{\rho}}} \le C\|P_n(\rho,\theta)\|^2_{0,\Gamma}. \qquad (7.3.44)$$

Combining (7.3.39), (7.3.43) and (7.3.44) gives (7.3.34). ■

Theorem 7.3.2. *Let the conditions in Theorem 7.3.1 hold. Assume that* $u \in \mathbf{H}^p(S)$ $(p \ge \frac{3}{2})$ *and choose the* N *as* (7.3.49) *below to satisfy*

$$T_n = \sqrt{n}\,\frac{|J_{N-n}(kr_{\max})J_{N-n}(kR)|}{\mathcal{T}_n} \le \frac{1}{n^{p-\frac{1}{2}}}. \qquad (7.3.45)$$

Then there exists the error bound,

$$\|P_n(\rho,\theta) - \Sigma_N(P_n;\rho,\theta)\|_{0,\Gamma} = O\left(\frac{1}{N^{p-\frac{1}{2}}}\|P_n(\rho,\theta)\|_{0,\Gamma}\right). \qquad (7.3.46)$$

Proof. When (7.3.45) is satisfied, the bound (7.3.46) is obtained from Theorem 7.3.1. Below, we find the detailed N. We may choose N with the help of (7.3.37), to have

$$\begin{aligned} T_n &\approx \frac{n^{1.5}}{N-n}\,\frac{\left(\frac{ekr_{\max}}{2(N-n)}\right)^{N-n}\left(\frac{ekR}{2(N-n)}\right)^{N-n}}{\left(\frac{ekr_{\min}}{2n}\right)^n\left(\frac{ekR}{2n}\right)^n} \\ &= \frac{n^{1.5}}{N-n}\,\frac{\left(\frac{e^2k^2r_{\max}R}{2^2(N-n)^2}\right)^{N-n}}{\left(\frac{e^2k^2r_{\min}R}{2^2n^2}\right)^n} = \frac{n^{1.5}}{N-n}\left(\frac{e^2k^2r_{\max}R}{2^2(N-n)^2}\right)^{N-2n}\left(\left(\frac{n}{N-n}\right)^2\frac{r_{\max}}{r_{\min}}\right)^n. \end{aligned}$$

Since $N > 2n$, we have $\frac{n}{N-n} < 1$ and $N-n > n$, to give

$$T_n \le \sqrt{n}\left(\frac{e^2k^2r_{\max}R}{2^2n^2}\right)^{N-2n}\left(\frac{r_{\max}}{r_{\min}}\right)^n. \tag{7.3.47}$$

To satisfy (7.3.45), we may request

$$\left(\frac{e^2k^2r_{\max}R}{2^2n^2}\right)^{N-2n}\left(\frac{r_{\max}}{r_{\min}}\right)^n \le \frac{1}{n^p}. \tag{7.3.48}$$

This gives

$$N \ge 2n + \frac{n\,\ln\left(\frac{r_{\max}}{r_{\min}}\right) + p\,\ln(n)}{\ln\left(\frac{2^2n^2}{e^2k^2r_{\max}R}\right)}. \tag{7.3.49}$$

Since

$$\frac{n\,\ln\left(\frac{r_{\max}}{r_{\min}}\right) + p\,\ln(n)}{\ln\left(\frac{2^2n^2}{e^2k^2r_{\max}R}\right)} \le Cn,$$

we may choose N such that $N < Cn$. Hence, from $N > 2n$ and $N \le Cn$, we conclude

$$N \asymp n, \tag{7.3.50}$$

where the notation "$a \asymp b$" denotes that there exist two constants $C_1(>0)$ and C_2 independent of n such that $C_1 b \le a \le C_2 b$. From Theorem 7.3.1 at $q = 0$ and (7.3.50), we obtain (7.3.46) and complete the proof of Theorem 7.3.2. ■

Since $P_n \approx u$, we have

$$\|P_n(\rho,\theta)\|_{0,\Gamma} \le C\|u\|_{0,\Gamma} \le C\|u\|_{\frac{1}{2},S} \le C\|u\|_{p,S}.$$

Then there exists the asymptote,

$$\|P_n(\rho,\theta) - u_N^*\|_{0,\Gamma} = O\left(\frac{1}{N^{p-\frac{1}{2}}}\|u\|_{p,S}\right). \tag{7.3.51}$$

We have from (7.3.51) and (7.3.11)

$$\|u - u_N\|_{0,\Gamma} \le \|u - u_N^*\|_{0,\Gamma} \le \|P_n(\rho,\theta) - u_N^*\|_{0,\Gamma} + \|R_n\|_{0,\Gamma} \le C\frac{1}{N^{p-\frac{1}{2}}}\|u\|_{p,S}. \tag{7.3.52}$$

We have the following theorem.

Theorem 7.3.3. *Suppose that* $u \in \mathbf{H}^p(S)$ $\left(p \ge \frac{3}{2}\right)$ *and the conditions in Theorem 7.3.1 hold. For small* k*, when the* N $(> 2n)$ *satisfies (7.3.49), the solution* u_N *by the MFS using Bessel functions has the optimal polynomial convergence rates,*

$$\|u - u_N\|_{0,\Gamma} = O\left(\frac{1}{N^{p-\frac{1}{2}}}\|u\|_{p,S}\right). \tag{7.3.53}$$

Remark 7.3.1. *Although Theorem 7.3.3 is similar to Theorem 2.3.2, the traditional well-known condition (7.2.10) is not supposed to be satisfied (e.g., we may choose* $R \le r_{\max}$*), while the bounds (7.3.48) and (7.3.49) still hold. This discovery is distinct from the MFS for Laplace's equation in Part I. The reason is the case of* $J_0(0) = 1$*, which is different from the singularity,* $\ln(r)|_{r\to 0} \to -\infty$ *for Laplace's equation.*

7.3.3 Exploration of Bounded k

The error analysis in Section 7.3.2 is for small k (*e.g.*, $kR \le 2$) to guarantee (7.3.32) and (7.3.33), which may not hold for bounded k. In this subsection, we explore the error analysis for bounded k. When k is bounded, we have to consider the case that k^2 is very close to one of eigenvalues $\{\lambda_\ell\}$. Denote the gap

$$\delta = \min_{\forall \ell}\left\{\frac{|k^2 - \lambda_\ell|}{\lambda_\ell}\right\} = \min_{\forall \ell}\left|1 - \frac{k^2}{\lambda_\ell}\right| > 0. \tag{7.3.54}$$

In the denominator of (7.3.40), $J_m(kR)J_m(k\tilde{\rho})$ may be very close to zero. The zeros of $J_n(kR) = 0$ occur if

$$k^2 = \lambda_{k^*} = \left(\frac{j_{n,k^*}}{R}\right)^2, \tag{7.3.55}$$

where j_{n,k^*} is the k^*th zero of $J_n(x)$. We have from (7.3.54)

$$\delta = \left|\frac{k^2 - \left(\frac{j_{n,k^*}}{R}\right)^2}{\left(\frac{j_{n,k^*}}{R}\right)^2}\right| = \left|\frac{(kR)^2 - (j_{n,k^*})^2}{(j_{n,k^*})^2}\right| = \left|1 - \frac{x^2}{(j_{n,k^*})^2}\right|, \tag{7.3.56}$$

where $x = kR$. Assume $\delta \ll 1$, then we have from (7.3.56)

$$x \approx j_{n,k^*}. \tag{7.3.57}$$

Note that the values $k^2 = \lambda_{k^*}$ in (7.3.55) are different from the eigenvalues λ_ℓ of eigenvalue problems, called spurious eigenvalues (see [35]). In this chapter, it is assumed that both $k^2 \ne \lambda_\ell$ and $k^2 \ne \lambda_{k^*}$. We have a lemma.

Lemma 7.3.4. *For* $\delta \ll 1$*, there exists an approximation,*

$$|J_n(x)| \approx \frac{2}{(n+1)!}\left(\frac{x}{2}\right)^{n+1}\delta. \tag{7.3.58}$$

Proof. There exists a formula from [198, p.235, 10.21.15],

$$J_n(x) = \frac{1}{n!}\left(\frac{x}{2}\right)^n \prod_{k=1}^{\infty}\left(1 - \frac{x^2}{j_{n,k}^2}\right). \tag{7.3.59}$$

We have

$$J_n(x) = \frac{1}{n!}\left(\frac{x}{2}\right)^n \left(1 - \frac{x^2}{j_{n,k^*}^2}\right)\mathcal{T} = \pm\delta \frac{1}{n!}\left(\frac{x}{2}\right)^n \mathcal{T}, \tag{7.3.60}$$

where

$$\mathcal{T} = \prod_{k=1 \wedge k \neq k^*}^{\infty} \left(1 - \frac{x^2}{j_{n,k}^2}\right). \tag{7.3.61}$$

By using the logarithmic differentiation, we have from (7.3.61)

$$\frac{1}{\mathcal{T}} = -2x \sum_{k=1 \wedge k \neq k^*}^{\infty} \frac{1}{j_{n,k}^2 - x^2}. \tag{7.3.62}$$

We cite an equality from Baricz *et al.* [19, (1.1)],

$$\sum_{k=1 \wedge k \neq k^*}^{\infty} \frac{1}{j_{n,k}^2 - j_{n,k^*}^2} = \frac{n+1}{2j_{n,k^*}^2}. \tag{7.3.63}$$

We have from (7.3.63) and (7.3.57)

$$\sum_{k=1 \wedge k \neq k^*}^{\infty} \frac{1}{j_{n,k}^2 - x^2} \approx \sum_{k=1 \wedge k \neq k^*}^{\infty} \frac{1}{j_{n,k}^2 - j_{n,k^*}^2} = \frac{n+1}{2j_{n,k^*}^2} \approx \frac{n+1}{2x^2}. \tag{7.3.64}$$

Combining (7.3.62) and (7.3.64) gives $\frac{1}{\mathcal{T}} \approx -2x \times \frac{n+1}{2x^2} = -\frac{n+1}{x}$, to have

$$\mathcal{T} \approx -\frac{x}{n+1}. \tag{7.3.65}$$

The desired result (7.3.58) follows from (7.3.60) and (7.3.65). ■

From [198, 10.9.4], there exists the formula of Bessel functions,

$$J_n(x) = \frac{2}{n!\pi}\left(\frac{x}{2}\right)^n \int_0^1 (1-t^2)^{n-1} \cos(xt)\, dt = \frac{2}{n!\pi}\left(\frac{x}{2}\right)^n G_n(x),$$

where

$$G_n(x) = \int_0^1 (1-t^2)^{n-1} \cos(xt)\, dt, \quad \forall n. \tag{7.3.66}$$

There also exists the upper bound,

$$|G_n(x)| \leq \int_0^1 (1-t^2)^{n-1} |\cos(xt)|\, dt \leq 1.$$

From (7.3.59) we have

$$G_n(x) = \int_0^1 (1-t^2)^{n-1} \cos(xt)\, dt = \frac{\pi}{2} \prod_{k=1}^{\infty} \left(1 - \frac{x^2}{j_{n,k}^2}\right).$$

Suppose that x is not approximated to any zero, $j_{n,k}, \forall n, k$. We may assume

$$|G_n(x)| \geq c_0 > 0, \tag{7.3.67}$$

where c_0 is a constant independent of n. Hence the equation (7.3.67) implies

$$|J_n(x)| \asymp \frac{1}{n!} \left(\frac{x}{2}\right)^n. \tag{7.3.68}$$

When small $x < j_{1,1} = 3.8317$,

$$J_n(x) \geq c_0 \frac{2}{n!\pi} \left(\frac{x}{2}\right)^n, \quad n \geq 1. \tag{7.3.69}$$

Note that the bound in (7.3.68) is consistent with (7.3.37) and (7.3.69) for small k.

When k is bounded, for the denominator, $J_m(kR)J_m(k\rho)$ with $\rho = \tilde{\rho}$, in (7.3.40), there exist two cases:

$$\min_m J_m(kR)J_m(k\rho) = 0, \tag{7.3.70}$$

$$\min_m J_m(kR)J_m(k\rho) \neq 0. \tag{7.3.71}$$

For (7.3.70), the case $J_m(k\rho) = 0$ may relate to true eigenvalues, but the case $J_m(kR) = 0$ responds to spurious eigenvalues. The algorithms bypassing all spurious eigenvalues are given in Chapters 8 and 9. Since the roots of $J_n(x) = 0$ are simple for $x > 0$, there are four cases for (7.3.71) as follows.

Case I:

$$\begin{aligned} &|G_m(kR)| \geq c_0, \\ &|G_m(k\rho)| \geq c_0, \quad \rho \in [r_{\min}, r_{\max}], \quad \forall m. \end{aligned}$$

Then the equivalence (7.3.68) holds for $x = kR, k\rho$.

Case II: There exists m^* such that

$$\begin{aligned} &|G_{m^*}(kR)| \approx 0, \\ &|G_m(k\rho)| \geq c_0, \quad \rho \in [r_{\min}, r_{\max}], \quad \forall m. \end{aligned} \tag{7.3.72}$$

Case III: There exists m^* such that

$$\begin{aligned} &|G_m(kR)| \geq c_0, \quad \forall m, \\ &|G_{m^*}(k\rho)| \approx 0, \quad \rho \in [r_{\min}, r_{\max}]. \end{aligned}$$

Case IV: There exists m^* for both:

$$\begin{aligned}&|G_{m^*}(kR)| \approx 0,\\&|G_{m^*}(k\rho)| \approx 0, \quad \rho \in [r_{\min}, r_{\max}].\end{aligned}$$

In computation, the radius R can be chosen differently. For a non-disk domain S, since $r_{\max} > r_{\min}$, the $\rho\,(=\tilde{\rho})$ in analysis may also be chosen deliberately. Since the zeros of Bessel functions are simple, it is possible to choose $J_n(k\rho) \neq 0$, except for the disk domains with radius $r_{\max} = r_{\min} = \rho$. For the disk domains, when $k\rho = j_{n,k^*}$, we have $J_n(k\rho) = J_n(j_{n,k^*}) = 0$, and then the true eigenvalue at $\lambda_\ell = k^2$ occurs. For Case I, all conclusions in Section 7.3.2 hold because of (7.3.68). Case IV happens rather rarely. Below, we focus on the analysis of Case II, since the analysis of Case III is similar. For Case II with $x = kR$, we assume $(x \neq j_{n,k^*}) \wedge (x \approx j_{n,k^*})$ with $\delta \ll 1$ as in (7.3.56). We have a lemma.

Lemma 7.3.5. *For Case II with* $n = m^*$, *there exist the lower bounds,*

$$|J_n(kR)J_n(k\rho)| \geq c_0\delta \frac{1}{(n+1)!}\left(\frac{kR}{2}\right)^{n+1} \times \frac{1}{n!}\left(\frac{k\rho}{2}\right)^n, \tag{7.3.73}$$

$$|J_n(kR)J_n(k\rho)| \geq c_0\delta \frac{1}{n^2}\left(\frac{ekR}{2n}\right)^n \left(\frac{ek\rho}{2n}\right)^n, \tag{7.3.74}$$

where $c_0\ (> 0)$ *is a constant independent of* n.

Proof. From Lemma 7.3.4, we have

$$|J_n(kR)| \geq c_0\delta \frac{1}{(n+1)!}\left(\frac{kR}{2}\right)^{n+1}. \tag{7.3.75}$$

Then for Case II, we have from (7.3.72)

$$|J_n(k\rho)| \geq c_0 \frac{1}{n!}\left(\frac{k\rho}{2}\right)^n. \tag{7.3.76}$$

Combining (7.3.75) and (7.3.76) gives the first desired result (7.3.73).

Next, from the Stirling formula: $n! \approx \sqrt{2\pi n}\left(\frac{n}{e}\right)^n$ in [1, p.257, (6.1.37)], we have

$$\frac{1}{n!}\left(\frac{x}{2}\right)^n \approx \frac{1}{\sqrt{2\pi n}}\left(\frac{ex}{2n}\right)^n.$$

Then the lower bound (7.3.73) can be expressed as

$$\begin{aligned}|J_n(kR)J_n(k\rho)| &\geq c_0\delta \frac{1}{(n+1)!}\left(\frac{kR}{2}\right)^{n+1} \times \frac{1}{n!}\left(\frac{k\rho}{2}\right)^n\\ &\geq c_0\delta \frac{1}{n}\frac{1}{(n!)^2}\left(\frac{kR}{2}\right)^n \times \left(\frac{k\rho}{2}\right)^n \geq c_0\delta \frac{1}{n^2}\left(\frac{ekR}{2n}\right)^n \left(\frac{ek\rho}{2n}\right)^n.\end{aligned}$$

This is the second desired (7.3.74). ■

We have the following theorem.

Theorem 7.3.4. *Let* $u \in \mathbf{H}^p(S)$ $(p > 1)$, *and the conditions (7.3.32) and (7.3.33) hold. Under Case II, there exists the bound,*

$$\begin{aligned}&\|P_n(\rho,\theta) - \Sigma_N(P_n;\rho,\theta)\|_{q,\Gamma}\\ &\le C\frac{1}{\delta}\sqrt{n}N^q\frac{|J_{N-n}(kr_{\max})J_{N-n}(kR)|}{\mathcal{T}_n^*}\|P_n(\rho,\theta)\|_{0,\Gamma},\end{aligned} \tag{7.3.77}$$

where

$$\mathcal{T}_n^* = \frac{1}{n^2}\left(\frac{ekR}{2n}\right)^n\left(\frac{ekr_{\min}}{2n}\right)^n. \tag{7.3.78}$$

Proof. The proof is analogous to that in Theorem 7.3.1, except that the lower bounds of the denominator in (7.3.40) are different. From Lemma 7.3.5, we have Case II with $m = m^*$

$$\begin{aligned}|J_m(kR)J_m(k\rho)| &\ge c_0\delta\frac{1}{(m+1)!}\left(\frac{kR}{2}\right)^{m+1}\times\frac{1}{m!}\left(\frac{k\rho}{2}\right)^m\\ &\approx c_0\delta\frac{1}{m^2}\left(\frac{ekR}{2m}\right)^m\left(\frac{ek\rho}{2m}\right)^m := Q_m(\rho).\end{aligned}$$

The functions $Q_m(\rho)$ are decreasing *via* m but increasing *via* ρ. We have for $m \le n$

$$Q_m(\rho) \ge Q_n(\rho) \ge Q_n(r_{\min}) = c_0\delta\frac{1}{n^2}\left(\frac{ekR}{2n}\right)^n\left(\frac{ek\,r_{\min}}{2n}\right)^n. \tag{7.3.79}$$

Then from (7.3.40) and (7.3.79), we obtain

$$\sum_{m=1}^{n}\frac{1}{J_m^2(k\widetilde{\rho})}\|E_m(\rho,\theta)\|^2_{q,\Gamma_\rho} \le C\frac{1}{\delta}nN^{2q}\left(\frac{J_{N-n}(kr_{\max})J_{N-n}(kR)}{\mathcal{T}_n^*}\right)^2. \tag{7.3.80}$$

Combining (7.3.39), (7.3.44) and (7.3.80) gives (7.3.77). ■

Compared with Theorem 7.3.1, there exists an additional factor $1/\delta$ in the upper bound. Similarly, we have the following theorem.

Theorem 7.3.5. *Let* $u \in \mathbf{H}^p(S)$ $\left(p \ge \frac{3}{2}\right)$, *and the conditions (7.3.32) and (7.3.33) hold. Suppose that the* N *satisfies*

$$II = \frac{1}{\delta}\sqrt{n}\frac{|J_{N-n}(kr_{\max})J_{N-n}(kR)|}{\mathcal{T}_n^*} \le \frac{1}{n^{p-\frac{1}{2}}}. \tag{7.3.81}$$

Then for Case II, there exists the error bound,

$$\|P_n(\rho,\theta) - \Sigma_N(P_n;\rho,\theta)\|_{0,\Gamma} = O\left(\frac{1}{N^{p-\frac{1}{2}}}\|P_n(\rho,\theta)\|_{0,\Gamma}\right).$$

Proof. For $q = 0$, we have from Lemma 7.3.5 and (7.3.35)

$$\begin{aligned} II &\approx \frac{1}{\delta}\frac{n^{2.5}}{N-n}\frac{\left(\frac{ekr_{\max}}{2(N-n)}\right)^{N-n}\left(\frac{ekR}{2(N-n)}\right)^{N-n}}{\left(\frac{ekr_{\min}}{2n}\right)^{n}\left(\frac{ekR}{2n}\right)^{n}} \\ &= \frac{1}{\delta}\frac{n^{2.5}}{N-n}\left(\frac{e^2k^2r_{\max}R}{2^2(N-n)^2}\right)^{N-2n}\left(\left(\frac{n}{N-n}\right)^2\frac{r_{\max}}{r_{\min}}\right)^{n}. \end{aligned}$$

Since $N > 2n$, we have $\frac{n}{N-n} < 1$ and $N - n > n$, to give

$$II \le \frac{1}{\delta}n^{1.5}\left(\frac{e^2k^2r_{\max}R}{2^2n^2}\right)^{N-2n}\left(\frac{r_{\max}}{r_{\min}}\right)^{n}. \tag{7.3.82}$$

To satisfy the bound of $II \le \frac{1}{n^{p-\frac{1}{2}}}$ in (7.3.82), we may request

$$\frac{1}{\delta}\left(\frac{e^2k^2r_{\max}R}{2^2n^2}\right)^{N-2n}\left(\frac{r_{\max}}{r_{\min}}\right)^{n} \le \frac{1}{n^{p+1}}.$$

This gives

$$N \ge 2n + \frac{\ln\frac{1}{\delta} + n\ln\left(\frac{r_{\max}}{r_{\min}}\right) + p\ln(n+1)}{\ln\left(\frac{2^2n^2}{e^2k^2r_{\max}R}\right)}. \tag{7.3.83}$$

■

Compared with (7.3.49) for small k in Section 7.3.2, a larger N given in (7.3.83) is needed to guarantee the optimal polynomial convergence. From Theorem 7.3.5 and (7.3.52), we have the following corollary.

Corollary 7.3.1. *Let all conditions in Theorem 7.3.5 hold. Then for Case II, there exists the error bound,*

$$\|u - u_N\|_{0,\Gamma} = O\left(\frac{1}{N^{p-\frac{1}{2}}}\|P_n(\rho,\theta)\|_{0,\Gamma}\right). \tag{7.3.84}$$

Case II may respond to the case near the spurious eigenvalues. For Case III, the zero, j_{m^*,k^*} $(= \lambda_\ell)$, may just be one true eigenvalue of Laplace's operator; this case occurs for disk domains, where $\rho = r_{\max} = r_{\min}$. For Case III, Corollary 7.3.1 also holds.

The above analysis is made for the boundary errors on Γ. For Laplace's equation, the maximal errors occur only on the domain boundary. It is, however, invalid for the Helmholtz equation. Hence, we need the error bounds in S. The Sobolev 1-norm is defined by $\|v\|_{1,S} = \sqrt{\iint_S\{v^2 + v_x^2 + v_y^2\}}$. For the Dirichlet problem, we can obtain the following lemma from Li *et al.* [149] and [169, p.281, Theorem 10.3.1].

Lemma 7.3.6. *Suppose that for* $v \in V_N$ *the following inverse property holds,*

$$\|v_\nu\|_{0,\Gamma} \leq CK_N \|v\|_{1,S}, \tag{7.3.85}$$

where K_N *may be unbounded as* $N \to \infty$*. Then for* $\delta > 0$ *in (7.3.54), there exists the bound,*

$$\|v\|_{1,S} \leq CK_N \left(1 + \frac{k}{\delta}\right) \|v\|_{0,\Gamma}, \quad v \in V_N. \tag{7.3.86}$$

We have the following corollary.

Corollary 7.3.2. *Consider the approximation* $k^2 \approx \lambda_\ell$ *with* $\delta \ll 1$ *in (7.3.54). Suppose that the equation (7.3.85) holds for* $(u - u_N)$*, and other conditions in Theorem 7.3.5 hold. For Cases II and III, when* N *is chosen as (7.3.83), there exists the bound,*

$$\|u - u_N\|_{1,S} \leq CK_N \left(1 + \frac{k}{\delta}\right) \frac{1}{N^{p-1}} \|u\|_{p,S}. \tag{7.3.87}$$

7.4 Stability Analysis for Disk Domains

For simplicity, consider the Dirichlet problem of (7.2.1) in a disk,

$$S_0 = \{(r, \theta) | 0 < r < \rho, 0 \leq \theta < 2\pi\}. \tag{7.4.1}$$

Choose the source and the collocation nodes on concentric circles,

$$Q_i = \{(x, y) | x = R\,\cos(ih), y = R\,\sin(ih)\}, \tag{7.4.2}$$

$$P_i = \{(x, y) | x = \rho\,\cos(ih), y = \rho\,\sin(ih)\}, \tag{7.4.3}$$

where $h = \frac{2\pi}{N}$. In the existing literature of the MFS, the condition $\rho < R$ is assumed for disk domains. From the error analysis in the previous section, this well-known condition $\rho < R$ may be violated.

Let the number of source nodes be equal to N. From the Dirichlet problem, the collocation equations at P_ℓ are obtained from (7.2.15),

$$\sum_{j=1}^{N} c_j \Phi_j(P_\ell) = f(P_\ell), \quad P_\ell \in \Gamma, \quad \ell = 1, 2, ..., N, \tag{7.4.4}$$

where $\Gamma = \{(r, \theta) | r = \rho, 0 \leq \theta \leq 2\pi\}$, $P_\ell = (\rho_\ell, \theta_\ell)$, c_i are the coefficients, and the fundamental solutions are

$$\Phi_j(P_\ell) = J_0(k|\overline{P_\ell Q_j}|) = J_0\left(k\sqrt{R^2 + \rho^2 - 2R\rho\,\cos(\ell - j)h}\right). \tag{7.4.5}$$

Denote (7.4.4) by $\mathbf{D}\mathbf{x} = \mathbf{f}$, where $\mathbf{x} = \{c_1, c_2, ..., c_N\}^T \in \mathbf{R}^N$and $\mathbf{f} = \{f(P_1), f(P_2), ..., f(P_N)\}^T \in \mathbf{R}^N$. The matrix $\mathbf{D} \in \mathbf{R}^{N\times N}$ is circulant,

$$\mathbf{D} = \begin{pmatrix} d_0 & d_1 & \cdots & d_{N-1} \\ d_{N-1} & d_0 & \cdots & d_{N-2} \\ \vdots & \vdots & \ddots & \vdots \\ d_1 & d_2 & \cdots & d_0 \end{pmatrix}, \tag{7.4.6}$$

with entries $d_i = J_0\left(k\sqrt{R^2 + \rho^2 - 2R\rho\,\cos(ih)}\right)$.

Based on Basic Lemmas A and B in Part I, the eigenvalues of matrix $\mathbf{D}$ are known as

$$\lambda_\ell = \sum_{j=0}^{N-1} d_j\,\cos(\ell jh), \quad \ell = 0, 1, ..., N-1. \tag{7.4.7}$$

In this section, we confine the disk domains for stability analysis. For the bounded simply-connected domains, the bounds of condition numbers can be derived by following Chapter 3; details are omitted. We have the following lemma.

Lemma 7.4.1. *Let $k^2 \neq \lambda_\ell$ and k is small such that*

$$J_i(k\rho) \neq 0, \quad J_i(kR) \neq 0, \quad i = 0, 1, 2, ... \tag{7.4.8}$$

There exist the approximations of λ_ℓ,

$$\lambda_0 \approx NJ_0(kR)J_0(k\rho), \tag{7.4.9}$$

$$\lambda_\ell \approx N\{J_\ell(kR)J_\ell(k\rho) + J_{N-\ell}(kR)J_{N-\ell}(k\rho)\}, \quad \ell = 1, 2, ..., N-1. \tag{7.4.10}$$

Proof. First, by following the proof in Chapters 2 and 3, we have

$$\begin{aligned} \lambda_0 &= \sum_{j=0}^{N-1} d_j = \frac{1}{h}\sum_{j=0}^{N-1} hJ_0\left(k\sqrt{R^2 + \rho^2 - 2R\rho\,\cos(jh)}\right) \\ &= \frac{1}{h}\int_0^{2\pi} J_0\left(k\sqrt{R^2 + \rho^2 - 2R\rho\,\cos(x)}\right)dx + \triangle\lambda_0. \end{aligned} \tag{7.4.11}$$

Form (7.3.4), there exists the equality,

$$\frac{1}{h}\int_0^{2\pi} J_0\left(k\sqrt{R^2 + \rho^2 - 2R\rho\,\cos(x)}\right)dx = NJ_0(kR)J_0(k\rho). \tag{7.4.12}$$

The error $\triangle\lambda_0$ can be obtained from Basic Lemmas A and B and (7.3.5),

$$\triangle\lambda_0 = \frac{1}{h}\triangle_N\left(J_0\left(k\sqrt{R^2+\rho^2-2R\rho\,\cos x}\right)\right) = \frac{2\pi}{h}\sum_{\mu=1}^{\infty}\alpha_{\mu N}, \tag{7.4.13}$$

where

$$\begin{aligned}\alpha_\ell &= \frac{1}{\pi}\int_0^{2\pi} J_0\left(k\sqrt{R^2+\rho^2-2R\rho\,\cos x}\right)\cos(\ell x)\,dx\\ &= 2J_\ell(kR)J_\ell(k\rho), \quad \ell = 0,1,2,....\end{aligned} \tag{7.4.14}$$

Since N is large, we have from (7.3.37)

$$\triangle\lambda_0 = \frac{4\pi}{h}\sum_{\mu=1}^{\infty} J_{\mu N}(kR)J_{\mu N}(k\rho) \approx 2NJ_N(kR)J_N(k\rho). \tag{7.4.15}$$

Hence, from (7.4.12) and (7.4.15), we have

$$\lambda_0 \approx N\{J_0(kR)J_0(k\rho) + 2J_N(kR)J_N(k\rho)\} \approx NJ_0(kR)J_0(k\rho).$$

This is the first result (7.4.9).

Next, consider λ_ℓ $(\ell = 1,2,...,N-1)$. From Basic Lemma A in Part I and (7.3.5), we have

$$\begin{aligned}\lambda_\ell = \sum_{j=0}^{N-1} d_j\,\cos(\ell jh) &= \frac{1}{h}\int_0^{2\pi} J_0\left(k\sqrt{R^2+\rho^2-2R\rho\,\cos(x)}\right)\cos(\ell x)\,dx + \triangle\lambda_\ell\\ &= NJ_\ell(kR)J_\ell(k\rho) + \triangle\lambda_\ell,\end{aligned} \tag{7.4.16}$$

where the error $\triangle\lambda_\ell$ can be obtained from Basic Lemmas A and B and (7.3.5),

$$\triangle\lambda_\ell = \frac{1}{h}\triangle_N\left(J_0\left(k\sqrt{R^2+\rho^2-2R\rho\,\cos x}\right)\cos(\ell x)\right) = \frac{\pi}{h}\sum_{\mu=1}^{\infty}(\alpha_{\mu N-\ell}+\alpha_{\mu N+\ell}),$$

where the coefficients α_ℓ are also given in (7.4.14). Since N is large, we also have from (7.3.37)

$$\begin{aligned}\triangle\lambda_\ell &= \frac{2\pi}{h}\sum_{\mu=1}^{\infty}\{J_{\mu N-\ell}(kR)J_{\mu N-\ell}(k\rho) + J_{\mu N+\ell}(kR)J_{\mu N+\ell}(k\rho)\}\\ &\approx NJ_{N-\ell}(kR)J_{N-\ell}(k\rho).\end{aligned} \tag{7.4.17}$$

Combining (7.4.16) and (7.4.17) gives $\lambda_\ell \approx N\{J_\ell(kR)J_\ell(k\rho) + J_{N-\ell}(kR)J_{N-\ell}\,(k\rho)\}$. This is the second result (7.4.10). ■

Theorem 7.4.1. *Let k be small such that*

$$kR, k\rho \le 2 < j_{0,1}, \tag{7.4.18}$$

or $k^2 \ne \lambda_\ell$ with not small gap δ denoted in (7.3.54). Then there exist the bounds,

$$\text{Cond} \leq C \frac{1}{J_{\frac{N}{2}}(kR) J_{\frac{N}{2}}(k\rho)}, \tag{7.4.19}$$

and

$$\text{Cond} \leq CN \left(\frac{N^2}{e^2 k^2 R\rho} \right)^{\frac{N}{2}}. \tag{7.4.20}$$

Proof. From (7.4.18), there exists the equivalence: $J_0(kR) \asymp O(1)$ and $J_0(k\rho) \asymp O(1)$. From (7.4.9), we have $\lambda_0 \asymp O(N)$. Without loss of generality, assume that N is even. We have from (7.4.10)

$$\min_{\ell} |\lambda_\ell| \geq \lambda_{\frac{N}{2}} \approx N J_{\frac{N}{2}}(kR) J_{\frac{N}{2}}(k\rho). \tag{7.4.21}$$

Hence, combining (7.4.10) and (7.4.21) gives

$$\text{Cond} = \frac{\max_\ell |\lambda_\ell|}{\min_\ell |\lambda_\ell|} = \frac{|\lambda_0|}{|\lambda_{\frac{N}{2}}|} \leq C \frac{1}{J_{\frac{N}{2}}(kR) J_{\frac{N}{2}}(k\rho)}. \tag{7.4.22}$$

This is the desired result (7.4.19). The bound (7.4.20) follows from (7.4.19) and (7.3.37), and this completes the proof of Theorem 7.4.1. ■

7.5 Application to BKM

Note that the well-known rule, $R > r_{\max}$, is unnecessary to obey. This implies that the source nodes may be located just on the domain boundary, thus bypassing the pseudo-boundary and leading to the boundary knot method (BKM). The BKM was applied to the Helmholtz equation in Chen and Hon [53, 100], where the Bessel function $J_0(kr)$ is chosen as the FS, and the source nodes are located just on the physical boundary Γ. High accuracy of solutions was obtained by using a few FS. Since then, there have appeared many numerical reports. There exists no analysis for the BKM so far; this section provides an analysis. High polynomial convergence rates can be obtained but very severe instability occurs. The bounds of Cond are derived for disk domains to show a super-exponential growth *via* the number of FS used. The instability of the BKM is much worse than the exponential growth rates of the MFS in Part I. However, good numerical solutions may be achieved by balancing stability and accuracy. Numerical experiments are carried out to support the analysis made. Efforts were also paid to reduce the severe ill-conditioning of the BKM by regularization and the effective condition numbers; see Zhang *et al.* [259], Wang *et al.* [235, 236] and Li *et al.* [161, 162].

The error bound in Corollary 7.3.2 is valid for the BKM. We are more interested in stability analysis to give the following theorem.

Theorem 7.5.1. *Suppose that the bounded k satisfies $\delta \geq \delta_0 > 0$, where δ_0 is a constant independent of N. There exists the bound for the disk domain with radius ρ,*

$$\text{Cond} \le CN\left(\frac{N}{ek\rho}\right)^N, \tag{7.5.1}$$

where C is a bounded constant independent of N. Also when $\delta \ll 1$,

$$\text{Cond} \le C\frac{1}{\delta}N^2\left(\frac{N}{ek\rho}\right)^N. \tag{7.5.2}$$

Proof. We obtain from (7.4.19) at $R = \rho$

$$\text{Cond} \le C\left(\frac{1}{J_{\frac{N}{2}}(k\rho)}\right)^2. \tag{7.5.3}$$

For large n, there exists an approximation from (7.3.37),

$$|J_n(k\rho)| \approx \frac{1}{\sqrt{2\pi n}}\left(\frac{ek\rho}{2n}\right)^n.$$

Hence we have

$$|J_{\frac{N}{2}}(k\rho)| \ge c_0\frac{1}{\sqrt{N}}\left(\frac{ek\rho}{N}\right)^{\frac{N}{2}}, \tag{7.5.4}$$

where c_0 (> 0) is also a constant independent of N. Combining (7.5.3) and (7.5.4) gives

$$\text{Cond} \le CN\left(\frac{N}{ek\rho}\right)^N.$$

This is the first desired result (7.5.1). For $\delta \ll 1$, there exists the lower bound from (7.3.74) at $R = \rho$,

$$J_n^2(k\rho) \ge c_0\delta\frac{1}{n^2}\left(\frac{ek\rho}{2n}\right)^{2n}. \tag{7.5.5}$$

The second desired result (7.5.2) follows from (7.5.3) and (7.5.5). ∎

Below, we consider the case of bounded k with $\delta \ge \delta_0 > 0$ for stability discussions. When ρ and k are given, the growth of Cond in (7.5.1) is faster than that of exponential rates, called "the super-exponential growth" in this book. Compared with the exponential growth by the MFS using the singular FS in Part I, the instability of the BKM is much worse.

Remark 7.5.1. *There arises a dilemma. How can the BKM with the super-exponential growth rates of Cond succeed in the real application as in [53, 100]? The polynomial convergence rates are obtained from (7.3.87), and high convergence rates are achieved for the highly smooth solutions. The fast convergence is essential and imperative for the BKM because satisfactory solutions must be obtained only under not large N, thus* *avoiding the huge Cond incurring from the super-exponential growth. The key to success for the BKM in the real application is to balance stability and accuracy; the same strategy for the MFS using singular FS is seen in Part I.*

Consider the Dirichlet problem on a square: $S = \{(x,y)| -1<x<1, -1<y<1\}$,

$$\Delta u + k^2 u = 0 \text{ in } S, \quad u(x,y) = f(x,y) \text{ on } \Gamma.$$

Choose the exact solution $u(x,y) = \frac{1}{2}(\cos kx + \cos ky)$ as in [177]. Then the boundary function is $f(x,y) = \frac{1}{2}(\cos kx + \cos ky)|_\Gamma$. Note that there does not exist a corner singularity. For the error $\epsilon = u - u_N$, define the boundary and the domain errors by

$$\|\epsilon\|_{\infty,\partial S} = \max_{\partial S} |\epsilon|, \quad \|\epsilon\|_{0,S} = \left\{\iint_S \epsilon^2 ds\right\}^{\frac{1}{2}}, \quad \|\epsilon\|_{1,S} = \left\{\iint_S (\epsilon^2 + \epsilon_x^2 + \epsilon_y^2) ds\right\}^{\frac{1}{2}}.$$

For the trapezoidal rule used on Γ, we find from Table 7.1 at $k = 2$,

$$\|\epsilon\|_{\infty,\partial S} = O((0.32)^N), \quad \|\epsilon\|_{0,S} = O((0.26)^N), \quad \|\epsilon\|_{1,S} = O((0.28)^N), \tag{7.5.6}$$

$$\text{Cond} = O((3.57)^N), \quad \text{Cond\_eff} = O((1.85)^N). \tag{7.5.7}$$

The equation (7.5.6) coincides with the high convergence rates in (7.3.87). For $N = 16, M = 32$, we choose different $k = 0.5 \sim 20$, and list the results in Table 7.2. We can see that when k increases, both accuracy and Cond decrease. The equation (7.5.7) displays an average exponential growth. The super-exponential growth is confirmed as follows. Let us scrutinize the growth of Cond, and take Table 7.1 at $k = 2$ for discussion. Since the square domain S is not far different from a disk, we may use the estimate of Cond in Theorem 7.5.1 for disk domains. Formulate an equivalent disk S° with the same area of S as $\pi(\rho^\circ)^2 = 4$, where the radius $\rho^\circ = \frac{2}{\sqrt{\pi}}$. For $k = 2$ with $\delta \geq \delta_0 > 0$, we have from (7.5.1)

$$\text{Cond} \leq CN\left(\frac{N}{ek\rho^\circ}\right)^N \leq CN\left(\frac{N}{ek\frac{2}{\sqrt{\pi}}}\right)^N = O(\text{Cond}^\circ),$$

Tab. 7.1 – The errors and the condition numbers by the trapezoidal rule at $k = 2$.

N	M	$\|\epsilon\|_{\infty,\partial S}$	$\|\epsilon\|_{0,S}$	$\|\epsilon\|_{1,S}$	Cond	Cond_eff	Cond$^\circ$	$\|\mathbf{x}\|$
4	8	2.95(−2)	3.98(−1)	8.12(−1)	5.66	1.00	7.23(−1)	3.12
8	16	2.17(−4)	2.43(−4)	1.30(−3)	8.77(1)	5.27	6.69(1)	5.79
12	24	2.02(−4)	1.94(−4)	1.19(−3)	1.32(4)	6.35(2)	3.77(4)	5.20
16	32	3.40(−8)	2.34(−8)	2.15(−7)	2.49(7)	1.65(3)	7.34(7)	3.12(3)
20	40	3.17(−8)	2.13(−8)	2.06(−7)	1.19(11)	7.68(6)	3.68(11)	2.82(3)
24	48	1.29(−8)	2.33(−8)	5.16(−8)	1.23(15)	1.00(7)	3.97(15)	2.02(7)

TAB. 7.2 – The errors and the condition numbers by the trapezoidal rule at $N = 16$ and $M = 32$.

k	$\|\epsilon\|_{\infty,\partial S}$	$\|\epsilon\|_{0,S}$	$\|\epsilon\|_{1,S}$	Cond	Cond_eff	$\|\mathbf{x}\|$
0.5	3.17(−8)	4.81(−8)	5.87(−8)	1.11(17)	6.16(8)	4.93(7)
1	6.19(−10)	9.93(−10)	1.38(−9)	2.38(12)	1.15(6)	7.47(5)
2	3.40(−8)	2.34(−8)	2.15(−7)	2.49(7)	1.65(3)	3.12(3)
5	1.20(−3)	7.29(−3)	3.82(−2)	2.81(3)	4.59(2)	3.72
10	9.13(−2)	1.39(−1)	1.59	5.95	2.18	3.76
15	6.17(−1)	9.99(−1)	3.12(1)	5.70	2.98	2.57
20	6.81(−1)	1.28	2.78(1)	1.40(1)	2.30	4.87

where

$$\text{Cond}^{\circ} = N\left(\frac{N}{ek\rho^{\circ}}\right)^{N} = N\left(\frac{N}{6.13}\right)^{N}. \tag{7.5.8}$$

When $N = 4, 8, 12, 16, 20, 24 := 4\ell$, we have from (7.5.8) and Table 7.1

$$\text{Cond}^{\circ} = 0.723, 6.69(1), 3.77(4), 7.34(7), 3.68(11), 3.97(15), \tag{7.5.9}$$

$$\text{Cond}_{\ell} = 5.66, 8.77(1), 1.32(4), 2.49(7), 1.19(11), 1.23(15), \tag{7.5.10}$$

$$\frac{\text{Cond}_{\ell+1}}{\text{Cond}_{\ell}} = 1.55(1), 1.51(2), 1.89(3), 4.78(3), 1.03(4). \tag{7.5.11}$$

The equation (7.5.9) is an excellent estimate for the numerical (7.5.10) as $N \geq 8$, thus verifying Theorem 7.5.1 perfectly. The super-exponential growth can be found from an increasing sequence of ratios (7.5.11). From (7.5.8), we have

$$\ln(\text{Cond}^{\circ}) = \ln N + \ln\left(\frac{N}{ek\rho^{\circ}}\right) \times N. \tag{7.5.12}$$

The equation (7.5.12) displays a super-linear function *via* N. The curves of Cond°, Cond and Cond_eff are drawn in Figure 7.2, where the scale of the vertical coordinate is *via* the logarithmic scale. A super-linear function of Cond can be seen in Figure 7.2, thus confirming the super-exponential growth again. Besides, the Cond_eff is much smaller than Cond, as shown in Figure 7.2. The effective condition number is a better criterion for stability analysis [162].

From Table 7.1 at $N = 16$ and $M = 32$, we find that Cond $= 2.49(7)$, the maximal boundary error $\|\epsilon\|_{\infty,\partial S} = 3.40(-8)$, and the domain error $\|\epsilon\|_{1,S} = 2.15(-7)$ in $\mathbf{H}^1$ norm (*cf.* [53, 100]). The Cond $= 2.49(7)$ in Figure 7.2 is large but not huge. From Table 7.1, the huge Cond at $N = 20, 24$ has greatly reduced the accuracy. Hence, for less smooth solutions (*e.g.*, $p = 2, 3$), the high accuracy of numerical solutions may not be obtained due to small N allowed. These numerical results also coincide with Remark 7.5.1. Note that the high accuracy as $O(10^{-7})$ has been achieved only by 16 fundamental solutions and 32 collocation equations only. A modest computational effort!

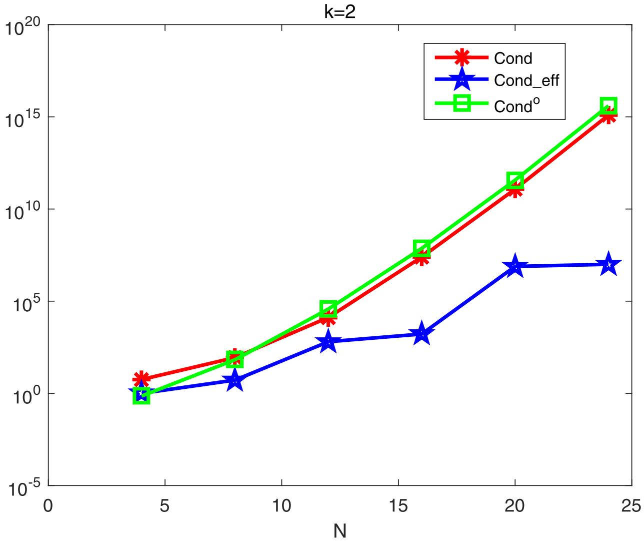

Fig. 7.2 – The curves of Cond°, Cond and Cond_eff for $k = 2$.

Chapter 8

Exterior Problems of Helmholtz Equation

For the exterior Dirichlet problems (EDP) of the Helmholtz equation in 2D, when the Sommerfeld radiation condition is satisfied, there always exists a unique solution. Denote by S_∞ the unbounded domain outside a bounded simply-connected domain, where the interior boundary Γ_{in} is non-circular and smooth. The standard MFS is first studied by using the complex Hankel function $H_0^{(1)}(kr)$ as the fundamental solutions (FS). However, some solutions cannot be obtained correctly (*e.g.*, the spurious eigenvalues called). This chapter is devoted to exploring spurious eigenvalues and their removals. For the non-circular interior boundary Γ_{in}, the error analysis is briefly made for the standard MFS, and some guidance is provided to bypass the spurious eigenvalues. Denote two nodes $P = (\rho, \theta)$ and $Q = (R, \phi)$, and $r = |\overline{PQ}| = \sqrt{R^2 + \rho^2 - 2R\rho\,\cos(\theta - \phi)}$. To eliminate all spurious eigenvalues, we solicit the new combined FS,

$$\left(\frac{\partial}{\partial R} \pm \mathbf{i}k\right) H_0^{(1)}(kr)$$

with $\mathbf{i} = \sqrt{-1}$, and propose the new modified MFS. The new algorithms are simple, and strict analysis may be made. The bounds of errors are derived and the polynomial convergence rates can be achieved. The bounds of condition numbers are derived for a circular Γ_{in}° only, to display the exponential growth *via* the number of the new FS used. Numerical experiments are carried out to support the analysis made. This chapter discusses the spurious eigenvalues and their removals by the MFS and focuses on the strict analysis of errors and stability. The materials of this chapter are adapted from [254].

8.1 Introduction

Consider the EDP of the Helmholtz equation $\Delta u + k^2 u = 0$ in 2D. When the Sommerfeld radiation condition in (8.2.3) is satisfied, there always exists a unique

DOI: 10.1051/978-2-7598-3171-5.c008
© Science Press, EDP Sciences, 2023

solution (*i.e.*, no true eigenvalues exist). By the MFS, however, the solutions at specific k cannot be obtained from the standard MFS for some fixed locations of source nodes; the spurious eigenvalues λ^- $(= k^2)$ are called in this chapter. Hence, the standard MFS also suffers from spurious eigenvalues as the boundary element method (BEM) (see Chapter 7). This chapter is devoted to exploring the spurious eigenvalues and their removals, and strict analysis of errors and stability.

Denote by S_∞ the unbounded domains outside a bounded simply-connected domain S, where the interior boundary $\mathbf{\Gamma}_{\text{in}}$ of S_∞ is non-circular and smooth. The source nodes $Q(R, \phi)$ are located within $\mathbf{\Gamma}_{\text{in}}$; the circular pseudo-boundary with radius R is chosen as in Figure 8.1 for analysis. The Hankel functions $H_0^{(1)}(kr)$ are used for the standard MFS, but the spurious eigenvalues occur at $J_n(kR) = 0$, where $J_n(z)$ is the Bessel function of order n. The error analysis of the standard MFS involves degeneracy as $J_n(kR) \approx 0$, and some guidance such as $kR < 2.4$ is provided to bypass the spurious eigenvalues. The standard MFS for exterior problems was studied in Ushijima and Chiba [230, 231], Chiba and Ushijima [61], and Ogata *et al.* [196], where the circular interior boundary $\mathbf{\Gamma}_{\text{in}}^{\circ}$ is confined. The exterior problems of the Helmholtz equation result from the scattering and radiation problems in acoustics, and a review of the MFS was given in Fairweather *et al.* [81] with an extensive list of references.

To eliminate all spurious eigenvalues is our goal. We solicit the new FS:

$$\mathcal{D}H_0^{(1)}(kr) = \left(\frac{\partial}{\partial R} \pm \mathbf{i}k\right) H_0^{(1)}(kr),$$

where $\mathbf{i} = \sqrt{-1}$. The new algorithms are called the modified MFS. In fact, the new FS is a combination of $H_0^{(1)}(kr)$ and $\frac{\partial}{\partial R} H_0^{(1)}(kr)$; a similar combination of the single-layer and the double-layer potentials was used in BEM [29, 30, 79, 210]. The new modified MFS is rather simple, and its strict analysis may be made. The bounds of errors are derived and polynomial convergence rates can be achieved. The bounds of condition numbers are derived for circular $\mathbf{\Gamma}_{\text{in}}^{\circ}$ only, to display an exponential growth *via* the number of the new FS used.

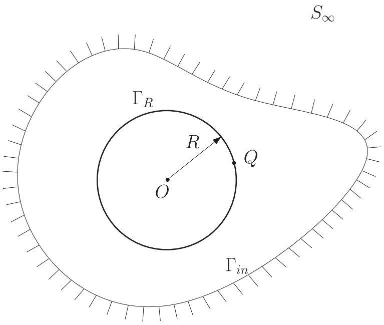

FIG. 8.1 – The unbounded domain S_∞ with an interior boundary $\mathbf{\Gamma}_{\text{in}}$, where the source nodes are located on a circle $\mathbf{\Gamma}_R$ with radius $R < \min \rho|_{\mathbf{\Gamma}_{\text{in}}}$.

There were many computational reports for exterior problems by the MFS; see Fairweather *et al.* [81]. The MFS suffers from spurious eigenvalues and the numerical characteristics are explored in Section 8.3. In this chapter, a comprehensive and advanced exploration has been developed from the spurious eigenvalues of the MFS and their removals. The study of this chapter can also be applied to the Helmholtz equation in multiply-connected domains [44, 46, 47]. See Chapter 9.

This chapter is organized as follows. In the next section, the standard MFS is discussed, and the error analysis is briefly provided in Section 8.2.2. In Section 8.3, the numerical characteristics of spurious eigenvalues are explored for the standard MFS. In Section 8.4, the new modified MFS is proposed, and the error and stability analysis is made in Sections 8.5 and 8.6. In Section 8.7, numerical experiments are carried out. In the last section, a few concluding remarks are made.

8.2 Standard MFS

8.2.1 Basic Algorithms

Consider the Helmholtz equation in an unbounded domain S_∞ with the Sommerfeld radiation condition at the infinity [196, 231] (see Figure 8.1):

$$\Delta u + k^2 u = 0 \text{ in } S_\infty, \tag{8.2.1}$$

$$u = f \text{ on } \Gamma_{\text{in}}, \tag{8.2.2}$$

$$\lim_{r\to\infty} \sqrt{r}\left\{\frac{\partial u}{\partial r} - \mathbf{i}ku\right\} = 0, \tag{8.2.3}$$

where $\mathbf{i} = \sqrt{-1}$, Γ_{in} is the smooth interior boundary of S_∞, and the known complex function $f \in \mathbf{C}$. Only the Dirichlet condition is studied in this chapter; other kinds of boundary conditions may be developed similarly. Note that equations (8.2.1)–(8.2.3) have the unique solution for all $k > 0$; see Sauter and Schwab [210, p.99] and Tikhonov and Samarskii [223, p.580].

Denote two nodes $P = (x, y) = (\rho, \theta)$ and $Q = (\xi, \eta) = (R, \phi)$, where (ρ, θ) and (R, ϕ) are polar coordinates. Then $x = \rho\cos\theta$, $y = \rho\sin\theta$, $\xi = R\cos\phi$, $\eta = R\sin\phi$, $\rho = \sqrt{x^2 + y^2}$, $R = \sqrt{\xi^2 + \eta^2}$, and $r = |\overline{PQ}| = \sqrt{R^2 + \rho^2 - 2R\rho\cos(\theta - \phi)}$. The complex FS are given by

$$\begin{aligned} \mathbf{\Phi}_j(\rho, \theta) &= H_0^{(1)}(kr_j) = J_0(kr_j) + \mathbf{i}\, Y_0(kr_j) \\ &= H_0^{(1)}\left(k\sqrt{R^2 + \rho^2 - 2R\rho\, \cos(\theta - \phi_j)}\right), \quad R < \rho, \end{aligned} \tag{8.2.4}$$

where $\phi_j = \frac{2\pi}{N} j$, and $H_0^{(1)}(x)$ is the Hankel function of order zero. In (8.2.4), $J_\mu(x)$ and $Y_\mu(x)$ are the Bessel and the Neumann functions of order μ, defined by

$$J_\mu(x) = \sum_{i=0}^{\infty} \frac{(-1)^i}{\Gamma(i+1)\Gamma(i+\mu+1)} \left(\frac{x}{2}\right)^{2i+\mu}, \tag{8.2.5}$$

$$Y_\mu(x) = \frac{J_\mu(x)\cos(\mu\pi) - J_{-\mu}(x)}{\sin(\mu\pi)}. \tag{8.2.6}$$

For (8.2.6), when μ is an integer, the right-hand side of (8.2.6) is defined by its limit. Denote $\mathbf{\Gamma}_{\text{in}} = \{(\rho,\theta)|\rho = \rho(\theta), 0 \le \theta \le 2\pi\}$, $r_{\min} = \min \rho|_{\Gamma_{\text{in}}}$ and $r_{\max} = \max \rho|_{\Gamma_{\text{in}}}$. Note that the source nodes $Q(R,\phi)$ must be located inside $\mathbf{\Gamma}_{\text{in}}$, to give

$$R < r_{\min}, \tag{8.2.7}$$

because when $r \to 0$, the singularity occurs from $H_0^{(1)}(kr) = \mathbf{i}\frac{2}{\pi}\ln\frac{1}{kr} + \cdots$. The condition (8.2.7) is against $R > r_{\max}$ for the bounded simply-connected domains in Part I. The linear combinations of FS are given by

$$u_N = \sum_{j=1}^{N} c_j \Phi_j(\rho,\theta), \tag{8.2.8}$$

where $c_j = \alpha_j + \mathbf{i}\beta_j \, (\alpha_j, \beta_j \in \mathbf{R})$ are the unknown coefficients.

The Hankel functions $H_0^{(1)}(kr)$ satisfy (8.2.1) and the Sommerfeld radiation condition (8.2.3). Hence, the coefficients c_j in (8.2.8) are sought by satisfying the interior boundary condition (8.2.2) only. Denote by V_N the set of FS as (8.2.8), the Trefftz method in [169] reads: to seek $u_N \in V_N$ such that

$$I(u_N) = \min_{v \in V_N} I(v), \quad I(v) = \int_{\Gamma_{\text{in}}} |v - f|^2, \tag{8.2.9}$$

where $|v|^2 = v\bar{v}$, and $\bar{v}$ is the conjugate of complex v. When the integral in (8.2.9) involves a numerical approximation, the Trefftz method reads: to seek $\tilde{u}_N \in V_N$ such that

$$\widehat{I}(\tilde{u}_N) = \min_{v \in V_N} \widehat{I}(v), \quad \widehat{I}(v) = \widehat{\int_{\Gamma_{\text{in}}}} |v - f|^2, \tag{8.2.10}$$

where $\widehat{\int_{\Gamma_{\text{in}}}}$ is the numerical approximation of $\int_{\Gamma_{\text{in}}}$ by the trapezoidal rule (or the Gaussian rule). Let $\mathbf{\Gamma}_{\text{in}}$ be divided into small $\mathbf{\Gamma}_{\text{in}}^{\ell}$ with the meshspacings $\triangle h_\ell$, then $\mathbf{\Gamma}_{\text{in}} = \bigcup_{\ell=1}^{M} \mathbf{\Gamma}_{\text{in}}^{\ell}$. We establish the boundary collocation equations,

$$\sqrt{\triangle h_\ell} \sum_{j=1}^{N} c_j \Phi_j(\rho_\ell, \theta_\ell) = \sqrt{\triangle h_\ell}\, f(\rho_\ell, \theta_\ell), \quad (\rho_\ell, \theta_\ell) \in \mathbf{\Gamma}_{\text{in}}^{\ell}, \quad \ell = 1, 2, \ldots, M. \tag{8.2.11}$$

The equations (8.2.11) are just equivalent to (8.2.10), where the trapezoidal rule is chosen for $\widehat{\int_{\Gamma_{\text{in}}}}$. We may assign other weights on both sides in (8.2.11) by the Gaussian rule [169].

In computation, we may choose the number M of collocation nodes to be larger than N. The equations (8.2.11) lead to an overdetermined system,

$$\mathbf{F}\mathbf{x} = \mathbf{b}, \tag{8.2.12}$$

where $\mathbf{F} \in \mathbf{C}^{M\times N}(M \geq N)$, $\mathbf{x} \in \mathbf{C}^N$ and $\mathbf{b} \in \mathbf{C}^M$. The FS in (8.2.8) and the coefficients c_j from (8.2.9) (or (8.2.11)) are called the standard MFS.

8.2.2 Brief Error Analysis

For complex solutions of (8.2.1)–(8.2.3), there are the expansions,

$$u(\rho,\theta) = P_n(\rho,\theta) + R_n(\rho,\theta), \tag{8.2.13}$$

where the particular solutions (PS) of degree n are given by

$$P_n(\rho,\theta) = a_0 H_0^{(1)}(k\rho) + \sum_{m=1}^{n} H_m^{(1)}(k\rho)[a_m \cos(m\theta) + b_m \sin(m\theta)], \tag{8.2.14}$$

and the residual

$$R_n(\rho,\theta) = \sum_{m=n+1}^{\infty} H_m^{(1)}(k\rho)[a_m \cos(m\theta) + b_m \sin(m\theta)], \tag{8.2.15}$$

where $H_m^{(1)}(x) = J_m(x) + \mathbf{i}\, Y_m(x)$, and a_m and b_m are the exact complex coefficients. The Sobolev norms are defined by

$$\|v\|^2_{0,\Gamma_{\text{in}}} = \int_{\Gamma_{\text{in}}} v\bar{v}, \quad \|v\|^2_{p,\Gamma_{\text{in}}} = \sum_{k=0}^{p} \|\nabla^k v\|^2_{0,\Gamma_{\text{in}}}. \tag{8.2.16}$$

Suppose that the exact solution satisfies $u \in \mathbf{H}^p(\boldsymbol{\Gamma}_{\text{in}})$, and there exist the bounds of residuals,

$$\|R_n(\rho,\theta)\|_{q,\Gamma_{\text{in}}} = O\left(\frac{1}{n^{p-q}}\|u\|_{p,\Gamma_{\text{in}}}\right), \quad q < p. \tag{8.2.17}$$

The addition theorem for $H_0^{(1)}(kr)$ is given in Watson [239, p.361],

$$\begin{aligned} H_0^{(1)}\left(k\sqrt{R^2+\rho^2-2R\rho\,\cos(\theta-\phi)}\right) &= \sum_{m=-\infty}^{\infty} H_m^{(1)}(k\rho) J_m(kR) \cos m(\theta-\phi) \\ &= H_0^{(1)}(k\rho)J_0(kR) + 2\sum_{m=1}^{\infty} H_m^{(1)}(k\rho)J_m(kR)\cos m(\theta-\phi), \quad R < \rho. \end{aligned} \tag{8.2.18}$$

Then, we have the following lemma from (8.2.18).

Lemma 8.2.1. *There exist the equalities for* $R<\rho$,

$$\int_0^{2\pi} H_0^{(1)}\left(k\sqrt{R^2+\rho^2-2R\rho\,\cos(\theta-\phi)}\right)d\phi = 2\pi H_0^{(1)}(k\rho)J_0(kR),$$
$$\int_0^{2\pi} H_0^{(1)}\left(k\sqrt{R^2+\rho^2-2R\rho\,\cos(\theta-\phi)}\right)\cos(m\phi)\,d\phi = 2\pi H_m^{(1)}(k\rho)J_m(kR)\cos(m\theta),$$
$$\int_0^{2\pi} H_0^{(1)}\left(k\sqrt{R^2+\rho^2-2R\rho\,\cos(\theta-\phi)}\right)\sin(m\phi)\,d\phi = 2\pi H_m^{(1)}(k\rho)J_m(kR)\sin(m\theta).$$

From Lemma 8.2.1, for $P_n(\rho,\theta)$ in (8.2.14), we can find the approximation,

$$P_n = P_n(\rho,\theta) \approx \sum_{j=1}^{N} c_j\Phi_j(\rho,\theta) = u_N^* := \Sigma_N(P_n;\rho,\theta), \tag{8.2.19}$$

where $\Phi_j(\rho,\theta)$ are given in (8.2.4), and the coefficients are

$$c_j = \frac{1}{N}\left\{\frac{a_0}{J_0(kR)} + \sum_{m=1}^{n}\frac{1}{J_m(kR)}\left[a_m\,\cos(mjh) + b_m\,\sin(mjh)\right]\right\}. \tag{8.2.20}$$

Since the Bessel functions have infinite zeros, it is assumed that all denominators in (8.2.20) are nonzero:

$$J_m(kR) \neq 0, \quad \forall m. \tag{8.2.21}$$

For the error bounds between FS and PS, since the continuity extension in Remark 2.3.1 in Chapter 2 is needed, we assume that the continuous solution $u\in C(S_\infty)$ holds, which may not be written in some lemmas and theorems. We have the following lemma similarly to Chapter 7.

Lemma 8.2.2. *For* $N\geq 2n$, *there exists the bound,*

$$\begin{aligned}&\|P_n(\rho,\theta)-\Sigma_N(P_n;\rho,\theta)\|_{q,\Gamma_{\text{in}}}^2\\ &\leq CN^{2q}\sum_{m=0}^{n}\left\{\frac{M_{N-m}(k\rho)J_{N-m}(kR)}{M_m(k\widetilde{\rho})J_m(kR)}\right\}^2\|P_n(\rho,\theta)\|_{0,\Gamma_{\text{in}}}^2,\end{aligned} \tag{8.2.22}$$

where $\widetilde{\rho}\in\{r_{\min},r_{\max}\}$.

The factors $M_m(k\widetilde{\rho})J_m(kR)$ appear in the denominator of (8.2.22), where the modular $M_m(k\widetilde{\rho}) = |H_m^{(1)}(k\widetilde{\rho})|>0$. The zeros of $J_m(kR)$ occur if $\lambda_i^- = (k^-)^2 = \left(\frac{j_{m,\ell}}{R}\right)^2$, where $j_{m,\ell}$ is the ℓth zero of $J_m(x)$. The λ_i^- is called the spurious eigenvalue. More discussions on the spurious eigenvalues of the standard MFS are given in Section 8.3. We then assume that $k\neq\frac{j_{m,\ell}}{R}$, $\forall m,\ell$. However, in computation, it often happens that kR is very close to one zero $j_{m,\ell}$. Denote the gap

$$\delta = \left| \frac{k^2 - \left(\frac{j_{m,\ell}}{R}\right)^2}{\left(\frac{j_{m,\ell}}{R}\right)^2} \right| = \left| \frac{(kR)^2 - (j_{m,\ell})^2}{(j_{m,\ell})^2} \right| = \left| 1 - \frac{x^2}{(j_{m,\ell})^2} \right|, \tag{8.2.23}$$

where $x = kR$. Assume $0 < \delta \ll 1$, then $x \approx j_{m,\ell}$ from (8.2.23); it is called the degeneracy of spurious eigenvalues. Similarly to Chapter 7, we have the following theorems.

Theorem 8.2.1. *Let $0 < \delta \ll 1$ hold. When N is large and $N \geq 2n$, there exists the bound,*

$$\begin{aligned} &\|P_n(\rho,\theta) - \Sigma_N(P_n;\rho,\theta)\|_{q,\Gamma_{\text{in}}} \\ &\leq C\frac{1}{\delta}\sqrt{n}N^q \left(\frac{R}{r_{\min}}\right)^{N-2n} \left(\frac{r_{\max}}{r_{\min}}\right)^n \|P_n(\rho,\theta)\|_{0,\Gamma_{\text{in}}}, \quad R < r_{\min}. \end{aligned} \tag{8.2.24}$$

Theorem 8.2.2. *Suppose that $0 < \delta \ll 1$ and $u \in \mathbf{H}^p(\Gamma_{\text{in}})$ $(p \geq 1)$ hold. When the large $N\,(> 2n)$ is chosen as*

$$N \geq 2n + \frac{\ln\left(\frac{1}{\delta}\right) + n\ln\left(\frac{r_{\max}}{r_{\min}}\right) + \left(p + \frac{1}{2}\right)\ln n}{\ln\left(\frac{r_{\min}}{R}\right)}, \tag{8.2.25}$$

the solution u_N in (8.2.8) by the standard MFS has the optimal polynomial convergence rates,

$$\|u - u_N\|_{0,\Gamma} = O\left(\frac{1}{N^p}\|u\|_{p,\Gamma_{\text{in}}}\right). \tag{8.2.26}$$

Remark 8.2.1. *To bypass the spurious eigenvalues, the condition (8.2.21) must hold. One way is that if we could choose R so small such that $kR < j_{0,1}$, where $j_{0,1} = 2.40482$ from [1, p.409]. The error analysis may follow Section 7.3.2. From Section 8.7, when $kR = 0.02$ (e.g., $k = 2$ and $R = 0.01$), the numerical solutions are satisfactory. Otherwise when $kR > j_{0,1}$, the annoying spurious eigenvalues may still exist. The better remedy is to develop the new modified MFS given in Section 8.4. In the next section, however, the spurious eigenvalues of the standard MFS are further explored.*

8.3 Numerical Characteristics of Spurious Eigenvalues by MFS

The standard MFS suffers from spurious eigenvalues for the Helmholtz equation. A view of the spurious eigenvalues in BEM was given by Chen *et al.* [46]. In this section, we will explore their numerical characteristics. For the exterior Dirichlet problems (EDP) in (8.2.1)–(8.2.3), there always exists a unique solution (*i.e.*, no true eigenvalues exist), which can be expressed in (8.2.13). If the PS in (8.2.14) is chosen instead of the FS in (8.2.8), the approximate solutions can also be found from (8.2.9) (or (8.2.11)). This is the method of particular solutions (MPS) in [169, Chapters 9 and 10]. By the MPS, for every bounded $k > 0$, the optimal convergence rates can be achieved. By the standard MFS, in contrast, for some specific k, the solutions cannot succeed at some pseudo-boundary of source nodes; the spurious eigenvalues (*i.e.*, the fictitious resonance frequencies) are called in this chapter.

For the sources nodes (R_j, ϕ_j), we have from the addition theorem (8.2.18)

$$\begin{aligned} &H_0^{(1)}\left(k\sqrt{R_j^2+\rho^2-2R_j\rho\,\cos(\theta-\phi_j)}\right) \\ &\quad = J_0(kR_j)H_0^{(1)}(k\rho)+2\sum_{m=1}^{\infty} J_m(kR_j)H_m^{(1)}(k\rho)\cos m(\theta-\phi_j). \end{aligned} \tag{8.3.1}$$

From (8.3.1), the equation (8.2.8) may lead to one solution $u^*(\rho,\theta)$ of (8.2.13),

$$\begin{aligned} u_N &= \sum_{j=1}^{N} c_j H_0^{(1)}\left(k\sqrt{R_j^2+\rho^2-2R_j\rho\,\cos(\theta-\phi_j)}\right) \\ &= H_0^{(1)}(k\rho)a_0^* + \sum_{m=1}^{\infty} H_m^{(1)}(k\rho)[a_m^*\,\cos(m\theta)+b_m^*\,\sin(m\theta)] := u^*(\rho,\theta), \end{aligned} \tag{8.3.2}$$

where the coefficients,

$$\begin{aligned} &a_0^* = \sum_{j=1}^{N} c_j J_0(kR_j), \quad a_m^* = 2\sum_{j=1}^{N} c_j J_m(kR_j)\cos(m\phi_j), \\ &b_m^* = 2\sum_{j=1}^{N} c_j J_m(kR_j)\sin(m\phi_j). \end{aligned} \tag{8.3.3}$$

First, consider the circular interior boundary $\Gamma_{\text{in}}^{\circ} = \{(r,\theta)|r=\rho, 0 \le \theta \le 2\pi\}$. For the standard MFS, the collocation equations (8.2.11) lead to

$$\sum_{j=1}^{N} c_j \Phi_j(P_\ell) = f(P_\ell), \quad P_\ell \in \Gamma_{\text{in}}^{\circ}, \quad \ell = 1, 2, \ldots, N. \tag{8.3.4}$$

The spurious eigenvalues are known for the sources nodes (R, ϕ_j) as $\lambda^- = (k^-)^2$ from (*cf.* (8.2.21)),

$$J_{m^*}(k^- R) = 0. \tag{8.3.5}$$

Define the relative error $\frac{\|u-u_N\|_{0,\Gamma_{\text{in}}^{\circ}}}{\|u\|_{0,\Gamma_{\text{in}}^{\circ}}}$. We have the following proposition.

Proposition 8.3.1. *For the source nodes* (R, ϕ_j)*, there exists the lower bound at (8.3.5),*

$$\frac{\|u-u_N\|_{0,\Gamma_{\text{in}}^{\circ}}}{\|u\|_{0,\Gamma_{\text{in}}^{\circ}}} \ge \frac{M_{m^*}(k^-\rho)\sqrt{a_{m^*}^2+b_{m^*}^2}}{\sqrt{2|a_0|^2 M_0^2(k^-\rho)+\sum_{m=1}^{\infty} M_m^2(k^-\rho)(|a_m|^2+|b_m|^2)}}, \tag{8.3.6}$$

where $b_0 = 0$ *for* $m^* = 0$.

Proof. We have from (8.2.13) and the orthogonality of trigonometric functions

$$\|u\|^2_{0,\Gamma^\circ_{\text{in}}} = \int_{\Gamma^\circ_{\text{in}}} u\bar{u}ds = \pi\rho\Big\{2|a_0|^2 M_0^2(k^-\rho) + \sum_{m=1}^{\infty} M_m^2(k^-\rho)(|a_m|^2 + |b_m|^2)\Big\}.$$

Under (8.3.5), we have $a^*_{m^*} = b^*_{m^*} = 0$ from (8.3.2) and (8.3.3), then the FS cannot present the true nonzero term,

$$v_{m^*} = H^{(1)}_{m^*}(k^-\rho)\{a_{m^*}\cos(m^*\theta) + b_{m^*}\sin(m^*\theta)\},$$

with a_{m^*} $(\neq 0)$ and b_{m^*} $(\neq 0)$. Hence, for the solution u_N in (8.2.8) missing the term v_{m^*}, we have

$$\|u - u_N\|^2_{0,\Gamma^\circ_{\text{in}}} \geq \int_{\Gamma^\circ_{\text{in}}} (v_{m^*})(\bar{v}_{m^*})ds = \pi\rho M^2_{m^*}(k^-\rho)\{|a_{m^*}|^2 + |b_{m^*}|^2\}, \quad m^* \geq 1, \tag{8.3.7}$$

$$\|u - u_N\|^2_{0,\Gamma^\circ_{\text{in}}} \geq 2\pi\rho|a_0|^2 M^2_{m^*}(k^-\rho), \quad m^* = 0. \tag{8.3.8}$$

The desired result (8.3.6) follows from (8.3.7) and (8.3.8). ■

Proposition 8.3.1 proves the divergence of the MFS at the spurious eigenvalues. The errors from (8.3.6) could be as small as $O(10^{-4})$, but they never diminish to the infinitesimal. Numerical examples are omitted. The divergence is the first numerical characteristic of spurious eigenvalues.

Next, consider stability. Denote (8.3.4) by

$$\mathbf{D}^*\mathbf{x} = \mathbf{f}, \tag{8.3.9}$$

where the matrix $\mathbf{D}^* = \text{circulant}(d_0^*, d_1^*, \ldots, d_{N-1}^*)$ is also circulant as in (8.6.3), where the entries $d_i^* = H_0^{(1)}\left(k\sqrt{R^2 + \rho^2 - 2R\rho\,\cos(ih)}\right)$. For large n, from (8.5.32) and (8.5.33) we have

$$|J_n(kR)|M_n(k\rho) \approx \frac{1}{\sqrt{2\pi n}}\left(\frac{ekR}{2n}\right)^n \times \sqrt{\frac{2}{\pi n}}\left(\frac{ek\rho}{2n}\right)^{-n} = \frac{1}{\pi n}\left(\frac{R}{\rho}\right)^n, \quad R < \rho. \tag{8.3.10}$$

We obtain the following lemma by following Chapter 7.

Lemma 8.3.1. *There exist approximations for the eigenvalues* λ_ℓ *of the matrix* $\mathbf{D}^*$ *in (8.3.9),*

$$\lambda_0 \approx N\{J_0(kR)H_0^{(1)}(k\rho) + 2J_N(kR)H_N^{(1)}(k\rho)\}, \tag{8.3.11}$$

$$\lambda_\ell \approx N\{J_\ell(kR)H_\ell^{(1)}(k\rho) + J_{N-\ell}(kR)H_{N-\ell}^{(1)}(k\rho)\}, \quad \ell = 1, 2, \ldots, N-1. \tag{8.3.12}$$

Similarly to Theorem 8.6.1 and Chapter 7, we have the following proposition.

Proposition 8.3.2. *For bounded k and the gap $\delta > 0$, there exists the bound,*

$$\text{Cond} = \text{Cond}(\mathbf{D}^*) \leq C\frac{1}{\delta}\frac{M_0(k\rho)|J_0(kR)|}{M_{\frac{N}{2}}(k\rho)|J_{\frac{N}{2}}(kR)|} \leq C\frac{1}{\delta}N\left(\frac{\rho}{R}\right)^{\frac{N}{2}}, \quad R < \rho.$$

Proposition 8.3.3. *For bounded k but under (8.3.5), there exists the bound,*

$$\text{Cond}^* \leq CN\left(\frac{\rho}{R}\right)^N. \tag{8.3.13}$$

Proof. The main differences are for the lower bound of λ_{m^*} in (8.3.11) and (8.3.12). Under (8.3.5), we have $|\lambda_{m^*}| \approx \varepsilon_{m^*} N|J_{N-m^*}(kR)|M_{N-m^*}(k\rho)$, where $\varepsilon_0 = 2$ and $\varepsilon_{m^*} = 1$ for $m^* \geq 1$. Then from (8.3.10), we obtain

$$\min_i |\lambda_i| \geq c_0 N|J_N(kR)|M_N(k\rho) \geq c_0\left(\frac{R}{\rho}\right)^N.$$

Since $\max_i |\lambda_i| = O(N)$, we have $\text{Cond}^* = \frac{\max_i |\lambda_i|}{\min_i |\lambda_i|} \leq CN\left(\frac{\rho}{R}\right)^N$. ■

When the gap $\delta \geq c_0 > 0$, we have $\text{Cond} = O\left(N\left(\frac{\rho}{R}\right)^{\frac{N}{2}}\right)$ from Proposition 8.3.2, and then $\text{Cond}^* = O\left(\frac{1}{N}(\text{Cond})^2\right)$ from Proposition 8.3.3. Hence, the ill-conditioning at spurious eigenvalues becomes much more severer. This is the second numerical characteristic of the spurious eigenvalues, which is like the Neumann problem of Laplace's equation by the standard MFS in Chapter 3 with the operator singularity. Since the spurious eigenvalues are known as (8.3.5), for the given k we may choose the R carefully to avoid them (*e.g.,* (8.7.6)).

Numerical experiments have been carried out, to verify Propositions 8.3.1 and 8.3.3; details are omitted. The spurious eigenvalues do exist numerically. Note that the spurious eigenvalues occur at the eigenvalues of the interior Dirichlet problem (IDP) on the pseudo-domain S^- ($\neq S$), where $S = 2D\backslash S_\infty$. Hence, the spurious eigenvalues of MFS and BEM are distinct. For the circular Γ_{in}°, the spurious eigenvalues of the BEM occur at $J_{m^*}(k\rho) = 0$ with $R < \rho$, differently from (8.3.5). Such conclusions are also supported by the numerical examples in [41].

There were many computational reports for the exterior problems by the MFS see [81, 129]. The MFS suffers from spurious eigenvalues (see Chapter 7). For source nodes (R_j, ϕ_j) on the non-circular pseudo-boundary ℓ_ε in (8.7.11), the explicit k of spurious eigenvalues (*i.e.*, the explicit eigenvalues of the IDP) are unknown. However, the unexpectedly huge Cond will indicate the existence of the spurious eigenvalues [46, 47]; see Proposition 8.3.3. In this chapter, we explore a comprehensive and advanced study of the spurious eigenvalues of the MFS and their removals.

When spurious eigenvalues occur, the gap between PS and FS cannot diminish. Both the MFS and the BEM stem from the FS so both suffer from spurious eigenvalues. However, the spurious eigenvalues of BEM and MFS are distinct; one originated from the interior boundary Γ_{in}, while the other from the pseudo-boundary $\Gamma\ (\neq \Gamma_{\text{in}})$ of source nodes. The numerical characteristics of spurious eigenvalues are important to the numerical Helmholtz solutions by the MFS as well as the BEM; see [44, 46, 47, 81, 129].

8.4 Modified MFS

To eliminate all spurious eigenvalues, we propose the new modified MFS. Denote a smooth closed curve Γ_R inside the interior boundary Γ_{in} satisfying (8.2.7). Let the source nodes be located on Γ_R, and choose Γ_R as the circle as in Figure 8.1. We have from the boundary integral equation (BIE) of the first kind on Γ_R

$$u(\rho,\theta) = \int_{\Gamma_R} H_0^{(1)}(kr)\sigma\, ds, \tag{8.4.1}$$

where the boundary density $\sigma = \sigma(R,\phi)$ on Γ_R.

The boundary integral equation of the first kind is expressed in [210, p.102] by $u(\rho,\theta) = \frac{\mathrm{i}}{4}\int_{\Gamma_R} H_0^{(1)}(kr)\sigma\, ds$, where the constant $\frac{\mathrm{i}}{4}$ is omitted for easy discussion. By the trapezoidal rule with equal meshspacing h, we have from (8.4.1)

$$u(\rho,\theta) \approx h\sum_{j=1}^{N} H_0^{(1)}(kr_j)\sigma_j = \sum_{j=1}^{N} c_j H_0^{(1)}(kr_j), \tag{8.4.2}$$

where $c_j = h\sigma_j$. This leads to the FS in (8.2.8) in the standard MFS. The MFS was viewed as the boundary integral equation method (BIEM) in Fairweather and Karageorghis [80].

The equation (8.4.1) is of the single-layer potential, and the alternative is to use the double-layer potential:

$$u(\rho,\theta) = \int_{\Gamma_R} \frac{\partial}{\partial \nu} H_0^{(1)}(kr)\sigma\, ds = -\int_{\Gamma_R} \frac{\partial}{\partial R} H_0^{(1)}(kr)\sigma\, ds, \tag{8.4.3}$$

where ν is the exterior normal to Γ_R, and $\frac{\partial}{\partial \nu} = -\frac{\partial}{\partial R}$. We have

$$\frac{\partial}{\partial R} H_0^{(1)}(kr) = -kH_1^{(1)}(kr)\frac{\partial r}{\partial R} = -\frac{k}{r}H_1^{(1)}(kr)(R-\rho\,\cos(\theta-\phi)). \tag{8.4.4}$$

By the trapezoidal rule, we may choose the other kind of FS,

$$u_N = \sum_{j=1}^{N} c_j \frac{\partial}{\partial R} H_0^{(1)}(kr_j), \tag{8.4.5}$$

instead of (8.2.8). Based on the error analysis (details omitted), the MFS using (8.4.5) also suffers from spurious eigenvalues at $J_n'(kR) = 0$. To avoid the spurious eigenvalues by the BEM, a combination of the single-layer and the double-layer potentials was used in Burton and Miller [30], Chen *et al.* [44], Engleder and Steinbach [77], Buffa and Hiptmair [29], and Sauter and Schwab [210, p.175]. We then use the new combined FS,

$$\begin{aligned}\boldsymbol{\Psi}_j(\rho,\theta) &= \left(\frac{\partial}{\partial R} \pm \mathbf{i}\eta\right) H_0^{(1)}(kr_j) = \mathcal{D}H_0^{(1)}(kr_j) \\ &= \mathcal{D}H_0^{(1)}\left(k\sqrt{R^2+\rho^2-2R\rho\,\cos(\theta-\phi_j)}\right),\end{aligned} \tag{8.4.6}$$

where the operator $\mathcal{D} = \left(\frac{\partial}{\partial R} \pm \mathbf{i}\eta\right)$. In this chapter, choose $\eta = k$ and $\phi_j = \frac{2\pi}{N}j$. The new FS are given by

$$u_N = \sum_{j=1}^{N} c_j \boldsymbol{\Psi}_j(\rho,\theta), \tag{8.4.7}$$

where c_j ($\in \mathbf{C}$) are the unknown coefficients. The collocation equations (8.2.11) are modified as

$$\sqrt{\triangle h_\ell}\sum_{j=1}^{N} c_j \boldsymbol{\Psi}_j(\rho_\ell,\theta_\ell) = \sqrt{\triangle h_\ell}\, f(\rho_\ell,\theta_\ell), \quad (\rho_\ell,\theta_\ell)\in \boldsymbol{\Gamma}_{\rm in}^{\ell}, \quad \ell = 1,2,\ldots,M, \tag{8.4.8}$$

where $M \geq N$. Once the complex coefficients c_j are found, we obtain the solutions from (8.4.7). The algorithms of (8.4.7) and (8.4.8) are called the modified MFS. In fact, the $\boldsymbol{\Gamma}_R$ is not necessary to be circular, and the numerical computation is given in Section 8.7.2. Note that the non-circular $\boldsymbol{\Gamma}_{\rm in}$ and $\boldsymbol{\Gamma}_R$, the new FS in (8.4.7) remain the same. Hence the new algorithms are simple, compared with the modified BEM in [29, 46, 77]. Since a smooth non-circular $\boldsymbol{\Gamma}_R$ may be chosen easily, we can avoid the complicated combined operators for the Lipschitz boundaries in [29, 77]. The remarkable advantage of the modified MFS is to bypass all spurious eigenvalues.

8.5 Error Analysis for Modified MFS

Since the modified MFS using $\mathcal{D}H_0^{(1)}(kr)$ as FS is more complicated than the standard MFS, the proofs involve more challenging techniques. To follow the proofs below more easily, let us address the outlines. Although the basic analytical framework follows Chapter 7, the key lemmas in Section 8.5.1 are important, and the proof techniques are intriguing. Since the non-zero factors $\mathcal{D}J_m(kR)$ appear in the denominator in (8.5.5) below, the estimation on the lower bounds of $|\mathcal{D}J_m(kR)|$ is essential to error analysis and is given in Lemma 8.5.3. Next, the estimation of the denominators $|\mathcal{D}J_m(kR)|M_m(k\widetilde{\rho})$ in (8.5.58) is also imperative and given in Lemma 8.5.5. From (8.5.4), the errors between FS and PS can be found by Fourier expansions, and their bounds are given in Theorem 8.5.1. The optimal polynomial convergence rates are finally obtained in Theorem 8.5.2.

8.5.1 Preliminary Lemmas

We have from the addition theorem (8.2.18) for $R<\rho$

$$\begin{aligned}&\frac{\partial}{\partial R}H_0^{(1)}\left(k\sqrt{R^2+\rho^2-2R\rho\,\cos(\theta-\phi)}\right)\\&=H_0^{(1)}(k\rho)\frac{\partial}{\partial R}J_0(kR)+2\sum_{m=1}^{\infty}H_m^{(1)}(k\rho)\cos m(\theta-\phi)\frac{\partial}{\partial R}J_m(kR).\end{aligned}\tag{8.5.1}$$

From (8.2.18) and (8.5.1), we have

$$\begin{aligned}\mathcal{D}H_0^{(1)}(kr)&=\mathcal{D}H_0^{(1)}\left(k\sqrt{R^2+\rho^2-2R\rho\,\cos(\theta-\phi)}\right)\\&=H_0^{(1)}(k\rho)\mathcal{D}J_0(kR)+2\sum_{m=1}^{\infty}H_m^{(1)}(k\rho)\cos m(\theta-\phi)\mathcal{D}J_m(kR),\quad R<\rho,\end{aligned}\tag{8.5.2}$$

where the combined operator $\mathcal{D}=\left(\frac{\partial}{\partial R}\pm\mathbf{i}k\right)$. Choose the new FS in (8.4.6),

$$\mathbf{\Psi}(R,\theta;\rho,\phi)=\mathcal{D}H_0^{(1)}\left(k\sqrt{R^2+\rho^2-2R\rho\,\cos(\theta-\phi)}\right).\tag{8.5.3}$$

From (8.5.2), we have the following lemma.

Lemma 8.5.1. *There exist the equalities,*

$$\begin{aligned}&\int_0^{2\pi}\mathbf{\Psi}(R,\theta;\rho,\phi)\,d\phi=2\pi H_0^{(1)}(k\rho)\mathcal{D}J_0(kR),\\&\int_0^{2\pi}\mathbf{\Psi}(R,\theta;\rho,\phi)\cos(m\phi)\,d\phi=2\pi H_m^{(1)}(k\rho)\mathcal{D}J_m(kR)\cos(m\theta),\\&\int_0^{2\pi}\mathbf{\Psi}(R,\theta;\rho,\phi)\sin(m\phi)\,d\phi=2\pi H_m^{(1)}(k\rho)\mathcal{D}J_m(kR)\sin(m\theta).\end{aligned}$$

From Lemma 8.5.1, for the polynomials $P_n(\rho,\theta)$ in (8.2.14), we can find an approximation,

$$P_n(\rho,\theta)\approx\sum_{j=1}^{N}c_j\mathbf{\Psi}_j(\rho,\theta)=u_N^*:=\mathbf{\Sigma}_N^+(P_n;\rho,\theta),\tag{8.5.4}$$

where $\mathbf{\Psi}_j(\rho,\theta)$ are given in (8.5.3), and the coefficients

$$c_j=\frac{1}{N}\left\{\frac{a_0}{\mathcal{D}J_0(kR)}+\sum_{m=1}^{n}\frac{1}{\mathcal{D}J_m(kR)}\left[a_m\,\cos(mjh)+b_m\,\sin(mjh)\right]\right\},\tag{8.5.5}$$

where

$$|\mathcal{D}J_m(kR)| = \left|\left(\frac{\partial}{\partial R} \pm \mathbf{i}k\right) J_m(kR)\right| = \left\{\left(\frac{\partial}{\partial R} J_m(kR)\right)^2 + k^2 J_m^2(kR)\right\}^{\frac{1}{2}}.$$

Since $J_m(kR)$ and $\frac{\partial}{\partial R} J_m(kR)$ have no common zeros, we conclude $|\mathcal{D}J_m(kR)| > 0$ with $\forall m, k$. Hence, no spurious eigenvalues exist for the modified MFS; this is a remarkable advantage over the standard MFS in Section 8.2.

Note that the denominator $\mathcal{D}J_m(kR)$ appears in (8.5.5). The bounds $|\mathcal{D}J_m(kR)|$ are essential in error analysis, and given in Lemmas 8.5.2 and 8.5.3 below. We have for $x = kR$

$$|\mathcal{D}J_n(kR)|^2 = k^2\{(J_n'(x))^2 + J_n^2(x)\}. \tag{8.5.6}$$

The zeros, $j_{m,\ell}$ of $J_m(x)$ and $j'_{m,\ell}$ of $J'_m(x)$, are simple and distinct to each other. For the given m, there exist the bounds in [1, p.370],

$$m \le j'_{m,\ell} < j_{m,\ell} < j'_{m,\ell+1} < j_{m,\ell+1}. \tag{8.5.7}$$

From Elbert [79, p.72], there exists the lower gap for a fixed $m \left(> \frac{1}{2}\right)$,

$$j_{m,\ell^*} - j_{m,\ell} > (\ell^* - \ell)\pi, \quad \ell^* > \ell.$$

Then we have the minimal gap among different $j_{m,\ell}$ for given $m \ge 0$,

$$\min_{\ell}(j_{m,\ell+1} - j_{m,\ell}) \ge c_0^*.$$

Denote the gap

$$\min_{m,\ell}\{|j'_{m,\ell} - j_{m,\ell}|, |j'_{m,\ell+1} - j_{m,\ell}|\} \ge d_0^*,$$

where $c_0^*\,(> 0)$ and $d_0^*\,(> 0)$ are two constants independent of m and ℓ. There exist two formulas from [1, p.370, 9.5.10, 9.5.11],

$$J_n(x) = \frac{1}{n!}\left(\frac{x}{2}\right)^n \prod_{k=1}^{\infty}\left(1 - \frac{x^2}{j_{n,k}^2}\right), \tag{8.5.8}$$

$$J_n'(x) = \frac{1}{2(n-1)!}\left(\frac{x}{2}\right)^{n-1} \prod_{k=1}^{\infty}\left(1 - \frac{x^2}{(j'_{n,k})^2}\right), \quad n \ge 1, \tag{8.5.9}$$

where $j_{n,k}$ and $j'_{n,k}$ are the kth zeros of $J_n(x)$ and $J'_n(x)$, respectively.

Lemma 8.5.2. *For the bounded k, there exist the bounds,*

$$|\mathcal{D}J_n(kR)| \le C\frac{1}{(n-1)!}\left(\frac{kR}{2}\right)^{n-1}, \quad n \ge 1, \tag{8.5.10}$$

$$|\mathcal{D}J_n(kR)| \ge c_0 \frac{1}{(n-1)!}\left(\frac{kR}{2}\right)^n, \quad \textit{for large } n, \tag{8.5.11}$$

where $c_0\,(>0)$ *and* C *are two constants independent of* n.

Proof. We have from (8.5.8) and (8.5.9) for $n \ge 1$

$$|J_n(x)| \le \frac{1}{n!}\left(\frac{x}{2}\right)^n, \quad |J_n'(x)| \le \frac{1}{2(n-1)!}\left(\frac{x}{2}\right)^{n-1},$$

to give from (8.5.6)

$$|\mathcal{D}J_n(kR)|^2 \le \frac{k^2}{4}\left\{\frac{\left(\frac{kR}{2}\right)^{n-1}}{(n-1)!}\right\}^2 + k^2\left\{\frac{\left(\frac{kR}{2}\right)^n}{n!}\right\}^2 \le C\left\{\frac{\left(\frac{kR}{2}\right)^{n-1}}{(n-1)!}\right\}^2.$$

This is the first desired result (8.5.10). Next, for the bounded $x = kR$ and a large n, we have from [1, p.365]

$$|J_n(x)| \approx \frac{1}{\sqrt{2\pi n}}\left(\frac{ex}{2n}\right)^n \approx \frac{1}{n!}\left(\frac{x}{2}\right)^n, \tag{8.5.12}$$

where we have used Stirling's formula $n! \approx \sqrt{2\pi n}\left(\frac{n}{e}\right)^n$ in [1, p.257, 6.1.37]. Then the derivatives have

$$|J_n'(x)| \approx \frac{1}{x(n-1)!}\left(\frac{x}{2}\right)^n, \quad x > 0,$$

to give from (8.5.6)

$$|\mathcal{D}J_n(kR)|^2 \approx \frac{1}{R^2}\left\{\frac{\left(\frac{kR}{2}\right)^n}{(n-1)!}\right\}^2 + k^2\left\{\frac{\left(\frac{kR}{2}\right)^n}{n!}\right\}^2 \ge c_0\left\{\frac{\left(\frac{kR}{2}\right)^n}{(n-1)!}\right\}^2.$$

This is the second desired result (8.5.11). ■

We give the following key lemma.

Lemma 8.5.3. *Let* k *be bounded. Suppose that* $x = kR$ *is closer to* $j_{n,\ell}$ *and* $x = kR \in [j'_{n,\ell}, j'_{n,\ell+1}]$. *There exists the lower bound for (8.5.6),*

$$|\mathcal{D}J_n(kR)| \ge c_0 \min\{|J_n(j'_{n,\ell+1})|, |J_n'(j_{n,\ell})|\}, \quad n \ge 0, \tag{8.5.13}$$

where $c_0\,(>0)$ *is a constant independent of* n *and* ℓ.

Proof. Define the positive function

$$f(x) = |\mathcal{D}J_n(kR)|^2 = k^2\{(J_n'(x))^2 + J_n^2(x)\}. \tag{8.5.14}$$

For $x \in [j'_{n,\ell}, j'_{n,\ell+1}]$, the minimal values of $f(x)$ may exist at $x = \bar{x}$, provided that

$$f'(\bar{x}) = 2k^2 J_n'(\bar{x})\{J_n''(\bar{x}) + J_n(\bar{x})\} = 0.$$

Then two possible values of extremum exist,

$$J'_n(\bar{x}) = 0, \tag{8.5.15}$$

$$J''_n(\bar{x}) + J_n(\bar{x}) = 0. \tag{8.5.16}$$

From (8.5.15), the minimum may occur at two boundary points $\bar{x} = j'_{n,\ell}, j'_{n,\ell+1}$. The other possible minimum is given from (8.5.16). The Bessel functions satisfy

$$x^2 J''_n(x) + xJ'_n(x) + (x^2 - n^2)J_n(x) = 0. \tag{8.5.17}$$

From (8.5.16) and (8.5.17), the root $\bar{x}^*(= \bar{x})$ is found from

$$n^2 J_n(\bar{x}^*) = \bar{x}^* J'_n(\bar{x}^*). \tag{8.5.18}$$

The roots of (8.5.18) are discussed in Engleder and Steinbach [77] for the upper bounds of the first root only. In $[j'_{n,\ell}, j'_{n,\ell+1}]$, the curve of $J_n(x)$ passes the zero at $j_{n,\ell}$. From (8.5.18), we have $\bar{x}^* \in (j'_{n,\ell}, j_{n,\ell}) \cup (j_{n,\ell}, j'_{n,\ell+1})$. In fact, the root $\bar{x}^*$ occurs only if the signs of both $J_n(x)$ and $J'_n(x)$ are the same: $J_n(\bar{x}^*)J'_n(\bar{x}^*) > 0$, so that $\bar{x}^* \in (j_{n,\ell}, j'_{n,\ell+1})$. This conclusion may be illustrated in Figure 8.2, where the root of $J_n(\bar{x}^*) = J'_n(\bar{x}^*)$ exists in the same section $\bar{x}^* \in (j_{n,\ell}, j'_{n,\ell+1})$ as (8.5.18). There exist two cases for (8.5.18) in $[j'_{n,\ell}, j'_{n,\ell+1}]$.

Case A. The curve of $J_n(x)$ is strictly increasing, then $J'_n(x) > 0$. The inequality $J_n(\bar{x}^*)J'_n(\bar{x}^*) > 0$ happens only in $(j_{n,\ell}, j'_{n,\ell+1})$. See Figure 8.2(a).

Case B. The curve of $J_n(x)$ is strictly decreasing, then $J'_n(x) < 0$. The inequality $J_n(\bar{x}^*)J'_n(\bar{x}^*) > 0$ also happens only in $(j_{n,\ell}, j'_{n,\ell+1})$. See Figure 8.2(b).

Hence we find the minimal value of function (8.5.14),

$$f(x) \geq \min\{f(\bar{x}^*), f(j'_{n,\ell}), f(j'_{n,\ell+1})\}. \tag{8.5.19}$$

Next, we have

$$f(j'_{n,\ell}) = k^2\{(J'_n(j'_{n,\ell}))^2 + J_n^2(j'_{n,\ell})\} = k^2 J_n^2(j'_{n,\ell}), \tag{8.5.20}$$

$$f(j'_{n,\ell+1}) = k^2\{(J'_n(j'_{n,\ell+1}))^2 + J_n^2(j'_{n,\ell+1})\} = k^2 J_n^2(j'_{n,\ell+1}). \tag{8.5.21}$$

Since $|J_n(j'_{n,\ell+1})| < |J_n(j'_{n,\ell})|$ from [1, p.411, Table 9.5], we have from (8.5.19)–(8.5.21)

$$f(x) \geq \min\{f(\bar{x}^*), k^2 J_n^2(j'_{n,\ell+1})\}. \tag{8.5.22}$$

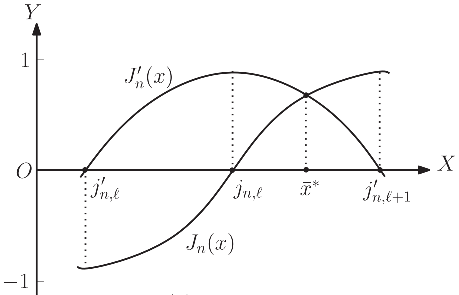

(a) *Case A*

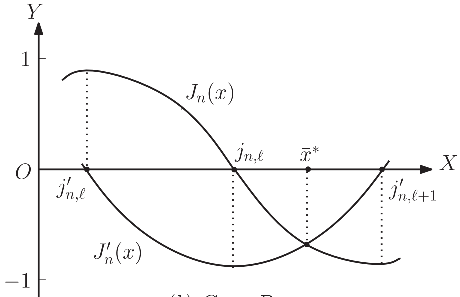

(b) *Case B*

FIG. 8.2 – The roots of $J_n(x) = J_n'(x)$ in $(j_{n,\ell}', j_{n,\ell+1}')$ in Case A(a) and Case B(b).

For $\bar{x}^* \in (j_{n,\ell}, j_{n,\ell+1}')$, first suppose

$$|\bar{x}^* - j_{n,\ell+1}'| \le \frac{1}{2}|j_{n,\ell+1}' - j_{n,\ell}|. \tag{8.5.23}$$

Then the $\bar{x}^*$ is closer to $j_{n,\ell+1}'$ than to $j_{n,\ell}$. Since $J_n''(\bar{x}) = -J_n(\bar{x})$ from (8.5.16), the function $J_n(\bar{x}^*)$ reaches the maximum (or the minimum) at **Case A** (or **Case B**). Take **Case A** in Figure 8.2 for example, where both $J_n(x) > 0$ and $J_n'(x) > 0$. From (8.5.17) and $x > j_{n,\ell} > n$ due to (8.5.7), we have

$$J_n''(x) = -\frac{1}{x}J_n'(x) - \frac{x^2 - n^2}{x^2}J_n(x) < 0, \tag{8.5.24}$$

and the curve of $J_n(x)$ in $(j_{n,\ell}, j_{n,\ell+1}')$ is convex. Then we have from (8.5.23)

$$\begin{aligned} |J_n(\bar{x}^*)| = J_n(\bar{x}^*) &\ge \frac{\bar{x}^* - j_{n,\ell}}{j_{n,\ell+1}' - j_{n,\ell}} J_n(j_{n,\ell+1}') \\ &= \left\{1 - \frac{|\bar{x}^* - j_{n,\ell+1}'|}{|j_{n,\ell+1}' - j_{n,\ell}|}\right\}|J_n(j_{n,\ell+1}')| \ge \frac{1}{2}|J_n(j_{n,\ell+1}')|, \end{aligned}$$

and then

$$f(\bar{x}^*) = k^2\{(J'_n(\bar{x}^*))^2 + J_n^2(\bar{x}^*)\} > k^2 J_n^2(\bar{x}^*) \ge \frac{k^2}{4} J_n^2(j'_{n,\ell+1}). \tag{8.5.25}$$

Otherwise, when the condition (8.5.23) is invalid, the $\bar{x}^*$ is closer to $j_{n,\ell}$. For **Case A**, the curve of $J'_n(x)$ in $(j_{n,\ell}, j'_{n,\ell+1})$ is also convex; see Remark 8.5.1. Similarly, we have $|J'_n(\bar{x}^*)| \ge \frac{1}{2}|J'_n(j_{n,\ell})|$ and then

$$f(\bar{x}^*) = k^2\{(J'_n(\bar{x}^*))^2 + J_n^2(\bar{x}^*)\} > k^2 (J'_n(\bar{x}^*))^2 \ge \frac{k^2}{4} (J'_n(j_{n,\ell}))^2. \tag{8.5.26}$$

For **Case B**, the bounds (8.5.25) and (8.5.26) also hold. Combining (8.5.22), (8.5.25) and (8.5.26) gives

$$f(x) = |\mathcal{D} J_n(kR)| \ge c_0 \min\{|J_n(j'_{n,\ell+1})|, |J'_n(j_{n,\ell})|\}.$$

This is the desired result (8.5.13) and completes the proof of Lemma 8.5.3. ■

Remark 8.5.1. *For $x \in (j_{n,\ell}, j'_{n,\ell+1})$ in **Case A** with both $J_n(x) > 0$ and $J'_n(x) > 0$, the curve of $J'_n(x)$ is also convex. This conclusion is confirmed by the following arguments. For small n, the convex curve of $J'_n(x)$ can be discovered in [198, p.218, Figures 10.3.1 and 10.3.3] with $J'_0(x) = -J_1(x)$ and $J'_5(x)$. Below, we prove that it is true for a suitable large n but bounded x. By differentiating (8.5.17), we have*

$$\begin{aligned} &\frac{d}{dx}\left\{x^2 J''_n(x) + x J'_n(x) + (x^2 - n^2) J_n(x)\right\} \\ &= x^2 J'''_n(x) + 3x J''_n(x) + (x^2 - n^2 + 1) J'_n(x) + 2x J_n(x) = 0. \end{aligned} \tag{8.5.27}$$

By using (8.5.24), the equation (8.5.27) leads to

$$x^2 J'''_n(x) = -(x^2 - n^2 - 2) J'_n(x) - \frac{1}{x}(3n^2 - x^2) J_n(x). \tag{8.5.28}$$

*From Watson [239, p.486], there exists the lower bound $j'_{n,\ell} \ge j'_{n,1} > \sqrt{n(n+2)}$. For $x \in (j_{n,\ell}, j'_{n,\ell+1})$ in **Case A**, we have $x > j_{n,\ell} > j'_{n,\ell} > \sqrt{n(n+2)}$, and then*

$$(x^2 - n^2 - 2) > n(n+2) - n^2 - 2 = 2(n-1) \ge 0, \quad n \ge 1.$$

*Since x is bounded, for a suitable large n such as $n \ge \frac{j'_{n,\ell+1}}{\sqrt{3}} \ge \frac{x}{\sqrt{3}}$, the other factor $\frac{1}{x}(3n^3 - x^2) \ge 0$ in (8.5.28). Hence for **Case A** with $J_n(x) > 0$ and $J'_n(x) > 0$, we conclude from (8.5.28) that $J'''_n(x) < 0$, and then the curve of $J'_n(x)$ in $x \in (j_{n,\ell}, j'_{n,\ell+1})$ is also convex. Since k and $R (< r_{\min})$ are bounded in our application, such a suitable $n^*(\ge 1)$ can be found as $n \ge n^* \ge \frac{kr_{\min}}{\sqrt{3}}$.*

Remark 8.5.2. *For the large* n*, the explicit expansions of* $J_n'(j_{n,\ell})$ *and* $J_n(j_{n,\ell}')$ *are given in [198, p.237] as*

$$j_{n,\ell} \approx n \sum_{k=0}^{\infty} \frac{\alpha_k}{n^{2k/3}}, \quad J_n'(j_{n,\ell}) \approx (-1)^{\ell} \frac{\left(\frac{2}{n}\right)^{\frac{2}{3}}}{\pi M(a_\ell)} \sum_{k=0}^{\infty} \frac{\beta_k}{n^{2k/3}}, \tag{8.5.29}$$

$$j_{n,\ell}' \approx n \sum_{k=0}^{\infty} \frac{\alpha_k'}{n^{2k/3}}, \quad J_n(j_{n,\ell}') \approx (-1)^{\ell-1} \frac{\left(\frac{2}{n}\right)^{\frac{1}{3}}}{\pi N(a_\ell')} \sum_{k=0}^{\infty} \frac{\beta_k'}{n^{2k/3}}, \tag{8.5.30}$$

where $\alpha_k, \alpha_k', \beta_k$ *and* β_k' *are the constants given in [198, p.236, p.237],* a_ℓ *and* a_ℓ' *are the* ℓ*th negative roots of the Airy functions* $Ai(x)$ *and* $Ai'(x)$*, respectively, and* $M(x)$ *and* $N(x)$ *are the modulus functions for the Airy functions and their derivatives, respectively. From Lemma 8.5.3, (8.5.29) and (8.5.30), the nonzero* $|\mathcal{D}J_n(kR)|$ *has the lower bound (also see [198, p.238, (10.21.42), (10.21.44)])*

$$|\mathcal{D}J_n(kR)| = k\Big\{(J_n'(x))^2 + J_n^2(x)\Big\}^{\frac{1}{2}} \geq c_0 n^{-\frac{2}{3}}, \tag{8.5.31}$$

where c_0 *is a constant independent of* n*. Therefore, no spurious eigenvalues exist for the modified MFS.*

Denote the modular of Hankel functions,

$$M_\mu^2(x) = |H_\mu^{(1)}(x)|^2 = J_\mu^2(x) + Y_\mu^2(x), \quad \mu \geq 0, x > 0.$$

For large μ, there exist the approximations from [198, p.231, 10.19.2],

$$J_\mu(x) \approx \frac{1}{\sqrt{2\pi\mu}} \left(\frac{ex}{2\mu}\right)^{\mu}, \quad Y_\mu(x) \approx -\mathbf{i}H_\mu^{(1)}(x) \approx -\sqrt{\frac{2}{\pi\mu}} \left(\frac{ex}{2\mu}\right)^{-\mu}. \tag{8.5.32}$$

Then we have for large μ,

$$M_\mu(x) \approx \sqrt{\frac{2}{\pi\mu}} \left(\frac{ex}{2\mu}\right)^{-\mu}. \tag{8.5.33}$$

From [198, p.225, 10.9.30] and [90, p.727, 6.664.4], there exists Nicholson's integral,

$$M_\mu^2(x) = \left|H_\mu^{(1)}(x)\right|^2 = \frac{8}{\pi^2} \int_0^\infty \mathcal{K}_0(2x \sinh(t)) \cosh(2\mu t)\, dt > 0, \quad \mu \geq 0, \tag{8.5.34}$$

where $\mathcal{K}_0(x) = \int_0^\infty e^{-x \cosh \eta} d\eta$ is the Bessel functions of the third kind [239, p.181].

Lemma 8.5.4. *For* $M_\mu(x)$ *defined in (8.5.34), there exist the bounds,*

$$M_\mu(x) < M_\nu(x), \quad 0 \leq \mu < \nu, \tag{8.5.35}$$

$$M_\mu(x) > M_\mu(y), \quad x < y. \tag{8.5.36}$$

Proof. By differentiating both sides of (8.5.34) with respect to μ, we have

$$2M_\mu(x)\frac{\partial}{\partial\mu}M_\mu(x) = \frac{16}{\pi^2}\int_0^\infty \mathcal{K}_0(2x\,\sinh(t))\sinh(2\mu t)t\ dt > 0,\ \ \mu \geq 0,$$

to give

$$\frac{\partial}{\partial\mu}M_\mu(x) = \frac{8}{\pi^2}\frac{1}{M_\mu(x)}\int_0^\infty \mathcal{K}_0(2x\,\sinh(t))\sinh(2\mu t)t\ dt > 0.$$

This gives the first result (8.5.35). Since $\mathcal{K}_0'(x) = -\mathcal{K}_1(x) < 0$, we also have from (8.5.34)

$$\frac{\partial}{\partial x}M_\mu(x) = -\frac{8}{\pi^2}\frac{1}{M_\mu(x)}\int_0^\infty \mathcal{K}_1(2x\,\sinh(t))\cosh(2\mu t)\sinh(t)\,dt < 0.$$

This gives the second result (8.5.36). ■

We give the other key lemma.

Lemma 8.5.5. *Let k be bounded. For $m \in [0, n]$, there exists the lower bound,*

$$\mathcal{T}_1^* = M_m(kR)|\mathcal{D}J_m(kr)| \geq c_0\left(\frac{R}{r_{\max}}\right)^n, \tag{8.5.37}$$

where $R < r_{\min} \leq r \leq r_{\max}$, and $c_0\ (> 0)$ is a constant independent of n.

Proof. There are two cases for $m \in [0, n]$ whether m is large or not. First, for large m, we have from (8.5.33) and the Stirling's formula $(m-1)! \approx \sqrt{\frac{2\pi}{m}}\left(\frac{m}{e}\right)^m$

$$M_m(x) \approx \sqrt{\frac{2}{\pi m}}\left(\frac{ex}{2m}\right)^{-m} \approx \frac{(m-1)!}{\pi}\left(\frac{x}{2}\right)^{-m}. \tag{8.5.38}$$

Hence for large m, we have from (8.5.38), (8.5.11) and $r \leq r_{\max}$

$$\begin{aligned}\mathcal{T}_1^* &= |\mathcal{D}J_m(kR)|M_m(kr) \\ &\geq c_0\frac{1}{(m-1)!}\left(\frac{kR}{2}\right)^m \times (m-1)!\left(\frac{kr}{2}\right)^{-m} \geq c_0\left(\frac{R}{r}\right)^m \geq c_0\left(\frac{R}{r_{\max}}\right)^n := I.\end{aligned} \tag{8.5.39}$$

Second, consider the challenging and imperative case of bounded m. Denote $x = kR \in [j'_{m,\ell}, j'_{m,\ell+1}] = [x^-, x^+]$, where $x^- = j'_{m,\ell}$, and $x^+ = j'_{m,\ell+1}$. First, we have $|\mathcal{D}J_0(x)| \geq c_0$. For $m \geq 1$, from Lemma 8.5.3 and (8.5.31),

$$|\mathcal{D}J_m(x)| = k\{(J_m'(x))^2 + J_m^2(x)\}^{\frac{1}{2}} \geq c_0 m^{-\frac{2}{3}} \geq c_0(kR)^{-\frac{2}{3}} \geq c_0, \quad m \geq 1, \tag{8.5.40}$$

where we have used $m \leq j_{m,1} \leq kR$ from (8.5.7). Besides, from Lemma 8.5.4

$$M_m(kR) \geq M_0(kR) \geq c_0, \quad m \geq 0. \tag{8.5.41}$$

Combining (8.5.40) and (8.5.41) gives

$$\mathcal{T}_1^* = M_m(kR)|\mathcal{D}J_m(x)| \geq c_0. \tag{8.5.42}$$

For two cases, we have from (8.5.39) and (8.5.42)

$$\mathcal{T}_1^* = M_m(kR)|\mathcal{D}J_m(kr)| \geq \min\{c_0, I\} = c_0\left(\frac{R}{r_{\max}}\right)^n. \tag{8.5.43}$$

This is the desired result (8.5.37). ■

8.5.2 Error Bounds

First, we estimate the errors in (8.5.4)

$$E(\rho,\theta) = P_n(\rho,\theta) - \sum_{j=1}^{N} c_j \Psi_j(\rho,\theta).$$

Denote the basic errors,

$$E_m(\rho,\theta) = \mathcal{D}H_m^{(1)}(k\rho)\cos(m\theta) - \sum_{j=1}^{N} \alpha_{jm}\Psi_j(\rho,\theta), \quad m = 0,\ 1, 2, \ldots, \tag{8.5.44}$$

$$E_m^*(\rho,\theta) = \mathcal{D}H_m^{(1)}(k\rho)\sin(m\theta) - \sum_{j=1}^{N} \beta_{jm}\Psi_j(\rho,\theta), \quad m = 1,\ 2, \ldots, \tag{8.5.45}$$

where the complex coefficients $\alpha_{jm} = \frac{1}{N}\frac{\cos(mjh)}{\mathcal{D}J_m(kR)}$ and $\beta_{jm} = \frac{1}{N}\frac{\sin(mjh)}{\mathcal{D}J_m(kR)}$ from (8.5.5).

Lemma 8.5.6. *There exist the bounds on the circle Γ_ρ with radius ρ,*

$$\|E_m(\rho,\theta)\|_{q,\Gamma_\rho}^2 \leq C\frac{N^{2q}}{|\mathcal{D}J_m(kR)|^2} M_{N-m}^2(k\rho)|\mathcal{D}J_{N-m}(kR)|^2, \tag{8.5.46}$$

$$\|E_m^*(\rho,\theta)\|_{q,\Gamma_\rho}^2 \leq C\frac{N^{2q}}{|\mathcal{D}J_m(kR)|^2} M_{N-m}^2(k\rho)|\mathcal{D}J_{N-m}(kR)|^2 \leq C\|E_m(\rho,\theta)\|_{q,\Gamma_\rho}^2. \tag{8.5.47}$$

Proof. We only prove (8.5.46), since the proof for (8.5.47) is similar. We expand (8.5.44) as a Fourier series,

$$E_m(\rho,\theta) = \frac{a_{0m}}{2} + \sum_{\ell=1}^{\infty}\{a_{\ell m}\cos(\ell\theta) + b_{\ell m}\sin(\ell\theta)\}, \tag{8.5.48}$$

where complex coefficients

$$\begin{aligned} a_{\ell m} &= \frac{1}{\pi}\int_0^{2\pi} E_m(\rho,\theta)\cos(\ell\theta)\,d\theta, \quad \ell = 0,\ 1\,, 2, \ldots, \\ b_{\ell m} &= \frac{1}{\pi}\int_0^{2\pi} E_m(\rho,\theta)\sin(\ell\theta)\,d\theta, \quad \ell = 1,\ 2, \ldots. \end{aligned} \tag{8.5.49}$$

For the Fourier coefficients in (8.5.48), based on Basic Lemma A in Part I and Lemma 8.5.1, there exist the equalities,

$$a_{\ell m} = \begin{cases} \pi \dfrac{H_\ell^{(1)}(k\rho)\mathcal{D}J_\ell(kR)}{\mathcal{D}J_m(kR)}, & \text{if } \ell = \pm m + \mu N,\ \mu = 1, 2, \ldots, \\ 0, & \text{otherwise,} \end{cases} \tag{8.5.50}$$

$$b_{\ell m} = 0, \quad \forall \ell, m. \tag{8.5.51}$$

When n is large and kr is bounded, we have from Lemma 8.5.2 and (8.5.12)

$$|\mathcal{D}J_n(kR)| \leq C \frac{\left(\frac{kR}{2}\right)^{n-1}}{(n-1)!} \leq Cn|J_n(kR)| \leq C\left(\frac{n}{\sqrt{2\pi n}}\right)\left(\frac{ekR}{2n}\right)^n. \tag{8.5.52}$$

From (8.5.33) and (8.5.52), when n is large, there exist the bounds,

$$T_n^*(r) = M_n(kr)|\mathcal{D}J_n(kR)| \leq C\sqrt{\frac{2}{\pi n}}\left(\frac{ekr}{2n}\right)^{-n} \times \left(\frac{n}{\sqrt{2\pi n}}\right)\left(\frac{ekR}{2n}\right)^n \leq C\left(\frac{R}{r}\right)^n. \tag{8.5.53}$$

For $R < r_{\min} \leq r$,

$$T_m^*(r) < T_n^*(r) \text{ for } m > n, \quad T_{n+N}^*(r) \ll T_n^*(r). \tag{8.5.54}$$

From (8.5.48)–(8.5.51), we have

$$\begin{aligned} \|E_m(\rho,\theta)\|_{q,\Gamma_\rho}^2 &\leq C\sum_{\ell=1}^{\infty} \ell^{2q}|a_{\ell m}|^2 = C\pi^2 \sum_{\ell=\pm m+\mu N} \ell^{2q}\left[\frac{\left|H_\ell^{(1)}(k\rho)\mathcal{D}J_\ell(kR)\right|}{|\mathcal{D}J_m(kR)|}\right]^2 \\ &= C\pi^2 \frac{1}{|\mathcal{D}J_m(kR)|^2}\left\{\sum_{\ell=-m+\mu N} \ell^{2q} M_\ell^2(k\rho)|\mathcal{D}J_\ell(kR)|^2 \right. \\ &\quad \left. + \sum_{\ell=m+\mu N} \ell^{2q} M_\ell^2(k\rho)|\mathcal{D}J_\ell(kR)|^2\right\}. \end{aligned} \tag{8.5.55}$$

Since n and $N\,(\geq 2n)$ are large, we have from (8.5.53) and (8.5.54)

$$\sum_{\ell=-m+\mu N} \ell^{2q} M_\ell^2(k\rho)|\mathcal{D}J_\ell(kR)|^2 \leq CN^{2q}M_{N-m}^2(k\rho)|\mathcal{D}J_{N-m}(kR)|^2, \tag{8.5.56}$$

$$\begin{aligned} \sum_{\ell=m+\mu N} \ell^{2q} M_\ell^2(kR)|\mathcal{D}J_\ell(k\rho)|^2 &\leq \sum_{\ell=-m+\mu N} \ell^{2q} M_\ell^2(kR)|\mathcal{D}J_\ell(k\rho)|^2 \\ &\leq CN^{2q}M_{N-m}^2(k\rho)|\mathcal{D}J_{N-m}(kR)|^2. \end{aligned} \tag{8.5.57}$$

Combining (8.5.55)–(8.5.57) gives

$$\|E_m(\rho,\theta)\|_{q,\Gamma_\rho}^2 \leq C\frac{N^{2q}}{|\mathcal{D}J_m(kR)|^2} M_{N-m}^2(k\rho)|\mathcal{D}J_{N-m}(kR)|^2.$$

This is the desired result (8.5.46). ■

Lemma 8.5.7. *For $N \geq 2n$, there exists the error bound for (8.5.4),*

$$\begin{aligned}&\|P_n(\rho,\theta) - \Sigma_N^+(P_n;\rho,\theta)\|_{q,\Gamma_{\text{in}}}\\ &\leq CN^q \left\{ \sum_{m=0}^{n} \left(\frac{M_{N-m}(k\rho)|\mathcal{D}J_{N-m}(kR)|}{M_m(k\widetilde{\rho})|\mathcal{D}J_m(kR)|} \right)^2 \right\}^{\frac{1}{2}} \|P_n(\rho,\theta)\|_{0,\Gamma_{\text{in}}},\end{aligned} \tag{8.5.58}$$

where $\widetilde{\rho} \in \{r_{\min}, r_{\max}\}$.

Proof. For $r_{\min} \leq \widetilde{\rho} \leq r_{\max}$, we have from Lemma 8.5.6 and the Schwarz inequality

$$\begin{aligned}&\|P_n(\rho,\theta) - \Sigma_N^+(P_n;\rho,\theta)\|^2_{q,\Gamma_\rho}\\ &= \left\| a_0E_0(\rho,\theta) + \sum_{m=1}^{n}(a_mE_m(\rho,\theta) + b_mE_m^*(\rho,\theta)) \right\|^2_{q,\Gamma_\rho}\\ &\leq \left\| a_0E_0(\rho,\theta)\frac{M_0(k\widetilde{\rho})}{M_0(k\widetilde{\rho})} + \sum_{m=1}^{n}[a_mE_m(\rho,\theta) + b_mE_m^*(\rho,\theta)]\frac{M_m(k\widetilde{\rho})}{M_m(k\widetilde{\rho})} \right\|^2_{q,\Gamma_\rho}\\ &\leq \left\{ |a_0|^2M_0^2(k\widetilde{\rho}) + \sum_{m=1}^{n}(|a_m|^2+|b_m|^2)M_m^2(k\widetilde{\rho}) \right\}\left\{ \sum_{m=0}^{n}\frac{\|E_m(\rho,\theta)\|^2_{q,\Gamma_\rho}}{M_m^2(k\widetilde{\rho})} \right\},\end{aligned} \tag{8.5.59}$$

where we have used (8.5.47). There also exists the bound,

$$|a_0|^2M_0^2(k\widetilde{\rho}) + \sum_{m=1}^{n}(|a_m|^2+|b_m|^2)M_m^2(k\widetilde{\rho}) \leq \|P_n(\widetilde{\rho},\theta)\|^2_{0,\Gamma_{\widetilde{\rho}}} \leq C\|P_n(\rho,\theta)\|^2_{0,\Gamma_{\text{in}}}, \tag{8.5.60}$$

where $P_n(\rho,\theta)$ are the complex polynomials of order n in (8.2.14). On the other hand, we have from (8.5.46)

$$\sum_{m=0}^{n}\frac{1}{M_m^2(k\widetilde{\rho})}\|E_m(\rho,\theta)\|^2_{q,\Gamma_\rho} \leq CN^{2q}\sum_{m=0}^{n}\left(\frac{|\mathcal{D}J_{N-m}(kR)|M_{N-m}(k\rho)}{|\mathcal{D}J_m(kR)|M_m(k\widetilde{\rho})} \right)^2. \tag{8.5.61}$$

Combining (8.5.59)–(8.5.61) leads to the desired result (8.5.58). ■

We have the following main theorem.

Theorem 8.5.1. *When N is large and $N \geq 2n$, there exists the error bound for (8.5.4),*

$$\|P_n(\rho,\theta) - \Sigma_N(P_n;\rho,\theta)\|_{q,\Gamma_{\text{in}}} \leq C\sqrt{n}N^q \left\{ \left(\frac{R}{r_{\min}}\right)^{N-2n}\left(\frac{r_{\max}}{r_{\min}}\right)^n \right\} \|P_n(\rho,\theta)\|_{0,\Gamma_{\text{in}}}. \tag{8.5.62}$$

Proof. When $N \geq 2n$ and N is large, then $(N-m)\,(\geq n)$ is large. For $m \leq n$ and $0 < R < r_{\min} \leq \rho \leq r_{\max}$, we have from (8.5.53) and (8.5.54)

$$\begin{aligned} &|\mathcal{D}J_{N-m}(kR)|M_{N-m}(k\rho) \leq |\mathcal{D}J_{N-n}(kR)|M_{N-n}(k\rho) \\ &\leq C\left(\frac{R}{\rho}\right)^{N-n} \leq C\left(\frac{R}{r_{\min}}\right)^{N-n}, \end{aligned} \tag{8.5.63}$$

where $\frac{R}{r_{\min}} < 1$. For $m \in [0, n]$ and bounded kR with $R < r_{\min}$, we have from Lemma 8.5.5 and (8.5.63)

$$\begin{aligned} &\sum_{m=0}^{n}\left(\frac{|\mathcal{D}J_{N-m}(kR)|M_{N-m}(k\rho)}{|\mathcal{D}J_m(kR)|M_m(k\widetilde{\rho})}\right)^2 \\ &\leq Cn\max_m\left(\frac{|\mathcal{D}J_{N-m}(kR)|M_{N-m}(kr_{\min})}{|\mathcal{D}J_m(kR)|M_m(kr_{\max})}\right)^2 \leq Cn\left\{\frac{\left(\frac{R}{r_{\min}}\right)^{N-n}}{\left(\frac{R}{r_{\max}}\right)^{n}}\right\}^2 \\ &= Cn\left\{\left(\frac{R}{r_{\min}}\right)^{N-n} \times \left(\frac{r_{\max}}{R}\right)^{n}\right\}^2 = Cn\left\{\left(\frac{R}{r_{\min}}\right)^{N-2n}\left(\frac{r_{\max}}{r_{\min}}\right)^{n}\right\}^2. \end{aligned} \tag{8.5.64}$$

The desired result (8.5.62) follows from Lemma 8.5.7 and (8.5.64). ■

Theorem 8.5.2. *Suppose that* $u \in \mathbf{H}^p(\Gamma_{\text{in}})$ $(p \geq 1)$ *and the conditions of Theorem 8.5.1 hold. When the large* $N\,(> 2n)$ *is chosen as in (8.5.69) below, the solution* u_N *in (8.4.7) by the modified MFS has the optimal polynomial convergence rates,*

$$\|u-u_N\|_{0,\Gamma_{\text{in}}} = O\left(\frac{1}{N^p}\|u\|_{p,\Gamma_{\text{in}}}\right). \tag{8.5.65}$$

Proof. We have

$$\begin{aligned} \|u-u_N\|_{0,\Gamma_{\text{in}}} &= \inf_{v\in V_N}\|u-v\|_{0,\Gamma_{\text{in}}} \leq \|u-\Sigma_N^+(P_n;\rho,\theta)\|_{0,\Gamma_{\text{in}}} \\ &\leq \|u-P_n(\rho,\theta)\|_{0,\Gamma_{\text{in}}} + \|P_n(\rho,\theta)-\Sigma_N^+(P_n;\rho,\theta)\|_{0,\Gamma_{\text{in}}}. \end{aligned} \tag{8.5.66}$$

From (8.2.17),

$$\|u-P_n(\rho,\theta)\|_{0,\Gamma_{\text{in}}} = \|R_n(\rho,\theta)\|_{0,\Gamma_{\text{in}}} \leq C\frac{1}{n^p}\|u\|_{p,\Gamma_{\text{in}}}. \tag{8.5.67}$$

There exists the bound,

$$\|P_n(\rho,\theta)\|_{0,\Gamma_{\text{in}}} \approx \|u\|_{0,\Gamma_{\text{in}}} \leq \|u\|_{p,\Gamma_{\text{in}}}, \quad p \geq 1. \tag{8.5.68}$$

Then we have from (8.5.66)–(8.5.68) and Theorem 8.5.1

$$\|u-u_N\|_{0,\Gamma_{\text{in}}} \leq C\left\{\frac{1}{n^p} + n^{\frac{1}{2}}\left(\frac{R}{r_{\min}}\right)^{N-2n}\left(\frac{r_{\max}}{r_{\min}}\right)^{n}\right\}\|u\|_{p,\Gamma_{\text{in}}}.$$

The desired result (8.5.65) follows if we choose the large N such that

$$n^{\frac{1}{2}}\left(\frac{R}{r_{\min}}\right)^{N-2n}\left(\frac{r_{\max}}{r_{\min}}\right)^{n}\leq n^{-p},$$

to give

$$N\geq 2n+\frac{(p+\frac{1}{2})\ln n+n\,\ln\left(\frac{r_{\max}}{r_{\min}}\right)}{\ln\left(\frac{r_{\min}}{R}\right)},\quad R<r_{\min}. \tag{8.5.69}$$

The equality of (8.5.69) also implies $n\geq c_0N$, where c_0 (>0) is also independent of n and N. This completes the proof of Theorem 8.5.2. ■

Remark 8.5.3. *The boundary errors are provided in Theorems 8.5.1 and 8.5.2. By using the weighted Sobolev norms in an unbounded domain* S_∞ *(see Hsiao and Wendland [104, p.191] and Sauter and Schwab [210, p.83]), the domain errors may be obtained from the boundary errors (see (7.3.87) in Chapter 7). For simplicity in computation, we may also evaluate the errors on a large circle* Γ_{R^*} *with a large radius, say* $R^*=100$*. The small boundary errors,* $\|\epsilon\|_{\infty,\Gamma_{\text{in}}}$ *and* $\|\epsilon\|_{\infty,\Gamma_{R^*}}$*, imply the small domain errors, as if the Dirichlet problem of the Helmholtz equation in annular domains were considered.*

8.6 Stability Analysis for Modified MFS

The stability analysis is made only for the circular interior boundary $\Gamma_{\text{in}}^{\circ}$ in this section. For the non-circular Γ_{in}, the stability analysis may follow Chapter 3. Consider the Dirichlet problem of (8.2.1) on the circle $\Gamma_{\text{in}}^{\circ}=\Gamma_\rho$, where $\Gamma_\rho=\{(\rho,\theta)|\rho=\text{constant},0\leq\theta\leq 2\pi\}$. Choose the following uniform source nodes and collocation nodes,

$$\begin{aligned}Q_i&=\{(x,y)|x=R\,\cos(ih),y=R\,\sin(ih)\},\\ P_i&=\{(x,y)|x=\rho\,\cos(ih),y=\rho\,\sin(ih)\},\end{aligned}\tag{8.6.1}$$

where $h=\frac{2\pi}{N}$ and $R<\rho$. The equation (8.4.8) leads to

$$\sum_{j=1}^{N}c_j\boldsymbol{\Psi}_j(P_\ell)=f(P_\ell),\quad P_\ell\in\Gamma_\rho,\quad \ell=1,\,2,\ldots,N, \tag{8.6.2}$$

where $P_\ell=(\rho_\ell,\theta_\ell)$, and c_i are the complex coefficients. Then the new FS are given from (8.4.6)

$$\boldsymbol{\Psi}_j(P_\ell)=\mathcal{D}H_0^{(1)}(k|\overline{P_\ell Q_j}|)=\left(\frac{\partial}{\partial R}\pm\mathbf{i}k\right)H_0^{(1)}\left(k\sqrt{R^2+\rho^2-2R\rho\,\cos(\ell-j)h}\right).$$

Denote (8.6.2) by $\mathbf{Dx} = \mathbf{f}$, where $\mathbf{D} \in \mathbf{C}^{N\times N}$, $\mathbf{x} = (c_1, c_2, \ldots, c_N)^T \in \mathbf{C}^N$ and $\mathbf{f} = (f(P_1), f(P_2), \ldots, f(P_N))^T \in \mathbf{C}^N$. The matrix $\mathbf{D}$ is circulant as

$$\mathbf{D} = \text{circulant}(d_0, d_1, \ldots, d_{N-1}) = \begin{pmatrix} d_0 & d_1 & \cdots & d_{N-1} \\ d_{N-1} & d_0 & \cdots & d_{N-2} \\ \vdots & \vdots & \ddots & \vdots \\ d_1 & d_2 & \cdots & d_0 \end{pmatrix}, \tag{8.6.3}$$

where the entries $d_i = \mathcal{D}H_0^{(1)}\left(k\sqrt{R^2 + \rho^2 - 2R\rho\,\cos(ih)}\right)$. Since $d_{N-i} = d_i$, the matrix $\mathbf{D}$ is symmetric but not Hermite, and the eigenvalues of (8.6.3) are complex. Denote the Fourier matrix

$$\mathbf{F}^*(\in \mathbf{C}^{N\times N}) = \frac{1}{\sqrt{N}} \begin{bmatrix} 1 & 1 & \cdots & 1 \\ 1 & \omega & \cdots & \omega^{N-1} \\ \vdots & \vdots & \ddots & \vdots \\ 1 & \omega^{N-1} & \cdots & \omega \end{bmatrix},$$

where $\omega = e^{\frac{2\pi}{N}\mathbf{i}} = \cos\frac{2\pi}{N} + \mathbf{i}\,\sin\frac{2\pi}{N}$.

Based on David [71, p.73], the eigenvalues $\lambda_\ell\,(\in \mathbf{C})$ of matrix $\mathbf{D}$ are given by

$$\lambda_\ell = \sum_{j=0}^{N-1} d_j(\cos(\ell jh) + \mathbf{i}\,\sin(\ell jh)), \quad \ell = 0, 1, \ldots, N-1. \tag{8.6.4}$$

From Basic Lemma A in Part I and (8.5.2), we have

$$\sum_{j=0}^{N-1} d_j\,\sin(\ell jh) = 0, \quad \ell = 0, 1, \ldots, N-1,$$

to give from (8.6.4)

$$\lambda_\ell = \sum_{j=0}^{N-1} d_j\,\cos(\ell jh), \quad \ell = 0, 1, \ldots, N-1.$$

Denote $\mathbf{D} = \mathbf{F}^*\text{diag}(\lambda_0, \lambda_1, \ldots, \lambda_{N-1})\mathbf{F}$, where $\sigma_{\max} = \max_j |\lambda_j|$ and $\sigma_{\min} = \min_j |\lambda_j|$. The condition number is defined by $\text{Cond} = \dfrac{\sigma_{\max}}{\sigma_{\min}} = \dfrac{\max_j |\lambda_j|}{\min_j |\lambda_j|}$. Similarly, we can prove the following lemma from Chapter 7.

Lemma 8.6.1. *There exist the approximations of complex* λ_ℓ*,*

$$\lambda_0 \approx NH_0^{(1)}(k\rho)\mathcal{D}J_0(kR),$$
$$\lambda_\ell \approx N[H_\ell^{(1)}(k\rho)\mathcal{D}J_\ell(kR) + H_{N-\ell}^{(1)}(k\rho)\mathcal{D}J_{N-\ell}(kR)], \quad \ell = 1, 2, \ldots, N-1.$$

Theorem 8.6.1. There exists the bound,

$$\mathrm{Cond} \le C\frac{M_0(k\rho)|\mathcal{D}J_0(kR)|}{M_{\frac{N}{2}}(k\rho)|\mathcal{D}J_{\frac{N}{2}}(kR)|} \le C\Big(\frac{\rho}{R}\Big)^{\frac{N}{2}}, \quad R<\rho, \tag{8.6.5}$$

where C is a constant independent of N.

Proof. From Lemma 8.6.1 we have

$$\mathrm{Cond} \le C\frac{M_0(k\rho)|\mathcal{D}J_0(kR)|}{M_{\frac{N}{2}}(k\rho)|\mathcal{D}J_{\frac{N}{2}}(kR)|}. \tag{8.6.6}$$

Since $M_0(k\rho) \le C$ and $|\mathcal{D}J_0(kR)| < C$,

$$\max_{\ell}|\lambda_\ell| = |\lambda_0| = N|\mathcal{D}J_0(kR)|M_0(k\rho) \le CN. \tag{8.6.7}$$

Let N be even without loss of generality. We have from Lemma 8.5.5

$$\min_{\ell}|\lambda_\ell| = \left|\lambda_{\frac{N}{2}}\right| \approx N\left|\mathcal{D}J_{\frac{N}{2}}(kR)\right|M_{\frac{N}{2}}(k\rho) \ge c_0 N\left(\frac{R}{\rho}\right)^{\frac{N}{2}}. \tag{8.6.8}$$

The desired result (8.6.5) is obtained from (8.6.6)–(8.6.8). ■

Remark 8.6.1. *From (8.5.62), the key factor $\left(\frac{R}{r_{\min}}\right)^{N-2n}$ implies that the smaller R is, the better accuracy is obtained. From (8.6.5), the smaller R is, the worse stability occurs. For the complicated Γ_{in} with a large ratio $\frac{r_{\max}}{r_{\min}}$, the circular pseudo-boundary will cause the huge Cond, so that satisfactory numerical solutions cannot be obtained. Hence, the non-circular pseudo-boundary near Γ_{in} as in Chapter 16 may be beneficial to reducing the ill-conditioning; see Section 8.7.2.*

8.7 Numerical Experiments

8.7.1 Circular Pseudo-Boundaries by Two MFS

Consider the EDP in (8.2.1)–(8.2.3). The interior boundary Γ_{in} is defined by the following parametric equation as in [222]

$$\Gamma_{\text{in}} = \{(x,y)|x = \rho(\theta)\cos\theta,\ y = \rho(\theta)\sin\theta,\ 0 \le \theta \le 2\pi\}, \tag{8.7.1}$$

where

$$\rho(\theta) = \sqrt{(a+b)^2 + 1 - 2(a+b)\cos(a\theta/b)}, \tag{8.7.2}$$

and a and b are constants. In computation, choose $a = 3$ and $b = 1$ with $\rho \in [3, 5]$, and the interior boundary Γ_{in} is drawn in Figure 8.3. Choose the complex solution,

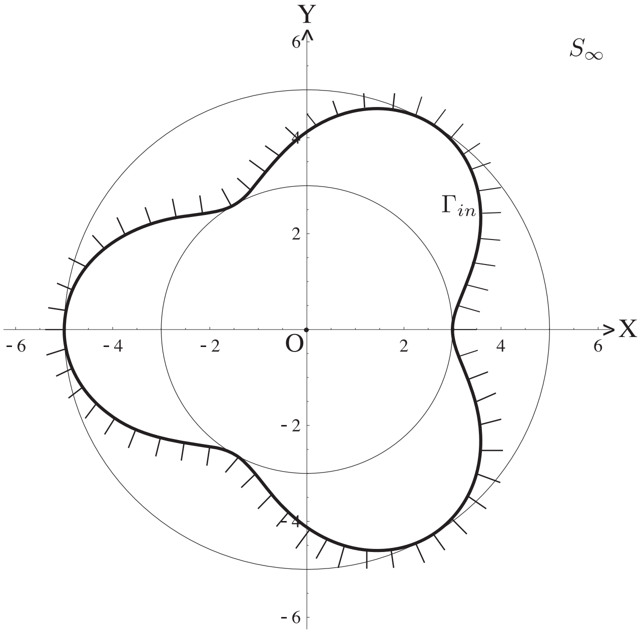

FIG. 8.3 – The interior boundary Γ_{in} of S_∞ as (8.7.1) and (8.7.2), where $a = 3$ and $b = 1$.

$$u(\rho, \theta) = \frac{H_n^{(1)}(k\rho)}{H_n^{(1)}(k\rho_0)} \cos(n\theta) \text{ in } S_\infty, \tag{8.7.3}$$

where $n = 4$ and $\rho_0 = 1$ in computation. The Dirichlet boundary condition is given by $f = u(\rho, \theta)|_{\Gamma_{\text{in}}}$. Choose (8.2.8) as the standard FS and (8.4.7) as the new FS, and use the collocation equations in (8.2.11) and (8.4.8). Denote the collocation nodes $P = (\rho \cos\theta, \rho \sin\theta)$ on Γ_{in}. Let the source nodes $Q_i = (R \cos\theta_i, R \sin\theta_i)$ with $\theta_i = \frac{2\pi i}{N}$ and $R < r_{\min} = 3$. There is always a unique solution for the EDP of the Helmholtz equation. For the circular Γ_R, however, the spurious eigenvalues happen just at $J_n(kR) = 0$ by the standard MFS in Section 8.2. The computed results by the standard MFS are given in Tables 8.1–8.3. In the tables, the $\|\epsilon\|_{\infty,\Gamma_{R^*}}$ denotes the maximal errors on the large circle Γ_{R^*} with radius $R^* = 100$; we will not compute the domain errors in S_∞ (see Remark 8.5.3). The numerical data in all tables in this chapter are computed by double precision with 16 decimal digits. In Table 8.3, when k increases, the errors increase but the Cond decreases. From Table 8.1, we can see the asymptotes,

$$\|\epsilon\|_{\infty,\Gamma_{\text{in}}} = O(0.57^N), \ \|\epsilon\|_{0,\Gamma_{\text{in}}} = O(0.56^N), \ \|\epsilon\|_{\infty,\Gamma_{R^*}} = O(0.52^N), \tag{8.7.4}$$

$$\text{Cond} = O(1.53^N), \quad \text{Cond\_eff} = O(1.53^N). \tag{8.7.5}$$

Note that when small $kR < j_{0,1} = 2.40482$, the condition (8.2.21) holds, and no spurious eigenvalues occur for the standard MFS (see Remark 8.2.1). For Table 8.2 at $k = 2$, there is no risk of spurious eigenvalues when $R < 1.2$. The curves of $\|\epsilon\|_{0,\Gamma_{\text{in}}}$, Cond and Cond_eff are drawn in Figure 8.4 from Table 8.2. Interestingly, the source nodes may be chosen to suitably shrink to origin O. When $R = 0.01$, the numerical solutions are still satisfactory, but when $R = 0.001$, they become poor, due to the huge $\text{Cond} = O(10^{16})$. The Cond_eff is smaller (even much smaller) than the Cond, and the Cond_eff may better measure the stability of the numerical coefficients c_j (*i.e.*, $\mathbf{x}$) from (8.2.12) than the Cond; see [162]. Figure 8.4 shows that Cond_eff $\ll$ Cond in the region without risk of spurious eigenvalues. When the working digits used more than 16 decimal digits, the R could be chosen smaller to bypass easily the spurious eigenvalues. For Table 8.2 and Figure 8.4 at $k = 2$ and $R < r_{\min} = 3$, we may find all zeros for $j_{m,\ell} = kR \le kr_{\min} = 6$ from [1, p.409, Table 9.5]. Hence, four spurious eigenvalues are found at

$$R = \frac{j_{m,\ell}}{k} = \frac{j_{m,\ell}}{2} = 1.20241,\ 1.91586,\ 2.56781,\ 2.76004,\ m \le 2. \tag{8.7.6}$$

In computation, when $k = 2$, the R should be chosen carefully to avoid (8.7.6) (*i.e.*, to satisfy (8.2.21)).

Next, for the modified MFS, the computed results are given in Tables 8.4–8.7. For the new FS with the operator $\mathcal{D} = \left(\frac{\partial}{\partial R} \pm \mathbf{i}k\right)$ in (8.5.3), Tables 8.4 and 8.5 show almost the same results. This verifies the analysis in Section 8.5 because of the same error bounds for $\mathcal{D} = \left(\frac{\partial}{\partial R} \pm \mathbf{i}k\right)$. Hence, we only choose $\mathcal{D} = \left(\frac{\partial}{\partial R} + \mathbf{i}k\right)$ for the rest of the computation by the modified MFS. The curves of $\|\epsilon\|_{0,\Gamma_{\text{in}}}$, Cond and Cond_eff from Table 8.6 are similar to those in Figure 8.4, but no spurious eigenvalues exist for all $R \in (0, r_{\min})$. From Table 8.4, we can see the asymptotes,

$$\|\epsilon\|_{\infty,\Gamma_{\text{in}}} = O(0.61^N),\ \|\epsilon\|_{0,\Gamma_{\text{in}}} = O(0.60^N),\ \|\epsilon\|_{\infty,\Gamma_{R^*}} = O(0.55^N), \tag{8.7.7}$$

$$\text{Cond} = O(1.39^N),\ \text{Cond\_eff} = O(1.35^N). \tag{8.7.8}$$

Compared with the standard MFS, the modified MFS offers a slightly slower convergence rate but slightly better stability. Such slightly better stability is consistent with Theorem 8.6.1 and Proposition 8.3.2. From (8.5.62), the dominant factor of errors is

TAB. 8.1 – The errors and the condition numbers by the standard MFS with $k = 2$ and $R = 2$.

N	M	$\|\epsilon\|_{\infty,\Gamma_{\text{in}}}$	$\|\epsilon\|_{0,\Gamma_{\text{in}}}$	$\|\epsilon\|_{\infty,\Gamma_{R^*}}$	Cond	Cond_eff	$\|\mathbf{x}\|$	$\sigma_{\min}$
6	12	1.15(−1)	3.17(−1)	2.30(−2)	3.66	3.08	2.06(−1)	6.50(−1)
12	24	3.69(−3)	9.77(−3)	4.91(−4)	6.95	4.65	2.62(−1)	3.40(−1)
18	36	9.51(−5)	1.56(−4)	3.16(−6)	1.19(2)	7.92(1)	2.14(−1)	2.44(−2)
24	48	4.17(−6)	6.76(−6)	8.74(−8)	1.37(3)	9.15(2)	1.86(−1)	2.45(−3)
30	60	1.70(−7)	3.25(−7)	3.57(−9)	1.51(4)	1.00(4)	1.66(−1)	2.50(−4)

Tab. 8.2 – The errors and the condition numbers by the standard MFS with $k = 2$, $M = 60$, $N = 30$, and different R. There is no risk of spurious eigenvalues when $R < 1.20241$.

R	$\|\epsilon\|_{\infty,\Gamma_{in}}$	$\|\epsilon\|_{0,\Gamma_{in}}$	$\|\epsilon\|_{\infty,\Gamma_{R^*}}$	Cond	Cond_eff	$\|\mathbf{x}\|$	$\sigma_{\min}$
2.95	5.47(−3)	9.12(−3)	8.55(−5)	1.45(2)	1.12(2)	1.57(−1)	2.36(−2)
2.9	3.11(−3)	5.30(−3)	4.00(−5)	1.71(2)	1.41(2)	1.45(−1)	2.02(−2)
2.7	3.56(−4)	6.55(−4)	4.87(−6)	3.56(2)	3.38(2)	1.21(−1)	1.02(−2)
2.5	4.25(−5)	8.12(−5)	7.07(−7)	8.13(2)	7.99(2)	1.20(−1)	4.34(−3)
2	1.70(−7)	3.25(−7)	3.57(−9)	1.51(4)	1.00(4)	1.66(−1)	2.50(−4)
1.5	2.28(−10)	4.18(−10)	4.84(−12)	9.78(5)	2.82(5)	3.53(−1)	4.17(−6)
1	2.65(−14)	4.62(−14)	2.27(−15)	4.54(8)	2.87(7)	1.37	1.05(−8)
0.5	9.19(−15)	2.46(−14)	3.31(−14)	1.87(13)	6.53(10)	1.88(1)	3.37(−13)
0.2	3.31(−13)	9.95(−13)	1.87(−12)	3.92(16)	1.62(12)	7.67(2)	3.34(−16)
0.1	6.22(−12)	1.67(−11)	1.75(−11)	3.40(16)	5.32(10)	1.40(4)	5.58(−16)
0.05	9.53(−11)	2.19(−10)	3.25(−10)	8.85(16)	5.67(9)	2.02(5)	3.62(−16)
0.01	7.97(−8)	1.69(−7)	2.18(−7)	4.15(16)	4.35(6)	1.49(8)	6.40(−16)
0.005	1.45(−6)	2.87(−6)	2.83(−6)	5.01(16)	3.37(5)	2.36(9)	5.23(−16)
0.001	5.19(−4)	1.16(−3)	3.36(−3)	6.44(16)	1.06(3)	1.49(12)	2.63(−16)

Tab. 8.3 – The errors and the condition numbers by the standard MFS with $M = 60$, $N = 30$, $R = 2$ and different k.

k	$\|\epsilon\|_{\infty,\Gamma_{\text{in}}}$	$\|\epsilon\|_{0,\Gamma_{\text{in}}}$	$\|\epsilon\|_{\infty,\Gamma_{R^*}}$	Cond	Cond_eff	$\|\mathbf{x}\|$	$\sigma_{\min}$
0.5	6.28(−8)	1.31(−7)	2.07(−10)	1.57(5)	3.28(3)	1.04(−1)	7.94(−5)
1	7.70(−8)	1.57(−7)	7.24(−10)	6.77(4)	5.96(3)	1.14(−1)	1.01(−4)
2	1.70(−7)	3.25(−7)	3.57(−9)	1.51(4)	1.00(4)	1.66(−1)	2.50(−4)
3	7.86(−7)	1.24(−6)	1.80(−8)	2.68(3)	2.57(3)	3.90(−1)	9.67(−4)
5	1.26(−5)	1.38(−5)	1.66(−7)	4.42(1)	2.89(1)	1.35	4.01(−2)
10	2.82(−2)	7.28(−2)	3.88(−3)	2.83(2)	1.12(2)	3.75	4.34(−3)
15	5.90(−1)	1.77	1.18(−1)	1.13(1)	1.95(1)	1.05	9.08(−2)
20	5.65(−1)	1.77	1.51(−1)	5.48	3.33	3.69	1.52(−1)

$$O\left(\left(\frac{R}{r_{\min}}\right)^N\right) = O\left(\left(\frac{2}{3}\right)^N\right) = O(0.67^N). \tag{8.7.9}$$

For the solution domain in Figure 8.3, $r_{\max} = 5$ and $\sqrt{\frac{r_{\max}}{R}} = \sqrt{\frac{5}{2}} = 1.58$ at $R = 2$. Then from (8.6.5), we have

$$\text{Cond} = O\left(\left(\sqrt{\frac{r_{\max}}{R}}\right)^N\right) = O(1.58^N). \tag{8.7.10}$$

The equations (8.7.7) and (8.7.8) coincide with (8.7.9) and (8.7.10) very well to support the theoretical analysis made.

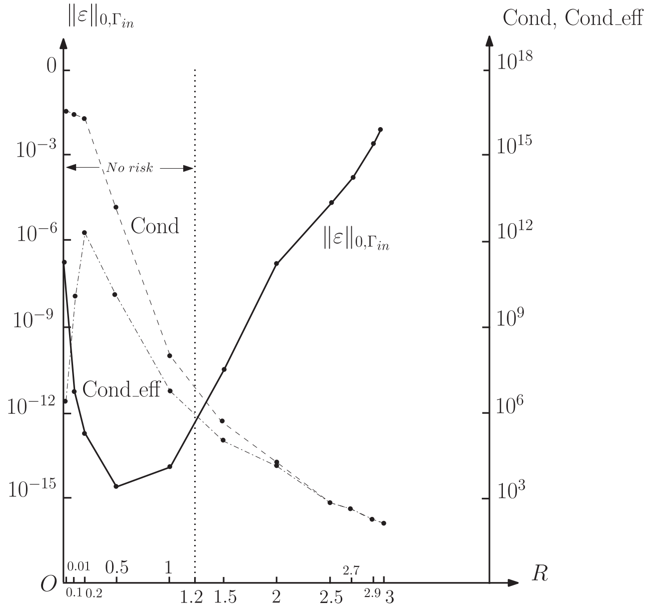

FIG. 8.4 – The curves of $\|\epsilon\|_{0,\Gamma_{\text{in}}}$, Cond and Cond_eff from Table 8.2 at $k = 2$, where no risk of spurious eigenvalues when $R < 1.2$.

TAB. 8.4 – The errors and the condition numbers by the modified MFS using $\mathcal{D} = \left(\frac{\partial}{\partial R} + \mathbf{i}k\right)$ with $k = 2$ and $R = 2$.

N	M	$\|\epsilon\|_{\infty,\Gamma_{\text{in}}}$	$\|\epsilon\|_{0,\Gamma_{\text{in}}}$	$\|\epsilon\|_{\infty,\Gamma_{R^*}}$	Cond	Cond_eff	$\|\mathbf{x}\|$	$\sigma_{\min}$
6	12	1.28(−1)	3.25(−1)	2.29(−2)	1.58	2.08	6.67(−2)	2.99
12	24	6.79(−3)	1.75(−2)	9.09(−4)	3.51	2.65	1.16(−1)	1.35
18	36	3.00(−4)	4.87(−4)	1.01(−5)	5.26(1)	3.95(1)	9.47(−2)	1.11(−1)
24	48	1.89(−5)	3.03(−5)	3.84(−7)	4.71(2)	3.53(2)	8.20(−2)	1.44(−2)
30	60	9.75(−7)	1.88(−6)	1.96(−8)	4.30(3)	3.22(3)	7.33(−2)	1.76(−3)

TAB. 8.5 – The errors and the condition numbers by the modified MFS using $\mathcal{D} = \left(\frac{\partial}{\partial R} - \mathbf{i}k\right)$ with $k = 2$ and $R = 2$.

N	M	$\|\epsilon\|_{\infty,\Gamma_{\text{in}}}$	$\|\epsilon\|_{0,\Gamma_{\text{in}}}$	$\|\epsilon\|_{\infty,\Gamma_{R^*}}$	Cond	Cond_eff	$\|\mathbf{x}\|$	$\sigma_{\min}$
6	12	9.47(−2)	3.28(−1)	2.16(−2)	1.58	2.10	6.30(−2)	3.13
12	24	6.50(−3)	1.76(−2)	8.80(−4)	3.56	2.66	1.16(−1)	1.35
18	36	3.01(−4)	4.88(−4)	1.01(−5)	5.27(1)	3.96(1)	9.47(−2)	1.11(−1)
24	48	1.89(−5)	3.03(−5)	3.92(−7)	4.71(2)	3.53(2)	8.20(−2)	1.44(−2)
30	60	9.75(−7)	1.88(−6)	2.02(−8)	4.30(3)	3.22(3)	7.33(−2)	1.76(−3)

TAB. 8.6 – The errors and the condition numbers by the modified MFS using $\mathcal{D} = (\frac{\partial}{\partial R} + \mathbf{i}k)$ with $k = 2$, $M = 60, N = 30$ and different R.

R	$\|\epsilon\|_{\infty,\Gamma_{\text{in}}}$	$\|\epsilon\|_{0,\Gamma_{\text{in}}}$	$\|\epsilon\|_{\infty,\Gamma_{R^*}}$	Cond	Cond_eff	$\|\mathbf{x}\|$	$\sigma_{\min}$
2.95	2.40(−2)	3.91(−2)	6.03(−4)	9.46(1)	6.37(1)	7.19(−2)	9.06(−2)
2.9	1.59(−2)	2.52(−2)	2.62(−4)	9.15(1)	7.62(1)	6.95(−2)	7.84(−2)
2.7	2.04(−3)	3.52(−3)	1.77(−5)	1.67(2)	1.49(2)	6.41(−2)	4.36(−2)
2.5	2.41(−4)	4.48(−4)	3.32(−6)	3.32(2)	3.20(2)	6.00(−2)	2.16(−2)
2.0	9.75(−7)	1.88(−6)	1.96(−8)	4.30(3)	3.22(3)	7.33(−2)	1.76(−3)
1.5	1.37(−9)	2.54(−9)	2.92(−11)	2.05(5)	8.09(4)	1.25(−1)	4.13(−5)
1.0	1.64(−13)	2.91(−13)	3.58(−15)	6.47(7)	7.87(6)	3.34(−1)	1.58(−7)
0.5	3.48(−15)	9.11(−15)	1.07(−14)	1.44(12)	1.75(10)	2.34	1.01(−11)
0.2	5.15(−14)	1.13(−13)	1.75(−13)	9.05(15)	5.48(12)	3.70(1)	2.05(−15)
0.1	4.19(−13)	1.25(−12)	1.28(−12)	2.07(16)	1.26(12)	3.09(2)	1.07(−15)
0.05	3.04(−12)	9.57(−12)	1.22(−11)	2.94(16)	2.19(11)	2.88(3)	6.59(−16)
0.01	7.08(−10)	2.37(−9)	1.31(−9)	5.70(16)	3.36(9)	3.81(5)	3.24(−16)
0.005	4.67(−9)	1.23(−8)	1.13(−8)	3.86(16)	2.14(8)	2.87(6)	6.77(−16)
0.001	4.57(−7)	1.23(−6)	1.57(−6)	2.83(16)	1.27(6)	4.09(8)	7.97(−16)

TAB. 8.7 – The errors and the condition numbers by the modified MFS using $\mathcal{D} = (\frac{\partial}{\partial R} + \mathbf{i}k)$ with $M = 60, N = 30$, $R = 2$ and different k.

k	$\|\epsilon\|_{\infty,\Gamma_{\text{in}}}$	$\|\epsilon\|_{0,\Gamma_{\text{in}}}$	$\|\epsilon\|_{\infty,\Gamma_{R^*}}$	Cond	Cond_eff	$\|\mathbf{x}\|$	$\sigma_{\min}$
0.5	4.14(−7)	8.56(−7)	1.27(−9)	1.39(4)	1.02(3)	5.19(−2)	5.17(−4)
1	4.96(−7)	1.01(−6)	4.39(−9)	1.08(4)	1.85(3)	5.56(−2)	6.67(−4)
2	9.75(−7)	1.88(−6)	1.96(−8)	4.30(3)	3.22(3)	7.33(−2)	1.76(−3)
3	3.22(−6)	5.10(−6)	7.42(−8)	1.12(3)	1.10(3)	1.23(−1)	7.18(−3)
5	2.76(−5)	3.00(−5)	3.63(−7)	2.93(1)	2.27(1)	2.25(−1)	3.06(−1)
10	2.57(−2)	6.93(−2)	3.98(−3)	2.01	1.08	2.71(−1)	6.22
15	6.22(−1)	1.41	1.13(−1)	2.06	1.89	1.20(−1)	8.15
20	3.35(−1)	8.58(−1)	1.75(−1)	2.72	1.29	2.32(−1)	6.24

8.7.2 Non-Circular Pseudo-Boundaries by Modified MFS

The modified MFS can also be applied to the non-circular pseudo-boundaries; no spurious eigenvalues existing are significant in the application. Choose the source nodes on the interior contour ℓ_ε as

$$\rho(\theta) = \varepsilon\left\{\sqrt{(a+b)^2 + 1 - 2(a+b)\cos(a\theta/b)}\right\}, \tag{8.7.11}$$

where $0<\varepsilon<1$. When $\varepsilon = 1$, the function (8.7.11) leads to (8.7.2) for $\mathbf{\Gamma}_{\text{in}}$. The results are given in Tables 8.8–8.10. From Table 8.8, we can see the asymptotes,

$$\|\epsilon\|_{\infty,\Gamma_{\text{in}}} = O(0.62^N), \ \|\epsilon\|_{0,\Gamma_{\text{in}}} = O(0.62^N), \ \|\epsilon\|_{\infty,\Gamma_{R^*}} = O(0.57^N), \tag{8.7.12}$$

$$\text{Cond} = O(1.44^N), \ \text{Cond\_eff} = O(1.39^N). \tag{8.7.13}$$

In Table 8.8, choose $\varepsilon = 0.5$ for comparisons. For ℓ_ε at $\varepsilon = 0.5$, the maximal and the minimal radii are 2.5 and 1.5, respectively; their mean is $R = 2$ as in Tables 8.1 and 8.4. Comparing (8.7.12) and (8.7.13) with (8.7.7) and (8.7.8), the non-circular pseudo-boundaries provide almost the same convergence rates and the same growth rates of Cond. Let us cite the data at $N = 30$ and $M = 60$ from Tables 8.1, 8.4, and 8.8,

$$\|\epsilon\|_{\infty,\Gamma_{\rm in}} = 1.70(-7),\ \|\epsilon\|_{0,\Gamma_{\rm in}} = 3.25(-7),\ \text{Cond} = 1.51(4), \tag{8.7.14}$$

$$\|\epsilon\|_{\infty,\Gamma_{\rm in}} = 9.75(-7),\ \|\epsilon\|_{0,\Gamma_{\rm in}} = 1.88(-6),\ \text{Cond} = 4.30(3), \tag{8.7.15}$$

$$\|\epsilon\|_{\infty,\Gamma_{\rm in}} = 1.47(-6),\ \|\epsilon\|_{0,\Gamma_{\rm in}} = 3.51(-6),\ \text{Cond} = 1.48(4). \tag{8.7.16}$$

We can see that the three cases offer almost the same numerical performance in errors and stability. The standard MFS provides slightly better accuracy, but the modified MFS eliminates all spurious eigenvalues. Hence, the modified MFS is significant for exterior problems of the Helmholtz equation.

To show the effects of the non-circular pseudo-boundaries, let us provide more numerical comparisons. When the source nodes are not close to $\Gamma_{\rm in}$, no evident

TAB. 8.8 – The errors and the condition numbers by the modified MFS using $\mathcal{D} = \left(\frac{\partial}{\partial R} + \mathbf{i}k\right)$ with the contour ℓ_ε of non-circular pseudo-boundaries at $k = 2$ and $\varepsilon = 0.5$.

N	M	$\|\epsilon\|_{\infty,\Gamma_{\rm in}}$	$\|\epsilon\|_{0,\Gamma_{\rm in}}$	$\|\epsilon\|_{\infty,\Gamma_{R^*}}$	Cond	Cond_eff	$\|\mathbf{x}\|$	$\sigma_{\min}$
6	12	1.37(−1)	3.49(−1)	2.25(−2)	2.03	2.72	5.87(−2)	2.59
12	24	9.56(−3)	2.68(−2)	1.36(−3)	3.76	2.29	1.33(−1)	1.36
18	36	2.35(−4)	6.00(−4)	2.12(−5)	7.33(1)	3.59(1)	1.38(−1)	8.41(−2)
24	48	2.27(−5)	4.51(−5)	8.09(−7)	1.07(3)	5.38(2)	1.16(−1)	6.68(−3)
30	60	1.47(−6)	3.51(−6)	4.71(−8)	1.48(4)	7.51(3)	1.03(−1)	5.37(−4)

TAB. 8.9 – The errors and the condition numbers by the modified MFS using $\mathcal{D} = \left(\frac{\partial}{\partial R} + \mathbf{i}k\right)$ with the contour ℓ_ε of non-circular pseudo-boundaries with $k = 2$ and $M = 60, N = 30$ and different ε.

ε	$\|\epsilon\|_{\infty,\Gamma_{\rm in}}$	$\|\epsilon\|_{0,\Gamma_{\rm in}}$	$\|\epsilon\|_{\infty,\Gamma_{R^*}}$	Cond	Cond_eff	$\|\mathbf{x}\|$	$\sigma_{\min}$
0.95	4.51(−2)	1.20(−1)	3.29(−3)	2.99	2.00	7.55(−2)	2.76
0.9	1.04(−2)	3.17(−2)	4.12(−4)	6.11	3.77	8.29(−2)	1.33
0.7	1.94(−4)	4.56(−4)	2.59(−6)	1.29(2)	8.82(1)	7.57(−2)	6.22(−2)
0.5	1.47(−6)	3.51(−6)	4.71(−8)	1.48(4)	7.51(3)	1.03(−1)	5.37(−4)
0.2	5.95(−12)	1.43(−11)	2.56(−13)	9.70(9)	3.69(8)	9.16(−1)	1.23(−9)
0.1	9.09(−15)	2.28(−14)	3.17(−14)	2.03(14)	8.21(11)	6.76	7.48(−14)
0.05	8.82(−14)	2.16(−13)	1.83(−13)	1.16(16)	5.26(12)	5.21(1)	1.52(−15)
0.01	8.99(−12)	2.31(−11)	2.78(−11)	1.61(16)	4.88(10)	6.17(3)	1.38(−15)
0.005	4.63(−11)	1.23(−10)	1.83(−10)	1.63(16)	6.67(9)	4.63(4)	1.35(−15)
0.001	4.79(−9)	1.12(−8)	1.49(−8)	1.76(16)	7.00(7)	4.67(6)	1.27(−15)

TAB. 8.10 – The errors and the condition numbers by the modified MFS using $\mathcal{D} = (\frac{\partial}{\partial R} + \mathbf{i}k)$ for different k and the contour ℓ_ε of non-circular pseudo-boundaries with $M = 60, N = 30$ and $\varepsilon = 0.5$.

k	$\|\epsilon\|_{\infty,\Gamma_{\rm in}}$	$\|\epsilon\|_{0,\Gamma_{\rm in}}$	$\|\epsilon\|_{\infty,\Gamma_{R^*}}$	Cond	Cond_eff	$\|\mathbf{x}\|$	$\sigma_{\min}$
0.5	4.66(−7)	9.94(−7)	1.04(−9)	2.98(4)	1.47(3)	7.62(−2)	2.43(−4)
1	5.74(−7)	1.26(−6)	4.56(−9)	2.55(4)	3.03(3)	8.03(−2)	2.82(−4)
2	1.47(−6)	3.51(−6)	4.71(−8)	1.48(4)	7.51(3)	1.03(−1)	5.37(−4)
3	7.53(−6)	1.62(−5)	4.37(−7)	4.74(3)	3.52(3)	1.51(−1)	1.82(−3)
5	1.02(−3)	3.59(−3)	2.12(−4)	6.99(1)	4.38(1)	2.61(−1)	1.37(−1)
10	3.57(−1)	9.09(−1)	7.64(−2)	2.43	1.65	2.13(−1)	5.16
15	5.49(−1)	1.09	1.03(−1)	2.58	1.42	2.00(−1)	6.55
20	4.35(−1)	1.17	1.18(−1)	3.49	1.76	1.69(−1)	6.30

advantage using (8.7.11) shows up from (8.7.14)–(8.7.16). However, when the source nodes are close to $\Gamma_{\rm in}$ (say $\varepsilon \geq 0.9$), better stability may gain evidently. First, we cite $\varepsilon = 0.9$ from Table 8.9, where the minimal distance $\triangle = 0.3$ between $\Gamma_{\rm in}$ and ℓ_ε,

$$\|\epsilon\|_{\infty,\Gamma_{\rm in}} = 1.04(-2),\ \|\epsilon\|_{0,\Gamma_{\rm in}} = 3.17(-2), \tag{8.7.17}$$

$$\text{Cond} = 6.11,\ \text{Cond\_eff} = 3.77,\ \sigma_{\min} = 1.33. \tag{8.7.18}$$

Next cite $R = 2.7$ in Table 8.6 with the same minimal distance $\triangle = 3 - R = 0.3$,

$$\|\epsilon\|_{\infty,\Gamma_{\rm in}} = 2.04(-3),\ \|\epsilon\|_{0,\Gamma_{\rm in}} = 3.52(-3), \tag{8.7.19}$$

$$\text{Cond} = 1.67(2),\ \text{Cond\_eff} = 1.49(2),\ \sigma_{\min} = 4.36(-2). \tag{8.7.20}$$

Comparing (8.7.17) and (8.7.18) with (8.7.19) and (8.7.20), the non-circular pseudo-boundaries offer much smaller Cond ($= O(1)$), but larger errors as $O(10^{-2})$. This comparison supports the discussions in Remark 8.6.1. More discussions for pseudo-boundaries near the boundary ∂S are given in Chapter 16.

8.8 Concluding Remarks

To close this chapter, let us draw several concluding remarks.

1. For the EDP (8.2.1)–(8.2.3) of the Helmholtz equation, the standard MFS using the Hankel functions (8.2.4) is first studied in Section 8.2. The error bounds involving degeneracy are provided in Theorem 8.2.1, and the optimal convergence rates are obtained in Theorem 8.2.2.
2. The standard MFS suffers from spurious eigenvalues at $J_n(kR) = 0$ for circular pseudo-boundaries. In some cases, the small R may be chosen so small such that $kR < j_{0,1} = 2.40482$ to avoid spurious eigenvalues. See Remark 8.2.1 and Figure 8.4. To eliminate all spurious eigenvalues for $R \in (0, r_{\min})$, the new combined FS as (8.4.6) is chosen. The new algorithms of the modified MFS are analogous to the combination of single-layer and double-layer potentials in the BEM [29, 30, 79, 210].

3. Numerical characteristics of spurious eigenvalues by the standard MFS are explored in Section 8.3. The divergence and the extremely large Cond are proved for spurious eigenvalues. Note that the spurious eigenvalues of the BEM and the MFS are distinct. One originated from the interior boundary Γ_{in}; the other from the pseudo-boundary $\Gamma \, (\neq \Gamma_{\text{in}})$ of source nodes. This study is important to the numerical Helmholtz solutions by the MFS as well as the BEM.
4. For the modified MFS, the error bounds are derived in Theorem 8.5.1, and the optimal convergence rates can be achieved in Theorem 8.5.2. The stability analysis is made for the circular $\Gamma^{\circ}_{\text{in}}$ only, given in Theorem 8.6.1. This chapter has explored the spurious eigenvalues by the MFS and their removals [44, 46, 47]. The strict theoretical analysis for the modified MFS is our focus; the proof techniques for lower bounds of some denominators in Section 8.5.1 are essential and intriguing.
5. Numerical experiments are carried out to support the theoretical analysis made. Numerical comparisons are also provided and some suggestions are given for dealing with spurious eigenvalues. The non-circular nodes (R_i, θ_i) are beneficial for better stability, which is supported when $\varepsilon \geq 0.9$ in (8.7.11) (*i.e.*, close to Γ_{in}), and they may be applied to some complicated Γ_{in} (*e.g.*, as a long strip-shaped curve). See Remark 8.6.1 and Section 8.7.2.

Chapter 9

Helmholtz Equations in Bounded Multiply-Connected Domains

9.1 Introduction

For the Helmholtz equation $\Delta u + k^2 u = 0$ in a 2D domain S, there exists a unique solution if k^2 is not exactly equal to an eigenvalue λ for the Laplace eigenvalue problem $\Delta u + \lambda u = 0$ in S. One important criterion for numerical methods is that there must exist no spurious (*i.e.*, superfluous) eigenvalues so that the unique solution can be obtained correctly. For exterior problems, the method of fundamental solutions (MFS) using the Hankel functions suffers from spurious eigenvalues. The new modified Hankel functions have been proposed in Chapter 8 to eliminate all spurious eigenvalues. In this chapter, we study the bounded multiply-connected domains. New MFS algorithms without spurious eigenvalues and their strict analysis are our goals. First, we study the bounded simply-connected domains by the MFS. The algorithms using the Hankel functions are free from spurious eigenvalues. A brief error analysis is provided. Next, we focus on the bounded multiply-connected domains and choose an annular domain for analysis. The Hankel functions and the modified Hankel functions in Chapter 8 are chosen as the exterior FS and the interior FS, respectively. Such combined FS eliminate all spurious eigenvalues, and new error and stability analyses are explored. The bounds of errors involve a degeneracy, and the bounds of condition numbers (Cond) involve a gap to eigenvalues. Numerical experiments are carried out to support the analysis made. The error and stability analyses in this chapter are essential and important. This chapter and Chapters 7 and 8 provide a solid theoretical basis for the MFS for the Helmholtz equation in the exterior problems and the interior problems with simply-connected and multiply-connected domains in 2D.

There exist many reports for the Helmholtz equation by the MFS using the Hankel functions (*e.g.*, [25, 87, 108, 207, 226]), but only Barnett and Betcke [20] involved some analysis for disk domains by using Katsurada's approaches [123]. The eigenvalues by the MFS were reported in many articles, such as Alves and Antunes [3], Antunes [10], Chen *et al.* [41], Karageorghis [115], Reutskiy [207], and Tsai *et al.*

DOI: 10.1051/978-2-7598-3171-5.c009
© Science Press, EDP Sciences, 2023

[226, 227]. The MFS is a meshless method with the pseudo-boundaries of source nodes. Other kinds of meshless methods without the pseudo-boundaries were introduced by Chen *et al.* [52], such as the boundary knot method and the singular boundary method. For the bounded multiply-connected domains by the MFS, the computations are reported in Antunes [10], Chen *et al.* [41, 44, 46, 47], Li [151], Reutskiy [207], and Tsangaris *et al.* [228]. Spurious eigenvalues for bounded multiply-connected domains by the BEM and the MFS were first studied by Chen and his group. See [46] in 2001 and [41] in 2005.

This chapter is organized as follows. In the next section, the MFS algorithms using Hankel functions are proposed for the bounded simply-connected domains, and the error bounds involving degeneracy are provided. Section 9.3 is for the bounded domains with interior holes, where the MFS algorithms without spurious eigenvalues are proposed. The error analysis is made for annular domains. In Section 9.4, the stability analysis is made for ring domains, and the bounds of the Cond involving a gap to eigenvalues are derived. In Section 9.5, numerical experiments are carried out for a bounded domain with four interior holes. In the last section, a few concluding remarks are made. The materials of this chapter are adapted from [258].

9.2 Bounded Simply-Connected Domains

9.2.1 Algorithms

Consider the Helmholtz equation with the interior Dirichlet problem (IDP),

$$\Delta u + k^2 u = 0 \text{ in } S, \quad u = f \text{ on } \Gamma, \tag{9.2.1}$$

where $\Delta = \frac{\partial^2}{\partial x^2} + \frac{\partial^2}{\partial y^2}$, S is a bounded simply-connected domain in 2D, and $\Gamma\,(= \partial S)$ the smooth boundary. In (9.2.1), $k\ (>0) \in \mathbf{R}$ but the known function $f \in \mathbf{C}$. The Hankel function of the first kind of order n is given by $H_n^{(1)}(z) = J_n(z) + \mathbf{i}\,Y_n(z)$, where $\mathbf{i} = \sqrt{-1}$, and $J_n(z)$ and $Y_n(z)$ are the Bessel and the Neumann functions of order n defined in (7.2.4) and (7.2.5) in Chapter 7, respectively. The complex fundamental solutions (FS) are given by the Hankel function $H_0^{(1)}(kr_j)$ of the first kind of zero-order, where $r_j = |\overline{PQ_j}|$, $P = \rho e^{\mathbf{i}\theta}$ and $Q_j = Re^{\mathbf{i}\phi_j}$. Denote

$$r_j = \sqrt{R^2 + \rho^2 - 2R\rho\,\cos(\theta - \phi_j)}, \quad R > \rho. \tag{9.2.2}$$

For real solutions, we may choose the Bessel (or Neumann) functions as FS in [177],

$$\Phi_j(\rho, \theta) = J_0(kr_j), \quad \psi_j(\rho, \theta) = Y_0(kr_j), \tag{9.2.3}$$

where $\phi_j = \frac{2\pi}{N} j$ and $Q_j(R, \phi_j)$ are the source nodes. By the MFS using the Bessel (or the Neumann) functions, there exist the spurious eigenvalues $\lambda^+ = k^2$ at $J_n(kR) = 0$ (or $Y_n(kR) = 0$). Further exploration for the spurious eigenvalues is provided in Chapter 8.

In this chapter, consider the complex solutions $u(x,y) = v(x,y) + \mathbf{i}w(x,y) \in \mathbf{C}$, where the functions $v(x,y), w(x,y) \in \mathbf{R}$. The complex FS for the Helmholtz equation are given by

$$\mathbf{\Psi}_j(\rho,\theta) = H_0^{(1)}(kr_j) = J_0(kr_j) + \mathbf{i}\,Y_0(kr_j) = \mathbf{\Phi}_j(\rho,\theta) + \mathbf{i}\psi_j(\rho,\theta). \tag{9.2.4}$$

The linear combinations of FS are chosen as

$$u_N = \sum_{j=1}^{N} c_j \mathbf{\Psi}_j(\rho,\theta) = \sum_{j=1}^{N} c_j(\mathbf{\Phi}_j(\rho,\theta) + \mathbf{i}\psi_j(\rho,\theta)), \tag{9.2.5}$$

where the functions $\mathbf{\Phi}_j(\rho,\theta)$ and $\psi_j(\rho,\theta)$ are given in (9.2.3), and the unknown complex coefficients $c_j = \alpha_j + \mathbf{i}\beta_j \in \mathbf{C}$ with $\alpha_j, \beta_j \in \mathbf{R}$. The complex coefficients c_j can also be sought by the Trefftz method (TM) in [169]. For the MFS using the Hankel functions (9.2.4), we have to choose the source nodes (R, ϕ_j) outside S (*i.e.*, $R > r_{\max} = \max\, r|_S$). However, for the MFS using the Bessel functions, such a condition is unnecessary to obey (see Chapter 7).

Denote by V_N the set of FS as (9.2.5). The TM reads: to seek $u_N \in V_N$ such that

$$I(u_N) = \min_{v \in V_N} I(v), \quad I(v) = \int_\Gamma |v-f|^2, \tag{9.2.6}$$

where $|v|^2 = v \cdot \bar{v}$, and $\bar{v}$ is the conjugate of complex v. When the integral in (9.2.6) involves a numerical approximation, the TM reads: to seek $\tilde{u}_N \in V_N$ such that

$$\widehat{I}(\tilde{u}_N) = \min_{v \in V_N} \widehat{I}(v), \quad \widehat{I}(v) = \widehat{\int_\Gamma} |v-f|^2, \tag{9.2.7}$$

where $\widehat{\int_\Gamma}$ is a numerical approximation of $\int_\Gamma$ by the trapezoidal rule (or the Gaussian rule). Let $\mathbf{\Gamma}$ be divided into small $\mathbf{\Gamma}_\ell$ with the meshspacings $\triangle h_\ell$, as $\mathbf{\Gamma} = \bigcup_{\ell=1}^{M} \mathbf{\Gamma}_\ell$. We give the collocation equations,

$$\sqrt{\triangle h_\ell} \sum_{j=1}^{N} c_j \mathbf{\Psi}_j(\rho_\ell,\theta_\ell) = \sqrt{\triangle h_\ell}\, f(\rho_\ell,\theta_\ell), \quad (\rho_\ell,\theta_\ell) \in \mathbf{\Gamma}_\ell, \quad \ell = 1,2,...,M. \tag{9.2.8}$$

The equation (9.2.8) is just equivalent to (9.2.7), where the central rule is chosen for $\widehat{\int_\Gamma}$. We may also assign other weights for two sides of (9.2.8) by the trapezoidal rule. In computation, we may choose the number M in (9.2.8) larger than N. The equation (9.2.8) leads to an overdetermined system $\mathbf{F}\mathbf{x} = \mathbf{b}$, where $\mathbf{F} \in \mathbf{C}^{M\times N} (M \geq N)$, $\mathbf{x} \in \mathbf{C}^N$ and $\mathbf{b} \in \mathbf{C}^M$.

9.2.2 Brief Error Analysis

The boundary $\mathbf{\Gamma}$ in (9.2.1) is supposed to be Lipschitz-continuous [91, p.5]. For analysis, we assume that the boundary $\mathbf{\Gamma}$ is smooth. In the bounded simply-connected domains, the complex solutions of the Helmholtz equation can be expressed by

$$u(\rho,\theta) = P_n(\rho,\theta) + R_n(\rho,\theta), \tag{9.2.9}$$

where the particular solutions (PS) of degree n are given by

$$P_n(\rho,\theta) = J_0(k\rho)a_0 + \sum_{m=1}^{n} J_m(k\rho)(a_m \cos(m\theta) + b_m \sin(m\theta)), \tag{9.2.10}$$

and the residual

$$R_n(\rho,\theta) = \sum_{m=n+1}^{\infty} J_m(k\rho)(a_m \cos(m\theta) + b_m \sin(m\theta)), \tag{9.2.11}$$

where the coefficients a_m and b_m are the exact complex coefficients. In fact, for the complex solutions of (9.2.1), the boundary complex function is denoted by $f = \mathcal{R}e(f) + \mathbf{i}\,\mathcal{I}m(f)$. For real $\mathcal{R}e(f)$ and real $\mathcal{I}m(f)$, the real solutions are also given by (9.2.10) from [177], where the real coefficients are just $\mathcal{R}e(a_m)\,\&\,\mathcal{R}e(b_m)$ and $\mathcal{I}m(a_m)\,\&\,\mathcal{I}m(b_m)$, respectively. This verifies the complex solutions (9.2.9). For a complex v, the Sobolev norms are defined as

$$\|v\|_{0,S}^2 = \int_S |v|^2 = \int_S v\bar{v}, \quad \|v\|_{p,S}^2 = \sum_{k=0}^{p} \|\nabla^k v\|_{0,S}^2,$$

where $\nabla = \frac{\partial}{\partial x} + \mathbf{i}\frac{\partial}{\partial y}$. Suppose that the complex solution $u \in \mathbf{H}^p(\mathbf{\Gamma})$, there also exist the bounds for the complex residual (9.2.11) in [149, 169],

$$\|R_n(\rho,\theta)\|_{q,S} = O\left(\frac{1}{n^{p-q}}\|u\|_{p,S}\right), \quad q < p. \tag{9.2.12}$$

From Chapters 7 and 8, we find an approximation to the complex polynomials (9.2.10),

$$P_n = P_n(\rho,\theta) \approx \sum_{j=1}^{N} c_j^* \mathbf{\Psi}_j(\rho,\theta) = u_N^* := \mathbf{\Sigma}_N(P_n;\rho,\theta), \tag{9.2.13}$$

where $\mathbf{\Psi}_j(\rho,\theta)$ are given in (9.2.4), and the complex coefficients

$$c_j^* = \frac{1}{N}\left\{\frac{a_0}{H_0^{(1)}(kR)} + \sum_{m=1}^{n} \frac{1}{H_m^{(1)}(kR)}(a_m \cos(mjh) + b_m \sin(mjh))\right\}, \tag{9.2.14}$$

where $h = \frac{2\pi}{N}$ and all $H_m^{(1)}(kR) \neq 0$. The non-zero denominator $H_m^{(1)}(kR)$ in (9.2.14) is distinct from the MFS using Bessel functions in Chapter 7, where the denominator $J_m(kR)$ may have infinite zeros.

From Remark 2.3.1 in Chapter 2, we assume the continuous solution $u \in C(S)$. From Chapters 7 and 8, we may prove the following lemma.

Lemma 9.2.1. *Let $u \in C(S)$ hold. For $N \geq 2n$ there exists the bound,*

$$\begin{aligned}&\|P_n(\rho,\theta) - \Sigma_N(P_n;\rho,\theta)\|_{q,\Gamma_\rho}\\ &\leq CN^q \sum_{m=0}^{n} \left(\frac{M_{N-m}(kR)J_{N-m}(k\rho)}{M_m(kR)J_m(k\tilde{\rho})}\right) \|P_n(\rho,\theta)\|_{0,\Gamma},\end{aligned} \tag{9.2.15}$$

where $J_m(k\tilde{\rho}) \neq 0$ with $\tilde{\rho} \in [r_{\min}, r_{\max}]$, $r_{\max} = \max \rho|_\Gamma$, $r_{\min} = \min \rho|_\Gamma$, $R > r_{\max}$ and C is a constant independent of N, m and n.

For the Helmholtz equation (9.2.1), the corresponding Dirichlet–Laplace's eigenvalue problem is given by

$$\Delta u + \lambda u = 0 \text{ in } S, \quad u = 0 \text{ on } \Gamma. \tag{9.2.16}$$

Assume that k^2 is not an eigenvalue of (9.2.16), but k^2 may be very close to one eigenvalue λ_ℓ, called degeneracy. Denote the gap

$$\delta = \min_{\forall \ell} \left\{\frac{|k^2 - \lambda_\ell|}{\lambda_\ell}\right\} = \min_{\forall \ell} \left|1 - \frac{k^2}{\lambda_\ell}\right| > 0. \tag{9.2.17}$$

The case of $\delta = 0$ responds to the exact eigenvalues: $\lambda_\ell = k^2$. When k^2 is not an eigenvalue of (9.2.16), the unique solutions can be expressed by (9.2.9). Then the unique solutions by the MFS can also be obtained from (9.2.13) with the coefficients (9.2.14). Therefore, no spurious eigenvalues exist. We write this important conclusion as a remark.

Remark 9.2.1. *For the 2D bounded simply-connected domains, the MFS using the complex $H_0^{(1)}(kr)$ as FS is free from spurious eigenvalues. This is distinct from the exterior problems in Chapter 8 suffering from spurious eigenvalues.*

For disk domains with $\tilde{\rho} = r_{\min} = r_{\max} = \rho$, we have $J_m(k\tilde{\rho}) = J_m(k\rho) \neq 0$ because the case of $J_m(k\rho) = 0$ corresponds to the exact eigenvalue: $k^2 = \lambda_{m,\ell} = \left(\frac{j_{m,\ell}}{\rho}\right)^2$. For the non-disk domains with $r_{\min} < r_{\max}$, since the roots of $J_n(x) = 0$ are simple and denumerable, there must exist a $\tilde{\rho} \in (r_{\min}, r_{\max})$ such that $J_m(k\tilde{\rho}) \neq 0$, $\forall m$. Such a $\tilde{\rho}$ is selected in our analysis. However, the value of $|J_m(k\tilde{\rho})|$ may be very close to zero; this is also degeneracy. Let $k^2 \approx \lambda_{k^*} = \left(\frac{j_{n,k^*}}{\rho}\right)^2$, where j_{n,k^*} is the k^*th zero of $J_n(x)$. Similarly to (9.2.17), denote the other gap for $x = k\rho$ by

$$\delta^* = \left|\frac{k^2 - \left(\frac{j_{n,k^*}}{\rho}\right)^2}{\left(\frac{j_{n,k^*}}{\rho}\right)^2}\right| = \left|\frac{(k\rho)^2 - (j_{n,k^*})^2}{(j_{n,k^*})^2}\right| = \left|1 - \frac{x^2}{(j_{n,k^*})^2}\right|. \tag{9.2.18}$$

When $x \approx j_{n,k^*}$ but $x \neq j_{n,k^*}$, then $0 < \delta^* \ll 1$ from (9.2.18). Below, we consider this degeneracy with $k^2 \approx \lambda_{k^*}$ in analysis.

To explain more about the degeneracy, let us cite some numerical results in Plagianakos *et al.* [201, p.552] as follows. Consider a bounded k, and denote $\bigcup_{n\geq 0,\ell\geq 1}\{j_{n,\ell}\} = \bigcup_{j=1}^{\infty}\{x_j\}$, where root x_j $(= j_{n,\ell})$ is the ℓth positive zero of $J_n(x)$ and $x_j < x_{j+1}$. Then root $x_j \to \infty$ as $j \to \infty$. They computed 1,054,942 zeros for $n \leq 2000$ and $0 \leq x_j \leq 3000$, to find the minimal and the maximal gaps,

$$d_0^* = \min_j (x_{j+1} - x_j) = 1.36(-9), \quad d_1^* = \max_j (x_{j+1} - x_j) = 1.43. \tag{9.2.19}$$

There exists the limit $\lim_{j\to\infty}(x_{j+1} - x_j) = 0$ in [79, p.75]. We assume that k is bounded in the analysis. Then there must exist a $\widetilde{\rho}$ $(= \rho)|_\Gamma \in (r_{\min}, r_{\max})$ with $0 < \delta^* \ll 1$ in (9.2.18) such that

$$\frac{d_0^*}{kr_{\max}} \leq \delta^* \leq \frac{d_1^*}{kr_{\min}}. \tag{9.2.20}$$

In fact, there exists the lower bound,

$$\min_{n,\ell} \frac{|j_{n,\ell} - k\tilde{\rho}|}{|j_{n,\ell}|} = \min_j \frac{|k\tilde{\rho} - x_j|}{x_j} = \frac{|k\tilde{\rho} - x_{j^*}|}{x_{j^*}} \geq \frac{1}{2}\frac{|x_{j^*\pm 1} - x_{j^*}|}{x_{j^*}} \geq \frac{1}{2}\frac{d_0^*}{kr_{\max}} > 0, \quad \forall n, \ell.$$

Since $k\tilde{\rho} \approx x_{j^*}$, we have from (9.2.18)

$$\begin{aligned}\delta^* &= \min_{n,\ell} \frac{|j_{n,\ell}^2 - (k\tilde{\rho})^2|}{|j_{n,\ell}^2|} = \frac{|(k\tilde{\rho})^2 - (x_{j^*})^2|}{(x_{j^*})^2} = \frac{|k\tilde{\rho} - x_{j^*}|}{x_{j^*}} \times \frac{|k\tilde{\rho} + x_{j^*}|}{x_{j^*}} \\ &\approx 2\frac{|k\tilde{\rho} - x_{j^*}|}{x_{j^*}} \geq \frac{d_0^*}{kr_{\max}} > 0.\end{aligned}$$

This is the lower bound of (9.2.20); the proof for the upper bound of (9.2.20) is similar.

For the MFS using Bessel functions, the value $\lambda^+ = k^2$ at $J_m(kR) = 0$ is a spurious eigenvalue (see [177]). For the MFS using Hankel functions, a specific $\tilde{\rho}$ is selected by $J_n(k\tilde{\rho}) \neq 0, \forall n, k$, so that no spurious eigenvalues exist. However, since $\delta^* = O(10^{-9})$ from (9.2.19) and (9.2.20), the degeneracy must be considered in the analysis. We summarize the above exploration as a remark.

Remark 9.2.2. *Although the Bessel functions $J_n(k\tilde{\rho})$ with $r_{\min} \leq \tilde{\rho} \leq r_{\max}$ appear in the denominator in the error bounds (9.2.15), since the $\tilde{\rho}$ may be selected deliberately, no spurious* eigenvalues *exist, but the degeneracy $0 < \delta^* \ll 1$ is inevitable.*

By following Chapters 7 and 8, we can prove the following theorems.

Theorem 9.2.1. *Let $u \in C(S)$ hold. For bounded k and $0 < \delta^* \ll 1$, when N $(\geq 2n)$ is large, there exists the bound,*

$$\|P_n(\rho,\theta) - \Sigma_N(P_n;\rho,\theta)\|_{q,\Gamma} \leq C\frac{1}{\delta^*}N^q\sqrt{n}\left(\frac{r_{\max}}{R}\right)^{N-2n}\left(\frac{r_{\max}}{r_{\min}}\right)^n \|P_n(\rho,\theta)\|_{0,\Gamma}, \tag{9.2.21}$$

where $R > r_{\max}$ and C is a constant independent of N and n.

Theorem 9.2.2. *Suppose that* $u \in \mathbf{H}^p(\Gamma)$ $\big(p > \frac{1}{2}\big)$ *and the conditions of Theorem 9.2.1 hold. The solution* u_N *in (9.2.5) by the MFS using Hankel functions has the optimal polynomial convergence rates,*

$$\|u - u_N\|_{0,\Gamma} = O\left(\frac{1}{n^p}\right)\|u\|_{p,\Gamma} = O\left(\frac{1}{N^p}\right)\|u\|_{p,\Gamma}, \tag{9.2.22}$$

provided that the N $(> 2n)$ *satisfies*

$$N \geq 2n + \frac{\ln\big(\frac{1}{\delta^*}\big) + n\,\ln\Big(\frac{r_{\max}}{r_{\min}}\Big) + \big(p + \frac{1}{2}\big)\ln n}{\ln\Big(\frac{R}{r_{\max}}\Big)}. \tag{9.2.23}$$

9.3 Bounded Multiply-Connected Domains

9.3.1 Algorithms

Denote an annular domain by $S_a = S_1 \backslash S_2$, where S_1 and S_2 are two bounded simply-connected domains with $S_2 \subset S_1$. Consider the Dirichlet problem in S_a,

$$\Delta u + k^2 u = 0 \text{ in } S_a, \quad u = g_{\text{out}} \text{ on } \Gamma_{\text{out}}, \quad u = g_{\text{in}} \text{ on } \Gamma_{\text{in}}, \tag{9.3.1}$$

where Γ_{out} and Γ_{in} are the exterior and the interior boundaries without any overlaps $\Gamma_{\text{out}} \cap \Gamma_{\text{in}} = \varnothing$. For analysis, let two boundaries Γ_{out} and Γ_{in} be smooth and star-shaped. Suppose that k^2 is not an eigenvalue λ of Laplace's operator:

$$\Delta u + \lambda u = 0 \text{ in } S_a, \quad u = 0 \text{ on } \Gamma_{\text{out}} \cup \Gamma_{\text{in}}. \tag{9.3.2}$$

The PS in S_a are given by

$$u = u(\rho, \theta; \bar{\rho}, \bar{\theta}) = u_1(\rho, \theta) + u_2(\bar{\rho}, \bar{\theta}), \tag{9.3.3}$$

where

$$u_1(\rho, \theta) = J_0(k\rho)a_0 + \sum_{i=1}^{\infty} J_i(k\rho)\{a_i \cos(i\theta) + b_i \sin(i\theta)\}, \tag{9.3.4}$$

$$u_2(\bar{\rho}, \bar{\theta}) = H_0^{(1)}(k\bar{\rho})\bar{a}_0 + \sum_{i=1}^{\infty} H_i^{(1)}(k\bar{\rho})\{\bar{a}_i \cos(i\bar{\theta}) + \bar{b}_i \sin(i\bar{\theta})\}, \tag{9.3.5}$$

where a_i, b_i, $\bar{a}_i$ and $\bar{b}_i$ are complex coefficients. Two systems of polar coordinates are denoted by (ρ, θ) and $(\bar{\rho}, \bar{\theta})$; they may have different origins. Denote nodes $P(\rho, \theta) \in \bar{S}_a$. For the exterior source nodes $Q(R, \theta)$ outside Γ_{out}, choose the FS as in Section 9.2,

$$\Psi_j(P) = H_0^{(1)}(k|\overline{PQ_j}|), \quad Q_j = (R, jh), \quad j = 1, 2, ..., N, \tag{9.3.6}$$

where $h = \frac{2\pi}{N}$ and $R > r_{\max} = \max \rho|_{\rho \in \Gamma_{\rm out}}$. For the interior source nodes $\bar{Q}(\bar{R}, \bar{\theta})$ inside $\mathbf{\Gamma}_{\rm in}$, however, the FS as $\mathbf{\Psi}_j(P)$ cause spurious eigenvalues (see Sections 8.2 and 8.3). Therefore, we choose the new modified FS,

$$\bar{\mathbf{\Psi}}_j(P) = \mathcal{D}H_0^{(1)}(k|\overline{P\bar{Q}_j}|) = \left(\frac{\partial}{\partial \bar{R}} \pm \mathbf{i}k\right) H_0^{(1)}(k|\overline{P\bar{Q}_j}|),\ \ \bar{Q}_j = \left(\bar{R}, j\bar{h}\right), j = 1, 2, ..., L, \tag{9.3.7}$$

where operator $\mathcal{D} = \left(\frac{\partial}{\partial \bar{R}} \pm \mathbf{i}k\right)$, $\bar{h} = \frac{2\pi}{L}$ and $\bar{R} < \bar{r}_{\min} = \min \bar{\rho}|_{\bar{\rho} \in \Gamma_{\rm in}}$ (see Section 8.4). For the annular domain S_a, the combined FS are given by

$$v_{N-L} = \sum_{j=1}^{N} c_j \mathbf{\Psi}_j(P) + \sum_{j=1}^{L} \bar{c}_j \bar{\mathbf{\Psi}}_j(P), \tag{9.3.8}$$

where c_j and $\bar{c}_j$ are the unknown complex coefficients.

Define the boundary norm,

$$\|v\|_{0,\partial S_a} = \|v\|_{0,\Gamma_{\rm out} \cup \Gamma_{\rm in}} = \left\{\|v\|^2_{0,\Gamma_{\rm out}} + \|v\|^2_{0,\Gamma_{\rm in}}\right\}^{\frac{1}{2}}. \tag{9.3.9}$$

Denote by V_{N-L} the set of (9.3.8). The unknown coefficients c_j and $\bar{c}_j$ can be sought by

$$\|u_{N-L} - u\|_{0,\Gamma_{\rm out} \cup \Gamma_{\rm in}} = \inf_{v \in V_{N-L}} \|v - u\|_{0,\Gamma_{\rm out} \cup \Gamma_{\rm in}}.$$

We may also employ the collocation equations directly to satisfy the Dirichlet conditions (9.3.1),

$$\sqrt{h} u_{N-L}(P_i) = \sqrt{h} g_{\rm out}(P_i), P_i \in \mathbf{\Gamma}_{\rm out};\ \sqrt{\bar{h}} u_{N-L}(\bar{P}_i) = \sqrt{\bar{h}} g_{\rm in}(\bar{P}_i), \bar{P}_i \in \mathbf{\Gamma}_{\rm in}, \tag{9.3.10}$$

where $P_i = (\rho_i, \theta_i)$ and $\bar{P}_i = (\bar{\rho}_i, \bar{\theta}_i)$. The equations (9.3.10) are called the MFS for annular domains.

Remark 9.3.1. *Note that for non-circular* $\mathbf{\Gamma}_{\rm in}$ *and* $\mathbf{\Gamma}_R$*, the new FS in (9.3.7) remains the same, and the new algorithms are simple compared with the modified BEM in [29, 46, 77]. In the BEM, the complicated combined operators for the Lipsichitz boundaries are proposed in [29, 77]. Spurious eigenvalues occur at special shapes of pseudo-boundaries by the MFS, not at those of* $\mathbf{\Gamma}_{\rm in}$ *by the BEM. Since the interior pseudo-boundary may be chosen to be smooth, it greatly simplifies the MFS algorithms. The remarkable advantage of the modified MFS in Chapter 8 and this chapter is to bypass easily all spurious eigenvalues.*

9.3.2 Error Analysis

Denote finite terms of PS in S_1 and S_2 by

$$P_n = P_n(\rho,\theta) = J_0(k\rho)a_0 + \sum_{i=1}^{n} J_i(k\rho)\{a_i \cos(i\theta) + b_i \sin(i\theta)\}, \ (\rho,\theta) \in S_1, \tag{9.3.11}$$

$$\bar{P}_\ell = \bar{P}_\ell(\bar{\rho},\bar{\theta}) = H_0^{(1)}(k\bar{\rho})\bar{a}_0 + \sum_{i=1}^{\ell} H_i^{(1)}(k\bar{\rho})\{\bar{a}_i \cos(i\bar{\theta}) + \bar{b}_i \sin(i\bar{\theta})\}, \ (\bar{\rho},\bar{\theta}) \in S_2. \tag{9.3.12}$$

The interior source nodes $\bar{Q}(\bar{R},\bar{\phi})$ are chosen inside Γ_{in} with $\bar{R} < \bar{r}_{\min} = \min \bar{\rho}|_{\Gamma_{\text{in}}}$. For the PS, $\bar{P}_\ell(\bar{\rho},\bar{\theta})$ in (9.3.12), we can find an approximation from (8.5.4) and (8.5.5) in Chapter 8,

$$\bar{P}_\ell = \bar{P}_\ell(\bar{\rho},\bar{\theta})) \approx \sum_{j=1}^{L} \bar{c}_j^* \bar{\mathbf{\Psi}}_j(\rho,\theta) = \bar{v}_L^* := \mathbf{\Sigma}_L(\bar{P}_\ell; \bar{\rho},\bar{\theta}), \tag{9.3.13}$$

where $\bar{\mathbf{\Psi}}_j(\rho,\theta)$ are given in (9.3.7), and the coefficients are

$$\bar{c}_j^* = \frac{1}{L}\left\{\frac{\bar{a}_0}{\mathcal{D}J_0(k\bar{R})} + \sum_{m=1}^{\ell} \frac{1}{\mathcal{D}J_m(k\bar{R})}(\bar{a}_m \cos(mj\bar{h}) + \bar{b}_m \sin(mj\bar{h}))\right\}, \tag{9.3.14}$$

where $\bar{h} = \frac{2\pi}{L}$, and

$$\left|\mathcal{D}J_m(k\bar{R})\right| = \left|\left(\frac{\partial}{\partial \bar{R}} \pm \mathbf{i}k\right) J_m(k\bar{R})\right| = \left\{\left(\frac{\partial}{\partial \bar{R}} J_m(k\bar{R})\right)^2 + k^2 J_m^2(k\bar{R})\right\}^{\frac{1}{2}}.$$

We cite a lemma from Theorem 8.5.1 of Chapter 8.

Lemma 9.3.1. *Let the Helmholtz solutions $u_2 \in C(S_a)$ hold, and choose $\bar{P}_\ell$ in (9.3.12) and $\bar{v}_L^*$ in (9.3.13). For bounded k and large $L\,(\geq 2\ell)$, there exists the error bound,*

$$\|\bar{P}_\ell - \bar{v}_L^*\|_{0,\Gamma_{\text{in}}} \leq C\sqrt{\ell}\left\{\left(\frac{\bar{R}}{\bar{r}_{\min}}\right)^{L-2\ell} \left(\frac{\bar{r}_{\max}}{\bar{r}_{\min}}\right)^{\ell}\right\}\|\bar{P}_\ell(\bar{\rho},\bar{\theta})\|_{0,\Gamma_{\text{in}}}, \tag{9.3.15}$$

where $\bar{R} < \bar{r}_{\min}$, and $\bar{r}_{\max}$ and $\bar{r}_{\min}$ are the maximal and the minimal radii of $\mathbf{\Gamma}_{\text{in}}$, respectively.

Error bounds for annular domains can be easily obtained by the decomposition techniques used in Section 4.3. Denote the error functions,

$$E = (P_n + \bar{P}_\ell) - (u_N^* + \bar{v}_L^*) := E_1 + E_2, \tag{9.3.16}$$

where

$$E_1 = P_n - u_N^* = P_n(\rho,\theta) - \sum_{i=1}^{N} c_i^* \mathbf{\Psi}_i(P), \ \ E_2 = \bar{P}_\ell - \bar{v}_L^* = \bar{P}_\ell(\bar{\rho},\bar{\theta}) - \sum_{i=1}^{L} \bar{c}_i^* \bar{\mathbf{\Psi}}_i(\bar{P}).$$

Theorem 9.3.1. *Suppose that the Helmholtz solutions satisfy* $u \in C(S_a)$*. For large* N *and* L*, there exist the error bounds between FS and PS,*

$$\begin{aligned} &\|(P_n + \bar{P}_\ell) - (u_N^* + \bar{v}_L^*)\|_{0,\Gamma_{\text{out}} \cup \Gamma_{\text{in}}} \\ &\le C\left\{ \frac{\sqrt{n}}{\delta^*} \left(\frac{r_{\max}}{R}\right)^{N-2n} \left(\frac{r_{\max}}{r_{\min}}\right)^n \|u_1\|_{0,\Gamma_{\text{out}}} + \sqrt{\ell}\left(\frac{\bar{R}}{\bar{r}_{\min}}\right)^{L-2\ell} \left(\frac{\bar{r}_{\max}}{\bar{r}_{\min}}\right)^\ell \|u_2\|_{0,\Gamma_{\text{in}}} \right\}, \end{aligned} \tag{9.3.17}$$

where P_n *is given in (9.3.11),* $\bar{P}_\ell$ *in (9.3.12),* u_N^* *in (9.2.13) and* $\bar{v}_L^*$ *in (9.3.13).*

Proof. We have

$$\|(P_n + \bar{P}_\ell) - (u_N^* + \bar{v}_L^*)\|_{0,\Gamma_{\text{out}} \cup \Gamma_{\text{in}}} \le \|P_n - u_N^*\|_{0,\Gamma_{\text{out}} \cup \Gamma_{\text{in}}} + \|\bar{P}_\ell - \bar{v}_L^*\|_{0,\Gamma_{\text{out}} \cup \Gamma_{\text{in}}}. \tag{9.3.18}$$

The distance from the interior source nodes $\bar{Q}_i$ to the interior boundary Γ_{in} is closer than that to the exterior boundary Γ_{out}. From (9.3.15) in Lemma 9.3.1, the errors $(\bar{P}_\ell - \bar{v}_L^*)$ on Γ_{in} are dominant,

$$\|\bar{P}_\ell - \bar{v}_L^*\|_{0,\Gamma_{\text{out}} \cup \Gamma_{\text{in}}} \le C\|\bar{P}_\ell - \bar{v}_L^*\|_{0,\Gamma_{\text{in}}}. \tag{9.3.19}$$

Similarly, from (9.2.21) in Theorem 9.2.1, the errors $(P_n - u_N^*)$ on Γ_{out} are dominant,

$$\|P_n - u_N^*\|_{0,\Gamma_{\text{out}} \cup \Gamma_{\text{in}}} \le C\|P_n - u_N^*\|_{0,\Gamma_{\text{out}}}. \tag{9.3.20}$$

Then we have from (9.3.18)–(9.3.20)

$$\|(P_n + \bar{P}_\ell) - (u_N^* + \bar{v}_L^*)\|_{0,\Gamma_{\text{out}} \cup \Gamma_{\text{in}}} \le C\Big\{\|P_n - u_N^*\|_{0,\Gamma_{\text{out}}} + \|\bar{P}_\ell - \bar{v}_L^*\|_{0,\Gamma_{\text{in}}}\Big\}. \tag{9.3.21}$$

The desired result (9.3.17) follows from Theorem 9.2.1 and Lemma 9.3.1. ■

Theorem 9.3.2. *Suppose that the Helmholtz solutions satisfy* $u \in C(S_a), u \in \mathbf{H}^p(\Gamma_{\text{out}})$ $\left(p > \frac{1}{2}\right)$ *and* $u \in \mathbf{H}^q(\Gamma_{\text{in}})$ $\left(q > \frac{1}{2}\right)$*. When the large* N *satisfies (9.2.23) and the large* L *satisfies (9.3.25) below, there exists the error bound for the annular domain by the MFS,*

$$\|u - u_{N-L}\|_{0,\Gamma_{\text{out}} \cup \Gamma_{\text{in}}} \le C\Big\{N^{-p}\|u\|_{p,\Gamma_{\text{out}}} + L^{-q}\|u\|_{q,\Gamma_{\text{in}}}\Big\}. \tag{9.3.22}$$

Proof. Denote $R_{n-\ell} = R_n + \bar{R}_\ell$, where the residuals $R_n = u_1 - P_n$ and $\bar{R}_\ell = u_2 - \bar{P}_\ell$ satisfy

$$\|R_n\|_{0,\Gamma_{\text{out}}} \le C\frac{1}{n^p}\|u_1\|_{p,\Gamma_{\text{out}}}, \quad \|\bar{R}_\ell\|_{0,\Gamma_{\text{in}}} \le C\frac{1}{\ell^q}\|u_2\|_{q,\Gamma_{\text{in}}}. \tag{9.3.23}$$

Then we have from (9.3.23)

$$\begin{aligned} \|R_{n-\ell}\|_{0,\Gamma_{\text{out}} \cup \Gamma_{\text{in}}} &\le \|R_n\|_{0,\Gamma_{\text{out}} \cup \Gamma_{\text{in}}} + \|\bar{R}_\ell\|_{0,\Gamma_{\text{out}} \cup \Gamma_{\text{in}}} \\ &\le C\Big\{\|R_n\|_{0,\Gamma_{\text{out}}} + \|\bar{R}_\ell\|_{0,\Gamma_{\text{in}}}\Big\} \le C\left\{\frac{1}{n^p}\|u_1\|_{p,\Gamma_{\text{out}}} + \frac{1}{\ell^q}\|u_2\|_{q,\Gamma_{\text{in}}}\right\}. \end{aligned} \tag{9.3.24}$$

Choose the u_N^* with coefficients c_j^* in (9.2.14) to approximate P_n, and the $\bar{v}_L^*$ with coefficients $\bar{c}_j^*$ in (9.3.14) to approximate $\bar{P}_\ell$. Then we have from (9.3.24) and Theorem 9.3.1

$$\begin{aligned}
&\|u-u_{N-L}\|_{0,\Gamma_{\text{out}}\cup\Gamma_{\text{in}}} \le \|u-v_{N-L}^*\|_{0,\Gamma_{\text{out}}\cup\Gamma_{\text{in}}}\\
&\le \|R_{n-\ell}\|_{0,\Gamma_{\text{out}}\cup\Gamma_{\text{in}}} + \|P_{n-\ell}-v_{N-L}^*\|_{0,\Gamma_{\text{out}}\cup\Gamma_{\text{in}}}\\
&\le C\left\{\frac{1}{n^p}\|u_1\|_{p,\Gamma_{\text{out}}} + \frac{1}{\ell^q}\|u_2\|_{q,\Gamma_{\text{in}}} + \frac{\sqrt{n}}{\delta^*}\left(\frac{r_{\max}}{R}\right)^{N-2n}\left(\frac{r_{\max}}{r_{\min}}\right)^n\|u_1\|_{0,\Gamma_{\text{out}}}\right.\\
&\quad\left. + \sqrt{\ell}\left(\frac{\bar{R}}{\bar{r}_{\min}}\right)^{L-2\ell}\left(\frac{\bar{r}_{\max}}{\bar{r}_{\min}}\right)^{\ell}\|u_2\|_{0,\Gamma_{\text{in}}}\right\}.
\end{aligned}$$

To reach the optimal convergence rates in (9.3.22), we choose the N satisfying (9.2.23) and the L satisfying (8.5.69) in Chapter 8.

$$L \ge 2\ell + \frac{(q+\frac{1}{2})\ln\ell + \ell\,\ln\left(\frac{\bar{r}_{\max}}{\bar{r}_{\min}}\right)}{\ln\left(\frac{\bar{r}_{\min}}{\bar{R}}\right)}, \quad \bar{R} < \bar{r}_{\min}. \tag{9.3.25}$$

Then we have

$$\|u-u_{N-L}\|_{0,\Gamma_{\text{out}}\cup\Gamma_{\text{in}}} \le C\left\{\frac{1}{n^p}\|u_1\|_{p,\Gamma_{\text{out}}} + \frac{1}{\ell^q}\|u_2\|_{q,\Gamma_{\text{in}}}\right\}. \tag{9.3.26}$$

From (9.2.23) and (9.3.25), we may choose $N \le Cn$ and $L \le C\ell$. Moreover, we have $\|u\|_{p,\Gamma_{\text{out}}} \asymp \|u_1\|_{p,\Gamma_{\text{out}}}$ and $\|u\|_{q,\Gamma_{\text{in}}} \asymp \|u_2\|_{q,\Gamma_{\text{in}}}$. The notation "$a \asymp b$" means that there exist two constants $c_0\,(>0)$ and C independent of N and L such that $c_0 b \le a \le Cb\,(b>0)$. Hence, the desired result (9.3.22) follows from (9.3.26). ■

9.4 Stability Analysis for Ring Domains

Consider a ring domain, $S_a^\circ = \{(\rho,\theta)|a<\rho<b, 0\le\theta<2\pi\}$, as in [46, 47, 228]. Denote by Γ_a° and Γ_b° two circles with radii a and b, respectively. The equation (9.3.1) is simplified as

$$\Delta u + k^2 u = 0 \text{ in } S_a^\circ, \quad u = g_{\text{out}} \text{ on } \Gamma_b^\circ, \quad u = g_{\text{in}} \text{ on } \Gamma_a^\circ. \tag{9.4.1}$$

Under $N = L$, the combined FS in (9.3.8) lead to

$$v_{N-N} = \sum_{j=1}^{N} c_j H_0^{(1)}(k|\overline{PQ_j}|) + \sum_{j=1}^{N} \bar{c}_j\left(\frac{\partial}{\partial\bar{R}} \pm \mathbf{i}k\right)H_0^{(1)}\left(k|\overline{P\bar{Q}_j}|\right), \tag{9.4.2}$$

where $Q_j = (R, jh)$, $\bar{Q}_j = (\bar{R}, jh)$, $h = \frac{2\pi}{N}$ and $\bar{R} < a < b < R$. Then the collocation equations (9.3.10) are simplified as

$$u_{N-N}(P_i) = g_{\text{out}}(P_i), P_i \in \Gamma_b^\circ; \quad u_{N-N}(\bar{P}_i) = g_{\text{in}}(\bar{P}_i),\ \bar{P}_i \in \Gamma_a^\circ, \tag{9.4.3}$$

where $P_i = (b, ih)$, $\bar{P}_i = (a, ih)$ and $h = \frac{2\pi}{N}$. The equation (9.4.3) is denoted by $\mathbf{Ax} = \mathbf{b}$, where the unknown vector $\mathbf{x} = \{c_1, ..., c_N, \bar{c}_1, ..., \bar{c}_N\}^T \in \mathbf{C}^{2N}$ and $\mathbf{b} \in \mathbf{C}^{2N}$. The matrix $\mathbf{A} \in \mathbf{C}^{2N \times 2N}$ is decomposed as

$$\mathbf{A} = \begin{bmatrix} \mathbf{A}_{11} & \mathbf{A}_{12} \\ \mathbf{A}_{21} & \mathbf{A}_{22} \end{bmatrix}. \tag{9.4.4}$$

The entries of submatrices, $\mathbf{A}_{11}, ..., \mathbf{A}_{22}$, are given by

$$(\mathbf{A}_{11})_{ij} = H_0^{(1)}\left(k\sqrt{R^2 + b^2 - 2Rb\cos(i-j)h}\right),$$

$$(\mathbf{A}_{12})_{ij} = \mathcal{D}H_0^{(1)}\left(k\sqrt{\bar{R}^2 + b^2 - 2\bar{R}b\cos(i-j)h}\right),$$

$$(\mathbf{A}_{21})_{ij} = H_0^{(1)}\left(k\sqrt{R^2 + a^2 - 2Ra\cos(i-j)h}\right),$$

$$(\mathbf{A}_{22})_{ij} = \mathcal{D}H_0^{(1)}\left(k\sqrt{\bar{R}^2 + a^2 - 2\bar{R}a\cos(i-j)h}\right).$$

To follow the proof more easily, let us address the outlines. The matrix $\mathbf{A}$ is a circulant-block matrix [71, p.181], and the eigenvalues may be sought by seeking 2×2 matrices. The challenging work is to explore the Cond involving a gap to eigenvalues; we first prove Lemma 9.4.1. Then the eigenvalues of all 2×2 matrices can be found in Lemmas 9.4.2 and 9.4.3. Finally, the bounds of the Cond are derived in Theorem 9.4.1. For the MFS in annular domains, stability analysis is more important than error analysis because Theorem 9.4.1 also provides a theoretical basis for the Dirichlet–Laplace eigenvalue problems. See Remark 9.4.2.

The submatrices, $\mathbf{A}_{11}, ..., \mathbf{A}_{22}$, are circulant. Denote the Fourier matrix (see Davis [71, p.32])

$$\mathbf{F}^*(\in \mathbf{C}^{N\times N}) = \frac{1}{\sqrt{N}}\begin{bmatrix} 1 & 1 & \cdots & 1 \\ 1 & \omega & \cdots & \omega^{n-1} \\ \vdots & \vdots & \ddots & \vdots \\ 1 & \omega^{n-1} & \cdots & \omega \end{bmatrix}, \tag{9.4.5}$$

where $\omega = e^{2\pi\mathbf{i}/N} = \cos(2\pi/N) + \mathbf{i}\sin(2\pi/N)$ with $\mathbf{i} = \sqrt{-1}$. Based on [71] we have

$$\mathbf{A}_{11} = \mathbf{F}^*\Lambda_{11}\mathbf{F},\ \mathbf{A}_{12} = \mathbf{F}^*\Lambda_{12}\mathbf{F},\ \mathbf{A}_{21} = \mathbf{F}^*\Lambda_{21}\mathbf{F},\ \mathbf{A}_{22} = \mathbf{F}^*\Lambda_{22}\mathbf{F}, \tag{9.4.6}$$

where $\mathbf{F}$ is unitary with $\mathbf{FF}^* = \mathbf{F}^*\mathbf{F} = \mathbf{I}$, and $\mathbf{I}$ is the identity matrix. In (9.4.6) the matrices,

$$\boldsymbol{\Lambda}_{pq} = \mathrm{diag}(\lambda_0^{(pq)}, \lambda_1^{(pq)}, ..., \lambda_{N-1}^{(pq)}),\ 1 \le p, q \le 2, \tag{9.4.7}$$

are diagonal. The diagonal entries of $\mathbf{\Lambda}_{11}$ and $\mathbf{\Lambda}_{12}$ are given by

$$\lambda_0^{(11)} \approx NH_0^{(1)}(kR)J_0(kb), \tag{9.4.8}$$

$$\lambda_\ell^{(11)} \approx N\{H_\ell^{(1)}(kR)J_\ell(kb) + H_{N-\ell}^{(1)}(kR)J_{N-\ell}(kb)\}, \quad \ell = 1, 2, ..., N-1, \tag{9.4.9}$$

and

$$\lambda_0^{(12)} \approx NH_0^{(1)}(kb)\mathcal{D}J_0(k\bar{R}), \tag{9.4.10}$$

$$\lambda_\ell^{(12)} \approx N[H_\ell^{(1)}(kb)\mathcal{D}J_\ell(k\bar{R}) + H_{N-\ell}^{(1)}(kb)\mathcal{D}J_{N-\ell}(k\bar{R})], \quad \ell = 1, 2, ..., N-1. \tag{9.4.11}$$

Also the diagonal entries of $\mathbf{\Lambda}_{21}$ and $\mathbf{\Lambda}_{22}$ are given from Lemma 8.6.1 of Chapter 8,

$$\lambda_0^{(21)} \approx NH_0^{(1)}(kR)J_0(ka), \tag{9.4.12}$$

$$\lambda_\ell^{(21)} \approx N\{H_\ell^{(1)}(kR)J_\ell(ka) + H_{N-\ell}^{(1)}(kR)J_{N-\ell}(ka)\}, \quad \ell = 1, 2, ..., N-1, \tag{9.4.13}$$

and

$$\lambda_0^{(22)} \approx NH_0^{(1)}(ka)\mathcal{D}J_0(k\bar{R}), \tag{9.4.14}$$

$$\lambda_\ell^{(22)} \approx N[H_\ell^{(1)}(ka)\mathcal{D}J_\ell(k\bar{R}) + H_{N-\ell}^{(1)}(ka)\mathcal{D}J_{N-\ell}(k\bar{R})], \quad \ell = 1, 2, ..., N-1. \tag{9.4.15}$$

By using matrix $\mathbf{F}^*$ in (9.4.5) we obtain from (9.4.6)

$$\mathbf{A} = \begin{bmatrix} \mathbf{A}_{11} & \mathbf{A}_{12} \\ \mathbf{A}_{21} & \mathbf{A}_{22} \end{bmatrix} = \begin{bmatrix} \mathbf{F}^* & \mathbf{O} \\ \mathbf{O} & \mathbf{F}^* \end{bmatrix} \begin{bmatrix} \mathbf{\Lambda}_{11} & \mathbf{\Lambda}_{12} \\ \mathbf{\Lambda}_{21} & \mathbf{\Lambda}_{22} \end{bmatrix} \begin{bmatrix} \mathbf{F} & \mathbf{O} \\ \mathbf{O} & \mathbf{F} \end{bmatrix}. \tag{9.4.16}$$

Since the eigenvalues of similar matrices are the same, the eigenvalues of $\mathbf{A}$ are just those of matrix Λ, denoted by

$$\mathbf{\Lambda} = \begin{bmatrix} \mathbf{\Lambda}_{11} & \mathbf{\Lambda}_{12} \\ \mathbf{\Lambda}_{21} & \mathbf{\Lambda}_{22} \end{bmatrix} = \begin{bmatrix} \text{diag}(\lambda_i^{(11)}) & \text{diag}(\lambda_i^{(12)}) \\ \text{diag}(\lambda_i^{(21)}) & \text{diag}(\lambda_i^{(22)}) \end{bmatrix}. \tag{9.4.17}$$

By a permutation transformation $\mathbf{P}$ we have

$$\mathbf{P}^T\mathbf{\Lambda}\mathbf{P} = \begin{bmatrix} \lambda_0^{(11)} & \lambda_0^{(12)} & & & \\ \lambda_0^{(21)} & \lambda_0^{(22)} & & \mathbf{O} & \\ & & \ddots & & \\ & \mathbf{O} & & \lambda_{N-1}^{(11)} & \lambda_{N-1}^{(12)} \\ & & & \lambda_{N-1}^{(21)} & \lambda_{N-1}^{(22)} \end{bmatrix}. \tag{9.4.18}$$

Hence the eigenvalues $\bar{\lambda}\,(=\bar{\lambda}_i^{\pm})$ of $\mathbf{\Lambda}$ can be found from the zero determinants,

$$\begin{vmatrix} \lambda_i^{(11)}-\bar{\lambda} & \lambda_i^{(12)} \\ \lambda_i^{(21)} & \lambda_i^{(22)}-\bar{\lambda} \end{vmatrix} = 0, \quad i=0,1,2,...,N-1. \tag{9.4.19}$$

The Dirichlet–Laplace eigenvalue problem of the ring domain S_a° is defined by

$$\Delta u + \lambda^\circ u = 0 \text{ in } S_a^\circ, \quad u=0 \text{ on } \mathbf{\Gamma}_b^\circ \cup \mathbf{\Gamma}_a^\circ. \tag{9.4.20}$$

Similarly to (9.2.17), define the gap

$$\delta^\circ = \min_{\forall n}\left\{\frac{|k^2-\lambda_n^\circ|}{\lambda_n^\circ}\right\}, \tag{9.4.21}$$

where λ_n° is an eigenvalue of (9.4.20). We will discuss the case of $0<\delta^\circ \ll 1$. In this chapter assume that k is bounded. The eigenfunctions are given from (9.3.3):

$$u_\ell(\rho,\theta) = J_\ell(k\rho)\{a_\ell \cos(\ell\theta) + b_\ell \sin(\ell\theta)\} + H_\ell^{(1)}(k\rho)\{\bar{a}_\ell \cos(\ell\theta) + \bar{b}_\ell \sin(\ell\theta)\}. \tag{9.4.22}$$

From $u(a,\theta)=u(b,\theta)=0$, we find the eigenvalues $\lambda_n^\circ\,(=k^2)$ satisfying

$$H_\ell^{(1)}(ka)J_\ell(kb) - J_\ell(ka)H_\ell^{(1)}(kb) = 0, \quad \ell=0,1,.... \tag{9.4.23}$$

Since

$$H_\ell^{(1)}(ka)J_\ell(kb) - J_\ell(ka)H_\ell^{(1)}(kb) = \mathbf{i}\{Y_\ell(ka)J_\ell(kb) - J_\ell(ka)Y_\ell(kb)\} = 0, \tag{9.4.24}$$

the equation (9.4.23) is also consistent with that in [41, 47, Table 1]. The zeros of (9.4.24) are also discussed in [1, p.374]. Define the functions *via* k by

$$g_\ell(k) = H_\ell^{(1)}(ka)J_\ell(kb) - H_\ell^{(1)}(kb)J_\ell(ka) = \mathbf{i}\{Y_\ell(ka)J_\ell(kb) - J_\ell(ka)Y_\ell(kb)\}. \tag{9.4.25}$$

Hence the functions $g_\ell(k)=0$ at $k=\sqrt{\lambda_n^\circ}$ for (9.4.23). Below, we use the notation $a \asymp O(b)$, which means that there exist two constants $c_0\ (>0)$ and C independent of ℓ and k such that $c_0 b \le a \le Cb\,(b>0)$.

By the method of separation of variables, the equation (9.4.20) leads to the Bessel differential equation [223, p.480],

$$-\frac{d}{d\rho}\left(\rho\frac{du(\rho)}{d\rho}\right) + \frac{\ell^2}{\rho}u(\rho) = \lambda\rho u(\rho), \quad u(a)=0, \quad u(b)=0, \tag{9.4.26}$$

where $0<a\le\rho\le b$. The equation (9.4.26) is a regular Sturm-Liouville problem. Based on the Sturm-Liouville theory in Courant and Hilbert [70, p.293], the eigenvalues for (9.4.26) are real, simple and denumerable,

$$0<\lambda_{\ell,1}<\lambda_{\ell,2}<\cdots<\lambda_{\ell,m}<\lambda_{\ell,m+1}<\cdots. \tag{9.4.27}$$

Then for functions (9.4.25), when $g_\ell(k)=0$ at $k=\sqrt{\lambda_{\ell,m}}\,(=\sqrt{\lambda_n^\circ})$, we have $|g'_\ell(k)|>0$ from (9.4.27). Below, we will confirm $|g'_\ell(k)|\geq c_0>0$ (*i.e.*, $|g'_\ell(k)|\asymp O(1)$). First, we give a preliminary lemma.

Lemma 9.4.1. *For bounded* k, *when* $g_\ell(k)=0$ *at* $k=\sqrt{\lambda_n^\circ}$, *we have* $|g'_\ell(k)|\asymp O(1)$.

Proof. Consider the Dirichlet and the Neumann conditions on $\mathbf{\Gamma}_a^\circ$ and $\mathbf{\Gamma}_b^\circ$, denoted by D-D, D-N, N-D and N-N, where the letters D- and N- before the hyphen denote the Dirichlet and the Neumann conditions on $\mathbf{\Gamma}_a^\circ$, respectively, and the letters -D and -N after the hyphen denote the Dirichlet and the Neumann conditions on $\mathbf{\Gamma}_b^\circ$, respectively. We rewrite (9.4.25) as

$$g_\ell(k)=\begin{vmatrix} J_\ell(kb) & J_\ell(ka) \\ H_\ell^{(1)}(kb) & H_\ell^{(1)}(ka) \end{vmatrix} := \mathbf{i}g_\ell^{D-D}(k),$$

and obtain the derivatives

$$\begin{aligned} g'_\ell(k) &= \begin{vmatrix} \dfrac{d}{dk}J_\ell(kb) & J_\ell(ka) \\ \dfrac{d}{dk}H_\ell^{(1)}(kb) & H_\ell^{(1)}(ka) \end{vmatrix} + \begin{vmatrix} J_\ell(kb) & \dfrac{d}{dk}J_\ell(ka) \\ H_\ell^{(1)}(kb) & \dfrac{d}{dk}H_\ell^{(1)}(ka) \end{vmatrix} \qquad (9.4.28) \\ &= b\begin{vmatrix} J'_\ell(kb) & J_\ell(ka) \\ J'_\ell(kb)+\mathbf{i}\,Y'_\ell(kb) & J_\ell(ka)+\mathbf{i}\,Y_\ell(ka) \end{vmatrix} + a\begin{vmatrix} J_\ell(kb) & J'_\ell(ka) \\ J_\ell(kb)+\mathbf{i}\,Y_\ell(kb) & J'_\ell(ka)+\mathbf{i}\,Y'_\ell(ka) \end{vmatrix} \\ &= \mathbf{i}b\begin{vmatrix} J'_\ell(kb) & J_\ell(ka) \\ Y'_\ell(kb) & Y_\ell(ka) \end{vmatrix} + \mathbf{i}a\begin{vmatrix} J_\ell(kb) & J'_\ell(ka) \\ Y_\ell(kb) & Y'_\ell(ka) \end{vmatrix} = \mathbf{i}\{bg_\ell^{D-N}(k)+ag_\ell^{N-D}(k)\}, \end{aligned}$$

where

$$g_\ell^{D-D}(k) = Y_\ell(ka)J_\ell(kb) - Y_\ell(kb)J_\ell(ka), \qquad (9.4.29)$$

$$g_\ell^{D-N}(k) = Y_\ell(ka)J'_\ell(kb) - Y'_\ell(kb)J_\ell(ka), \qquad (9.4.30)$$

$$g_\ell^{N-D}(k) = Y'_\ell(ka)J_\ell(kb) - Y_\ell(kb)J'_\ell(ka), \qquad (9.4.31)$$

$$g_\ell^{N-N}(k) = Y'_\ell(ka)J'_\ell(kb) - Y'_\ell(kb)J'_\ell(ka). \qquad (9.4.32)$$

The eigenvalues for the D-N, the N-D and the N-N conditions are given by $\lambda^\circ\ (=k^2)$ satisfying $g_\ell^{D-N}(k)=0$, $g_\ell^{N-D}(k)=0$ and $g_\ell^{N-N}(k)=0$, respectively. For bounded k, we have from (9.4.28)

$$|g'_\ell(k)| \geq \Big| b|g_\ell^{D-N}(k)| - a|g_\ell^{N-D}(k)| \Big| > 0, \qquad (9.4.33)$$

$$|g'_\ell(k)| \leq b|g_\ell^{D-N}(k)| + a|g_\ell^{N-D}(k)| \leq C. \qquad (9.4.34)$$

Next, from the formula of cross-product in [1, 9.1.34, p.361], we have

$$g_\ell^{D-D}(k)g_\ell^{N-N}(k) - g_\ell^{D-N}(k)g_\ell^{N-D}(k) = \frac{4}{\pi k^2 ab}. \qquad (9.4.35)$$

When the function $g_\ell(k) = \mathbf{i} g_\ell^{D-D}(k) = 0$, the equation (9.4.35) leads to

$$g_\ell^{D-N}(k) g_\ell^{N-D}(k) = -\frac{4}{\pi k^2 ab}, \tag{9.4.36}$$

to give $g_\ell^{D-N}(k) \neq 0$ and $g_\ell^{N-D}(k) \neq 0$. The eigenvalues of the D-N and the N-D conditions must be distinct from those of the D-D condition; see [1, Table 9.7]. Moreover, two functions are bounded from (9.4.29)–(9.4.32): $|g_\ell^{D-N}(k)| \leq |Y_\ell(ka) J'_\ell(kb)| + |J_\ell(ka) Y'_\ell(kb)| \leq C$ and $|g_\ell^{N-D}(k)| \leq C$. Hence we have from (9.4.36)

$$|g_\ell^{N-D}(k)| = \frac{4}{\pi k^2 ab |g_\ell^{D-N}(k)|} \geq c_0 > 0.$$

Similarly, we have $|g_\ell^{D-N}(k)| \geq c_0 > 0$. Since $b|g_\ell^{D-N}(k)| \geq c_0 > 0$, $a|g_\ell^{N-D}(k)| \geq c_0 > 0$ and $|g'_\ell(k)| > 0$, we conclude $|g'_\ell(k)| \geq c_0 > 0$ and then $|g'_\ell(k)| \asymp O(1)$ from (9.4.33). This completes the proof of Lemma 9.4.1. ■

Under bounded k we only consider the bounded $\lambda_n^\circ \, (= \lambda_{\ell,m}) \approx k^2$. First, we seek the leading eigenvalues $\bar{\lambda}_0^\pm$ of $\mathbf{T}_0$ given by

$$\mathbf{T}_0 = \begin{bmatrix} \lambda_0^{(11)} & \lambda_0^{(12)} \\ \lambda_0^{(21)} & \lambda_0^{(22)} \end{bmatrix} \approx N \begin{bmatrix} H_0^{(1)}(kR) J_0(kb) & H_0^{(1)}(kb) \mathcal{D} J_0(k\bar{R}) \\ H_0^{(1)}(kR) J_0(ka) & H_0^{(1)}(ka) \mathcal{D} J_0(k\bar{R}) \end{bmatrix}, \tag{9.4.37}$$

where the entries are given from (9.4.19) and (9.4.8)–(9.4.15).

Lemma 9.4.2. *Let* $0 < \delta^\circ \ll 1$ *and the matrix* $\mathbf{T}_0$ *in (9.4.37) be given. There exist the bounds,*

$$|\bar{\lambda}_0^+| \leq CN, \quad |\bar{\lambda}_0^-| \geq c_0 \delta^\circ N. \tag{9.4.38}$$

Proof. Denote $\lambda_n^\circ \, (\approx k^2)$ and $\varepsilon = |k - \sqrt{\lambda_n^\circ}|$. For bounded k and λ_n°, we have from (9.4.21)

$$\delta^\circ = \frac{|k^2 - \lambda_n^\circ|}{\lambda_n^\circ} = \frac{|k + \sqrt{\lambda_n^\circ}|}{\lambda_n^\circ} \times \left| k - \sqrt{\lambda_n^\circ} \right| \asymp O(\varepsilon). \tag{9.4.39}$$

From the assumption $0 < \delta^\circ \ll 1$, there exist the bounds,

$$0 < \varepsilon \ll 1, \quad \varepsilon \asymp O(\delta^\circ). \tag{9.4.40}$$

From calculus we have

$$g_\ell(k) \approx g_\ell\left(\sqrt{\lambda_n^\circ}\right) + g'_\ell\left(\sqrt{\lambda_n^\circ}\right)\left(k - \sqrt{\lambda_n^\circ}\right) = g'_\ell\left(\sqrt{\lambda_n^\circ}\right)\left(k - \sqrt{\lambda_n^\circ}\right). \tag{9.4.41}$$

Based on Lemma 9.4.1 and (9.4.40),

$$|g_\ell(k)| \approx \left| g'_\ell\left(\sqrt{\lambda_n^\circ}\right) \right| \varepsilon \asymp O(\varepsilon) \asymp O(\delta^\circ). \tag{9.4.42}$$

For (9.4.37) we have the key determinant,

$$\begin{aligned} t_0 &= \begin{vmatrix} H_0^{(1)}(kR)J_0(kb) & H_0^{(1)}(kb)\mathcal{D}J_0(k\bar{R}) \\ H_0^{(1)}(kR)J_0(ka) & H_0^{(1)}(ka)\mathcal{D}J_0(k\bar{R}) \end{vmatrix} \\ &= H_0^{(1)}(kR)\mathcal{D}J_0(k\bar{R})\begin{vmatrix} J_0(kb) & H_0^{(1)}(kb) \\ J_0(ka) & H_0^{(1)}(ka) \end{vmatrix} = H_0^{(1)}(kR)\mathcal{D}J_0(k\bar{R})g_0(k). \end{aligned} \tag{9.4.43}$$

Since $|H_0^{(1)}(kR)\mathcal{D}J_0(k\bar{R})| = M_0(kR)|\mathcal{D}J_0(k\bar{R})| \asymp O(1)$ from Lemma 8.5.5 in Chapter 8, we have from (9.4.43) and (9.4.42)

$$|t_0| = M_0(kR)|\mathcal{D}J_0(k\bar{R})| \times |g_0(k)| \asymp O(\delta^\circ). \tag{9.4.44}$$

Then we obtain from (9.4.37) and (9.4.44)

$$|\mathrm{Det}(\mathbf{T}_0)| = N^2|t_0| \asymp N^2 O(\delta^\circ). \tag{9.4.45}$$

Consider the quadratic equation $x^2 + bx + c = 0$, where $c = \mathrm{Det}(\mathbf{T}_0)$. We have $x^\pm = \frac{1}{2}\left\{-b \pm \sqrt{b^2 - 4c}\right\}$ and then $x^+ \le |b| + \sqrt{|c|}$. See Section 10.4. Hence, we obtain two eigenvalues $\bar{\lambda}_0^\pm$ of matrix $\mathbf{T}_0$,

$$\begin{aligned} &|\bar{\lambda}_0^+| \le NM_0(kR)|\mathcal{D}J_0(k\bar{R})|(M_0(ka) + |J_0(kb)|) + \sqrt{|\mathrm{Det}(\mathbf{T}_0)|} \le C(N + N\sqrt{\delta^\circ}) \le CN, \\ &|\bar{\lambda}_0^-| = \frac{|\mathrm{Det}(\mathbf{T}_0)|}{|\bar{\lambda}_0^+|} \ge c_0\delta^\circ N. \end{aligned}$$

This completes the proof of Lemma 9.4.2. ■

Next, consider the following submatrices from (9.4.19) and (9.4.8)–(9.4.15),

$$\begin{aligned} T_i &= \begin{bmatrix} \lambda_i^{(11)} & \lambda_i^{(12)} \\ \lambda_i^{(21)} & \lambda_i^{(22)} \end{bmatrix} \\ &\approx N\begin{bmatrix} H_i^{(1)}(kR)J_i(kb) + H_{N-i}^{(1)}(kR)J_{N-i}(kb) & H_i^{(1)}(kb)\mathcal{D}J_i(k\bar{R}) + H_{N-i}^{(1)}(kb)\mathcal{D}J_{N-i}(k\bar{R}) \\ H_i^{(1)}(kR)J_i(ka) + H_{N-i}^{(1)}(kR)J_{N-i}(ka) & H_i^{(1)}(ka)\mathcal{D}J_i(k\bar{R}) + H_{N-i}^{(1)}(ka)\mathcal{D}J_{N-i}(k\bar{R}) \end{bmatrix}. \end{aligned} \tag{9.4.46}$$

Lemma 9.4.3. *Let $0 < \delta^\circ \ll 1$ and bounded k. Consider the eigenvalues $\lambda_i^\pm$ of matrix $\mathbf{T}_i$ in (9.4.46) with $i = 1, 2, ..., N-1$. For small i there exist the bounds,*

$$|\bar{\lambda}_i^+| \le CN, \quad |\bar{\lambda}_i^-| \ge c_0\delta^\circ N. \tag{9.4.47}$$

For large $i \le \frac{N}{2}$,

$$|\bar{\lambda}_i^+| \le CN\max\left\{\frac{1}{i}\left(\frac{b}{R}\right)^i, \left(\frac{\bar{R}}{a}\right)^i\right\}, \quad |\bar{\lambda}_i^-| \ge c_0N\min\left\{\frac{1}{i}\left(\frac{b}{R}\right)^i, \left(\frac{\bar{R}}{a}\right)^i\right\}. \tag{9.4.48}$$

Proof. For large n, since $\bar{R}<a<b<R$, there exist the bounds,

$$\left|H_n^{(1)}(kR)J_n(ka)\right| = M_n(kR)|J_n(ka)| \approx \frac{1}{n\pi}\left(\frac{a}{R}\right)^n, \tag{9.4.49}$$

$$\left|H_n^{(1)}(kR)J_n(kb)\right| \approx \frac{1}{n\pi}\left(\frac{b}{R}\right)^n \gg \left|H_n^{(1)}(kR)J_n(ka)\right|. \tag{9.4.50}$$

Also for large n, we have from (8.5.53) in Chapter 8

$$\left|H_n^{(1)}(kb)\mathcal{D}J_n(k\bar{R})\right| = M_n(kb)|\mathcal{D}J_n(k\bar{R})| \approx \frac{1}{\pi}\left(\frac{\bar{R}}{b}\right)^n, \tag{9.4.51}$$

$$\left|H_n^{(1)}(ka)\mathcal{D}J_n(k\bar{R})\right| \approx \frac{1}{\pi}\left(\frac{\bar{R}}{a}\right)^n \gg \left|H_n^{(1)}(kb)\mathcal{D}J_n(k\bar{R})\right|. \tag{9.4.52}$$

For small i, there may exist the eigenvalues $\lambda_n^\circ(\approx\sqrt{k})$ of (9.4.20), where k is bounded. From (9.4.46) and (9.4.49)–(9.4.52), we have

$$\mathbf{T}_i = \begin{bmatrix} \lambda_i^{(11)} & \lambda_i^{(12)} \\ \lambda_i^{(21)} & \lambda_i^{(22)} \end{bmatrix} \approx N\begin{bmatrix} H_i^{(1)}(kR)J_i(kb) & H_i^{(1)}(kb)\mathcal{D}J_i(k\bar{R}) \\ H_i^{(1)}(kR)J_i(ka) & H_i^{(1)}(ka)\mathcal{D}J_i(k\bar{R}) \end{bmatrix}. \tag{9.4.53}$$

For (9.4.53) we have the key determinant,

$$\begin{aligned} t_i &= \begin{vmatrix} H_i^{(1)}(kR)J_i(kb) & H_i^{(1)}(kb)\mathcal{D}J_i(k\bar{R}) \\ H_i^{(1)}(kR)J_i(ka) & H_i^{(1)}(ka)\mathcal{D}J_i(k\bar{R}) \end{vmatrix} \\ &= H_i^{(1)}(kR)\mathcal{D}J_i(k\bar{R})\begin{vmatrix} J_i(kb) & H_i^{(1)}(kb) \\ J_i(ka) & H_i^{(1)}(ka) \end{vmatrix} = H_i^{(1)}(kR)\mathcal{D}J_i(k\bar{R})g_i(k), \end{aligned}$$

where the functions $g_i(k)$ are given in (9.4.25). Moreover, we have

$$\left|H_i^{(1)}(kR)\mathcal{D}J_i(k\bar{R})\right| = M_i(kR)\left|\mathcal{D}J_i(k\bar{R})\right| \asymp O(1)$$

from Lemma 8.5.5 of Chapter 8. By following the arguments of Lemma 9.4.2, we also have from (9.4.42)

$$\left|\bar{\lambda}_i^+\right| \le CN, \quad \left|\bar{\lambda}_i^-\right| \ge c_0\delta^\circ N, \quad \text{for small } i. \tag{9.4.54}$$

This is the first result (9.4.47).

Next for large i, the bounded k^2 is not close to any eigenvalue, and then $\delta^\circ \ge c_0 > 0$. We obtain from (9.4.46) and (9.4.49)–(9.4.52),

$$\begin{aligned} \mathbf{T}_i = \begin{bmatrix} \lambda_i^{(11)} & \lambda_i^{(12)} \\ \lambda_i^{(21)} & \lambda_i^{(22)} \end{bmatrix} &\approx N\begin{bmatrix} H_i^{(1)}(kR)J_i(kb) & H_i^{(1)}(kb)\mathcal{D}J_i(k\bar{R}) \\ H_i^{(1)}(kR)J_i(ka) & H_i^{(1)}(ka)\mathcal{D}J_i(k\bar{R}) \end{bmatrix} \\ \approx N\begin{bmatrix} H_i^{(1)}(kR)J_i(kb) & 0 \\ 0 & H_i^{(1)}(ka)\mathcal{D}J_i(k\bar{R}) \end{bmatrix} &\approx \mathbf{T}_{N-i}. \end{aligned} \tag{9.4.55}$$

Then we only consider $i \leq \frac{N}{2}$, and obtain the following eigenvalues from (9.4.55) and (9.4.49)–(9.4.52),

$$|\bar{\lambda}_i^-| \geq N\min\left\{\left|H_i^{(1)}(kR)J_i(kb)\right|, \left|H_i^{(1)}(ka)\mathcal{D}J_i(k\bar{R})\right|\right\} \geq c_0 N\min\left\{\frac{1}{i}\left(\frac{b}{R}\right)^i, \left(\frac{\bar{R}}{a}\right)^i\right\}.$$

Similarly, we have

$$|\bar{\lambda}_i^+| \leq CN\max\left\{\frac{1}{i}\left(\frac{b}{R}\right)^i, \left(\frac{\bar{R}}{a}\right)^i\right\}.$$

This gives the second result (9.4.48) and completes the proof of Lemma 9.4.3. ■

Theorem 9.4.1. *Let $0 < \delta^\circ \ll 1$ and matrix $\mathbf{A}$ in (9.4.4) be given. For bounded k there exists the bound,*

$$\text{Cond}(\mathbf{A}) \leq C\max\left\{\frac{1}{\delta^\circ}, N\left(\frac{R}{b}\right)^{\frac{N}{2}}, \left(\frac{a}{\bar{R}}\right)^{\frac{N}{2}}\right\}. \tag{9.4.56}$$

Proof. From Lemmas 9.4.2 and 9.4.3, we have

$$\sigma_{\max} = \max_i |\bar{\lambda}_i^\pm| \leq C|\bar{\lambda}_0^+| \leq CN, \tag{9.4.57}$$

$$\sigma_{\min} = \min_i |\bar{\lambda}_i^\pm| \geq \min\left\{c_0|\bar{\lambda}_0^-|, \left|\bar{\lambda}_{\frac{N}{2}}^-\right|\right\} \geq c_0 N\min\left\{\delta^\circ, \frac{1}{N}\left(\frac{b}{R}\right)^{\frac{N}{2}}, \left(\frac{\bar{R}}{a}\right)^{\frac{N}{2}}\right\}. \tag{9.4.58}$$

Combining (9.4.57) and (9.4.58) gives[1]

$$\text{Cond}(\mathbf{A}) = \frac{\max_i |\bar{\lambda}_i^\pm|}{\min_i |\bar{\lambda}_i^\pm|} \leq C\ \max\left\{\frac{1}{\delta^\circ}, N\left(\frac{R}{b}\right)^{\frac{N}{2}}, \left(\frac{a}{\bar{R}}\right)^{\frac{N}{2}}\right\}. \tag{9.4.59}$$

■

When k^2 is not close to any eigenvalue λ_ℓ° (*i.e.*, $\delta^\circ \geq c_0 > 0$), we have from (9.4.56)

$$\text{Cond}(\mathbf{A}) \leq C\ \max\left\{N\left(\frac{R}{b}\right)^{\frac{N}{2}}, \left(\frac{a}{\bar{R}}\right)^{\frac{N}{2}}\right\}. \tag{9.4.60}$$

By following [163, 222], the stability analysis above can be extended to annular domains, provided that the source nodes are located on two concentric circles (*i.e.*, $Q_j = (R, jh)$, $\bar{Q}_j = (\bar{R}, jh)$, $h = \frac{2\pi}{N}$ and $\bar{R} < \min \rho|_{S_a} < \max \rho|_{S_a} < R$). For the bounded and fixed N, once an eigenvalue occurs (*i.e.*, $\delta^\circ = 0$), there occurs $\text{Cond} = \infty$ from Theorem 9.4.1. This gives a basic approach to seeking eigenvalues; see Remark 9.4.2 below. In Chen *et al.* [41, 44, 46, 47], numerical eigenvalues were reported for ring domains by the MFS and the boundary element method (BEM), and the exact (and spurious) eigenvalues were found based on $\sigma_{\min} \approx 0$.

---

[1] The condition number in spectral norm is used in (9.4.59), and the related discussions are given in Remarks 10.4.1 and 10.4.2 in Chapter 10.

Remark 9.4.1. *Note that the MFS-QR in Antunes [8, 9] is irrelevant to the MFS, because it is only a variant of the MPS (see Section 14.3). For simplicity, we only discuss the bounded simply-connected domains in Section 9.2. The conclusions for the bounded multiply-connected domains remain the same. Based on Section 14.3, we can prove that the following particular solutions are used in the MFS-QR algorithms in [9],*

$$P_n^{MFS-QR}(\rho, \theta) = \pm \frac{a_0}{\sqrt{N}} J_0(k\rho) + \sum_{m=1}^{n} J_m(k\rho) \left(\pm \sqrt{\frac{2}{N}} a_m \cos(m\theta) \pm \sqrt{\frac{2}{N}} b_m \sin(m\theta) \right), \tag{9.4.61}$$

where $N = 2n + 1$. *Note that the functions (9.4.61) are the very PS in (9.2.10) with the scale factors,* $\pm \frac{1}{\sqrt{N}}$ *and* $\pm \sqrt{\frac{2}{N}}$. *For disk domains, the* $\text{Cond} = O(1)$ *can be proved to display an excellent stability. The MFS-QR in Antunes [9] is a variant of the MPS in Li [149] but not a variant of the MFS in Section 9.2. Hence, the stability analysis in this chapter is important and indispensable for the MFS.*

Remark 9.4.2. *For the bounded multiply-connected domains, the MFS algorithms without spurious eigenvalues in this chapter are also useful for solving the Dirichlet–Laplace eigenvalue problems. The MFS offers a unique solution with the optimal convergence rates provided that* $k^2 \neq \lambda$. *Otherwise, the unique solutions cannot be found due to the matrix singularity with* $\sigma_{\min}(\mathbf{F}) = 0$ *even for small* N*; see Theorem 9.4.1. For the eigenvalue problem, the discrete matrix* $\mathbf{F}$ *is the same as the Helmholtz equation. Hence the matrix* $\mathbf{F}$ *is singular, if and only if an eigenvalue as* $\lambda_\ell \, (= k^2)$ *occurs. By following [148, 172] and [169, Chapter 9], eigenvalues and eigenfunctions can be obtained. For the eigenvalue problem in the bounded multiply-connected domains, however, we strongly recommend the combined algorithms (9.3.8) and (9.3.10), to eliminate all spurious eigenvalues. Hence, the study in this chapter is also important to the Dirichlet–Laplace eigenvalue problems.*

9.5 Numerical Experiments

Denote by S_{holes} a bounded domain with four interior holes, where the exterior boundary Γ_{out} is defined as in Chapter 8,

$$\Gamma_{\text{out}} = \{(x, y) | x = \rho(\theta)\cos\theta, y = \rho(\theta)\sin\theta, \ 0 \leq \theta \leq 2\pi\},$$

where $\rho(\theta) = \sqrt{(a+b)^2 + 1 - 2(a+b)\cos(a\theta/b)}$ with two constants a and b. In computation, choose $a = 3$ and $b = 1$ with $\rho \in [3, 5]$. There are four interior circular holes $\bar{S}_\ell$ with the same radius $\bar{r}_0^{\text{in}} = 0.5$. The centers of these four circles are given by $(x, y) = (0, 0), (-2.5, 0)$ and $(1.25, \pm 1.25\sqrt{3})$ (see Figure 9.1). The equation (9.3.1) is modified as

$$\Delta^2 u + k^2 u = 0 \text{ in } S_{\text{holes}}, \quad u = f \text{ on } \mathbf{\Gamma}_{\text{out}}, \quad u = g_\ell \text{ on } \mathbf{\Gamma}_{\text{in}}^\ell, \quad \ell = 1, 2, 3, 4. \quad (9.5.1)$$

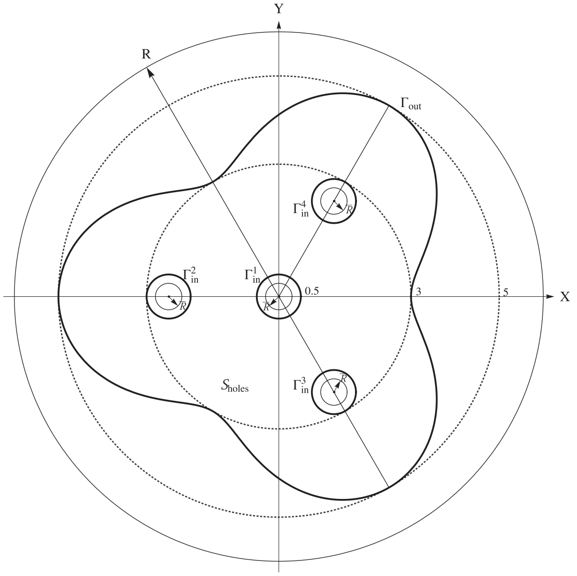

FIG. 9.1 – The bounded domain S_{holes} with four interior holes.

Let the interior boundary $\mathbf{\Gamma}_{\text{in}} = \cup_\ell \mathbf{\Gamma}_{\text{in}}^\ell = \cup_\ell \partial \bar{S}_\ell$, then $\partial S_{\text{holes}} = \mathbf{\Gamma}_{\text{out}} \cup \mathbf{\Gamma}_{\text{in}}$. Denote by $(\bar{\rho}^\ell, \bar{\theta}^\ell)$ four local polar coordinates and choose their origins at the centers of $\bar{S}_\ell$. For the exterior source nodes $Q(R, \theta)$ outside $\mathbf{\Gamma}_{\text{out}}$, we choose (9.3.6) as the FS with $R > r_{\max} = \max \rho|_{\rho \in \mathbf{\Gamma}_{\text{out}}}$. For the interior source nodes $\bar{Q}(\bar{R}^\ell, \bar{\theta}^\ell)$ inside $\mathbf{\Gamma}_{\text{in}}^\ell$, choose the modified FS in (9.3.7),

$$\begin{aligned} \bar{\mathbf{\Psi}}_j^\ell(P) &= \mathcal{D} H_0^{(1)}\left(k|\overline{P\bar{Q}_j^\ell}|\right) = \left(\frac{\partial}{\partial \bar{R}^\ell} + \mathbf{i}k\right) H_0^{(1)}\left(k|\overline{P\bar{Q}_j^\ell}|\right), \\ \bar{Q}_j^\ell &= (\bar{R}^\ell, j\bar{h}), \ \ell = 1, 2, 3, 4, \end{aligned}$$

where $\bar{h} = 2\pi/L$, $\bar{R} = \bar{R}^\ell < \bar{r}_{\min}^\ell = \bar{r}_0^{\text{in}} = 0.5$, and the operator $\mathcal{D} = \left(\frac{\partial}{\partial \bar{R}^\ell} + \mathbf{i}k\right)$ in computation. The combined FS for the domain S_{holes} are given by

$$v_{N-L} = \sum_{j=1}^{N} c_j \Psi_j(P) + \sum_{\ell=1}^{4} \sum_{j=1}^{L} \bar{c}_j^{\ell} \bar{\Psi}_j^{\ell}(P). \tag{9.5.2}$$

We employ the collocation equations directly from the Dirichlet conditions (9.5.1),

$$\sqrt{h} u_{N-L}(P_i) = \sqrt{h}\, f(P_i), \quad P_i \in \Gamma_{\text{out}}, \tag{9.5.3}$$

$$\sqrt{\bar{h}} u_{N-L}(\bar{P}_i^{\ell}) = \sqrt{\bar{h}}\ g_{\ell}(\bar{P}_i^{\ell}), \quad \bar{P}_i^{\ell} \in \Gamma_{\text{in}}^{\ell}, \quad \ell = 1, 2, 3, 4, \tag{9.5.4}$$

where $P_i = (\rho_i, \theta_i)$ and $\bar{P}_i^{\ell} = (\bar{\rho}_i^{\ell}, \bar{\theta}_i^{\ell})$.

Choose the complex solution $u(x, y) = \frac{1}{2}\{\exp(-\mathbf{i}kx) + \exp(-\mathbf{i}ky)\}$, where $\mathbf{i} = \sqrt{-1}$. Define the boundary and the domain errors by

$$\|\epsilon\|_{\infty,\partial S_{\text{holes}}} = \max_{\partial S_{\text{holes}}} |\epsilon|, \quad \|\epsilon\|_{\infty,S_{\text{holes}}} = \max_{S_{\text{holes}}} |\epsilon|, \quad \|\epsilon\|_{0,\partial S_{\text{holes}}} = \left\{ \int_{\partial S_{\text{holes}}} |\epsilon|^2 ds \right\}^{\frac{1}{2}},$$

where the complex errors $\epsilon = u - u_N$ and $|\epsilon|^2 = \epsilon\bar{\epsilon}$. Denote by N and M the numbers of the source and the collocation nodes, respectively. For simplicity, we fix 160 exterior collocation equations on Γ_{out} and 40 interior collocation equations on each $\Gamma_{\text{in}}^{\ell}$ with $\ell = 1, 2, 3, 4$. The total number of collocation equations is $M = 160 + 4 \times 40 = 320$. The results are given in Tables 9.1 and 9.2 for $k = 2$. From Table 9.1, we can see the asymptotes,

$$\|\epsilon\|_{\infty,\partial S_{\text{holes}}} = O(0.69^N), \quad \|\epsilon\|_{0,\partial S_{\text{holes}}} = O(0.69^N), \quad \|\epsilon\|_{\infty,S_{\text{holes}}} = O(0.68^N), \tag{9.5.5}$$

$$\text{Cond} = O(1.41^N), \quad \text{Cond\_eff} = O(1.41^N). \tag{9.5.6}$$

The exponential convergence/growth rates are observed.

For S_{holes} in Figure 9.1, there exist the ratios: $\frac{r_{\max}}{R} = \frac{5}{5+\sqrt{3}} = 0.74$ and $\frac{\bar{R}}{\bar{r}_0^{\text{in}}} = \frac{0.25}{0.5} = 0.5$. The dominant errors are given from Theorems 9.3.1 and 9.3.2 by

$$\max\{O(0.74^N),\ O(0.5^N)\} = O(0.74^N). \tag{9.5.7}$$

TAB. 9.1 – The errors and the condition numbers by the combined MFS in S_{holes} at $k = 2$ with $R = 5 + \sqrt{3}$ and $\bar{R} = 0.25$.

N	L	$\|\epsilon\|_{\infty,\partial S_{\text{holes}}}$	$\|\epsilon\|_{0,\partial S_{\text{holes}}}$	$\|\epsilon\|_{\infty,S_{\text{holes}}}$	Cond	Cond_eff	$\|\mathbf{x}\|$	$\sigma_{\min}$
20	10	2.40(−1)	4.86(−1)	1.90(−1)	5.66(3)	3.08(2)	3.27	8.40(−3)
30	15	1.75(−3)	5.27(−3)	1.25(−3)	1.37(5)	7.12(3)	2.79	3.47(−4)
40	20	4.71(−5)	1.22(−4)	3.20(−5)	6.39(6)	3.27(5)	2.46	7.44(−6)
50	25	1.14(−6)	3.03(−6)	6.46(−7)	1.49(8)	7.61(6)	2.19	3.20(−7)
60	30	7.44(−8)	1.42(−7)	2.75(−8)	6.76(9)	3.46(8)	2.00	7.04(−9)
70	35	2.91(−9)	5.17(−9)	8.45(−10)	1.56(11)	7.98(9)	1.85	3.05(−10)

The numerical errors in (9.5.5) are coincident with (9.5.7). Also for S_{holes} in Figure 9.1, there exist the ratios: $\sqrt{\frac{R}{r_{\min}}} = \sqrt{\frac{5+\sqrt{3}}{3}} = 1.498$ and $\sqrt{\frac{\bar{r}_0^{\text{in}}}{\bar{R}}} = \sqrt{\frac{0.5}{0.25}} = \sqrt{2} = 1.414$. The theoretical estimate for Cond is given from (9.4.60),

$$\text{Cond} = \max\{O(N \times 1.498^N),\ O(1.414^N)\} = O(N \times 1.498^N). \qquad (9.5.8)$$

TAB. 9.2 – The errors and the condition numbers by the combined MFS in S_{holes} at $k = 2$ with $\bar{R} = 0.25$, $N = 40$ and $L = 20$.

R	$\Vert\epsilon\Vert_{\infty,\partial S_{\text{out}}}$	$\Vert\epsilon\Vert_{\infty,\partial S_{\text{in}}}$	$\Vert\epsilon\Vert_{0,\partial S_{\text{holes}}}$	$\Vert\epsilon\Vert_{\infty,S_{\text{holes}}}$	Cond	Cond_eff	$\Vert\mathbf{x}\Vert$	$\sigma_{\min}$
5.50	6.32(−3)	3.30(−5)	1.43(−2)	3.36(−3)	6.39(6)	3.73(5)	2.15	7.44(−6)
$5+\sqrt{3}$	4.71(−5)	1.08(−6)	1.22(−4)	3.20(−5)	6.39(6)	3.27(5)	2.46	7.44(−6)
9.00	1.39(−6)	7.69(−8)	3.88(−6)	1.04(−6)	6.39(6)	2.49(5)	3.23	7.44(−6)
13.00	3.36(−7)	2.67(−8)	1.66(−6)	3.14(−7)	6.39(6)	1.88(5)	4.26	7.44(−6)
14.00	3.30(−7)	2.40(−8)	1.55(−6)	2.87(−7)	6.55(6)	1.84(5)	4.47	7.26(−6)
17.00	3.20(−7)	2.28(−8)	1.32(−6)	2.34(−7)	7.75(6)	1.94(5)	5.01	6.13(−6)
20.00	3.02(−7)	2.11(−8)	1.16(−6)	2.26(−7)	8.70(6)	1.99(5)	5.48	5.46(−6)

The numerical growth rates of Cond in (9.5.6) are also coincident with (9.5.8). From Table 9.2, the larger R is, the smaller the errors are. However, the condition numbers vary insignificantly as $R \leq 13$. When the interior pseudo-boundaries with radius $\bar{R}\,(=\bar{R}^{\ell}) = 0.25$ is given, the obvious effects of R on Cond can be found when $R \geq 14$. The reason is that the interior pseudo-boundaries play a dominant role in stability; see (9.5.6) and (9.5.8). For $k = 4$ the numerical results are given in Table 9.3. From Table 9.3, we can see the asymptotes,

$$\Vert\epsilon\Vert_{\infty,\partial S_{\text{holes}}} = O(0.67^N), \quad \Vert\epsilon\Vert_{0,\partial S_{\text{holes}}} = O(0.66^N), \quad \Vert\epsilon\Vert_{\infty,S_{\text{holes}}} = O(0.72^N), \quad (9.5.9)$$

$$\text{Cond} = O(1.62^N), \quad \text{Cond\_eff} = O(1.52^N), \quad \alpha = 1.16. \qquad (9.5.10)$$

For different k, the results are given in Table 9.4. When k increases, the errors enlarge and the Cond declines; but the enlarging rates of the errors are much higher than the declining rates of the Cond. Such conclusions are reasonable because the derivatives become larger (also see [254]).

TAB. 9.3 – The errors and the condition numbers for S_{holes} at $k = 4$ with $R = 9$ and $\bar{R} = 0.25$.

N	L	$\Vert\epsilon\Vert_{\infty,\partial S_{\text{holes}}}$	$\Vert\epsilon\Vert_{0,\partial S_{\text{holes}}}$	$\Vert\epsilon\Vert_{\infty,S_{\text{holes}}}$	Cond	Cond_eff	$\Vert\mathbf{x}\Vert$	$\sigma_{\min}$
20	10	6.16(−1)	1.90	1.29	3.45(3)	1.77(1)	2.88(1)	1.67(−2)
30	15	5.09(−1)	1.47	1.07	1.08(5)	2.78(2)	4.67(1)	5.33(−4)
40	20	9.02(−2)	2.70(−1)	7.74(−2)	5.78(6)	3.67(4)	1.64(1)	9.96(−6)
50	25	2.51(−3)	4.85(−3)	1.46(−3)	1.42(8)	2.58(6)	5.12	4.06(−7)
60	30	4.99(−6)	1.45(−5)	3.26(−6)	6.76(9)	1.16(8)	4.95	8.52(−9)
70	35	1.20(−8)	3.72(−8)	7.79(−9)	1.60(11)	2.64(9)	4.75	3.61(−10)
80	40	1.50(−11)	3.65(−11)	5.10(−9)	1.57(16)	1.68(12)	6.82(2)	3.69(−15)

TAB. 9.4 – The errors and the condition numbers for S_{holes} at different k with $R = 9$, $\bar{R} = 0.25$, $N = 70$ and $L = 35$.

k	$\Vert\epsilon\Vert_{\infty,\partial S_{\text{holes}}}$	$\Vert\epsilon\Vert_{0,\partial S_{\text{holes}}}$	$\Vert\epsilon\Vert_{\infty,S_{\text{holes}}}$	Cond	Cond_eff	$\Vert\mathbf{x}\Vert$	$\sigma_{\min}$
1	4.66(−15)	1.67(−14)	4.66(−15)	1.38(13)	1.46(12)	1.26	2.51(−12)
2	1.42(−14)	4.10(−14)	8.83(−15)	3.51(12)	1.36(11)	2.45	1.36(−11)
3	9.54(−12)	1.94(−11)	5.01(−12)	1.68(11)	4.23(9)	3.65	3.08(−10)
4	1.20(−8)	3.72(−8)	7.79(−9)	1.60(11)	2.64(9)	4.75	3.61(−10)
5	9.32(−6)	2.73(−5)	9.86(−6)	1.59(11)	2.08(9)	5.58	4.10(−10)
6	1.42(−3)	4.14(−3)	2.35(−3)	1.41(11)	2.43(8)	4.00(1)	4.79(−10)
8	3.59(−1)	7.56(−1)	7.76(−1)	1.08(11)	4.79(4)	1.32(5)	7.19(−10)
10	4.99(−1)	1.17	1.99	5.81(10)	4.14(3)	8.99(5)	1.24(−9)
15	5.84(−1)	2.08	1.29	7.47(9)	2.07(1)	2.13(7)	1.06(−8)

9.6 Concluding Remarks

To close this chapter, let us address its novelties.

1. For the Helmholtz equation in 2D bounded simply-connected domains, the complex MFS using the Hankel functions (9.2.4) is first studied. The error bounds involving degeneracy are derived in Theorem 9.2.1, and the optimal polynomial convergence rates can be achieved in Theorem 9.2.2. The MFS using Hankel functions is free from spurious eigenvalues for 2D bounded simply-connected domains; see Section 9.2.2.
2. In Section 9.3, the combined algorithms of the MFS are proposed for annular domains, where the Hankel functions and the modified Hankel functions in Chapter 8 are chosen for the exterior FS and the interior FS, respectively. The remarkable advantage is free from spurious eigenvalues. The error bounds are derived in Theorems 9.3.1 and 9.3.2, and the optimal polynomial convergence rates can also be achieved. Numerical experiments are carried out in this section to support the theoretical analysis made.
3. The bounds of Cond are derived in Theorem 9.4.1 for a ring domain to give

$$\text{Cond}(\mathbf{A}) \le C \max\left\{\frac{1}{\delta^\circ},\ N\left(\frac{R}{b}\right)^{\frac{N}{2}},\ \left(\frac{a}{\bar{R}}\right)^{\frac{N}{2}}\right\},$$

   where gap δ° is defined in (9.4.21). For not large N, the huge Cond (*i.e.*, the infinitesimal $\sigma_{\min}$) indicates an exact eigenvalue occurring. Note that the MFS-QR in Antunes [8, 9] is irrelevant to the stability of the MFS (see Remark 9.4.1). Hence Theorem 9.4.1 is important to the MFS for the Helmholtz equation and the Dirichlet–Laplace eigenvalue problems in bounded multiply-connected domains.
4. In summary, the error and stability analysis in this chapter is new and essential. This chapter and Chapters 7 and 8 provide a solid theoretical basis for the MFS for the Helmholtz equation in exterior and interior problems in 2D.

Chapter 10

Biharmonic Equations

The error and stability analysis of the method of fundamental solutions (MFS) is explored for biharmonic equations in this chapter. The bounds of errors are derived for the fundamental solutions (FS) using $r^2\ln r$ in the bounded simply-connected domains, and polynomial convergence rates are obtained for certain smooth solutions. The bounds of condition numbers are also derived to show the exponential growth rates for disk domains. Numerical experiments are carried out to support the analysis made. The materials of this chapter are adapted from [73, 166].

10.1 Introduction

Consider the biharmonic equation with the clamped boundary conditions,

$$\Delta^2 u = 0, \text{ in } S, \tag{10.1.1}$$

$$u = f, \text{ on } \Gamma, \tag{10.1.2}$$

$$u_\nu = \frac{\partial u}{\partial \nu} = g, \text{ on } \Gamma, \tag{10.1.3}$$

where $\Delta = \frac{\partial^2}{\partial x^2} + \frac{\partial^2}{\partial y^2}$, S is the bounded simply-connected domain, Γ its smooth boundary, u_ν the exterior normal derivative to Γ, and f and g are the given functions with certain smoothness. Denote $r = |\overline{PQ}|$, $P = \rho e^{\mathbf{i}\theta}$, $Q = Re^{\mathbf{i}\phi}$, and $\mathbf{i} = \sqrt{-1}$. The FS of biharmonic equations in 2D are well-known as

$$\Phi(\rho, \theta) = r^2 \ln r, \quad r = |\overline{PQ}| = \sqrt{R^2 + \rho^2 - 2R\rho \cos(\theta - \phi)}, \tag{10.1.4}$$

where Q is the source node outside S. Denote two kinds of FS at $Q_j = Re^{\mathbf{i}\phi_j}$ by

$$\Phi_j(\rho, \theta) = r_j^2 \ln r_j, \quad \Psi_j(\rho, \theta) = \ln r_j,$$

where $r_j = |\overline{PQ_j}| = \sqrt{R^2 + \rho^2 - 2R\rho \cos(\theta - \phi_j)}$. Hence we choose the linear combination,

DOI: 10.1051/978-2-7598-3171-5.c010
© Science Press, EDP Sciences, 2023

$$u_N = \sum_{j=1}^{N} \{ c_j \Phi_j(\rho, \theta) + d_j \Psi_j(\rho, \theta) \}, \tag{10.1.5}$$

where $\{c_j\}$ and $\{d_j\}$ are the unknown coefficients to be determined by the boundary conditions (10.1.2) and (10.1.3). Denote by V_N the set of (10.1.5). We may solicit the Trefftz method (TM) in [169]: to seek the numerical solution u_N by

$$I(u_N) = \min_{v \in V_N} I(v), \quad I(v) = \int_\Gamma (v - f)^2 + w^2 \int_\Gamma (v_\nu - g)^2, \tag{10.1.6}$$

where w is the weight, which may be chosen as $w = \frac{1}{N}$ (see [169]).

Almansi's FS for biharmonic equations are obtained directly from the general particular solutions $u(\rho, \theta) = \rho^2 v + z$, where v and z are harmonic functions, to give $\Phi^A(\rho, \theta) = \rho^2 \ln r$. We may choose the other linear combination

$$u_N^A = \sum_{j=1}^{N} \{ c_j \Phi_j^A(\rho, \theta) + d_j \Psi_j(\rho, \theta) \}, \tag{10.1.7}$$

to replace (10.1.5), where $\Phi_j^A(\rho, \theta) = \rho^2 \ln r_j$, and the coefficients c_j and d_j are also obtained from (10.1.6). The equation (10.1.6) with (10.1.7) is called the MFS using Almansi's FS: $\rho^2 \ln r$. For the biharmonic equation, the MFS using $\rho^2 \ln r$ was introduced in Karageorghis and Fairweather [80, 117, 118]. The analysis of the MFS for Laplace's equations is given in Part I. A preliminary analysis of error and stability was given in [166] for the MFS using $\rho^2 \ln r$. Note that the analysis for the MFS using $r^2 \ln r$ in this chapter is more important and challenging.

Let us summarize the important theoretical results in this chapter. The error and stability analysis is explored for biharmonic equations by the MFS using $r^2 \ln r$. The error bounds are derived as

$$\|u - u_N\|_H = O\left(\frac{1}{N^{p-\frac{1}{2}}} \right) \|u\|_{p,S},$$

to show the polynomial convergence rates, where the norm $\|v\|_H = \{ \int_\Gamma (v^2 + w^2 v_\nu^2) \}^{\frac{1}{2}}$. This chapter is the advanced study of [166], where a preliminary analysis was made for the MFS using simple FS: $\rho^2 \ln r$. For circular domains, the condition number grows exponentially, as

$$\text{Cond} \asymp O\left(N^3 \left(\frac{R}{\rho} \right)^{\frac{N}{2}} \right).$$

For the bounded simply-connected domains and under other boundary conditions, similar bounds of condition number can also be derived by following [163] and Chapter 3.

This chapter is organized as follows. In Sections 10.2 and 10.3, preliminary lemmas and the main theorems are derived for error bounds, respectively. In Section 10.4, the bounds of condition numbers are derived for circular domains. In the last section, numerical experiments are reported to illustrate our results.

10.2 Preliminary Lemmas

The general biharmonic solutions are given by $u(\rho,\theta)=\rho^2 v+w$, where v and w are harmonic functions,

$$u(\rho,\theta)=\rho^2\left\{\frac{a_0^*}{2}+\sum_{i=1}^{\infty}\rho^i(a_i^*\cos i\theta+b_i^*\sin i\theta)\right\}+\frac{a_0}{2}+\sum_{i=1}^{\infty}\rho^i(a_i\ \cos i\theta+b_i\ \sin i\theta),$$

where a_i^*, b_i^*, a_i and b_i are the exact coefficients. Denote two kinds of harmonic polynomials of degree n,

$$P_n^H(\rho,\theta)=\frac{a_0^*}{2}+\sum_{i=1}^{n}\rho^i(a_i^*\cos i\theta+b_i^*\sin i\theta),\ P_n^h(\rho,\theta)=\frac{a_0}{2}+\sum_{i=1}^{n}\rho^i(a_i\ \cos i\theta+b_i\ \sin i\theta),$$

and their residuals,

$$R_n^H(\rho,\theta)=\sum_{i=n+1}^{\infty}\rho^i(a_i^*\ \cos i\theta+b_i^*\ \sin i\theta), R_n^h(\rho,\theta)=\sum_{i=n+1}^{\infty}\rho^i(a_i\ \cos i\theta+b_i\ \sin i\theta).$$

Then we have

$$u_B(\rho,\theta)=P_n^B+R_n^B, \tag{10.2.1}$$

where

$$\begin{aligned}P_n^B&=P_n^B(\rho,\theta)=\rho^2P_n^H(\rho,\theta)+P_n^h(\rho,\theta),\\ R_n^B&=R_n^B(\rho,\theta)=\rho^2R_n^H(\rho,\theta)+R_n^h(\rho,\theta).\end{aligned} \tag{10.2.2}$$

Suppose that the solution satisfies $u\in\mathbf{H}^\sigma(S)$ with $\sigma\geq\frac{5}{2}$. Then there exist the bounds of the residuals in [33],

$$\begin{aligned}\|R_n^B(\rho,\theta)\|_{k,S}&\leq C\frac{1}{n^{\sigma-k}}\|u\|_{\sigma,S},\\ \|R_n^H(\rho,\theta)\|_{k,S},\ \|R_n^h(\rho,\theta)\|_{k,S}&\leq C\frac{1}{n^{\sigma-k}}\|u\|_{\sigma,S},\end{aligned} \tag{10.2.3}$$

where $\|u\|_{\sigma,S}$ are the Sobolev norms. We give the addition theorem (*i.e.*, the series expansions).

Lemma 10.2.1 (Addition Theorem). *For $\rho<R$, there exists the series expansion for the FS of biharmonic equation in (10.1.4),*

$$\begin{aligned}\Phi(\rho,\theta)=&R^2\ln R+\rho^2(1+\ln R)+R^2\sum_{m=1}^{\infty}\frac{\beta_m}{m}\left(\frac{\rho}{R}\right)^m\cos m(\theta-\phi)\\ &-\rho^2\sum_{m=1}^{\infty}\frac{1}{m(m+1)}\left(\frac{\rho}{R}\right)^m\cos m(\theta-\phi),\end{aligned} \tag{10.2.4}$$

where $\beta_1=-(1+2\ \ln R)$ and $\beta_m=\frac{1}{m-1}(m\geq2)$.

Proof. From addition theorem for $\ln r$ in Lemma I.3 in Part I, there exists the expansion of the FS of Laplace's equation,

$$\ln r = \ln R - \sum_{n=1}^{\infty} \frac{1}{n}\left(\frac{\rho}{R}\right)^n \cos n(\theta-\phi), \quad \rho < R. \tag{10.2.5}$$

For biharmonic equations, the traditional FS using $r^2 \ln r$ is expressed by

$$\Phi(\rho,\theta) = (R^2+\rho^2-2R\rho\,\cos(\theta-\phi))\left\{\ln R - \sum_{n=1}^{\infty}\frac{1}{n}\left(\frac{\rho}{R}\right)^n \cos n(\theta-\phi)\right\}. \tag{10.2.6}$$

From the trigonometric formula, $2\cos\theta\,\cos n\theta = \cos(n+1)\theta + \cos(n-1)\theta$, we have

$$\begin{aligned}
&2\cos(\theta-\phi)\sum_{n=1}^{\infty}\frac{1}{n}\left(\frac{\rho}{R}\right)^n \cos n(\theta-\phi)\\
&= \sum_{n=1}^{\infty}\frac{1}{n}\left(\frac{\rho}{R}\right)^n (\cos(n+1)(\theta-\phi)+\cos(n-1)(\theta-\phi)) \qquad (10.2.7)\\
&= \sum_{m=2}^{\infty}\frac{1}{m-1}\left(\frac{\rho}{R}\right)^{m-1}\cos m(\theta-\phi) + \sum_{m=0}^{\infty}\frac{1}{m+1}\left(\frac{\rho}{R}\right)^{m+1}\cos m(\theta-\phi),
\end{aligned}$$

where we have used transformation $n \pm 1 = m$. Hence we obtain from (10.2.6)

$$\begin{aligned}
\Phi(\rho,\theta) &= (R^2+\rho^2-2R\rho\,\cos(\theta-\phi))\left\{\ln R - \sum_{n=1}^{\infty}\frac{1}{n}\left(\frac{\rho}{R}\right)^n \cos n(\theta-\phi)\right\}\\
&= (R^2+\rho^2-2R\rho\,\cos(\theta-\phi))\ln R - (R^2+\rho^2)\sum_{n=1}^{\infty}\frac{1}{n}\left(\frac{\rho}{R}\right)^n \cos n(\theta-\phi)\\
&\quad + 2R\rho\,\cos(\theta-\phi)\sum_{n=1}^{\infty}\frac{1}{n}\left(\frac{\rho}{R}\right)^n \cos n(\theta-\phi)\\
&= [R^2+\rho^2-2R\rho\,\cos(\theta-\phi)]\ln R\\
&\quad + R^2\sum_{m=2}^{\infty}\left(\frac{1}{m-1}-\frac{1}{m}\right)\left(\frac{\rho}{R}\right)^m \cos m(\theta-\phi) - R^2\left(\frac{\rho}{R}\right)\cos(\theta-\phi)\\
&\quad + \rho^2\sum_{m=1}^{\infty}\left(\frac{1}{m+1}-\frac{1}{m}\right)\left(\frac{\rho}{R}\right)^m \cos m(\theta-\phi) + R\rho\left(\frac{\rho}{R}\right)\\
&= R^2\ln R + \rho^2(1+\ln R) + R^2\sum_{m=1}^{\infty}\frac{\beta_m}{m}\left(\frac{\rho}{R}\right)^m \cos m(\theta-\phi)\\
&\quad -\rho^2\sum_{m=1}^{\infty}\frac{1}{m(m+1)}\left(\frac{\rho}{R}\right)^m \cos m(\theta-\phi).
\end{aligned}$$

This is the desired result (10.2.4). ■

Lemma 10.2.2. *For $R > \rho$ and $R \neq \frac{1}{e}$, there exist the integration formulas,*

$$\rho^2 = \frac{1}{2\pi(1+\ln R)}\left\{\int_0^{2\pi} r^2 \ln r\, d\phi - R^2\int_0^{2\pi}\ln r\, d\phi\right\}, \tag{10.2.8}$$

$$\begin{aligned}\rho^{m+2}\begin{pmatrix}\cos m\theta\\ \sin m\theta\end{pmatrix} &= -\frac{R^m(m(m+1))}{\pi}\left\{\int_0^{2\pi} r^2\ln r\begin{pmatrix}\cos m\phi\\ \sin m\phi\end{pmatrix}d\phi\right.\\ &\qquad \left.+\beta_m R^2\int_0^{2\pi}\ln r\begin{pmatrix}\cos m\phi\\ \sin m\phi\end{pmatrix}d\phi\right\},\quad m\geq 1,\end{aligned}\tag{10.2.9}$$

where $r=|\overline{PQ}|$, $P=\rho e^{\mathbf{i}\theta}$, $Q=Re^{\mathbf{i}\phi}$ *and* $\mathbf{i}=\sqrt{-1}$.

Proof. By using the orthogonality of trigonometric functions, we have from (10.2.4)

$$\begin{aligned}\int_0^{2\pi} r^2\ln r d\phi &= \int_0^{2\pi}\Phi(\rho,\theta)d\phi = 2\pi(R^2\ln R+\rho^2(1+\ln R))\\ &= R^2\int_0^{2\pi}\ln r d\phi+2\pi\rho^2(1+\ln R),\end{aligned}\tag{10.2.10}$$

where we have used the equality: $2\pi\ln R=\int_0^{2\pi}\ln r d\phi$ from (10.2.5). This gives the first result (10.2.8).

Next, from (10.2.5) there exists the equality for $m\geq 1$,

$$\int_0^{2\pi}\ln r\begin{pmatrix}\cos m\phi\\ \sin m\phi\end{pmatrix}d\phi=-\frac{\pi}{m}\left(\frac{\rho}{R}\right)^m\begin{pmatrix}\cos m\theta\\ \sin m\theta\end{pmatrix}.\tag{10.2.11}$$

From (10.2.4) and (10.2.11) for $m\geq 1$, we have

$$\begin{aligned}&\int_0^{2\pi} r^2\ln r\begin{pmatrix}\cos m\phi\\ \sin m\phi\end{pmatrix}d\phi\\ &=\frac{\beta_m\pi R^2}{m}\left(\frac{\rho}{R}\right)^m\begin{pmatrix}\cos m\theta\\ \sin m\theta\end{pmatrix}-\pi\rho^2\frac{1}{m(m+1)}\left(\frac{\rho}{R}\right)^m\begin{pmatrix}\cos m\theta\\ \sin m\theta\end{pmatrix}\\ &=-\beta_m R^2\int_0^{2\pi}\ln r\begin{pmatrix}\cos m\phi\\ \sin m\phi\end{pmatrix}d\phi-\pi\rho^2\frac{1}{m(m+1)}\left(\frac{\rho}{R}\right)^m\begin{pmatrix}\cos m\theta\\ \sin m\theta\end{pmatrix},\end{aligned}$$

to give

$$\begin{aligned}\rho^{m+2}\begin{pmatrix}\cos m\theta\\ \sin m\theta\end{pmatrix} &= -\frac{R^m m(m+1)}{\pi}\left\{\int_0^{2\pi} r^2\ln r\begin{pmatrix}\cos m\phi\\ \sin m\phi\end{pmatrix}d\phi\right.\\ &\qquad \left.+\beta_m R^2\int_0^{2\pi}\ln r\begin{pmatrix}\cos m\phi\\ \sin m\phi\end{pmatrix}d\phi\right\}.\end{aligned}$$

This is the second result (10.2.9) and completes the proof of Lemma 10.2.2. ■

Based on Lemma 10.2.2, we seek (10.1.5) with some special coefficients $\bar{c}_i$ and $\bar{d}_i$, to approximate the major term $\rho^2P_n^H$ of u in (10.2.1). Choose the source nodes Q_j located uniformly on the circle $\{(\rho,\theta)|\rho=R,0\leq\theta\leq 2\pi\}$, where $Q_j=(R\cos(jh),R\sin(jh))$ with $h=\frac{2\pi}{N}$. By the trapezoidal rule, we have the approximation from (10.2.8),

$$\begin{aligned}\rho^2 &\approx \frac{h}{2\pi(1+\ln R)}\left\{\sum_{j=1}^{N} r_j^2 \ln r_j - R^2\sum_{j=1}^{N}\ln r_j\right\}\\ &= \frac{h}{2\pi(1+\ln R)}\left\{\sum_{j=1}^{N}\mathbf{\Phi}_j(\rho,\theta) - R^2\sum_{j=1}^{N}\mathbf{\Psi}_j(\rho,\theta)\right\},\end{aligned} \tag{10.2.12}$$

where $\mathbf{\Phi}_j(\rho,\theta) = r_j^2\ln r_j$, $\mathbf{\Psi}_j(\rho,\theta) = \ln r_j$, $r_j = |\overline{PQ_j}|$ and $P = (\rho\cos\theta, \rho\sin\theta)$. Similarly, we have from (10.2.9)

$$\begin{aligned}\rho^{m+2}\begin{pmatrix}\cos(m\theta)\\ \sin(m\theta)\end{pmatrix} \approx -\frac{R^m m(m+1)}{\pi} h\Bigg\{&\sum_{j=1}^{N}\mathbf{\Phi}_j(\rho,\theta)\begin{pmatrix}\cos(mjh)\\ \sin(mjh)\end{pmatrix}\\ &+\beta_m R^2\sum_{j=1}^{N}\mathbf{\Psi}_j(\rho,\theta)\begin{pmatrix}\cos(mjh)\\ \sin(mjh)\end{pmatrix}\Bigg\}, \quad m\ge 1.\end{aligned} \tag{10.2.13}$$

From (10.2.2), (10.2.12) and (10.2.13), we have

$$\begin{aligned}\rho^2 P_n^H(\rho,\theta) &= \frac{a_0^*}{2}\rho^2 + \sum_{m=1}^{n}\rho^{m+2}\{a_m^*\cos(m\theta) + b_m^*\sin(m\theta)\}\\ &\approx \sum_{k=1}^{N}\{c_k^*\mathbf{\Phi}_k(\rho,\theta) + d_k^*\mathbf{\Psi}_k(\rho,\theta)\},\end{aligned} \tag{10.2.14}$$

where the coefficients are given by

$$c_k^* = \frac{h}{4\pi(1+\ln R)}a_0^* - \frac{h}{\pi}\sum_{m=1}^{n} R^m m(m+1)\{a_m^*\cos(mkh) + b_m^*\sin(mkh)\}, \tag{10.2.15}$$

$$\begin{aligned}d_k^* &= -\frac{R^2 h}{4\pi(1+\ln R)}a_0^*\\ &\quad + \frac{R^2 h}{\pi}\sum_{m=1}^{n}\beta_m R^m m(m+1)\{a_m^*\cos(mhk) + b_m^*\sin(mkh)\}, \quad R \neq \frac{1}{e}.\end{aligned} \tag{10.2.16}$$

From Chapter 2 we find an approximation,

$$P_n^h(\rho,\theta) = \frac{a_0}{2} + \sum_{m=1}^{n}\rho^m\{a_m\cos(m\theta) + b_m\sin(m\theta)\} \approx \sum_{k=1}^{N} d_k^h\mathbf{\Psi}_k(r,\theta), \tag{10.2.17}$$

where

$$d_k^h = \frac{h}{4\pi\ln R}a_0 - \frac{h}{\pi}\sum_{m=1}^{n} mR^m\{a_m\cos(mkh) + b_m\sin(mkh)\}, \quad R\neq 1. \tag{10.2.18}$$

Hence from (10.2.14)–(10.2.18), when $R \neq \frac{1}{e}$ and $R \neq 1$, we have found an approximation for P_N^B in (10.2.2),

$$P_n^B \approx \mathbf{\Sigma}_N(P_n^B;\rho,\theta) := \sum_{i=1}^N c_i^* \mathbf{\Phi}_i(\rho,\theta) + \sum_{i=1}^N \bar{d}_i \mathbf{\Psi}_i(\rho,\theta), \tag{10.2.19}$$

where $\bar{d}_i = d_k^h + d_k^*$, and d_k^h and d_k^* are the coefficients in (10.2.18) and (10.2.16), respectively.

Based on Basic Lemmas A and B in Part I, the errors of the trapezoidal rule can be found for four terms: $\rho^{m+2}\cos(m\theta)$, $\rho^{m+2}\sin(m\theta)$, $\rho^m\cos(m\theta)$ $(m \geq 1)$ and $\rho^m \sin(m\theta)$ $(m \geq 1)$. Since the errors of harmonic polynomials $\rho^m\cos(m\theta)$ and $\rho^m \sin(\mathrm{m}\theta)$ are given from Chapter 2, we derive the bounds of the following errors,

$$\begin{aligned} &\rho^2 P_n^H(\rho,\theta) - \mathbf{\Sigma}_N(\rho^2 P_n^H;\rho,\theta) \\ &= \sum_{i=1}^n a_i^*\{\rho^{i+2}\cos i\theta - \mathbf{\Sigma}_N(\rho^{i+2}\cos i\theta;\rho,\theta)\} \\ &\quad + \sum_{i=1}^n b_i^*\{\rho^{i+2}\sin i\theta - \mathbf{\Sigma}_N(\rho^{i+2}\sin i\theta;\rho,\theta)\}. \end{aligned} \tag{10.2.20}$$

We will derive the error bounds only for the first term in (10.2.20) because those for the second term are the same.

From (10.2.13) we have

$$\begin{aligned} &\mathbf{\Sigma}_N(\rho_m^{m+2}\cos m\theta;\rho,\theta) \\ &= -\frac{R^m m(m+1)h}{\pi}\left\{\sum_{j=1}^N \cos(mjh)\mathbf{\Phi}_j(\rho,\theta) - R^2\sum_{j=1}^N \beta_m \cos(mjh)\mathbf{\Psi}_j(\rho,\theta)\right\}, \quad m \geq 1. \end{aligned} \tag{10.2.21}$$

Denote the errors

$$E(\rho^{m+2}\cos(m\theta)) = \rho^{m+2}\cos(m\theta) - \mathbf{\Sigma}_N(\rho^{m+2}\cos(m\theta);\rho,\theta), \tag{10.2.22}$$

where $\mathbf{\Sigma}_N$ is also the discrete approximation from the trapezoidal rule. Below, we estimate the bounds of (10.2.22) by the Fourier series. For the circle $\mathbf{\Gamma}_\rho = \{(r,\theta)|r = \rho, 0 \leq \theta \leq 2\pi\}$, we have

$$E(\rho^{m+2}\cos(m\theta)) = \frac{a_{0,m}}{2} + \sum_{k=1}^\infty \{a_{k,m}\cos(k\theta) + b_{k,m}\sin(k\theta)\}, \tag{10.2.23}$$

where

$$a_{k,m} = \frac{1}{\pi}\int_0^{2\pi} E(\rho^{m+2}\cos(m\theta))\cos(k\theta)d\theta, \quad k = 0,\, 1, \ldots, \tag{10.2.24}$$

$$b_{k,m} = \frac{1}{\pi}\int_0^{2\pi} E(\rho^{m+2}\cos(m\theta))\sin(k\theta)d\theta, \quad k = 1,\, 2, \ldots. \tag{10.2.25}$$

From Basic Lemma A in Part I, we have

$$b_{k,m} = 0, \quad \forall k, m. \tag{10.2.26}$$

To estimate the bounds of $a_{k,m}$, we have the following lemma.

Lemma 10.2.3. *For the Fourier expansion (10.2.23), the coefficients are given by*

$$a_{k,m}\ (m \geq 1) = \begin{cases} R^m m(m+1)\left(\frac{\rho}{R}\right)^k \left(\frac{R^2}{k}(\beta_m + \beta_k) - \frac{\rho^2}{k(k+1)}\right), & \text{if } k = \pm m + vN, \\ 0, & \text{if } k \neq \pm m + vN, \end{cases} \tag{10.2.27}$$

where $v = 1,\ 2, \ldots,\ \ \beta_1 = -(1 + 2\ln R),\ \ \beta_m = \frac{1}{m-1}\ (m \geq 2)$, *and*

$$a_{k,0} = \begin{cases} \frac{\left(\frac{\rho}{R}\right)^k}{(1+\ln R)}\left(\frac{R^2}{k}(1+\beta_k) - \frac{\rho^2}{k(k+1)}\right), & \text{if } k = vN, v = 1,\ 2, \ldots, \\ 0, & \text{otherwise.} \end{cases} \tag{10.2.28}$$

Proof. First, for $m \geq 1$ we have from (10.2.13)

$$\begin{aligned} a_{k,m} &= \frac{1}{\pi}\int_0^{2\pi} \rho^{m+2} \cos(m\theta) \cos(k\theta)\, d\theta - \frac{1}{\pi}\Big\{ - \frac{R^m m(m+1)h}{\pi} \\ &\quad \times \Big[\sum_{j=1}^{N} \int_0^{2\pi} \cos(jmh)\boldsymbol{\Phi}_j(\rho,\theta) \cos(k\theta)\, d\theta \\ &\quad - R^2 \sum_{j=1}^{N} \int_0^{2\pi} \beta_m \cos(jmh)\boldsymbol{\Psi}_j(\rho,\theta) \cos(k\theta)\, d\theta\Big]\Big\} \\ &:= T_1 - T_2. \end{aligned} \tag{10.2.29}$$

In (10.2.29) the second term T_2 is just an approximation of the first term

$$T_1 = \frac{1}{\pi}\int_0^{2\pi} \rho^{m+2} \cos(m\theta) \cos(k\theta)\, d\theta,$$

by the trapezoidal rule. We may express $T_1\,(m \geq 1)$ as

$$\begin{aligned} T_1 &= \frac{1}{\pi^2} R^m m(m+1) \int_0^{2\pi} \Big\{ \int_0^{2\pi} r^2 \ln r \cos(k\theta)\, d\theta \\ &\quad + \beta_m R^2 \int_0^{2\pi} \ln r \cos(k\theta)\, d\theta \Big\} \cos(m\phi)\, d\phi \\ &= \frac{1}{\pi} R^m m(m+1) \left(\frac{\rho}{R}\right)^k \Big\{ \beta_k \frac{R^2}{k} - \frac{\rho^2}{k(k+1)} + \beta_m \frac{R^2}{k} \Big\} \int_0^{2\pi} \cos(m\phi) \cos(k\phi)\, d\phi, \end{aligned} \tag{10.2.30}$$

where we have used (10.2.4) and (10.2.5). Hence, from Basic Lemma B we obtain

$$\begin{aligned}
a_{k,m} &= T_1 - T_2\\
&= \frac{1}{\pi} R^m m(m+1)\left(\frac{\rho}{R}\right)^k \left\{\frac{R^2}{k}(\beta_k+\beta_m) - \frac{\rho^2}{k(k+1)}\right\}\triangle_N(\cos(m\phi)\cos(k\phi)),
\end{aligned}$$

where $\triangle_N(g) = T_N(g) - \int_0^{2\pi} g(x)\,dx$ and T_N is the trapezoidal rule. Then we have for $k = \pm m + \nu N$

$$a_{k,m} = R^m m(m+1)\left(\frac{\rho}{R}\right)^k \left\{\frac{R^2}{k}(\beta_m+\beta_k) - \frac{\rho^2}{k(k+1)}\right\},$$

otherwise $a_{k,m} = 0$. This is the result (10.2.27).

Next, for $m = 0$ there exists the equality from (10.2.8):

$$\begin{aligned}
a_{k,0} =& \frac{1}{\pi}\int_0^{2\pi} \rho^2 \cos(k\theta)\,d\theta - \frac{h}{2\pi(1+\ln R)}\int_0^{2\pi}\left\{\sum_{i=1}^N \Phi(\rho,\theta) - R^2\sum_{i=1}^N \Psi_i(\rho,\theta)\right\}\cos(k\theta)\,d\theta\\
:=& T_1 - T_2. \qquad (10.2.31)
\end{aligned}$$

For T_1 we have, similarly from (10.2.5) and (10.2.4),

$$\begin{aligned}
T_1 &= \frac{1}{\pi}\int_0^{2\pi} \rho^2 \cos(k\theta)\,d\theta\\
&= \frac{1}{2\pi^2(1+\ln R)}\int_0^{2\pi}\left\{\int_0^{2\pi} r^2 \ln r \cos(k\theta)\,d\theta - R^2\int_0^{2\pi} \ln r \cos(k\theta)\,d\theta\right\}d\phi\\
&= \frac{\left(\frac{\rho}{R}\right)^k}{2\pi(1+\ln R)}\int_0^{2\pi}\left\{\left(\frac{R^2}{k}\beta_k - \frac{\rho^2}{k(k+1)}\right) + R^2\frac{1}{k}\right\}\cos(k\phi)\,d\phi.
\end{aligned}$$

Hence we obtain

$$a_{k,0} = \frac{\left(\frac{\rho}{R}\right)^k}{2\pi(1+\ln R)}\left\{\frac{R^2}{k}(1+\beta_k) - \frac{\rho^2}{k(1+k)}\right\}\triangle_N(\cos(k\phi)),$$

and from Basic Lemma A for $k \geq 1$,

$$\begin{cases}
a_{k,0} = \frac{1}{(1+\ln R)}\left(\frac{\rho}{R}\right)^k\left(\frac{R^2}{k}(1+\beta_k) - \frac{\rho^2}{k(k+1)}\right), & \text{if } k = \nu N,\ \nu = 1, 2, \ldots,\\
a_{k,0} = 0, & \text{otherwise.}
\end{cases} \qquad (10.2.32)$$

For $m = 0$ and $k = 0$ we have

$$a_{0,0} = \frac{1}{2\pi}\left\{\int_0^{2\pi} \rho^2\,d\theta - \frac{h}{2\pi(1+\ln R)}\int_0^{2\pi}\left\{\sum_{i=1}^N \Phi_i(\rho,\theta) - R^2\sum_{i=1}^N \Psi_i(\rho,\theta)\right\}d\theta\right\},$$

to give

$$a_{0,0} = \rho^2 \triangle_N(1) = 0. \tag{10.2.33}$$

Combining (10.2.32) and (10.2.33) gives the third desired results (10.2.28). This completes the proof of Lemma 10.2.3. ■

Lemma 10.2.4. *Let $N > 2n$ and $n \geq m$. The Fourier coefficients in (10.2.27) and (10.2.28) have the bounds,*

$$|a_{k,m}| \leq CR^{m-k}\rho^k, \tag{10.2.34}$$

where $k = \pm m + vN$, $v = 1, 2, \ldots,$ and C is a constant independent of N.

Proof. From Lemma 10.2.3, we have

$$|a_{k,m}| \leq CR^{m-k}\rho^k \left\{ \frac{m}{k}(m+1)(|\beta_m| + |\beta_k|) + \frac{m}{k}\frac{(m+1)}{(k+1)} \right\}, \quad m \geq 1. \tag{10.2.35}$$

Firstly, let $k = vN - m$ for $v \geq 1$. Since $k = vN - m \geq N - m \geq m$, it is easy to see that the constants in the brackets of (10.2.35) are bounded by noting $\beta_1 = -(1 + 2\ln R)$ and $\beta_m = \frac{1}{m-1}(m \geq 2)$. Detailed proof is given in [152]. Secondly, let $k = vN + m$. Since $vN + m > vN - m$, the equation (10.2.34) also holds. This completes the proof of Lemma 10.2.4. ■

10.3 Error Bounds

We are ready to give the main theorems.

Theorem 10.3.1. *Let $u \in C(S)$ hold. For large N there exists the bound for $q \geq 0$,*

$$\begin{aligned} &\|\rho^2 P_n^H(\rho,\theta) - \Sigma_N(\rho^2 P_n^H(\rho,\theta);\rho,\theta)\|^2_{q,\Gamma_\rho} \\ &\leq CN^q \left(\frac{R}{r_{\max}}\right)^{2n-N} \left(\frac{r_{\max}}{r_{\min}}\right)^n \|\rho^2 P_n^H(r,\theta)\|_{0,\Gamma}, \end{aligned} \tag{10.3.1}$$

where $r_{\max} = \max_S r$, $r_{\min}$ is the maximal radius of disk S_ρ $(\subseteq S)$, and C is a constant independent of N.

Proof. From (10.2.23), (10.2.26) and Lemmas 10.2.3 and 10.2.4, we have for large N

$$\begin{aligned} &\|E(\rho^{m+2}\cos(m\theta))\|^2_{q,\Gamma_\rho} \leq C\sum_{k=1}^{\infty} a^2_{k,m}k^{2q} \\ &\leq C \sum_{k=\pm m + vN}^{\infty} R^{2(m-k)}\rho^{2k}k^{2q} \leq CN^{2q}\left(\frac{R}{\rho}\right)^{2(m-N)} R^{2m}. \end{aligned} \tag{10.3.2}$$

Similarly, we have

$$\|E(\rho^{m+2}\sin(m\theta))\|^2_{q,\Gamma_\rho} \le CN^{2q}\left(\frac{R}{\rho}\right)^{2(m-N)} R^{2m} = \|E(\rho^{m+2}\cos(m\theta))\|^2_{q,\Gamma_\rho}, \quad m \ge 1.$$

For $0 < \rho_0 \le \tilde{\rho} \le \rho$, from (10.2.20) and the Schwarz inequality,

$$\begin{aligned} &\|\rho^2 P_n^H(\rho,\theta) - \Sigma_N(\rho^2 P_n^H(\rho,\theta);\rho,\theta)\|^2_{q,\Gamma_\rho} \qquad (10.3.3)\\ &= \left\| \frac{a_0^*}{2}E(\rho^2) + \sum_{m=1}^{n}\left\{a_m^* E(\rho^{m+2}\cos(m\theta)) + b_m^* E(\rho^{m+2}\sin(m\theta))\right\}\right\|^2_{q,\Gamma_\rho}\\ &\le C\tilde{\rho}^4\left\{\left(\frac{a_0^*}{2}\right)^2 + \sum_{m=1}^{\infty}\tilde{\rho}^{2m}\left[(a_m^*)^2 + (b_m^*)^2\right]\right\} \times \sum_{m=0}^{n}\frac{1}{\tilde{\rho}^{2m+2}}\left\|E(\rho^{m+2}\cos(m\theta))\right\|^2_{q,\Gamma_\rho}. \end{aligned}$$

From (10.2.14) and the continuity extension in Remark 2.3.1 in Chapter 2, we have

$$\tilde{\rho}^4\left\{\left(\frac{a_0^*}{2}\right)^2 + \sum_{m=1}^{\infty}\tilde{\rho}^{2m}\left[(a_m^*)^2 + (b_m^*)^2\right]\right\} = \|\rho^2 P_n^H(\rho,\theta)\|^2_{0,\Gamma_{\tilde{\rho}}} \le C\|\rho^2 P_n^H(\rho,\theta)\|^2_{0,\Gamma}, \tag{10.3.4}$$

and from (10.3.2)

$$\begin{aligned} &\sum_{m=0}^{n}\frac{1}{\tilde{\rho}^{2m+2}}\|E(\rho^{m+2}\cos(m\theta))\|^2_{q,\Gamma_\rho} \le C\sum_{m=1}^{n} N^{2q}\left(\frac{R}{\rho}\right)^{4(m-N)}\left(\frac{\rho}{\tilde{\rho}}\right)^{2m}\\ &\le CN^{2q}\left(\frac{R}{\rho}\right)^{4n-2N}\left(\frac{\rho}{\tilde{\rho}}\right)^{2n} \le CN^{2q}\left(\frac{R}{r_{\max}}\right)^{4n-2N}\left(\frac{r_{\max}}{r_{\min}}\right)^{2n}. \end{aligned} \tag{10.3.5}$$

The desired result (10.3.1) follows from (10.3.3)–(10.3.5), and this completes the proof of Theorem 10.3.1. ■

Theorem 10.3.2. *Let $u \in C(S)$ and $P_n^B = \rho^2 P_n^H + P_n^h$ in (10.2.1) hold. Then there exists the bound,*

$$\|P_n^B - \Sigma_N(P_n^B;\rho,\theta)\|_{q,\Gamma_\rho} \le CN^q\left(\frac{R}{r_{\max}}\right)^{2n-N}\left(\frac{r_{\max}}{r_{\min}}\right)^{n}\|P_n^B\|_{0,\Gamma}. \tag{10.3.6}$$

Proof. From Chapter 2 we have

$$\|P_n^h - \Sigma_N(P_n^h;\rho,\theta)\|_{q,\Gamma_\rho} \le CN^q\left(\frac{R}{r_{\max}}\right)^{2n-N}\left(\frac{r_{\max}}{r_{\min}}\right)^{2n}\|P_n^h\|_{0,\Gamma}. \tag{10.3.7}$$

Hence we have from (10.3.3) and (10.3.7)

$$\begin{aligned}\|P_n^B - \Sigma_N(P_n^B;\rho,\theta)\|_{q,\Gamma_\rho} &\le CN^q\left(\frac{R}{r_{\max}}\right)^{2n-N}\left(\frac{r_{\max}}{r_{\min}}\right)^n\left\{\|\rho^2 P_n^H\|_{0,\Gamma}^2 + \|P_n^h\|_{0,\Gamma}^2\right\}^{\frac{1}{2}}\\ &\le CN^q\left(\frac{R}{r_{\max}}\right)^{2n-N}\left(\frac{r_{\max}}{r_{\min}}\right)^{2n}\|P_n^B\|_{0,\Gamma}.\end{aligned}$$

This is the desired result (10.3.6). ■

We need the error bounds of solution derivatives. Define the norm

$$\left\|\frac{\partial}{\partial v}f(\theta)\right\|_{q,\Gamma_\rho}^2 = \pi\rho\left\{\sum_{m=1}^{\infty} m^{2q+2}\rho^{2m-2}(a_m^2 + b_m^2)\right\}, \quad q \ge 0, \tag{10.3.8}$$

where $f(\theta) = \frac{a_0}{2} + \sum_{i=1}^{\infty}\rho^i\{a_i\cos(i\theta) + b_i\sin(i\theta)\}$. From the arguments in Theorems 10.3.1 and 10.3.2, we have the following theorem.

Theorem 10.3.3. *Let* $u \in C(S)$. *There exists the bound for* $q \ge 0$,

$$\left\|\frac{\partial}{\partial v}(P_n^B - \Sigma_N(P_n^B;\rho,\theta))\right\|_{q,\Gamma_\rho} \le CN^{q+1}\left(\frac{R}{r_{\max}}\right)^{2n-N}\left(\frac{r_{\max}}{r_{\min}}\right)^n\|P_n^B\|_{0,\Gamma}. \tag{10.3.9}$$

Denote

$$[u,v]_H = \int_\Gamma uv + w^2\int_\Gamma u_v v_v, \tag{10.3.10}$$

where the norm $\|v\|_H = \sqrt{[u,v]_H}$. The MFS for (10.1.1)–(10.1.3) reads: to seek the solution u_N such that

$$\|u - u_N\|_H = \min_{v\in V_N}\|u - v\|_H. \tag{10.3.11}$$

Since there exists the orthogonality $[u - u_N, v]_H = 0$, we have

$$[u_N, v]_H = \int_\Gamma fv + w^2\int_\Gamma g\cdot v_v, \quad \forall v \in V_N. \tag{10.3.12}$$

Theorem 10.3.4. *Suppose that* $u \in \mathbf{H}^p(S)$ $\left(p \ge \frac{5}{2}\right)$, *and the* N *is chosen such that*

$$\left(\frac{R}{r_{\max}}\right)^{2n-N}\left(\frac{r_{\max}}{r_{\min}}\right)^n \le \frac{1}{n^{p+\frac{1}{2}}}. \tag{10.3.13}$$

When $w = \frac{1}{N}$, *there exists the error bound,*

$$\|u - u_N\|_H = O\left(\frac{1}{N^{p-\frac{1}{2}}}\right)\|u\|_{p,S}. \tag{10.3.14}$$

Proof. For the residuals in (10.2.1), there exist the bounds,

$$\|R_n^B\|_{q,S} \le C\frac{1}{n^{p-q}}\|u\|_{p,S}, \quad \left\|\frac{\partial R_n^B}{\partial \nu}\right\|_{q,S} \le C\frac{1}{n^{p-q-1}}\|u\|_{p,S}. \tag{10.3.15}$$

Choose $\bar{u}\,(\in V_N) = \Sigma_N(P_n^B;\rho,\theta)$. From (10.3.11) we have

$$\|u-u_N\|_H \le \|u-\bar{u}\|_H \le \|P_n^B - \Sigma_N(P_n^B;\rho,\theta)\|_H + \|R_n^B\|_H. \tag{10.3.16}$$

From (10.3.15) and $w=\frac{1}{N}$,

$$\|R_n^B\|_H \le \|R_n^B\|_{0,\Gamma} + w\left\|\frac{\partial R_n^B}{\partial \nu}\right\|_{0,\Gamma} \le C\frac{1}{n^{p-q}}\|u\|_{p,S}. \tag{10.3.17}$$

Denote $z = P_n^B - \Sigma_N(P_n^B;\rho,\theta)$. From the embedding theorem [15, 91, 195],

$$\left\|\frac{\partial^q z}{\partial \nu^q}\right\|_{k,\Gamma} \le C\|z\|_{k+q+\frac{1}{2},S}, \quad k,\, q \ge 0,$$

we have

$$\begin{aligned}\|P_n^B - \Sigma_N(P_n^B;\rho,\theta)\|_H = \|z\|_H &\le \left\{\|z\|_{0,\Gamma} + w\left\|\frac{\partial z}{\partial \nu}\right\|_{0,\Gamma}\right\}\\ &\le \|z\|_{\frac{1}{2},S} + w\|z\|_{\frac{3}{2},S} \le \|z\|_{\frac{1}{2},S_{\max}} + w\|z\|_{\frac{3}{2},S_{\max}},\end{aligned}$$

where $S_{\max} = \{(r,\theta)|r<r_{\max}, 0\le\theta<2\pi\}$.

For $\Delta z = 0$ with the Dirichlet condition $u=f$ on Γ (or the Neumann condition $u_\nu = g$ on Γ), there exist the bounds (Oden [195] and Babuska and Aziz [15]),

$$\|z\|_{\frac{1}{2}+q,S_{\max}} \le C\|f\|_{q,\partial S_{\max}} \left(\text{or } \|z\|_{\frac{1}{2}+q,S_{\max}} \le C\|g\|_{q-1,\partial S_{\max}}\right), \quad q\ge 0.$$

Also for (10.1.1)–(10.1.3), there exists the bound (see Grisvard [91]),

$$\|z\|_{\frac{1}{2}+q,S_{\max}} \le C\left(\|z\|_{q,\partial S_{\max}} + \left\|\frac{\partial z}{\partial \nu}\right\|_{q-1,\partial S_{\max}}\right), \quad q\ge 0. \tag{10.3.18}$$

Hence, we obtain from (10.3.10) and (10.3.18)

$$\begin{aligned}\|z\|_H &\le C\left\{\|z\|_{0,\partial S_{\max}} + \left\|\frac{\partial z}{\partial \nu}\right\|_{-1,\partial S_{\max}} + w\left(\|z\|_{1,\partial S_{\max}} + \left\|\frac{\partial z}{\partial \nu}\right\|_{0,\partial S_{\max}}\right)\right\}\\ &\le C\left\{\|z\|_{0,\partial S_{\max}} + w\|z\|_{1,\partial S_{\max}} + \left\|\frac{\partial z}{\partial \nu}\right\|_{0,\partial S_{\max}} + w\left\|\frac{\partial z}{\partial \nu}\right\|_{0,\partial S_{\max}}\right\}.\end{aligned}$$

From Theorems 10.3.2 and 10.3.3, when $w=\frac{1}{N}$ we have for $q=0,\,1$

$$\|z\|_H \le CN\left(\frac{R}{r_{\max}}\right)^{2n-N}\left(\frac{r_{\max}}{r_{\min}}\right)^n \|P_n^B\|_{0,\Gamma}. \tag{10.3.19}$$

Since

$$\|P_n^B\|_{0,\Gamma} \le C\|u\|_{0,\Gamma} \le C\|u\|_{p,S}, \tag{10.3.20}$$

we have from (10.3.19) and (10.3.20)

$$\|P_n^B - \Sigma_N(P_n^B;\rho,\theta)\|_H \le CN\left(\frac{R}{r_{\max}}\right)^{2n-N}\left(\frac{r_{\max}}{r_{\min}}\right)\|u\|_{p,S}. \tag{10.3.21}$$

Combining (10.3.16), (10.3.17) and (10.3.21) gives

$$\|u-u_N\|_H \le C\left\{N\left(\frac{R}{r_{\max}}\right)^{2n-N}\left(\frac{r_{\max}}{r_{\min}}\right)^n + \frac{1}{n^{p-\frac{1}{2}}}\right\}\|u\|_{p,S}. \tag{10.3.22}$$

Hence from (10.3.13) we have

$$\|u-u_N\|_H = O\left(\frac{1+\frac{N}{n}}{n^{p-\frac{1}{2}}}\|u\|_{p,S}\right) = O\left(\frac{1}{N^{p-\frac{1}{2}}}\|u\|_{p,S}\right), \tag{10.3.23}$$

where we have used $N \le Cn$. This completes the proof of Theorem 10.3.4. ■

10.4 Stability Analysis for Circular Domains

10.4.1 Approaches for Seeking Eigenvalues

Consider only the circular domains. For the non-circular domains, stability analysis may follow Chapter 3. Denote the circular domain by $S^\circ = \{(\varrho,\theta)|0 \le \varrho < \rho, 0 \le \theta < 2\pi\}$. From (10.1.5) we have

$$u_N = u_N(\varrho,\theta) = \sum_{j=1}^{N}\{c_j\Phi_j(\varrho,\theta) + d_j\Psi_j(\varrho,\theta)\}, \tag{10.4.1}$$

where c_j and d_j are the unknown coefficients. Then we have $2N$ collocation equations on ∂S:

$$u_N(\rho,\theta_k) = \sum_{j=1}^{N} c_j\Phi_j(\rho,\theta_k) + \sum_{j=1}^{N} d_j\Psi_j(\rho,\theta_k) = f(\rho,\theta_k), \quad k = 1, 2, \ldots, N, \tag{10.4.2}$$

$$\begin{aligned} w\frac{\partial}{\partial\rho}u_N(\rho,\theta) &= w\sum_{j=1}^{N} c_j\frac{\partial}{\partial\rho}\Phi_j(\rho,\theta_k) + w\sum_{j=1}^{N} d_j\frac{\partial}{\partial\rho}\Psi_j(\rho,\theta_k) \\ &= wg(\rho,\theta_k), \quad k = 1, 2, \ldots, N, \end{aligned} \tag{10.4.3}$$

where $\theta_k = kh$, $h = \frac{2\pi}{N}$ and $w = \frac{1}{N}$. Hence the $2N$ coefficients c_j and d_j can be obtained by (10.4.2) and (10.4.3) if the system of linear algebraic equations is nonsingular. Denote (10.4.2) and (10.4.3) by $\mathbf{Ax} = \mathbf{b}$, where the vectors $\mathbf{x} = \{c_1, c_2, \ldots, c_N, d_1, d_2, \ldots, d_N\}^T$ and $\mathbf{b} = \{f_1, f_2, \ldots, f_N, wg_1, wg_2, \ldots, wg_N\}^T$, and the matrix $\mathbf{A} \in \mathbf{R}^{2N\times 2N}$ is decomposed into

$$\mathbf{A} = \begin{bmatrix} \mathbf{A}_{11}(\mathbf{\Phi}) & \mathbf{A}_{12}(\mathbf{\Psi}) \\ w\mathbf{A}_{21}(D\mathbf{\Phi}) & w\mathbf{A}_{22}(D\mathbf{\Psi}) \end{bmatrix}. \tag{10.4.4}$$

In (10.4.4) the matrices $\mathbf{A}_{11}(\mathbf{\Phi}), \mathbf{A}_{12}(\mathbf{\Psi}), \mathbf{A}_{21}(D\mathbf{\Phi}), \mathbf{A}_{22}(D\mathbf{\Psi}) \in \mathbf{R}^{N\times N}$ are given by

$$\begin{aligned}
\mathbf{A}_{11}(\mathbf{\Phi}) &= \begin{bmatrix} \mathbf{\Phi}_1(\theta_1) & \cdots & \mathbf{\Phi}_N(\theta_1) \\ \vdots & \ddots & \vdots \\ \mathbf{\Phi}_1(\theta_N) & \cdots & \mathbf{\Phi}_N(\theta_N) \end{bmatrix}, \\
\mathbf{A}_{12}(\mathbf{\Psi}) &= \begin{bmatrix} \mathbf{\Psi}_1(\theta_1) & \cdots & \mathbf{\Psi}_N(\theta_1) \\ \vdots & \ddots & \vdots \\ \mathbf{\Psi}_1(\theta_N) & \cdots & \mathbf{\Psi}_N(\theta_N) \end{bmatrix}, \\
\mathbf{A}_{21}(D\mathbf{\Phi}) &= \begin{bmatrix} \frac{\partial}{\partial\rho}\mathbf{\Phi}_1(\theta_1) & \cdots & \frac{\partial}{\partial\rho}\mathbf{\Phi}_N(\theta_1) \\ \vdots & \ddots & \vdots \\ \frac{\partial}{\partial\rho}\mathbf{\Phi}_1(\theta_N) & \cdots & \frac{\partial}{\partial\rho}\mathbf{\Phi}_N(\theta_N) \end{bmatrix}, \\
\mathbf{A}_{22}(D\mathbf{\Psi}) &= \begin{bmatrix} \frac{\partial}{\partial\rho}\mathbf{\Psi}_1(\theta_1) & \cdots & \frac{\partial}{\partial\rho}\mathbf{\Psi}_N(\theta_1) \\ \vdots & \ddots & \vdots \\ \frac{\partial}{\partial\rho}\mathbf{\Psi}_1(\theta_N) & \cdots & \frac{\partial}{\partial\rho}\mathbf{\Psi}_N(\theta_N) \end{bmatrix}.
\end{aligned} \tag{10.4.5}$$

The matrices $\mathbf{A}_{12}(\mathbf{\Psi})$ and $\mathbf{A}_{22}(D\mathbf{\Psi})$ result from the Dirichlet and the Neumann problems of Laplace's equations in circular domains, which are given in Chapters 2 and 3, respectively. All four sub-matrices $\mathbf{A}_{11}(\mathbf{\Phi})$, $\mathbf{A}_{12}(\mathbf{\Psi})$, $\mathbf{A}_{21}(D\mathbf{\Phi})$ and $\mathbf{A}_{22}(D\mathbf{\Psi})$ are circulant. Denote the Fourier matrix (see Davis [71, p.32])

$$\mathbf{F}^*(\in \mathbf{C}^{N\times N}) = \frac{1}{\sqrt{N}} \begin{bmatrix} 1 & 1 & \cdots & 1 \\ 1 & \omega & \cdots & \omega^{n-1} \\ \vdots & \vdots & \ddots & \vdots \\ 1 & \omega^{n-1} & \cdots & \omega \end{bmatrix}, \tag{10.4.6}$$

where $\omega = e^{2\pi \mathbf{i}/N} = \cos\left(\frac{2\pi}{N}\right) + \mathbf{i}\sin\left(\frac{2\pi}{N}\right)$ with $\mathbf{i} = \sqrt{-1}$. Based on Davis [71] we have

$$\begin{aligned}
&\mathbf{A}_{11}(\mathbf{\Phi}) = \mathbf{F}^*\Lambda_{11}(\mathbf{\Phi})\mathbf{F},\ \mathbf{A}_{12}(\mathbf{\Psi}) = \mathbf{F}^*\Lambda_{12}(\mathbf{\Psi})\mathbf{F}, \\
&\mathbf{A}_{21}(D\mathbf{\Phi}) = \mathbf{F}^*\Lambda_{21}(D\mathbf{\Phi})\mathbf{F},\ \mathbf{A}_{22}(D\mathbf{\Psi}) = \mathbf{F}^*\Lambda_{22}(D\mathbf{\Psi})\mathbf{F},
\end{aligned} \tag{10.4.7}$$

where $\mathbf{F}$ is unitary with $\mathbf{FF}^* = \mathbf{F}^*\mathbf{F} = \mathbf{I}$, and $\mathbf{I}$ is the identity matrix. In (10.4.7) the matrices

$$\begin{aligned}
&\Lambda_{11}(\Phi) = \mathrm{diag}(\lambda_0(\Phi), \lambda_1(\Phi), \ldots, \lambda_{N-1}(\Phi)),\\
&\Lambda_{12}(\Psi) = \mathrm{diag}(\lambda_0(\Psi), \lambda_1(\Psi), \ldots, \lambda_{N-1}(\Psi)),\\
&\Lambda_{21}(D\Phi) = \mathrm{diag}(\lambda_0(D\Phi), \lambda_1(D\Phi), \ldots, \lambda_{N-1}(D\Phi)), \text{ and}\\
&\Lambda_{22}(D\Psi) = \mathrm{diag}(\lambda_0(D\Psi), \lambda_1(D\Psi), \ldots, \lambda_{N-1}(D\Psi))
\end{aligned}$$

are diagonal matrices. We have from Chapters 2 and 3 and [163, 167]

$$\begin{aligned}
&\lambda_0(\Psi) = N\,\ln R + \varepsilon, \quad \varepsilon \approx -\left(\frac{\rho}{R}\right)^N,\\
&\lambda_k(\Psi) \approx -\frac{N}{2}\left(\frac{1}{k}\left(\frac{\rho}{R}\right)^k + \frac{1}{N-k}\left(\frac{\rho}{R}\right)^{N-k}\right), \quad k = 1, 2, \ldots, N-1,\\
&\lambda_0(D\Psi) = -\frac{N}{\rho}\left(\frac{\rho}{R}\right)^N,\\
&\lambda_k(D\Psi) \approx -\frac{N}{2\rho}\left(\left(\frac{\rho}{R}\right)^k + \left(\frac{\rho}{R}\right)^{N-k}\right), \quad k = 1, 2, \ldots, N-1.
\end{aligned} \tag{10.4.8}$$

The new eigenvalues $\lambda_k(\Phi)$ and $\lambda_k(D\Phi)$ will be sought in the next subsection.

By using matrix $\mathbf{F}^*$ in (10.4.6), we obtain from (10.4.7)

$$\begin{aligned}
\mathbf{A} &= \begin{bmatrix} \mathbf{A}_{11}(\Phi) & \mathbf{A}_{12}(\Psi) \\ w\mathbf{A}_{21}(D\Phi) & w\mathbf{A}_{22}(D\Psi) \end{bmatrix}\\
&= \begin{bmatrix} \mathbf{F}^* & \mathbf{O} \\ \mathbf{O} & \mathbf{F}^* \end{bmatrix} \begin{bmatrix} \Lambda_{11}(\Phi) & \Lambda_{12}(\Psi) \\ w\Lambda_{21}(D\Phi) & w\Lambda_{22}(D\Psi) \end{bmatrix} \begin{bmatrix} \mathbf{F} & \mathbf{O} \\ \mathbf{O} & \mathbf{F} \end{bmatrix}.
\end{aligned} \tag{10.4.9}$$

Since the eigenvalues of similar matrices are the same, the eigenvalues of $\mathbf{A}$ are just those of matrix Λ, denoted by

$$\Lambda = \begin{bmatrix} \Lambda_{11}(\Phi) & \Lambda_{12}(\Psi) \\ w\Lambda_{21}(D\Phi) & w\Lambda_{22}(D\Psi) \end{bmatrix} = \begin{bmatrix} \mathrm{diag}(\lambda_i(\Phi)) & \mathrm{diag}(\lambda_i(\Psi)) \\ w\ \mathrm{diag}(\lambda_i(D\Phi)) & w\ \mathrm{diag}(\lambda_i(D\Psi) \end{bmatrix}.$$

By a permutation transformation $\mathbf{P}$, we have

$$\mathbf{P}^T\Lambda\mathbf{P} = \begin{bmatrix} \lambda_0(\Phi) & \lambda_0(\Psi) & & & & \\ w\lambda_0(D\Phi) & w\lambda_0(D\Psi) & & & & \\ & & \ddots & \mathbf{O} & & \\ & \mathbf{O} & & \lambda_i(\Phi) & \lambda_i(\Psi) & \\ & & & w\lambda_i(D\Phi) & w\lambda_i(D\Psi) & \\ & & & & & \ddots \end{bmatrix}. \tag{10.4.10}$$

Hence the eigenvalues $\lambda_i^{\pm}$ of Λ can be found from the zero determinants,

$$\det\begin{vmatrix} \lambda_i(\Phi) - \lambda & \lambda_i(\Psi) \\ w\lambda_i(D\Phi) & w\lambda_i(D\Psi) - \lambda \end{vmatrix} = 0, \quad i = 0, 1, 2, \ldots, N-1. \tag{10.4.11}$$

10.4.2 Eigenvalues $\lambda_k(\Phi)$ and $\lambda_k(D\Phi)$

Firstly, consider the matrix in (10.4.5)

$$\mathbf{A}_{11}(\Phi) = \begin{bmatrix} \Phi_1(\theta_1) & \cdots & \Phi_N(\theta_1) \\ \vdots & \ddots & \vdots \\ \Phi_1(\theta_N) & \cdots & \Phi_N(\theta_N) \end{bmatrix}.$$

Since $\Phi_i(\theta_j) = \Phi_i(\rho, \theta_j)$, the matrix $\mathbf{A}_{11}(\Phi)$ is circulant, denoted by

$$\mathbf{A}_{11}(\Phi) = \text{circulant}(b_0, b_1, \ldots, b_{N-1}),$$

where the entries are

$$b_j = r_j^2 \ln r_j = (R^2 + \rho^2 - 2R\rho \cos(jh))\ln\sqrt{R^2 + \rho^2 - 2R\rho \cos(jh)}.$$

Based on Circulant Lemma in Part I, the eigenvalues of $\mathbf{A}_{11}(\Phi)$ are given by

$$\lambda_k = \sum_{j=0}^{N-1} b_j \cos(kjh), \quad k = 0, 1, \ldots, N-1. \tag{10.4.12}$$

Lemma 10.4.1. *When $\rho < R$, there exist the approximations of $\lambda_k(\Phi)$ for large N,*

$$\lambda_0(\Phi) \approx N(R^2 \ln R + \rho^2(1 + \ln R)) + \left(\frac{\rho}{R}\right)^N \left(\frac{R^2}{N-1} - \frac{\rho^2}{N+1}\right), \tag{10.4.13}$$

$$\begin{aligned} \lambda_1(\Phi) \approx & -\frac{N}{2}\left((1 + 2\ln R)R^2 + \frac{\rho^2}{2}\right)\left(\frac{\rho}{R}\right) \\ & + \frac{N}{2(N-1)}\left(\frac{\rho}{R}\right)^{N-1}\left(\frac{R^2}{N-2} - \frac{\rho^2}{N}\right), \end{aligned} \tag{10.4.14}$$

$$\begin{aligned} \lambda_k(\Phi) \approx & \frac{N}{2k}\left(\frac{\rho}{R}\right)^k \left(\frac{R^2}{k-1} - \frac{\rho^2}{k+1}\right) \\ & + \frac{N}{2(N-k)}\left(\frac{\rho}{R}\right)^{N-k}\left(\frac{R^2}{N-k-1} - \frac{\rho^2}{N-k+1}\right), \ k = 2, 3, \ldots, N-1. \end{aligned} \tag{10.4.15}$$

Proof. Firstly for $\lambda_0(\Phi)$, we have from (10.4.12)

$$\lambda_0(\Phi) = \sum_{j=0}^{N-1} b_j = \frac{1}{h}\sum_{j=1}^{N} h r_j^2 \ln r_j, \tag{10.4.16}$$

where $r_j = \sqrt{R^2 + \rho^2 - 2R\rho \cos(jh)}$. Also from (10.2.4) there exists the expansion,

$$
\begin{aligned}
&(R^2+\rho^2-2R\rho\ \cos x)\ln\sqrt{R^2+\rho^2-2R\rho\ \cos x} \qquad (10.4.17)\\
&= R^2\ \ln R+\rho^2(1+\ln R)-(1+2\ \ln R)R\rho\ \cos x\\
&\quad + R^2\sum_{m=2}^{\infty}\frac{1}{m(m-1)}\left(\frac{\rho}{R}\right)^m\cos(mx)-\rho^2\sum_{m=1}^{\infty}\frac{1}{m(m+1)}\left(\frac{\rho}{R}\right)^m\cos(mx).
\end{aligned}
$$

Then, from Basic Lemma A in Part I we have

$$
\begin{aligned}
\lambda_0(\Phi) &= \frac{1}{h}\int_0^{2\pi}(R^2+\rho^2-2R\rho\ \cos x)\ln\sqrt{R^2+\rho^2-2R\rho\ \cos x}\ dx+\triangle\lambda_0(\Phi)\\
&= \frac{1}{h}2\pi(R^2\ \ln R+\rho^2(1+\ln R))+\triangle\lambda_0(\Phi), \qquad (10.4.18)
\end{aligned}
$$

where the increments are obtained directly from (10.4.17) and Basic Lemma A,

$$
\begin{aligned}
\triangle\lambda_0(\Phi) &= \frac{2\pi}{h}\left\{R^2\sum_{m=vN}\frac{1}{m(m-1)}\left(\frac{\rho}{R}\right)^m-\rho^2\sum_{m=vN}\frac{1}{m(m+1)}\left(\frac{\rho}{R}\right)^m\right\} \qquad (10.4.19)\\
&\approx N\left\{\frac{R^2}{N(N-1)}\left(\frac{\rho}{R}\right)^N-\rho^2\frac{1}{N(N+1)}\left(\frac{\rho}{R}\right)^N\right\}=\left(\frac{\rho}{R}\right)^N\left(\frac{R^2}{N-1}-\frac{\rho^2}{N+1}\right).
\end{aligned}
$$

Combining (10.4.18) and (10.4.19) gives

$$
\lambda_0(\Phi)\approx N\{R^2\ \ln R+\rho^2(1+\ln R)\}+\left(\frac{\rho}{R}\right)^N\left(\frac{R^2}{N-1}-\frac{\rho^2}{N+1}\right).
$$

This is the first result (10.4.13).

Next for $\lambda_1(\Phi)$, we have from Basic Lemma A, (10.4.12) and (10.4.17)

$$
\begin{aligned}
\lambda_1(\Phi) &= \sum_{j=1}^{N-1}b_j\ \cos(jh)=\frac{1}{h}\sum_{j=1}^{N}hb_j\ \cos(jh)=\frac{1}{h}\sum_{j=1}^{N}hr_j^2\ \ln r_j\ \cos(jh)\\
&= \frac{1}{h}\int_0^{2\pi}(R^2+\rho^2-2R\rho\ \cos x)\sqrt{R^2+\rho^2-2R\rho\ \cos x}\times\cos x\ dx+\triangle\lambda_1(\Phi)\\
&= \frac{\pi}{h}\left\{-(1+2\ \ln R)R\rho-\frac{\rho^3}{2R}\right\}+\triangle\lambda_1(\Phi)\\
&= -\frac{N}{2}\left[\left((1+2\ \ln R)R^2+\frac{\rho^2}{2}\right)\left(\frac{\rho}{R}\right)\right]+\triangle\lambda_1(\Phi). \qquad (10.4.20)
\end{aligned}
$$

Also the increments are given directly from Basic Lemma B in Part I and (10.4.17),

$$\begin{aligned}\triangle\lambda_1(\Phi) &= \frac{\pi}{h}\left\{R^2\sum_{m=\pm 1+vN}\frac{1}{m(m-1)}\left(\frac{\rho}{R}\right)^m - \rho^2\sum_{m=\pm 1+vN}\frac{1}{m(m+1)}\left(\frac{\rho}{R}\right)^m\right\}\\ &\approx \frac{N}{2}\left\{R^2\frac{1}{(N-1)(N-2)}\left(\frac{\rho}{R}\right)^{N-1} - \rho^2\frac{1}{N(N-1)}\left(\frac{\rho}{R}\right)^{N-1}\right\}\\ &= \frac{N}{2(N-1)}\left(\frac{\rho}{R}\right)^{N-1}\left\{\frac{R^2}{N-2}-\frac{\rho^2}{N}\right\}. \qquad (10.4.21)\end{aligned}$$

Combining (10.4.20) and (10.4.21) gives the second result (10.4.14).

Finally, for $\lambda_k(\Phi)$ $(k = 2, \ldots, N-1)$, we have similarly

$$\begin{aligned}\lambda_k(\Phi) &= \frac{1}{h}\sum_{j=1}^{N} hb_j\cos(kjh)\\ &= \frac{1}{h}\int_0^{2\pi}(R^2+\rho^2-2R\rho\cos x)\sqrt{R^2+\rho^2-2R\rho\cos x}\cos(kx)\,dx + \triangle\lambda_k(\Phi)\\ &= \frac{\pi}{h}\left\{R^2\frac{1}{k(k-1)}\left(\frac{\rho}{R}\right)^k - \rho^2\frac{1}{k(k+1)}\left(\frac{\rho}{R}\right)^k\right\} + \triangle\lambda_k(\Phi)\\ &= \frac{N}{2k}\left(\frac{\rho}{R}\right)^k\left(\frac{R^2}{k-1}-\frac{\rho^2}{k+1}\right) + \triangle\lambda_k(\Phi), \qquad (10.4.22)\end{aligned}$$

where $\triangle\lambda_k(\Phi)$ is obtained from Basic Lemma B and (10.4.17),

$$\begin{aligned}\triangle\lambda_k(\Phi) &= \frac{\pi}{h}\left\{R^2\sum_{m=\pm k+vN}\frac{1}{m(m-1)}\left(\frac{\rho}{R}\right)^m - \rho^2\sum_{m=\pm k+vN}\frac{1}{m(m+1)}\left(\frac{\rho}{R}\right)^m\right\}\\ &\approx \frac{N}{2}\left\{\frac{R^2}{(N-k)(N-k-1)}\left(\frac{\rho}{R}\right)^{N-k} - \frac{\rho^2}{(N-k)(N-k+1)}\left(\frac{\rho}{R}\right)^{N-k}\right\}\\ &= \frac{N}{2(N-k)}\left(\frac{\rho}{R}\right)^{N-k}\left(\frac{R^2}{N-k-1}-\frac{\rho^2}{N-k+1}\right). \qquad (10.4.23)\end{aligned}$$

Combining (10.4.22) and (10.4.23) gives the desired result (10.4.15) and completes the proof of Lemma 10.4.1. ■

We need the expansions of the normal derivatives $\frac{\partial}{\partial\rho}(r^2 \ln r)$. The following lemma follows from (10.4.17).

Lemma 10.4.2. *For* $\rho < R$ *there exists the expansion,*

$$\begin{aligned}&\frac{\partial}{\partial\rho}\left((R^2+\rho^2-2R\rho\cos x)\sqrt{R^2+\rho^2-2R\rho\cos x}\right)\\ &= 2\rho(1+\ln R) - (1+2\ln R)R\cos x + R\sum_{m=2}^{\infty}\frac{1}{m-1}\left(\frac{\rho}{R}\right)^{m-1}\cos(mx) \qquad (10.4.24)\\ &\quad - \rho\sum_{m=1}^{\infty}\frac{m+2}{m(m+1)}\left(\frac{\rho}{R}\right)^m\cos(mx).\end{aligned}$$

The matrix in (10.4.5) is expressed by

$$\mathbf{A}_{21}(D\Phi) = \begin{bmatrix} \frac{\partial}{\partial\rho}\Phi_1(\theta_1) & \cdots & \frac{\partial}{\partial\rho}\Phi_N(\theta_1) \\ \vdots & \ddots & \vdots \\ \frac{\partial}{\partial\rho}\Phi(\theta_N) & \cdots & \frac{\partial}{\partial\rho}\Phi_N(\theta_N) \end{bmatrix},$$

which is also circulant: $\mathbf{A}_{21}(D\Phi) = \text{circulant}(d_0, d_1, \ldots, d_{N-1})$, where

$$d_j = \frac{\partial}{\partial\rho}\left\{(R^2+\rho^2-2R\rho\,\cos(jh))\ln\sqrt{R^2+\rho^2-2R\rho\,\cos(jh)}\right\}. \tag{10.4.25}$$

Based on Circulant Lemma in Part I, the eigenvalues of $\mathbf{A}_{21}(D\Phi)$ are given by

$$\lambda_k = \sum_{j=0}^{N-1} d_j\,\cos(kjh), \quad k=0,1,\ldots,N-1. \tag{10.4.26}$$

Lemma 10.4.3. *When $\rho<R$, there exist the approximations of $\lambda_k(D\Phi)$ for large N,*

$$\lambda_0(D\Phi) \approx 2N\rho(1+\ln R) + \frac{N}{N-1}\left(\frac{\rho}{R}\right)^{N-1}\frac{1}{R}\left\{R^2 - \frac{(N+2)(N-1)}{(N+1)N}\rho^2\right\}, \tag{10.4.27}$$

$$\begin{aligned}\lambda_1(D\Phi) &\approx -\frac{N}{2R}\left\{(1+2\,\ln R)R^2+\frac{3}{2}\rho^2\right\}\\ &\quad+\frac{N}{2(N-2)}\left(\frac{\rho}{R}\right)^{N-2}\frac{1}{R}\left\{R^2-\frac{(N+1)(N-2)}{N(N-1)}\rho^2\right\},\end{aligned} \tag{10.4.28}$$

$$\begin{aligned}\lambda_k(D\Phi) &\approx \frac{N}{2(k-1)}\left(\frac{\rho}{R}\right)^{k-1}\frac{1}{R}\left\{R^2-\frac{(k+2)(k-1)}{k(k+1)}\rho^2\right\}\\ &\quad+\frac{N}{2(N-k-1)}\left(\frac{\rho}{R}\right)^{N-k-1}\frac{1}{R}\left\{R^2-\frac{(N-k+2)(N-k+1)}{(N-k)(N-R+1)}\rho^2\right\},\\ &\quad k=2,3,\ldots,N-1.\end{aligned} \tag{10.4.29}$$

Proof. Firstly for $\lambda_0(D\Phi)$, we have from (10.4.24) similarly

$$\begin{aligned}\lambda_0(D\Phi) &= \sum_{j=0}^{N-1} d_j = \frac{1}{h}\sum_{j=1}^{N} hd_j\\ &= \frac{1}{h}\int_0^{2\pi}\frac{\partial}{\partial\rho}\left\{(R^2+\rho^2-2R\rho\,\cos x)\sqrt{R^2+\rho^2-2R\rho\,\cos x}\right\}dx + \triangle\lambda_0(D\Phi)\\ &= \frac{2\pi}{h}2\rho(1+\ln R)+\triangle\lambda_0(D\Phi) = 2N\rho(1+\ln R)+\triangle\lambda_0(D\Phi),\end{aligned} \tag{10.4.30}$$

where

$$\begin{aligned}\triangle\lambda_0(D\Phi) &= \frac{2\pi}{h}\left\{R\sum_{m=vN}\frac{1}{m-1}\left(\frac{\rho}{R}\right)^{m-1} - \rho\sum_{m=vN}\left(\frac{m+2}{m(m+1)}\right)\left(\frac{\rho}{R}\right)^{m}\right\}\\ &\approx N\left\{R\frac{1}{N-1}\left(\frac{\rho}{R}\right)^{N-1} - \rho\frac{N+2}{N(N+1)}\left(\frac{\rho}{R}\right)^{N}\right\}\\ &= \frac{N}{N-1}\left(\frac{\rho}{R}\right)^{N-1}\frac{1}{R}\left\{R^2 - \frac{(N+2)(N-1)}{N(N+1)}\rho^2\right\}.\end{aligned} \tag{10.4.31}$$

Combining (10.4.30) and (10.4.31) gives the first result (10.4.27).

Next for $\lambda_1(D\Phi)$, we have from Basic Lemma B in Part I, (10.4.25) and (10.4.26)

$$\begin{aligned}\lambda_1(D\Phi) &= \sum_{j=0}^{N-1} d_j\ \cos jh = \frac{1}{h}\sum_{j=1}^{N} hd_j\ \cos jh\\ &= \frac{1}{h}\int_0^{2\pi}\frac{\partial}{\partial\rho}\left\{(R^2+\rho^2-2R\rho\ \cos x)\sqrt{R^2+\rho^2-2R\rho\ \cos x}\right\}\cos x\ dx + \triangle\lambda_1(D\Phi)\\ &= \frac{\pi}{h}\left\{-(1+2\ \ln R)R - \rho\frac{3}{2}\left(\frac{\rho}{R}\right)\right\} + \triangle\lambda_1(D\Phi),\end{aligned} \tag{10.4.32}$$

where $\triangle\lambda_1(D\Phi)$ is obtained from Basic Lemma B in Part I and (10.4.24),

$$\begin{aligned}\triangle\lambda_1(D\Phi) &= \frac{\pi}{h}\left\{R\sum_{m=\pm1+vN}\frac{1}{m-1}\left(\frac{\rho}{R}\right)^{m-1} - \rho\sum_{m=\pm1+vN}\frac{(m+2)}{m(m+1)}\left(\frac{\rho}{R}\right)^{m}\right\}\\ &\approx \frac{N}{2}\left\{\frac{R}{N-2}\left(\frac{\rho}{R}\right)^{N-2} - \rho\frac{N+1}{N(N-1)}\left(\frac{\rho}{R}\right)^{N-1}\right\}\\ &= \frac{N}{2(N-2)}\left(\frac{\rho}{R}\right)^{N-2}\frac{1}{R}\left\{R^2 - \frac{(N+1)(N-2)}{N(N-1)}\rho^2\right\}.\end{aligned} \tag{10.4.33}$$

Combining (10.4.32) and (10.4.33) gives the second result (10.4.28).

Finally, for $\lambda_k(D\Phi)$ $(k = 2, 3, \ldots, N-1)$, we have similarly

$$\lambda_k(D\Phi) = \frac{1}{h}\sum_{j=1}^{N} hd_j\ \cos(kjh) \tag{10.4.34}$$

$$\begin{aligned}&= \frac{1}{h}\int_0^{2\pi}\frac{\partial}{\partial\rho}\left\{(R^2+\rho^2-2R\rho\ \cos x)\sqrt{R^2+\rho^2-2R\rho\ \cos x}\right\}\cos(kx)\,dx + \triangle\lambda_k(D\Phi)\\ &= \frac{\pi}{h}\left\{\frac{R}{k-1}\left(\frac{\rho}{R}\right)^{k-1} - \rho\frac{k+2}{k(k+1)}\left(\frac{\rho}{R}\right)^{k}\right\} + \triangle\lambda_k(D\Phi)\\ &= \frac{N}{2(k-1)R}\left(\frac{\rho}{R}\right)^{k-1}\left\{R^2 - \frac{(k+2)(k-1)}{k(k+1)}\rho^2\right\} + \triangle\lambda_k(D\Phi),\ \ k = 2, 3, \ldots, N-1,\end{aligned}$$

where

$$\begin{aligned}\triangle\lambda_k(D\Phi) &= \frac{\pi}{h}\left\{\sum_{m=\pm k+\nu N}\frac{R}{m-1}\left(\frac{\rho}{R}\right)^{m-1} - \rho\sum_{m=\pm k+\nu N}\frac{m+2}{m(m+1)}\left(\frac{\rho}{R}\right)^{m}\right\} \\ &\approx \frac{N}{2}\left\{\frac{R}{N-k-1}\left(\frac{\rho}{R}\right)^{N-k-1} - \frac{\rho(N-k+2)}{(N-k)(N-k+1)}\left(\frac{\rho}{R}\right)^{N-k}\right\} \\ &= \frac{N}{2(N-k-1)}\left(\frac{\rho}{R}\right)^{N-k-1}\frac{1}{R}\times\left\{R^2 - \frac{(N-k+2)(N-k-1)}{(N-k)(N-k+1)}\rho^2\right\}.\end{aligned} \tag{10.4.35}$$

Combining (10.4.34) and (10.4.35) gives the last result (10.4.29), and this completes the proof of Lemma 10.4.3. ■

10.4.3 Bounds of Condition Number

The notation $a \asymp O(b)$ denotes that there exist two constants C_1 (>0) and C_2 such that $C_1 b \le |a| \le C_2 b$ with $b > 0$. Since the eigenvalues $\lambda_j(\Psi)$, $\lambda_j(\Phi)$, $\lambda_j(D\Psi)$ and $\lambda_j(D\Phi)$ are provided in (10.4.8) and Lemmas 10.4.1 and 10.4.3, we can derive the approximate eigenvalues of the MFS.

Lemma 10.4.4. *Let $\rho < R$ and $w = \frac{1}{N}$. When $R \ne 1$ and $R \ne \frac{1}{e}$, there exist the asymptotes of the leading eigenvalues: $\lambda_0^+ \asymp O(N)$ and $\lambda_0^- \asymp O(1)$.*

Proof. From (10.4.10), the $\lambda_0^\pm$ result from the eigenvalues of the 2×2 matrix

$$\mathbf{A}_F^0 = \begin{bmatrix}\lambda_0(\Psi) & \lambda_0(\Phi) \\ w\lambda_0(D\Psi) & w\lambda_0(D\Phi)\end{bmatrix} \approx \begin{bmatrix} N\ln R & N[R^2\ln R + \rho^2(1+\ln R)] \\ -\frac{1}{\rho}\left(\frac{\rho}{R}\right)^N & 2\rho(1+\ln R)\end{bmatrix}. \tag{10.4.36}$$

One entry has $-\frac{1}{\rho}\left(\frac{\rho}{R}\right)^N \approx 0$ for $\rho < R$ and large N. When $R \ne 1$ and $R \ne \frac{1}{e}$, the eigenvalues of $\mathbf{A}_F^0$ are given by $\lambda_0^+ \approx N\ln R$ and $\lambda_0^- \approx 2\rho(1+\ln R)$. ■

Lemma 10.4.5. *Let $\rho < R$ and $w = \frac{1}{N}$. For even N there exist asymptotes,*

$$\lambda_1^+ \asymp O(N), \quad \lambda_1^- \asymp O(1), \tag{10.4.37}$$

$$\lambda_k^+ \asymp O\left(\frac{N}{k}\left(\frac{\rho}{R}\right)^k\right), \quad \lambda_k^- \asymp O\left(\frac{1}{k^2}\left(\frac{\rho}{R}\right)^k\right), \quad k = 2, 3, \ldots, \frac{N}{2}, \tag{10.4.38}$$

$$\lambda_{N-k}^\pm = \lambda_k^\pm, \quad k = 2, 3, \ldots, \frac{N}{2} - 1. \tag{10.4.39}$$

Proof. From (10.4.8) and Lemmas 10.4.1 and 10.4.3, we have the matrix for $\lambda_1^{\pm}$,

$$\mathbf{A}_F^{(1)} = \begin{bmatrix} \lambda_1(\boldsymbol{\Psi}) & \lambda_1(\boldsymbol{\Phi}) \\ w\lambda_1(D\boldsymbol{\Psi}) & w\lambda_1(D\boldsymbol{\Phi}) \end{bmatrix}$$
$$= -\frac{N}{2}\left(\frac{\rho}{R}\right)\begin{bmatrix} 1 & (1+2\,\ln R)R^2+\frac{\rho^2}{2} \\ \frac{1}{N\rho} & \frac{1}{N\rho}\left((1+2\,\ln R)R^2+\frac{3}{2}\rho^2\right) \end{bmatrix} = cN\mathbf{B}^{(1)},$$

where $c = -\frac{1}{2}\frac{\rho}{R}$, and

$$\mathbf{B}^{(1)} = \begin{bmatrix} a_1 & a_2 \\ a_3 & a_4 \end{bmatrix}, a_1 = 1, a_2 = (1+2\,\ln R)R^2 + \frac{\rho^2}{2},$$
$$a_3 = \frac{1}{N\rho}, a_4 = \frac{1}{N\rho}\left\{(1+2\,\ln R)R^2 + \frac{3}{2}\rho^2\right\}. \tag{10.4.40}$$

Firstly, the determinant of $\mathbf{B}^{(1)}$ is given by

$$\det(\mathbf{B}^{(1)}) = a_1a_4 - a_2a_3$$
$$= \frac{1}{N\rho}\left\{(1+2\,\ln R)R^2 + \frac{3}{2}\rho^2 - \left((1+2\,\ln R)R^2+\frac{\rho^2}{2}\right)\right\} = \frac{\rho}{N} > 0.$$

Denote by $\lambda^{\pm}$ the eigenvalues of $\mathbf{B}^{(1)}$ in (10.4.40). We have

$$\lambda^{\pm} = \frac{1}{2}\left((a_1+a_4) \pm \sqrt{(a_1-a_4)^2 + 4a_2a_3}\right). \tag{10.4.41}$$

When N is large, we have $a_1 = 1$, $|a_4| \le C\frac{1}{N}$, and $|a_2a_3| \le C\frac{1}{N}$ to give $a_1 \gg |a_4|$ and $4|a_2a_3| \ll (a_1-a_4)^2$. We conclude that $\lambda_1^+ > \lambda_1^- > 0$, to obtain from (10.4.41)

$$\lambda_1^+ \asymp O(1), \quad \lambda_1^- = \frac{\det(\mathbf{B}^{(1)})}{\lambda^+} \asymp O\left(\frac{1}{N}\right).$$

This is the first result (10.4.37).

Next, we examine the matrix

$$\mathbf{A}_F^{(k)} = \begin{bmatrix} \lambda_k(\boldsymbol{\Psi}) & \lambda_k(\boldsymbol{\Phi}) \\ w\lambda_k(D\boldsymbol{\Psi}) & w\lambda_k(D\boldsymbol{\Phi}) \end{bmatrix}, \ k = 2, 3, \ldots, N-1. \tag{10.4.42}$$

The entries of $\mathbf{A}_F^{(k)}$ in (10.4.42) are given from (10.4.8) and Lemmas 10.4.1 and 10.4.3,

$$\lambda_k(\boldsymbol{\Psi}) \approx -\frac{N}{2}\left\{\frac{1}{k}\left(\frac{\rho}{R}\right)^k + \frac{1}{N-k}\left(\frac{\rho}{R}\right)^{N-k}\right\} \approx -\alpha_k\frac{N}{2}\frac{1}{k}\left(\frac{\rho}{R}\right)^k, \tag{10.4.43}$$

$$\lambda_k(D\boldsymbol{\Psi}) \approx -\frac{N}{2\rho}\left\{\left(\frac{\rho}{R}\right)^k + \left(\frac{\rho}{R}\right)^{N-k}\right\} \approx -\alpha_k\frac{N}{2\rho}\left(\frac{\rho}{R}\right)^k, \tag{10.4.44}$$

$$\begin{aligned}
\lambda_k(\Phi) &\approx \frac{N}{2k}\left(\frac{\rho}{R}\right)^k\left(\frac{R^2}{k-1}-\frac{\rho^2}{k+1}\right)+\frac{N}{2(N-k)}\left(\frac{\rho}{R}\right)^{N-k}\left(\frac{R^2}{N-k-1}-\frac{\rho^2}{N-k+1}\right)\\
&\approx \alpha_k\frac{N}{2k}\left(\frac{\rho}{k}\right)^k\left(\frac{R^2}{k-1}-\frac{\rho^2}{k+1}\right), \qquad (10.4.45)
\end{aligned}$$

$$\begin{aligned}
\lambda_k(D\Phi) &\approx \frac{N}{2k-1}\left(\frac{\rho}{R}\right)^{k-1}\frac{1}{R}\left\{R^2-\frac{(k+2)(k+1)}{k(k+1)}\rho^2\right\}\\
&\quad+\frac{N}{2(N-k-1)}\left(\frac{\rho}{R}\right)^{N-k-1}\frac{1}{k}\left\{R^2-\frac{(N-k+2)(N-k+1)}{(N-k)(k-N+1)}\rho^2\right\}\\
&\approx \alpha_k\frac{N}{2(k-1)}\left(\frac{\rho}{R}\right)^{k-1}\frac{1}{R}\left\{R^2-\frac{(k+2)(k-1)}{k(k+1)}\rho^2\right\}, \qquad (10.4.46)
\end{aligned}$$

where $\alpha_k = 1$ for $k \neq \frac{N}{2}$ and $\alpha_k = 2$ for $k = \frac{N}{2}$. For even N there exist equalities,

$$\mathbf{A}_F^{(N-k)} = \mathbf{A}_F^{(k)}, \quad k = 1,\, 2, \ldots, \frac{N}{2},$$

and $\lambda^{\pm}_{N-k} = \lambda^{\pm}_k$ for $k = 1,\, 2, \ldots, \frac{N}{2}-1$.

Denote the matrix

$$\mathbf{A}_F^{(k)} = \alpha_k\frac{N}{2}\left(\frac{\rho}{R}\right)^k \times \mathbf{B}^*, \quad \mathbf{B}^* = \begin{pmatrix} a_1^* & a_2^* \\ a_3^* & a_4^* \end{pmatrix}, \qquad (10.4.47)$$

where the entries are given from (10.4.42)–(10.4.46),

$$\begin{aligned}
a_1^* &= -\frac{1}{k}, \quad a_2^* = \frac{1}{k(k-1)}\left\{R^2-\frac{k-1}{k+1}\rho^2\right\},\\
a_3^* &= -\frac{1}{N\rho}, \quad a_4^* = \frac{1}{N(k-1)}\frac{1}{\rho}\left\{R^2-\frac{(k+2)(k-1)}{k(k+1)}\rho^2\right\}.
\end{aligned} \qquad (10.4.48)$$

Since $\frac{(k+2)(k-1)}{k(k+1)} < 1$, the bracket of a_4^* in (10.4.48) is positive for $\rho < R$, to give

$$R^2-\frac{(k+2)(k-1)}{k(k+1)}\rho^2 \asymp O(1).$$

Hence we conclude $a_1^* < 0$, $a_2^* > 0$, $a_3^* < 0$ and $a_4^* > 0$. The determinant of $\mathbf{A}_F^{(k)}$ is given by

$$\begin{aligned}
\det(\mathbf{B}^*) &= a_1^*a_4^* - a_2^*a_3^*\\
&= -\frac{1}{N\rho}\frac{1}{k(k-1)}\left\{R^2-\frac{(k+2)(k-1)}{k(k+1)}\rho^2\right\}+\frac{1}{N\rho}\frac{1}{k(k-1)}\left\{R^2-\frac{k-1}{k+1}\rho^2\right\}\\
&= \frac{2\rho}{Nk^2(k+1)} \asymp O\left(\frac{1}{Nk^3}\right). \qquad (10.4.49)
\end{aligned}$$

Next, we obtain the eigenvalues of $\mathbf{B}^*$ from (10.4.48):

$$\begin{aligned}\lambda_*^{\pm} &= (a_1^* + a_4^*) \pm \sqrt{(a_1^* - a_4^*)^2 + 4a_2^* a_3^*} \\ &= O\left(\frac{1}{k}\right) + O\left(\frac{1}{Nk}\right) \pm \sqrt{\left\{O\left(\frac{1}{k}\right) + O\left(\frac{1}{Nk}\right)\right\}^2 + O\left(\frac{1}{Nk^2}\right)}.\end{aligned}$$

Similarly, we have

$$\lambda_*^+ \asymp O\left(\frac{1}{k}\right), \quad \lambda_*^- = \frac{\det(\mathbf{B}^*)}{\lambda_*^+} \asymp O\left(\frac{1}{Nk^2}\right). \tag{10.4.50}$$

Then from (10.4.47) and (10.4.50), the eigenvalues of $\mathbf{A}_F^{(k)}$ have the asymptotes

$$\lambda_k^+ \asymp O\left(\frac{N}{k}\left(\frac{\rho}{R}\right)^k\right), \quad \lambda_k^- \asymp O\left(\frac{1}{k^2}\left(\frac{\rho}{R}\right)^k\right).$$

The desired results (10.4.38) follow. This completes the proof of Lemma 10.4.5. ■

Theorem 10.4.1. *Suppose that* $\rho < R$, $w = \frac{1}{N}$ *and even* $N\,(\gg 1)$. *When* $R \neq 1$ *and* $R \neq \frac{1}{e}$, *there exists the asymptote*

$$\text{Cond} = O\left(N^3\left(\frac{R}{\rho}\right)^{\frac{N}{2}}\right). \tag{10.4.51}$$

Proof. From Lemmas 10.4.4 and 10.4.5, we obtain

$$\lambda_{\max}|\lambda_i^{\pm}| = |\lambda_0^+| \asymp O(N), \quad \lambda_{\min}|\lambda_i^{\pm}| = |\lambda_{\frac{N}{2}}^-| \asymp O\left(\frac{1}{N^2}\left(\frac{\rho}{R}\right)^{N/2}\right),$$

to give

$$\text{Cond} = \frac{\lambda_{\max}|\lambda_i^{\pm}|}{\lambda_{\min}|\lambda_i^{\pm}|} = \frac{O(N)}{|\lambda_{\frac{N}{2}}^-|} = O\left(N^3\left(\frac{R}{\rho}\right)^{N/2}\right).$$

This is the desired result (10.4.51) and completes the proof of Theorem 10.4.1. ■

When N is odd, we can prove $\text{Cond} = O(N^3(R/\rho)^{\lfloor N/2 \rfloor})$, where $\lfloor x \rfloor$ is the largest integer less than (or equal to) x. Note that the Cond in (10.4.51) is similar to $\text{Cond} = O\left(N\left(\frac{R}{\rho}\right)^{\frac{N}{2}}\right)$ for Laplace's equation in Chapter 2. By following [163] and Chapter 3, the bounds of Cond can be derived for the simply-connected domains, and extended for other boundary conditions, such as the simply supported boundary condition and the mixed type of different boundary conditions. Details are omitted.

Remark 10.4.1. *The traditional condition number of the matrix* $\mathbf{A}$ *in 2-norm is given by* $\mathrm{Cond}_2(\mathbf{A}) = \frac{\sigma_{\max}(\mathbf{A})}{\sigma_{\min}(\mathbf{A})}$. *For symmetric (or circulant) matrices, we have*

$$\mathrm{Cond}_2(\mathbf{A}) = \frac{\max_i |\lambda_i(\mathbf{A})|}{\min_i |\lambda_i(\mathbf{A})|} := \mathrm{Cond}^*(\mathbf{A}). \tag{10.4.52}$$

The $\mathrm{Cond}^*(\mathbf{A})$ *is called the condition number in spectral radius since the spectral radius* $\rho(\mathbf{A}) = \max_i |\lambda_i(\mathbf{A})|$. *For the matrix (10.4.9) of circulant blocks, sub-matrices* $\mathbf{A}_{11}(\Phi) \neq w\mathbf{A}_{22}(D\Psi)$, *and the eigenvalues from (10.4.10) are not the singular values of matrix* $\mathbf{A}$. *See Davis [71, Theorem 5.7.3]. Since the singular values of* $\mathbf{A}$ *and* Λ *are the same, we may find*

$$\sigma_i(\mathbf{A}) = \sigma_i(\Lambda) = \sqrt{\lambda_i(\Lambda^T\Lambda)}. \tag{10.4.53}$$

There exists the bound in Atkinson [13, p.489],

$$\rho(\mathbf{A}) \leq \|\mathbf{A}\|, \tag{10.4.54}$$

where $\|\mathbf{A}\|$ *is any matrix norm. We have* $\rho(\mathbf{A}^{-1}) \leq \|\mathbf{A}^{-1}\|$ *and then give*

$$\mathrm{Cond}^*(\mathbf{A}) = \rho(\mathbf{A})\rho(\mathbf{A}^{-1}) \leq \|\mathbf{A}\|\|\mathbf{A}^{-1}\| = \mathrm{Cond}(\mathbf{A}). \tag{10.4.55}$$

However, for a square matrix $\mathbf{A}$, *if* $\epsilon > 0$ *is given, there exists a matrix norm* $\|\mathbf{A}\|_\epsilon$ *such that (also see [13, p.489])*

$$\|\mathbf{A}\|_\epsilon \leq \rho(\mathbf{A}) + \epsilon. \tag{10.4.56}$$

Then we have similarly

$$\mathrm{Cond}_\epsilon(\mathbf{A}) = \|\mathbf{A}\|_\epsilon \|\mathbf{A}^{-1}\|_\epsilon \leq \mathrm{Cond}^*(\mathbf{A}) + \delta, \tag{10.4.57}$$

where $\delta\ (>0) \to 0$ *as* $\epsilon \to 0$. *From the norm equivalence, there exist the bounds,*

$$c_0 \mathrm{Cond}^*(\mathbf{A}) \leq \mathrm{Cond}_2(\mathbf{A}) \leq C_1 \mathrm{Cond}^*(\mathbf{A}), \tag{10.4.58}$$

where the constants $c_0 = N^{-v}$ *and* $C_1 = N^v$ *with small* $v\ (\geq 0)$. *Note that the key part of Cond in (10.4.51) is the exponential growth* $O\left(\left(\frac{R}{\rho}\right)^{\frac{N}{2}}\right)$; *while the polynomial growth* $O(N^{3+v})$ *is less important. Therefore, we may simply use* $\mathrm{Cond}^*(\mathbf{A})$ *in (10.4.52) for stability analysis.*

Remark 10.4.2. *Let us consider the matrix in (10.4.10), which consists of diagonal sub-matrices with* $\mathbf{R}^{2\times 2}$. *We will prove that the constant* $C_1 = O(1)$ *with* $v = 0$ *in (10.4.58). We first derive the singular values based on (10.4.53). The matrix* $\mathbf{A}_F^{(k)}$ *in (10.4.42) and (10.4.47) is denoted by*

$$\mathbf{A}_F^{(k)} = \begin{bmatrix} \lambda_k(\Psi) & \lambda_k(\Phi) \\ w\lambda_k(D\Psi) & w\lambda_k(D\Phi) \end{bmatrix} = \alpha_k \frac{N}{2}\left(\frac{\rho}{R}\right)^k \times B^*, \quad k = 2, 3, \ldots, N-1, \tag{10.4.59}$$

where the matrix

$$\mathbf{B}^* = \begin{pmatrix} a_1^* & a_2^* \\ a_3^* & a_4^* \end{pmatrix}, \tag{10.4.60}$$

and the entries are expressed by

$$|a_1^*| \asymp O\left(\frac{1}{k}\right), \quad |a_2^*| \asymp O\left(\frac{1}{k^2}\right), \quad |a_3^*| \asymp O\left(\frac{1}{N}\right), \quad |a_4^*| \asymp O\left(\frac{1}{Nk}\right). \tag{10.4.61}$$

In (10.4.61), the notation $a \asymp O(b)$ *means that there exist two constants* $c_0\,(>0)$ *and* C *independent of* N *and* k *such as* $c_0 b \le a \le Cb$. *Denote by* $\lambda^\pm$ *and* $\sigma^\pm$ *the eigenvalues and the singular values of matrix* $\mathbf{B}^*$*, respectively. From (10.4.49) we have*

$$\sigma^+\sigma^- = |\lambda^+||\lambda^-| = |\det(\mathbf{B}^*)| \asymp O\left(\frac{1}{Nk^3}\right). \tag{10.4.62}$$

Also we have

$$(\mathbf{B}^*)^T\mathbf{B}^* = \begin{pmatrix} (a_1^*)^2 + (a_3^*)^2 & a_1^* a_2^* + a_3^* a_4^* \\ a_1^* a_2^* + a_3^* a_4^* & (a_2^*)^2 + (a_4^*)^2 \end{pmatrix}, \tag{10.4.63}$$

and give

$$\begin{aligned}(\sigma^+)^2 + (\sigma^-)^2 &= (a_1^*)^2 + (a_2^*)^2 + (a_3^*)^2 + (a_4^*)^2 \\ &\asymp O\left(\frac{1}{k^2} + \frac{1}{k^4} + \frac{1}{N^2} + \frac{1}{N^2k^2}\right) \asymp O\left(\frac{1}{k^2} + \frac{1}{N^2}\right).\end{aligned} \tag{10.4.64}$$

Then we find one singular value

$$(\sigma^+)^2 \asymp O\left(\frac{1}{k^2} + \frac{1}{N^2}\right), \quad \sigma^+ \asymp O\left(\frac{1}{k} + \frac{1}{N}\right) \asymp O\left(\frac{k+N}{kN}\right). \tag{10.4.65}$$

The other singular value is found from (10.4.62) and (10.4.65)

$$\sigma^- = \frac{|\det(\mathbf{B}^*)|}{\sigma^+} \asymp O\left(\frac{1}{Nk^3}\frac{kN}{k+N}\right) \asymp O\left(\frac{1}{k^2(k+N)}\right). \tag{10.4.66}$$

Hence, we have two singular values from (10.4.59), (10.4.65) and (10.4.66)

$$\sigma_k^\pm = \alpha_k \frac{N}{2}\left(\frac{\rho}{R}\right)^k \times \sigma^\pm, \tag{10.4.67}$$

to give

$$\sigma_k^+ \asymp O\left(\frac{k}{k+N}\left(\frac{\rho}{R}\right)^k\right), \quad \sigma_k^- \asymp O\left(\frac{N}{k^2(k+N)}\left(\frac{\rho}{R}\right)^k\right). \tag{10.4.68}$$

Next for matrix $\mathbf{A}_F^0$ *in (10.4.36), we have for* $R \ne 1$ *and* $R \ne \frac{1}{e}$

$$\mathbf{A}_F^0 = \begin{bmatrix} \lambda_0(\mathbf{\Psi}) & \lambda_0(\mathbf{\Phi}) \\ w\lambda_0(D\mathbf{\Psi}) & w\lambda_0(D\mathbf{\Phi}) \end{bmatrix} = \begin{pmatrix} a_1 & a_2 \\ a_3 & a_4 \end{pmatrix} := \mathbf{B}, \tag{10.4.69}$$

where the entries are

$$|a_1| \asymp O(N), \quad |a_2| \asymp O(N), \quad |a_3| \asymp O\left(\left(\frac{\rho}{R}\right)^N\right), \quad |a_4| \asymp O(1). \tag{10.4.70}$$

By following the above approaches, we have

$$\sigma_0^+ \asymp O(N), \quad \sigma_0^- \asymp O(1). \tag{10.4.71}$$

The bound of the traditional Cond_2 *is obtained by*

$$\text{Cond}_2 = \frac{\max\ \sigma_i^\pm}{\min\ \sigma_i^\pm} = \frac{\sigma_0^+}{\sigma_{\frac{N}{2}}^-} = O\left(N^3\left(\frac{R}{\rho}\right)^{N/2}\right), \tag{10.4.72}$$

where $\sigma_0^+ \asymp O(N)$ *and* $\sigma_{\frac{N}{2}}^-$ *from (10.4.68)*

$$\sigma_{\frac{N}{2}}^- \asymp O\left(\frac{1}{N^2}\left(\frac{\rho}{R}\right)^{N/2}\right). \tag{10.4.73}$$

Note that the bound of Cond_2 *in (10.4.72) are the same as that in (10.4.51) in Theorem 10.4.1. In Chapter 9, we have also used the* $\text{Cond}^*(\mathbf{A})$ *in (10.4.52); we may prove that the bound of* Cond_2 *is the same as that in Theorem 9.4.1.*

10.5 Numerical Experiments

Consider the biharmonic equation (10.1.1) in square domain $S = \{(x, y)| -1 < x < 1, -1 < y < 1\}$, and choose the following exact solution:

$$u(x, y) = \exp(x)\ \cos y + (x^2 + y^2)\exp(y)\ \cos x. \tag{10.5.1}$$

Consider the mixed type of the clamped and the simply supported boundary conditions on Γ, then the boundary condition (10.1.3) is replaced by

$$u_\nu = g \text{ on } \Gamma_1, \quad u_{\nu\nu} = g^* \text{ on } \Gamma_2, \tag{10.5.2}$$

where $\Gamma_1 \cup \Gamma_2 = \Gamma$ and $\Gamma_1 \cap \Gamma_2 = \emptyset$. The admissible functions (10.1.5) are expressed as

$$u_N = u_N(\rho, \theta) = \sum_{j=1}^N c_j(r_j^2\ \ln r_j) + \sum_{j=1}^N d_j\ \ln r_j = \sum_{j=1}^N (c_j\Phi_j(\rho, \theta) + d_j\Psi_j(\rho, \theta)),$$

where c_j and d_j are the unknown coefficients, and $r_j = |\overline{PQ_j}|$. Choose the uniform source nodes $Q_j = (R, \varphi_j)$, where $\varphi_j = \frac{2\pi j}{N}$. The energy $I(v)$ in (10.1.6) is replaced by

$$I^*(v) = \int_\Gamma (v - f)^2 + w^2\int_{\Gamma_1} (v_\nu - g)^2 + (w_1^*)^2\int_{\Gamma_2} (v_{\nu\nu} - g^*)^2, \tag{10.5.3}$$

where weights $w = \frac{1}{N}$ and $w_1^* = \frac{1}{N^2}$ as in [169]. Next, we formulate the collocation equations directly from (10.1.2) and (10.5.2), and obtain the collocation equations at nodes $(\rho_k, \theta_k) \in \Gamma$ for the mixed type of boundary conditions,

$$u_N(\rho_k, \theta_k) = \sum_{j=1}^{N} \{c_j \Phi_j(\rho_k, \theta_k) + d_j \Psi_j(\rho_k, \theta_k)\} = f(\rho_k, \theta_k), \quad (\rho_k, \theta_k) \in \Gamma, \quad (10.5.4)$$

$$\begin{aligned} w\frac{\partial}{\partial v} u_N(\rho_k, \theta_k) &= w \sum_{j=1}^{N} \left\{ c_j \frac{\partial}{\partial v} \Phi_j(\rho_k, \theta_k) + d_j \frac{\partial}{\partial v} \Psi_j(\rho_k, \theta_k) \right\} \\ &= wg(\rho_k, \theta_k), \quad (\rho_k, \theta_k) \in \Gamma_1, \end{aligned} \quad (10.5.5)$$

$$\begin{aligned} w^2\frac{\partial^2}{\partial v^2} u_N(\rho_k, \theta_k) &= w^2 \sum_{j=1}^{N} \left\{ c_j \frac{\partial^2}{\partial v^2} \Phi_j(\rho_k, \theta_k) + d_j \frac{\partial^2}{\partial v^2} \Psi_j(\rho_k, \theta_k) \right\} \\ &= w^2 g^*(\rho_k, \theta_k), \quad (\rho_k, \theta_k) \in \Gamma_2, \end{aligned} \quad (10.5.6)$$

where v is the normal of Γ_1 and Γ_2, and $w = \frac{1}{N}$. For the collocation equations (10.5.4)–(10.5.6), the number of collocation nodes is often chosen to be larger than that of source nodes. Then we obtain an overdetermined system of linear algebraic equations

$$\mathbf{F}\mathbf{x} = \mathbf{b}, \quad (10.5.7)$$

where matrix $\mathbf{F} \in \mathbf{R}^{m \times n}$ $(m \geq n)$, and vectors $\mathbf{x} \in \mathbf{R}^n$ and $\mathbf{b} \in \mathbf{R}^m$. The boundary errors are given by $\|\epsilon\|_B = \|u - u_N\|_B = \sqrt{I(u_N)}$ or $\sqrt{I^*(u_N)}$, where $I(v)$ and $I^*(v)$ are defined in (10.1.6) and (10.5.3), respectively.

When $\Gamma_2 = \emptyset$, the mixed type is reduced to the purely clamped boundary conditions. For the clamped boundary conditions, the errors and condition numbers are listed in Table 10.1, where M denotes the number of uniform collocation nodes along each edge of ∂S. Then $n = 2N$ and $m = 8M$ in (10.5.7). From Table 10.1, we can see the asymptotes for $R = 2$,

$$\|\epsilon\|_B = O(0.65^N), \quad \|\epsilon\|_{0,S} = O(0.66^N), \quad \|\epsilon\|_{1,S} = O(0.61^N), \quad (10.5.8)$$

$$\text{Cond} = O(1.4^N), \ \text{Cond\_eff} = O(1.3^N), \quad (10.5.9)$$

and for $R = 5$,

$$\|\epsilon\|_B = O(0.37^N), \quad \|\epsilon\|_{0,S} = O(0.37^N), \quad \|\epsilon\|_{1,S} = O(0.35^N), \quad (10.5.10)$$

$$\text{Cond} = O(2.3^N), \ \text{Cond\_eff} = O(2.2^N). \quad (10.5.11)$$

The errors decrease exponentially via the number of FS used; the exponential convergence rates result from the highly smooth solution (10.5.1). On the other hand, the condition numbers grow also exponentially. By noting $\sqrt{R/r_{\min}} = \sqrt{R} = \sqrt{2}$ (or $\sqrt{5}$), the Cond in (10.5.9) and (10.5.11) coincides with (10.4.51) very well.

Let us scrutinize (10.4.51) more carefully. Choose $R = 5$, and find the numerical growth of Cond between $N_1 = 31$ and $N_2 = 11$ from Table 10.1,

$$T_1 = \frac{\text{Cond}|_{N_1=31}}{\text{Cond}|_{N_2=11}} = \frac{4.41(14)}{2.27(7)} = 1.94(7).$$

On the other hand, the theoretical growth of Cond is evaluated from (10.4.51) by

$$T_2 = \left(\frac{N_1}{N_2}\right)^3 \times R^{\frac{N_1-N_2}{2}} = \left(\frac{31}{11}\right)^3 \times 5^{\frac{31-11}{2}} = (2.82)^3 \times 5^{10} = 2.19(7).$$

The relative error of T_1 is given by

$$\frac{|T_1 - T_2|}{T_2} = \frac{|1.94(7) - 2.19(7)|}{2.19(7)} = 11.5\%,$$

to show a remarkable consistency of stability between theory and computation. The effective condition number is a better criterion for stability in numerical partial differential equations (PDE); see [162]. We obtain the ratio from Table 10.1 at $R = 5$ and $N = 31$,

$$\frac{\text{Cond}}{\text{Cond\_eff}} = \frac{4.41(14)}{1.79(9)} = 2.46(5),$$

to show that the effective condition number is much smaller than the traditional condition number. The bounds of the effective condition may be derived by following [162]; details are omitted.

Next, we still choose the exact solution (10.5.1), but use the mixed type of the clamped and the simply supported boundary conditions,

$$\begin{aligned} u &= f, \quad u_\nu = g, \ \text{on } x = \pm 1, \\ u &= f, \quad u_{\nu\nu} = g^*, \ \text{on } y = \pm 1, \end{aligned}$$

where ν is the exterior normal of ∂S. The errors and the condition numbers of the MFS are listed in Table 10.2. The asymptotes of errors and conditions are similar to

TAB. 10.1 – The errors and the condition numbers for the biharmonic equation with the clamped boundary condition by the MFS, where $\epsilon = u - u_N$.

	N	M	$\|\epsilon\|_B$	$\|\epsilon\|_{0,S}$	$\|\epsilon\|_{1,S}$	Cond	Cond_eff	$\|\mathbf{x}\|$
$R = 2$	11	5	2.25(−1)	8.77(−2)	6.08(−1)	1.54(4)	86.0	27.3
	21	10	2.16(−3)	4.46(−4)	6.89(−3)	1.28(6)	5.95(3)	23.6
	31	15	2.89(−5)	4.33(−6)	9.07(−5)	4.10(7)	1.89(5)	19.6
	41	20	6.03(−7)	3.72(−8)	1.94(−6)	1.32(9)	6.24(6)	16.6
$R = 5$	11	5	2.86(−2)	1.11(−2)	8.73(−2)	2.22(7)	1.69(2)	2.33(3)
	21	10	1.46(−6)	5.35(−7)	5.89(−6)	1.64(11)	6.68(5)	3.14(3)
	31	15	3.10(−11)	1.71(−11)	8.48(−11)	4.41(14)	1.79(9)	2.59(3)

TAB. 10.2 – The errors and the condition numbers for the biharmonic equation with the mixed type of the clamped and simply supported boundary conditions by the MFS, where $\epsilon = u - u_N$.

	N	M	$\|\epsilon\|_B$	$\|\epsilon\|_{0,S}$	$\|\epsilon\|_{1,S}$	Cond	Cond_eff	$\|\mathbf{x}\|$
$R = 2$	11	5	1.87(−1)	2.27(−1)	1.07	1.83(4)	1.37(2)	20.3
	21	10	2.01(−3)	1.05(−3)	8.23(−3)	1.46(6)	6.48(3)	24.1
	31	15	2.62(−5)	6.33(−6)	1.08(−4)	4.87(7)	2.24(5)	19.6
	41	20	5.77(−7)	5.71(−8)	2.32(−6)	1.52(9)	7.20(6)	16.6
$R = 5$	11	5	2.48(−2)	1.19(−2)	8.91(−2)	3.35(7)	2.59(2)	2.28(3)
	21	10	1.28(−6)	7.39(−7)	6.93(−6)	2.00(11)	8.14(5)	3.14(3)
	31	15	4.87(−11)	3.59(−11)	1.28(−10)	4.72(14)	1.92(9)	2.59(3)

(10.5.8)–(10.5.11). In summary, numerical experimenters are carried out for the simply supported boundary conditions and the mixed type of boundary conditions to coincide with the analysis made in this chapter.

Chapter 11

Elastic Problems

11.1 Introduction

In this chapter, we will apply the basic analysis in Part I to linear elastostatics in 2D satisfying the Cauchy–Navier equation. The mixed types of displacement and the traction boundary conditions are dealt with, and both the direct collocation techniques and the Lagrange multiplier are used to couple the boundary conditions. The method of fundamental solutions (MFS) and the method of particular solutions (MPS) are used for the direct collocation techniques, and the hybrid Trefftz method (HTM) in Jirousek [109–111] for the Lagrange multiplier. We explore the error analysis of the MFS and the HTM using fundamental solutions (FS) to achieve optimal convergence rates. The MFS algorithms are introduced in Wang and Qin [237, Chapter 6], and the strict error analysis is given in this chapter.

This chapter is organized as follows. In Section 11.2, some basic mathematics for elastostatics problems in 2D is introduced, and then the fundamental solutions are provided. In Section 11.3, the collocation Trefftz method (CTM) and the HTM are described. In Section 11.4, the errors between FS and PS are derived, and in Section 11.5, the error estimates of the MFS and the HTM using FS are obtained. In Section 11.6, numerical experiments are reported, and in Appendix 11.7, new addition theorems for linear elastostatics are derived. The materials of this chapter are adapted from [159, 164].

11.2 Linear Elastostatics Problems in 2D

11.2.1 Basic Theory

Consider the linear elastostatics problem in 2D. Denote the displacements by $\vec{w} = \mathbf{w} = (w_1(\mathbf{x}), w_2(\mathbf{x}))^T = (u(x,y), v(x,y))^T$, where $\mathbf{x} = (x_1, x_2) = (x, y)$. The linear strain tensor is given by

DOI: 10.1051/978-2-7598-3171-5.c011
© Science Press, EDP Sciences, 2023

$$\epsilon_{ij}(\mathbf{x}) = \frac{1}{2}\left\{\frac{\partial w_i(\mathbf{x})}{\partial x_j} + \frac{\partial w_j(\mathbf{x})}{\partial x_i}\right\}, \quad 1 \le i, j \le 2. \tag{11.2.1}$$

Let $\sigma_{ij}\,(1 \le i, j \le 2)$ denote the stress tensor at $\mathbf{x}$. For an isotropic homogeneous Hookean solid, there exist the stress-strain relations

$$\sigma_{ij} = \lambda(\nabla \cdot \vec{w})\delta_{ij} + 2\mu\epsilon_{ij}, \quad 1 \le i, j \le 2, \tag{11.2.2}$$

where "$\nabla\cdot$" is the divergence operator, δ_{ij} are the Kronecker delta, and λ and μ are the Lamé constants. When there exists a body force $\vec{f}$, we have

$$\mu\Delta\vec{w} + (\lambda + \mu)\nabla(\nabla \cdot \vec{w}) + \vec{f} = 0 \text{ in } S. \tag{11.2.3}$$

When $\vec{f} \equiv \vec{0}$, we obtain the homogeneous equation, called the Cauchy–Navier equation of linear elastostatics for the isotropic body.

For linear elastostatics in 2D, define the Sobolev norm

$$\|\mathbf{v}\|_{1,\Omega}^2 = \sum_{i,j=1}^{2} \int_\Omega \left(\frac{\partial v_i}{\partial x_j}\right)^2 d\mathbf{x} + \sum_{i=1}^{2} \int_\Omega v_i^2\, d\mathbf{x}.$$

For $\mathbf{v} = (v_1, v_2)^T$, norm $\|\mathbf{v}\|_{1,\Omega}^2 = \|v_1\|_{1,\Omega}^2 + \|v_2\|_{1,\Omega}^2$. We cite the Korn inequality from [28, 51].

Lemma 11.2.1 (Korn Inequality). *For a bounded open domain Ω in 2D (or 3D) with the regular boundary $\partial\Omega$, there exist two constants $c_0\ (>0)$ and C independent of $\mathbf{v}$ such that*

$$c_0(\lambda, \mu)\|\mathbf{v}\|_{1,\Omega}^2 \le \sum_{i,j=1}^{2} \int_\Omega \epsilon_{ij}^2(\mathbf{v})\, d\mathbf{x} + \sum_{i=1}^{2} \int_\Omega v_i^2\, d\mathbf{x} \le C(\lambda, \mu)\|\mathbf{v}\|_{1,\Omega}^2,$$

where $\epsilon_{ij}(\mathbf{v}) = \frac{1}{2}\left\{\frac{\partial v_i}{\partial x_j} + \frac{\partial v_j}{\partial x_i}\right\}$.

Let $\mathbf{M}(\mathbf{x})$ denote the space of a rigid motion, *e.g.*, translation and rotation, given by $\vec{w}(\mathbf{x}) = (d_1 - ay, d_2 + ax)^T$, where d_1, d_2 and a are constants. Define the quotient space $\mathbf{H}_1^* = (\mathbf{H}^1(\Omega))^2/\mathbf{M}(\mathbf{x})$ equipped with the norm

$$|\mathbf{v}|_1^* = \inf_{\mathbf{m} \in \mathbf{M}(\mathbf{x})} \|\mathbf{v} + \mathbf{m}\|_{1,\Omega}.$$

We have the following theorem [28, 51, 192].

Theorem 11.2.1. *There exist two constants $C_1 = C_1(\lambda, \mu)$ and $C_2 = C_2(\lambda, \mu)$ such that*

$$C_1 A(\vec{v}, \vec{v}) \le (|\mathbf{v}|_1^*)^2 \le C_2 A(\vec{v}, \vec{v}),$$

where

$$A(\vec{w}, \vec{v}) = \int_\Omega \left\{\lambda(\nabla \cdot \vec{w})(\nabla \cdot \vec{v}) + \frac{1}{2}\sum_{i,j=1}^{2}\left(\frac{\partial w_i}{\partial x_j} + \frac{\partial w_j}{\partial x_i}\right)\left(\frac{\partial v_i}{\partial x_j} + \frac{\partial v_j}{\partial x_i}\right)\right\} d\mathbf{x}. \tag{11.2.4}$$

The strain energy of an elastostatic solid satisfying (11.2.3) is given by

$$\epsilon(\vec{w}) = \frac{1}{2}\int_\Omega \left\{ \lambda(\nabla\cdot\vec{w})^2 + \frac{\mu}{2}\sum_{i,j=1}^{2}\left(\frac{\partial w_j}{\partial x_i} + \frac{\partial w_i}{\partial x_j}\right)^2 \right\} d\mathbf{x}.$$

Theorem 11.2.2. *There exist the Gauss–Green formulas,*

$$A(\vec{w},\vec{v}) - \int_\Omega [\mu\Delta\vec{w} + (\lambda+\mu)\nabla(\nabla\cdot\vec{w})]\cdot\vec{v}\,d\mathbf{x} = \int_{\partial\Omega} \vec{\tau}(\vec{w})\cdot\vec{v}\,d\sigma, \tag{11.2.5}$$

$$\begin{aligned}&\int_\Omega \{[\mu\Delta\vec{w} + (\lambda+\mu)\nabla(\nabla\cdot\vec{w})]\cdot\vec{v} - [\mu\Delta\vec{v} + (\lambda+\mu)\nabla(\nabla\cdot\vec{v})]\cdot\vec{w}\}\,d\mathbf{x}\\ &= \int_{\partial\Omega}\{\vec{\tau}(\vec{w})\cdot\vec{v} - \vec{\tau}(\vec{v})\cdot\vec{w}\}\,d\sigma,\end{aligned} \tag{11.2.6}$$

where the traction vector $\vec{\tau}(\vec{w})(\mathbf{x}) = (\tau_1(\mathbf{x}), \tau_2(\mathbf{x}))^T$ *with* $\tau_j(\mathbf{x}) = \sum_{i=1}^{2}\sigma_{ij}(\mathbf{x})n_i(\mathbf{x})$, $j = 1, 2$, *and* $n_i(\mathbf{x}) = \cos(\vec{n}, x_i)$ *with* $i = 1, 2$, *where* $\vec{n}$ *is the normal vector.*

Theorem 11.2.3 ([51, 104, 210, 246]). *The general solutions of the linear elastostatic equations (11.2.3) in 2D and 3D are given by*

$$\vec{w}(\vec{x}) = \vec{h}(\vec{x}) - \kappa\nabla[\vec{x}\cdot\vec{h}(\vec{x}) + q(\vec{x})], \tag{11.2.7}$$

where $\vec{h}(\vec{x})$ *is the harmonic vector,* $q(\vec{x})$ *a harmonic function, and the constant*

$$\kappa = \frac{1}{4(1-\nu)}. \tag{11.2.8}$$

The PS and the FS of the Cauchy–Navier equation can be obtained from (11.2.7) and given in Sections 11.2.3 and 11.2.4. The general solutions of (11.2.7) are important to the study of algorithms and error bounds of MFS for linear elastostatics. The analysis in this chapter is more advanced than Part I because the linear elastostatics is more complicated and because new addition theorems of the FS are explored in Section 11.7.

11.2.2 Traction Boundary Conditions

Denote $\vec{w} = (u, v)^T$ and $\vec{x} = (x, y)^T$. The Cauchy–Navier equation is obtained from (11.2.3) with $\vec{f} \equiv \vec{0}$, and it is given explicitly as

$$\mu\Delta u + (\lambda+\mu)\left\{\frac{\partial^2 u}{\partial x^2} + \frac{\partial^2 v}{\partial x\partial y}\right\} = 0 \text{ in } S, \tag{11.2.9}$$

$$\mu\Delta v + (\lambda+\mu)\left\{\frac{\partial^2 u}{\partial x\partial y} + \frac{\partial^2 v}{\partial y^2}\right\} = 0 \text{ in } S, \tag{11.2.10}$$

or

$$\Delta u + \frac{1}{1-2\nu}\left\{\frac{\partial^2 u}{\partial x^2} + \frac{\partial^2 v}{\partial x \partial y}\right\} = 0 \text{ in } S, \tag{11.2.11}$$

$$\Delta v + \frac{1}{1-2\nu}\left\{\frac{\partial^2 u}{\partial x \partial y} + \frac{\partial^2 v}{\partial y^2}\right\} = 0 \text{ in } S, \tag{11.2.12}$$

where S is the solution domain in 2D, and ν is the Poisson ratio given by

$$\nu = \frac{\lambda}{2(\lambda+\mu)}, \quad 0 < \nu < \frac{1}{2}.$$

The traction on ∂S is given by

$$\vec{\tau}(\vec{w})(\mathbf{x}) = (\tau_1(u,v), \tau_2(u,v))^T, \tag{11.2.13}$$

where

$$\tau_1(u,v) = \lambda\left(\frac{\partial u}{\partial x} + \frac{\partial v}{\partial y}\right)n_1 + 2\mu\frac{\partial u}{\partial \nu} + \mu n_2\left(\frac{\partial v}{\partial x} - \frac{\partial u}{\partial y}\right), \tag{11.2.14}$$

$$\tau_2(u,v) = \lambda\left(\frac{\partial u}{\partial x} + \frac{\partial v}{\partial y}\right)n_2 + 2\mu\frac{\partial v}{\partial \nu} - \mu n_1\left(\frac{\partial v}{\partial x} - \frac{\partial u}{\partial y}\right), \tag{11.2.15}$$

and $n_1 = \cos(\vec{n}, x)$ and $n_2 = \cos(\vec{n}, y)$.

11.2.3 Fundamental Solutions

The FS in 2D can be derived from (11.2.7), and they are given in [51, p.520] (also refer to [39, 87, 133, 202, 209]) by

$$E_2(\mathbf{x},\mathbf{y}) = \frac{\lambda+3\mu}{4\pi\mu(\lambda+2\mu)}\left\{-\ln r_{\mathbf{xy}} I_2 + \frac{\lambda+\mu}{\lambda+3\mu}\frac{1}{r^2_{\mathbf{xy}}}[(\mathbf{x}-\mathbf{y})(\mathbf{x}-\mathbf{y})^T]\right\}, \tag{11.2.16}$$

where $r_{\mathbf{xy}} = |\mathbf{x}-\mathbf{y}|$ and I_2 is the identity matrix. The FS in (11.2.16) satisfy

$$\mu\Delta E_2(\mathbf{x},\mathbf{y}) + (\lambda+\mu)\nabla_{\mathbf{x}}[\nabla_{\mathbf{x}} \cdot E_2(\mathbf{x},\mathbf{y})] = -\delta(\mathbf{x}-\mathbf{y})I_2.$$

Choose the source nodes $\mathbf{y}_i = (\xi_i, \eta_i)$ to be uniformly located on a larger circle outside the 2D domain S, and denote the collocation points by $\mathbf{x} = P(x,y)$, where

$$x = r\cos\theta, \quad y = r\sin\theta,$$
$$\xi_i = R\cos\phi_i, \quad \eta_i = R\sin\phi_i, \quad i = 1, 2, ..., N,$$

where $R > \max_S r$, $r = \sqrt{x^2+y^2}$, $R = \sqrt{\xi_i^2 + \eta_i^2}$ and $\phi_i = \frac{2\pi}{N}i$. Then the distance between two points $\mathbf{x}$ and $\mathbf{y}_i$ is given by

$$r_i = r_{\mathbf{xy}_i} = \sqrt{R^2 + r^2 - 2Rr\cos(\theta - \phi_i)}.$$

Denote vectors $\vec{u}_i = (u_i, v_i)^T$ and $\vec{d}_i = (a_i, b_i)$ with two constants a_i and b_i. We have the FS: $\vec{u}_i = E_2(\mathbf{x}, \mathbf{y}_i)\vec{d}_i$, where

$$u_i = a_i\left\{-A \ \ln r_i + B\frac{(x-\xi_i)^2}{r_i^2}\right\} + b_i B\frac{(x-\xi_i)(y-\eta_i)}{r_i^2},$$
$$v_i = a_i B\frac{(x-\xi_i)(y-\eta_i)}{r_i^2} + b_i\left\{-A \ \ln r_i + B\frac{(y-\eta_i)^2}{r_i^2}\right\},$$

and the constants $A = \frac{\lambda+3\mu}{4\pi\mu(\lambda+2\mu)}$ and $B = \frac{\lambda+\mu}{4\pi\mu(\lambda+2\mu)}$. From Theorem 11.2.3, by adding the other FS: $\nabla(\ln r) = \left(\frac{x}{r^2}, \frac{y}{r^2}\right)^T$, we obtain the general linear combination of FS,

$$\begin{aligned} u_N &= u_N(x,y) \qquad (11.2.17)\\ &= \sum_{i=1}^{N}\left\{a_i\left(-\ln r_i + D\frac{(x-\xi_i)^2}{r_i^2}\right) + b_i D\frac{(x-\xi_i)(y-\eta_i)}{r_i^2} + c_i\frac{(x-\xi_i)}{r_i^2}\right\},\end{aligned}$$

$$\begin{aligned} v_N &= v_N(x,y) \qquad (11.2.18)\\ &= \sum_{i=1}^{N}\left\{a_i D\frac{(x-\xi_i)(y-\eta_i)}{r_i^2} + b_i\left(-\ln r_i + D\frac{(y-\eta_i)^2}{r_i^2}\right) + c_i\frac{(y-\eta_i)}{r_i^2}\right\},\end{aligned}$$

where a_i, b_i and c_i are the coefficients, and the constant

$$D = \frac{B}{A} = \frac{\lambda+\mu}{\lambda+3\mu} = \frac{1}{3-4\nu} = \frac{\kappa}{1-\kappa}, \qquad (11.2.19)$$

and κ is given in (11.2.8). For the plane stress problem,

$$D = \frac{1}{3-4\nu} = \frac{1+\hat{\nu}}{3-\hat{\nu}}, \quad \nu = \frac{\hat{\nu}}{1+\hat{\nu}}. \qquad (11.2.20)$$

11.2.4 Particular Solutions

From Jirousek and Wroblewski [111] and Qin [203], the smooth PS from (11.2.7) are given by

$$\begin{aligned} u_L = \sum_{k=1}^{L}\rho^k\{&a_k[-\sin(k\theta) + Dk \ \sin(k-2)\theta] \\ &+ b_k[\cos(k\theta) - Dk \ \cos(k-2)\theta] + c_k \ \sin(k\theta) - d_k \ \cos(k\theta)\} - d_0, \end{aligned} \qquad (11.2.21)$$

$$\begin{aligned} v_L = \sum_{k=1}^{L}\rho^k\{&a_k[\cos(k\theta) + Dk \ \cos(k-2)\theta] \\ &+ b_k[\sin(k\theta) + Dk \ \sin(k-2)\theta] + c_k \ \cos(k\theta) + d_k \ \sin(k\theta)\} + c_0, \end{aligned} \qquad (11.2.22)$$

where D is given in (11.2.19) or (11.2.20), and a_k, b_k, c_k and d_k are the coefficients.

11.3 HTM, MFS and MPS

11.3.1 Algorithms of HTM

We discuss three methods: (1) The hybrid Trefftz method (HTM), (2) The method of fundamental solution (MFS), and (3) The method of particular solution (MPS). The error analysis of the HTM using FS and the MFS is the goal of this chapter (see Section 11.5); the analysis for the HTM using PS and the MPS was provided in [153] already. Consider the mixed type of displacement-traction conditions,

$$\vec{w}(\mathbf{x}) = \vec{f}(\mathbf{x}) \text{ on } \mathbf{\Gamma}_D, \tag{11.3.1}$$

$$\vec{\tau}(\vec{w}) = \vec{g}(\mathbf{x}) \text{ on } \mathbf{\Gamma}_N, \tag{11.3.2}$$

where $\partial\mathbf{\Omega} = \mathbf{\Gamma}_D \cup \mathbf{\Gamma}_N$, $\mathbf{\Gamma}_D \cap \mathbf{\Gamma}_N = \emptyset$, and the traction vector $\vec{\tau}(\vec{w})$ is given in (11.2.13). For simplicity in exposition, let $\mathbf{\Gamma}_D \neq \emptyset$. Then the solution $\vec{w}$ of (11.2.9), (11.2.10), (11.3.1) and (11.3.2) exists uniquely, and a rigid motion is included in the solution $\vec{w}$. Also, assume that the solution $\vec{w}$ is smooth enough so that the FS in Section 11.2 can be used directly. For corner singularity, the singular solutions and their numerical algorithms are explored in [138, 156]. Hence the admissible functions satisfy the Cauchy–Navier equations exactly. Based on the minimum principle of complementary strain energy [62, 98, 209], when the traction condition (11.3.2) is satisfied, the displacement condition (11.3.1) is a natural consequence. Hence we may use the Lagrange multiplier $\vec{\xi}$ to deal with (11.3.2). In fact, the exact value of $\vec{\xi}$ is just the solution $\vec{w}$ on $\mathbf{\Gamma}_N$ (see [153]). We choose the FS in (11.2.17) and (11.2.18). Hence the admissible functions $\vec{v}$ also satisfy equations (11.2.9) and (11.2.10). Denote its space by $V_N \subset (\mathbf{H}^1(\mathbf{\Omega}))^3$. Also, choose the piecewise polynomial of order p for the Lagrange multiplier $\vec{\xi}$ on $\mathbf{\Gamma}_N$, and denote its space by $\mathbf{T}_p = \mathbf{T}_p(\mathbf{\Gamma}_N)$. Then the HTM reads: to seek $\vec{w}_N \in V_N$ and $\vec{\xi}_p \in \mathbf{T}_p \subset \left(\mathbf{H}^{\frac{1}{2}}(\mathbf{\Gamma}_N)\right)^3$ such that

$$\begin{aligned} &A(\vec{w}_N, \vec{v}) - \int_{\Gamma_D} \vec{f} \cdot \vec{\tau}(\vec{v}) d\sigma - \int_{\Gamma_N} [\vec{\tau}(\vec{w}_N) - \vec{g}] \cdot \vec{\eta} d\sigma - \int_{\Gamma_N} \vec{\tau}(\vec{v}) \cdot \vec{\xi}_p d\sigma = 0, \\ &\forall \vec{v} \in V_N, \vec{\eta} \in \mathbf{T}_p, \end{aligned} \tag{11.3.3}$$

where $A(\vec{w}, \vec{v})$ is given in (11.2.4). The HTM was first proposed in Jirousek [109] and then discussed in [83, 110, 111, 203]. The error analysis of the HTM using PS is provided in [153], and the analysis of the HTM using FS will be made in Section 11.5.2.

11.3.2 Algorithms of MFS and MPS

Since the Lagrange multiplier in HTM is an extra variable in computation, we may replace it by using direct collocation techniques. The collocation Trefftz method is described as follows. Let $\vec{f} = (f_1, f_2)^T$ in (11.3.1) and $\vec{g} = (g_1, g_2)^T$ in (11.3.2). Define the boundary energy

$$I(u,v) = \int_{\Gamma_D} [(u - f_1)^2 + (v - f_2)^2] + \omega^2 \int_{\Gamma_N} [(\tau_1(u,v) - g_1)^2 + (\tau_2(u,v) - g_2)^2], \tag{11.3.4}$$

where ω is a weight to balance two terms in (11.3.4), and $\tau_1(u,v)$ and $\tau_2(u,v)$ are given in (11.2.14) and (11.2.15). Denote by V_N the set of all linear combinations in (11.2.17) and (11.2.18). In computation, we may choose $\omega = \frac{1}{N}$. The CTM reads: to seek $(u_N, v_N) \in V_N$ such that

$$I(u_N, v_N) = \min_{(u,v) \in V_N} I(u,v). \tag{11.3.5}$$

When the integrals in (11.3.4) involve a numerical approximation, we have

$$\widehat{I}(u,v) = \widehat{\int_{\Gamma_D}} [(u - f_1)^2 + (v - f_2)^2] + \omega^2 \widehat{\int_{\Gamma_N}} [(\tau_1(u,v) - g_1)^2 + (\tau_2(u,v) - g_2)^2], \tag{11.3.6}$$

where $\widehat{\int}$ is a numerical approximation of $\int$ by some quadrature rules, such as the central or the Gaussian rule. The equation (11.3.5) leads to

$$\widehat{I}(u_N, v_N) = \min_{(u,v) \in V_N} \widehat{I}(u,v). \tag{11.3.7}$$

We may establish the collocation equations directly from the boundary conditions (11.3.1) and (11.3.2),

$$\begin{aligned} &u_N(P_j) = f_1(P_j), \quad v_N(P_j) = f_2(P_j), \quad P_j \in \boldsymbol{\Gamma}_D, \\ &\tau_1(u_N(P_j),\, v_N(P_j)) = g_1(P_j), \quad \tau_2(u_N(P_j),\, v_N(P_j)) = g_2(P_j), \quad P_j \in \boldsymbol{\Gamma}_N. \end{aligned}$$

Let $\boldsymbol{\Gamma}_D$ and $\boldsymbol{\Gamma}_N$ be divided into small sections $\triangle\boldsymbol{\Gamma}_j$ with the meshspacings $\triangle h_j$. We obtain from (11.3.1) and (11.3.2) with suitable weights

$$\sqrt{\triangle h_j} u_N(P_j) = \sqrt{\triangle h_j} f_1(P_j), \quad \sqrt{\triangle h_j} v_N(P_j) = \sqrt{\triangle h_j} f_2(P_j), \quad P_j \in \boldsymbol{\Gamma}_D, \tag{11.3.8}$$

$$\omega\sqrt{\triangle h_j}\tau_1(u_N(P_j), v_N(P_j)) = \omega\sqrt{\triangle h_j} g_1(P_j), \quad P_j \in \boldsymbol{\Gamma}_N, \tag{11.3.9}$$

$$\omega\sqrt{\triangle h_j}\tau_2(u_N(P_j), v_N(P_j)) = \omega\sqrt{\triangle h_j} g_2(P_j), \quad P_j \in \boldsymbol{\Gamma}_N. \tag{11.3.10}$$

If choosing the middle nodes of $\triangle\boldsymbol{\Gamma}_j$ as the boundary collocation nodes P_j, the equations (11.3.8)–(11.3.10) are just the equation (11.3.7) with the central rule (see [169]). When the number M of collocation nodes is equal to (or larger than) N, we obtain an overdetermined system,

$$\mathbf{Fz} = \mathbf{b}, \tag{11.3.11}$$

where $\mathbf{F} \in \mathbf{R}^{2M\times 2N}(M \geq N)$ and $\mathbf{z} = (..., a_i, b_i, ...)^T$. We may use the singular value decomposition (SVD) or the QR decomposition to solve (11.3.11). The CTM (11.3.7) using the FS is called the MFS. When the FS in (11.2.17) and (11.2.18) are replaced by the PS in (11.2.21) and (11.2.22), the equation (11.3.7) (or (11.3.8)–(11.3.10)) is called the method of particular solutions (MPS). In the MPS, the number of unknown coefficients in (11.2.21) and (11.2.22) is $(4L+2)$, and the weight $\omega = \frac{1}{L}$.

11.4 Errors Between FS and PS

11.4.1 Preliminary Lemmas

Our error analysis is also related to Laplace's equation in Chapter 2. Consider Laplace's equation with the Dirichlet boundary condition,

$$\Delta u = \frac{\partial^2 u}{\partial x^2} + \frac{\partial^2 u}{\partial y^2} = 0 \text{ in } S, \quad u = f \text{ on } \Gamma, \tag{11.4.1}$$

where S is a bounded simply-connected domain with the boundary $\partial S = \Gamma$. Denote $r_{\max} = \max r|_S$ and $r_{\min} = \max\limits_{S_{\text{in}}\,(S_{\text{in}} \subseteq S)} r$, where S_{in} is a disk inside S. A circle surrounding S is given by

$$\ell_R = \{(r, \theta) | r = R, 0 \leq \theta \leq 2\pi\}, \quad R > r_{\max}.$$

Let the source (charge) nodes Q be located outside S, then the FS

$$\phi(r, \theta) = \ln|\overline{PQ}|, \quad P \in S \cup \partial S,$$

are harmonic functions, where $P = \{(x, y) | x = r\cos\theta, y = r\sin\theta\}$. The source nodes $Q_i = \{(x, y) | x = R\cos(ih), y = R\sin(ih)\}$ may be located uniformly on ℓ_R, where $R > r_{\max}$ and $h = \frac{2\pi}{N}$. We obtain the FS

$$\phi_i(P) = \ln|\overline{PQ_i}|, \quad i = 1, 2, ..., N,$$

and the numerical solutions are found by a linear combination

$$u_N = \sum_{i=1}^{N} c_i \phi_i(P),$$

where c_i are the unknown coefficients to be determined. Since u_N satisfies Laplace's equation in S already, the coefficients c_i can be determined by enforcing the boundary condition in (11.4.1) only. We may use the MFS or the HTM.

Denote the harmonic polynomials

$$\bar{P}_n(\rho, \theta) = \bar{a}_0 + \sum_{k=1}^{n} \rho^k \{\bar{a}_k \cos(k\theta) + \bar{b}_k \sin(k\theta)\}, \tag{11.4.2}$$

where $\bar{a}_k$ and $\bar{b}_k$ are the coefficients. For error bounds between FS and PS, since the continuity extension in Remark 2.3.1 in Chapter 2 is needed, we always assume the solution $u \in \mathbf{H}^p(S)$ $(p > 1)$, which may not be written in some lemmas and theorems. We have two lemmas from Chapter 2.

Lemma 11.4.1 (Addition Theorem). *There exists the series expansion for* $\rho < R$,

$$\ln r = \ln\sqrt{\rho^2 - 2\rho R\cos(\theta-\phi) + R^2} = \ln R - \sum_{n=1}^{\infty}\frac{1}{n}\left(\frac{\rho}{R}\right)^n \cos n(\theta-\phi).$$

Lemma 11.4.2. *For* $R > \rho$ *and* $R \neq 1$, *there exist the equalities*

$$\bar{P}_n(\rho,\theta) = \frac{\bar{a}_0}{2\pi\,\ln R}\int_0^{2\pi}\ln r\ d\phi - \frac{1}{\pi}\sum_{k=1}^{n} kR^k\int_0^{2\pi}(\bar{a}_k\cos(k\phi) + \bar{b}_k\sin(k\phi))\ln r\ d\phi,$$

where $r^2 = R^2 + \rho^2 - 2\rho R\cos(\phi - \theta)$.

For the periodical functions $f(x+2\pi) = f(x)$, the trapezoidal rule is given by

$$\int_0^{2\pi} f(x)\,dx \approx \widehat{\int_0^{2\pi}} f(x)\,dx = h\sum_{i=0}^{N-1} f(ih),$$

where $h = \frac{2\pi}{N}$. Then the harmonic polynomials $\bar{P}_n(\rho,\theta)$ in (11.4.2) can be approximated by $\ln r_i$,

$$\bar{P}_n(r,\theta) \approx \sum_{i=1}^{N}\bar{\alpha}_i\ \ln r_i,$$

where $r_i^2 = R^2 + \rho^2 - 2\rho R\cos(\theta - \phi_i)$, $\phi_i = \frac{2\pi}{N}i$, and the constants

$$\bar{\alpha}_i = \frac{h}{2\pi\,\ln R}\bar{a}_0 - \frac{h}{\pi}\sum_{k=1}^{n} kR^k\{\bar{a}_k\cos(k\phi_i) + \bar{b}_k\sin(k\phi_i)\}. \tag{11.4.3}$$

Denote this specific FS of $\ln r_i$ by

$$\Sigma_N(\bar{P}_n, \ln r; \rho,\theta) = \sum_{i=1}^{N}\bar{\alpha}_i\ \ln r_i.$$

Lemma 11.4.3. *For large* $N\,(> 2n)$, *there exist the bounds,*

$$\|\bar{P}_n(\rho,\theta) - \Sigma_N(\bar{P}_n, \ln r;\rho,\theta)\|_{q,\Gamma} \le CN^q\left(\frac{R}{r_{\max}}\right)^{2n-N}\left(\frac{r_{\max}}{r_{\min}}\right)^n\|\bar{P}_n(\rho,\theta)\|_{0,\Gamma}, \tag{11.4.4}$$

$$\begin{aligned}&\left\|\frac{\partial}{\partial \nu}(\bar{P}_n(\rho,\theta) - \Sigma_N(\bar{P}_n, \ln r;\rho,\theta))\right\|_{q,\Gamma}\\ &\le CN^{q+1}\left(\frac{R}{r_{\max}}\right)^{2n-N}\left(\frac{r_{\max}}{r_{\min}}\right)^n\|\bar{P}_n(\rho,\theta)\|_{0,\Gamma},\end{aligned} \tag{11.4.5}$$

where v *is the normal of* $\Gamma = \partial S$*, and* C *is a constant independent of* n *and* N*.*

Proof. The first result (11.4.4) is cited from Chapter 2. Denote the Fourier expansion for v,

$$v = \frac{a_0}{2} + \sum_{k=1}^{n} \rho^k \{a_k \cos(k\theta) + b_k \sin(k\theta)\},$$

where a_k and b_k are the Fourier coefficients. The Sobolev norms are given by

$$\left\| \frac{\partial^m}{\partial v^m} v \right\|_{q,\Gamma} \leq C \left\{ \sum_{k=1}^{n} k^{2(q+m)} (a_k^2 + b_k^2) \right\}^{\frac{1}{2}}, \quad m = 0, 1, \ldots. \tag{11.4.6}$$

By using (11.4.6), the second result (11.4.5) can be proved similarly. ■

Below, we discuss linear elastostatics and derive the errors of the MFS. To this end, we need the series expansions of the FS. For the simple FS and the principal FS with $\rho < R$, we cite two lemmas from addition theorems of FS in elastic problems in Appendix 11.7.

Lemma 11.4.4 (Addition Theorem A^e). *Let* $\rho < R$ *and* $r^2 = R^2 + \rho^2 - 2\rho R \times \cos(\phi - \theta)$*. There exist the series expansions of the simple FS by* $\nabla \ln r = \left(\frac{x-\xi}{r^2}, \frac{y-\eta}{r^2}\right)^T$*,*

$$\kappa \begin{pmatrix} \frac{x-\xi}{r^2} \\ \frac{y-\eta}{r^2} \end{pmatrix} = \frac{\kappa}{R} \sum_{n=0}^{\infty} \left(\frac{\rho}{R}\right)^n \begin{pmatrix} -\cos(n(\theta - \phi) - \phi) \\ \sin(n(\theta - \phi) - \phi) \end{pmatrix}.$$

Lemma 11.4.5 (Addition Theorem B^e). *Let* $\rho < R$*,* $a = \frac{\rho}{R}$ *and* $r^2 = R^2 + \rho^2 - 2\rho R \times \cos(\phi - \theta)$*. There exist the series expansions of the principal FS in (11.2.16),*

$$E_2(\mathbf{x}, \mathbf{y}) = \begin{pmatrix} T_{11} & T_{12} \\ T_{12} & T_{22} \end{pmatrix},$$

where the entries

$$\begin{aligned} T_{11} = (1 - \kappa) \Bigg\{ &- \left[\ln R - \sum_{n=1}^{\infty} \frac{1}{n} \left(\frac{\rho}{R}\right)^n \cos n(\theta - \phi) \right] \\ &+ D \left[\frac{1}{2} - \frac{a}{2} \cos(\theta + \phi) + \frac{1 - a^2}{2} \sum_{n=0}^{\infty} \left(\frac{\rho}{R}\right)^n \cos(n(\theta - \phi) - 2\phi) \right] \Bigg\}, \\ T_{22} = (1 - \kappa) \Bigg\{ &- \left[\ln R - \sum_{n=1}^{\infty} \frac{1}{n} \left(\frac{\rho}{R}\right)^n \cos n(\theta - \phi) \right] \\ &+ D \left[\frac{1}{2} + \frac{a}{2} \cos(\theta + \phi) - \frac{1 - a^2}{2} \sum_{n=0}^{\infty} \left(\frac{\rho}{R}\right)^n \cos(n(\theta - \phi) - 2\phi) \right] \Bigg\}, \\ T_{12} = (1 - \kappa) D &\left[-\frac{a}{2} \sin(\theta + \phi) - \frac{1 - a^2}{2} \sum_{n=0}^{\infty} \left(\frac{\rho}{R}\right)^n \sin(n(\theta - \phi) - 2\phi) \right]. \end{aligned}$$

11.4.2 Polynomials ∇P_n Approximated by $\left(\frac{x-\xi}{r^2}\right)$ and $\left(\frac{y-\eta}{r^2}\right)$

First, consider the simple FS of linear elastostatics. Denote the harmonic polynomials in (11.2.21) and (11.2.22) by

$$P_n(\rho,\theta) = d_0 + \sum_{k=1}^{n} \rho^k\{c_k \sin(k\theta) + d_k \cos(k\theta)\}, \tag{11.4.7}$$

where c_k and d_k are the coefficients. Denote the simple FS by

$$\vec{\Phi} = \nabla \ln r = \left(\frac{x-\xi}{r^2}, \frac{y-\eta}{r^2}\right)^T, \tag{11.4.8}$$

where $\nabla = \left(\frac{\partial}{\partial x}, \frac{\partial}{\partial y}\right)^T = \left(\frac{\partial}{\partial \rho}, \frac{\partial}{\rho \partial \theta}\right)^T$. Also we have

$$\nabla P_n(\rho,\theta) = \left(\frac{\partial P_n(\rho,\theta)}{\partial x}, \frac{\partial P_n(\rho,\theta)}{\partial y}\right)^T,$$

where

$$\begin{aligned}\frac{\partial P_n(\rho,\theta)}{\partial x} &= \sum_{k=1}^{n} k\rho^{k-1}\{c_k \sin(k-1)\theta + d_k \cos(k-1)\theta\},\\ \frac{\partial P_n(\rho,\theta)}{\partial y} &= \sum_{k=1}^{n} k\rho^{k-1}\{c_k \cos(k-1)\theta - d_k \sin(k-1)\theta\}.\end{aligned}$$

From Lemma 11.4.2, we have

$$\begin{aligned}\nabla P_n(\rho,\theta) = &\frac{d_0}{2\pi \ln R}\int_0^{2\pi} \nabla \ln r \; d\phi\\ &-\frac{1}{\pi}\sum_{k=1}^{n} kR^k \int_0^{2\pi} (\nabla \ln r)(c_k \sin(k\phi) + d_k \cos(k\phi))\, d\phi.\end{aligned} \tag{11.4.9}$$

In (11.4.9), the first term on the right-hand side is zero,

$$\int_0^{2\pi} \frac{x-\xi}{r^2}\, d\phi = \int_0^{2\pi} \frac{y-\eta}{r^2}\, d\phi = 0,$$

based on Lemma 11.4.4. By the trapezoidal rule we have

$$\begin{aligned}\nabla P_n(\rho,\theta) \approx &\frac{d_0}{2\pi \ln R}\widehat{\int_0^{2\pi}} \nabla \ln r \; d\phi\\ &-\frac{1}{\pi}\sum_{k=1}^{n} kR^k \widehat{\int_0^{2\pi}} (\nabla \ln r)(c_k \sin(k\phi) + d_k \cos(k\phi))\, d\phi = \sum_{i=1}^{n} \hat{\alpha}_i \vec{\Phi}_i,\end{aligned}$$

where $\vec{\Phi}_i$ is given in (11.4.8), and the constants are given from (11.4.3)

$$\hat{\alpha}_i = \frac{h}{2\pi \ln R} d_0 - \frac{h}{\pi} \sum_{k=1}^{n} k R^k \{c_k \sin(k\phi_i) + d_k \cos(k\phi_i)\}. \tag{11.4.10}$$

We also have

$$P_n(\rho, \theta) \approx \sum_{i=1}^{n} \hat{\alpha}_i \ln r_i.$$

Denote the special FS by

$$\Sigma_N(\nabla P_n, \vec{\Phi}; \rho, \theta) = \sum_{i=1}^{N} \hat{\alpha}_i \vec{\Phi}_i, \quad \Sigma_N(P_n, \ln r; \rho, \theta) = \sum_{i=1}^{N} \hat{\alpha}_i \ln r_i.$$

Theorem 11.4.1. *There exists the bound for $N > 2n$,*

$$\|\nabla P_n(\rho, \theta) - \Sigma_N(\nabla P_n, \vec{\Phi}; \rho, \theta)\|_{q,\Gamma} \leq C N^{q+1} \left(\frac{R}{r_{\max}}\right)^{2n-N} \left(\frac{r_{\max}}{r_{\min}}\right)^n \|P_n(\rho, \theta)\|_{0,\Gamma}, \tag{11.4.11}$$

where C is a constant independent of n and N.

Proof. We have

$$\nabla P_n(\rho, \theta) - \Sigma_N(\nabla P_n, \vec{\Phi}; \rho, \theta) = \nabla(P_n(\rho, \theta) - \Sigma_N(P_n, \ln r_i; \rho, \theta)).$$

Since $\nabla = \vec{n}\frac{\partial}{\partial n} + \vec{s}\frac{\partial}{\partial s}$, where $\vec{n}$ and $\vec{s}$ are the normal and the tangent directions of Γ, respectively, we have from Lemma 11.4.3

$$\begin{aligned}
&\|\nabla P_n(\rho, \theta) - \Sigma_N(\nabla P_n, \vec{\Phi}; \rho, \theta)\|_{q,\Gamma} \\
&\leq C\left\{ \|P_n(\rho, \theta) - \Sigma_N(P_n, \ln r; \rho, \theta)\|_{q+1,\Gamma} + \left\| \frac{\partial}{\partial v}(P_n(\rho, \theta) - \Sigma_N(P_n, \ln r; \rho, \theta)) \right\|_{q,\Gamma} \right\} \\
&\leq C N^{q+1} \left(\frac{R}{r_{\max}}\right)^{2n-N} \left(\frac{r_{\max}}{r_{\min}}\right)^n \|P_n(\rho, \theta)\|_{0,\Gamma}.
\end{aligned}$$

■

11.4.3 Other Proof for Theorem 11.4.1

Take the functions $\rho^m \sin(m\theta)$ in (11.4.7) for example. We derive the errors approximated by FS in (11.4.8). Using the orthogonality, we have from Lemma 11.4.4

$$\int_0^{2\pi} \frac{x - \xi}{r^2} \sin(n\phi)\, d\phi = -\frac{\pi}{R}\left(\frac{\rho}{R}\right)^{n-1} \sin(n-1)\theta,$$
$$\int_0^{2\pi} \frac{y - \eta}{r^2} \sin(n\phi)\, d\phi = -\frac{\pi}{R}\left(\frac{\rho}{R}\right)^{n-1} \cos(n-1)\theta.$$

Then we obtain

$$\begin{aligned}\nabla(\rho^m \sin(m\theta)) &= m\rho^{m-1}\begin{pmatrix}\sin(m-1)\theta\\ \cos(m-1)\theta\end{pmatrix}\\ &= -\frac{1}{\pi}mR^m\int_0^{2\pi}\begin{pmatrix}\frac{x-\xi}{r^2}\\ \frac{y-\eta}{r^2}\end{pmatrix}\sin(m\phi)\,d\phi \qquad (11.4.12)\\ &\approx -\frac{1}{\pi}mR^m\widehat{\int_0^{2\pi}}\begin{pmatrix}\frac{x-\xi}{r^2}\\ \frac{y-\eta}{r^2}\end{pmatrix}\sin(m\phi)\,d\phi.\end{aligned}$$

Also from Lemma 11.4.4,

$$\begin{aligned}&\int_0^{2\pi}\frac{x-\xi}{r^2}\sin(m\phi)\,d\phi\\ &= -\frac{1}{R}\int_0^{2\pi}\sum_{n=1}^{\infty}\left(\frac{\rho}{R}\right)^{n-1}\{\cos(n-1)\theta\ \cos(n\phi)+\sin(n-1)\theta\ \sin n\phi\}\sin(m\phi)\,d\phi.\end{aligned}$$

By the trigonometric formulas,

$$\begin{aligned}\cos(n\phi)\ \sin(m\phi) &= \frac{1}{2}(\sin(m+n)\phi-\sin(m-n)\phi),\\ \sin(n\phi)\ \sin(m\phi) &= \frac{1}{2}(-\cos(m+n)\phi+\cos(m-n)\phi),\end{aligned}$$

we have from Basic Lemma A in Part I

$$\begin{aligned}&\left(\int_0^{2\pi}-\widehat{\int_0^{2\pi}}\right)\frac{x-\xi}{r^2}\sin(m\phi)\,d\phi\\ &= -\frac{\pi}{R}\left\{-\sum_{n=-m+vN}^{\infty}\left(\frac{\rho}{R}\right)^{n-1}\sin(n-1)\theta+\sum_{n=m+vN}^{\infty}\left(\frac{\rho}{R}\right)^{n-1}\sin(n-1)\theta\right\}\\ &= \sum_{v=1}^{\infty}a^-_{v,m,n}\ \sin(n^- -1)\theta-\sum_{v=1}^{\infty}a^+_{v,m,n}\ \sin(n^+ -1)\theta, \qquad (11.4.13)\end{aligned}$$

where the integers and the coefficients are given by

$$\begin{aligned}&n^- = -m+vN-1, \quad n^+ = m+vN-1,\\ &a^-_{v,m,n} = \frac{\pi}{R}\left(\frac{\rho}{R}\right)^{-m+vN-1}, \quad a^+_{v,m,n} = \frac{\pi}{R}\left(\frac{\rho}{R}\right)^{m+vN-1}.\end{aligned}$$

Then we obtain from (11.4.12) and (11.4.13)

$$\begin{aligned}
ES1_m(\rho,\theta) &= \left\| \nabla \rho^m \sin(m\theta) - \left\{ -\frac{1}{\pi} mR^m \widehat{\int_0^{2\pi}} \frac{x-\xi}{r^2} \sin(m\phi)\, d\phi \right\} \right\|_{q,\Gamma} \\
&\le CmR^m \left\| \left(\int_0^{2\pi} - \widehat{\int_0^{2\pi}} \right) \frac{x-\xi}{r^2} \sin(m\phi)\, d\phi \right\|_{q,\Gamma} \\
&\le CmR^m \left\{ \sum_{v=1}^{\infty} (-m+vN)^{2q} (a^-_{v,m,n})^2 + \sum_{v=1}^{\infty} (m+vN)^{2q} (a^+_{v,m,n})^2 \right\}^{\frac{1}{2}} \\
&\le CmR^m \left\{ \sum_{v=1}^{\infty} (-m+vN)^{2q} \left(\frac{\rho}{R}\right)^{2(-m+vN-1)} + \sum_{v=1}^{\infty} (m+vN)^{2q} \left(\frac{\rho}{R}\right)^{2(m+vN-1)} \right\}^{\frac{1}{2}} \\
&\le CmR^m N^q \left(\frac{\rho}{R}\right)^{-m} \left\{ \sum_{v=1}^{\infty} v^{2q} \left(\frac{\rho}{R}\right)^{2vN} \right\}^{\frac{1}{2}} \le CmN^q R^m \left(\frac{\rho}{R}\right)^{N-m}. \qquad (11.4.14)
\end{aligned}$$

Similarly, we have

$$\begin{aligned}
&\left(\int_0^{2\pi} - \widehat{\int_0^{2\pi}} \right) \frac{y-\eta}{r^2} \sin(m\phi)\, d\phi \\
&= \frac{\pi}{2R} \left\{ \sum_{n=-m+vN}^{\infty} \left(\frac{\rho}{R}\right)^{n-1} \cos(n-1)\theta - \sum_{n=m+vN}^{\infty} \left(\frac{\rho}{R}\right)^{n-1} \cos(n-1)\theta \right\},
\end{aligned} \qquad (11.4.15)$$

to give

$$\begin{aligned}
ES2_m(\rho,\theta) &= \left\| m\rho^m \cos(m\theta) - \left\{ -\frac{1}{\pi} mR^m \widehat{\int_0^{2\pi}} \frac{y-\eta}{r^2} \sin(m\phi)\, d\phi \right\} \right\|_{q,\Gamma} \\
&\le CmN^q R^m \left(\frac{\rho}{R}\right)^{N-m}.
\end{aligned} \qquad (11.4.16)$$

For $0 < \tilde{\rho} \le \rho$, by the Schwarz inequality we have from (11.4.7), (11.4.12) and (11.4.14)–(11.4.16)

$$\begin{aligned}
&\|\nabla P(\rho,\theta) - \Sigma_N(\nabla P_n, \Phi; \rho, \theta)\|_{q,\Gamma} \\
&\le \sum_{m=1}^{n} \left\{ |c_m| \|ES1_m(\rho,\theta)\|_{q,\Gamma} + |d_m| \|ES2_m(\rho,\theta)\|_{q,\Gamma} \right\} \\
&= \sum_{m=1}^{n} \left\{ (|c_m|\tilde{\rho}^m) \frac{\|ES1_m(\rho,\theta)\|_{q,\Gamma}}{\tilde{\rho}^m} + (|d_m|\tilde{\rho}^m) \frac{\|ES2_m(\rho,\theta)\|_{q,\Gamma}}{\tilde{\rho}^m} \right\} \\
&\le \left\{ \sum_{m=1}^{n} c_m^2 \tilde{\rho}^{2m} \sum_{m=1}^{n} \frac{\|ES1_m(\rho,\theta)\|^2_{q,\Gamma}}{\tilde{\rho}^{2m}} \right\}^{\frac{1}{2}} + \left\{ \sum_{m=1}^{n} d_m^2 \tilde{\rho}^{2m} \sum_{m=1}^{n} \frac{\|ES2_m(\rho,\theta)\|^2_{q,\Gamma}}{\tilde{\rho}^{2m}} \right\}^{\frac{1}{2}}.
\end{aligned}$$

From (11.4.14) there exist the bounds,

$$\begin{aligned}\sum_{m=1}^{n}\frac{\|ES1_m(\rho,\theta)\|_{q,\Gamma}^2}{\tilde{\rho}^{2m}} &\le CN^{2q}\left(\frac{R}{\rho}\right)^{-2N}\sum_{m=1}^{n} m^2\frac{R^{2m}}{\tilde{\rho}^{2m}}\left(\frac{R}{\rho}\right)^{2m}\\ &\le CN^{2q}\left(\frac{R}{\rho}\right)^{-2N}\sum_{m=1}^{n} m^2\left(\frac{\rho}{\tilde{\rho}}\right)^{2m}\left(\frac{R}{\rho}\right)^{4m}\\ &\le CN^{2q}\left(\frac{R}{\rho}\right)^{-2N} n^2\left(\frac{\rho}{\tilde{\rho}}\right)^{2n}\left(\frac{R}{\rho}\right)^{4n}\\ &\le CN^{2q}n^2\left(\frac{R}{\rho}\right)^{4n-2N}\left(\frac{\rho}{\tilde{\rho}}\right)^{2n}.\end{aligned}$$

Similarly,

$$\sum_{m=1}^{n}\frac{\|ES2_m(\rho,\theta)\|_{q,\Gamma}^2}{\tilde{\rho}^{2m}} \le CN^{2q}n^2\left(\frac{R}{\rho}\right)^{4n-2N}\left(\frac{\rho}{\tilde{\rho}}\right)^{2n}.$$

Hence we have

$$\begin{aligned}\|\nabla P(\rho,\theta)-\Sigma_N(\nabla P_n,\Phi;\rho,\theta)\|_{q,\Gamma}^2 &\le CN^{2q}n^2\left(\frac{R}{\rho}\right)^{4n-2N}\left(\frac{\rho}{\tilde{\rho}}\right)^{2n}\times\sum_{m=1}^{n}\tilde{\rho}^{2m}(c_m^2+d_m^2)\\ &\le CN^{2q}n^2\left(\frac{R}{\rho}\right)^{4n-2N}\left(\frac{\rho}{\tilde{\rho}}\right)^{2n}\|P_n\|_{0,\Gamma}.\end{aligned}$$

We obtain for $2n<N$

$$\|\nabla P_n(\rho,\theta)-\Sigma_N(\nabla P_n,\vec{\Phi};\rho,\theta)\|_{q,\Gamma}\le CN^{q+1}\left(\frac{R}{r_{\max}}\right)^{2n-N}\left(\frac{r_{\max}}{r_{\min}}\right)^{n}\|P_n(\rho,\theta)\|_{0,\Gamma}.$$

This is the desired bound (11.4.11) in Theorem 11.4.1. ■

11.4.4 The Polynomials $\mathcal{L}P_n$ Approximated by Principal FS

Denote the principal FS vectors by $\vec{\Psi}_I=(\Psi_{1,1},\Psi_{1,2})^T$ and $\vec{\Psi}_{II}=(\Psi_{2,1},\Psi_{2,2})^T$, where the components are given by

$$\Psi_{1,1}=-\ln r+\frac{(x-\xi)^2}{r^2},\quad \Psi_{2,2}=-\ln r+\frac{(y-\eta)^2}{r^2},\quad \Psi_{1,2}=\Psi_{2,1}=\frac{(x-\xi)(y-\eta)}{r^2}.$$

Let the source nodes $(\xi_i,\eta_i)=(R\cos\phi_i, R\sin\phi_i)$ with $\phi_i=\frac{2\pi}{N}i$, and denote

$$\vec{\Psi}_I^{(i)}=(\Psi_{1,1}^{(i)},\Psi_{1,2}^{(i)})^T,\quad \vec{\Psi}_{II}^{(i)}=(\Psi_{2,1}^{(i)},\Psi_{2,2}^{(i)})^T,$$

where

$$\boldsymbol{\Psi}^{(i)}_{1,1} = -\ln r_i + \frac{(x-\xi_i)^2}{r_i^2}, \quad \boldsymbol{\Psi}^{(i)}_{2,2} = -\ln r_i + \frac{(y-\eta_i)^2}{r_i^2},$$
$$\boldsymbol{\Psi}^{(i)}_{1,2} = \boldsymbol{\Psi}^{(i)}_{2,1} = \frac{(x-\xi_i)(y-\eta_i)}{r_i^2},$$

and $r_i^2 = R^2 + \rho^2 - 2\rho R\cos(\phi_i - \theta)$. Denote the harmonic solutions by $\vec{u}^H = (\bar{u}, \bar{v})^T$. When $q(\vec{x}) = 0$, the solutions of the Cauchy–Navier equation are given from Theorem 11.2.3,

$$\vec{w} = \mathcal{L}\vec{u}^H = (1-\kappa)\begin{pmatrix} \bar{u} \\ \bar{v} \end{pmatrix} + \kappa \begin{pmatrix} x\frac{\partial \bar{u}}{\partial x} + y\frac{\partial \bar{v}}{\partial x} \\ x\frac{\partial \bar{u}}{\partial y} + y\frac{\partial \bar{v}}{\partial y} \end{pmatrix}, \tag{11.4.17}$$

where the operator is

$$\mathcal{L} = (1-\kappa)I_2 + \kappa\vec{x}\cdot\nabla. \tag{11.4.18}$$

For the harmonic solutions $\vec{u}^H$, the derivatives satisfy

$$\frac{\partial \bar{u}}{\partial x} = \frac{\partial \bar{v}}{\partial y}, \quad \frac{\partial \bar{v}}{\partial x} = -\frac{\partial \bar{u}}{\partial y}. \tag{11.4.19}$$

Let the harmonic polynomials of $\bar{u}$ and $\bar{v}$ be chosen as in (11.2.21) and (11.2.22),

$$\bar{u} = \hat{P}_n = b_0 + \sum_{k=1}^{L} r^k\{-a_k \sin(k\theta) + b_k \cos(k\theta)\}, \tag{11.4.20}$$

$$\bar{v} = \hat{Q}_n = a_0 + \sum_{k=1}^{L} r^k\{a_k \cos(k\theta) + b_k \sin(k\theta)\}. \tag{11.4.21}$$

For (11.4.20), denote the special combinations of FS by

$$\boldsymbol{\Sigma}_N(\mathcal{L}\hat{P}_n, \vec{\boldsymbol{\Psi}}_I; \rho, \theta) = \sum_{i=1}^{N} \hat{\beta}_i \vec{\boldsymbol{\Psi}}^{(i)}_I, \quad \boldsymbol{\Sigma}_N(\hat{P}_n, \ln r; \rho, \theta) = \sum_{i=1}^{N} \hat{\beta}_i \ln r_i, \tag{11.4.22}$$

where the coefficients $\hat{\beta}_i$ are also provided from (11.4.3),

$$\hat{\beta}_i = \frac{h}{2\pi \ln R} b_0 - \frac{h}{\pi}\sum_{k=1}^{n} kR^k\{-a_k \sin(k\phi_i) + b_k \cos(k\phi_i)\}. \tag{11.4.23}$$

Theorem 11.4.2. *For large $N\,(> 2n)$, there exists the bound,*

$$\left\| \begin{pmatrix} \mathcal{L}\hat{P}_n \\ 0 \end{pmatrix} - \boldsymbol{\Sigma}_N(\mathcal{L}\hat{P}_n, \vec{\boldsymbol{\Psi}}_I; \rho, \theta) \right\|_{q,\Gamma} \le CN^{q+1}\left(\frac{R}{r_{\max}}\right)^{2n-N}\left(\frac{r_{\max}}{r_{\min}}\right)^{n} \|\hat{P}_n(\rho,\theta)\|_{0,\Gamma},$$

where C is a constant independent of n and N.

Proof. The proof follows from that in Theorem 11.4.1. We have from Lemma 11.4.2

$$\begin{aligned}\begin{pmatrix}\mathcal{L}\hat{P}_n\\0\end{pmatrix} &= \frac{b_0}{2\pi\ \ln R}\int_0^{2\pi}\mathcal{L}\ln r\ d\phi - \frac{1}{\pi}\sum_{k=1}^{n}kR^k\int_0^{2\pi}(\mathcal{L}\ln r)\{-a_k\ \sin(k\phi)+b_k\ \cos(k\phi)\}d\phi\\ &\approx \frac{b_0}{2\pi\ \ln R}\widehat{\int_0^{2\pi}}\mathcal{L}\ln r\ d\phi - \frac{1}{\pi}\sum_{k=1}^{n}kR^k\widehat{\int_0^{2\pi}}(\mathcal{L}\ln r)\{-a_k\ \sin(k\phi)+b_k\ \cos(k\phi)\}d\phi\\ &= \sum_{i=1}^{N}\hat{\beta}_i\vec{\Psi}_I^{(i)} = \Sigma_N(\mathcal{L}\hat{P}_n,\vec{\Psi}_I;\rho,\theta).\end{aligned}$$

Then by noting the operator $\mathcal{L}$ in (11.4.18),

$$\begin{aligned}&\left\|\begin{pmatrix}\mathcal{L}\hat{P}_n\\0\end{pmatrix} - \Sigma_N(\mathcal{L}\hat{P}_n,\vec{\Psi}_I;\rho,\theta)\right\|_{q,\Gamma} = \|\mathcal{L}\hat{P}_n - \Sigma_N(\hat{P}_n,\ln r;\rho,\theta)\|_{q,\Gamma}\\ &\le C\left\{\left\|\frac{\partial}{\partial v}(\hat{P}_n - \Sigma_N(\hat{P}_n,\ln r;\rho,\theta))\right\|_{q,\Gamma} + \|\hat{P}_n - \Sigma_N(\hat{P}_n,\ln r;\rho,\theta)\|_{q+1,\Gamma}\right\}\\ &\le CN^{q+1}\left(\frac{R}{r_{\max}}\right)^{2n-N}\left(\frac{r_{\max}}{r_{\min}}\right)^{n}\|\hat{P}_n(\rho,\theta)\|_{0,\Gamma}.\end{aligned}$$

■

Next for $\hat{Q}_n$ in (11.4.21), denote

$$\Sigma_N(\mathcal{L}\hat{Q}_n,\vec{\Psi}_{II};\rho,\theta) = \sum_{i=1}^{N}\hat{\gamma}_i\vec{\Psi}_{II}^{(i)},\quad \Sigma_N(\hat{Q}_n,\ln r;\rho,\theta) = \sum_{i=1}^{N}\hat{\gamma}_i\ \ln r_i,$$

where

$$\hat{\gamma}_i = \frac{h}{2\pi\ \ln R}a_0 - \frac{h}{\pi}\sum_{k=1}^{n}kR^k\{a_k\ \cos(k\phi_i)+b_k\ \sin(k\phi_i)\}. \tag{11.4.24}$$

Similarly, we have the following theorem.

Theorem 11.4.3. *For large $N\,(> 2n)$, there exists the bound,*

$$\left\|\begin{pmatrix}0\\\mathcal{L}\hat{Q}_n\end{pmatrix} - \Sigma_N(\mathcal{L}\hat{Q}_n,\vec{\Psi}_{II};\rho,\theta)\right\|_{q,\Gamma} \le CN^{q+1}\left(\frac{R}{r_{\max}}\right)^{2n-N}\left(\frac{r_{\max}}{r_{\min}}\right)^{n}\|\hat{Q}_n(\rho,\theta)\|_{0,\Gamma}.$$

Combining Theorems 11.4.2 and 11.4.3 gives the following theorem.

Theorem 11.4.4. *For large $N\,(> 2n)$, there exists the bound,*

$$\left\|\begin{pmatrix}\mathcal{L}\hat{P}_n - \Sigma_N(\mathcal{L}\hat{P}_n,\vec{\Psi}_I;\rho,\theta)\\\mathcal{L}\hat{Q}_n - \Sigma_N(\mathcal{L}\hat{Q}_n,\vec{\Psi}_{II};\rho,\theta)\end{pmatrix}\right\|_{q,\Gamma} \le CN^{q+1}\left(\frac{R}{r_{\max}}\right)^{2n-N}\left(\frac{r_{\max}}{r_{\min}}\right)^{n}\Big(\|\hat{P}_n\|_{0,\Gamma} + \|\hat{Q}_n\|_{0,\Gamma}\Big).$$

We may also use Lemma 11.4.5 to derive the error bounds as done in Section 11.4.3; details are omitted.

11.5 Error Bounds for MFS and HTM

11.5.1 The MFS

We will derive the error bounds of the CTM using FS in (11.3.5) without integration approximation, and those of the MFS with integration approximation may follow [169] to obtain similar error bounds.

The harmonic solutions are given by $(u^H, v^H)^T$ and q^H in (11.2.7), and in general, two kinds of FS are also needed. The solutions are denoted by

$$\vec{w} = \mathcal{L}\begin{pmatrix} u^H \\ v^H \end{pmatrix} = \mathcal{L}\begin{pmatrix} \hat{P}_n \\ \hat{Q}_n \end{pmatrix} + \nabla P_n + \mathcal{L}\vec{\hat{R}}_n + \nabla R_n,$$

where the operator $\mathcal{L}$ is given in (11.4.18), and the residual terms are given by

$$\vec{\hat{R}}_n = \begin{pmatrix} \sum\limits_{k=n+1}^{\infty} \rho^k\{-a_k \sin(k\theta) + b_k \cos(k\theta)\} \\ \sum\limits_{k=n+1}^{\infty} \rho^k\{a_k \cos(k\theta) + b_k \sin(k\theta)\} \end{pmatrix},$$

$$R_n = \sum_{k=n+1}^{\infty} \rho^k\{c_k \sin(k\theta) + d_k \cos(k\theta)\}.$$

Assume that for harmonic solutions, there exist the regularities,

$$u^H, v^H, q^H \in \mathbf{H}^{t+1}(S) \ \left(t \geq \frac{3}{2}\right). \tag{11.5.1}$$

Then there exist the bounds of the residuals,

$$\|\mathcal{L}\vec{\hat{R}}_n\|_{k,S} \leq C\frac{1}{n^{(t-k)}}\left(\|u^H\|_{t+1,S} + \|v^H\|_{t+1,S}\right),$$

$$\|\nabla R_n\|_{k,S} \leq C\frac{1}{n^{(t-k)}}\|q^H\|_{t+1,S}.$$

In the MFS, choose the general FS in (11.2.17) and (11.2.18) as

$$\vec{w}_N = \sum_{i=1}^{N}\{\beta_i\vec{\Psi}_I^{(i)} + \gamma_i\vec{\Psi}_{II}^{(i)} + \alpha_i\vec{\Phi}_i\}, \tag{11.5.2}$$

where α_i, β_i and γ_i are constants. Denote by V_N the set of all FS in (11.5.2), and a specific FS by

$$\mathbf{\Sigma}_N = \mathbf{\Sigma}_N(\hat{P}_n, \hat{Q}_n, P_n; \vec{\mathbf{\Psi}}_I, \vec{\mathbf{\Psi}}_{II}, \vec{\mathbf{\Phi}}; \rho, \theta) = \sum_{i=1}^{N} \{\hat{\beta}_i \vec{\mathbf{\Psi}}_I^{(i)} + \hat{\gamma}_i \vec{\mathbf{\Psi}}_{II}^{(i)} + \hat{\alpha}_i \vec{\mathbf{\Phi}}_i\}, \tag{11.5.3}$$

where the coefficients $\hat{\beta}_i$, $\hat{\gamma}_i$ and $\hat{\alpha}_i$ are given in (11.4.23), (11.4.24) and (11.4.10), respectively. Evidently, we have $\mathbf{\Sigma}_N \subset V_N$. Denote $\vec{w} = (u, v)^T$, $\vec{w}_N = (u_N, v_N)^T$ and $\|\vec{w}\|_{0,\Gamma}^2 = \|u\|_{0,\Gamma}^2 + \|v\|_{0,\Gamma}^2$.

Theorem 11.5.1. *Let (11.5.1) hold. For large $N\,(> 2n)$, the solutions $\vec{w}$ by the MFS have the error bound,*

$$\|\vec{w} - \vec{w}_N\|_{0,\Gamma} \le C \left\{ \frac{1}{n^{t-\frac{1}{2}}} + N \left(\frac{R}{r_{\max}} \right)^{2n-N} \left(\frac{r_{\max}}{r_{\min}} \right)^n \right\}, \tag{11.5.4}$$

where C is a constant independent of n and N.

Proof. From the MFS using FS in (11.3.5) we have

$$\|\vec{w} - \vec{w}_N\|_{0,\Gamma} \le C \inf_{\vec{v} \in V_N} \|\vec{w} - \vec{v}\|_{0,\Gamma}.$$

We choose the specific admissible functions $\vec{v} = \mathbf{\Sigma}_N$, and obtain

$$\begin{aligned} \|\vec{w} - \vec{w}_N\|_{0,\Gamma} &\le C \|\vec{w} - \mathbf{\Sigma}_N\|_{0,\Gamma} \\ &\le C \Big\{ \|\mathcal{L}\hat{P}_n - \mathbf{\Sigma}_N(\mathcal{L}\hat{P}_n; \vec{\mathbf{\Psi}}_I; \rho, \theta)\|_{0,\Gamma} + \|\mathcal{L}\hat{Q}_n - \mathbf{\Sigma}_N(\mathcal{L}\hat{Q}_n; \vec{\mathbf{\Psi}}_{II}; \rho, \theta)\|_{0,\Gamma} \\ &\quad + \|\nabla P_n - \mathbf{\Sigma}_N(\nabla P_n; \vec{\mathbf{\Phi}}; \rho, \theta)\|_{0,\Gamma} + \|\mathcal{L}\vec{\hat{R}}_n\|_{0,\Gamma} + \|\nabla R_n\|_{0,\Gamma} \Big\}. \end{aligned} \tag{11.5.5}$$

By the embedding theorem

$$\|v\|_{0,\Gamma} \le C \|v\|_{\frac{1}{2},S} \le C \sqrt{\|v\|_{0,S} \|v\|_{1,S}},$$

we obtain the bound from the assumption (11.5.1),

$$\|\mathcal{L}\vec{\hat{R}}_n\|_{0,\Gamma} + \|\nabla R_n\|_{0,\Gamma} \le C \frac{1}{n^{t-\frac{1}{2}}} \left\{ \|u^H\|_{t+1,S} + \|v^H\|_{t+1,S} + \|q^H\|_{t+1,S} \right\}.$$

Since the other terms in (11.5.5) are the errors between FS and PS, which are obtained from Theorems 11.4.1 and 11.4.4 by noting $\|P_n(\rho, \theta)\|_{0,\Gamma}$, $\|\hat{P}_n(\rho, \theta)\|_{0,\Gamma}$, $\|\hat{Q}_n(\rho, \theta)\|_{0,\Gamma} \le C$. The desired bound (11.5.4) is obtained. ■

Corollary 11.5.1. *Let the conditions in Theorem 11.5.1 hold. Choose $N = O(n)$ such that*

$$\left(\frac{R}{r_{\max}} \right)^{2n-N} \left(\frac{r_{\max}}{r_{\min}} \right)^n = O\left(\frac{1}{n^{t+\frac{1}{2}}} \right).$$

Then there exists the bound,

$$\|u - u_N\|_{0,\Gamma} + \|v - v_N\|_{0,\Gamma} \le C\frac{1}{N^{t-\frac{1}{2}}}.$$

Proof. Choose

$$\left(\frac{R}{r_{\max}}\right)^{2n-N}\left(\frac{r_{\max}}{r_{\min}}\right)^{n} = \frac{1}{n^{t+\frac{1}{2}}}.$$

We have

$$(2n - N)\ln\left(\frac{R}{r_{\max}}\right) + n\,\ln\left(\frac{r_{\max}}{r_{\min}}\right) = -\left(t + \frac{1}{2}\right)\ln n,$$

to give

$$N = 2n + \frac{1}{\ln\left(\frac{R}{r_{\max}}\right)}\left\{n\,\ln\left(\frac{r_{\max}}{r_{\min}}\right) + \left(t + \frac{1}{2}\right)\ln n\right\} \le Cn.$$

Hence we have

$$N\left(\frac{R}{r_{\max}}\right)^{2n-N}\left(\frac{r_{\max}}{r_{\min}}\right)^{n} \le C\frac{1}{n^{t-\frac{1}{2}}}.$$

This completes the proof of Corollary 11.5.1 by noting $\frac{1}{n} \le C\frac{1}{N}$. ■

11.5.2 The HTM Using FS

Consider a 2D solution domain S, and denote its boundary by $\Gamma\,(= \partial S)$. By following [153], we will derive the error bounds of the HTM using FS for the mixed boundary conditions with $\Gamma_D \neq \emptyset$. For the pure traction condition (*i.e.*, $\Gamma = \Gamma_N$), the analysis is similar (see [153]). For the HTM (11.3.3), we assume that the following three conditions hold.

(A1) For $A(\vec{w}, \vec{v})$ in (11.2.4), there exist the bounds,

$$c_0\|\vec{v}\|^2_{1,\Omega} \le A(\vec{v}, \vec{v}), \quad |A(\vec{w}, \vec{v})| \le C\|\vec{w}\|_{1,S}\|\vec{v}\|_{1,S}, \quad \forall \vec{v} \in V_N.$$

(A2) For $\int_{\Gamma_N}\vec{\tau}(\vec{v})\cdot\vec{\eta}$, where $\vec{\tau}(\vec{v})$ is the traction given in (11.2.14) and (11.2.15), the Ladyzhenskaya-Babuska-Brezzi (LBB) condition holds: $\forall\vec{\eta}_p \in \mathbf{T}_p$, $\exists\vec{v}_N \in V_N$, $\vec{v}_N \neq 0$ such that

$$\left|\int_{\Gamma_N}\vec{\tau}(\vec{v}_N)\cdot\vec{\eta}_p d\sigma\right| \ge c_0\|\vec{v}_N\|_{1,S}\|\vec{\eta}_p\|_{\frac{1}{2},\Gamma_N}.$$

(A3) Also the following bound holds,

$$\left|\int_{\Gamma_N}\vec{\tau}(\vec{v})\cdot\vec{\xi}d\sigma\right| \le C\|\vec{\xi}\|_{\frac{1}{2},\Gamma_N}\|\vec{v}\|_{1,S}, \quad \vec{v} \in V_N.$$

In **(A1)**, **(A2)** and **(A3)**, c_0 and C are positive constants independent of N and p.

We cite a theorem from Li *et al.* [153].

Theorem 11.5.2. *Let* **(A1)**–**(A3)** *and* $\mathbf{\Gamma}_D \neq \emptyset$ *hold. There exists the error bound,*

$$\|\vec{w} - \vec{w}_N\|_{1,\Omega} + \|\vec{\xi} - \vec{\xi}_p\|_{\frac{1}{2},\Gamma_N} \leq C\left\{\inf_{\vec{v}\in V_N} \|\vec{w} - \vec{v}\|_{1,\Omega} + \inf_{\vec{\eta}\in \mathbf{T}_p} \|\vec{\xi} - \vec{\eta}\|_{\frac{1}{2},\Gamma_N}\right\}.$$

Below, we will derive the explicit error bounds from Theorem 11.5.2. Choose $\vec{\eta} = \vec{\xi}_p^{\,*} \in \mathbf{T}_p$, where $\vec{\xi}_p^{\,*}$ is the interpolation polynomial of order p. When the assumptions (11.5.1) hold, we have $\vec{\xi}\,(= \vec{w}) \in \mathbf{H}^{t-\frac{1}{2}}(\mathbf{\Gamma}_N)$. Then there exists the bound,

$$\|\vec{\xi} - \vec{\xi}_p\|_{\frac{1}{2},\Gamma_N} \leq C\frac{1}{p^{t-1}}\|\vec{\xi}\|_{t-\frac{1}{2},\Gamma_N}.$$

Also let $\mathbf{\Sigma}_N = \mathbf{\Sigma}_N(\hat{P}_n, \hat{Q}_n, P_n; \vec{\mathbf{\Psi}}_I, \vec{\mathbf{\Psi}}_{II}, \vec{\mathbf{\Phi}})$ in (11.5.3). We have from Theorem 11.5.2

$$\begin{aligned}
&\|\vec{w} - \vec{w}_N\|_{1,\Omega} + \|\vec{\xi} - \vec{\xi}_p\|_{\frac{1}{2},\Gamma_N} \leq C\left\{\|\vec{w} - \mathbf{\Sigma}_N\|_{1,\Omega} + \|\vec{\xi} - \vec{\eta}_p^{\,*}\|_{\frac{1}{2},\Gamma_N}\right\}\\
&\leq C\Big\{\|\mathcal{L}\hat{P}_n - \mathbf{\Sigma}_N(\mathcal{L}\hat{P}_n, \vec{\mathbf{\Psi}}_I; \rho, \theta)\|_{1,S} + \|\mathcal{L}\hat{Q}_n - \mathbf{\Sigma}_N(\mathcal{L}\hat{Q}_n, \vec{\mathbf{\Psi}}_{II}; \rho, \theta)\|_{1,S}\\
&\quad + \|\nabla P_n - \mathbf{\Sigma}_N(\nabla P_n; \vec{\mathbf{\Phi}}; \rho, \theta)\|_{1,S} + \|\mathcal{L}\vec{\hat{R}}_n\|_{1,S} + \|\nabla R_n\|_{1,S} + O\left(\frac{1}{p^{t-1}}\right)\Big\}.
\end{aligned}$$

When the equations (11.5.1) hold, there also exist the bounds,

$$\|\mathcal{L}\vec{\hat{R}}_n\|_{1,S} \leq C\frac{1}{n^{t-1}}\left(\|u^H\|_{t+1,S} + \|v^H\|_{t+1,S}\right), \quad \|\nabla R_n\|_{1,S} \leq C\frac{1}{n^{t-1}}\|q^H\|_{t+1,S}.$$

Lemma 11.5.1. *Let* $\Gamma_D \neq \emptyset$ *and* $\vec{v}$ *satisfy (11.2.9) and (11.2.10). There exists the bound,*

$$\|\vec{v}\|_{1,S}^2 \leq C\|\vec{v}\|_{0,\Gamma}\left\{\|\vec{v}\|_{1,\Gamma} + \left\|\frac{\partial}{\partial \nu}\vec{v}\right\|_{0,\Gamma}\right\}.$$

Proof. For $\mathbf{\Gamma}_D \neq \emptyset$, the norms $|\vec{v}|_{1,S}$ and $\|\vec{v}\|_{1,S}$ are equivalent to each other ([195]). Since $\vec{v}$ satisfies the governing equations (11.2.9) and (11.2.10), we have from Theorem 11.2.1 and (11.2.5)

$$\begin{aligned}
\|\vec{v}\|_{1,S}^2 &\leq CA(\vec{v}, \vec{v}) = C\int_\Gamma \vec{\tau}(\vec{v}) \cdot \vec{v}\, d\sigma\\
&\leq C\|\vec{v}\|_{0,\Gamma}\, \|\, \vec{\tau}(\vec{v})\|_{0,\Gamma} \leq C\|\vec{v}\|_{0,\Gamma}\left\{\|\vec{v}\|_{1,\Gamma} + \left\|\frac{\partial}{\partial \nu}\vec{v}\right\|_{0,\Gamma}\right\},
\end{aligned}$$

by noting (11.2.14) and (11.2.15). This completes the proof of Lemma 11.5.1. ■

We may prove the following lemma similarly.

Lemma 11.5.2. *For large $N\,(>2n)$, there exist the bounds,*

$$\left\|\frac{\partial}{\partial v}\begin{pmatrix}\mathcal{L}\hat{P}_n-\Sigma_N(\mathcal{L}\hat{P}_n,\vec{\Psi}_I;\rho,\theta)\\ \mathcal{L}\hat{Q}_n-\Sigma_N(\mathcal{L}\hat{Q}_n,\vec{\Psi}_{II};\rho,\theta)\end{pmatrix}\right\|_{q,\Gamma}$$

$$\leq CN^{q+2}\left(\frac{R}{r_{\max}}\right)^{2n-N}\left(\frac{r_{\max}}{r_{\min}}\right)^{n}\left(\|\hat{P}_n\|_{0,\Gamma}+\|\hat{Q}_n\|_{0,\Gamma}\right),$$

$$\left\|\frac{\partial}{\partial v}\{\nabla P_n-\Sigma_N(\nabla P_n,\vec{\Phi};\rho,\theta)\}\right\|_{q,\Gamma}\leq CN^{q+2}\left(\frac{R}{r_{\max}}\right)^{2n-N}\left(\frac{r_{\max}}{r_{\min}}\right)^{n}\|P_n\|_{0,\Gamma}.$$

Based on Lemmas 11.5.1, 11.5.2 and Theorems 11.4.1, 11.4.4, we have

$$\left\|\begin{pmatrix}\mathcal{L}\hat{P}_n-\Sigma_N(\mathcal{L}\hat{P}_n,\vec{\Psi}_I;\rho,\theta)\\ \mathcal{L}\hat{Q}_n-\Sigma_N(\mathcal{L}\hat{Q}_n,\vec{\Psi}_{II};\rho,\theta)\end{pmatrix}\right\|_{q,S}$$

$$\leq CN^{q+\frac{3}{2}}\left(\frac{R}{r_{\max}}\right)^{2n-N}\left(\frac{r_{\max}}{r_{\min}}\right)^{n}\left(\|\hat{P}_n\|_{0,\Gamma}+\|\hat{Q}_n\|_{0,\Gamma}\right),$$

$$\|\nabla P_n-\Sigma_N(\nabla P_n,\vec{\Phi};\rho,\theta)\|_{q,S}\leq CN^{q+\frac{3}{2}}\left(\frac{R}{r_{\max}}\right)^{2n-N}\left(\frac{r_{\max}}{r_{\min}}\right)^{n}\|P_n\|_{0,\Gamma}.$$

Hence we have the following theorem.

Theorem 11.5.3. *Let (11.5.1) hold. For large $N\,(>2n)$, the solutions $\vec{w}_N$ and $\vec{\xi}_p$ by the HTM have the error bound,*

$$\|\vec{w}-\vec{w}_N\|_{1,S}+\|\vec{\xi}-\vec{\xi}_p\|_{\frac{1}{2},\Gamma_N}\leq C\left\{\frac{1}{n^{t-1}}+\frac{1}{p^{t-1}}+N^{\frac{3}{2}}\left(\frac{R}{r_{\max}}\right)^{2n-N}\left(\frac{r_{\max}}{r_{\min}}\right)^{n}\right\},$$

where C is a constant independent of n and N.

Corollary 11.5.2. *Let the conditions in Theorem 11.5.3 hold. Choose $p=O(n)$ and N such that $\left(\frac{R}{r_{\max}}\right)^{2n-N}\left(\frac{r_{\max}}{r_{\min}}\right)^{n}=O\left(\frac{1}{n^{t+\frac{1}{2}}}\right)$. Then there exists the error bound,*

$$\|\vec{w}-\vec{w}_N\|_{1,S}+\|\vec{\xi}-\vec{\xi}_p\|_{\frac{1}{2},\Gamma_N}=O\left(\frac{1}{N^{t-1}}\right).$$

11.6 Numerical Experiments

In the unit square domain $S=\{(x,y)|0<x<1,0<y<1\}$, choose the following exact solutions of (11.2.9) and (11.2.10),

$$\begin{aligned}\begin{pmatrix} u \\ v \end{pmatrix} = (1-\kappa)&\begin{pmatrix} e^x \cos y \\ e^x \sin y \end{pmatrix} \\ -\kappa&\left[\begin{pmatrix} xe^x \cos y + ye^x \sin y \\ -xe^x \sin y + ye^x \cos y \end{pmatrix} + \begin{pmatrix} -\pi\ \sin(\pi x)\cosh(\pi y) \\ \pi\ \cos(\pi x)\sinh(\pi y) \end{pmatrix}\right].\end{aligned} \tag{11.6.1}$$

Consider the mixed type of the displacement and the traction boundary conditions in Figure 11.1,

$$u = \bar{u}, \quad v = \bar{v} \text{ on } \overline{AB} \cup \overline{CD} \cup \overline{DA},$$
$$\tau_1 = \bar{\tau}_1, \quad \tau_2 = \bar{\tau}_2 \text{ on } \overline{BC},$$

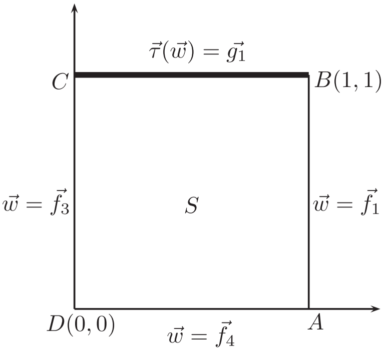

FIG. 11.1 – The solution domain S.

where the traction conditions in (11.2.14) and (11.2.15) are simplified as

$$\tau_1 = \mu(u_y + v_x), \quad \tau_2 = \lambda u_x + (\lambda + 2\mu) v_y, \tag{11.6.2}$$

and $\bar{u}, \bar{v}$, $\bar{\tau}_1$ and $\bar{\tau}_2$ are given directly from (11.6.1).

In computation, let $\lambda = \mu = 1$ and $D = 0.5$. Choose the general fundamental solutions in (11.2.17) and (11.2.18), where $R = 1.2$, and a_i, b_i and c_i are unknown coefficients to be sought. Let m denote the number of collocation nodes of each edge of ∂S, and choose $m = 50$. We obtain the over-determined system (11.3.11). Denote the errors $\varepsilon = \vec{w} - \vec{w}_N = \{(u - u_N)^2 + (v - v_N)^2\}^{\frac{1}{2}}$, and

$$\|\varepsilon\|_{0,S} = \left\{\iint_S \varepsilon^2 ds\right\}^{\frac{1}{2}}, \quad |\varepsilon|_{1,S} = \left\{\iint_S ({\varepsilon_x}^2 + {\varepsilon_y}^2) ds\right\}^{\frac{1}{2}},$$

where ${\varepsilon_x}^2 = [u_x - (u_N)_x]^2 + [v_x - (v_N)_x]^2$ and ${\varepsilon_y}^2 = [u_y - (u_N)_y]^2 + [v_y - (v_N)_y]^2$. Denote the maximal boundary errors on Γ,

$$\|\varepsilon\|_{\infty,\Gamma} = \max_{\Gamma}\{(u - u_N)^2 + (v - v_N)^2\}^{\frac{1}{2}},$$

$$\|\vec{\tau}-\vec{\tau}_N\|_{\infty,\Gamma}=\max_{\Gamma}\{[\tau_x-(\tau_x)_N]^2+[\tau_y-(\tau_y)_N]^2\}^{\frac{1}{2}},$$

where $\boldsymbol{\Gamma}=\partial S=\overline{AB}\cup\overline{BC}\cup\overline{CD}\cup\overline{DA}$.

The errors and the condition numbers by the MFS are given in Table 11.1. All computations are performed by using 50 decimal working digits. From Table 11.1 we can see

$$\begin{aligned}&\|\varepsilon\|_{\infty,\Gamma}=O(0.83^{3N}),\quad \|\varepsilon\|_{0,S}=O(0.81^{3N}),\quad |\varepsilon|_{1,S}=O(0.83^{3N}),\\ &\|\tau-\tau_N\|_{\infty,\overline{BC}}=O(0.85^{3N}),\quad \text{Cond}=O(1.25^{3N}),\quad \text{Cond\_eff}=O(1.22^{3N}).\end{aligned}\tag{11.6.3}$$

TAB. 11.1 – The errors and the condition numbers for the mixed type of displacement and traction conditions by the MFS using FS in (11.2.17) and (11.2.18).

N	$\|\varepsilon\|_{\infty,\Gamma}$	$\|\varepsilon\|_{0,S}$	$\|\varepsilon\|_{1,S}$	$\|\vec{\tau}-\vec{\tau}_L\|_{\infty,\overline{BC}}$	Cond	Cond_eff	$\|\mathbf{y}\|$
6	1.57	0.573	5.44	13.3	78.9	4.84	87.5
10	0.200	4.70 (−2)	0.781	2.05	1.30 (3)	66.5	59.2
14	6.97 (−2)	6.51 (−3)	0.139	0.955	1.95 (4)	177	244
18	4.58 (−3)	1.82 (−4)	5.72 (−3)	0.157	3.22 (5)	3.50 (3)	167
22	4.82 (−4)	5.33 (−6)	2.12 (−4)	1.61 (−2)	5.11 (6)	5.46 (4)	148
26	3.83 (−5)	1.40 (−7)	7.99 (−6)	1.27 (−3)	6.54 (7)	7.29 (5)	127
30	3.41 (−6)	5.40 (−9)	3.26 (−7)	1.19 (−4)	7.75 (8)	7.51 (6)	134

Next, we try to choose a_i and b_i only (*i.e.*, $c_i=0$) in (11.2.17) and (11.2.18), and the numerical results by the MFS are listed in Table 11.2. We can also see from Table 11.2

$$\begin{aligned}&\|\varepsilon\|_{\infty,\Gamma}=O(0.76^{2N}),\quad \|\varepsilon\|_{0,S}=O(0.74^{2N}),\quad |\varepsilon|_{1,S}=O(0.76^{2N}),\\ &\|\tau-\tau_N\|_{\infty,\overline{BC}}=O(0.78^{2N}),\quad \text{Cond}=O(1.21^{2N}),\quad \text{Cond\_eff}=O(1.20^{2N}).\end{aligned}\tag{11.6.4}$$

TAB. 11.2 – The errors and the condition numbers for the mixed type of displacement and traction conditions by the MFS using FS in (11.2.17) and (11.2.18) with $c_i=0$.

N	$\|\varepsilon\|_{\infty,\Gamma}$	$\|\varepsilon\|_{0,S}$	$\|\varepsilon\|_{1,S}$	$\|\vec{\tau}-\vec{\tau}_L\|_{\infty,\overline{BC}}$	Cond	Cond_eff	$\|\mathbf{y}\|$
9	3.67	0.989	8.23	41.4	88.0	4.67	112
15	0.353	7.71 (−2)	0.769	6.38	751	44.2	62.8
21	1.22 (−2)	2.05 (−3)	3.58 (−2)	0.312	8.68 (3)	378	66.0
27	1.72 (−4)	2.30 (−5)	6.68 (−4)	1.57 (−2)	7.70 (4)	3.04 (3)	61.8
33	9.54 (−6)	9.28 (−7)	2.91 (−5)	8.22 (−4)	8.16 (5)	3.17 (4)	55.7
39	3.34 (−7)	2.58 (−8)	1.04 (−6)	3.35 (−5)	8.54 (6)	3.27 (5)	51.2
45	1.13 (−8)	7.06 (−10)	3.11 (−8)	1.01 (−6)	8.25 (7)	3.14 (6)	47.7

Comparing (11.6.4) with (11.6.3), we conclude that using two coefficients a_i and b_i yields better accuracy and stability. Hence we may simply choose a_i and b_i only.

Third, we choose the MPS using the PS in (11.2.21) and (11.2.22), where a_k, b_k, c_k and d_k are the unknown coefficients to be sought. The numerical results are listed in Table 11.3. We can see from Table 11.3

$$\begin{aligned}&\|\varepsilon\|_{\infty,\Gamma} = O(0.65^{4L}), \quad \|\varepsilon\|_{0,S} = O(0.64^{4L}), \quad |\varepsilon|_{1,S} = O(0.66^{4L}),\\ &\|\tau - \tau_L\|_{\infty,\overline{BC}} = O(0.66^{4L}), \quad \text{Cond} = O(1.15^{4L}), \quad \text{Cond\_eff} = O(1.13^{4L}).\end{aligned} \tag{11.6.5}$$

TAB. 11.3 – The errors and the condition numbers for the mixed type of displacement and traction conditions by the CTM using (11.2.21) and (11.2.22).

L	$\|\varepsilon\|_{\infty,\Gamma}$	$\|\varepsilon\|_{0,S}$	$\|\varepsilon\|_{1,S}$	$\|\vec{\tau} - \vec{\tau}_L\|_{\infty,\overline{BC}}$	Cond	Cond_eff	$\|\mathbf{y}\|$
3	3.33	0.965	8.86	30.9	5.57	3.14	23.8
5	0.486	0.109	1.29	2.38	16.6	5.92	24.3
7	1.76 (−2)	3.65 (−3)	6.99 (−2)	0.317	51.8	14.7	23.8
9	8.75 (−4)	1.29 (−4)	3.01 (−3)	5.50 (−3)	159	38.7	23.7
11	1.41 (−5)	2.53 (−6)	7.05 (−5)	4.19 (−4)	482	106	23.7
13	4.11 (−7)	4.12 (−8)	1.40 (−6)	2.97 (−6)	1.45 (3)	296	23.7
15	3.50 (−9)	5.20 (−10)	1.88 (−8)	1.34 (−7)	4.37 (3)	851	23.7

Comparing (11.6.5) with (11.6.4), the MPS offers a better numerical performance in both accuracy and stability. The numerical results (11.6.3)–(11.6.5) support the analysis made in this chapter. The numerical results of the HTM are reported in [153]. For the corner and crack singularity, the leading singular solutions are added in the basic FS, and the combined methods of the MFS and the MPS are designed. The numerical experiments are given in [138].

In summary, in this chapter, we provide strict error analysis of the MFS and the HTM using FS and PS. Optimal convergence rates can be achieved. Numerical experiments are coincident with the error analysis made. Moreover, additional theorems of FS in linear elastostatics are derived in appendix below.

11.7 Appendix: Addition Theorems of FS in Linear Elastostatics

Series expansions of fundamental solutions (called addition theorems) are essential to algorithms and analysis of the MFS. For linear elastostatics, new addition theorems of FS are derived directly from integration. The new expansions of the FS are simpler than those in Chen *et al.* [43]. The materials of this appendix are adapted from [164].

11.7.1 Preliminary Lemmas

Denote two nodes by $P(x, y)$ and $Q(\xi, \eta)$ with $x = \rho \cos\theta$, $y = \rho \sin\theta$, $\xi = R \cos\phi$, and $\eta = R \sin\phi$. Then $\rho = \sqrt{x^2 + y^2}$, $R = \sqrt{\xi^2 + \eta^2}$ and $r = |\overline{PQ}| = \sqrt{\rho^2 - 2\rho R \cos(\theta - \phi) + R^2}$.

From (11.2.16)–(11.2.18), the simple FS is $\kappa\nabla(\ln r) = \kappa\{\frac{x}{r^2}, \frac{y}{r^2}\}^T$, and the principal FS in (11.2.16) is expressed in the matrix form

$$\begin{aligned} E_2(\mathbf{x},\mathbf{y}) &:= \begin{pmatrix} -\ln r(1-\kappa) + \kappa\dfrac{x^2}{r^2} & \kappa\dfrac{xy}{r^2} \\ \kappa\dfrac{xy}{r^2} & -\ln r(1-\kappa) + \kappa\dfrac{y^2}{r^2} \end{pmatrix} \\ &= (1-\kappa)\begin{pmatrix} -\ln r + D\dfrac{x^2}{r^2} & D\dfrac{xy}{r^2} \\ D\dfrac{xy}{r^2} & -\ln r + D\dfrac{y^2}{r^2} \end{pmatrix}. \end{aligned} \tag{11.7.1}$$

Addition theorem for $\ln r$ is given in Lemma I.3 in Part I. The main work is to derive the new expansions for $\frac{x}{r^2}$, $\frac{y}{r^2}$, $\frac{x^2}{r^2}$, $\frac{y^2}{r^2}$ and $\frac{xy}{r^2}$. First, let us derive the basic series expansions of $\frac{1}{r^2}$.

Lemma 11.7.1. *There exist the integrals,*

$$\int_0^{2\pi} \frac{\cos nx}{1+a^2-2a\cos x}\,dx = \begin{cases} \dfrac{2\pi a^n}{1-a^2}, & a^2<1, \\ \dfrac{2\pi a^{-n}}{a^2-1}, & a^2>1, \end{cases} \tag{11.7.2}$$

$$\int_0^{2\pi} \frac{\sin nx}{1+a^2-2a\cos x}\,dx = 0. \tag{11.7.3}$$

Proof. From Gradsheyan and Ryzhik [90, p.366],

$$\int_0^{\pi} \frac{\cos nx}{1+a^2-2a\cos x}\,dx = \begin{cases} \dfrac{\pi a^n}{1-a^2}, a^2<1, \\ \dfrac{\pi a^{-n}}{a^2-1}, a^2>1, \end{cases} \tag{11.7.4}$$

we have

$$\begin{aligned} \int_0^{2\pi} \frac{\cos nx}{1+a^2-2a\cos x}\,dx &= \int_{-\pi}^{\pi} \frac{\cos nx}{1+a^2-2a\cos x}\,dx \\ &= \left(\int_{-\pi}^{0} + \int_0^{\pi}\right) \frac{\cos nx}{1+a^2-2a\cos x}\,dx. \end{aligned} \tag{11.7.5}$$

Letting $x=-t$ and $dx=-dt$, we have

$$\begin{aligned} \int_{-\pi}^{0} \frac{\cos nx}{1+a^2-2a\cos x}\,dx &= -\int_{\pi}^{0} \frac{\cos nx}{1+a^2-2a\cos x}\,dx \\ &= \int_0^{\pi} \frac{\cos nx}{1+a^2-2a\cos x}\,dx. \end{aligned} \tag{11.7.6}$$

Combining (11.7.4)–(11.7.6) gives

$$\int_0^{2\pi} \frac{\cos nx}{1+a^2-2a\,\cos x}\,dx = 2\int_0^{\pi} \frac{\cos nx}{1+a^2-2a\,\cos x}\,dx = \begin{cases} \dfrac{2\pi a^n}{1-a^2}, & a^2<1, \\ \dfrac{2\pi a^n}{a^2-1}, & a^2>1. \end{cases}$$

This is the first desired result (11.7.2).

Next we have

$$\int_0^{2\pi} \frac{\sin nx}{1+a^2-2a\,\cos x}\,dx = \left(\int_{-\pi}^{0} + \int_0^{\pi}\right) \frac{\sin nx}{1+a^2-2a\,\cos x}\,dx = 0,$$

since the following equality holds,

$$\int_{-\pi}^{0} \frac{\sin nx}{1+a^2-2a\,\cos x}\,dx = -\int_0^{\pi} \frac{\sin nx}{1+a^2-2a\,\cos x}\,dx = 0.$$

This is the second desired result (11.7.3) and completes the proof of Lemma 11.7.1. ■

Lemma 11.7.2. *For* $a^2<1$*, there exist the Fourier expansions,*

$$\frac{1}{1+a^2-2a\,\cos x} = \frac{2}{1-a^2}\left(\frac{1}{2} + \sum_{n=1}^{\infty} a^n \cos nx\right). \tag{11.7.7}$$

For $a^2>1$*,*

$$\frac{1}{1+a^2-2a\,\cos x} = \frac{2}{a^2-1}\left(\frac{1}{2} + \sum_{n=1}^{\infty} a^{-n} \cos nx\right). \tag{11.7.8}$$

Proof. Denote the Fourier series

$$\frac{1}{1+a^2-2a\,\cos x} = \frac{a_0}{2} + \sum_{k=1}^{\infty}(a_k\,\cos kx + b_k\,\sin kx), \tag{11.7.9}$$

where the Fourier coefficients a_k and b_k are obtained:

$$a_k = \frac{1}{\pi}\int_0^{2\pi} \frac{\cos kx}{1+a^2-2a\,\cos x}\,dx, \qquad k=0,1,2,\ldots,$$
$$b_k = \frac{1}{\pi}\int_0^{2\pi} \frac{\sin kx}{1+a^2-2a\,\cos x}\,dx, \qquad k=1,2,\ldots.$$

Then from Lemma 11.7.1 we obtain for $a^2<1$

$$a_k = \frac{2}{\pi}\frac{\pi a^k}{1-a^2} = \frac{2a^k}{1-a^2}, \qquad k=0,1,\ldots,$$
$$b_k = 0, \qquad k=1,2,\ldots.$$

Substituting the coefficients a_k and b_k into (11.7.9) gives the first desired result (11.7.7) with $a^2 < 1$. Similarly, the equation (11.7.8) with $a^2 > 1$ also holds. ■

Lemma 11.7.3. *There exist the Fourier expansions,*

$$\frac{1}{r^2} = \frac{2}{R^2 - \rho^2}\left\{\frac{1}{2} + \sum_{n=1}^{\infty}\left(\frac{\rho}{R}\right)^n \cos n(\phi - \theta)\right\}, \quad \rho < R, \tag{11.7.10}$$

$$\frac{1}{r^2} = \frac{2}{\rho^2 - R^2}\left\{\frac{1}{2} + \sum_{n=1}^{\infty}\left(\frac{R}{\rho}\right)^n \cos n(\phi - \theta)\right\}, \quad \rho > R, \tag{11.7.11}$$

where $r^2 = R^2 + \rho^2 - 2\rho R\cos(\phi - \theta)$, $\mathbf{x} = (x, y) = (\rho\cos\theta, \rho\sin\theta)$ *and* $\mathbf{y} = (\xi, \eta) = (R\cos\phi, R\sin\phi)$.

Proof. Since $r^2 = R^2(1 + a^2 - 2a\cos(\phi - \theta))$ with $a = \frac{\rho}{R}$, we obtain (11.7.10) from Lemma 11.7.2 by noting $x = \phi - \theta$. The equation (11.7.11) follows from (11.7.10) by the symmetry between ρ and R. ■

Lemma 11.7.4. *Let* $\rho < R$, $a = \frac{\rho}{R}$ *and* $r^2 = R^2 + \rho^2 - 2\rho R\cos(\phi - \theta)$. *There exist the Fourier expansions,*

$$\begin{aligned} T_1^e = \frac{x - \xi}{r^2} &= -\frac{1}{R}\sum_{n=1}^{\infty}\left(\frac{\rho}{R}\right)^{n-1}\{\cos(n-1)\theta\,\cos n\phi + \sin(n-1)\theta\,\sin n\phi\} \\ &= -\frac{1}{R}\sum_{n=0}^{\infty}\left(\frac{\rho}{R}\right)^n \cos(n(\theta - \phi) - \phi), \end{aligned} \tag{11.7.12}$$

$$\begin{aligned} T_2^e = \frac{y - \eta}{r^2} &= \frac{1}{R}\sum_{n=1}^{\infty}\left(\frac{\rho}{R}\right)^{n-1}\{\sin(n-1)\theta\,\cos n\phi - \cos(n-1)\theta\,\sin n\phi\} \\ &= \frac{1}{R}\sum_{n=0}^{\infty}\left(\frac{\rho}{R}\right)^n \sin(n(\theta - \phi) - \phi), \end{aligned} \tag{11.7.13}$$

where the superscripts "e" and "i" denote the cases of $\rho < R$ *and* $\rho > R$*, respectively.*

Proof. We have the Fourier expansion,

$$\frac{x - \xi}{r^2} = \frac{\alpha_0}{2} + \sum_{n=1}^{\infty}(\alpha_n \cos n\phi + \beta_n \sin n\phi) := f, \tag{11.7.14}$$

where

$$\alpha_n = \frac{1}{\pi}\int_0^{2\pi} f\,\cos n\phi\,d\phi, \quad \beta_n = \frac{1}{\pi}\int_0^{2\pi} f\,\sin n\phi\,d\phi. \tag{11.7.15}$$

The explicit coefficients α_n and β_n in (11.7.15) can be obtained from direct integration based on Lemma 11.7.3. There exist the equalities,

$$\begin{aligned}(x-\xi)\cos n\phi &= (\rho\,\cos\theta - R\,\cos\phi)\cos n\phi\\ &= \rho\,\cos\theta\,\cos n\phi - \frac{R}{2}(\cos(n-1)\phi+\cos(n+1)\phi).\end{aligned}$$

From Lemma 11.7.3 and the orthogonality of trigonometric functions, we have

$$\begin{aligned}&\int_0^{2\pi}\frac{x-\xi}{r^2}\cos n\phi\, d\phi\\ &= \frac{2\pi}{R^2(1-a^2)}\left\{\rho\,\cos\theta a^n\cos n\theta - \frac{R}{2}(a^{n-1}\cos(n-1)\theta + a^{n+1}\cos(n+1)\theta)\right\}\\ &= \frac{2\pi}{R^2(1-a^2)}\left\{\frac{\rho a^n}{2}(\cos(n-1)\theta+\cos(n+1)\theta)\right.\\ &\quad\left.-\frac{R}{2}(a^{n-1}\cos(n-1)\theta + a^{n+1}\cos(n+1)\theta)\right\}\\ &= \frac{2\pi}{R^2(1-a^2)}\,a^{n-1}\left(\frac{\rho a}{2}-\frac{R}{2}\right)\cos(n-1)\theta.\end{aligned}$$

Since

$$\frac{\rho a}{2}-\frac{R}{2} = \frac{\rho^2}{2R}-\frac{R}{2} = \frac{1}{2R}(\rho^2-R^2) = \frac{R}{2}(a^2-1),$$

we obtain

$$\int_0^{2\pi}\frac{x-\xi}{r^2}\cos n\phi\, d\phi = -\frac{\pi}{R}\left(\frac{\rho}{R}\right)^{n-1}\cos(n-1)\theta. \tag{11.7.16}$$

Similarly, we have

$$\int_0^{2\pi}\frac{x-\xi}{r^2}\,d\phi = 0,\ \int_0^{2\pi}\frac{x-\xi}{r^2}\sin n\phi\, d\phi = -\frac{\pi}{R}\left(\frac{\rho}{R}\right)^{n-1}\sin(n-1)\theta. \tag{11.7.17}$$

From (11.7.15), (11.7.16) and (11.7.17), we obtain the first expansions of the right-hand side in (11.7.12). Letting $n-1=k$, we obtain

$$\begin{aligned}\frac{x-\xi}{r^2} &= -\frac{1}{R}\sum_{k=1}^{\infty}\left(\frac{\rho}{R}\right)^k\{\cos k\theta\,\cos(k+1)\phi + \sin k\theta\,\sin(k+1)\phi\}\\ &= -\frac{1}{R}\sum_{k=0}^{\infty}\left(\frac{\rho}{R}\right)^k\cos(k(\theta-\phi)-\phi).\end{aligned}$$

The proof for (11.7.13) is similar and this completes the proof of Lemma 11.7.4. ■

Next for the principal FS with $\rho<R$, we have their expansions by direct integration.

Lemma 11.7.5. *Let* $\rho<R$, $a=\frac{\rho}{R}$ *and* $r^2 = R^2+\rho^2-2\rho R\cos(\phi-\theta)$. *There exist the Fourier expansions,*

$$\begin{aligned}\frac{(x-\xi)^2}{r^2} &= \frac{1}{2}-\frac{a}{2}\cos(\theta+\phi)+\frac{1-a^2}{2}\sum_{n=2}^{\infty}\left(\frac{\rho}{R}\right)^{n-2}\{\cos(n-2)\theta\,\cos n\phi+\sin(n-2)\theta\,\sin n\phi\}\\ &= \frac{1}{2}-\frac{a}{2}\cos(\theta+\phi)+\frac{1-a^2}{2}\sum_{n=0}^{\infty}\left(\frac{\rho}{R}\right)^{n}\cos(n(\theta-\phi)-2\phi), \qquad (11.7.18)\end{aligned}$$

$$\begin{aligned}\frac{(y-\eta)^2}{r^2} &= \frac{1}{2}+\frac{a}{2}\cos(\theta+\phi)-\frac{1-a^2}{2}\sum_{n=2}^{\infty}\left(\frac{\rho}{R}\right)^{n-2}\{\cos(n-2)\theta\,\cos n\phi+\sin(n-2)\theta\,\sin n\phi\}\\ &= \frac{1}{2}+\frac{a}{2}\cos(\theta+\phi)-\frac{1-a^2}{2}\sum_{n=0}^{\infty}\left(\frac{\rho}{R}\right)^{n}\cos(n(\theta-\phi)-2\phi), \qquad (11.7.19)\end{aligned}$$

$$\begin{aligned}&\frac{(x-\xi)(y-\eta)}{r^2}\\ &= -\frac{a}{2}\sin(\theta+\phi)+\frac{1-a^2}{2}\sum_{n=2}^{\infty}\left(\frac{\rho}{R}\right)^{n-2}\{-\sin(n-2)\theta\,\cos n\phi+\cos(n-2)\theta\,\sin n\phi\}\\ &= -\frac{a}{2}\sin(\theta+\phi)-\frac{1-a^2}{2}\sum_{n=0}^{\infty}\left(\frac{\rho}{R}\right)^{n}\sin(n(\theta-\phi)-2\phi). \qquad (11.7.20)\end{aligned}$$

Proof. There exist the equalities of trigonometric functions,

$$\begin{aligned}(x-\xi)^2 &= (\rho\,\cos\theta-R\,\cos\phi)^2=\rho^2\cos^2\theta+R^2\cos^2\phi-2\rho R\,\cos\theta\,\cos\phi\\ &= \rho^2\frac{1+\cos2\theta}{2}+R^2\frac{1+\cos2\phi}{2}-2\rho R\,\cos\theta\,\cos\phi, \qquad (11.7.21)\end{aligned}$$

and

$$\begin{aligned}(x-\xi)^2\cos n\phi &= \rho^2\left(\frac{1+\cos2\theta}{2}\right)\cos n\phi+R^2\left(\frac{1+\cos2\phi}{2}\right)\cos n\phi-2\rho R\,\cos\theta\,\cos\phi\,\cos n\phi\\ &= \frac{\rho^2+R^2}{2}\cos n\phi+\rho^2\left(\frac{\cos2\theta}{2}\right)\cos n\phi+\frac{R^2}{4}\{\cos(n+2)\phi+\cos(n-2)\phi\}\\ &\quad-\rho R\,\cos\theta\{\cos(n+1)\phi+\cos(n-1)\phi\}. \qquad (11.7.22)\end{aligned}$$

Letting $f=\frac{(x-\xi)^2}{r^2}$, we can derive the Fourier expansions from (11.7.14) and (11.7.15). From Lemma 11.7.3 and the orthogonality of trigonometric functions, we have the integral for $n\geq 2$,

$$\begin{aligned}\int_0^{2\pi}\frac{(x-\xi)^2}{r^2}\cos n\phi\,d\phi &= \frac{2\pi}{R^2(1-a^2)}\Bigg\{\frac{\rho^2+R^2}{2}a^n\cos n\theta+\rho^2\left(\frac{\cos2\theta}{2}\right)a^n\cos n\theta\\ &\quad+\frac{R^2}{4}[a^{n+2}\cos(n+2)\theta+a^{n-2}\cos(n-2)\theta]\\ &\quad-\rho R\,\cos\theta[a^{n+1}\cos(n+1)\theta+a^{n-1}\cos(n-1)\theta]\Bigg\}\end{aligned}$$

$$\begin{aligned}
&= \frac{2\pi}{R^2(1-a^2)}\left\{\frac{\rho^2+R^2}{2}\,a^n\cos n\theta + \frac{\rho^2}{4}\,a^n[\cos(n+2)\theta+\cos(n-2)\theta]\right.\\
&\quad + \frac{R^2}{4}[a^{n+2}\cos(n+2)\theta + a^{n-2}\cos(n-2)\theta] \qquad (11.7.23)\\
&\quad \left. - \frac{\rho R}{2}\,a^{n+1}[\cos(n+2)\theta+\cos n\theta] - \frac{\rho R}{2}\,a^{n-1}[\cos n\theta+\cos(n-2)\theta]\right\}.
\end{aligned}$$

Note that in (11.7.23), the final coefficients in front of $\cos n\theta$ and $\cos(n+2)\theta$ are just zero. Then we obtain

$$\int_0^{2\pi}\frac{(x-\xi)^2}{r^2}\cos n\phi\, d\phi = \frac{\pi a^{n-2}}{2R^2(1-a^2)}\left(R^2+\frac{\rho^4}{R^2}-2\rho^2\right)\cos(n-2)\theta. \qquad (11.7.24)$$

There exists the equality,

$$\begin{aligned}
R^2+\frac{\rho^4}{R^2}-2\rho^2 &= R^2-\rho^2+\rho^2\left(\frac{\rho^2}{R^2}-1\right)\\
&= (R^2-\rho^2)\left(1-\frac{\rho^2}{R^2}\right) = R^2(1-a^2)^2.
\end{aligned} \qquad (11.7.25)$$

Combining (11.7.24) and (11.7.25) gives

$$\int_0^{2\pi}\frac{(x-\xi)^2}{r^2}\cos n\phi\, d\phi = \frac{\pi}{2}(1-a^2)\left(\frac{\rho}{R}\right)^{n-2}\cos(n-2)\theta, \quad n\geq 2. \qquad (11.7.26)$$

Similarly we have

$$\int_0^{2\pi}\frac{(x-\xi)^2}{r^2}\sin n\phi\, d\phi = \frac{\pi}{2}(1-a^2)\left(\frac{\rho}{R}\right)^{n-2}\sin(n-2)\theta, \quad n\geq 2. \qquad (11.7.27)$$

Moreover, we have the integrations

$$\int_0^{2\pi}\frac{(x-\xi)^2}{r^2}\, d\phi = \pi, \qquad (11.7.28)$$

$$\int_0^{2\pi}\frac{(x-\xi)^2}{r^2}\cos\phi\, d\phi = -\frac{\pi}{2}\,a\,\cos\theta, \quad \int_0^{2\pi}\frac{(x-\xi)^2}{r^2}\sin\phi\, d\phi = \frac{\pi}{2}\,a\,\sin\theta. \qquad (11.7.29)$$

The first expansion (11.7.18) for $f=\frac{(x-\xi)^2}{r^2}$ is obtained from (11.7.26)–(11.7.29). The proof for expansions (11.7.19) and (11.7.20) is similar; details are given in [164]. This completes the proof of Lemma 11.7.5. ■

11.7.2 Addition Theorems

Based on the preliminary lemmas above, we provide new series expansions of the FS for linear elastostatics in 2D. For the simple FS with $\rho < R$, we have their series expansions from Lemma 11.7.4.

Theorem 11.7.1 (Addition Theorem A^e). *Let* $\rho < R$ *and* $r^2 = R^2 + \rho^2 - 2\rho R\cos(\phi - \theta)$. *There exist the series expansions of the simple FS,*

$$\kappa\begin{pmatrix}\frac{x-\xi}{r^2}\\ \frac{y-\eta}{r^2}\end{pmatrix} = \frac{\kappa}{R}\sum_{n=0}^{\infty}\left(\frac{\rho}{R}\right)^n\begin{pmatrix}-\cos(n(\theta-\phi)-\phi)\\ \sin(n(\theta-\phi)-\phi)\end{pmatrix}.$$

Next for the principal FS with $\rho < R$, we have their series expansions from Lemmas 11.7.5 and 11.4.1.

Theorem 11.7.2 (Addition Theorem B^e). *Let* $\rho < R, a = \frac{\rho}{R}$ *and* $r^2 = R^2 + \rho^2 - 2\rho R\cos(\phi - \theta)$. *There exist the series expansions of the principal FS,*

$$E_2^e(\mathbf{x}, \mathbf{y}) = \begin{pmatrix} T_{11}^e & T_{12}^e\\ T_{12}^e & T_{22}^e\end{pmatrix},$$

where the entries

$$\begin{aligned}
T_{11}^e &= (1-\kappa)\Bigg\{-\left[\ln R - \sum_{n=1}^{\infty}\frac{1}{n}\left(\frac{\rho}{R}\right)^n\cos n(\theta-\phi)\right]\\
&\quad + D\left[\frac{1}{2} - \frac{a}{2}\cos(\theta+\phi) + \frac{1-a^2}{2}\sum_{n=0}^{\infty}\left(\frac{\rho}{R}\right)^n\cos(n(\theta-\phi)-2\phi)\right]\Bigg\},\\
T_{22}^e &= (1-\kappa)\Bigg\{-\left[\ln R - \sum_{n=1}^{\infty}\frac{1}{n}\left(\frac{\rho}{R}\right)^n\cos n(\theta-\phi)\right]\\
&\quad + D\left[\frac{1}{2} + \frac{a}{2}\cos(\theta+\phi) - \frac{1-a^2}{2}\sum_{n=0}^{\infty}\left(\frac{\rho}{R}\right)^n\cos(n(\theta-\phi)-2\phi)\right]\Bigg\},\\
T_{12}^e &= (1-\kappa)D\left[-\frac{a}{2}\sin(\theta+\phi) - \frac{1-a^2}{2}\sum_{n=0}^{\infty}\left(\frac{\rho}{R}\right)^n\sin(n(\theta-\phi)-2\phi)\right].
\end{aligned}$$

For $\rho > R$ we have the following theorem.

Theorem 11.7.3 (Addition Theorem A^i). *Let* $\rho > R$ *and* $r^2 = R^2 + \rho^2 - 2\rho R \times \cos(\phi - \theta)$. *There exist the series expansions of the simple FS,*

$$\kappa\begin{pmatrix}\frac{x-\xi}{r^2}\\ \frac{y-\eta}{r^2}\end{pmatrix} = \frac{\kappa}{\rho}\sum_{n=0}^{\infty}\left(\frac{R}{\rho}\right)^n\begin{pmatrix}\cos(n(\phi-\theta)-\theta)\\ -\sin(n(\phi-\theta)-\theta)\end{pmatrix}. \tag{11.7.30}$$

Proof. We will use Theorem 11.7.1 *via* symmetry. When $\rho > R$, we have

$$\frac{x-\xi}{r^2} = \frac{\rho\cos\theta - R\cos\phi}{R^2+\rho^2-2\rho R\cos(\phi-\theta)} = -\frac{R\cos\phi - \rho\cos\theta}{R^2+\rho^2-2\rho R\cos(\theta-\phi)}. \tag{11.7.31}$$

If switching (ρ, θ) and (R, ϕ), from Theorem 11.7.1 and (11.7.31), we obtain the first component of the vector in (11.7.30):

$$\kappa\frac{x-\xi}{r^2} = \frac{\kappa}{\rho}\sum_{n=0}^{\infty}\left(\frac{R}{\rho}\right)^n\cos(n(\phi-\theta)-\theta). \tag{11.7.32}$$

The proof for the second component of the vector in (11.7.30) is similar. ■

Similarly, we have the following series expansions from Theorem 11.7.2 *via* symmetry.

Theorem 11.7.4 (Addition Theorem B^i). *Let* $\rho > R$, $a = \frac{\rho}{R}$ *and* $r^2 = R^2 + \rho^2 - 2\rho R\cos(\phi - \theta)$. *There exist the series expansions of the principal FS,*

$$E_2^i(\mathbf{x}, \mathbf{y}) = \begin{pmatrix} T_{11}^i & T_{12}^i \\ T_{12}^i & T_{22}^i \end{pmatrix},$$

where the entries are given by

$$\begin{aligned} T_{11}^i &= (1-\kappa)\Bigg\{-\left[\ln\rho - \sum_{n=1}^{\infty}\frac{1}{n}\left(\frac{R}{\rho}\right)^n \cos n(\theta-\phi)\right] \\ &\quad + D\left[\frac{1}{2} - \frac{a^{-1}}{2}\cos(\theta+\phi) + \frac{1-a^{-2}}{2}\sum_{n=0}^{\infty}\left(\frac{R}{\rho}\right)^n \cos(n(\phi-\theta)-2\theta)\right]\Bigg\}, \\ T_{22}^i &= (1-\kappa)\Bigg\{-\left[\ln\rho - \sum_{n=1}^{\infty}\frac{1}{n}\left(\frac{R}{\rho}\right)^n \cos n(\theta-\phi)\right] \\ &\quad + D\left[\frac{1}{2} + \frac{a^{-1}}{2}\cos(\theta+\phi) - \frac{1-a^{-2}}{2}\sum_{n=0}^{\infty}\left(\frac{R}{\rho}\right)^n \cos(n(\phi-\theta)-2\theta)\right]\Bigg\}, \\ T_{12}^i &= (1-\kappa)D\left[-\frac{a^{-1}}{2}\sin(\theta+\phi) - \frac{1-a^{-2}}{2}\sum_{n=0}^{\infty}\left(\frac{R}{\rho}\right)^n \sin(n(\phi-\theta)-2\theta)\right]. \end{aligned}$$

Chapter 12

Cauchy Problems

12.1 Introduction

The systematic analysis of the MFS has been completed for the classic 2D problems in previous chapters; they may be applied to more complicated problems. In this chapter, we consider Cauchy problems of Laplace's equation, which are highly ill-posed with severe instability. We use the method of particular solutions (MPS) and the method of fundamental solutions (MFS), but focus on the analysis of the MFS. The basic analysis of errors and stability in Chapter 2 can be applied to the Cauchy data. The regularization may also be adopted as in [255, 259]. There exist many reports on numerical Cauchy problems [58, 119]; most of them are of computational aspects. The strict analysis of this chapter may, to a certain degree, fill up the existing gap between the theory and the computation of Cauchy problems by the MFS and the MPS.

This chapter is organized as follows. In the next section, the MPS and the MFS are introduced. In Section 12.3, the existence and uniqueness is discussed for Cauchy problems, and the ill-posedness is defined. In Section 12.4, the error and stability analysis is made for the MFS. In Section 12.5, the basic analysis is applied to Cauchy data. In the last section, numerical experiments are reported, and a few concluding remarks are made. The materials of this chapter are adapted from [255], where more numerical experiments and comparisons are provided.

12.2 Algorithms of Collocation Trefftz Methods

Consider the Cauchy problem of Laplace's equation in [58, 94, 119, 240, 248],

$$\Delta u = \frac{\partial^2 u}{\partial x^2} + \frac{\partial^2 u}{\partial y^2} = 0 \text{ in } S, \tag{12.2.1}$$

$$u = f \text{ on } \Gamma^*, \tag{12.2.2}$$

DOI: 10.1051/978-2-7598-3171-5.c012
© Science Press, EDP Sciences, 2023

$$\frac{\partial u}{\partial \nu} = g \text{ on } \mathbf{\Gamma}^*, \tag{12.2.3}$$

where $S = (0, a)^2$ is a square domain, where $a = 1$ in computation, ν the exterior normal, and a partial boundary $\mathbf{\Gamma}^* \subset \partial S$. For the non-square domains, the algorithms and analysis are similar. The algorithms and analysis of this chapter can be developed for the problems with some over-specified boundary conditions in Chen and Chen [40], where the Cauchy conditions (12.2.2) and (12.2.3) are enforced on $\mathbf{\Gamma}^*$, while the Dirichlet and Neumann conditions are still given on a portion of the remaining boundary $\partial S \backslash \mathbf{\Gamma}^*$. See the problem (12.3.3)–(12.3.5) in the next section.

Below, consider a unit square $S = (0, 1)^2$. The exact solution for the Cauchy problem is chosen as

$$u_n(x, y) = \frac{1}{n^k} \sin(nx) \cosh(ny), \quad k \geq 0. \tag{12.2.4}$$

The simple Cauchy data in (12.2.2) and (12.2.3) at the bottom edge $y = 0$ are given by both the Dirichlet and the Neumman boundary conditions

$$f = \frac{1}{n^k} \sin(nx), \; \frac{\partial u}{\partial y} = g = 0 \quad \text{at } y = 0, \tag{12.2.5}$$

and the remaining three edges are free, *i.e.*, no boundary conditions are given at the top, the left and the right edges. In this chapter, we also consider three-edge Cauchy data: the condition (12.2.5) plus

$$f = 0, \; \frac{\partial u}{\partial x} = -g = \frac{1}{n^{k-1}} \cosh(ny) \text{ at } x = 0, \tag{12.2.6}$$

$$f = \frac{1}{n^k} \sin(n) \cosh(ny), \; \frac{\partial u}{\partial x} = g = \frac{1}{n^{k-1}} \cos(n) \cosh(ny) \text{ at } x = 1, \tag{12.2.7}$$

and only the top edge is free. The Cauchy conditions in (12.2.5) and (12.2.5)–(12.2.7) are called Cauchy Models I and II in this chapter, respectively. See Figure 12.1.

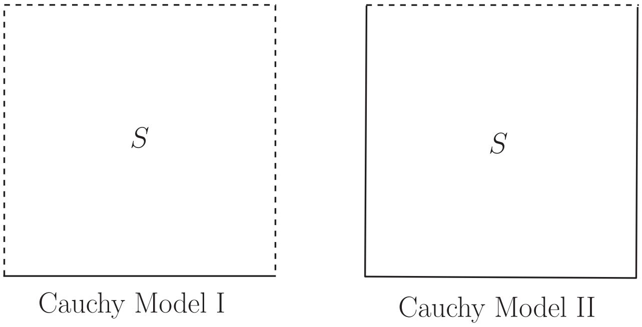

FIG. 12.1 – The Cauchy data in Cauchy Models I and II on ∂S.

In the Cauchy problem, we assume that the boundary conditions in (12.2.2) and (12.2.3) are given to guarantee the existence and uniqueness of the solution. Otherwise, the solution space is enlarged or enforced (see Kirsch [124]), so that a unique solution can be found. Note that by the MFS, there always exists a numerical solution. When the equations (12.2.2) and (12.2.3) are inconsistent, the least-squares solutions exist, although the exact solutions may not exist (see Section 12.3.1). Hence, the set of fundamental solutions (FS) is regarded as a modified space in which a unique solution exists.

Let S be a bounded simply-connected domain with the boundary ∂S, and $\mathbf{\Gamma}^*$ be part of ∂S, *i.e.*, $\mathbf{\Gamma}^* \subset \partial S$. Denote $r_{\max} = \max_S r$ and $r_{\min} = \max\limits_{S_{\text{in}}\,(S_{\text{in}} \subseteq S)} r$, where S_{in} is an inscribed disk of S. Let the source (charge) nodes Q be located outside S. The FS

$$\phi(r,\theta) = \ln|\overline{PQ}|, \quad P \in S \cup \partial S, \tag{12.2.8}$$

are harmonic, where $P = \{(x,y)|x = r\ \cos\theta, y = r\ \sin\theta\}$. A circle surrounding S is given by $\ell_R = \{(r,\theta)|r = R, 0 \leq \theta \leq 2\pi\}$ with $R > r_{\max}$. The source nodes Q_i may be simply located uniformly on ℓ_R:

$$Q_i = \{(x,y)|x = R\ \cos(ih),\ y = R\ \sin(ih)\}, \tag{12.2.9}$$

where $R > r_{\max}$ and $h = \frac{2\pi}{N}$. We obtain the fundamental solutions

$$\phi_i(P) = \ln|\overline{PQ_i}|, \quad i = 1,\ 2, \ldots, N, \tag{12.2.10}$$

and the numerical solution as the linear combination

$$u_N = \sum_{i=1}^{N} c_i \phi_i(P), \tag{12.2.11}$$

where c_i are the unknown coefficients to be determined. Since u_N satisfies Laplace's equation in S already, the coefficients c_i can be sought by satisfying the Cauchy boundary conditions (12.2.2) and (12.2.3) only. We will follow the Trefftz method (TM) to seek u_N (*i.e.*, c_i). Denote the energy

$$I(v) = \int_{\Gamma^*} \left\{ (v-f)^2 + w^2 \left(\frac{\partial v}{\partial \nu} - g \right)^2 \right\}, \tag{12.2.12}$$

where the weight $w = \frac{1}{N}$ in computation (see [169]). Also denote by V_N the set of (12.2.11). Then the numerical solution u_N can be obtained by

$$I(u_N) = \min_{v \in V_N} I(v). \tag{12.2.13}$$

When the integrals in (12.2.12) involve approximation, denote

$$\widehat{I}(v) = \widehat{\int}_{\Gamma^*} \left\{ (v-f)^2 + w^2 \left(\frac{\partial v}{\partial \nu} - g \right)^2 \right\}, \tag{12.2.14}$$

where $\widehat{\int}_{\Gamma^*}$ is a numerical approximation of $\int_{\Gamma^*}$ by some quadrature rules, such as the central or the Gaussian rule. Hence, the numerical solution $\tilde{u}_N \in V_N$ is obtained by

$$\widehat{I}(\tilde{u}_N) = \min_{v \in V_N} \widehat{I}(v). \tag{12.2.15}$$

We may establish the collocation equations directly from (12.2.2) and (12.2.3), to yield

$$\sum_{i=1}^{N} c_i \phi_i(P_j) = f(P_j), \quad P_j \in \mathbf{\Gamma}^*, \tag{12.2.16}$$

$$\sum_{i=1}^{N} c_i \frac{\partial}{\partial v} \phi_i(P_j) = g(P_j), \quad P_j \in \mathbf{\Gamma}^*. \tag{12.2.17}$$

Let $\mathbf{\Gamma}^*$ be divided into small sections $\mathbf{\Gamma}_j^*$ with the meshspacings $\triangle h_j$, then $\mathbf{\Gamma}^* = \bigcup_{j=1}^{M} \mathbf{\Gamma}_j^*$. We obtain from (12.2.16) and (12.2.17) with weights $\sqrt{\triangle h_j}$

$$\sqrt{\triangle h_j} \sum_{i=1}^{N} c_i \phi_i(P_j) = \sqrt{\triangle h_j}\, f(P_j), \quad P_j \in \mathbf{\Gamma}_j^*, \quad j = 1, 2, \ldots, M, \tag{12.2.18}$$

$$w\sqrt{\triangle h_j} \sum_{i=1}^{N} c_i \frac{\partial}{\partial v} \phi_i(P_j) = w\sqrt{\triangle h_j}\, g(P_j), \quad P_j \in \mathbf{\Gamma}_j^*, \quad j = 1, 2, \ldots, M, \tag{12.2.19}$$

where for simplicity, P_j are located at the midpoints of $\mathbf{\Gamma}_j^*$. Following [169], the equations (12.2.18) and (12.2.19) are just equivalent to (12.2.15), where the central rule is chosen for $\widehat{\int}_{\mathbf{\Gamma}^*}$. In computation, we may choose the number of collocation nodes to be equal to (or larger than) that of source nodes, *i.e.*, $2M \geq N$. When the Gaussian rule is chosen, the following collocation equations are obtained,

$$\beta_j \sum_{i=1}^{N} c_i \phi_i(P_j) = \beta_j\, f(P_j), \quad P_j \in \mathbf{\Gamma}^*, \tag{12.2.20}$$

$$\beta_j w \sum_{i=1}^{N} c_i \frac{\partial}{\partial v} \phi_i(P_j) = \beta_j w\, g(P_j), \quad P_j \in \mathbf{\Gamma}^*, \tag{12.2.21}$$

where P_j are the Gaussian nodes, weights $\beta_j = O(\sqrt{\triangle h})$ and $\triangle h = \max_j \triangle h_j$.

12.3 Characteristics

12.3.1 Existence and Uniqueness

First, we discuss the existence and uniqueness of the solutions to Cauchy problems. In John [112, Chapter 3], the Cauchy boundary conditions are discussed for partial differential equations (PDE). Based on the systems of quasi-linear equations of the first order and their characteristic lines, the existence and the uniqueness of solutions are proved, which are sufficient and complete for the hyperbolic and parabolic equations, but not for the Cauchy conditions of elliptic equations. We may, however, draw from [112] some useful conclusions of existence and uniqueness. Based on the Cauchy-Kowalevski Theorem in [112, pp.61–77], for the Cauchy conditions on a smooth boundary $\boldsymbol{\Gamma}^*$ with the real analytic functions f and g, there must exist a neighboring domain $\boldsymbol{\Omega}^*$ including $\boldsymbol{\Gamma}^*$ such that a real analytic function satisfying (12.2.2) and (12.2.3) exists uniquely. Suppose that for Laplace's equation, the harmonic functions on $\boldsymbol{\Omega}^*$ can be expressed by the Laurent series,

$$\begin{aligned} u(r,\theta) = a_0 + \sum_{i=1}^{\infty} r^i \{a_i \cos(i\theta) + b_i \sin(i\theta)\} \\ + \bar{a}_0 \ln r + \sum_{i=1}^{\infty} r^{-i} \{\bar{a}_i \cos(i\theta) + \bar{b}_i \sin(i\theta)\}, \quad (r,\theta) \in \boldsymbol{\Omega}^*, \end{aligned} \tag{12.3.1}$$

where a_i, b_i, $\bar{a}_i$ and $\bar{b}_i$ are the coefficients, and (r,θ) are the polar coordinates with the origin $O = (0, 0)$. Through an analytic extension, the enlarged domain $\boldsymbol{\Omega}$ of $\boldsymbol{\Omega}^*$ excluding origin O is defined, where $\boldsymbol{\Gamma}^* \subset \boldsymbol{\Omega}^* \subset \boldsymbol{\Omega}$ and $O \notin \boldsymbol{\Omega}^*$. If the solution domain S (12.2.1) is given *a priori* and satisfies

$$S \subset \boldsymbol{\Omega}, \quad (i.e., \ \partial S \subset \boldsymbol{\Omega}), \tag{12.3.2}$$

then the Cauchy problem (12.2.1)–(12.2.3) has a unique solution. Therefore, for any analytic data f and g, there must exist S satisfying (12.3.2) to guarantee the unique solutions to Cauchy problems.

The existence and uniqueness of Cauchy problems are equivalent to the trivial (*i.e.*, zero) solution under the homogenous Cauchy conditions $f = g = 0$. The Uniqueness Theorem of Holmgren (1901) in [112, pp.80–88] stated that the zero solutions on $\boldsymbol{\Gamma}^*$ can be extended to some $\boldsymbol{\Omega}$ with $\boldsymbol{\Gamma}^* \subset \boldsymbol{\Omega}$. The existence and uniqueness of Cauchy problems also depend on (12.3.2). For the Cauchy problem (12.2.1)–(12.2.3), the existence and the uniqueness are discussed only for special cases in Ohe and Ohnaka [197] and Wei and Zhou [241], where the Cauchy conditions are given on the exterior boundary of a disk, and S is an annular domain. Note that the center of the disk is excluded from S. For the general Cauchy data f and g in (12.2.2) and (12.2.3) and for arbitrary simply-connected domains S, however, uncertainty remains to guarantee (12.3.2).

To support the above analysis, let us cite from John [112, p.76]: *"The Theorem of Cauchy-Kowalevski is local in character, and applies only to analytic solutions of analytic Cauchy problems. It does not guarantee global existence of solutions."* More study on the existence of solutions to the Cauchy problem for PDE is given in Calderon [31].

Let us cite Holmgrens's theorem from Kress [130, p.99]. Let S be a class of C^1, and the solution $u \in C^2(S) \cap C^1(\overline{S})$ be harmonic such that

$$u = \frac{\partial u}{\partial \nu} = 0, \text{ in } \mathbf{\Gamma}^*,$$

where $\mathbf{\Gamma}^* \subset \mathbf{\Gamma}$. Then there occurs the zero solution $u \equiv 0$ in S. From Holmgrens's theorem, the existence of solutions to Cauchy problems implies uniqueness. In real applications [146], S is often chosen as a polygon, and $\mathbf{\Gamma}^*$ may be piecewise straight lines, as in Model II. Moreover, the harmonic solutions may be singular with unbounded derivatives. Below, we give a counter-example to show that arbitrary Cauchy data on two edges of a corner may cause no solutions to exist.

Denote the rectangular domain $S^* = \{(x, y) | -1 < x < 1, 0 < y < 1\}$, and consider the over-specified boundary condition as in [40],

$$\Delta u = 0 \text{ in } S^*, \tag{12.3.3}$$

$$u = f(x), \ \frac{\partial u}{\partial y} = 0, \ (y = 0) \cap (0 < x \leq 1), \tag{12.3.4}$$

$$u = 0, \ (y = 0) \cap (-1 \leq x < 0). \tag{12.3.5}$$

The origin $O = (0, 0)$ can be regarded as a corner with an interior angle π. The Cauchy data are assigned only on one edge $(y = 0) \cap (0 < x \leq 1)$, but not on two edges simultaneously. When the Dirichlet or the Neumann condition is assigned to the corner edges, the harmonic solutions are derived in detail in [169]. For the following mixed boundary conditions,

$$\frac{\partial u}{\partial y} = 0 \text{ at } (y = 0) \cap (0 < x \leq 1), \quad u = 0 \text{ at } (y = 0) \cap (-1 \leq x < 0), \tag{12.3.6}$$

the harmonic solutions are given from [146, 169] by

$$u(r, \theta) = \sum_{k=0}^{\infty} d_k r^{k+\frac{1}{2}} \cos\left(k + \frac{1}{2}\right)\theta, \ (r, \theta) \in S^*, \tag{12.3.7}$$

where d_k are the real coefficients, and (r, θ) are the polar coordinates with the origin O. The coefficients d_i can be determined uniquely by the left condition in (12.3.4),

$$u = f(x) \text{ at } (y = 0) \cap (0 < x \leq 1). \tag{12.3.8}$$

Hence, we can not assign more Cauchy data on the other edge,

$$\frac{\partial u}{\partial y} = g, \quad (y = 0) \cap (-1 \leq x < 0). \tag{12.3.9}$$

Suppose that the function $w(r) = \frac{f(r)}{\sqrt{r}}$ is analytic and expandable by the Taylor series,

$$\frac{f(r)}{\sqrt{r}} = w(r) = \sum_{k=0}^{\infty} \frac{w^{(k)}(0)}{k!} r^k. \tag{12.3.10}$$

Comparing (12.3.10) with (12.3.8) and (12.3.7) at $\theta = 0$, we obtain the coefficients in (12.3.7)

$$d_k = \frac{w^{(k)}(0)}{k!}, \quad k = 0, 1, \ldots. \tag{12.3.11}$$

In particular, when $w(0) \neq 0$, we have $d_0 = w(0) \neq 0$. Then the harmonic solutions (12.3.7) lead to

$$u(r, \theta) \approx d_0 r^{\frac{1}{2}} \cos\left(\frac{\theta}{2}\right), \quad r \to 0. \tag{12.3.12}$$

Then when $\theta = \pi$ for $(y = 0) \cap (-1 \leq x < 0)$, we have

$$g = \frac{\partial u}{\partial y}(r, \pi) = \frac{d_0}{2} r^{-\frac{1}{2}} \to \infty, \quad r \to 0. \tag{12.3.13}$$

Hence, for $d_0 \neq 0$, it is impossible to add (12.3.9) with any bounded function g to guarantee the existence of the solutions satisfying (12.3.3)–(12.3.5) and (12.3.9).

This counter-example implies an uncertainty of existence for the Cauchy problems on $\mathbf{\Gamma}^* \subset \partial S$ with the arbitrary Cauchy data, at least for polygons S. Therefore, there may exist inconsistency among Cauchy data. The consistent Cauchy conditions in (12.2.2) and (12.2.3) must have the regularities of second-order elliptic equations (see [15, 195]),

$$f \in \mathbf{H}^{\frac{1}{2}}(\mathbf{\Gamma}^*), \quad g \in \mathbf{H}^{-\frac{1}{2}}(\mathbf{\Gamma}^*), \tag{12.3.14}$$

where $\mathbf{H}^{\pm\frac{1}{2}}(\mathbf{\Gamma}^*)$ are the Sobolev spaces. Obviously, the random noise data violate (12.3.14), and no solution exists. However, since the random noise data can be regarded as perturbation errors, we may obtain their error bounds by the stability analysis below.

12.3.2 Ill-Posedness of Inverse Problems

Below, we always consider the consistent Cauchy conditions. First, in this subsection, we explore the relationship of the Cauchy data to the entire boundary data of harmonic functions, to indicate the ill-posedness of the inverse problems. Denote the norms,

$$\|v\|_B = \left\{\int_{\Gamma_*} (v^2 + w^2 v_\nu^2)\right\}^{\frac{1}{2}}, \quad \|v\|_{\partial S} = \left\{\int_{\partial S} (v^2 + w^2 v_\nu^2)\right\}^{\frac{1}{2}}, \tag{12.3.15}$$

where $v_\nu = \frac{\partial v}{\partial \nu}$ and weight $w \in (0, 1]$. Since $\mathbf{\Gamma}^* \subset \partial S$, we have

$$\|v\|_B \leq \|v\|_{\partial S}.$$

Suppose that there exists an inverse inequality,

$$\|v\|_{\partial S} \leq C_a(v, w)\|v\|_B, \tag{12.3.16}$$

where the function $C_a(v, w)$ (≥ 1) may be dependent on v and w.

Lemma 12.3.1. *Let (12.3.16) hold. For the harmonic function $v \in \mathbf{H}^2(S)$, there exists the bound,*

$$\|v\|_{1,S} \leq \frac{C}{\sqrt{w}} C_a(v, w)\|v\|_B, \tag{12.3.17}$$

where C is a constant independent of v, and $\|v\|_{k,S}$ and $|v|_{k,S}$ are the Sobolev norms.

Proof. From (12.3.15), there exist the bounds,

$$\|v\|_{0,\partial S} \leq \|v\|_{\partial S}, \quad \|v_\nu\|_{0,\partial S} \leq \frac{1}{w}\|v\|_{\partial S}.$$

For the solution v of Laplace's equation, we have from the Green formula [15]

$$|v|_{1,S}^2 = \iint_S \left(v_x^2 + v_y^2\right) = \int_{\partial S} v v_\nu \leq \|v\|_{0,\partial S}\|v_\nu\|_{0,\partial S} \leq \frac{1}{w}\|v\|_{\partial S}^2, \tag{12.3.18}$$

where $v_x = \frac{\partial v}{\partial x}$ and $v_y = \frac{\partial v}{\partial y}$. Since for $\mathbf{\Gamma}^* \neq \emptyset$ of the Dirichlet condition, the norms $|v|_{1,S}$ and $\|v\|_{1,S}$ are equivalent to each other [15], we have from (12.3.18) and the assumption (12.3.16)

$$\|v\|_{1,S}^2 \leq C|v|_{1,S}^2 \leq \frac{C}{w}\|v\|_{\partial S}^2 \leq \frac{C}{w} C_a^2(v, w)\|v\|_B^2. \tag{12.3.19}$$

This gives the desired result (12.3.17). ■

For the exact solution (12.2.4) with Cauchy Model I in (12.2.5), we show that for large n, the function bound has

$$C_a^I(u, w) = O((1 + wn)e^{na}) > 1. \tag{12.3.20}$$

In fact, the derivatives are given from (12.2.4),

$$\frac{\partial u_n(x, y)}{\partial x} = \frac{1}{n^{k-1}}\cos(nx)\cosh(ny), \tag{12.3.21}$$

$$\frac{\partial u_n(x, y)}{\partial y} = \frac{1}{n^{k-1}}\sin(nx)\sinh(ny). \tag{12.3.22}$$

Then we obtain

$$\|u\|_B^2 = \int_0^a (u^2 + w^2 u_y^2)(x, 0)\,dx = \frac{1}{n^{2k}}\int_0^a (\sin(nx))^2\,dx \geq c_0\frac{1}{n^{2k}}, \tag{12.3.23}$$

where c_0 (> 0) is a constant independent of n. Moreover, we have

$$\int_0^a (u^2 + w^2 u_y^2)(x, a)\, dx = \frac{1}{n^{2k}} \{(\cosh(na))^2 + (wn)^2 (\sinh(na))^2\} \int_0^a (\sin(nx))^2\, dx,$$
$$\int_0^a \left(u^2 + w^2 u_x^2\right)(0, y)\, dy = \frac{1}{n^{2k}} (wn)^2 \int_0^a (\cosh(ny))^2\, dy,$$
$$\int_0^a \left(u^2 + w^2 u_x^2\right)(a, y)\, dy = \frac{1}{n^{2k}} \{(\sin(na))^2 + (wn)^2 (\cos(na))^2\} \int_0^a (\cosh(ny))^2\, dy.$$

For large n there exist the approximations,

$$\cosh(na) \approx \frac{e^{na}}{2}, \quad \sinh(na) \approx \frac{e^{na}}{2}, \quad \int_0^a (\cosh(ny))^2\, dy \approx \frac{e^{2na}}{8n}.$$

Hence we have

$$\begin{aligned}
\|u\|_{\partial S}^2 &= \|u\|_B^2 + \int_0^a (u^2 + w^2 u_y^2)(x, a)\, dx \\
&\quad + \int_0^a (u^2 + w^2 u_x^2)(0, y)\, dy + \int_0^a (u^2 + w^2 u_x^2)(a, y)\, dy \\
&= \frac{1}{n^{2k}} \{1 + (\cosh(na))^2 + (wn)^2 (\sinh(na))^2\} \int_0^a (\sin(nx))^2\, dx \\
&\quad + \frac{1}{n^{2k}} \{(wn)^2 + (\sin(na))^2 + (wn)^2 (\cos(na))^2\} \int_0^a (\cosh(ny))^2\, dy \\
&\le C\{1 + (wn)^2\} e^{2na} \|u\|_B^2,
\end{aligned}$$

where we have used (12.3.23). The desired bound (12.3.20) is proved by letting $v = u$.

In computation of the MFS, choose $w = \frac{1}{N}$ (see [176]), and $N > n$ or even $N \gg n$, then $wn = \frac{n}{N} < 1$. The bound (12.3.20) is simplified as

$$C_a^I\left(u, \frac{1}{N}\right) = O(e^{na}), \quad N > n > 1. \tag{12.3.24}$$

For Cauchy Model II, it is easy to show

$$C_a^{II}\left(u, \frac{1}{N}\right) = O(1). \tag{12.3.25}$$

Consider the harmonic function at $a = 1$ as in [248],

$$u(x, y) = x^3 - 3xy^2 + e^{2y} \sin(2x) - e^x \cos(y), \text{ in } S, \tag{12.3.26}$$

where the solution domain and the Cauchy boundary are given by

$$S = (0, 1)^2, \quad \Gamma^* = \partial S \cap (y = 0), \tag{12.3.27}$$

$$S = \{(x, y) | x^2 + y^2 < 1\}, \quad \Gamma^* = \{(x, y) | x^2 + y^2 = 1, x > 0, y > 0\}. \tag{12.3.28}$$

For the Cauchy problem with (12.3.26) and (12.3.27) (or (12.3.28)), it is easy to show

$$C_a(u, w) = O((1 + wn)) = O(1). \tag{12.3.29}$$

Hence, this Cauchy problem and Cauchy Model II are not ill-posed themselves. The $\|v\|_{\partial S}$ in (12.3.15) may be defined differently by

$$\|v\|_{\partial S} = \left\{ \|v\|_B^2 + \int_{\partial S \backslash \Gamma^*} v^2 \right\}^{\frac{1}{2}}, \text{ or } \|v\|_{\partial S} = \left\{ \|v\|_B^2 + w^2 \int_{\partial S \backslash \Gamma^*} v_\nu^2 \right\}^{\frac{1}{2}},$$

where $\partial S \backslash \Gamma^*$ denotes ∂S excluding the Cauchy boundary Γ^*. The analysis can be performed similarly.

12.4 Error and Stability Analysis

12.4.1 Error Analysis

Consider the Cauchy problem (12.2.1)–(12.2.3) on a bounded simply-connected domain S with $\Gamma^* \subset \partial S$. Suppose that for $w = \frac{1}{N}$, there exists an inverse inequality,

$$\|v\|_{\partial S} \le C_V(N) \|v\|_B, \quad \forall v \in V_N, \tag{12.4.1}$$

where the function $C_V(N)\ (\ge 1)$ is independent of v. Compared with (12.3.16), there exists the equation,

$$C_V(N) = \max_{\forall v \in V_N} C_a\left(v, \frac{1}{N}\right). \tag{12.4.2}$$

From Lemma 12.3.1, we have the following lemma.

Lemma 12.4.1. *Let (12.4.1) hold. When $w = \frac{1}{N}$, there exists the bound,*

$$\|v\|_{1,S} \le C\sqrt{N} C_V(N) \|v\|_B, \quad \forall v \in V_N,$$

where C is a constant independent of v.

From Chapters 2 and 3, we have the following theorem; detailed proof is given in [255].

Theorem 12.4.1. *Let $u \in \mathbf{H}^p(S)$ $\left(p \ge \frac{3}{2}\right)$ hold. For large N there exists the bound,*

$$\|u - u_N\|_B \le C(1 + Mw) \left\{ \left(\frac{R}{r_{\max}}\right)^{2M-N} \left(\frac{r_{\max}}{r_{\min}}\right)^M \|u\|_{0,\Gamma} + \frac{1}{M^{p-\frac{1}{2}}} \|u\|_{p,S} \right\},$$

where C is a constant independent of M and N.

Corollary 12.4.1. *Let the conditions in Theorem 12.4.1 hold. Suppose that N satisfies*

$$\left(\frac{R}{r_{\max}}\right)^{2M-N} \left(\frac{r_{\max}}{r_{\min}}\right)^M = \frac{1}{M^{p-\frac{1}{2}}}.$$

For the solution of the Cauchy problem by the MFS, when $w = \frac{1}{N}$, *there exist the error bounds,*

$$\|u - u_N\|_B \le C \frac{1}{N^{p-\frac{1}{2}}} \|u\|_{p,S}, \tag{12.4.3}$$

$$\|u - u_N\|_{1,S} \le C \frac{C_a(u,w)}{N^{p-1}} \|u\|_{p,S}, \tag{12.4.4}$$

where the function $C_a(u,w)$ *is given by (12.3.16), and* C *is a constant independent of* N.

Remark 12.4.1. *Note that when* $C_a(u,w) \gg 1$, *the small errors* $\|u - u_N\|_B$ *on* $\mathbf{\Gamma}^*$ *may not imply the convergence of the Cauchy solution. Based on (12.4.4), the number* N *of FS in (12.2.11) should be chosen so large such that*

$$N^{p-1} \gg C_a(u,w)\|u\|_{p,S}, \tag{12.4.5}$$

thus guaranteeing the convergence of the Cauchy solution. However, the large N *used in the MFS cause severe instability.*

Remark 12.4.2. *From (12.4.4), the bounds of errors of the Cauchy problem (12.2.1)–(12.2.3) will be enlarged by factor* $C_a(u,w)$, *compared with the regular boundary value problems of Laplace's equation in Part I. Note that* $C_a^I(u,w)$ *in (12.3.20) is large for Cauchy Model I with large n; but* $C_a^{II}(u,w)$ *in (12.3.25) is not for Cauchy Model II.*

12.4.2 Stability Analysis

12.4.2.1 Trefftz Methods

First, we study stability of the CTM (12.2.13) without integration approximation to obtain the normal equation $\mathbf{Bx} = \mathbf{d}$, where $\mathbf{x} = (c_1, c_2, \ldots, c_N)^T$ and $\mathbf{d} \in \mathbf{R}^N$. The matrix $\mathbf{B} \in \mathbf{R}^{N\times N}$ is symmetric and positive definite, given by

$$\mathbf{x}^T\mathbf{Bx} = \int_{\Gamma^*} \left\{ v^2 + w^2 \left(\frac{\partial v}{\partial \nu}\right)^2 \right\} = \|v\|_B^2. \tag{12.4.6}$$

Hence, the maximal and the minimal eigenvalues of $\mathbf{B}$ are expressed by

$$\lambda_{\max}(\mathbf{B}) = \max_{\mathbf{x}\neq 0} \frac{\mathbf{x}^T\mathbf{Bx}}{\mathbf{x}^T\mathbf{x}} = \max_{\substack{\mathbf{x}\neq 0\\ v\in V_N}} \frac{\|v\|_B^2}{\|\mathbf{x}\|^2}, \tag{12.4.7}$$

$$\lambda_{\min}(\mathbf{B}) = \min_{\mathbf{x}\neq 0} \frac{\mathbf{x}^T\mathbf{Bx}}{\mathbf{x}^T\mathbf{x}} = \min_{\substack{\mathbf{x}\neq 0\\ v\in V_N}} \frac{\|v\|_B^2}{\|\mathbf{x}\|^2}. \tag{12.4.8}$$

Lemma 12.4.2. *For $R > r_{\max}$, there exists the bound,*

$$\lambda_{\max}(\mathbf{B}) \le CN, \tag{12.4.9}$$

where C is a constant independent of N.

Proof. When $R > r_{\max}$, since functions $\phi_i(P)$ and derivatives $\frac{\partial \phi_i}{\partial v}(P)$ are bounded on Γ^*, we have from the Schwarz inequality

$$\begin{aligned}\int_{\Gamma^*} v^2 &= \int_{\Gamma^*}\Big(\sum_{i=1}^N c_i\phi_i(P)\Big)^2 \le \Big(\sum_{i=1}^N |c_i|\int_{\Gamma^*}|\phi_i(P)|\Big)^2\\ &\le \sum_{i=1}^N c_i^2 \sum_{i=1}^N \Big(\int_{\Gamma^*}|\phi_i(P)|\Big)^2 \le CN\sum_{i=1}^N c_i^2 = CN\|\mathbf{x}\|^2.\end{aligned} \tag{12.4.10}$$

Similarly we have

$$\int_{\Gamma^*}\left(\frac{\partial v}{\partial v}\right)^2 = \int_{\Gamma^*}\left\{\sum_{i=1}^N c_i\left(\frac{\partial \phi_i}{\partial v}(P)\right)\right\}^2 \le CN\|\mathbf{x}\|^2. \tag{12.4.11}$$

For $w = \frac{1}{N} \le 1$, we obtain from (12.4.6), (12.4.7), (12.4.10) and (12.4.11)

$$\lambda_{\max}(\mathbf{B}) = \max_{\substack{\mathbf{x}\neq 0\\ v\in V_n}}\frac{\|v\|_B^2}{\|\mathbf{x}\|^2} = \max_{\substack{\mathbf{x}\neq 0\\ v\in V_n}}\frac{\int_{\Gamma^*}\left\{v^2 + w^2\left(\frac{\partial v}{\partial v}\right)^2\right\}}{\|\mathbf{x}\|^2} \le CN(1+w^2) \le 2CN. \tag{12.4.12}$$

This is the desired result (12.4.9). ■

The challenging work is to estimate the lower bound of $\lambda_{\min}(\mathbf{B})$ in (12.4.8). For simplicity, we assume $R \neq 1$. Hence the matrix $\mathbf{B}$ is nonsingular, and then $\lambda_{\min}(\mathbf{B}) > 0$. Denote the inscribed disk $S_0 \subseteq S$ and its boundary by $S_0 = \{(r,\theta) | r < r_{\min}, 0 \le \theta < 2\pi\}$ and $\Gamma_0 = \{(r,\theta) | r = r_{\min}, 0 \le \theta \le 2\pi\}$. Choose the collocation nodes uniformly on Γ_0,

$$P_\ell^* = \{(x,y) | x = r_{\min}\cos(\ell h), y = r_{\min}\sin(\ell h)\}, \tag{12.4.13}$$

where $h = \frac{2\pi}{N}$. It is shown in [169] that the integrals, $\int_{\Gamma_0} v^2$ and $\widehat{\int}_{\Gamma_0} v^2$, are equivalent to each other,

$$\overline{\|v\|}_{0,\Gamma_0}^2 \asymp \|v\|_{0,\Gamma_0}^2, \tag{12.4.14}$$

even by the central rule, where $\overline{\|v\|}_{0,\Gamma_0}^2 = \widehat{\int}_{\Gamma_0} v^2$. In (12.4.14), the notation $a \asymp b$ (or $a \asymp O(b)$) means that there exist two positive constants c_0 and C_1 such that $c_0 b \le |a| \le C_1 b$, $b > 0$. We have the following lemma.

Lemma 12.4.3. *Let* $R > r_{\max} > r_{\min}$*, and the collocation and the source nodes be chosen as (12.4.13) and (12.2.9), respectively. Then there exists the lower bound,*

$$\|v\|^2_{0,\Gamma_0} \geq c_0 \frac{1}{N} \left(\frac{r_{\min}}{R}\right)^N \mathbf{x}^T\mathbf{x}, \tag{12.4.15}$$

where $c_0\,(> 0)$ *is a constant independent of* N.

Proof. We have for $P \in \Gamma_0$

$$\|v\|^2_{0,\Gamma_0} = \int_{\Gamma_0} v^2 = \int_{\Gamma_0} \left\{\sum_{i=1}^N c_i\phi_i(P)\right\}^2 = \sum_{i,j=1}^N c_ic_j \int_{\Gamma_0} \phi_i(P)\phi_j(P). \tag{12.4.16}$$

Denote $P^*_\ell = (r_{\min}\cos(\ell h), r_{\min}\sin(\ell h))$ with $\ell = 1, 2, \ldots, N$. Combining (12.4.16) and (12.4.14) gives

$$\begin{aligned} \|v\|^2_{0,\Gamma_0} \geq c_0\overline{\|v\|}^2_{0,\Gamma_0} &= c_0hr_{\min} \sum_{i,j=1}^N \left\{ c_ic_j \sum_{\ell=1}^N \phi_i(P^*_\ell)\phi_j(P^*_\ell) \right\} \\ &= c_0hr_{\min}\mathbf{x}^T\mathbf{A}^T\mathbf{A}\mathbf{x} = \bar{c}_0\frac{1}{N}\mathbf{x}^T\mathbf{A}^T\mathbf{A}\mathbf{x}, \end{aligned} \tag{12.4.17}$$

where $h = \frac{2\pi}{N}$, and $\bar{c}_0 > 0$ is a constant independent of N. The matrix $\mathbf{A}$ is symmetric and circulant, which is obtained from the MFS, where the collocation nodes are located uniformly on the circle Γ_0 with radius $\rho = r_{\min}$. For the disk S_0, the sharp bound, $\lambda_{\min}(\mathbf{A}) \geq c_0\left(\frac{r_{\min}}{R}\right)^{\frac{N}{2}}$, is cited from [163] and Chapter 2. We have

$$\frac{\mathbf{x}^T\mathbf{A}^T\mathbf{A}\mathbf{x}}{\mathbf{x}^T\mathbf{x}} \geq (\lambda_{\min}(\mathbf{A}))^2 \geq c_0\left(\frac{r_{\min}}{R}\right)^N. \tag{12.4.18}$$

Combining (12.4.17) and (12.4.18) gives the desired result (12.4.15). ■

Theorem 12.4.2. *Let* $R \neq 1$*, and the conditions (12.4.1) and (12.4.14) hold. Then when* $w = \frac{1}{N}$ *there exists the bound,*

$$\lambda_{\min}(\mathbf{B}) \geq \frac{c_0}{C_V^2(N)}\frac{1}{N^2}\left(\frac{r_{\min}}{R}\right)^N, \tag{12.4.19}$$

where $C_V(N)$ *is defined in (12.4.2), and* $c_0\,(> 0)$ *is a constant independent of* N.

Proof. Since $S_0 \subseteq S$, we have from the imbedding theorem [15, 195]

$$\|v\|_{0,\Gamma_0} = \|v\|_{0,\partial S_0} \leq C\|v\|_{1,S_0} \leq C\|v\|_{1,S}. \tag{12.4.20}$$

Under (12.4.1) we have from Lemma 12.4.1

$$\|v\|_B \geq c_0\frac{1}{\sqrt{N}C_V(N)}\|v\|_{1,S}, \quad \forall v \in V_{\mathrm{N}}. \tag{12.4.21}$$

Combining (12.4.20) and (12.4.21) gives

$$\|v\|_B \geq c_0 \frac{1}{\sqrt{N} C_V(N)} \|v\|_{0,\Gamma_0}. \tag{12.4.22}$$

From (12.4.8) and (12.4.22) and Lemma 12.4.3, we obtain

$$\lambda_{\min}(\mathbf{B}) = \max_{\substack{\mathbf{x}\neq 0 \\ v\in V_n}} \frac{\|v\|_B^2}{\|\mathbf{x}\|^2} \geq \frac{c_0}{C_V^2(N)N} \frac{\|v\|_{0,\Gamma_0}^2}{\|\mathbf{x}\|^2} \geq \frac{c_0}{C_V^2(N)} \frac{1}{N^2} \left(\frac{r_{\min}}{R}\right)^N.$$

This is the desired result (12.4.19) and completes the proof of Theorem 12.4.2. ■

From Lemma 12.4.2 and Theorem 12.4.2, we obtain the following corollary.

Corollary 12.4.2. *Let the conditions in Theorem 12.4.2 hold. When* $w = \frac{1}{N}$, *there exists the bound,*

$$\text{Cond}(\mathbf{B}) \leq C C_V^2(N) N^3 \left(\frac{R}{r_{\min}}\right)^N.$$

12.4.2.2 Collocation Trefftz Methods

In computation, we use (12.2.18) and (12.2.19) (or (12.2.20) and (12.2.21)) to give an overdetermined system

$$\mathbf{F}\mathbf{x} = \mathbf{b}, \tag{12.4.23}$$

where vectors $\mathbf{x} = (c_1, c_2, \ldots, c_N)^T$ and $\mathbf{b} \in \mathbf{R}^{2M}$, and matrix $\mathbf{F} \in \mathbf{R}^{2M\times N}(2M \geq N)$. We have

$$\mathbf{x}^T\mathbf{F}^T\mathbf{F}\mathbf{x} = \overline{\|v\|}_B^2,\ \overline{\|v\|}_B^2 = \widehat{\int}_{\Gamma^*} \left\{ v^2 + w^2 \left(\frac{\partial v}{\partial \nu}\right)^2 \right\},$$

where $\widehat{\int}_{\Gamma^*}$ is a numerical approximation of $\int_{\Gamma^*}$ by the central or the Gaussian rule. From [169], assume that the following equivalent norms hold,

$$\overline{\|v\|}_{0,\Gamma^*} \asymp \|v\|_{0,\Gamma^*}. \tag{12.4.24}$$

Denote the singular values σ_i of $\mathbf{F}$ in (12.4.23), the maximal singular value $\sigma_{\max} = \max_i \sigma_i$ and the minimal singular value $\sigma_{\min} = \min_i \sigma_i \,(> 0)$.

Theorem 12.4.3. *Let* $R \neq 1$, *and the conditions (12.4.1), (12.4.14) and (12.4.24) hold. For the MFS in (12.2.18) and (12.2.19) (or (12.2.20) and (12.2.21)), there exist the bounds,*

$$\sigma_{\max}(\mathbf{F}) \leq C N^{\frac{1}{2}}, \tag{12.4.25}$$

$$\sigma_{\min}(\mathbf{F}) \geq c_0 \frac{1}{C_V(N)} \frac{1}{N} \left(\frac{r_{\min}}{R}\right)^{\frac{N}{2}}. \tag{12.4.26}$$

Proof. From (12.4.24) we have

$$\overline{\|v\|}_B \asymp \|v\|_B. \tag{12.4.27}$$

From (12.4.12) and (12.4.27), there exist the bounds,

$$\lambda_{\max}(\mathbf{F}^T\mathbf{F}) = \max_{\mathbf{x}\neq 0}\frac{\mathbf{x}^T\mathbf{F}^T\mathbf{F}\mathbf{x}}{\mathbf{x}^T\mathbf{x}} = \max_{\substack{x\neq 0\\ v\in V_N}}\frac{\overline{\|v\|}_B^2}{\|\mathbf{x}\|^2} \leq C\max_{\substack{x\neq 0\\ v\in V_N}}\frac{\|v\|_B^2}{\|\mathbf{x}\|^2} \leq \bar{C}N, \tag{12.4.28}$$

where $\bar{C}$ is a constant independent of N. Next, from Theorem 12.4.2 and (12.4.27), we obtain

$$\begin{aligned}\lambda_{\min}(\mathbf{F}^T\mathbf{F}) &= \min_{\mathbf{x}\neq 0}\frac{\mathbf{x}^T\mathbf{F}^T\mathbf{F}\mathbf{x}}{\mathbf{x}^T\mathbf{x}} = \min_{\substack{x\neq 0\\ v\in V_N}}\frac{\overline{\|v\|}_B^2}{\|\mathbf{x}\|^2}\\ &\geq c_0\min_{\substack{x\neq 0\\ v\in V_N}}\frac{\|v\|_B^2}{\|\mathbf{x}\|^2} \geq \overline{c}_0\frac{1}{C_V^2(N)}\frac{1}{N^2}\left(\frac{r_{\min}}{R}\right)^N,\end{aligned} \tag{12.4.29}$$

where $\overline{c}_0 > 0$ is a constant independent of N. The desired results (12.4.25) and (12.4.26) follow from (12.4.28), (12.4.29) and the following equalities,

$$\sigma_{\max}(\mathbf{F}) = \{\lambda_{\max}(\mathbf{F}^T\mathbf{F})\}^{\frac{1}{2}}, \quad \sigma_{\min}(\mathbf{F}) = \{\lambda_{\min}(\mathbf{F}^T\mathbf{F})\}^{\frac{1}{2}}.$$

This completes the proof of Theorem 12.4.3. ■

Corollary 12.4.3. *Let the conditions in Theorem 12.4.3 hold. For* $w = \frac{1}{N}$ *there exists the bound,*

$$\text{Cond}(\mathbf{F}) \leq CC_V(N)N^{\frac{3}{2}}\left(\frac{R}{r_{\min}}\right)^{\frac{N}{2}}. \tag{12.4.30}$$

The severe numerical instability is caused by Cauchy problems and the MFS. The regularization in [95, 161] may be used to improve stability for Cauchy problems by the MFS; see [255, 259].

12.5 Applications to Cauchy Data

In application, the sensitivity of errors for Cauchy data is the focus of research. In this section, we will apply the theoretical results in Section 12.4 to Cauchy data, and provide more analysis for Model I with the boundary noise.

12.5.1 Errors on Cauchy Boundary

From the definitions (12.3.15) we have

$$\begin{aligned}\|u - u_N\|_B &= \left\{\int_{\Gamma_*}(f - u_N)^2 + w^2(g - (u_N)_\nu)^2\right\}^{\frac{1}{2}}\\ &= \left\{\|f - u_N\|_{0,\Gamma^*}^2 + w^2\|g - (u_N)_\nu\|_{0,\Gamma^*}^2\right\}^{\frac{1}{2}}.\end{aligned} \tag{12.5.1}$$

From (12.5.1) and (12.4.3),

$$\|u-u_N\|_B \le C\frac{1}{N^{p-\frac{1}{2}}}\|u\|_{p,S}. \tag{12.5.2}$$

The equation (12.5.2) displays explicitly the error bounds on the Cauchy boundary, to give the polynomial converge rates.

As Remark 12.4.1 pointed out, the small errors on the Cauchy boundary may not imply the convergence of the exact solution when $C_a(u,w) \gg 1$. A sufficient condition of convergent solutions is derived in (12.4.5). Hence the mere investigation of the errors of Cauchy conditions is valid for Model II, but not for Model I with $n \ge 5$. This is a distinct feature of error analysis from that of Dirichlet problems in Chapter 2.

12.5.2 Sensitivity of Solutions on Cauchy Data

The collocation equations on the Cauchy boundary yield an overdetermined system (12.4.23), and the stability analysis in Section 12.4 also illustrates a sensitivity to Cauchy data. Below, we provide a detailed explanation. Consider the overdetermined system (12.4.23), where $\text{rank}(\mathbf{F}) = n$. The traditional and the effective condition numbers in the 2-norm are defined by $\text{Cond} = \frac{\sigma_{\max}}{\sigma_{\min}}$ and $\text{Cond\_eff} = \frac{\|\mathbf{b}\|}{\sigma_{\min}\|\mathbf{x}\|}$, where $\sigma_{\max}$ and $\sigma_{\min}$ are the maximal and the minimal singular values of $\mathbf{F}$, respectively, and $\|\mathbf{x}\|$ is the 2-norm. There always exist bounds, $\text{Cond\_eff} \le \text{Cond}$ or even $\text{Cond\_eff} \ll \text{Cond}$.

From the collocation equations (12.2.18) and (12.2.19) (or (12.2.20) and (12.2.21)), the known vector $\mathbf{b}$ results just from the Cauchy data on Γ^* in (12.2.2) and (12.2.3) to give

$$\|\mathbf{b}\|^2 \approx \|f\|^2_{0,\Gamma^*} + w^2\|g\|^2_{0,\Gamma^*} = \|u\|^2_B. \tag{12.5.3}$$

When there exist perturbations of $\mathbf{b}$ and $\mathbf{F}$, the practical computation for (12.4.23) is carried out by

$$\mathbf{F}(\mathbf{x}+\triangle\mathbf{x}) = \mathbf{b}+\triangle\mathbf{b}, \tag{12.5.4}$$

$$(\mathbf{F}+\triangle\mathbf{F})(\mathbf{x}+\triangle\mathbf{x}) = \mathbf{b}+\triangle\mathbf{b}, \tag{12.5.5}$$

where $\triangle\mathbf{F} \in \mathbf{R}^{m\times n}$ $(m \ge n)$, $\triangle\mathbf{x} \in \mathbf{R}^n$ and $\triangle\mathbf{b} \in \mathbf{R}^m$. Suppose that $\triangle\mathbf{F}$ is small so that $\text{rank}(\mathbf{F}) = \text{rank}(\mathbf{F}+\triangle\mathbf{F}) = n$. For (12.5.4) (*i.e.*, $\triangle\mathbf{F} = 0$), there exist the bounds of relative errors,

$$\frac{\|\triangle\mathbf{x}\|}{\|\mathbf{x}\|} \le \text{Cond} \times \frac{\|\triangle\mathbf{b}\|}{\|\mathbf{b}\|}, \quad \frac{\|\triangle\mathbf{x}\|}{\|\mathbf{x}\|} \le \text{Cond\_eff} \times \frac{\|\triangle\mathbf{b}\|}{\|\mathbf{b}\|}. \tag{12.5.6}$$

For the perturbations in (12.5.5), there exists the bound (see [162, 242]),

$$\frac{\|\triangle\mathbf{x}\|}{\|\mathbf{x}\|} \le \frac{\text{Cond\_eff}}{1-\delta}\left\{\sqrt{2}\ \text{Cond} \times \frac{\|\triangle\mathbf{F}\|}{\|\mathbf{F}\|} + \frac{\|\triangle\mathbf{b}\|}{\|\mathbf{b}\|}\right\}, \tag{12.5.7}$$

where $\delta = \frac{\|\triangle \mathbf{F}\|}{\|\mathbf{F}\|} < 1$. Based on (12.5.3), the $\frac{\|\triangle \mathbf{b}\|}{\|\mathbf{b}\|}$ denotes the errors of Cauchy data on $\mathbf{\Gamma}^*$, and bounds (12.5.6) and (12.5.7) illustrate quantitatively the sensitivity of the solution $\mathbf{x}$ on Cauchy data. For linear algebraic equations, the bound $\frac{\|\triangle \mathbf{b}\|}{\|\mathbf{b}\|}$ may be smaller than $\frac{\|\triangle \mathbf{F}\|}{\|\mathbf{F}\|}$ from the solution methods, so that the condition number may play a dominant role in (12.5.7). However, for the MPS and the MFS, the noise $\frac{\|\triangle \mathbf{b}\|}{\|\mathbf{b}\|}$ of the Cauchy data are much larger than $\frac{\|\triangle \mathbf{F}\|}{\|\mathbf{F}\|}$, so the effective condition number will play a dominant role in (12.5.7). Details are given in [162].

The bounds (12.5.6) and (12.5.7) yield the perturbation errors of solutions from the errors of Cauchy data. More specifically, the relative errors of the solution $\mathbf{x}$ may be enlarged from the errors of the Cauchy conditions by Cond (or Cond_eff), which provides precisely the sensitivity (*i.e.*, stability) of the solutions on Cauchy conditions. In Section 12.4, the bounds of Cond are derived theoretically, and given in (12.4.30), which are also important and significant to the stability study of Cauchy data.

12.6 Numerical Experiments and Concluding Remarks

Consider (12.2.1)–(12.2.7) with $n = 5, k = 1$ and $a = 1$. We only use the MFS for Cauchy Models I and II, and choose the Dirichlet problem with $u = f$ on ∂S for comparison. Define the Sobolev errors in the entire domain S by

$$\|\epsilon\|_{0,S} = \sqrt{\int_S \epsilon^2 \, ds}, \quad \|\epsilon\|_{1,S} = \sqrt{\int_S \left\{ \epsilon^2 + \left(\frac{\partial \epsilon}{\partial x}\right)^2 + \left(\frac{\partial \epsilon}{\partial y}\right)^2 \right\} ds}, \tag{12.6.1}$$

where $\epsilon = u - u_N$. Choose the polar coordinates (ρ, θ) with the center $\left(\frac{1}{2}, \frac{1}{2}\right)$. In computation, we choose $R = 2 \left(> \frac{1}{\sqrt{2}}\right)$ in (12.2.9). We use the FS in (12.2.11) with the vector norm $\|\mathbf{x}\| = \left(\sum_{i=1}^N c_i^2\right)^{\frac{1}{2}}$. The collocation equations (12.2.18) and (12.2.19) are used on the Cauchy boundary. On each Cauchy edge, 40 collocation nodes are chosen, and the total number of collocation equations is given by $2M$, where $M = \ell \times 40$. When $\ell = 1$ and $\ell = 3$, we have Cauchy Models I and II, respectively. For Cauchy Model I, the errors and the condition numbers are listed in Table 12.1. All computations and tables in this chapter are conducted in Matlab with double precision. From Table 12.1, we can find the following asymptotes:

$$\|\epsilon\|_B = O(0.510^N), \quad \|\epsilon\|_{\partial S} = O(0.868^N), \quad \|\epsilon\|_{0,S} = O(0.749^N), \tag{12.6.2}$$

$$\text{Cond} = O(1.89^N), \quad \text{Cond\_eff} = O(1.89^N). \tag{12.6.3}$$

From (12.6.2) we have

$$\frac{\|\epsilon\|_{\partial S}}{\|\epsilon\|_B} = O(1.7^N). \tag{12.6.4}$$

The equations (12.6.2) and (12.6.4) imply that we should seek the MFS solutions with much smaller errors $\|\epsilon\|_B$ on the Cauchy boundary, to achieve the approximate solutions on the entire boundary and in the entire domains (*i.e.*, $\|\epsilon\|_{\ell,S}, \ell = 0, 1$). This coincides with the analysis in Section 12.4. Note that in Table 12.1, when N grows, $\sigma_{\max} = O(\sqrt{N})$, but $\sigma_{\min}$ diminishes exponentially, leading to the exponential growth of Cond. They are also consistent with the analysis in Section 12.4. The bounds of Cond are greatly dependent on R, similarly to those in the Dirichlet, the Neumann problems, and their mixed boundary problems in Chapters 2–4. We only report those with $R = 2$; other results are omitted.

For Cauchy Model II, the errors and condition numbers are listed in Table 12.2. From Table 12.2, we find

$$\|\epsilon\|_B = O(0.440^N), \quad \|\epsilon\|_{\partial S} = O(0.437^N), \quad \|\epsilon\|_{0,S} = O(0.441^N), \tag{12.6.5}$$

$$\text{Cond} = O(2.03^N), \quad \text{Cond\_eff} = O(1.97^N), \tag{12.6.6}$$

and

$$\frac{\|\epsilon\|_{\partial S}}{\|\epsilon\|_B} = O(0.993^N) \approx O(1). \tag{12.6.7}$$

The equation (12.6.7) implies that almost the same accuracy of the Cauchy and the entire boundary errors can be achieved, thus verifying the analysis in Section 12.3 (see (12.3.25)).

To verify the estimated bound (12.4.30), we cite the data in Tables 12.1 and 12.2 at $N = 36$ of the MFS, respectively

$$\sigma_{\min} = 9.42(-18), \quad \text{Cond} = 7.21(16), \quad \text{Cond\_eff} = 1.14(11), \tag{12.6.8}$$

$$\sigma_{\min} = 4.44(-12), \quad \text{Cond} = 2.57(11), \quad \text{Cond\_eff} = 8.56(6). \tag{12.6.9}$$

Cond = 7.21(16) of Model I is larger than Cond = 2.57(11) of Model II. By noting different bounds of $C_V(N)$, these computed results coincide with the theoretical estimate (12.4.30).

We also carry out the computation for the Dirichlet problem for comparisons, and list the results in Table 12.3. We find

$$\|\epsilon\|_{0,\partial S} = O(0.462^N), \quad \|\epsilon\|_{0,S} = O(0.467^N), \tag{12.6.10}$$

$$\text{Cond} = O(1.89^N), \quad \text{Cond\_eff} = O(1.85^N). \tag{12.6.11}$$

Comparing $\|\epsilon\|_{0,S} = O(0.441^N)$ of Model II with $\|\epsilon\|_{0,S} = O(0.467^N)$ of the Dirichlet problem, the numerical performance of Model II is very satisfactory. Obviously, the MFS for Cauchy Model II is more efficient than Cauchy Model I. We have computed the cases with $n = 10$; both errors and condition numbers are much larger. However, Tab. 12.1 – The errors and the condition numbers of Cauchy Model I by the MFS with $R = 2$.

N	$\|\epsilon\|_B$	$\|\epsilon\|_{\partial S}$	$\|\epsilon\|_{0,S}$	$\|\epsilon\|_{1,S}$	Cond_eff	Cond	$\sigma_{\max}$	$\sigma_{\min}$	$\|\mathbf{x}\|$
20	4.16(−6)	2.36	4.61(−1)	5.92	5.89(5)	2.87(11)	5.06(−1)	1.76(−12)	2.21(4)
24	1.52(−7)	1.86	3.55(−1)	5.07	3.37(7)	6.17(13)	5.54(−1)	8.99(−15)	7.58(4)
28	5.30(−9)	9.58(−1)	1.68(−1)	3.56	1.09(9)	1.23(16)	5.99(−1)	4.86(−17)	4.33(5)
32	2.43(−10)	1.66(−1)	2.99(−2)	5.92(−1)	2.18(10)	6.57(16)	6.40(−1)	9.74(−18)	1.08(5)
36	1.78(−11)	1.32(−2)	2.31(−3)	4.29(−2)	1.14(11)	7.21(16)	6.79(−1)	9.42(−18)	2.14(4)
40	5.96(−12)	8.48(−3)	1.44(−3)	3.21(−2)	2.22(11)	1.04(17)	7.15(−1)	6.87(−18)	1.51(4)

Tab. 12.2 – The errors and the condition numbers of Cauchy Model II by the MFS with $R = 2$.

N	$\|\epsilon\|_B$	$\|\epsilon\|_{\partial S}$	$\|\epsilon\|_{0,S}$	$\|\epsilon\|_{1,S}$	Cond_eff	Cond	$\sigma_{\max}$	$\sigma_{\min}$	$\|\mathbf{x}\|$
20	1.85(−3)	1.12(−1)	2.97(−2)	3.14(−1)	2.00(2)	2.88(6)	8.52(−1)	2.95(−7)	1.25(4)
24	1.24(−4)	6.94(−3)	1.67(−3)	2.22(−2)	2.70(3)	6.17(7)	9.33(−1)	1.51(−8)	1.78(4)
28	2.31(−6)	5.84(−4)	1.35(−4)	2.01(−3)	2.69(4)	7.40(8)	1.01	1.36(−9)	1.98(4)
32	8.77(−8)	2.68(−5)	5.95(−6)	9.84(−5)	5.04(5)	1.49(10)	1.08	7.23(−11)	1.98(4)
36	8.15(−10)	7.16(−7)	1.46(−7)	2.93(−6)	8.56(6)	2.57(11)	1.14	4.44(−12)	1.89(4)
40	1.05(−11)	1.99(−8)	3.92(−9)	8.60(−8)	1.08(8)	3.25(12)	1.21	3.71(−13)	1.80(4)
44	5.13(−12)	2.62(−10)	4.89(−11)	1.23(−9)	2.40(9)	7.27(13)	1.26	1.74(−14)	1.71(4)

TAB. 12.3 – The errors and the condition numbers of the Dirichlet problem by the MFS with $R = 2$.

N	$\|\epsilon\|_{0,\partial S}$	$\|\epsilon\|_{0,S}$	$\|\epsilon\|_{1,S}$	Cond_eff	Cond	$\sigma_{\max}$	$\sigma_{\min}$	$\|\mathbf{x}\|$
20	2.27(−2)	4.42(−3)	1.04(−1)	2.87(2)	2.20(6)	3.92(1)	1.78(−5)	1.44(4)
24	1.30(−3)	2.40(−4)	8.25(−3)	2.46(3)	2.69(7)	4.30(1)	1.60(−6)	1.88(4)
28	7.24(−5)	1.25(−5)	4.31(−4)	3.12(4)	3.98(8)	4.64(1)	1.17(−7)	2.03(4)
32	2.32(−6)	3.96(−7)	1.83(−5)	3.61(5)	4.82(9)	4.96(1)	1.03(−8)	1.99(4)
36	7.31(−8)	1.16(−8)	5.45(−7)	4.93(6)	6.65(10)	5.26(1)	7.92(−10)	1.89(4)
40	1.45(−9)	2.34(−10)	1.35(−8)	6.00(7)	8.10(11)	5.55(1)	6.85(−11)	1.80(4)
44	3.09(−11)	7.98(−12)	2.43(−10)	7.83(8)	1.06(13)	5.82(1)	5.50(−12)	1.71(4)
48	9.78(−12)	2.65(−12)	5.83(−11)	9.69(9)	1.31(14)	6.07(1)	4.64(−13)	1.64(4)

the above conclusions and comparisons of Models I and II and Dirichlet problems remain invariant. Details are omitted. Numerical experiments for Cauchy data with noise are provided in [255].

To close this chapter, let us make a few concluding remarks.

1. The Cauchy problems can be solved numerically by the MFS and the MPS. Based on Lemmas 12.3.1 and 12.4.1, the bounds of errors and condition numbers of Cauchy problems by the MFS have been derived in Theorems 12.4.1 and 12.4.3. The analysis for the MPS can also be obtained similarly.
2. For $S = (0, 1)^2$, the Cauchy Models I and II are designed with Cauchy data on one edge and three edges of ∂S, respectively. Numerical experiments in Section 12.6 are carried out for these two Cauchy Models and the Dirichlet problem by the MFS. The numerical results support the analysis in Section 12.4.
3. Cauchy Model II is more effective than Cauchy Model I, and the MPS is superior to the MFS. The MFS owns simplicity of algorithms but may incur worse instability. For Cauchy problems, the less Cauchy data are assigned on ∂S, the worse instability occurs causing larger errors. Moreover, the numerical performance of well-posed Cauchy problems is as good as that of Dirichlet problems. Hence, the study of numerical methods for ill-posed Cauchy problems is imperative and significant.
4. For Cauchy problems, the existence and uniqueness of the solutions is discussed in Section 12.3.1, and the ill-posedness of Cauchy problems can be denoted by the functions $C_a(v, w)$ in (12.3.16). The large and the small bounds of $C_a(v, w)$ define the ill-posed and the well-posed Cauchy problems, respectively. The study of Cauchy problems should focus on the ill-posed Cauchy problems, such as Model I with $n \geq 5$. The error and stability analysis of this chapter may, to a certain degree, fill up the existing gap between theory and computation [58, 119] of Cauchy problems by the MFS and the MPS.

Chapter 13

3D Problems

In this chapter, we will develop the basic analysis of the method of fundamental solutions (MFS) in Part I for Laplace's equation in the bounded simply-connected domains Ω in three dimensions (3D). Although some numerical computations can be found in Chen *et al.* [38], the theoretical analysis is much behind (Li [143] only for convergence in the unit sphere Ω). Our efforts are devoted to exploring the strict error analysis of the MFS. The error bounds are derived and the optimal polynomial convergence rates can also be achieved. Numerical experiments are carried out to support the analysis made, and several useful locations of source nodes are investigated numerically. The analysis in this chapter may lay a theoretical basis for the MFS for 3D problems, as in the previous chapters for 2D problems. Besides, the method of particular solutions (MPS) in [169] is also studied by using the spherical harmonic functions (SHF). Optimal polynomial convergence rates and exponential growth of condition numbers (Cond) are obtained. The source nodes are located on surfaces based on the abscissas of quadrature rules; they are "*grid-like*", where the source nsodes are located at their intersections. Since most 3D problems, in reality, can not be simplified to 2D problems, and since the MFS has more advantages for 3D problems in algorithm simplicity and wide application, the study in this chapter is essential and important to the MFS. The materials of this chapter are adapted from [249].

13.1 Introduction

In this chapter, we study the MFS for Laplace's equation in the bounded simply-connected domains Ω in 3D. For Laplace's equation in 3D, the fundamental solutions (FS) are simple as $\frac{1}{|PQ|}$, where $P \in \bar{\Omega}$ and the source nodes $Q\,(\neq P)$ are located outside Ω. Our efforts are devoted to the error analysis of the MFS for 3D problems. The strategy is to link the FS to the SHF so that the error bounds between FS and SHF can be derived. Hence, we will first study the MPS by using the SHF in Section 13.2. Bounds of both errors and Cond are derived by the MPS, and the optimal polynomial convergence rates and the exponential growth of Cond are attained. This error and

DOI: 10.1051/978-2-7598-3171-5.c013

© Science Press, EDP Sciences, 2023

stability analysis in this chapter is also a new development of the book [169], where the MPS was discussed only for 2D problems.

The source nodes can be simply located on a sphere outside $\boldsymbol{\Omega}$. By using the addition theorems, the solutions by the MFS can be chosen to approximate those by the MPS, and the same optimal polynomial convergence rates can be achieved. Numerical experiments are carried out to support the analysis made. For 3D problems by the MFS, numerical experiments are reported in Chen *et al.* [38], Chi [60], and Saavedra and Power [208]. There exists no strict analysis; the convergence was provided in Li [143] only for the unit sphere $\boldsymbol{\Omega}$. This chapter is the first time to give a strict error analysis of the MFS for 3D problems, to establish a theoretical framework as Chapter 2 for 2D problems.

Numerical experiments are carried out to support the analysis made. The locations of source nodes are important in real applications [38]. In Section 13.5, three kinds of locations for source nodes are investigated numerically. The source nodes are located on surfaces outside $\boldsymbol{\Omega}$ based on the abscissas of quadrature rules; they are "*grid-like*", where the source nodes are located at their intersections. The remarkable reward is the polynomial convergence rates, and even the exponential convergence rates if the solution is analytic.

This chapter is organized as follows. In the next section, the MPS is first discussed by using the spherical harmonic functions (SHF). In Section 13.3, the algorithms of the MFS are described. In Section 13.4, the error analysis for the MFS is made for the source nodes on a sphere. In Section 13.5, numerical experiments for 3D problems are reported. In Section 13.6, a few concluding remarks are made. In Appendix 13.7, the techniques in this chapter may be applied to 3D Helmholtz equations.

13.2 Method of Particular Solutions

Since the analysis of the MFS is closely related to that of the MPS in [169], we will first discuss the MPS in this section, and start to study the MFS in the next section.

Let Ω be a bounded simply-connected domain in 3D with a smooth boundary $\Gamma\,(=\partial\Omega)$. Consider the Dirichlet problem,

$$\nabla^2 u(x,y,z)=0, \quad (x,y,z)\in\boldsymbol{\Omega}, \tag{13.2.1}$$

$$u(x,y,z)=f(x,y,z), \quad (x,y,z)\in\Gamma. \tag{13.2.2}$$

The spherical coordinates (ρ,θ,ϕ) are denoted by $(x,y,z)=(\rho\,\sin\theta\,\cos\phi,\rho\,\sin\theta\,\sin\phi,\rho\,\cos\theta)$ (see Figure 13.1). The Laplace operator is written in the spherical coordinates as

$$\nabla^2 u=\frac{1}{\rho^2}\left(\frac{\partial}{\partial\rho}\left(\rho^2\frac{\partial u}{\partial\rho}\right)+\frac{1}{\sin\theta}\frac{\partial}{\partial\theta}\left(\sin\theta\frac{\partial u}{\partial\theta}\right)+\frac{1}{\sin^2\theta}\frac{\partial^2 u}{\partial\phi^2}\right). \tag{13.2.3}$$

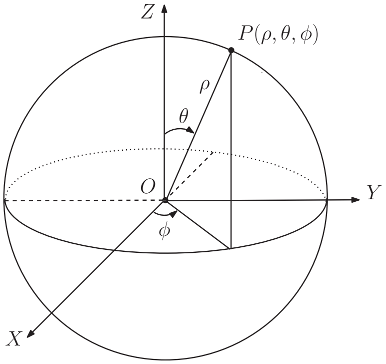

FIG. 13.1 – The spherical coordinates (ρ, θ, ϕ).

The solutions of (13.2.3) are given by (see Tikhonov and Samarskii [223])

$$u(\rho,\theta,\phi) = \sum_{n=0}^{\infty} \rho^n Y_n(\theta,\phi), \tag{13.2.4}$$

where $Y_n(\theta,\phi)$ are the SHF,

$$Y_n(\theta,\phi) = A_n P_n(\cos\theta) + \sum_{m=1}^{n} P_n^{(m)}(\cos\theta)\{A_{n,m}\cos(m\phi) + B_{n,m}\sin(m\phi)\}, \tag{13.2.5}$$

and A_n, $A_{n,m}$ and $B_{n,m}$ are real coefficients. In (13.2.5), $P_n(x)$ are the Legendre polynomials defined by

$$P_n(x) = \frac{1}{2^n n!}\frac{d^n}{dx^n}[(x^2-1)^n], \tag{13.2.6}$$

and $P_n^{(m)}(x)$ with $0 \le m \le n$ are the associated functions defined by

$$P_n^{(m)}(x) = (1-x^2)^{\frac{m}{2}}\frac{d^m}{dx^m}[P_n(x)]. \tag{13.2.7}$$

Then the functions $P_n^{(0)}(x) = P_n(x)$. There exists the orthogonality,

$$\int_{-1}^{1} P_n(x)P_k(x)\,dx = \delta_{nk}\frac{2}{2n+1}, \tag{13.2.8}$$

$$\int_{-1}^{1} P_n^{(m)}(x)P_k^{(m)}(x)\,dx = \delta_{nk}\frac{2}{2n+1}\frac{(n+m)!}{(n-m)!}, \tag{13.2.9}$$

where $\delta_{nn} = 1$ and $\delta_{nk} = 0$ for $n \ne k$. Define spheres,

$$S_\rho = \{(\rho,\theta,\phi)|\rho = \text{const}, 0 \le \theta \le \pi, 0 \le \phi \le 2\pi\},$$
$$U = \{(\rho,\theta,\phi)|\rho = 1, 0 \le \theta \le \pi, 0 \le \phi \le 2\pi\}.$$

In (13.2.5), the spherical harmonic functions, $P_n(\cos\theta)$, $P_n^{(m)}(\cos\theta)\cos(m\phi)$ and $P_n^{(m)}(\cos\theta)\sin(m\phi)$, are orthogonal in the integration on the unit sphere U, *e.g.*,

$$\begin{aligned}
&\iint_U (P_n^{(m)}(\cos\theta)\cos(m\phi))(P_k^{(\ell)}(\cos\theta)\cos(\ell\phi))\,ds \\
&= \int_0^\pi \left\{ \int_0^{2\pi} (P_n^{(m)}(\cos\theta)\cos(m\phi))(P_k^{(\ell)}(\cos\theta)\cos(\ell\phi))\,d\phi \right\} \sin\theta\,d\theta \qquad (13.2.10) \\
&= \delta_{nk}\delta_{m\ell}\varepsilon_m \frac{2\pi}{2n+1}\frac{(n+m)!}{(n-m)!},
\end{aligned}$$

where $ds = \sin\theta\,d\theta\,d\phi$, $\varepsilon_0 = 2$ and $\varepsilon_m = 1$ for $m \ge 1$.

Suppose that solution $u(\rho,\theta,\phi)$ on the sphere S_ρ is known, the exact coefficients A_n, $A_{n,m}$ and $B_{n,m}$ can be found from (13.2.4), (13.2.8), (13.2.9) and (13.2.10) explicitly as

$$\begin{aligned}
A_n &= \frac{1}{\rho^n \frac{4\pi\rho^2}{2n+1}} \iint_{S_\rho} u(\rho,\theta,\phi) P_n(\cos\theta)\,ds, \\
A_{n,m} &= \frac{1}{\rho^n \frac{2\pi\rho^2}{2n+1}\frac{(n+m)!}{(n-m)!}} \iint_{S_\rho} u(\rho,\theta,\phi) P_n^{(m)}(\cos\theta)\cos(m\phi)\,ds, \\
B_{n,m} &= \frac{1}{\rho^n \frac{2\pi\rho^2}{2n+1}\frac{(n+m)!}{(n-m)!}} \iint_{S_\rho} u(\rho,\theta,\phi) P_n^{(m)}(\cos\theta)\sin(m\phi)\,ds,
\end{aligned}$$

where $ds = \rho^2 \sin\theta\,d\theta\,d\phi$. The SHF was first discussed by MacRobert [186] and developed by Atkinson and Han [14]. For the Dirichlet problem in (13.2.1) and (13.2.2), where $\mathbf{\Omega}$ is not a sphere, we may choose the truncated terms of (13.2.4),

$$\begin{aligned}
u_N = u_N(\rho,\theta,\phi) &= \sum_{n=0}^{N} \rho^n Y_n(\theta,\phi) \qquad (13.2.11) \\
&= \sum_{n=0}^{N} \rho^n \{A_n P_n(\cos\theta) + \sum_{m=1}^{n} P_n^{(m)}(\cos\theta)[A_{n,m}\cos(m\phi) + B_{n,m}\sin(m\phi)]\},
\end{aligned}$$

where the coefficients, A_n, $A_{n,m}$ and $B_{n,m}$, are unknown. There are $(N+1)^2$ unknown coefficients. The functions (13.2.11) are the spherical harmonic polynomials of order N. Denote the set of (13.2.11) by V_N. By the Trefftz method (TM) in [169], we seek the unknown coefficients (*i.e.*, u_N) such that

$$\|u_N - f\|_{0,\Gamma} = \inf_{v \in V_N} \|v - f\|_{0,\Gamma}, \qquad (13.2.12)$$

where $\|v\|_{0,\Gamma} = \sqrt{\iint_\Gamma v^2\,ds}$. We may also use the collocation equations directly to satisfy the Dirichlet condition (13.2.2),

$$\sqrt{\omega_{k,i,j}}\; u_N(\rho_k,\theta_i,\phi_j) = \sqrt{\omega_{k,i,j}}\; f(\rho_k,\theta_i,\phi_j), \quad (\rho_k,\theta_i,\phi_j) \in \Gamma, \qquad (13.2.13)$$

where $\omega_{k,i,j}\,(>0)$ are suitable weights, and the detailed nodes $(\rho_k, \theta_i, \phi_j)$ will be introduced in Section 13.5.1. The total number of the collocation equations in (13.2.13) may be chosen to be larger than $(N+1)^2$. From (13.2.12) and (13.2.13), the unknown coefficients A_n, $A_{n,m}$ and $B_{n,m}$ in (13.2.11) can be sought. This is called the method of particular solutions (MPS) in this chapter.

Denote the normalized Legendre polynomials,

$$\hat{P}_n(x) = \left\{\frac{2n+1}{2}\right\}^{\frac{1}{2}} P_n(x), \quad \hat{P}_n^{(m)}(x) = \left\{\frac{2n+1}{2}\frac{(n-m)!}{(n+m)!}\right\}^{\frac{1}{2}} P_n^{(m)}(x). \tag{13.2.14}$$

The orthogonality of (13.2.14) and (13.2.10) leads to

$$\int_{-1}^{1} \hat{P}_n(x)\hat{P}_k(x)\,dx = \delta_{nk}, \quad \int_{-1}^{1} \hat{P}_n^{(m)}(x)\hat{P}_k^{(m)}(x)\,dx = \delta_{nk}, \tag{13.2.15}$$

$$\iint_U \left\{\hat{P}_n^{(m)}(\cos\theta)\cos(m\phi)\right\}\left\{\hat{P}_k^{(\ell)}(\cos\theta)\cos(\ell\phi)\right\} ds = \pi\varepsilon_m \delta_{nk}\delta_{m\ell}. \tag{13.2.16}$$

Then solution (13.2.11) is rewritten as

$$u_N = u_N(\rho, \theta, \phi) = \sum_{n=0}^{N} \rho^n Y_n^{\circ}(\theta, \phi), \tag{13.2.17}$$

where

$$\begin{aligned} Y_n^{\circ}(\theta, \phi) &= a_n \hat{P}_n(\cos\theta) + \sum_{m=1}^{n} \hat{P}_n^{(m)}(\cos\theta)\{a_{n,m}\cos(m\phi) + b_{n,m}\sin(m\phi)\}, \\ a_n &= \left\{\frac{2}{2n+1}\right\}^{\frac{1}{2}} A_n, \quad a_{n,m} = \left\{\frac{2}{2n+1}\frac{(n-m)!}{(n+m)!}\right\}^{\frac{1}{2}} A_{n,m}, \\ b_{n,m} &= \left\{\frac{2}{2n+1}\frac{(n-m)!}{(n+m)!}\right\}^{\frac{1}{2}} B_{n,m}. \end{aligned}$$

The Sobolev norms are defined by

$$\|u\|_{p,\Gamma} = \left\{\sum_{k=0}^{p} |u|_{k,\Gamma}^2\right\}^{\frac{1}{2}}, \quad |u|_{k,\Gamma} = \left\{\iint_\Gamma (D^k u)^2\right\}^{\frac{1}{2}}.$$

The Sobolev norms on U can be denoted equivalently by (see Atkinson [13] and Chen [55])

$$\|u\|_{k,U} = \left\{\sum_{n=0}^{\infty}(2n+1)^{2k}\left[a_n^2 + \sum_{m=1}^{n}(a_{n,m}^2 + b_{n,m}^2)\right]\right\}^{\frac{1}{2}}.$$

On sphere $\mathbf{\Gamma}_\rho$, the Sobolev norms may be denoted equivalently by

$$\|u\|_{k,\Gamma_\rho} = \left\{ \sum_{n=0}^{\infty} \rho^{2n}(2n+1)^{2k} \left[a_n^2 + \sum_{m=1}^{n} (a_{n,m}^2 + b_{n,m}^2) \right] \right\}^{\frac{1}{2}}. \tag{13.2.18}$$

Define the semi-norm

$$\|v\|_{\frac{1}{2},\mathbf{\Omega}} = \left\{ \|v\|_{0,\mathbf{\Omega}}^2 + \int_{\mathbf{\Omega}}\int_{\mathbf{\Omega}} \frac{[v(P)-v(Q)]^2}{|\overline{PQ}|^3} dv(Q)dv(P) \right\}^{\frac{1}{2}}.$$

Proposition 13.2.1. *Suppose that* $u \in \mathbf{H}^p(\mathbf{\Gamma})$ $(p>1)$ *can be analytically extended to sphere* $\mathbf{\Gamma}_\rho$ *with* $\rho = r_{\max} = \max \rho|_{\mathbf{\Gamma}}$. *Then the solution from the MPS in (13.2.12) has the optimal convergence rates,*

$$\|u_N - u\|_{0,\Gamma} \leq C \frac{1}{(2N)^p} \|u\|_{p,\Gamma}, \tag{13.2.19}$$

where C *is a constant independent of* N.

Proof. Let $\bar{u}_N$ be (13.2.17), where a_n, $a_{n,m}$ and $b_{n,m}$ are the exact coefficients. Then we have for $k \leq p$

$$\begin{aligned} \|u-\bar{u}_N\|_{k,\Gamma_\rho}^2 &= \sum_{n=N+1}^{\infty} (2n+1)^{2k} \rho^{2n} \left\{ a_n^2 + \sum_{m=1}^{n} (a_{n,m}^2 + b_{n,m}^2) \right\} \\ &= \sum_{n=N+1}^{\infty} \frac{(2n+1)^{2k}}{(2n+1)^{2p}} (2n+1)^{2p} \rho^{2n} \left\{ a_n^2 + \sum_{m=1}^{n} (a_{n,m}^2 + b_{n,m}^2) \right\} \\ &\leq \frac{(2N+3)^{2k}}{(2N+3)^{2p}} \sum_{n=N+1}^{\infty} (2n+1)^{2p} \rho^{2n} \left\{ a_n^2 + \sum_{m=1}^{n} (a_{n,m}^2 + b_{n,m}^2) \right\} \\ &\leq \frac{1}{(2N+3)^{2(p-k)}} \sum_{n=0}^{\infty} (2n+1)^{2p} \rho^{2n} \left\{ a_n^2 + \sum_{m=1}^{n} (a_{n,m}^2 + b_{n,m}^2) \right\} \\ &\leq \frac{1}{(2N)^{2(p-k)}} \|u\|_{p,\Gamma_\rho}^2. \end{aligned} \tag{13.2.20}$$

Next, we have from (13.2.12)

$$\|u_N - u\|_{0,\Gamma} \leq \inf_{v \in V_N} \|v-u\|_{0,\Gamma} \leq \|u - \bar{u}_N\|_{0,\Gamma}. \tag{13.2.21}$$

Let the ball $\mathbf{\Omega}_\rho$ denote the spherical surface S_ρ with radius $\rho = r_{\max}$, where $r_{\max} = \max \rho|_{\rho \in \mathbf{\Omega}}$. Then $\mathbf{\Omega} \subseteq \mathbf{\Omega}_\rho$. Since the functions $v\,(=u-\bar{u}_N)$ satisfy Laplace's equation, we have from Oden and Reddy [195, Theorem 5.7 at p.189]

$$\|v\|_{0,\Gamma} \leq C\|v\|_{\frac{1}{2},\mathbf{\Omega}} \leq C\|v\|_{\frac{1}{2},\mathbf{\Omega}_\rho} \leq C\|v\|_{0,\Gamma_\rho}. \tag{13.2.22}$$

Hence from (13.2.20)–(13.2.22), we have

$$\|u-u_N\|_{0,\Gamma} \le \|u-\bar{u}_N\|_{0,\Gamma} \le C\|u-\bar{u}_N\|_{0,\Gamma_\rho} \le C\frac{1}{(2N)^p}\|u\|_{p,\Gamma_\rho} \le C\frac{1}{(2N)^p}\|u\|_{p,\Gamma}.$$

The desired result (13.2.19) is obtained. ■

Below, we discuss the stability. For the bounded simply-connected domain $\mathbf{\Omega}$, denote the maximal and the minimal radii by $r_{\max} = \min \rho|_{\mathbf{\Omega}\subset\mathbf{\Omega}_\rho}$ and $r_{\min} = \max \rho|_{\mathbf{\Omega}_\rho\subset\mathbf{\Omega}}$, respectively. Then $\mathbf{\Omega}_{r_{\min}} \subseteq \mathbf{\Omega} \subseteq \mathbf{\Omega}_{r_{\max}}$, where $\mathbf{\Omega}_{r_{\max}}$ and $\mathbf{\Omega}_{r_{\min}}$ are the balls with radii $r_{\max}$ and $r_{\min}$, respectively. Denote two spherical surfaces by $S_{r_{\max}} = \partial\mathbf{\Omega}_{r_{\max}}$ and $S_{r_{\min}} = \partial\mathbf{\Omega}_{r_{\min}}$. For easy analysis and computation, choose the following normalized Legendre polynomials,

$$\begin{aligned} u(\rho,\theta,\phi) &= \sum_{n=0}^{\infty}\left(\frac{\rho}{r_{\max}}\right)^n Y_n^{\circ}(\theta,\phi) \\ &= \sum_{n=0}^{\infty}\left(\frac{\rho}{r_{\max}}\right)^n \left\{a_n\hat{P}_n(\cos\theta) + \sum_{m=1}^{n}\hat{P}_n^{(m)}(\cos\theta)[a_{n,m}\cos(m\phi)+b_{n,m}\sin(m\phi)]\right\}, \end{aligned}$$

where a_n, $a_{n,m}$ and $b_{n,m}$ are unknown coefficients. The admissible functions (13.2.17) are rewritten as

$$\begin{aligned} u_N = u_N(\rho,\theta,\phi) &= \sum_{n=0}^{N}\left(\frac{\rho}{r_{\max}}\right)^n Y_n^{\circ}(\theta,\phi) \qquad (13.2.23) \\ &= \sum_{n=0}^{N}\left(\frac{\rho}{r_{\max}}\right)^n \left\{a_n\hat{P}_n(\cos\theta) + \sum_{m=1}^{n}\hat{P}_n^{(m)}(\cos\theta)[a_{n,m}\cos(m\phi)+b_{n,m}\sin(m\phi)]\right\}. \end{aligned}$$

Denote $\|u\|_{0,\Gamma}^2 = \mathbf{x}^T\mathbf{A}\mathbf{x}$, where the symmetric and positive matrix $\mathbf{A} \in \mathbf{R}^{(N+1)^2\times(N+1)^2}$, and the vector $\mathbf{x} \in \mathbf{R}^{(N+1)^2}$ consists of coefficients a_n, $a_{n,m}$ and $b_{n,m}$. The condition number is defined by $\text{Cond}(\mathbf{A}) = \frac{\lambda_{\max}(\mathbf{A})}{\lambda_{\min}(\mathbf{A})}$, where $\lambda_{\max}$ and $\lambda_{\min}$ are the maximal and the minimal eigenvalues of matrix $\mathbf{A}$, respectively.

Proposition 13.2.2. *Suppose that the admissible solutions (13.2.23) are chosen for (13.2.12), there exists the bound,*

$$\text{Cond}(\mathbf{A}) \le C\left(\frac{r_{\max}}{r_{\min}}\right)^{2N}. \qquad (13.2.24)$$

Proof. Since the SHF satisfy Laplace's equation, there exist the bounds from [195, p.189],

$$\|u\|_{0,\Gamma} \le C\|u\|_{\frac{1}{2},\mathbf{\Omega}} \le C\|u\|_{\frac{1}{2},\mathbf{\Omega}_{r_{\max}}} \le C\|u\|_{0,S_{r_{\max}}}.$$

Then we obtain from (13.2.23) and the orthogonality (13.2.16)

$$\mathbf{x}^T\mathbf{A}\mathbf{x} = \|v_N\|^2_{0,\Gamma} \leq C\|v_N\|^2_{0,S_{r_{\max}}} \leq C\left\|\sum_{n=0}^{N} Y_n^\circ(\theta,\phi)\right\|^2_{0,U} \leq C\mathbf{x}^T\mathbf{x},$$

where $\mathbf{x}^T\mathbf{x} = \|\mathbf{x}\|^2 = \sum_{n=0}^{N}\left\{a_n^2 + \sum_{m=1}^{n}(a_{n,m}^2 + b_{n,m}^2)\right\}$. This implies

$$\lambda_{\max} = \max_{\mathbf{x}\neq 0}\frac{\mathbf{x}^T\mathbf{A}\mathbf{x}}{\mathbf{x}^T\mathbf{x}} \leq C. \tag{13.2.25}$$

On the other hand, from [195, p.189] we have

$$\|u\|_{0,\Gamma} \geq c_0\|u\|_{\frac{1}{2},\mathbf{\Omega}} \geq c_0\|u\|_{\frac{1}{2},\mathbf{\Omega}_{r_{\min}}} \geq c_0\|u\|_{0,S_{r_{\min}}}.$$

Then we obtain

$$\begin{aligned}\mathbf{x}^T\mathbf{A}\mathbf{x} &\geq c_0\|v_N\|^2_{0,S_{r_{\min}}} \geq c_0\left\|\sum_{n=0}^{N}\left(\frac{r_{\min}}{r_{\max}}\right)^{2n} Y_n^\circ(\theta,\phi)\right\|^2_{0,U} \\ &\geq c_0\left(\frac{r_{\min}}{r_{\max}}\right)^{2N}\left\|\sum_{n=0}^{N} Y_n^\circ(\theta,\phi)\right\|^2_{0,U} \geq c_0\left(\frac{r_{\min}}{r_{\max}}\right)^{2N}\mathbf{x}^T\mathbf{x},\end{aligned}$$

to give

$$\lambda_{\min} = \min_{\mathbf{x}\neq 0}\frac{\mathbf{x}^T\mathbf{A}\mathbf{x}}{\mathbf{x}^T\mathbf{x}} \geq c_0\left(\frac{r_{\min}}{r_{\max}}\right)^{2N}. \tag{13.2.26}$$

Combining (13.2.25) and (13.2.26) gives the desired result (13.2.24). ■

For the admissible functions (13.2.23), the collocation equations are given as (13.2.13), denoted by $\mathbf{F}\mathbf{x} = \mathbf{b}$, where $\mathbf{F} \in \mathbf{R}^{\bar{M}\times(N+1)^2}$ with $\bar{M} \geq (N+1)^2$. When the suitable weights $\omega_{k,i,j}$ in (13.2.13) are chosen such that

$$\mathbf{x}^T\mathbf{F}^T\mathbf{F}\mathbf{x} = \widehat{\iint_\Gamma} v^2\,ds, \tag{13.2.27}$$

where $\widehat{\iint}_\Gamma$ is the integration approximation of $\iint_\Gamma$, we may assume that

$$\widehat{\iint_\Gamma} v^2\,ds \asymp \iint_\Gamma v^2\,ds, \quad v \in V_N, \tag{13.2.28}$$

where the notation $a \asymp b$ denotes that there exist two constants $c_0\,(>0)$ and C independent of n and m such that $c_0 b \leq a \leq Cb$. Since $\mathbf{x}^T\mathbf{F}^T\mathbf{F}\mathbf{x} \asymp \mathbf{x}^T\mathbf{A}\mathbf{x}$, we have the following proposition.

Proposition 13.2.3. *Suppose that equivalence (13.2.28) holds. When the functions (13.2.23) are used in (13.2.13), there exist the bounds of condition number,*

$$\mathrm{Cond}(\mathbf{F}) = \frac{\sigma_{\max}(\mathbf{F})}{\sigma_{\min}(\mathbf{F})} \le C\left\{\frac{\lambda_{\max}(\mathbf{A})}{\lambda_{\min}(\mathbf{A})}\right\}^{\frac{1}{2}} = C\{\mathrm{Cond}(\mathbf{A})\}^{\frac{1}{2}} \le C\left(\frac{r_{\max}}{r_{\min}}\right)^N,$$

where $\sigma_{\max}$ *and* $\sigma_{\min}$ *are the maximal and the minimal singular values of matrix* $\mathbf{F}$, *respectively.*

Remark 13.2.1. *The assumption (13.2.28) holds for the centroid rule, and for the trapezoidal and Gauss–Legendre rules in (13.3.1) below on the unit sphere* U *with* $M > N$, *based on Lemma 13.4.2. Besides, Proposition 13.2.1 is consistent with [13, 14] when* $\Gamma = U$. *For the collocation equations (13.2.13), some errors in the infinity norm are given in [14, p.201] via the rule (13.3.1). Denote the discrete norm* $\overline{\|v\|}_{0,\Gamma} = \sqrt{\widehat{\iint_\Gamma} v^2 ds}$. *Similarly to (13.2.12), we have* $\overline{\|u_N - f\|}_{0,\Gamma} = \inf_{v \in V_N} \overline{\|v - f\|}_{0,\Gamma}$. *For (13.2.13), the polynomial convergence rates can also be obtained by following Quarteroni and Valli [204, Chapter 4]; details are omitted.*

13.3 Method of Fundamental Solutions

13.3.1 Algorithms

The quadrature rules on the surfaces are important not only for algorithms but also for analysis of the MFS. For the unit sphere U, the trapezoidal and the Gauss–Legendre rules are composed as

$$\begin{aligned}\iint_U f(\theta,\phi)\,ds &= \int_0^\pi \left\{\int_0^{2\pi} f(\theta,\phi)\,d\phi\right\} \sin\theta\, d\theta \\ &\approx \widehat{\iint_\Gamma} f(\theta,\phi)\,ds = h \sum_{i=1}^{M} \sum_{j=1}^{2M} w_i f(\theta_i, \phi_j),\end{aligned} \tag{13.3.1}$$

where $h = \frac{\pi}{M}$, $\phi_j = jh$, and $\cos\theta_i$ and $w_i\,(>0)$ are the abscissas and weights of the Gauss–Legendre rule, respectively. The rule (13.3.1) was given in Stroud [220] and it has the precision of degree $2M-1$. In Atkinson [13] the errors are given by

$$\left| \iint_U f(\theta,\phi)\,ds - \widehat{\iint_U} f(\theta,\phi)\,ds \right| \le C \frac{1}{(2M)^p}, \quad M \ge 1,$$

provided that function $f(\theta,\phi)(\in C^p(U))$ has the p-order continuous derivatives on U.

For Laplace's equation in 3D, the FS is known as $\frac{1}{|\overline{PQ}|}$ with $P \ne Q$, where $|\overline{PQ}|$ denotes the Euclidean distance between nodes $P\,(\in \bar{\mathbf{\Omega}})$ and the source nodes Q outside $\mathbf{\Omega}$. Denote (see Figure 13.2)

$$P(x,y,z) = (\rho\,\sin\theta\,\cos\phi, \rho\,\sin\theta\,\sin\phi, \rho\,\cos\theta) := P(\rho,\theta,\phi),$$
$$Q(x,y,z) = (r\,\sin\xi\,\cos\eta, r\,\sin\xi\,\sin\eta, r\,\cos\xi) := Q(r,\xi,\eta),$$

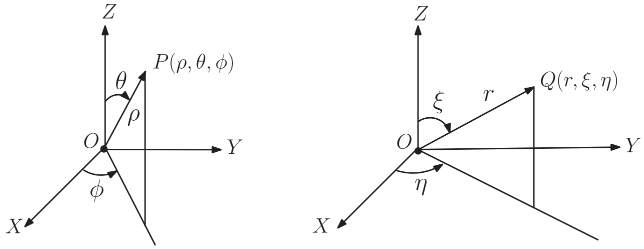

FIG. 13.2 – The node $P(\rho, \theta, \phi) \in \bar{\Omega}$ and the source node $Q(r, \xi, \eta) \notin \bar{\Omega}$.

where $r > r_{\max} = \max \rho|_{\rho \in \Omega}$. The source nodes Q_{ij} may be simply located on a larger pseudo-sphere S_R with radius $R > r_{\max}$. Based on rule (13.3.1), we choose the $2M^2$ fundamental solutions as

$$\Phi_{ij}(P) = \frac{1}{|\overline{PQ_{ij}}|}, \quad Q_{ij} = (R, \xi_i, \eta_j),$$

where $\eta_j \, (= jh)$ and $\cos\xi_i$ are the abscissas from the trapezoidal and the Gauss–Legendre rules, respectively. Note that the source nodes (R, ξ_i, η_j) of the MFS are chosen just as the same integration nodes on sphere S_R from the rule (13.3.1). Then a linear combination of FS is given by

$$v_M = \sum_{i=1}^{M} \sum_{j=1}^{2M} c_{ij} \Phi_{ij}(P), \quad P \in \bar{\Omega}, \tag{13.3.2}$$

where c_{ij} are the unknown coefficients to be sought.

The coefficients c_{ij} can be found by the Trefftz method as (13.2.12), or the collocation Trefftz method as (13.2.13) in [169], where the total number of the collocation equations may be chosen to be larger than $2M^2$.

13.3.2 Link to MPS

For $P(\rho, \theta, \phi)$ and $Q(r, \xi, \eta)$, denote $|\overline{PQ}| = \sqrt{r^2 + \rho^2 - 2\rho r \cos(\Theta)}$, where the angle Θ between vectors $\overrightarrow{OQ}$ and $\overrightarrow{OP}$ is shown in Figure 13.3. We have

$$\cos(\Theta) = \cos\theta \, \cos\xi + \sin\theta \, \sin\xi \, \cos(\phi - \eta).$$

From Tikhonov and Samarskii [223, p.687], we have

$$\frac{1}{|\overline{PQ}|} = \frac{1}{\sqrt{r^2 + \rho^2 - 2\rho r \cos(\Theta)}} = \begin{cases} \dfrac{1}{\rho} \displaystyle\sum_{n=0}^{\infty} \left(\frac{r}{\rho}\right)^n P_n(\cos\Theta), & \rho > r, \\ \dfrac{1}{r} \displaystyle\sum_{n=0}^{\infty} \left(\frac{\rho}{r}\right)^n P_n(\cos\Theta), & r > \rho, \end{cases} \tag{13.3.3}$$

where $P_n(x)$ are the Legendre polynomials of order n. From [90, p.1015, 8.814],

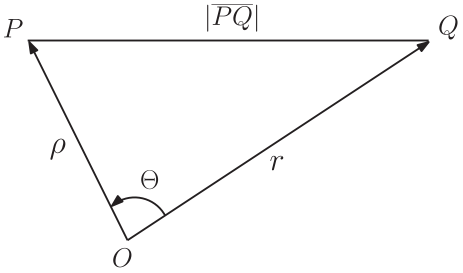

FIG. 13.3 – The angle Θ between vectors $\overrightarrow{OQ}$ and $\overrightarrow{OP}$.

$$P_n(\cos\Theta) = P_n(\cos\theta)P_n(\cos\xi) + 2\sum_{m=1}^{n}\frac{(n-m)!}{(n+m)!}P_n^{(m)}(\cos\theta)P_n^{(m)}(\cos\xi)\cos m(\phi-\eta), \tag{13.3.4}$$

where $P_n^{(m)}(x)$ are the associated functions defined in (13.2.7). From (13.3.3) and (13.3.4), we have the following addition theorem.

Theorem 13.3.1 (Addition Theorem). *The FS in 3D has the expansions,*

$$\frac{1}{|\overline{PQ}|} = \begin{cases} \frac{1}{\rho}\sum_{n=0}^{\infty}\left(\frac{r}{\rho}\right)^n\{P_n(\cos\theta)P_n(\cos\xi) \\ \quad +2\sum_{m=1}^{n}\frac{(n-m)!}{(n+m)!}P_n^{(m)}(\cos\theta)P_n^{(m)}(\cos\xi)\cos m(\phi-\eta)\}, & \rho > r, \\ \frac{1}{r}\sum_{n=0}^{\infty}\left(\frac{\rho}{r}\right)^n\{P_n(\cos\theta)P_n(\cos\xi) \\ \quad +2\sum_{m=1}^{n}\frac{(n-m)!}{(n+m)!}P_n^{(m)}(\cos\theta)P_n^{(m)}(\cos\xi)\cos m(\phi-\eta)\}, & r > \rho. \end{cases} \tag{13.3.5}$$

By using the normalized Legendre polynomials in (13.2.14), the second expansion in (13.3.5) with $r = R$ is rewritten as

$$\begin{aligned} \frac{1}{|\overline{PQ}|} = \frac{1}{R}\sum_{n=0}^{\infty}\frac{2}{2n+1}\left(\frac{\rho}{R}\right)^n\Big\{\hat{P}_n(\cos\theta)\hat{P}_n(\cos\xi) \\ +2\sum_{m=1}^{n}\hat{P}_n^{(m)}(\cos\theta)\hat{P}_n^{(m)}(\cos\xi)\cos m(\phi-\eta)\Big\}, \quad \rho < R, \end{aligned} \tag{13.3.6}$$

where the source nodes $Q(R,\xi,\eta)$ are located on a larger sphere S_R with radius $R > r_{\max}$. The addition theorem (13.3.6) is important not only to link the MFS with the MPS but also to the error analysis given in Section 13.4.

Lemma 13.3.1. *Let* $S_R\,(=(r,\xi,\eta)|_{r=R})$ *be a larger pseudo-sphere with the radius* $R > r_{\max} = \max\rho|_{\rho\in\Gamma}$. *There exist equalities,*

$$\iint_{S_R} \frac{\hat{P}_n(\cos\xi)}{|\overline{PQ}|}\, ds_Q = \frac{4\pi R}{2n+1}\left(\frac{\rho}{R}\right)^n \hat{P}_n(\cos\theta), \tag{13.3.7}$$

$$\iint_{S_R} \frac{\hat{P}_n^{(m)}(\cos\xi)\cos(m\eta)}{|\overline{PQ}|}\, ds_Q = \frac{4\pi R}{2n+1}\left(\frac{\rho}{R}\right)^n \hat{P}_n^{(m)}(\cos\theta)\cos(m\phi), \tag{13.3.8}$$

$$\iint_{S_R} \frac{\hat{P}_n^{(m)}(\cos\xi)\sin(m\eta)}{|\overline{PQ}|}\, ds_Q = \frac{4\pi R}{2n+1}\left(\frac{\rho}{R}\right)^n \hat{P}_n^{(m)}(\cos\theta)\sin(m\phi), \tag{13.3.9}$$

where $ds_Q = R^2 \sin\xi\, d\xi\, d\eta = R^2\, ds_U$.

Proof. We only prove (13.3.8) since the proof for (13.3.7) and (13.3.9) is similar. From (13.3.6) and the orthogonality (13.2.16) of the SHF, we have

$$\begin{aligned}
&\iint_{S_R} \frac{\hat{P}_n^{(m)}(\cos\xi)\cos(m\eta)}{|\overline{PQ}|}\, ds_Q \\
&= \iint_{S_R} \hat{P}_n^{(m)}(\cos\xi)\cos(m\eta)\left\{\frac{1}{R}\sum_{\bar{n}=0}^{\infty}\frac{2}{2\bar{n}+1}\left(\frac{\rho}{R}\right)^{\bar{n}}[\hat{P}_{\bar{n}}(\cos\theta)\hat{P}_{\bar{n}}(\cos\xi)\right. \\
&\quad \left. + 2\sum_{\bar{m}=1}^{\bar{n}} \hat{P}_{\bar{n}}^{(\bar{m})}(\cos\theta)\hat{P}_{\bar{n}}^{(\bar{m})}(\cos\xi)\cos\bar{m}(\phi-\eta)]\right\} ds_Q \\
&= \frac{4\pi R}{2n+1}\left(\frac{\rho}{R}\right)^n \hat{P}_n^{(m)}(\cos\theta)\cos(m\phi), \quad m \geq 1.
\end{aligned}$$

■

The SHF is used in the MPS in Section 13.2, which can be approximated by a specific linear combination (13.3.2) of FS. Denote the finite terms of (13.2.17) by

$$\mathcal{P}_N = \mathcal{P}_N(\rho,\theta,\phi) = \sum_{n=0}^{N} \rho^n Y_n^{\circ}(\theta,\phi). \tag{13.3.10}$$

Denote the following integration approximation on the pseudo-sphere S_R from the rule (13.3.1) as,

$$\begin{aligned}
\iint_{S_R} f(r,\theta,\phi)\, ds &= R^2 \int_0^{2\pi}\int_0^{\pi} f(R,\theta,\phi)\sin\theta\, d\theta\, d\phi \\
&\approx \widehat{\iint_{S_R}} f(R,\theta,\phi)\, ds = hR^2 \sum_{j=1}^{2M}\sum_{i=1}^{M} w_i f(R,\theta_i,\phi_j).
\end{aligned} \tag{13.3.11}$$

To approximate the function $\rho^n \hat{P}_n^{(m)}(\cos\theta)\cos m\phi$ in (13.3.10) by the FS, we have from (13.3.8)

$$\begin{aligned}\rho^n \hat{P}_n^{(m)}(\cos\theta)\cos(m\phi) &= \frac{2n+1}{4\pi R} R^n \iint_{S_R} \frac{\hat{P}_n^{(m)}(\cos\xi)\cos(m\eta)}{|\overline{PQ}|}\, ds \\ &\approx \frac{2n+1}{4\pi} R^{n-1} \widehat{\iint_{S_\rho}} \frac{\hat{P}_n^{(m)}(\cos\xi)\cos(m\eta)}{|\overline{PQ}|}\, ds_Q \\ &= \frac{2n+1}{4\pi} R^{n+1} h \sum_{i=1}^{M} w_i \sum_{j=1}^{2M} \frac{\hat{P}_n^{(m)}(\cos\xi_i)\cos(m\eta_j)}{|\overline{PQ_{ij}}|} = \sum_{i=1}^{M}\sum_{j=1}^{2M} c_{ij}\Phi_{ij}(P),\end{aligned}$$

where $h = \frac{\pi}{M}$ and $c_{ij} = w_i \frac{2n+1}{4M} R^{n+1} \hat{P}_n^{(m)}(\cos\xi_i)\cos(m\eta_j)$. Similarly, by counting the coefficients c_{ij} from the approximations of $\rho^n \hat{P}_n(\cos\theta)$ and $\rho^n \hat{P}_n^{(m)}(\cos\theta)\sin(m\phi)$, we find a specific approximate combination of FS as

$$v_M^* = \sum_{i=1}^{M}\sum_{j=1}^{2M} c_{ij}^*\Phi_{ij}(P) \approx \mathcal{P}_N = \mathcal{P}_N(\rho,\theta,\phi), \tag{13.3.12}$$

where the coefficients

$$\begin{aligned} c_{ij}^* = w_i \frac{1}{4M} \sum_{n=0}^{N} (2n+1) R^{n+1} \Big\{ a_n \hat{P}_n(\cos\xi_i) \\ + \sum_{m=1}^{n} \hat{P}_n^{(m)}(\cos\xi_i)[a_{m,n}\cos(m\eta_j) + b_{m,n}\sin(m\eta_j)]\Big\}.\end{aligned} \tag{13.3.13}$$

When $M > N$ and $2M^2 \geq (N+1)^2$, the non-trivial c_{ij}^* can be obtained from a_n, $a_{m,n}$ and $b_{m,n}$ uniquely. We write these important conclusions as a proposition.

Proposition 13.3.1. *For the spherical harmonic functions $\mathcal{P}_N$ in (13.3.10) of order N, when $M > N$, an approximation v_M^* to $\mathcal{P}_N$ in (13.3.12) and (13.3.13) is found.*

For Laplace's equation in 2D in Part I, by using $\ln|\overline{PQ}|$ as FS, the MFS suffers from the algorithm singularity in [137]. For Laplace's equation in 3D, by using $\frac{1}{|\overline{PQ}|}$ as FS, no degenerate scales exist. This is one advantage of the MFS for Laplace's equation in 3D.

13.4 Error Analysis for MFS

This section is devoted to deriving the error bounds; the outlines of proofs are stated as follows. From proposition 13.3.1, we will first find the errors between the FS in (13.3.2) and the SHF in (13.3.10). The errors of two kinds of SHF from the rule (13.3.1) are given in the key Lemma 13.4.2. Based on expansions *via* the SHF on spheres, the related errors are derived in Lemmas 13.4.3 and 13.4.4. The errors between the solution (13.3.2) and the SHF are provided in Theorem 13.4.1, and the optimal polynomial convergence rates are attained in Theorem 13.4.2 for the MFS solutions. It is the first time to yield the strict error analysis of the MFS for 3D problems. The proof techniques in this chapter are more challenging and imperative than the 2D problems in Part I.

13.4.1 Preliminary Lemmas

Choose the $2M^2$ source nodes Q_{ij} on a larger pseudo-sphere S_R,

$$Q_{ij} = \left(R, \xi_i, \eta_j\right), \quad R > r_{\max}, \quad i = 1, 2, ..., M, \quad j = 1, 2, ..., 2M, \tag{13.4.1}$$

where $\eta_j = jh = j\frac{\pi}{M}$, and $\cos\xi_i$ are the zeros of the Legendre polynomials of order M as in rule (13.3.1). The error analysis will be made for the source nodes (13.4.1). For $I(g) = \int_0^{2\pi} g(x)\,dx$, the trapezoidal rule is given by

$$\widehat{I}_{2M}(g) = \widehat{\int_0^{2\pi}} g(x)\,dx = h \sum_{k=1}^{2M} g(kh),$$

where $h = \frac{\pi}{M}$. Denote the errors

$$\triangle_{2M}(g) = \widehat{I}_{2M}(g) - I(g) = \widehat{\int_0^{2\pi}} g(x)\,dx - \int_0^{2\pi} g(x)\,dx.$$

We have the following lemma from Basic Lemma A in Part I.

Lemma 13.4.1. *For the 2π-periodic function $g = g(x)$, there exist equalities:*

$$\triangle_{2M}(\sin mx) = 0, m = 1, 2, ...,$$
$$\triangle_{2M}(\cos mx) = \begin{cases} 2\pi, & \text{if } m = 2vM, v = 1, 2, ..., \\ 0, & \text{otherwise.} \end{cases}$$

The rule (13.3.1) is the product of the trapezoidal and the Gauss–Legendre rules in 2D domain $\{(x,\eta)| -1<x<1, 0\leq\eta\leq 2\pi\}$. The Gauss–Legendre rule is given by

$$\int_{-1}^{1} f(x)\,dx \approx \widehat{\int_{-1}^{1}} f(x)\,dx = \sum_{k=1}^{M} w_k f(x_k), \tag{13.4.2}$$

where x_k are the zeros of the Legendre polynomials of order M, and w_k the weights,

$$w_k = \frac{2}{(1-x_k)^2 (P'_M(x_k))^2} > 0,$$

to satisfy $\sum_{k=1}^{M} w_k = 2$. The rule (13.4.2) is exact for the polynomials of order $2M-1$, called the precision of order $2M-1$. Hence, for the Gauss–Legendre rule in (13.4.2) we have

$$\widehat{\int_{-1}^{1}} f(x)\,dx = \int_{-1}^{1} f(x)\,dx, \quad \forall f(x) \in \mathcal{P}_{2M-1}, \tag{13.4.3}$$

where $\mathcal{P}_M$ is the set of all polynomials of order M *via* x. Denote

$$\iint_U f(\cos\xi,\eta)\,ds_U = \int_0^{\pi}\int_0^{2\pi} f(\cos\xi,\eta)\sin\xi\,d\eta\,d\xi = \int_{-1}^{1}\int_0^{2\pi} f(x,\eta)\,d\eta\,dx,$$

where $x=\cos\xi$. We have

$$\int_{-1}^{1}\int_0^{2\pi} - \widehat{\int}_{-1}^{1}\widehat{\int}_0^{2\pi} = \left(\int_{-1}^{1} - \widehat{\int}_{-1}^{1}\right)\int_0^{2\pi} + \widehat{\int}_{-1}^{1}\left(\int_0^{2\pi} - \widehat{\int}_0^{2\pi}\right), \tag{13.4.4}$$

where $\widehat{\int}_{-1}^{1} = \widehat{\int}_{-1}^{1}\cdot\,dx$ and $\widehat{\int}_0^{2\pi} = \widehat{\int}_0^{2\pi}\cdot\,d\eta$ are the Gaussian and the trapezoidal rules, respectively. For two kinds of SHF, we have the following key lemma.

Lemma 13.4.2. *Let* $m \le n \le N < M$ *and* $\bar m \le \bar n < \infty$, *there exist the bounds,*

$$|ECC_{n,m;\bar n,\bar m}| := \left|\left(\iint_U - \widehat{\iint_U}\right)[\hat P_n^{(m)}(\cos\xi)\cos(m\eta)] \times [\hat P_{\bar n}^{(\bar m)}(\cos\xi)\cos(\bar m\eta)]\,ds_U\right| \tag{13.4.5}$$

$$= \begin{cases} \varepsilon_m\pi\left|\widehat{\int}_{-1}^{1}\hat P_n^{(m)}(x)\hat P_{\bar n}^{(\bar m)}(x)\,dx\right| \le \varepsilon_m\pi\sqrt{\frac{2\bar n+1}{2}}, & \textit{if } \bar n \ge 2M-n \textit{ and} \\ & \bar m \pm m = 2vM,\ v=0,1,2,..., \\ 0, & \textit{otherwise}, \end{cases}$$

where $\varepsilon_0 = 2$ *and* $\varepsilon_m = 1$ *for* $m \ge 1$, *and*

$$|ESS_{n,m;\bar n,\bar m}| := \left|\left(\iint_U - \widehat{\iint_U}\right)[\hat P_n^{(m)}(\cos\xi)\sin(m\eta)] \times [\hat P_{\bar n}^{(\bar m)}(\cos\xi)\sin(\bar m\eta)]\,ds_U\right|$$

$$= \left|ECC_{n,m;\bar n,\bar m}\right|, \quad m,\bar m \ge 1. \tag{13.4.6}$$

Besides, the trivial integrals exist for all $n, m, \bar n$ *and* $\bar m$,

$$ECS_{n,m;\bar n,\bar m} := \left(\iint_U - \widehat{\iint_U}\right)[\hat P_n^{m}(\cos\xi)\cos(m\eta)] \times [\hat P_{\bar n}^{\bar m}(\cos\xi)\sin(\bar m\eta)]\,ds_U \tag{13.4.7}$$

$$= ESC_{n,m;\bar n,\bar m} := \left(\iint_U - \widehat{\iint_U}\right)[\hat P_n^{m}(\cos\xi)\sin(m\eta)] \times [\hat P_{\bar n}^{\bar m}(\cos\xi)\cos(\bar m\eta)]\,ds_U = 0.$$

Proof. We only prove (13.4.5) since the proof for (13.4.6) and (13.4.7) is similar. First, we have $ECC_{n,m;\bar n,\bar m} = 0$ for $\bar n < 2M-n$ because the polynomials of x in the integrand have order $\le 2M-1$. We have from (13.4.4)

$$\begin{aligned} ECC_{n,m;\bar{n},\bar{m}} = {} & \left(\int_{-1}^{1} - \widehat{\int_{-1}^{1}}\right)\hat{P}_n^{(m)}(x)\hat{P}_{\bar{n}}^{(\bar{m})}(x)\,dx \times \int_0^{2\pi}\cos(m\eta)\cos(\bar{m}\eta)\,d\eta \\ & + \widehat{\int_{-1}^{1}}\hat{P}_n^{(m)}(x)\hat{P}_{\bar{n}}^{(\bar{m})}(x)\,dx \times \left(\int_0^{2\pi} - \widehat{\int_0^{2\pi}}\right)\cos(m\eta)\cos(\bar{m}\eta)\,d\eta. \end{aligned} \tag{13.4.8}$$

From Lemma 13.4.1, the second term on the right-hand side in (13.4.8) leads to

$$\begin{aligned} II &= \widehat{\int_{-1}^{1}}\hat{P}_n^{(m)}(x)\hat{P}_{\bar{n}}^{(\bar{m})}(x)\,dx \times \left(\int_0^{2\pi} - \widehat{\int_0^{2\pi}}\right)\cos(m\eta)\cos(\bar{m}\eta)\,d\eta \\ &= \varepsilon_m\pi\widehat{\int_{-1}^{1}}\hat{P}_n^{(m)}(x)\hat{P}_{\bar{n}}^{(\bar{m})}(x)\,dx, \quad \text{for } \bar{m}\pm m = 2vM, v = 1,2,\ldots. \end{aligned} \tag{13.4.9}$$

The first term on the right-hand side in (13.4.8) is nonzero only for $m = \bar{m}$ and $\bar{n} \geq 2M - n$. We have from the orthogonality (13.2.15)

$$\begin{aligned} I &= \left(\int_{-1}^{1} - \widehat{\int_{-1}^{1}}\right)\hat{P}_n^{(m)}(x)\hat{P}_{\bar{n}}^{(\bar{m})}(x)\,dx \times \int_0^{2\pi}\cos(m\eta)\cos(\bar{m}\eta)\,d\eta \\ &= \varepsilon_m\pi\left(\int_{-1}^{1} - \widehat{\int_{-1}^{1}}\right)\hat{P}_n^{(m)}(x)\hat{P}_{\bar{n}}^{(m)}(x)\,dx \\ &= \varepsilon_m\pi\left\{\int_{-1}^{1}\hat{P}_n^{(m)}(x)\hat{P}_{\bar{n}}^{(m)}(x)\,dx - \widehat{\int_{-1}^{1}}\hat{P}_n^{(m)}(x)\hat{P}_{\bar{n}}^{(m)}(x)\,dx\right\} \\ &= -\varepsilon_m\pi\left\{\widehat{\int_{-1}^{1}}\hat{P}_n^{(m)}(x)\hat{P}_{\bar{n}}^{(m)}(x)\,dx\right\}, \end{aligned} \tag{13.4.10}$$

where we have used $\bar{n} \neq n$ from $\bar{n} = 2M - n > 2N - n \geq n$ with $M > N$. Hence from (13.4.8)–(13.4.10), we have

$$\begin{aligned} & \left|\left(\iint_U - \widehat{\iint_U}\right)[\hat{P}_n^{(m)}(\cos\xi)\cos(m\eta)][\hat{P}_{\bar{n}}^{(\bar{m})}(\cos\xi)\cos(\bar{m}\eta)]\,ds_U\right| \\ & = \varepsilon_m\pi\left|\widehat{\int_{-1}^{1}}\hat{P}_n^{(m)}(x)\hat{P}_{\bar{n}}^{(\bar{m})}(x)\,dx\right|, \end{aligned}$$

where $\bar{m} \pm m = 2vM$ with $v = 0,1,2,\ldots$. We will show below

$$\left|\widehat{\int_{-1}^{1}}\hat{P}_n^{(m)}(x)\hat{P}_{\bar{n}}^{(\bar{m})}(x)\,dx\right| \leq \sqrt{\frac{2\bar{n}+1}{2}}, \tag{13.4.11}$$

and obtain the desired result (13.4.5).

Denote the norm $\|v\|_0 = \|v\|_{0,(-1,1)} = \left\{\int_{-1}^{1} v^2\,dx\right\}^{\frac{1}{2}}$. Simply denote $v = \hat{P}_n^{(m)}(x)$, $m \leq n \leq N < M$ and $u = \hat{P}_{\bar{n}}^{(\bar{m})}(x)$, $\bar{m} \leq \bar{n}$, $\bar{n} \geq 2M - n \geq 2M - N > M$. Then we have $\|v\|_0 = \|u\|_0 = 1$. Since $v \in \mathcal{P}_{M-1}$ we have from the Schwarz inequality and (13.4.3)

$$\begin{aligned}\left|\widehat{\int_{-1}^{1}} \hat{P}_n^{(m)}(x)\hat{P}_{\bar{n}}^{(\bar{m})}(x)\,dx\right| &= \left|\widehat{\int_{-1}^{1}} uv dx\right| \le \left\{\widehat{\int_{-1}^{1}} u^2\,dx\right\}^{\frac{1}{2}} \times \left\{\widehat{\int_{-1}^{1}} v^2\,dx\right\}^{\frac{1}{2}} \\ = \left\{\widehat{\int_{-1}^{1}} u^2\,dx\right\}^{\frac{1}{2}} \times \left\{\int_{-1}^{1} v^2\,dx\right\}^{\frac{1}{2}} &= \left\{\widehat{\int_{-1}^{1}} u^2\,dx\right\}^{\frac{1}{2}} \times \|v\|_0 = \left\{\widehat{\int_{-1}^{1}} u^2\,dx\right\}^{\frac{1}{2}}.\end{aligned} \tag{13.4.12}$$

From Lohofer [183, p.179, (5)], we have

$$\frac{1}{\sqrt{2n+1}} \le \max_{-1\le x\le 1}\left|P_n^{(m)}(x)\right|\sqrt{\frac{(n-m)!}{(n+m)!}} \le \frac{1}{\sqrt{2}},$$

and from (13.2.14)

$$\frac{1}{\sqrt{2}} \le \max_{-1\le x\le 1}\left|\hat{P}_n^{(m)}(x)\right| \le \frac{\sqrt{2n+1}}{2}. \tag{13.4.13}$$

Since $\sum_{k=1}^{M} w_k = 2$ and (13.4.13), we have from (13.4.2)

$$\widehat{\int_{-1}^{1}} u^2\,dx = \sum_{k=1}^{M} w_k\left\{\hat{P}_{\bar{n}}^{(\bar{m})}(\cos\theta_k)\right\}^2 \le \max_{-1\le x\le 1}\left|\hat{P}_{\bar{n}}^{(\bar{m})}(x)\right|^2 \times \sum_{k=1}^{M} w_k \le \frac{2\bar{n}+1}{2}. \tag{13.4.14}$$

The bound (13.4.11) is obtained from (13.4.12) and (13.4.14). ■

From Lemma 13.3.1, we have

$$\rho^n Y_n^{\circ}(\theta,\phi) = \frac{(2n+1)R^n}{4\pi R}\iint_{S_R}\frac{Y_n^{\circ}(\xi,\eta)}{|\overline{PQ}|}\,ds_Q, \tag{13.4.15}$$

where $ds_Q = R^2 \sin\xi\, d\xi\, d\phi = R^2\, ds_U$ and $Y_n^{\circ}(\theta,\phi)$ are given in (13.2.17). Then we have from (13.4.15), (13.3.6) and (13.3.10)

$$\mathcal{P}_N = \sum_{n=0}^{N}\rho^n Y_n^{\circ}(\theta,\phi) = \frac{1}{4\pi R}\iint_{S_R}\sum_{n=0}^{N}(2n+1)R^n\frac{Y_n^{\circ}(\xi,\eta)}{|\overline{PQ}|}\,ds_Q := \iint_{S_R} T_N\,ds_Q,$$

where

$$\begin{aligned}T_N = \frac{1}{4\pi R}\sum_{n=0}^{N}(2n+1)R^n &\Bigg\{\Big(a_n\hat{P}_n(\cos\xi) + \sum_{m=1}^{n}\hat{P}_n^{(m)}(\cos\xi)[a_{n,m}\cos(m\eta) + b_{n,m}\sin(m\eta)]\Big) \\ &\times\frac{1}{R}\sum_{\bar{n}=0}^{\infty}\frac{2}{2\bar{n}+1}\left(\frac{\rho}{R}\right)^{\bar{n}}\left\{\hat{P}_{\bar{n}}(\cos\theta)\hat{P}_{\bar{n}}(\cos\xi) + 2\sum_{\bar{m}=1}^{\bar{n}}\hat{P}_{\bar{n}}^{(\bar{m})}(\cos\theta)\hat{P}_{\bar{n}}^{(\bar{m})}(\cos\xi)\cos\bar{m}(\phi-\eta)\right\}\Bigg\}.\end{aligned}$$

The errors between the FS and the SHF are given by

$$|\mathcal{P}_N - v_M| = \left| \left(\widehat{\iint_{S_R}} - \iint_{S_R} \right) T_N \, ds_Q \right|, \quad M > N. \tag{13.4.16}$$

Denote $a_{n,0} = a_n$ and $T_{n,0} = T_n$. Then we have

$$\begin{aligned} \left(\widehat{\iint_{S_R}} - \iint_{S_R} \right) T_N \, ds_Q &= \sum_{n=0}^{N} \left\{ \sum_{m=0}^{n} a_{n,m} \triangle T_{n,m} + \sum_{m=1}^{n} b_{n,m} \triangle T^*_{n,m} \right\} \\ &= \sum_{n=0}^{N} \left\{ \sum_{m=0}^{n} a_{n,m} \left(\widehat{\iint_{S_R}} - \iint_{S_R} \right) T_{n,m} \, ds_Q \right. \\ &\quad \left. + \sum_{m=1}^{n} b_{n,m} \left(\widehat{\iint_{S_R}} - \iint_{S_R} \right) T^*_{n,m} \, ds_Q \right\}, \end{aligned} \tag{13.4.17}$$

where the basis errors,

$$\triangle T_{n,m} = \triangle T_{n,m}(\theta, \phi) = \left(\widehat{\iint_{S_R}} - \iint_{S_R} \right) T_{n,m} \, ds_Q, \tag{13.4.18}$$

$$\triangle T^*_{n,m} = \triangle T^*_{n,m}(\theta, \phi) = \left(\widehat{\iint_{S_R}} - \iint_{S_R} \right) T^*_{n,m} \, ds_Q, \tag{13.4.19}$$

and

$$\begin{aligned} T_{n,m} &= \frac{1}{4\pi R}(2n+1) R^n \hat{P}_n^{(m)}(\cos\xi)\cos(m\eta) \\ &\quad \times \frac{1}{R} \sum_{\bar{n}=2M-n}^{\infty} \frac{2}{2\bar{n}+1} \left(\frac{\rho}{R} \right)^{\bar{n}} \left\{ \sum_{\bar{m}=0}^{\bar{n}} \gamma_{\bar{m}} \hat{P}_{\bar{n}}^{(\bar{m})}(\cos\theta) \hat{P}_{\bar{n}}^{(\bar{m})}(\cos\xi)\cos(\bar{m}\phi)\cos(\bar{m}\eta) \right\}, \end{aligned} \tag{13.4.20}$$

where $\gamma_0 = 1$, $\gamma_{\bar{m}} = 2$ for $\bar{m} \geq 1$ with $\gamma_{\bar{m}} \varepsilon_{\bar{m}} = 2$, $\varepsilon_0 = 2$ and $\varepsilon_{\bar{m}} = 1$ for $\bar{m} \geq 1$, and

$$\begin{aligned} T^*_{n,m} &= \frac{1}{4\pi R}(2n+1) R^n \hat{P}_n^{(m)}(\cos\xi)\sin(m\eta) \\ &\quad \times \frac{1}{R} \sum_{\bar{n}=2M-n}^{\infty} \frac{2}{2\bar{n}+1} \left(\frac{\rho}{R} \right)^{\bar{n}} \left\{ \sum_{\bar{m}=1}^{\bar{n}} \hat{P}_{\bar{n}}^{(\bar{m})}(\cos\theta) \hat{P}_{\bar{n}}^{(\bar{m})}(\cos\xi)\sin(\bar{m}\phi)\sin(\bar{m}\eta) \right\}. \end{aligned} \tag{13.4.21}$$

Note that the non-zero summation $\sum_{\bar{n}=2M-n}^{\infty}$ in (13.4.20) and (13.4.21) starts from $\bar{n} = 2M - n$ since rule (13.3.1) has the precision of order $2M - 1$.

To estimate the basic errors of (13.4.18) (or (13.4.19)), we expand them by the SHF,

$$\begin{aligned} &\triangle T_{n,m}(\theta, \phi) \\ &\quad = \sum_{k=0}^{\infty} \{ \alpha_{n,m;k} \hat{P}_k(\cos\theta) + \sum_{\ell=1}^{k} \hat{P}_k^{(\ell)}(\cos\theta)[\alpha_{n,m;k,\ell} \cos(\ell\phi) + \beta_{n,m;k,\ell} \sin(\ell\phi)] \}, \end{aligned} \tag{13.4.22}$$

where the expanded coefficients are given by

$$\alpha_{n,m;k} = \frac{1}{2\pi}\iint_U \triangle T_{n,m}(\theta,\phi)\hat{P}_k(\cos\theta)\,ds_U, \tag{13.4.23}$$

$$\alpha_{n,m;k,\ell} = \frac{1}{\pi}\iint_U \triangle T_{n,m}(\theta,\phi)\hat{P}_k^{(\ell)}(\cos\theta)\cos(\ell\phi)\,ds_U, \quad m = 1,2,..., \tag{13.4.24}$$

$$\beta_{n,m;k,\ell} = \frac{1}{\pi}\iint_U \triangle T_{n,m}(\theta,\phi)\hat{P}_k^{(\ell)}(\cos\theta)\sin(\ell\phi)\,ds_U, \quad m = 1,2,..., \tag{13.4.25}$$

where we have used the orthogonality (13.2.16).

Lemma 13.4.3. *For the expanded coefficients, there exist the bounds,*

$$|\alpha_{n,m;k,\ell}| \le CR^n(2n+1)\frac{1}{\sqrt{k+\frac{1}{2}}}\left(\frac{\rho}{R}\right)^k, \tag{13.4.26}$$

$$|\beta_{n,m;k,\ell}| \le CR^n(2n+1)\frac{1}{\sqrt{k+\frac{1}{2}}}\left(\frac{\rho}{R}\right)^k, \tag{13.4.27}$$

where $k \ge 2M - n$ *and* $\ell \pm m = 2vM$, $v = 0,1,2,....$ *Otherwise,* $\alpha_{n,m;k,\ell} = \beta_{n,m;k,\ell} = 0$.

Proof. We only prove (13.4.26) since the proof of (13.4.27) is similar. From

$$\begin{aligned}\iint_{S_R} f(r,\cos\xi,\eta)\,ds_Q &= R^2\int_0^{\pi}\int_0^{2\pi} f(R,\cos\xi,\eta)\sin\xi\,d\eta\,d\xi \\ &= R^2\iint_U f(R,\cos\xi,\eta)\,ds_U = R^2\int_{-1}^{1}\int_0^{2\pi} f(R,x,\eta)\,d\eta\,dx,\end{aligned} \tag{13.4.28}$$

we have from (13.4.18) and (13.4.20)

$$\begin{aligned}\triangle T_{n,m}(\theta,\phi) &= \left(\iint_{S_R} - \widehat{\iint_{S_R}}\right) T_{n,m}\,ds_Q \\ &= R^2\left(\int_0^{\pi}\int_0^{2\pi} - \widehat{\int_0^{\pi}}\widehat{\int_0^{2\pi}}\right)\frac{1}{4\pi R}(2n+1)R^n(\hat{P}_n^{(m)}(\cos\xi)\cos(m\eta)) \\ &\quad\times\left\{\frac{1}{R}\sum_{\bar{n}=2M-n}^{\infty}\frac{2}{2\bar{n}+1}\left(\frac{\rho}{R}\right)^{\bar{n}}\sum_{\bar{m}=0}^{\bar{n}}\gamma_{\bar{m}}\left(\hat{P}_{\bar{n}}^{(\bar{m})}(\cos\theta)\cos(\bar{m}\phi)\right)\right. \\ &\quad\times\left.\left(\hat{P}_{\bar{n}}^{(\bar{m})}(\cos\xi)\cos(\bar{m}\eta)\right)\right\}\sin\xi\,d\eta\,d\xi,\end{aligned}$$

where the integrals are trivial for $\bar{n} < 2M - n$. Based on Lemma 13.4.2, the nonzero integrals occur only for $\bar{m} \pm m = 2vM$ with $v = 0,1,2,...,$

$$\begin{aligned}\triangle T_{n,m}(\theta,\phi) = {} & \frac{\varepsilon_m}{2}(2n+1)R^n \\ & \times \left\{ \sum_{\bar n=2M-n}^{\infty} \frac{1}{2\bar n+1}\left(\frac{\rho}{R}\right)^{\bar n} \sum_{\bar m=0}^{\bar n} \gamma_{\bar m} \hat P_{\bar n}^{(\bar m)}(\cos\theta)\cos(\bar m\phi) \right. \\ & \left. \times \left(\int_{-1}^{1} - \widehat{\int_{-1}^{1}} \right) \hat P_n^{(m)}(x) \hat P_{\bar n}^{(\bar m)}(x)\,dx \right\}.\end{aligned}$$

From (13.4.5) and the orthogonality (13.2.16), the coefficients (13.4.24) lead to

$$\begin{aligned}\left|\alpha_{n,m;k,\ell}\right| &= \frac{1}{\pi}\left| \iint_U \triangle T_{n,m}(\theta,\phi)\hat P_k^{(\ell)}(\cos\theta)\cos(\ell\phi)\,ds_U \right| \\ &= \frac{\varepsilon_m}{2}(2n+1)R^n \sum_{\bar n=2M-n}^{\infty} \frac{1}{2\bar n+1}\left(\frac{\rho}{R}\right)^{\bar n} \\ &\quad \times \left| \sum_{\bar m=0}^{\bar n} \gamma_{\bar m} \iint_U \left[\hat P_k^{(\ell)}(\cos\theta)\cos(\ell\phi)\right]\left[\hat P_{\bar n}^{(\bar m)}(\cos\theta)\cos(\bar m\phi)\right] ds_U \right. \\ &\quad \left. \times \left(\int_{-1}^{1} - \widehat{\int_{-1}^{1}} \right) \hat P_n^{(m)}(x)\hat P_{\bar n}^{(\bar m)}(x)\,dx \right| \\ &\le CR^n(2n+1) \sum_{\bar n=2M-n}^{\infty} \frac{\sqrt{2\bar n+1}}{2\bar n+1}\left(\frac{\rho}{R}\right)^{\bar n} \sum_{\bar m=0}^{\bar n} \delta_{k,\bar n}\delta_{\ell,\bar m} \\ &\le CR^n(2n+1) \sum_{\bar n=2M-n}^{\infty} \frac{1}{\sqrt{\bar n+\frac12}}\left(\frac{\rho}{R}\right)^{\bar n} \sum_{\bar m=0}^{\bar n} \delta_{k,\bar n}\delta_{\ell,\bar m}.\end{aligned} \tag{13.4.29}$$

Since $\sum_{\bar n=2M-n}^{\infty}\delta_{k,\bar n} = 1$ with $k=\bar n$, we have from (13.4.29)

$$\left|\alpha_{n,m;k,\ell}\right| \le CR^n(2n+1)\frac{1}{\sqrt{k+\frac12}}\left(\frac{\rho}{R}\right)^k \sum_{\bar m=0}^{k}\delta_{\ell,\bar m}.$$

Also since $\sum_{\bar m=0}^{k}\delta_{\ell,\bar m} = 1$ with $\ell=\bar m$, we have

$$\left|\alpha_{n,m;k,\ell}\right| \le CR^n(2n+1)\frac{1}{\sqrt{k+\frac12}}\left(\frac{\rho}{R}\right)^k,$$

where $\ell \pm m = \bar m \pm m = 2vM$, $v = 0,1,2,\ldots$. This gives the first desired result (13.4.26). ■

Lemma 13.4.4. *For (13.4.18) and (13.4.19) there exist the bounds,*

$$\begin{aligned}\|\triangle T_{n,m}\|_{0,S_\rho} &= \left\| \left(\widehat{\iint_{S_R}} - \iint_{S_R} \right) T_{n,m}\,ds_Q \right\|_{0,S_\rho} \\ &\le C\frac{R^n}{\sqrt{M}}(2n+1)\left(\frac{\rho}{R}\right)^{2M-n}, \quad n=0,1,2,\ldots,\end{aligned} \tag{13.4.30}$$

$$\begin{aligned}\|\triangle T^*_{n,m}\|_{0,S_\rho} &= \left\| \left(\widehat{\iint_{S_R}} - \iint_{S_R} \right) T^*_{n,m}\, ds_Q \right\|_{0,S_\rho} \\ &\le C \frac{R^n}{\sqrt{M}} (2n+1) \left(\frac{\rho}{R}\right)^{2M-n}, \quad n = 1, 2, ...,\end{aligned} \tag{13.4.31}$$

where $T_{n,m}$ and $T^*_{n,m}$ are given in (13.4.20) and (13.4.21), respectively.

Proof. From (13.4.28) and the expansions (13.4.22), we have from (13.2.16)

$$\begin{aligned}\|\triangle T_{n,m}\|^2_{0,S_\rho} &= \|\triangle T_{n,m}(\theta,\phi)\|^2_{0,S_\rho} = \rho^2 \iint_U (\triangle T_{n,m}(\theta,\phi))^2\, ds_U \\ &= \rho^2 \pi \sum_{k=0}^{\infty} \left\{ 2\alpha^2_{n,m;k} + \sum_{\ell=1}^{k} (\alpha^2_{n,m;k,\ell} + \beta^2_{n,m;k,\ell}) \right\}.\end{aligned} \tag{13.4.32}$$

From Lemma 13.4.3, $\rho < R$, and $\ell \pm m = 2\nu M$,

$$\begin{aligned}\sum_{k=0}^{\infty} \left\{ 2\alpha^2_{n,m;k} + \sum_{\ell=1}^{k} (\alpha^2_{n,m;k,\ell} + \beta^2_{n,m;k,\ell}) \right\} &\le 2 \sum_{k=0}^{\infty} \sum_{\ell=0}^{k} \alpha^2_{n,m;k,\ell} \\ &\le CR^{2n}(2n+1)^2 \sum_{k=2M-n}^{\infty} \sum_{\ell=0}^{k} \frac{1}{k+\frac{1}{2}} \left(\frac{\rho}{R}\right)^{2k} \\ &\le CR^{2n}(2n+1)^2 \sum_{k=2M-n}^{\infty} \frac{k}{2M} \frac{1}{k+\frac{1}{2}} \left(\frac{\rho}{R}\right)^{2k} \\ &\le C \frac{R^{2n}}{M} (2n+1)^2 \sum_{k=2M-n}^{\infty} \left(\frac{\rho}{R}\right)^{2k} \\ &\le C \frac{R^{2n}}{M} (2n+1)^2 \left(\frac{\rho}{R}\right)^{2(2M-n)}.\end{aligned} \tag{13.4.33}$$

From (13.4.32) and (13.4.33), we obtain the first desired result (13.4.30). The proof for (13.4.31) is similar. ■

13.4.2 Error Bounds

Theorem 13.4.1. *Suppose that Laplace's solutions $u \in \mathbf{C}(\mathbf{\Omega})$. For $\mathcal{P}_N$ in (13.3.10) and v^*_M in (13.3.12), when $M\,(> N)$ and N are large, there exists the error bound,*

$$\|\mathcal{P}_N - v^*_M\|_{0,\Gamma} \le CN \left(\frac{r_{\max}}{R}\right)^{2(M-N)} \left(\frac{r_{\max}}{r_{\min}}\right)^N \|u\|_{0,\Gamma}, \tag{13.4.34}$$

where C is a constant independent of N and M, and $r_{\max}$ and $r_{\min}$ are the maximal and the minimal radii of $\mathbf{\Omega}$, respectively.

Proof. From (13.4.16)–(13.4.21) and the Schwarz inequality, we have

$$\begin{aligned}\|\mathcal{P}_N - v_M^*\|^2_{0,S_\rho} &= \left\| \sum_{n=0}^{N} \left\{ a_n \triangle T_n + \sum_{m=1}^{n} (a_{n,m}\triangle T_{n,m} + b_{n,m}\triangle T^*_{n,m}) \right\} \right\|^2_{0,S_\rho} \\ &\le \left(\sum_{n=0}^{N} \left\{ |a_n| \|\triangle T_n\|_{0,S_\rho} + \sum_{m=1}^{n} \Big(|a_{n,m}| \|\triangle T_{n,m}\|_{0,S_\rho} + |b_{n,m}| \|\triangle T^*_{n,m}\|_{0,S_\rho} \Big) \right\} \right)^2 \\ &\le \sum_{n=0}^{N} \frac{1}{\tilde{\rho}^{2n}} \left\{ \|\triangle T_n\|^2_{0,S_\rho} + \sum_{m=1}^{n} \Big(\|\triangle T_{n,m}\|^2_{0,S_\rho} + \|\triangle T^*_{n,m}\|^2_{0,S_\rho} \Big) \right\} \\ &\quad \times \sum_{n=0}^{N} \tilde{\rho}^{2n} \left\{ a_n^2 + \sum_{m=1}^{n} (a^2_{n,m} + b^2_{n,m}) \right\}, \end{aligned} \tag{13.4.35}$$

where $r_{\min} \le \tilde{\rho} \le r_{\max}$. We have from (13.2.18),

$$\sum_{n=0}^{N} \tilde{\rho}^{2n} \left\{ a_n^2 + \sum_{m=1}^{n} (a^2_{n,m} + b^2_{n,m}) \right\} \le \|u\|^2_{0,S_{\tilde{\rho}}} \le C\|u\|^2_{0,\Gamma}. \tag{13.4.36}$$

In the last bound in (13.4.36), we have used the continuity extension in Remark 2.3.1 in Chapter 2. When $u \in \mathbf{C}(\mathbf{\Omega})$, we have $\|u\|_{0,S_{\tilde{\rho}}} \le C\|u\|_{0,\Gamma}$. From Lemma 13.4.4 and $2M - n > N \ge n$, we have for $\rho < R$

$$\begin{aligned}&\sum_{n=0}^{N} \frac{1}{\tilde{\rho}^{2n}} \left\{ \|\triangle T_n\|^2_{0,S_\rho} + \sum_{m=1}^{n} \Big(\|\triangle T_{n,m}\|^2_{0,S_\rho} + \|\triangle T^*_{n,m}\|^2_{0,S_\rho} \Big) \right\} \\ &\le C \frac{1}{M} \sum_{n=0}^{N} \frac{1}{\tilde{\rho}^{2n}} \sum_{m=0}^{n} R^{2n} (2n+1)^2 \left(\frac{\rho}{R}\right)^{4M-2n} \\ &\le C \frac{1}{M} \sum_{n=0}^{N} (2n+1)^2 (n+1) \left(\frac{\rho}{R}\right)^{4M-2n} \left(\frac{R}{\tilde{\rho}}\right)^{2n} \\ &\le C \frac{1}{M} (2N+1)^3 \left(\frac{\rho}{R}\right)^{4M-2N} \left(\frac{R}{\tilde{\rho}}\right)^{2N} \\ &= CN^2 \left(\frac{\rho}{R}\right)^{4(M-N)} \left(\frac{R}{\tilde{\rho}}\right)^{2N}, \end{aligned} \tag{13.4.37}$$

where we have used $M \ge c_0 N$, and $c_0\,(>0)$ is a constant independent of N and M. Since $\|u\|_{0,\tilde{\rho}} \le C\|u\|_{0,\Gamma}$, we have from (13.4.35)–(13.4.37)

$$\|\mathcal{P}_N - v_M^*\|_{0,\Gamma} \le CN \left(\frac{r_{\max}}{R}\right)^{2(M-N)} \left(\frac{r_{\max}}{r_{\min}}\right)^{N} \|u\|_{0,\Gamma}.$$

This is the desired result (13.4.34). ■

Denote by V_M the set of (13.3.2). The $2M^2$ unknown coefficients c_{ij} can be sought by (13.2.12):

$$\|v_M - f\|_{0,\Gamma} = \inf_{v \in V_M} \|v - f\|_{0,\Gamma}. \tag{13.4.38}$$

Theorem 13.4.2. *Suppose that Laplace's solutions satisfy* $u \in \mathbf{C}(\Omega)$ *and* $u \in \mathbf{H}^p(\Gamma)$ $(p > 1)$. *When the* $M\,(> N)$ *is chosen large enough to satisfy (13.4.42) below, there exist the error bounds by the MFS,*

$$\|u - v_M\|_{0,\Gamma} = O\left(\frac{1}{(2N)^p}\right)\|u\|_{p,\Gamma} = O\left(\frac{1}{(2M)^p}\right)\|u\|_{p,\Gamma}. \tag{13.4.39}$$

Proof. Choose the special v_M^* with the coefficients c_{ij}^* in (13.3.13) to approximate $\mathcal{P}_N$. From (13.4.38) we have $\|u - v_M\|_{0,\Gamma} \le \|u - v_M^*\|_{0,\Gamma}$. Then we obtain

$$\|u - v_M\|_{0,\Gamma} \le \|u - \mathcal{P}_N\|_{0,\Gamma} + \left\|\mathcal{P}_N - v_M^*\right\|_{0,\Gamma}.$$

From Proposition 13.2.1,

$$\|R_N\|_{0,\Gamma} = \|u - \mathcal{P}_N\|_{0,\Gamma} \le C\frac{1}{(2N)^p}\|u\|_{p,\Gamma}. \tag{13.4.40}$$

Moreover, we have from Theorem 13.4.1 and (13.4.40)

$$\begin{aligned}\|u - v_M\|_{0,\Gamma} &\le \|u - v_M^*\|_{0,\Gamma} \le \|R_N\|_{0,\Gamma} + \|\mathcal{P}_N - v_M^*\|_{0,\Gamma}\\ &\le C\left\{\frac{1}{(2N)^p} + N\left(\frac{r_{\max}}{R}\right)^{2(M-N)}\left(\frac{r_{\max}}{r_{\min}}\right)^N\right\}\|u\|_{p,\Gamma}.\end{aligned}$$

To reach the optimal convergence rates in (13.4.39), choose M large enough such that

$$N\left(\frac{r_{\max}}{R}\right)^{2(M-N)}\left(\frac{r_{\max}}{r_{\min}}\right)^N \le \frac{1}{(2N)^p}. \tag{13.4.41}$$

It is sufficient to choose

$$M \ge N + \frac{\ln N + p\,\ln(2N) + N\,\ln\left(\frac{r_{\max}}{r_{\min}}\right)}{2\,\ln\left(\frac{R}{r_{\max}}\right)}. \tag{13.4.42}$$

Then we have

$$\|u - v_M\|_{0,\Gamma} = O\left(\frac{1}{(2N)^p}\right)\|u\|_{p,\Gamma}. \tag{13.4.43}$$

From (13.4.42) we may choose $M \le CN$, and then $M \asymp N$. The desired result (13.4.39) follows from (13.4.43). ∎

Remark 13.4.1. *The rule (13.3.1) is composed of the trapezoidal rule along* θ *and the Gauss–Legendre rule along* z. *Other quadrature rules along* z *may be chosen, such as the Chebyshev rule. For the quadrature rules introduced in Lebedev [134] and Beetjes [21], the number of nodes is about* $\frac{2}{3}$ *of that in (13.3.1). More quadrature rules are given in [11, 14, 210]. All those integration nodes (i.e., the abscissas) may be used for source nodes* Q_{ij} *of the MFS; the error bounds of the MFS can be derived if the errors of quadrature rules may be evaluated.*

13.5 Numerical Experiments

The purposes of numerical experiments are twofold: to verify the analysis made, and to pursue better locations of source nodes for the MFS. First, let us describe the collocation equations.

13.5.1 Collocation Equations on $\boldsymbol{\Gamma}$

For (13.2.1) we choose a cylinder as the solution domain $\boldsymbol{\Omega}$ in cylindrical coordinates,

$$\boldsymbol{\Omega} = \left\{ (\rho, \phi, z) | 0 \le \rho < 1, 0 \le \phi < 2\pi, -\frac{H}{2} < z < \frac{H}{2} \right\}, \tag{13.5.1}$$

where $H = 1$ and $(x, y, z) = (\rho \cos\phi, \rho \sin\phi, z)$. In computation, choose the following cylindrical harmonic functions as the exact solution (see [60]),

$$u(P) = u(\rho, \phi, z) = \sinh(kz)\cos(n\phi) J_n(k\rho), \quad n = k = 1, 4, \tag{13.5.2}$$

where $J_n(\rho)$ are the Bessel functions with order n, defined by

$$J_n(\rho) = \sum_{i=0}^{\infty} \frac{(-1)^i}{i!(i+n)!} \left(\frac{\rho}{2}\right)^{2i+n}.$$

Note that the solutions (13.5.2) are smooth, and there exists no corner singularity for cylinder $\boldsymbol{\Omega}$ in (13.5.1). Let us establish the collocation equations (13.2.13) on $\boldsymbol{\Gamma}$. Denote the domain boundary by $\boldsymbol{\Gamma} = S_1 \cup S_2$, where S_1 are two cover disks, and S_2 is one surrounding cylindrical surface. For two cover disks: $S_1 = S_1^{\pm} = \{(r, \phi) | 0 \le r \le 1, 0 \le \phi \le 2\pi\}$ at $z = \pm \frac{H}{2}$, the 2D integration is given by

$$\iint_{S_1} f(r, \phi)\, ds = \int_0^1 \left\{ \int_0^{2\pi} f(r, \phi)\, d\phi \right\} r dr.$$

For the integral $\int_0^{2\pi} f(\phi)\, d\phi$, choose the trapezoidal rule, but for the other integral,

$$\int_0^1 f(r) r dr \approx \widehat{\int_0^1} f(r) r dr = \sum_{k=1}^{M} w_k^*\, f(r_k),$$

choose the Gauss-Jacobi rule (*i.e.*, the Gaussian integration of moments with order one), where (r_k, w_k^*) are the abscissas and weights given in [1, p.921]. By using the composite rule in [72] we have

$$\iint_{S_1} f(r, \phi)\, ds \approx h \sum_{k=1}^{M} \sum_{i=1}^{2M} w_k^*\, f(r_k, \phi_i),$$

where $\phi_i = ih$ and $h = \frac{\pi}{M}$. For two top-bottom disks $S_1^{\pm}$, the collocation equations in (13.2.13) are modified as

$$\sqrt{h w_k^*} u_M \left(r_k, \phi_i, \pm \frac{H}{2} \right) = \sqrt{h w_k^*}\, f \left(r_k, \phi_i, \pm \frac{H}{2} \right), \quad (r_k, \phi_i) \in S_1^{\pm}. \tag{13.5.3}$$

For $S_2 = \left\{(\theta, z) | 0 \le \theta \le 2\pi, -\frac{H}{2} \le z \le \frac{H}{2}\right\}$, the collocation equations in (13.2.13) are modified as

$$\sqrt{hw_j} u_M\big(1, \phi_i, z_j\big) = \sqrt{hw_j}\, f\big(1, \phi_i, z_j\big), \quad (\phi_i, z_j) \in S_2, \tag{13.5.4}$$

where h and ϕ_i are the same as in (13.5.3), but (z_j, w_j) are the abscissas and weights of the Gauss–Legendre rule. The numerical integration used in (13.5.3) and (13.5.4) is called the Jacobi-trapezoidal-Legendre rules in this chapter.

In computation, the number M_{tol} of collocation equations (13.5.3) and (13.5.4) may be larger than the number N_{tol} of FS (or SHF) (*i.e.*, $M_{\text{tol}} \ge N_{\text{tol}}$), to give an overdetermined system, $\mathbf{F}\mathbf{x} = \mathbf{b}$, where $\mathbf{F} \in \mathbf{R}^{M_{\text{tol}} \times N_{\text{tol}}} (M_{\text{tol}} \ge N_{\text{tol}})$ and $\mathbf{b} \in \mathbf{R}^{M_{\text{tol}}}$. The traditional and the effective condition numbers are defined in [162] as Cond $= \frac{\sigma_{\max}}{\sigma_{\min}}$ and Cond_eff $= \frac{\|\mathbf{b}\|}{\sigma_{\min}\|\mathbf{x}\|}$, respectively, where the $\sigma_{\max}$ and the $\sigma_{\min}$ are the maximal and the minimal singular values, respectively. Define the errors

$$\|\epsilon\|_\infty = \max_S |\epsilon|, \quad \|\epsilon\|_0 = \left\{ \iint_S \epsilon^2 \, ds \right\}^{\frac{1}{2}}, \quad \epsilon = u - \tilde{u}_{N_{\text{tol}}}.$$

For the Jacobi-trapezoidal-Legendre rules, denote the collocation equations by $C(m_1, m_2, m_3)$, where m_1, m_2, m_3 are the partition numbers along r, ϕ, z, respectively, and the total number $M_{\text{tol}} = 2m_1 m_2 + m_2 m_3$. In computation, we simply choose $C(m_1, m_2, m_3) = (8, 24, 12)$ with $M_{\text{tol}} = 672$.

13.5.2 By MFS

First, we test the source nodes Q_{ij} given in (13.4.1) (see Figure 13.4). Choose the solution (13.5.2) at $k = n = 1$ with $\|u\|_\infty = 0.228$ and $\|u\|_0 = 0.377$. The numerical results are given in Table 13.1, where $n_1 (= M)$ and $n_2 (= 2M)$ are the partition numbers along θ and ϕ, respectively. Then the total number of FS used is $N_{\text{tot}} = n_1 n_2$. All tables in this chapter are computed by double precision. For $R = \sqrt{2}$, we have from Table 13.1

$$\|\epsilon\|_\infty = O(0.78^{n_2}), \ \|\epsilon\|_0 = O(0.75^{n_2}), \ \text{Cond} = O(5.3^{n_2}), \ \text{Cond\_eff} = O(1.4^{n_2}). \tag{13.5.5}$$

For $R = 2$, we have from Table 13.1

$$\|\epsilon\|_\infty = O(0.60^{n_2}), \ \|\epsilon\|_0 = O(0.57^{n_2}), \ \text{Cond} = O(8.1^{n_2}), \ \text{Cond\_eff} = O(1.9^{n_2}). \tag{13.5.6}$$

Based on Theorem 13.4.1, when $r_{\max} = \sqrt{1 + 0.5^2} = 1.118$, we have the key convergence rates at $R = \sqrt{2}, 2$, as

$$O\left(\left(\frac{r_{\max}}{R}\right)^{2M}\right) = O\left(\left(\frac{1.118}{\sqrt{2}}\right)^{n_2}\right) = O((0.79)^{n_2}), \tag{13.5.7}$$

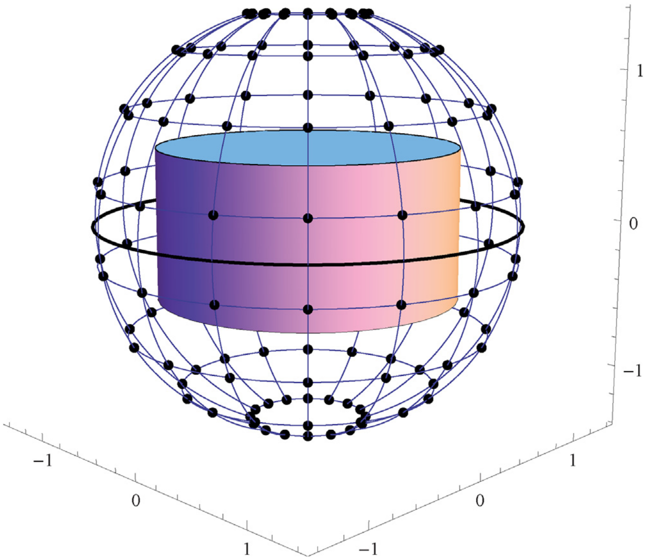

FIG. 13.4 – The source nodes Q_{ij} located on the sphere S_R with radius R, based on (13.4.1) at $M = 8$.

TAB. 13.1 – The errors and the condition numbers for spherical source nodes *via* the trapezoidal-Gauss rules at $R = \sqrt{2}, 2$ and $n = k = 1$ with $C(8, 24, 12)$.

R	n_1	n_2	$\|\epsilon\|_\infty$	$\|\epsilon\|_0$	$\sigma_{\max}$	$\sigma_{\min}$	$\|\mathbf{x}\|$	Cond	Cond_eff
$\sqrt{2}$	4	8	5.58(−3)	5.78(−3)	1.25	8.79(−6)	1.17	1.42(5)	3.96(3)
	10	20	3.93(−4)	2.23(−4)	3.10	8.18(−17)	1.69(9)	3.79(16)	2.94(5)
	12	24	1.07(−4)	5.92(−5)	3.72	7.01(−17)	4.19(8)	5.31(16)	1.39(6)
2	4	8	2.72(−3)	2.85(−3)	9.69(−1)	1.70(−6)	2.81	5.71(5)	8.55(3)
	6	12	5.36(−4)	4.15(−4)	1.45	3.43(−11)	2.79	4.24(10)	4.26(8)
	8	16	6.18(−5)	4.03(−5)	1.93	1.50(−16)	1.01(8)	1.29(16)	2.70(6)
	10	20	5.73(−6)	3.40(−6)	2.42	5.46(−17)	5.40(7)	4.43(16)	1.38(7)
	12	24	1.73(−7)	9.36(−8)	2.90	5.57(−17)	3.06(6)	5.21(16)	2.40(8)

$$O\left(\left(\frac{r_{\max}}{R}\right)^{2M}\right) = O\left(\left(\frac{1.118}{2}\right)^{n_2}\right) = O((0.56)^{n_2}). \qquad (13.5.8)$$

The numerical convergence rates in (13.5.5) and (13.5.6) coincide with (13.5.7) and (13.5.8) very well, thus supporting the error analysis in Section 13.4.

Besides (13.4.1), we test other locations of the source nodes Q_{ij} on the same pseudo-sphere. We do not implement Lebedev [134] and Beetjes [21] in computation because their algorithms are rather complicated. The following uniform partitions on the sphere are simpler than (13.4.1), $Q_{ij} := (x_{ij}, y_{ij}, z_i) = (R\,\sin\theta_i\,\cos\phi_j, R\,\sin\theta_i\,\sin\phi_j, R\,\cos\theta_i)$, where the uniform partitions in both θ and ϕ are given by

$$\theta_i = \left(i - \frac{1}{2}\right)\bar{h}, \quad i = 1, 2, ..., n_1, \quad \bar{h} = \frac{\pi}{n_1}, \quad n_1 = M, \tag{13.5.9}$$

$$\phi_j = \left(j - \frac{1}{2}\right)h, \quad j = 1, 2, ..., n_2, \quad h = \frac{2\pi}{n_2}, \quad n_2 = 2M. \tag{13.5.10}$$

The uniform rule (13.5.10) is of the trapezoidal rule along $\phi \in [0, 2\pi]$. The Gauss–Chebyshev rule is given in [72, p.98, (2.7.13)],

$$\widehat{\int_{-1}^{1}} f(x)\,dx = \frac{\pi}{M}\sum_{i=1}^{M} f(x_i),$$

where $x_i = \cos\left(\frac{2i-1}{2M}\pi\right) = \cos\theta_i$ with $i = 1, 2, ..., M$. Hence the θ_i in (13.5.9) is of the Gauss–Chebyshev rule. Both the Gauss–Chebyshev rule and the Gauss–Legendre rule have the same precision of degree $2M - 1$ (see [72]). Choose the uniform partitions in (13.5.9) and (13.5.10), and the numerical results are given in Table 13.2. For $R = \sqrt{2}$, we have from Table 13.2

$$\|\epsilon\|_\infty = O(0.53^{n_2}), \quad \|\epsilon\|_0 = O(0.51^{n_2}), \quad \text{Cond} = O(6.4^{n_2}), \quad \text{Cond\_eff} = O(4.8^{n_2}). \tag{13.5.11}$$

For $R = 2$,

$$\|\epsilon\|_\infty = O(0.41^{n_2}), \quad \|\epsilon\|_0 = O(0.39^{n_2}), \quad \text{Cond} = O(7.8^{n_2}), \quad \text{Cond\_eff} = O(3.9^{n_2}). \tag{13.5.12}$$

Comparing (13.5.11) and (13.5.12) with (13.5.5) and (13.5.6), we conclude that the uniform partitions in (13.5.9) and (13.5.10) provide a better performance in accuracy and stability than (13.4.1); the error analysis may be developed by following Section 13.4.

TAB. 13.2 – The errors and the condition numbers for spherical source nodes *via* the uniform rules in (13.5.9) and (13.5.10) at $R = \sqrt{2}, 2$ and $n = k = 1$ with $C(8, 24, 12)$.

R	n_1	n_2	$\|\epsilon\|_\infty$	$\|\epsilon\|_0$	$\sigma_{\max}$	$\sigma_{\min}$	$\|\mathbf{x}\|$	Cond	Cond_eff
$\sqrt{2}$	4	8	8.55(−3)	9.48(−3)	1.27	1.09(−4)	9.53(−1)	1.17(4)	3.94(2)
	6	12	5.93(−4)	5.60(−4)	1.90	1.89(−7)	5.58(−1)	1.00(7)	3.86(5)
	8	16	2.73(−5)	2.50(−5)	2.53	1.41(−10)	1.49(2)	1.79(10)	1.94(6)
	10	20	3.75(−6)	2.65(−6)	3.17	5.91(−14)	1.05(1)	5.36(13)	6.58(10)
2	4	8	2.87(−3)	3.13(−3)	9.79(−1)	1.90(−5)	2.09	5.16(4)	1.03(3)
	6	12	1.02(−4)	7.39(−5)	1.47	1.50(−8)	1.34	9.79(7)	2.02(6)
	8	16	1.12(−5)	7.73(−6)	1.96	5.37(−12)	3.96(1)	3.64(11)	1.92(8)
	10	20	6.07(−8)	4.25(−8)	2.45	9.89(−16)	3.28(3)	2.47(15)	1.26(10)

Since $\boldsymbol{\Omega}$ in (13.5.1) is a cylinder, it is natural to choose the source nodes on a cylindrical pseudo-surface S^* (see Figure 13.5). Denote $S^* = S_1^* \cup S_2^*$ with an equal distance $\triangle\,(>0)$ to the domain boundary Γ, where two cover disks $S_1^* = \{(r,\phi)|0 \le r \le 1+\triangle, 0 \le \phi \le 2\pi\}$ at $z = \pm\left(\frac{H}{2}+\triangle\right)$, and the surrounding cylindrical surface $S_2^* = \left\{(\phi,z)|0 \le \phi \le 2\pi, -\left(\frac{H}{2}+\triangle\right) \le z \le \frac{H}{2}+\triangle\right\}$. The cylindrical source nodes $Q_{ij} \in S^*$ are chosen *via* the Jacobi-trapezoidal-Legendre rules as in (13.5.3) and (13.5.4). The numerical results are given in Table 13.3, where n_1, n_2, n_3 are the partition numbers along r, ϕ, z, respectively. Then the total number of FS used is $N_{\text{tot}} = 2n_1n_2 + n_2n_3$. For $\triangle = 0.5$, we have from Table 13.3

$$\|\epsilon\|_\infty = O(0.55^{n_2}), \quad \|\epsilon\|_0 = O(0.55^{n_2}), \quad \text{Cond} = O(4.4^{n_2}), \quad \text{Cond\_eff} = O(3.3^{n_2}), \tag{13.5.13}$$

and for $\triangle = 1$,

$$\|\epsilon\|_\infty = O(0.37^{n_2}), \quad \|\epsilon\|_0 = O(0.37^{n_2}), \quad \text{Cond} = O(8.1^{n_2}), \quad \text{Cond\_eff} = O(6.9^{n_2}). \tag{13.5.14}$$

To compare the spherical and the cylindrical source nodes, we count the convergence rates and the growth rates of Cond *via* a number of total FS used by $N_{\text{tol}} = n_1n_2$ and $N_{\text{tol}} = 2n_1n_2 + n_2n_3$, respectively. We have from Table 13.1 at $R = 2$ and from Table 13.3 at $\triangle = 1$

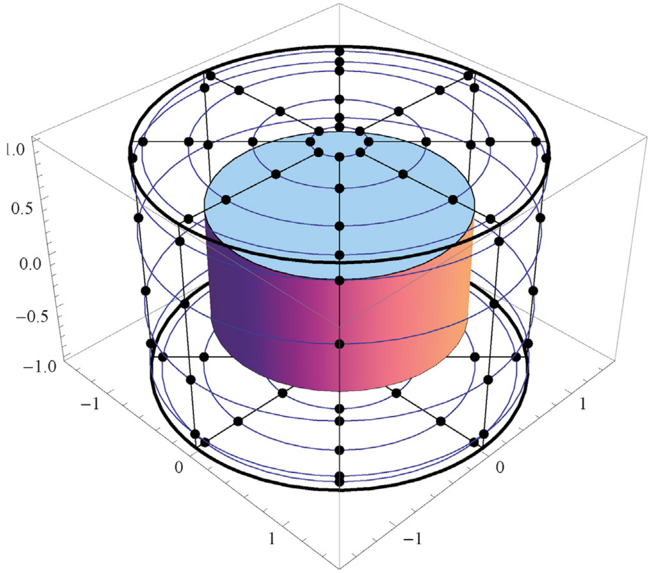

FIG. 13.5 – The source nodes Q_{ij} located on the outside cylindrical surface S^* with $\Delta = 0.5$ at $(n_1, n_{2,3}) = (4, 8, 4)$.

Tab. 13.3 – The errors and the condition numbers for cylindrical source nodes *via* the Jacobi-trapezoidal-Legendre rules at $\triangle = 0.5, 1$ and $n = k = 1$ with $C(8, 24, 12)$.

$\triangle$	n_1	n_2	n_3	$\|\epsilon\|_\infty$	$\|\epsilon\|_0$	$\sigma_{\max}$	$\sigma_{\min}$	$\|\mathbf{x}\|$	Cond	Cond_eff
0.5	2	4	2	7.76(−2)	7.83(−2)	1.39	2.29(−3)	2.18	6.06(2)	8.17
	4	8	4	1.82(−3)	1.38(−3)	2.80	3.80(−5)	2.17	7.36(4)	4.94(2)
	6	12	6	4.82(−4)	2.86(−4)	4.21	6.11(−9)	2.04	6.90(8)	3.27(6)
	8	16	8	6.21(−5)	5.93(−5)	5.63	1.59(−10)	1.85(1)	3.53(10)	1.38(7)
1	2	4	2	1.34(−2)	2.10(−2)	1.01	1.65(−4)	7.87	6.12(3)	3.14(1)
	4	8	4	3.62(−5)	3.48(−5)	2.05	2.52(−7)	5.42	8.14(6)	2.98(4)
	6	12	6	2.99(−6)	1.70(−6)	3.10	3.01(−12)	6.79	1.03(12)	1.99(9)
	8	16	8	8.93(−8)	1.25(−7)	4.15	8.37(−15)	1.32(1)	4.98(14)	3.68(11)

$$\|\epsilon\|_0 = O(0.963^{N_{\text{tol}}}), \quad \text{Cond} = O(1.10^{N_{\text{tol}}}), \tag{13.5.15}$$

$$\|\epsilon\|_0 = O(0.967^{N_{\text{tol}}}), \quad \text{Cond} = O(1.07^{N_{\text{tol}}}). \tag{13.5.16}$$

From (13.5.15) and (13.5.16), the slower convergence rates but better stability result from the cylindrical pseudo-surface. One criterion for stability may be viewed by $\|\mathbf{x}\| = \sqrt{\sum_{ij} c_{ij}^2}$. Comparing $\|\mathbf{x}\|$ among three different source nodes in Tables 13.1–13.3, the spherical pseudo-surface *via* the trapezoidal-Gauss rules in Table 13.1 offers the largest, but the cylindrical pseudo-surface *via* the Jacobi-trapezoidal-Legendre rules in Table 13.3 offers the smallest. Furthermore, when severer instability occurs, the truncated singular value decomposition (TSVD) may be solicited to seek better numerical solutions (see [162, Chapter 13] and [167, 259]).

The case of $k = n = 1$ represents the highly smooth solutions (more results were reported in Chi [60] *via* uniform partitions). We also choose the solution (13.5.2) at $k = n = 4$ with $\|u\|_\infty = 1.02$ and $\|u\|_0 = 1.28$. The numerical results are given in Tables 13.4–13.6. The convergence rates and the growth rates of Cond at $n = k = 4$ are similar to those at $n = k = 1$; details of discussions are omitted. Denote the relative errors by $\frac{\|\epsilon\|_0}{\|u\|_0}$ and $\frac{\|\epsilon\|_\infty}{\|u\|_\infty}$. From Tables 13.1–13.6, the relative errors with 10(−7) at $n = k = 1$ and 10(−5) at $n = k = 4$ can be obtained from 288 (or 384) FS with 672 collocation equations; a modest computational effort for 3D problems.

Tab. 13.4 – The errors and the condition numbers for spherical source nodes *via* the trapezoidal-Gauss rule at $R = 2$ and $n = k = 4$ with $C(8, 24, 12)$.

n_1	n_2	$\|\epsilon\|_\infty$	$\|\epsilon\|_0$	$\sigma_{\max}$	$\sigma_{\min}$	$\|\mathbf{x}\|$	Cond	Cond_eff
6	12	3.11(−3)	5.52(−3)	1.45	3.43(−11)	1.48(5)	4.24(10)	2.85(4)
8	16	9.51(−4)	7.76(−4)	1.93	1.43(−16)	5.28(9)	1.39(16)	1.93(5)
10	20	9.23(−5)	6.31(−5)	2.42	3.62(−17)	2.53(9)	2.30(17)	1.58(6)

TAB. 13.5 – The errors and the condition numbers for spherical source nodes *via* the uniform rules in (13.5.9) and (13.5.10) at $R = 2$ and $n = k = 4$ with $C(8, 24, 12)$.

n_1	n_2	$\|\epsilon\|_\infty$	$\|\epsilon\|_0$	$\sigma_{\max}$	$\sigma_{\min}$	$\|\mathbf{x}\|$	Cond	Cond_eff
6	12	4.02(−3)	5.80(−3)	1.47	1.50(−8)	8.45(3)	9.79(7)	1.15(3)
8	16	2.75(−4)	2.55(−4)	1.96	5.37(−12)	6.74(3)	3.64(11)	4.01(6)
10	20	6.08(−5)	4.16(−5)	2.45	9.89(−16)	1.17(6)	2.51(15)	1.26(8)

TAB. 13.6 – The errors and the condition numbers for cylindrical source nodes *via* the Jacobi-trapezoidal-Legendre rules at $\triangle = 1$ and $n = k = 4$ with $C(8, 24, 12)$.

n_1	n_2	n_3	$\|\epsilon\|_\infty$	$\|\epsilon\|_0$	$\sigma_{\max}$	$\sigma_{\min}$	$\|\mathbf{x}\|$	Cond	Cond_eff
2	4	2	5.27(−1)	7.80(−1)	1.01	1.65(−4)	1.70(2)	6.12(3)	5.19
4	8	4	1.36(−4)	1.30(−4)	2.05	2.52(−7)	1.63(2)	8.14(6)	3.53(3)
8	16	8	8.52(−5)	8.47(−5)	4.15	8.37(−15)	1.55(4)	4.98(14)	1.12(9)

Remark 13.5.1. *Let us give some comments on the choices of source nodes.*

1. *The source nodes are located, based on the abscissas of quadrature rules, on pseudo-surfaces outside* $\mathbf{\Omega}$*. Since the integration errors are part of numerical errors, the product rules of the trapezoidal and Gaussian rules will yield higher accuracy. In fact, for the MFS in 2D, the source nodes are located uniformly on the pseudo-circles, which are, indeed, of the trapezoidal rule (see Lemma 13.4.1). The fast convergence is imperative for the MFS to reach satisfactory solutions for scientific/engineering problems because a less number of FS is used so that rounding errors would not pollute the final numerical solutions. This is one efficient way to handle the severe instability of the MFS for wide applications [150, p.47].*

2. *In 3D problems, the source nodes are located at the intersections of coordinate grids, based on the abscissas of quadrature rules, called "the grid-like" source nodes in this chapter; see Figures 13.4 and 13.5 (ref. [204, p.125, Figure 4.5.1]). For the smooth pseudo-surfaces outside* $\mathbf{\Omega}$*, the grid-like source nodes can also be found from the latitude and longitude of the unit sphere U via the parameter mapping as in the BEM in [13, 55]. The grid-like source nodes without extra-computation are not "meshes", and they are simple, effective, and significant for the MFS in 3D problems. Even for the radial basis function (RBF), the grid-like source nodes may yield high convergence rates; see [169, Chapter 7].*

13.5.3 By MPS

For the MPS using the SHF in (13.2.23), no source nodes exist. The results are given in Table 13.7. For $n = k = 1$ we find

$$\|\epsilon\|_\infty = O(0.15^N), \quad \|\epsilon\|_0 = O(0.15^N), \quad \text{Cond} = O(1.8^N), \quad \text{Cond\_eff} = O(1.7^N). \tag{13.5.17}$$

Tab. 13.7 – The errors and the condition numbers by the MPS using (13.2.23) at $k = n = 1, 4$ with $C(8, 24, 12)$.

$k = n$	N	$\Vert\epsilon\Vert_\infty$	$\Vert\epsilon\Vert_0$	$\sigma_{\max}$	$\sigma_{\min}$	$\Vert\mathbf{x}\Vert$	Cond	Cond_eff
1	4	4.65(−4)	5.09(−4)	4.45(−1)	2.83(−2)	2.58(−1)	1.57(1)	5.60
	8	1.08(−7)	7.50(−8)	5.02(−1)	4.55(−3)	2.59(−1)	1.10(2)	3.46(1)
	12	4.51(−12)	2.54(−12)	5.80(−1)	8.84(−4)	2.59(−1)	6.56(2)	1.78(2)
	16	6.28(−14)	6.07(−14)	9.75(−1)	6.82(−5)	2.59(−1)	1.43(4)	2.31(3)
4	8	5.22(−2)	5.85(−2)	5.02(−1)	4.55(−3)	6.78(−1)	1.10(2)	4.71(1)
	12	6.65(−4)	6.65(−4)	5.80(−1)	8.84(−4)	8.23(−1)	6.56(2)	1.99(2)
	16	2.97(−6)	2.26(−6)	9.75(−1)	6.82(−5)	8.27(−1)	1.43(4)	2.57(3)
	20	3.36(−9)	3.67(−9)	1.30	1.35(−8)	8.27(−1)	9.66(7)	1.30(7)

For the boundary Γ, ratio $\frac{r_{\max}}{r_{\min}} = \frac{1.118}{0.5} = 2.236$. The theoretical bound of the Cond is given from Proposition 13.2.3,

$$\text{Cond} = O\left(\left(\frac{r_{\max}}{r_{\min}}\right)^N\right) = O(2.23^N). \tag{13.5.18}$$

The numerical Cond in (13.5.17) is coincident with (13.5.18). Comparing the MPS with the MFS, the errors are smaller, and the relative errors 10(−13) at $k = n = 1$ and 10(−8) at $k = n = 4$ can be obtained under double precision. More importantly, the moderate Cond and $\Vert\mathbf{x}\Vert = O(1)$ can be achieved. The numerical performance of the MPS is superior, but users must own the knowledge of the SHF in (13.2.4). In contrast, the algorithms of the MFS are simple and efficient by using the grid-like source nodes (see Remark 13.5.1); users need only to know the quadrature rules. It is due to the modest human effort needed that the MFS has become an attractive and competitive method for scientific/engineering computing.

In summary, the algorithms, the error analysis, and the computation in this chapter have established a theoretical foundation of the MFS for 3D problems as Chapter 2 for 2D problems. They may be applied to the modified Helmholtz equation [222] and the Helmholtz equation [177] in 3D problems as in Section 13.7. In Remark 13.5.1, the grid-like source nodes are simple and efficient, since the mathematical analysis and the numerical experiments have been provided in this chapter.

13.6 Concluding Remarks

To close this chapter, we provide a few concluding remarks.

1. For the MFS in 3D Laplace's equation, the error bounds are derived in Theorems 13.4.1 and 13.4.2; the optimal polynomial convergence can be achieved. This chapter gives a strict error analysis of the MFS for 3D problems.
2. For the MPS, the optimal convergence rates and the exponential growth rates of Cond are derived in Propositions 13.2.1 and 13.2.3 This error and stability

analysis is also a new development of the book [169], where the MPS was discussed only for 2D problems.

3. Numerical results in Section 13.5 support the theoretical analysis made. Besides, the source nodes Q_{ij} are located on spherical and cylindrical pseudo-surfaces outside $\mathbf{\Omega}$, with numerical comparisons. The grid-like source nodes are simple and efficient; see Remark 13.5.1
4. The algorithms, the error analysis, and the computation in this chapter have established a theoretical foundation of the MFS for 3D problems as Part I for 2D problems. Their applications to 3D Helmholtz equations are given in the appendix below.

13.7 Appendix: 3D Problems of Helmholtz Equations

The algorithms and analysis of the MFS in this chapter may be developed for 3D problems of Helmholtz equations. In this section, we only give the PS, the FS, and the important addition theorems. The error bounds may be derived similarly; details are omitted.

13.7.1 Interior Dirichlet Problems

Consider the interior Dirichlet problem (IDP),

$$\nabla^2 u + k^2 u = 0, \quad (x, y, z) \text{ in } \mathbf{\Omega}, \tag{13.7.1}$$

$$u = g, \quad (x, y, z) \text{ on } S, \tag{13.7.2}$$

where $\mathbf{\Omega}$ is the 3D bounded simply-connected domain, $S = \partial\mathbf{\Omega}$, $g \in \mathbf{C}$, and k^2 (> 0) is not an eigenvalue of Laplace's operator. The particular solutions of (13.7.1) are given in [223, p.721],

$$\begin{aligned} u(\rho, \theta, \phi) &= \sum_{n=0}^{\infty} j_n(k\rho)\, Y_n^{\circ}(\theta, \phi) \\ &\approx \sum_{n=0}^{N} j_n(k\rho) \left\{ a_n \hat{P}_n(\cos\theta) + \sum_{m=1}^{n} \hat{P}_n^{(m)}(\cos\theta)(a_{n,m}\cos(m\phi) + b_{n,m}\sin(m\phi)) \right\}, \end{aligned}$$

where the complex coefficients $a_n, a_{n,m}, b_{n,m} \in \mathbf{C}$, $j_n(z) = \sqrt{\frac{\pi}{2z}} J_{n+\frac{1}{2}}(z)$ are the spherical Bessel functions, and $Y_n^{\circ}(\theta, \phi)$ are the spherical harmonic functions in (13.2.17). From [1, p.437], we have

$$j_n(z) = \sqrt{\frac{\pi}{2z}} J_{n+\frac{1}{2}}(z), \quad y_n(z) = \sqrt{\frac{\pi}{2z}} Y_{n+\frac{1}{2}}(z),$$

$$h_n^{(1)}(z) = j_n(z) + \mathbf{i} y_n(z), \quad h_n^{(1)}(z) = \sqrt{\frac{\pi}{2z}} H_{n+\frac{1}{2}}^{(1)}(z).$$

From [1, p.440], we have the addition theorem.

Theorem 13.7.1 (Addition Theorem A). *For $\rho < r$, the FS in 3D have the expansions,*

$$\frac{e^{\mathbf{i}k|\overline{PQ}|}}{|\overline{PQ}|} = \mathbf{i}\pi \sum_{n=0}^{\infty}(2n+1)\frac{J_{n+\frac{1}{2}}(k\rho)}{\sqrt{\rho}}\frac{H^{(1)}_{n+\frac{1}{2}}(kr)}{\sqrt{r}}\Bigg\{P_n(\cos\theta)P_n(\cos\xi)$$

$$+2\sum_{m=1}^{n}\frac{(n-m)!}{(n+m)!}P_n^{(m)}(\cos\theta)P_n^{(m)}(\cos\xi)\cos m(\phi-\eta)\Bigg\}$$

$$= \mathbf{i}2k\sum_{n=0}^{\infty} j_n(k\rho)h_n^{(1)}(kr)\Bigg\{\hat{P}_n(\cos\theta)\hat{P}_n(\cos\xi)$$

$$+2\sum_{m=1}^{n}\hat{P}_n^{(m)}(\cos\theta)\hat{P}_n^{(m)}(\cos\xi)\cos m(\phi-\eta)\Bigg\}, \quad \rho < r,$$

where the normalized functions $\hat{P}_n^{(m)}(x)$ are defined in (13.2.14).

13.7.2 Exterior Dirichlet Problems

Consider the exterior Dirichlet problem (EDP) in the unbounded $\mathbf{\Omega}_\infty$ with the smooth interior boundary S_{in},

$$\nabla^2 u + k^2 u = 0, \quad (x, y, z) \in \mathbf{\Omega}_\infty, \tag{13.7.3}$$

$$u = g, \quad (x, y, z) \in S_{\text{in}}, \tag{13.7.4}$$

$$\lim_{r\to\infty} r\left\{\frac{\partial u}{\partial r} - \mathbf{i}ku\right\} = 0, \tag{13.7.5}$$

where $g \in \mathbf{C}$. The equation (13.7.5) is called Sommerfeld radiation conditions at infinity. For (13.7.3)–(13.7.5), there always exist unique solutions. The particular solutions of (13.7.3) and (13.7.5) are given in [223, p.721],

$$u(\rho,\theta,\phi) = \sum_{n=0}^{\infty} h_n^{(1)}(k\rho)\, Y_n^{\circ}(\theta,\phi)$$

$$\approx \sum_{n=0}^{N} h_n^{(1)}(k\rho)\Bigg\{a_n\hat{P}_n(\cos\theta) + \sum_{m=1}^{n}\hat{P}_n^{(m)}(\cos\theta)(a_{n,m}\cos(m\phi) + b_{n,m}\sin(m\phi))\Bigg\}.$$

From Sauter and Schwab [210, p.102], the FS satisfying (13.7.3) is given by $G_k(|\overline{PQ}|) = \frac{e^{\mathrm{i}k|\overline{PQ}|}}{|\overline{PQ}|}$. From Theorem 13.7.1, we have the addition theorem,

$$\frac{e^{\mathbf{i}k|\overline{PQ}|}}{|\overline{PQ}|} = \mathbf{i}2k\sum_{n=0}^{\infty} h_n^{(1)}(k\rho)j_n(kr)\Big\{\hat{P}_n(\cos\theta)\hat{P}_n(\cos\xi)$$

$$+2\sum_{m=1}^{n}\hat{P}_n^{(m)}(\cos\theta)\hat{P}_n^{(m)}(\cos\xi)\cos m(\phi-\eta)\Big\}, \quad \rho > r.$$

Note that when the source nodes are located on a sphere $S_{\bar{R}}$ with radius $\bar{R} < \min \rho|_{S_{\text{in}}}$, the function $j_n(k\bar{R}) = 0$ (*i.e.*, $J_{n+\frac{1}{2}}(k\bar{R}) = 0$) causes the spurious eigenvalues. By the following Chapter 8, we choose the new combined FS,

$$\mathbf{\Psi}(\rho, \theta) = \left(\frac{\partial}{\partial \bar{R}} + \mathbf{i}k\right) G_k(|\overline{PQ}|) = \mathcal{D} G_k\left(\sqrt{(\bar{R}^2 + \rho^2 - 2\bar{R}\rho \cos(\Theta)}\right), \qquad (13.7.6)$$

where the operator $\mathcal{D} = \left(\frac{\partial}{\partial \bar{R}} + \mathbf{i}k\right)$ and $\cos(\Theta) = \cos\theta \cos\xi + \sin\theta \sin\xi \cos(\phi - \eta)$. In (13.7.6) the derivatives are

$$\begin{aligned}\frac{\partial}{\partial R} G_k(|\overline{PQ}|) &= \frac{\partial}{\partial |\overline{PQ}|} G_k(|\overline{PQ}|) \times \frac{\partial}{\partial \bar{R}} |\overline{PQ}| \\ &= \big(\mathbf{i}k|\overline{PQ}| - 1\big) \frac{e^{\mathbf{i}k|\overline{PQ}|}}{|\overline{PQ}|^2} \times \frac{(\bar{R} - \rho\cos\Theta)}{|\overline{PQ}|} = \big(\mathbf{i}k|\overline{PQ}| - 1\big)(\bar{R} - \rho\cos\Theta) \frac{e^{\mathbf{i}k|\overline{PQ}|}}{|\overline{PQ}|^3}.\end{aligned}$$

The linear combinations of the new FS are given by

$$u_N = \sum_{j=1}^{N} c_j \mathbf{\Psi}_j(\rho, \theta), \quad \mathbf{\Psi}_j(\rho, \theta) = \mathcal{D} G_k(|PQ_j|), \qquad (13.7.7)$$

where $c_j \in \mathbf{C}$ are the complex unknown coefficients. The collocation equations are given by

$$\sqrt{\triangle h_\ell} \sum_{j=1}^{N} c_j \mathbf{\Psi}_j(\rho_\ell, \theta_\ell) = \sqrt{\triangle h_\ell}\, f(\rho_\ell, \theta_\ell), \quad (\rho_\ell, \theta_\ell) \in S_{\text{in}}^{\ell}, \quad \ell = 1, 2, ..., M,$$

where $M > N$. Once the coefficients c_j are found, we obtain the solutions from (13.7.7). The remarkable advantage of the modified MFS is free from spurious eigenvalues.

Theorem 13.7.2 (Addition Theorem B). *For $\rho > \bar{R}$, the FS in 3D has the expansions,*

$$\begin{aligned}\mathcal{D}\left\{\frac{e^{\mathbf{i}k|\overline{PQ}|}}{|\overline{PQ}|}\right\} = \mathbf{i}2k \sum_{n=0}^{\infty} h_n^{(1)}(k\rho) \mathcal{D} j_n(k\bar{R}) \Bigg\{ &\hat{P}_n(\cos\theta) \hat{P}_n(\cos\xi) \\ &+ 2 \sum_{m=1}^{n} \hat{P}_n^{(m)}(\cos\theta) \hat{P}_n^{(m)}(\cos\xi) \cos m(\phi - \eta) \Bigg\}.\end{aligned}$$

Part III

Selection of Source Nodes and Related Topics

Heaven's net is indeed vast.
Though its meshes are wide,
it misses nothing.
Lao-Tzu, c.571-c.471 B.C.

Seeking better source nodes is the goal of Part III, which consists of four chapters. In Chapter 14, comparisons are first discussed for the method of fundamental solutions (MFS), the method of particular solutions (MPS) and the MFS-QR in [10], and then for different source nodes. The MFS-QR also plays a role in bridging the MFS to the MPS. The sensitivity index in (III.2) is proposed to be a criterion for better methods and better source nodes. In Chapter 15, stability analysis is made for the smooth closed pseudo-boundaries. Better pseudo-boundaries for amoeba-like domains are reported in [253]. In Chapter 16, we discuss the singularity problems from the source functions as the source nodes are located near Γ. Reduced convergence rates are derived for the MPS and the MFS. Then new removal techniques are proposed to recover the optimal convergence rates. In Chapter 17, new locations of the source nodes are proposed. Since the algorithms using one pseudo radial-line are divergent, we propose the algorithms using two pseudo radial-lines. Since the success of the MFS mainly depends on stability, both the lower and the upper bounds of condition numbers (Cond) are derived. Numerical results are encouraging and promising. The new algorithms using pseudo radial-lines may also become a new competent boundary method in the MFS family.

Since the source nodes in the MFS are located outside the solution domain S, an essential issue in computation is how to select the source nodes. For the MFS, high accuracy and ill-conditioning coexist in computation. We propose the sensitivity index in Chapter 14. Suppose that the errors and the Cond can be expressed exponentially,

$$\|\epsilon\|_{0,\Gamma} = O(a^N), a<1, \quad \text{Cond} = O(b^N),\ b\geq 1, \tag{III.1}$$

where a and b are two constants independent of N. Define the sensitivity index by Cond *via* errors as

$$\kappa = -\frac{\ln b}{\ln a}. \tag{III.2}$$

The index κ also indicates the severity of ill-conditioning. The smaller κ is, the better stability occurs, and so is the better numerical performance. Better source nodes are also related to solution regularity and domain shapes. In general 2D domains, the circular pseudo-boundaries are the first choice. For elliptic domains, peanut-like domains, and long-narrow domains, the elliptic pseudo-boundaries are better. When the source nodes move away from boundary Γ, the errors of solutions decrease but the Cond also increases. For singularity solutions, the pseudo-boundaries near Γ will offer a better numerical performance based on the sensitivity index. However, once the singularity is removed as in Chapters 1, 5 and 16, the circular/elliptic pseudo-boundaries become optimal, and the basic analysis in error and stability has been established in Parts I and II.

For the analysis of better source nodes, stability is more imperative than accuracy, and the elliptic coordinates will play a key role. The elliptic coordinates are discussed in Li *et al.* [180] and employed in Chapter 6 for elliptic pseudo-boundaries. Below, we give some basic formulas, which are often used in Chapters 14–16. The elliptic coordinates are defined in [180] by (see Figure 14.1)

$$x = \sigma \cosh\rho \cos\theta, \; y = \sigma \sinh\rho \sin\theta, \tag{III.3}$$

where $\sigma > 0$, and two coordinates (ρ, θ) with ranges $0 \le \rho < \infty$ and $0 \le \theta < 2\pi$. When $\rho = \rho_0 \in (0, \infty)$, the equation (III.3) leads to an ellipse

$$\frac{x^2}{\sigma^2 \cosh^2(\rho_0)} + \frac{y^2}{\sigma^2 \sinh^2(\rho_0)} = 1,$$

where two semi-axes are $a = \sigma \cosh(\rho_0)$ and $b = \sigma \sinh(\rho_0)$. For the given node P with the Cartesian coordinates (x, y), their elliptic coordinates can be found from [180]:

$$\rho = \sinh^{-1}(F(x, y; \sigma)), \quad \theta = \arccos\left(\frac{x}{\sigma \cosh\rho}\right), \tag{III.4}$$

where $F(x, y; \sigma) = \frac{1}{\sqrt{2}\sigma}\sqrt{(x^2 + y^2 - \sigma^2) + \sqrt{(x^2 + y^2 - \sigma^2)^2 + 4\sigma^2 y^2}}$.

Addition theorem (*i.e.*, the series expansions) of the FS is also *essential* to stability analysis for better selection of the source nodes. The elliptic coordinates (III.3) can be expressed by the complex number,

$$z = x + \mathbf{i}y = \sigma \cosh w, \tag{III.5}$$

where $w = \rho + \mathbf{i}\theta$ and $\mathbf{i} = \sqrt{-1}$. Denote the other node in the same elliptic coordinate system (III.5) by

$$z_0 = x_0 + \mathbf{i}y_0 = \sigma \cosh w_0, \tag{III.6}$$

where $w_0 = r + \mathbf{i}\phi$. We give the addition theorem for the logarithmic function in elliptic coordinates.

Lemma III.1 (Addition Theorem). *In the same elliptic coordinate system (III.3), denote two nodes z and z_0 by (III.5) and (III.6), respectively. There exist the series expansions,*

$$\ln|z - z_0| = r + \ln\left(\frac{\sigma}{2}\right) \tag{III.7}$$

$$- 2\sum_{n=1}^{\infty} \frac{1}{n} e^{-nr}\{\cosh(n\rho)\cos(n\theta)\cos(n\phi) + \sinh(n\rho)\sin(n\theta)\sin(n\phi)\}, \ \rho < r,$$

$$\ln|z - z_0| = \rho + \ln\left(\frac{\sigma}{2}\right) \tag{III.8}$$

$$- 2\sum_{n=1}^{\infty} \frac{1}{n} e^{-n\rho}\{\cosh(nr)\cos(n\theta)\cos(n\phi) + \sinh(nr)\sin(n\theta)\sin(n\phi)\}, \ \rho > r.$$

Chapter 14

Comparisons of MFS and MPS

14.1 Introduction

The estimates of errors and condition numbers (Cond) by the method of fundamental solutions (MFS) are derived in Chapter 6 for elliptic pseudo-boundaries, and criteria for evaluating different numerical techniques are provided. Although accuracy and stability are the most important criteria, high accuracy and good stability can not succeed simultaneously for one method, except for some methods, such as the null field method in [180] that is confined only to circular/elliptic domains. For the method of particular solutions (MPS) and the MFS, the high convergence rates can be achieved only for highly smooth solutions and circular/elliptic domains. For non-circular/non-elliptic domains, however, the Cond of both the MPS and the MFS grow exponentially (see Section 14.2). A balance between accuracy and stability must be taken to reach satisfactory solutions. In particular, severe ill-conditioning is a critical issue for the MFS in applications. In this chapter and Chapter 15, new estimates of Cond are provided in (14.2.18) for arbitrary pseudo-boundaries.

When the source nodes move away from the domain boundary, the errors reduce but the Cond grows. Questions arise: how can we balance accuracy and stability and how can we choose better pseudo-boundaries? To respond to these questions, we propose a new sensitivity index of growth/convergence rates of the Cond *via* errors in (14.2.21). Better source nodes can be found based on the sensitivity index. For five-pedal-flower-like domains, different non-circular/non-elliptic pseudo-boundaries are tested numerically. Circular pseudo-boundaries are optimal for highly smooth solutions, but the pseudo-boundaries near the domain boundary may be better for singular solutions. This is the first goal of this chapter.

The second goal is to compare the MFS, the MPS, and the MFS-QR in Antunes [8]. First, let us compare the MFS with the MPS. Both the MFS and the MPS have the optimal polynomial convergence rates and the exponential growth rates of the Cond. However, the Cond by the MFS grows faster than that by the MPS. As pointed out in Chapter 13, although the MPS is superior to the MFS in accuracy and stability, the MFS is attractive in wide applications since uniform and simple fundamental functions are used and since only a modest human effort is needed.

DOI: 10.1051/978-2-7598-3171-5.c014
© Science Press, EDP Sciences, 2023

Next, we compare the MFS-QR with the MFS and the MPS. After exploration, the new basic functions in Antunes [8] are the very particular solutions (PS), and the MFS-QR may be regarded as a special MPS. The MFS-QR is not a variant of the MFS but a variant of the MPS. The MFS-QR also plays a role in bridging the MFS to the MPS. Both the MFS and the MPS can also be recognized as twins *via* the MFS-QR in the Trefftz family (see [169, 178]).

In this chapter, we consider Laplace's equation and choose the elliptic coordinates as in Chapter 6 for comparisons. This chapter is organized as follows. In the next section, the MFS and the MPS are discussed. In Section 14.3, the MFS-QR is applied for elliptic coordinates, and the characteristics of the MFS-QR are explored. In Section 14.4, numerical experiments and comparisons are carried out for five-pedal-flower-like domains, and different pseudo-boundaries are investigated for highly smooth and strongly singular boundary data. In the last section, a few concluding remarks are made. The materials of this chapter are adapted from [178, 251].

14.2 Two Basis Boundary Methods

14.2.1 Method of Particular Solutions

In this chapter, we solicit the elliptic coordinates (ρ, θ) defined in Chapter 6 and [180] by

$$x = \sigma \,\cosh\rho \,\cos\theta, \;\; y = \sigma \,\sinh\rho \,\sin\theta, \tag{14.2.1}$$

where $\sigma > 0$, $0 \le \rho < \infty$ and $0 \le \theta < 2\pi$ (see Figure 14.1). When $\rho = \rho_0 \in (0, \infty)$, the equation (14.2.1) leads to an ellipse:

$$\frac{x^2}{\sigma^2 \,\cosh^2\rho_0} + \frac{y^2}{\sigma^2 \,\sinh^2\rho_0} = 1,$$

where two semi-axes are $a = \sigma \,\cosh\rho_0$ and $b = \sigma \,\sinh\rho_0$. When the Cartesian coordinates (x, y) are known, the elliptic coordinates are defined from (14.2.1), and the converted formulas are derived in [180, p.92] as (III.4) in Part III. For exploring the stability and the errors of arbitrary pseudo-boundaries, the elliptic coordinates with two parameters a and b are more effective. After the Cond are obtained from Lemmas 14.2.2 and 14.2.3, they may be converted to Cartesian coordinates in Propositions 14.2.1 and 14.2.2 for easy application.

Consider Laplace's equation with the Dirichlet boundary condition,

$$\Delta u = 0 \text{ in } S, u = f \text{ on } \Gamma, \tag{14.2.2}$$

where S is a bounded simply-connected domain, and $\Gamma = \partial S$ its boundary. The PS in elliptic coordinates are given from Chapter 6 and [180],

$$u(\rho, \theta) = \alpha_0 + \sum_{k=1}^{\infty} e^{-k\rho_0}(\alpha_k \,\cosh k\rho \,\cos k\theta + \beta_k \,\sinh k\rho \,\sin k\theta) := P_n + R_n,$$

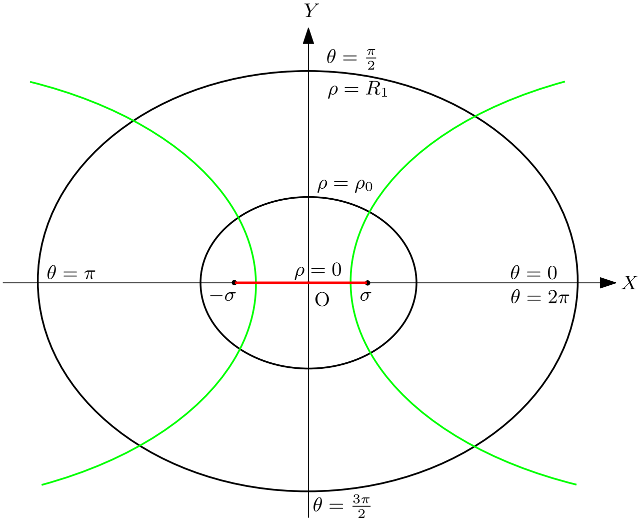

FIG. 14.1 – The elliptic coordinates with (ρ, θ), where $R_1 > \rho_0$.

where ρ_0 is a parameter, and the PS of degree n and the residuals are given by

$$P_n = P_n(\rho, \theta) = \alpha_0 + \sum_{k=1}^{n} e^{-k\rho_0}(\alpha_k \cosh k\rho \cos k\theta + \beta_k \sinh k\rho \sin k\theta), \tag{14.2.3}$$

$$R_n = R_n(\rho, \theta) = \sum_{k=n+1}^{\infty} e^{-k\rho_0}(\alpha_k \cosh k\rho \cos k\theta + \beta_k \sinh k\rho \sin k\theta), \tag{14.2.4}$$

where $\{\alpha_k\}_{k=0}^{n}$ and $\{\beta_k\}_{k=1}^{n}$ are the expansion coefficients. Let $\mathbf{\Gamma}$ be divided into small $\mathbf{\Gamma}_\ell$ with the meshspacings $\triangle h_\ell$, *i.e.*, $\mathbf{\Gamma} = \bigcup_{\ell=1}^{M} \mathbf{\Gamma}_\ell$. For simplicity, choose (ρ_ℓ, θ_ℓ) as the midpoints of $\mathbf{\Gamma}_\ell$. By using the PS in (14.2.3), we have the following collocation equations,

$$\begin{aligned} &\sqrt{\triangle h_\ell}\{P_n(\rho_\ell, \theta_\ell)\} \\ &= \sqrt{\triangle h_\ell}\left\{\alpha_0 + \sum_{k=1}^{n} e^{-k\rho_0}\{\alpha_k \cosh(k\rho_\ell)\cos(k\theta_\ell) + \beta_k \sinh(k\rho_\ell)\sin(k\theta_\ell)\}\right\} \\ &= \sqrt{\triangle h_\ell}\, f(\rho_\ell, \theta_\ell), \quad (\rho_\ell, \theta_\ell) \in \mathbf{\Gamma}_\ell,\ \ell = 1, 2, \ldots, M. \end{aligned} \tag{14.2.5}$$

The equation (14.2.5) is denoted by

$$\mathbf{P}\mathbf{y} = \mathbf{b}, \tag{14.2.6}$$

where matrix $\mathbf{P} \in \mathbf{R}^{M \times N}(M \geq N)$ and vector $\mathbf{y}\,(\in \mathbf{R}^N) = \{\alpha_0, \alpha_1, \beta_1, \ldots, \alpha_n, \beta_n\}^T$ with $N = 2n+1$. The algorithms of (14.2.5) are called the method of particular solutions (MPS).

The errors of the MPS are provided in Chapter 6 as

$$\|u-u_n\|_{0,\Gamma}=O\left(\frac{1}{n^{p-\frac{1}{2}}}\|u\|_{p,S}\right),\quad p\geq 1,\tag{14.2.7}$$

where $\|u\|_{p,S}$ are the Sobolev norms. The equation (14.2.7) is called the optimal convergence rates. Let $r_{\min}=\min\rho|_{\Gamma}$ and $r_{\max}=\max\rho|_{\Gamma}$. Denote two ellipses by S_ρ at $\rho=r_{\min}$ and $\rho=r_{\max}$. Also denote two semi-axes of $S_{r_{\min}}$ by $a_{\min}$ and $b_{\min}$, and two semi-axes of $S_{r_{\max}}$ by $a_{\max}$ and $b_{\max}$. We have the following theorem, whose proof is given in [251].

Theorem 14.2.1. *Let (14.2.3) at* $\rho_0=r_{\min}$ *be chosen. There exists the bound,*

$$\text{Cond}(\mathbf{P})=O(e^{n(r_{\max}-r_{\min})})=O\left(\left(\frac{a_{\max}+b_{\max}}{a_{\min}+b_{\min}}\right)^n\right).\tag{14.2.8}$$

For the elliptic domain S *with* $r_{\max}=r_{\min}$, $\text{Cond}(\mathbf{P})=O(1)$.

The Cond in (14.2.8) has the exponential growth *via* n, and it is valid for a non-elliptic boundary Γ. In [169] the MPS are discussed in Cartesian and polar coordinates. Moreover, the null field method is studied in elliptic coordinates in [180], but it is confined to elliptic domains. The MPS in this section is also a development of [169, 180].

14.2.2 Method of Fundamental Solutions

Denote node $P=(\rho,\theta)$ and source nodes $Q_j=(R_j,\phi_j)$. The source nodes Q_j are located on a closed pseudo-boundary Γ_R outside S. Choose the fundamental solution (FS),

$$\Phi_j(\rho,\theta)=\ln|\overline{PQ_j}|,\quad |\overline{PQ_j}|=\sqrt{R_j^2+\rho^2-2R_j\rho\cos(\theta-\phi_j)}.\tag{14.2.9}$$

We obtain a linear combination of FS as

$$u_N=\sum_{j=1}^{N}c_j\ln|\overline{PQ_j}|=\sum_{j=1}^{N}c_j\Phi_j(\rho,\theta),\tag{14.2.10}$$

where c_j are the coefficients. From the Dirichlet boundary condition in (14.2.2), the collocation equations are given by

$$\sqrt{\triangle h_\ell}\sum_{j=1}^{N}c_j\Phi_j(\rho_\ell,\theta_\ell)=\sqrt{\triangle h_\ell}\,f(\rho_\ell,\theta_\ell),\ (\rho_\ell,\theta_\ell)\in\Gamma,\ \ell=1,2,\ldots,M,\tag{14.2.11}$$

where $M\geq N$. The equation (14.2.11) leads to an overdetermined system,

$$\mathbf{F}\mathbf{x}=\mathbf{b},\tag{14.2.12}$$

where matrix $\mathbf{F}\in\mathbf{R}^{M\times N}(M\geq N)$, and vectors $\mathbf{x}=\{c_1,c_2,\ldots,c_N\}^T\in\mathbf{R}^N$ and $\mathbf{b}\in\mathbf{R}^M$.

The error and stability analysis in Chapter 6 is explored for elliptic pseudo-boundaries. Suppose that the source nodes are located on an outside ellipse Γ_R at $\rho = R > r_{\max} = \max\, \rho|_\Gamma$. Denote two semi-axes of Γ_R by a_R and b_R. To guarantee the non-singularity of the matrix $\mathbf{F}$ in (14.2.12), we assume (see Chapter 6)

$$R + \ln\left(\frac{\sigma}{2}\right) = \ln\left(\frac{a_R + b_R}{2}\right) \neq 0, \;\; i.e.,\; a_R + b_R \neq 2. \tag{14.2.13}$$

We have the following lemma from Chapter 6.

Lemma 14.2.1. *Let the solution $u \in \mathbf{H}^p(S)$ with $p > 1$ and (14.2.13) be given. When N is large, for the elliptic pseudo-boundary at $\rho = R$, there exists the bound,*

$$\|u - u_N\|_{0,\Gamma} \le C\left\{ e^{-(R - r_{\max})(N-2n)} e^{n(r_{\max} - r_{\min})} + \frac{1}{n^{p-\frac{1}{2}}}\right\} \|u\|_{p,S}, \tag{14.2.14}$$

where $r_{\max} = \max\, \rho|_\Gamma$, $r_{\min} = \min\, \rho|_\Gamma$, and C is a bounded constant independent of N and n. Also there exist the optimal polynomial convergence rates,

$$\|u - u_N\|_{0,\Gamma} = O\left(\frac{1}{n^{p-\frac{1}{2}}}\|u\|_{p,S}\right) = O\left(\frac{1}{N^{p-\frac{1}{2}}}\|u\|_{p,S}\right),$$

provided that the $N\,(> 2n)$ satisfies $N \ge 2n + \dfrac{n(r_{\max} - r_{\min}) + (p - 1/2)\ln n}{R - r_{\max}}$.

Note that the relaxed assumption $u \in \mathbf{H}^p(S)$ with $p > 1$ is given in Lemma 14.2.1 as in Chapter 6. This relaxed assumption is imperative for the strongly singular boundary data discussed in Sections 14.4.2 and 14.4.3, where the solutions only have $u \in \mathbf{H}^{1+\delta}(S)$ with $0 < \delta \ll 1$. Note that under (14.2.13), a constant is unnecessary to add in the FS in (14.2.10) based on Lemma 14.2.1. For the circular pseudo-boundaries with radius $R \neq 1$, the constant is also unnecessary. However, for the non-circular/non-elliptic pseudo-boundaries ℓ_R, for which the degenerate scales may occur, adding the constant may be helpful in the convergence and non-singularity of the discrete matrices.

Below, we discuss stability. Denote two semi-axes a_R and b_R for the elliptic pseudo-boundary at $\rho = R$, and denote the elliptic boundary Γ at ρ with two semi-axes a and b satisfying $a + b < a_R + b_R$. We cite Theorem 6.4.1 in Chapter 6 as a lemma.

Lemma 14.4.2. *Under (14.2.13), for the elliptic boundary Γ, there exists the bound,*

$$\text{Cond}(\mathbf{F}) \le C\max\left\{\frac{1}{\ln\left(\frac{a_R + b_R}{2}\right)}, N\right\} \times \left(\frac{e^R}{e^\rho}\right)^{\frac{N}{2}} \le CN \times \left(\frac{a_R + b_R}{a + b}\right)^{\frac{N}{2}}.$$

Consider a non-elliptic Γ. Suppose that there exists a positive constant $\mu\,(\ge 1)$ independent of N such that

$$\|v\|_{1,\Gamma} \le CN^\mu \|v\|_{0,\Gamma}, \quad v \in V_N, \tag{14.2.15}$$

where V_N is the set of (14.2.10), and C a bounded constant independent of N. Denote an ellipse $\Gamma_{\min}$ at $\rho = r_{\min} = \min \rho|_\Gamma$, and its semi-axes by $a_{\min}$ and $b_{\min}$. We cite Theorem 6.4.2 in Chapter 6 as a lemma.

Lemma 14.2.3. *Under (14.2.13) and (14.2.15), for the non-elliptic boundary* Γ*, there exists the bound,*

$$\begin{aligned}\mathrm{Cond}(\mathbf{F}) &\leq CN^{\frac{\mu}{2}} \max\left\{\frac{1}{\ln\left(\frac{a_R+b_R}{2}\right)}, N\right\} \times \left(\frac{e^R}{e^{r_{\min}}}\right)^{\frac{N}{2}} \\ &\leq CN^{1+\frac{\mu}{2}} \times \left(\frac{a_R+b_R}{a_{\min}+b_{\min}}\right)^{\frac{N}{2}}.\end{aligned} \tag{14.2.16}$$

Let us compare the MFS with the MPS at $N = 2n+1$. From (14.2.7) and Lemma 14.2.1, both the MFS and the MPS have optimal polynomial convergence rates, although the MFS has some extra errors. When the solutions are analytic, both methods may reach exponential convergence rates. Although the theoretical convergence rates are the same, the numerical convergence rates of the MPS are faster. From Theorem 14.2.1, Lemmas 14.2.2 and 14.2.3, both the MFS and the MPS have exponential growth rates of Cond. However, the MFS has a larger Cond because a larger base occurs: $a_R + b_R > a_{\max} + b_{\max}$. Then we give the following corollary.

Corollary 14.2.1. *Both the MFS and the MPS have optimal polynomial convergence rates and the exponential growth rates of Cond. However, the MPS is superior to the MFS in accuracy and stability.*

Since the PS may satisfy partially the boundary conditions, the MPS can offer better numerical performance in accuracy and stability. In particular, when corner singularity occurs, the singular particular solutions can be chosen as in [169]. The MPS is more advantageous to deal with singularity problems than the MFS. The combination of both FS and PS is a good technique for singularity problems. For corner singularities, some additional techniques may be employed for the MFS (see Chapter 1 and Section 6.6). For a given governing equation, since the FS is uniform and unchanged, the algorithms and programs of the MFS are simple. It is due to the modest human effort needed that the MFS has become an attractive and competitive method for scientific/engineering computing.

The estimates in (14.2.16) involving elliptic coordinates may not be convenient in application. Below, we provide a simplified estimate for Cond in Cartesian coordinates. To avoid confusion, denote the polar coordinates as (ρ°, ϕ°) with the superscript "∘" in this section. Suppose that the domain boundary Γ is star-like, which can be denoted by a single-valued function $\rho^\circ = \rho^\circ(\phi^\circ)$, where $\rho^\circ_{\min} \leq \rho^\circ(\phi^\circ) \leq \rho^\circ_{\max}$. We have the following proposition, whose proof is given in Chapter 15.

Proposition 14.2.1. *Let the conditions in Lemma 14.2.3 be given. For the elliptic pseudo-boundary at* $R\,(> r_{\max})$ *with semi-axes* a_R *and* b_R*, there exists the bound,*

$$\mathrm{Cond}(\mathbf{F}) \leq C\left(\frac{a_R+b_R}{\rho^\circ_{\max}+\rho^\circ_{\min}}\right)^{\beta N}, \quad \beta > \frac{1}{2}.$$

We are interested in an arbitrary pseudo-boundary $\mathbf{\Gamma}^*$. Choose the source nodes $(R_i, \phi_i) \in \mathbf{\Gamma}^*$ with $R_i \leq R$, and also denote an ellipse by $\mathbf{\Gamma}_R$ at $\rho = R$ with semi-axes a_R and b_R. Suppose that the $\mathbf{\Gamma}^*$ can also be denoted by $(\bar{\rho}^\circ(\phi^\circ), \phi^\circ)$ with $\bar{\rho}^\circ_{\min} \leq \bar{\rho}^\circ \leq \bar{\rho}^\circ_{\max}$. There also exist the bounds,

$$\bar{\rho}^\circ_{\max} \leq a_R,\ \bar{\rho}^\circ_{\min} \leq b_R,\ \bar{\beta} = \frac{a_R + b_R}{\bar{\rho}^\circ_{\max} + \bar{\rho}^\circ_{\min}} \geq 1.$$

In Chapter 15, the estimates (14.2.16) are proved for the source nodes (R_i, ϕ_i) on a non-circular/non-elliptic pseudo-boundary $\mathbf{\Gamma}^*$. We give the following proposition for arbitrary pseudo-boundaries.

Proposition 14.2.2. *Choose the source nodes* $(R_i, \phi_i) \in \mathbf{\Gamma}^*$ *with* $R_i \leq R$, *and denote* $\bar{\rho}^\circ_{\max} = \max\, \rho^\circ|_{\Gamma^*}$ and $\bar{\rho}^\circ_{\min} = \min\, \rho^\circ|_{\Gamma^*}$. *Suppose that there exist no degenerate scales for* $\mathbf{\Gamma}^*$*, then we have the bound,*

$$\text{Cond}(\mathbf{F}) \leq CN^{\left(1+\frac{\mu}{2}\right)} \left(\frac{\bar{\rho}^\circ_{\max} + \bar{\rho}^\circ_{\min}}{\rho^\circ_{\max} + \rho^\circ_{\min}}\right)^{(1+\gamma)N/2}, \tag{14.2.17}$$

where $\gamma > 0$, $\rho^\circ_{\min} \leq \rho^\circ \leq \rho^\circ_{\max}$ *and* $\bar{\rho}^\circ_{\min} \leq \bar{\rho}^\circ \leq \bar{\rho}^\circ_{\max}$. *Moreover,*

$$\text{Cond}(\mathbf{F}) \leq C\left(\frac{\bar{\rho}^\circ_{\max} + \bar{\rho}^\circ_{\min}}{\rho^\circ_{\max} + \rho^\circ_{\min}}\right)^{\beta N},\ \beta > \frac{1}{2}. \tag{14.2.18}$$

For general pseudo-boundaries, the Cond in (14.2.18) is also exponential, which is coincident with circular/elliptic pseudo-boundaries in Chapters 2 and 6. How to balance accuracy and stability and how to compare different pseudo-boundaries are essential in computation and application [150]. Suppose that the solutions are analytic; we have the exponential convergence rates from Lemma 14.2.1,

$$\|\epsilon\|_{0,\Gamma} = O\big(a^N\big),\ a<1,\ \epsilon = u - u_N. \tag{14.2.19}$$

The exponential growth rates of Cond are also denoted as

$$\text{Cond} = O\big(b^N\big), \quad b \geq 1. \tag{14.2.20}$$

Definition 14.2.1. *Let the convergence/growth rates of errors and Cond be given in (14.2.19) and (14.2.20). Define a sensitivity index* κ *of* Cond *via errors,*

$$\kappa = -\frac{\ln b}{\ln a} > 0,\ a<1 \leq b. \tag{14.2.21}$$

The index κ also indicates the severity of ill-conditioning. The smaller κ is, the better stability *via* accuracy occurs. In particular, the index $\kappa = 0$ indicates the excellent stability with Cond $= O(1)$. The larger κ is, the worse instability *via* accuracy occurs. When $\kappa \leq 1$, the Cond growth rates are not faster than the convergence rates, at least half of the working digits will serve for accuracy. Suppose that double precision (*i.e.*, 16 decimal significant digits) is used in computation, and the errors with $O(10^{-8})$

can be achieved. The numerical algorithms may be regarded as "*good*" in stability. When $1 < \kappa \le 2$, at least, about one-third of working digits will serve for accuracy, then the errors with $O(10^{-5})$ can be obtained by double precision. The errors with $O(10^{-5})$ may satisfy the requirement in most engineering problems. In general, for small N, assume that $\|\epsilon\|_{0,\Gamma} = O(1)$ and $\text{Cond} = O(1)$. For the general sensitivity index κ, about $\frac{1}{1+\kappa} \times 16$ significant digits of numerical solutions can be obtained. We list the corresponding accuracy of numerical solutions *via* κ in Table 14.1.

The sensitivity index is used in statistics for signal detection theory in [234]. The sensitivity index is also used in this chapter as the new definition in (14.2.21) by the severity of stability *via* accuracy for comparing different numerical methods and techniques. A significant application of the sensitivity index is for a better selection of pseudo-boundaries in the MFS. See Section 14.4.

To measure the effects of ill-conditioning in the MFS, we proposed a ratio power κ^* in [150, (2.81)]

$$\text{Cond} = O\left(\frac{1}{\|\epsilon\|_{0,\Gamma}}\right)^{\kappa^*}. \tag{14.2.22}$$

From (14.2.22) define the original sensitivity index as $\kappa^* = -\frac{\ln(\text{Cond})}{\ln(\|\epsilon\|_{0,\Gamma})} > 0$. We can show $\kappa \approx \kappa^*$ for large $N(\gg 1)$ in [251].

We will invoke the sensitivity index κ for selecting better pseudo-boundaries in the MFS: the smaller κ is, the better pseudo-boundaries are. We may also use the original sensitivity index κ^* to select better pseudo-boundaries and better regularization parameters in the Tikhonov regularization (TR) [259]. Moreover, the sensitivity index can also be used to compare the MFS, the MPS, and the spectral method. The advantages of the sensitivity index will be illustrated in numerical examples in Section 14.4.

TAB. 14.1 – Significant digits of the numerical solutions obtained by double precision *via* the sensitivity index κ with some comments on stability/instability.

κ	0	$\left(0, \frac{1}{4}\right]$	$\left(\frac{1}{4}, \frac{1}{2}\right]$	$\left(\frac{1}{2}, 1\right]$	(1, 2]	(2, 3]
Significant digits	16	12	10	8	5	4
Stability	excellent	excellent	very good	good		
Instability					severe	very severe

14.3 The MFS-QR

14.3.1 Algorithms in Elliptic Coordinates

To reduce the severe ill-conditioning, Antunes [8] proposed the MFS-QR algorithm. Based on the QR decomposition, some new good basis functions were sought instead of the FS basis functions. The source nodes of the MFS-QR are confined to circles/ellipses with uniform distribution. The source nodes on circles are discussed in [8] and Section 14.4 below. In this section, consider source nodes on an ellipse at $\rho = R$. Elliptic coordinates in (14.2.1) can be expressed by the complex $z = x + \mathbf{i}y = \sigma\ \cosh w$, where $w = \rho + \mathbf{i}\theta$ and $\mathbf{i} = \sqrt{-1}$. Denote the other node in the same elliptic system by $z_0 = x_0 + \mathbf{i}y_0 = \sigma\ \cosh w_0$ with $w_0 = r + \mathbf{i}\phi$. Also, denote $P = (\rho, \theta)$ and $Q = (r, \phi)$. We have from addition theorem in Lemma III.1 in Part III

$$\begin{aligned} \ln|z - z_0| &= \ln|\overline{PQ}| \qquad (14.3.1)\\ &= r + \ln\left(\frac{\sigma}{2}\right) - 2\sum_{n=1}^{\infty}\frac{1}{n}e^{-nr}(\cosh n\rho\ \cos n\theta\ \cos n\phi + \sinh n\rho\ \sin n\theta\ \sin n\phi), \quad \rho < r. \end{aligned}$$

Choose the source nodes $Q_j = (R, \phi_j)$ with $R > r_{\max} = \max\ \rho|_\Gamma$. From (14.3.1) we have

$$\ln|\overline{PQ_j}| = R + \ln\left(\frac{\sigma}{2}\right) - 2\sum_{n=1}^{\infty}\frac{1}{n}e^{-nR}(\cosh n\rho\ \cos n\theta\ \cos n\phi_j + \sinh n\rho\ \sin n\theta\ \sin n\phi_j).$$

We choose the PS of degree n from (14.2.3) with parameter $\rho_0\ (\leq R)$,

$$P_n = P_n(\rho, \theta) = \alpha_0 + \sum_{k=1}^{n} e^{-k\rho_0}(\alpha_k\ \cosh k\rho\ \cos k\theta + \beta_k\ \sinh k\rho\ \sin k\theta). \qquad (14.3.2)$$

The coefficients between the MFS and the MPS are found from Chapter 6 as

$$c_j = \frac{1}{N}\left\{\frac{\alpha_0}{R + \ln\left(\frac{\sigma}{2}\right)} - \sum_{m=1}^{n} m e^{m(R-\rho_0)}(\alpha_m\ \cos(mjh) + \beta_m\ \sin(mjh))\right\}. \qquad (14.3.3)$$

Under condition (14.2.13), the coefficients c_j can be determined uniquely, and the matrix $\mathbf{F}$ in (14.2.12) is nonsingular. Otherwise, if $a_R + b_R = 2$, the degenerate scales are called in Chapter 6. Denote vectors $\mathbf{x} = \{c_1, \ldots, c_N\}^T$ and $\mathbf{y}\ (\in \mathbf{R}^N) = \{\alpha_0, \alpha_1, \beta_1, \ldots, \alpha_n, \beta_n\}^T$ with $N = 2n + 1$. The coefficient relations (14.3.3) are denoted by

$$\mathbf{x} = \mathbf{GDy}, \qquad (14.3.4)$$

where the diagonal matrices,

$$\mathbf{D} = \frac{1}{N}\mathrm{diag}\left\{\frac{1}{R + \ln\left(\frac{\sigma}{2}\right)}, -e^{\delta}, -e^{\delta}, -2e^{2\delta}, -2e^{2\delta}, \ldots, -ne^{n\delta}, -ne^{n\delta}\right\}, \qquad (14.3.5)$$

$$\mathbf{D}^{-1} = N\mathrm{diag}\left\{R + \ln\left(\frac{\sigma}{2}\right), -e^{-\delta}, -e^{-\delta}, -\frac{1}{2}e^{-2\delta}, -\frac{1}{2}e^{-2\delta}, \ldots, -\frac{1}{n}e^{-n\delta}, -\frac{1}{n}e^{-n\delta}\right\},$$

where $\delta = R - \rho_0$, and

$$\mathbf{G} = \begin{pmatrix} 1 & \cos\phi_1 & \sin\phi_1 & \cos 2\phi_1 & \sin 2\phi_1 & \cdots & \cos n\phi_1 & \sin n\phi_1 \\ 1 & \cos\phi_2 & \sin\phi_2 & \cos 2\phi_2 & \sin 2\phi_2 & \cdots & \cos n\phi_2 & \sin n\phi_2 \\ \vdots & \vdots & \vdots & \vdots & \vdots & \vdots & \vdots & \vdots \\ 1 & \cos\phi_N & \sin\phi_N & \cos 2\phi_N & \sin 2\phi_N & \cdots & \cos n\phi_N & \sin n\phi_N \end{pmatrix}, \quad (14.3.6)$$

where $\phi_j = jh$. Note that the matrix $\mathbf{G}$ is the same as "$-\mathbf{B}$" in [8] and "$\mathbf{B}$" in [9], but the diagonal matrix $\mathbf{D}$ is different in elliptic coordinates. For the matrix $\mathbf{G}$ by the QR decomposition, we have

$$\mathbf{G} = \mathbf{QR}, \quad (14.3.7)$$

where $\mathbf{Q}$ and $\mathbf{R}$ are the orthogonal and the upper-triangular matrices, respectively. Hence, we have from (14.3.4)

$$\mathbf{x} = \mathbf{QRDy}. \quad (14.3.8)$$

From [8], we use the following transformation from $\mathbf{x}$ to a new unknown vector $\mathbf{z}$

$$\mathbf{z} = \mathbf{D}^{-1}\mathbf{Q}^T\mathbf{x}, \quad (14.3.9)$$

to give

$$\mathbf{z} = \mathbf{D}^{-1}\mathbf{Q}^T\mathbf{x} = \mathbf{D}^{-1}\mathbf{Q}^T(\mathbf{QRDy}) = \mathbf{D}^{-1}\mathbf{RDy}. \quad (14.3.10)$$

By using the Hadamard product $\circ$ of matrices, the equation (14.3.10) is rewritten as

$$\mathbf{z} = \mathbf{D}^{-1}\mathbf{RDy} = (\mathbf{T}_L \circ \mathbf{R} \circ \mathbf{T}_R)\mathbf{y} = (\mathbf{T}_L \circ \mathbf{T}_R \circ \mathbf{R})\mathbf{y} = (\tilde{\mathbf{T}} \circ \mathbf{R})\mathbf{y} = \tilde{\mathbf{R}}\mathbf{y}, \quad (14.3.11)$$

where the upper-triangular matrix $\tilde{\mathbf{T}} = \mathbf{T}_L \circ \mathbf{T}_R$ is given by

$$\tilde{\mathbf{T}} = \begin{pmatrix} 1 & \frac{-e^{-\delta}}{R+\ln(\frac{\sigma}{2})} & \frac{-e^{-\delta}}{R+\ln(\frac{\sigma}{2})} & \frac{-e^{-2\delta}}{2(R+\ln(\frac{\sigma}{2}))} & \frac{-e^{-2\delta}}{2(R+\ln(\frac{\sigma}{2}))} & \cdots & \frac{-e^{-n\delta}}{n(R+\ln(\frac{\sigma}{2}))} & \frac{-e^{-n\delta}}{n(R+\ln(\frac{\sigma}{2}))} \\ 0 & 1 & 1 & \frac{1}{2}e^{-\delta} & \frac{1}{2}e^{-\delta} & \cdots & \frac{1}{n}e^{-(n-1)\delta} & \frac{1}{n}e^{-(n-1)\delta} \\ 0 & 0 & 1 & \frac{1}{2}e^{-\delta} & \frac{1}{2}e^{-\delta} & \cdots & \frac{1}{n}e^{-(n-1)\delta} & \frac{1}{n}e^{-(n-1)\delta} \\ 0 & 0 & 0 & 1 & 1 & \cdots & \frac{2}{n}e^{-(n-2)\delta} & \frac{2}{n}e^{-(n-2)\delta} \\ 0 & 0 & 0 & 0 & 1 & \cdots & \frac{2}{n}e^{-(n-2)\delta} & \frac{2}{n}e^{-(n-2)\delta} \\ \vdots & \vdots & \vdots & \vdots & \vdots & \vdots & \vdots & \vdots \\ 0 & 0 & 0 & 0 & 0 & \cdots & 1 & 1 \\ 0 & 0 & 0 & 0 & 0 & \cdots & 0 & 1 \end{pmatrix}, \quad (14.3.12)$$

where $\delta = R - \rho_0$.

Define the vector of the basis functions for PS in (14.3.2) by

$$\begin{aligned} \tilde{\psi}(\rho,\theta) &= \{\psi_1(\rho,\theta), \psi_2(\rho,\theta), \ldots, \psi_{2n+1}(\rho,\theta)\}^T \quad (14.3.13) \\ &= \{1, e^{-\rho_0}\cosh\rho\,\cos\theta, e^{-\rho_0}\sinh\rho\,\sin\theta, \ldots, e^{-n\rho_0}\cosh n\rho\,\cos n\theta, e^{-n\rho_0}\sinh n\rho\,\sin n\theta\}^T. \end{aligned}$$

The family of the MPS is called if the basis functions consist of (14.3.13) with a scaling. Let us summarize the original MFS-QR as follows:

Step I. Let $N = 2n+1$, formulate matrices $\mathbf{D}$ and $\mathbf{G}$ in (14.3.5) and (14.3.6), respectively.

Step II. Carry out the QR decomposition (14.3.7) for $\mathbf{G} = \mathbf{QR}$.

Step III. The conversion (14.3.11) is chosen, and the new basis functions are found as

$$\tilde{\chi}(\rho,\theta) = \{\mathbf{\Psi}_1(\rho,\theta), \mathbf{\Psi}_2(\rho,\theta), \ldots, \mathbf{\Psi}_N(\rho,\theta)\}^T = (\tilde{\mathbf{T}} \circ \mathbf{R})^{-1}\tilde{\psi}(\rho,\theta), \quad (14.3.14)$$

where $N = 2n+1$ and $\tilde{\psi}(\rho,\theta)$ are the PS in (14.3.13).

Step IV. The collocation equations of the MFS-QR are given by

$$\sqrt{\triangle h_\ell}\sum_{j=1}^{N} d_j \mathbf{\Psi}_j(\rho_\ell,\theta_\ell) = \sqrt{\triangle h_\ell}\, f(\rho_\ell,\theta_\ell), \quad \ell = 1,\, 2, \ldots, N, \quad (14.3.15)$$

where d_j are the unknown coefficients to be sought. The equation (14.3.15) is rewritten as

$$\mathbf{\Omega z} = \mathbf{b}, \quad (14.3.16)$$

where matrix $\mathbf{\Omega} \in \mathbf{R}^{N\times N}$ and the unknown vector $\mathbf{z} = \{d_1, d_2, \ldots, d_N\}^T$.

14.3.2 Characteristics of MFS-QR

First, we examine matrices $\mathbf{G}$ in (14.3.6) and $\tilde{\mathbf{T}}$ in (14.3.12). The matrices $\mathbf{G}$ and $\tilde{\mathbf{T}}$ are independent of and dependent on source nodes, respectively. The Cond of the MFS is huge for large R in Chapter 6. When $R \to \infty$, however, the matrix $\tilde{\mathbf{R}}\,(= \tilde{\mathbf{T}} \circ \mathbf{R})$ leads to

$$\tilde{\mathbf{R}} = \begin{pmatrix} R_{1,1} & 0 & 0 & 0 & 0 & \cdots & 0 & 0 \\ 0 & R_{2,2} & R_{2,3} & 0 & 0 & \cdots & 0 & 0 \\ 0 & 0 & R_{3,3} & 0 & 0 & \cdots & 0 & 0 \\ \vdots & \vdots & \vdots & \vdots & \vdots & \vdots & \vdots & \vdots \\ 0 & 0 & 0 & 0 & 0 & \cdots & R_{N-1,N-1} & R_{N-1,N} \\ 0 & 0 & 0 & 0 & 0 & \cdots & 0 & R_{N,N} \end{pmatrix}, \quad (14.3.17)$$

where $R_{i,j}\,(i \le j)$ are the upper-triangular entries of matrix $\mathbf{R}$ in (14.3.7), which is independent of source nodes. We give the following lemma.

Lemma 4.3.1. *Let assumption (14.2.13) and an elliptic pseudo-boundary at* $\rho = R \in [\rho_0, \infty)$ *be given. The MFS-QR eliminates the effects of source nodes on stability, based on similar transformation. For the MFS-QR, the new basis functions* $\tilde{\chi}(\rho,\theta)$ *are a linear combination of the PS:* $\tilde{\psi}(\rho,\theta)$ *in (14.3.14), but the stability is not better than that of the MPS in (14.2.5).*

Proof. We have from (14.3.10)

$$\mathbf{y} = \mathbf{D}^{-1}\mathbf{R}^{-1}\mathbf{D}\mathbf{z}. \tag{14.3.18}$$

Substituting (14.3.18) into (14.2.6) gives

$$\mathbf{P}\mathbf{D}^{-1}\mathbf{R}^{-1}\mathbf{D}\mathbf{z} = \mathbf{b}. \tag{14.3.19}$$

Comparing (14.3.16) with (14.3.19), we have

$$\mathbf{\Omega} = \mathbf{P}\mathbf{D}^{-1}\mathbf{R}^{-1}\mathbf{D} = \mathbf{P}\mathbf{H}. \tag{14.3.20}$$

Since matrix $\mathbf{D}$ in (14.3.5) is nonsingular under (14.2.13), matrices $\mathbf{H} = \mathbf{D}^{-1}\mathbf{R}^{-1}\mathbf{D}$ and $\mathbf{R}^{-1}$ are similar to each other. The similar matrices $\mathbf{H}$ and $\mathbf{R}^{-1}$ have the same eigenvalues, which are independent of source nodes. Hence we obtain from (14.3.20)

$$\text{Cond}(\mathbf{\Omega}) = \text{Cond}(\mathbf{PH}) \le \text{Cond}(\mathbf{P}) \times \text{Cond}(\mathbf{H}) \le C\text{Cond}(\mathbf{P}),$$

by noting $C = \text{Cond}(\mathbf{H}) \ge 1$. This confirms the statements in Lemma 14.3.1. ■

The numerical experiments in [8] had shown no effects of source nodes on stability. On the other hand, the PS may be converted to harmonic kernels in Schaback [101, 213], which have source nodes but do not need a pseudo-boundary. The MFS-QR acted as if the source nodes and their pseudo-boundaries were eliminated, an inverse action of harmonic kernels.

Below, let us scrutinize the MFS-QR algorithm when the source nodes are located uniformly on an outside ellipse: $Q_j = (R, \phi_j)$ with $\phi_j = jh$ and $h = \frac{2\pi}{N}$. We have the following lemma.

Lemma 14.3.2. *The upper-triangular matrix* $\mathbf{R}$ *in (14.3.7) from the QR decomposition is, indeed, a diagonal matrix.*

Proof. Matrix $\mathbf{A}$ is orthogonal if $\mathbf{A}^T\mathbf{A} = \mathbf{I}$, where matrix $\mathbf{A}^T$ is the transpose of $\mathbf{A}$, and $\mathbf{I}$ is the identity matrix. We have $\mathbf{A}^T = \mathbf{A}^{-1}$. Since $(\mathbf{A}^T)^T = (\mathbf{A}^{-1})^T = (\mathbf{A}^T)^{-1}$, the matrix $\mathbf{A}^T$ is also orthogonal. Define a matrix $\mathbf{Q}_1$ by

$$\mathbf{Q}_1 = \sqrt{\frac{2}{N}} \begin{pmatrix} \frac{1}{\sqrt{2}} & \frac{1}{\sqrt{2}} & \cdots & \frac{1}{\sqrt{2}} \\ \cos\phi_1 & \cos\phi_2 & \cdots & \cos\phi_N \\ \sin\phi_1 & \sin\phi_2 & \cdots & \sin\phi_N \\ \vdots & \vdots & \vdots & \vdots \\ \cos(n\phi_1) & \cos(n\phi_2) & \cdots & \cos(n\phi_N) \\ \sin(n\phi_1) & \sin(n\phi_2) & \cdots & \sin(n\phi_N) \end{pmatrix}, \tag{14.3.21}$$

where $N = 2n + 1$ and $\phi_j = j\frac{2\pi}{N}$. We conclude that matrix $\mathbf{Q}_1$ is orthogonal. We have from (14.3.6) and (14.3.21)

$$\mathbf{Q}_1\mathbf{G} = \text{diag}\left\{\sqrt{N}, \sqrt{\frac{N}{2}}, \ldots, \sqrt{\frac{N}{2}}\right\} := \mathbf{D}_1, \tag{14.3.22}$$

where $\mathbf{D}_1$ is a diagonal matrix. Then we have

$$\mathbf{G} = (\mathbf{Q}_1)^T\mathbf{D}_1. \tag{14.3.23}$$

The matrix $(\mathbf{Q}_1)^T$ is also orthogonal. From (14.3.23), matrix $\mathbf{G}$ is a product of an orthogonal matrix $(\mathbf{Q}_1)^T$ and a diagonal matrix $\mathbf{D}_1$. Since the diagonal matrix is also an upper-triangular matrix, the equation (14.3.23) is of the QR decomposition for matrix $\mathbf{G}$. From [12, p.614], the QR decomposition is unique in the sense that the diagonal entries of $\mathbf{R}$ and $\mathbf{Q}_1$ may have sign differences. When the diagonal entries of $\mathbf{R}$ are positive, the QR decomposition as (14.3.23) is unique (see [88, p.230, Theorem 5.2.2]). Hence, the upper-triangular matrix $\mathbf{R}$ in (14.3.7) is a diagonal matrix. ■

Theorem 14.3.1. *The basis functions of MFS-QR are given in (14.3.27) below, which are converted from (14.3.13), by the scaling with factors* $\frac{1}{\sqrt{N}}$ *and* $\sqrt{\frac{2}{N}}$. *Then there exists the bound,*

$$\mathrm{Cond}(\boldsymbol{\Omega}) \le \sqrt{2}\ \mathrm{Cond}(\mathbf{P}), \tag{14.3.24}$$

where matrices $\boldsymbol{\Omega}$ *and* $\mathbf{P}$ *are given in (14.3.16) and (14.2.6), respectively. Hence the MFS-QR algorithms can be classified into the family of the MPS. The MFS-QR is not a variant of the MFS but a variant of the MPS.*

Proof. From (14.3.9) we have $\mathbf{z} = \mathbf{D}^{-1}\mathbf{Q}_1\mathbf{x}$. The equations (14.3.8) and (14.3.10) are simplified as

$$\mathbf{x} = \mathbf{G}\mathbf{D}\mathbf{y} = (\mathbf{Q}_1)^T\mathbf{D}_1\mathbf{D}\mathbf{y}, \tag{14.3.25}$$

$$\mathbf{z} = \mathbf{D}^{-1}\mathbf{Q}_1\mathbf{x} = \mathbf{D}^{-1}\mathbf{Q}_1[(\mathbf{Q}_1)^T\mathbf{D}_1\mathbf{D}\mathbf{y}] = \mathbf{D}^{-1}(\mathbf{D}_1\mathbf{D})\mathbf{y} = \mathbf{D}_1\mathbf{y}. \tag{14.3.26}$$

From (14.3.26), (14.3.22) and (14.3.13), the explicit basis functions of the MFS-QR are found as

$$\begin{aligned}\tilde{\chi}(\rho,\theta) = \mathbf{D}_1^{-1}\tilde{\psi}(\rho,\theta) = \Bigg\{&\frac{1}{\sqrt{N}}, \sqrt{\frac{2}{N}}e^{-\rho_0}\cosh\rho\ \cos\theta, \sqrt{\frac{2}{N}}e^{-\rho_0}\sinh\rho\ \sin\theta, \ldots,\\ &\sqrt{\frac{2}{N}}e^{-n\rho_0}\cosh n\rho\ \cos n\theta, \sqrt{\frac{2}{N}}e^{-n\rho_0}\sinh n\rho\ \sin n\theta\Bigg\}^T\\ &:= \{\boldsymbol{\Psi}_1(\rho,\theta), \boldsymbol{\Psi}_2(\rho,\theta), \ldots, \boldsymbol{\Psi}_N(\rho,\theta)\}^T,\end{aligned} \tag{14.3.27}$$

where $N = 2n+1$. We have from (14.3.20) with $\mathbf{R} = \mathbf{D}_1$

$$\boldsymbol{\Omega} = \mathbf{P}\mathbf{D}^{-1}\mathbf{R}^{-1}\mathbf{D} = \mathbf{P}\mathbf{D}_1^{-1}, \tag{14.3.28}$$

where matrix $\mathbf{D}_1$ is given in (14.3.22). Then we have

$$\mathrm{Cond}(\boldsymbol{\Omega}) \le \mathrm{Cond}(\mathbf{P}) \times \mathrm{Cond}(\mathbf{D}_1^{-1}) \le \sqrt{2}\ \mathrm{Cond}(\mathbf{P}), \tag{14.3.29}$$

where we have used $\mathrm{Cond}(\mathbf{D}_1^{-1}) = \sqrt{2}$. ■

Denote the solution from (14.3.27) by

$$v_N = v_N(\rho,\theta) = \sum_{i=1}^{N} d_i \mathbf{\Psi}_i(\rho,\theta), \tag{14.3.30}$$

where the coefficients d_i are obtained from (14.3.15) by the MFS-QR. Also, denote the solution u_n from (14.2.3) by

$$u_n = u_n(\rho,\theta) = \alpha_0 + \sum_{k=1}^{n} e^{-k\rho_0}\{\alpha_k \cosh(k\rho)\cos(k\theta) + \beta_k \sinh(k\rho)\sin(k\theta)\}, \tag{14.3.31}$$

where the coefficients α_k and β_k are obtained from (14.2.5) by the MPS. We have the following corollary.

Corollary 14.3.1. *Let the solutions* v_N *and* u_n *be obtained from the MFS-QR and the MPS, respectively. There exists the approximation,*

$$v_N(\rho,\theta) \approx u_n(\rho,\theta), \tag{14.3.32}$$

where $N = 2n+1$, *and the coefficients have the following relations from (14.3.26),*

$$d_1 \approx \sqrt{N}\alpha_0,\, d_2 \approx \sqrt{\frac{N}{2}}\alpha_1,\, d_3 \approx \sqrt{\frac{N}{2}}\beta_2, \ldots,\, d_{2n} \approx \sqrt{\frac{N}{2}}\alpha_n,\, d_{2n+1} \approx \sqrt{\frac{N}{2}}\beta_n. \tag{14.3.33}$$

Remark 14.3.1. *Note that the transformation (14.3.26) is slightly different from that via (14.3.10) as in [8]. The original basis functions (14.3.14) are replaced by (14.3.27), called the simplified MFS-QR in this chapter. To display their differences, we give numerical examples. Letting* $n = 3$ *and* $N = 7$, *we provide the explicit matrices* $\mathbf{G}_1$, $\mathbf{Q}$, $\mathbf{R}$, $\mathbf{Q}_1$ *and* $\mathbf{D}_1$, *as follows:*

$$\mathbf{G}_1 = \begin{pmatrix} 1 & 0.6235 & 0.7818 & -0.2225 & 0.9749 & -0.9010 & 0.4339 \\ 1 & -0.2225 & 0.9749 & -0.9010 & -0.4339 & 0.6235 & -0.7818 \\ 1 & -0.9010 & 0.4339 & 0.6235 & -0.7818 & -0.2225 & 0.9749 \\ 1 & -0.9010 & -0.4339 & 0.6235 & 0.7818 & -0.2225 & -0.9749 \\ 1 & -0.2225 & -0.9749 & -0.9010 & 0.4339 & 0.6235 & 0.7818 \\ 1 & 0.6235 & -0.7818 & -0.2225 & -0.9749 & -0.9010 & -0.4339 \\ 1 & 1.0000 & -0.0000 & 1.0000 & -0.0000 & 1.0000 & -0.0000 \end{pmatrix},$$

$$\mathbf{Q} = \begin{pmatrix} -0.3780 & 0.3333 & 0.4179 & 0.1189 & -0.5211 & -0.4816 & -0.2319 \\ -0.3780 & -0.1189 & 0.5211 & 0.4816 & 0.2319 & 0.3333 & 0.4179 \\ -0.3780 & -0.4816 & 0.2319 & -0.3333 & 0.4179 & -0.1189 & -0.5211 \\ -0.3780 & -0.4816 & -0.2319 & -0.3333 & -0.4179 & -0.1189 & 0.5211 \\ -0.3780 & -0.1189 & -0.5211 & 0.4816 & -0.2319 & 0.3333 & -0.4179 \\ -0.3780 & 0.3333 & -0.4179 & 0.1189 & 0.5211 & -0.4816 & 0.2319 \\ -0.3780 & 0.5345 & -0.0000 & -0.5345 & 0.0000 & 0.5345 & 0.0000 \end{pmatrix},$$

$$\mathbf{R} = \mathrm{diag}\{-2.6458,\, 1.8708,\, 1.8708,\, -1.8708,\, -1.8708,\, 1.8708,\, -1.8708\},$$

$$\mathbf{Q}_1 = \begin{pmatrix} 0.3780 & 0.3780 & 0.3780 & 0.3780 & 0.3780 & 0.3780 & 0.3780 \\ 0.3333 & -0.1189 & -0.4816 & -0.4816 & -0.1189 & 0.3333 & 0.5345 \\ 0.4179 & 0.5211 & 0.2319 & -0.2319 & -0.5211 & -0.4179 & -0.0000 \\ -0.1189 & -0.4816 & 0.3333 & 0.3333 & -0.4816 & -0.1189 & 0.5345 \\ 0.5211 & -0.2319 & -0.4179 & 0.4179 & 0.2319 & -0.5211 & -0.0000 \\ -0.4816 & 0.3333 & -0.1189 & -0.1189 & 0.3333 & -0.4816 & 0.5345 \\ 0.2319 & -0.4179 & 0.5211 & -0.5211 & 0.4179 & -0.2319 & -0.0000 \end{pmatrix},$$

$$\mathbf{D}_1 = \text{diag}\{2.6458,\ 1.8708,\ 1.8708,\ 1.8708,\ 1.8708,\ 1.8708,\ 1.8708\}.$$

The equalities, $\mathbf{R} = \mathbf{D}_1$ and $\mathbf{Q} = \mathbf{Q}_1^T$*, hold if different signs of entries are allowed. Since* $\sqrt{N} = \sqrt{7} = 2.6458$ *and* $\sqrt{\frac{N}{2}} = \sqrt{3.5} = 1.8708$*, Lemma 14.3.2 is supported numerically, and so does Theorem 14.3.1. For the original conversion (14.3.10), the explicit basis functions (14.3.27) are modified as*

$$\begin{aligned} \tilde{\chi}(\rho,\theta) &= \Big\{\pm\tfrac{1}{\sqrt{N}}, \pm\sqrt{\tfrac{2}{N}}e^{-\rho_0}\cosh\rho\,\cos\theta, \pm\sqrt{\tfrac{2}{N}}e^{-\rho_0}\sinh\rho\,\sin\theta, \ldots, \\ &\qquad \pm\sqrt{\tfrac{2}{N}}e^{-n\rho_0}\cosh n\rho\,\cos n\theta, \pm\sqrt{\tfrac{2}{N}}e^{-n\rho_0}\sinh n\rho\,\sin n\theta\Big\}^T \\ &:= \{\Psi_1(\rho,\theta), \Psi_2(\rho,\theta), \ldots, \Psi_N(\rho,\theta)\}^T, \end{aligned} \tag{14.3.34}$$

where $N = 2n+1$*. Moreover, the approximations (14.3.33) are modified as*

$$d_1 \approx \pm\sqrt{N}\alpha_0,\ d_2 \approx \pm\sqrt{\frac{N}{2}}\alpha_1,\ d_3 \approx \pm\sqrt{\frac{N}{2}}\beta_2, \ldots,\ d_{2n} \approx \pm\sqrt{\frac{N}{2}}\alpha_n,\ d_{2n+1} \approx \pm\sqrt{\frac{N}{2}}\beta_n, \tag{14.3.35}$$

where the signs in (14.3.34) and (14.3.35) may be different in computation. The analysis above remains the same.

Remark 14.3.2. *The MFS-QR was designed from the MFS in [8] via the transformation (14.3.14) to pursue better basis functions. The terminal algorithms fall into the MPS family. The MFS-QR is not a variant of the MFS but a variant of the MPS. The MFS-QR was also applied to the Helmholtz equation in [9]; it is not a variant of the MFS but a variant of the MPS in [149]. See Remark 9.4.1. However, the MFS-QR plays a role in bridging the MFS to the MPS; an inverse action of harmonic kernels in Schaback [101, 213]. The MFS and the MPS can also be recognized as twins via the MFS-QR in the Trefftz family [169]. The MFS and the MPS are two basic boundary methods, and the study of the MFS-QR in this chapter provides deep comparisons to enhance their applications.*

Remark 14.3.3. *The QR decomposition is used for orthogonalization in solving the least-squares problems, which is an important solution method to (14.2.12) from the MFS. The solution methods do not change any stability of (14.2.12), based on the stability analysis in Golub and van Loan [88, Chapter 5], Higham [99, Chapters 18, 19] and Li et al. [162, Chapter 1].*

Remark 14.3.4. *In Fornberg and Piret [82], the flat radial basis functions on spheres were transformed into the spherical harmonic functions (SHF) called the RBF-QR techniques. The MPS is discussed in Chapter 13 (also see [249]) for Laplace's equation in the 3D bounded simply-connected domains, where the SHF are chosen as basis functions. The optimal polynomial convergence rates and the exponential growth rates of Cond are proved. For ball domains, the stability is excellent as* Cond $= O(1)$. *From the analysis above, the RBF-QR techniques also fall into the MPS family.*

14.4 Numerical Experiments and Comparisons

Numerical verification for the MFS-QR in Section 14.3.2 and comparisons among the MPS, the MFS, and the MFS-QR are provided in [251]. In this section, different pseudo-boundaries are compared *via* the sensitivity index, to seek a better selection of source nodes (see Chapter 6). Five-pedal-flower-like domains as in Figure 14.2 are chosen, and numerical experiments and comparisons are made. We first choose highly smooth harmonic functions for the Dirichlet boundary data and then an auxiliary logarithmic function in the next subsection. The boundary Γ is defined by the following parametric equation (see Figure 14.2),

$$\Gamma = \{(x,y)|x = \rho(\theta)\cos\theta, y = \rho(\theta)\sin\theta,\ 0 \le \theta \le 2\pi\}, \tag{14.4.1}$$

where

$$\rho(\theta) = \rho(\rho_{\max}, \rho_{\min}, \theta) = \sqrt{\rho_{\min}^2 + \frac{1}{2}(\rho_{\max}^2 - \rho_{\min}^2)(1-\cos(5\theta))},\ \ \rho_{\max} > \rho_{\min} > 0. \tag{14.4.2}$$

The domain with the boundary Γ defined by (14.4.1) and (14.4.2) is five-pedal-flower-like (or starfish-like). From (14.4.1) and (14.4.2) we have

$$\rho'(\theta) = \frac{5}{4}\frac{1}{\rho(\theta)}\left(\rho_{\max}^2 - \rho_{\min}^2\right)\sin(5\theta),\ \ ds = \sqrt{(\rho'(\theta))^2 + \rho^2(\theta)}\,d\theta. \tag{14.4.3}$$

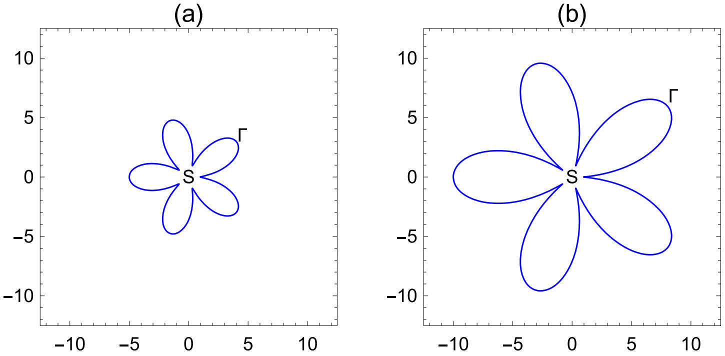

FIG. 14.2 – The boundaries Γ are defined by (14.4.2) with (a) $(\rho_{\max}, \rho_{\min}) = (5,1)$ and (b) $(\rho_{\max}, \rho_{\min}) = (10,1)$.

We establish the collocation equations

$$\sqrt{\triangle h_\ell}\sum_{j=1}^{N} c_j\Phi_j(\rho_\ell,\theta_\ell) = \sqrt{\triangle h_\ell}\, f(\rho_\ell,\theta_\ell),\ \ \ell = 1,2,\ldots,M, \tag{14.4.4}$$

where $\triangle h_\ell = \bar{h}\sqrt{(\rho'(\ell\bar{h}))^2 + \rho^2(\ell\bar{h})}$ and $\bar{h} = \frac{2\pi}{M}$. Choose the pseudo-boundaries outside Γ as

$$\bar{\rho}(\theta) = \bar{\rho}(\bar{\rho}_{\max},\bar{\rho}_{\min},\theta) = \sqrt{\bar{\rho}_{\min}^2 + \frac{1}{2}(\bar{\rho}_{\max}^2 - \bar{\rho}_{\min}^2)(1-\cos(5\theta))},\ \bar{\rho}_{\max} > \bar{\rho}_{\min} > 0, \tag{14.4.5}$$

where $\bar{\rho}_{\max} > \rho_{\max}$ and $\bar{\rho}_{\min} > \rho_{\min}$. When $\bar{\rho}_{\max} = \bar{\rho}_{\min}$, the equation (14.4.5) leads to a circular pseudo-boundary.

14.4.1 Highly Smooth Boundary Data

Choose the harmonic solution $u(x,y) = e^y\cos x$ and $u(x,y) = e^{\frac{y}{2}}\cos\frac{x}{2}$ for the boundary Γ with $(\rho_{\max},\rho_{\min}) = (5,1)$ and (10,1), respectively. The numerical results are given in [251]. We only list the summaries in Tables 14.2 and 14.3, which show a "good" stability as in Table 14.1. Since index $\kappa = 0.74$ is the smallest among all pseudo-boundaries in Table 14.2, the circular pseudo-boundary is optimal for four pseudo-boundaries on the left side in Figure 14.3 for $(\rho_{\max},\rho_{\min}) = (5,1)$. For $(\rho_{\max},\rho_{\min}) = (10,1)$, the circular pseudo-boundary is also optimal in Table 14.3. Note that for the MFS, by using the circular pseudo-boundary, the sensitivity index

TAB. 14.2 – Comparisons between the MFS and the MPS for $(\rho_{\max},\rho_{\min}) = (5,1)$, where κ and β are given in (14.2.21) and (14.2.18), respectively.

$(\bar{\rho}_{\max},\bar{\rho}_{\min})$	(6, 2)	(8, 4)	(8, 6)	(8, 8)	MPS
$\Vert\epsilon\Vert_{0,\Gamma}$	$O(0.93^N)$	$O(0.85^N)$	$O(0.73^N)$	$O(0.63^N)$	$O(0.54^N)$
Cond	$O(1.12^N)$	$O(1.34^N)$	$O(1.36^N)$	$O(1.41^N)$	$O(1.29^N)$
β	0.39	0.42	0.36	0.35	/
Index κ	1.56	1.80	0.98	0.74	0.41

TAB. 14.3 – Comparisons between the MFS and the MPS for $(\rho_{\max},\rho_{\min}) = (10,1)$, where κ and β are given in (14.2.21) and (14.2.18), respectively.

$(\bar{\rho}_{\max},\bar{\rho}_{\min})$	(11, 2)	(14, 4)	(14, 9)	(14, 14)	MPS
$\Vert\epsilon\Vert_{0,\Gamma}$	$O(0.96^N)$	$O(0.91^N)$	$O(0.82^N)$	$O(0.72^N)$	$O(0.67^N)$
Cond	$O(1.06^N)$	$O(1.19^N)$	$O(1.25^N)$	$O(1.32^N)$	$O(1.34^N)$
β	0.35	0.35	0.30	0.30	/
Index κ	1.43	1.84	1.12	0.85	0.73

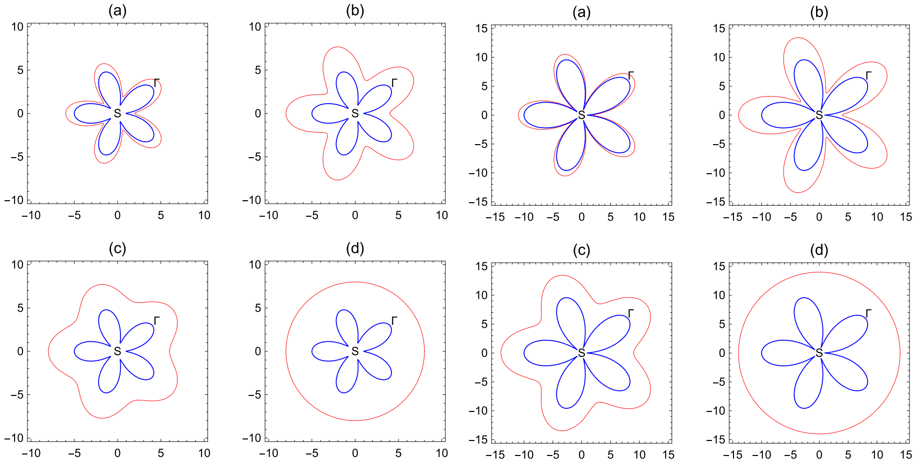

FIG. 14.3 – The pseudo-boundaries defined by (14.4.5) with $(\bar{\rho}_{\max}, \bar{\rho}_{\min}) = (6,2), (8,4), (8,6)$ and $(8,8)$ (The left side), and $(\bar{\rho}_{\max}, \bar{\rho}_{\min}) = (11,2), (14,4), (14,9)$ and $(14,14)$ (The right side).

is $\kappa|_{MFS} = 0.85$, which is slightly larger than $\kappa|_{MPS} = 0.73$. Then the numerical performance of the MFS is only a little behind that of the MPS (*cf.* [168]).

Remark 14.4.1. *Since the accuracy of the MFS depends on the boundary value problem (i.e., the Dirichlet problem of Laplace's equation in (14.2.2)), the sensitivity index is different for different* Γ, f *and pseudo-boundaries, and so are better pseudo-boundaries. For highly smooth solutions and singular solutions, better pseudo-boundaries are different (see the next subsection). Hence, the selection of pseudo-boundaries should be studied for each specified problem. The better selection is similar to the effective condition number that depends on the known vector* $\mathbf{b}$ *in (14.2.6) [162].*

14.4.2 Boundary Data with Strong Singularity

Define the logarithmic function

$$u^* = u^*(r^*, \phi^*) = \ln|\overline{PQ^*}| = \ln\sqrt{(x - x^*)^2 + (y - y^*)^2} := u^*(x, y), \tag{14.4.6}$$

where point $Q^* = (x^*, y^*)$ is outside but close to Γ, $P \in \bar{S}$, and $r^* = \sqrt{(x^*)^2 + (y^*)^2}$. The Dirichlet boundary data in (14.2.2) are generated by (14.4.6) as $f = u^*(r^*, \phi^*)|_{\Gamma}$. In fact, the solutions from (14.2.2) have a strong singularity only with $u \in \mathbf{H}^{1+\delta}(S)$ with $0 < \delta \ll 1$ as Q^* is close to Γ but $Q^* \notin \Gamma$. Hence, the convergence rates are very slowly, such as $O\left(\frac{1}{\sqrt{N}}\right)$ for arbitrary Γ; more discussions are given in Chapter 16. For the five-pedal-flower-like domain with $(\rho_{\max}, \rho_{\min}) = (5, 1)$ in Figure 14.2, we choose the following function with five points (x_i^*, y_i^*) in symmetry (see Figure 14.4):

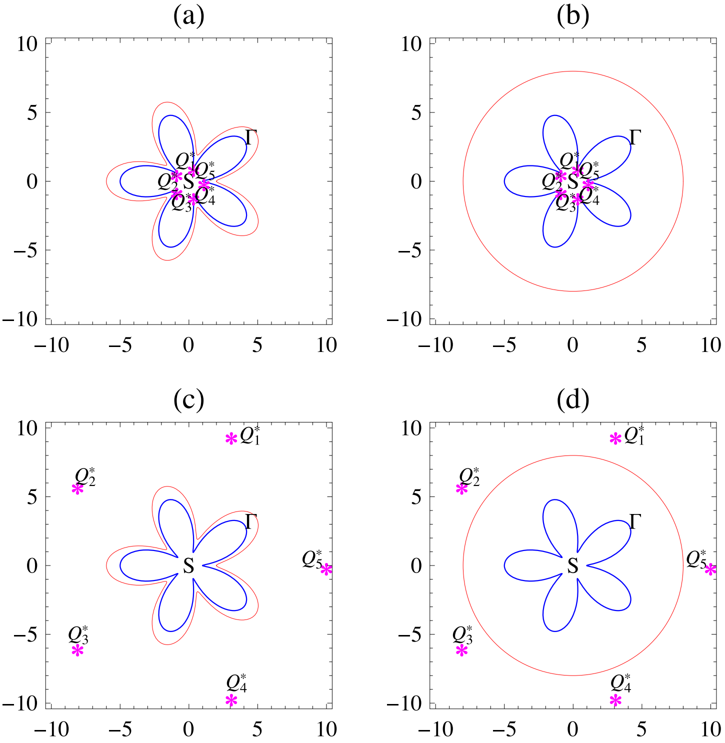

FIG. 14.4 – Locations of five points $Q_i^* = (r^*, \phi_i^*)$ at $r^* = 1.1, 10$, and two pseudo-boundaries: $(\bar{\rho}_{\max}, \bar{\rho}_{\min}) = (6, 2)$ and $(8, 8)$.

$$u^*(x, y) = \sum_{i=1}^{5} \ln\sqrt{(x - x_i^*)^2 + (y - y_i^*)^2} = \sum_{i=1}^{5} \ln|\overline{PQ_i^*}|, \qquad (14.4.7)$$

where $Q_i^* = (x_i^*, y_i^*) = (r^*, \phi_i^*)$, $r^* = 1.1, 10$ and $\phi_i^* = i\frac{2\pi}{5}$ at $i = 1, 2, 3, 4, 5$. Only the MFS is employed in computation. We have tested different $r^* \in [1.1,\ 15]$ for $(\bar{\rho}_{\max}, \bar{\rho}_{\min}) = (6, 2)$ and $(8,\ 8)$, and list the numerical results in [251]. The curves of $\|\epsilon\|_{0,\Gamma}$, Cond and Cond_eff *via* r^* are drawn in Figures 14.5 and 14.6. First, we note that for $(\bar{\rho}_{\max}, \bar{\rho}_{\min}) = (6, 2)$ (or $(8,\ 8)$), the Cond remains the same for different r^*, and the Cond = 1.15(5) for $(\bar{\rho}_{\max}, \bar{\rho}_{\min}) = (6, 2)$ is much smaller than the Cond = 5.66(12) for $(\bar{\rho}_{\max}, \bar{\rho}_{\min}) = (8, 8)$. The Cond_eff are changeable and smaller than the Cond. Second, when $r^* \geq 8$, the solutions are highly smooth, the errors for $(\bar{\rho}_{\max}, \bar{\rho}_{\min}) = (8,\ 8)$ are very small as $O(10^{-14})$. Third, when $r^* \leq 3$, the accuracy of solutions is very poor for both $(\bar{\rho}_{\max}, \bar{\rho}_{\min}) = (6, 2)$ and $(8,\ 8)$. However, there is an exception that the error $O(10^{-14})$ occurs for $(\bar{\rho}_{\max}, \bar{\rho}_{\min}) = (8, 2)$ at $r^* = 2$. When five points $Q^* = \left(2, i\frac{2\pi}{5}\right)$ are just chosen as the source nodes, the zero errors are rewarded, and the singularity of solutions can be removed completely. Note that the nonzero errors $O(10^{-14})$ are reasonable in computation of double precision since

Cond $= O(10^5)$. For $r^* = 8$, these five points $Q_i^* = \left(8, i\frac{2\pi}{5}\right)$ are also chosen as the source nodes for $(\bar{\rho}_{\max}, \bar{\rho}_{\min}) = (8, 8)$, but no better effects on errors are rendered because the errors are already as small as $O(10^{-14})$.

14.4.3 Better Pseudo-Boundaries

Let us look at Figures 14.5 and 14.6 again. When r^* increases in [1.1, 15], the errors for $(\bar{\rho}_{\max}, \bar{\rho}_{\min}) = (8, 8)$ decline significantly but those for $(\bar{\rho}_{\max}, \bar{\rho}_{\min}) = (6, 2)$ do not. This is a numerical reason why the better pseudo-boundaries are switched from $(\bar{\rho}_{\max}, \bar{\rho}_{\min}) = (6, 2)$ to (8, 8). Below, we intend to find theoretical reasons for this switch. The regularity of solutions depends on the locations of points $Q_i^* = \left(r^*, i\frac{2\pi}{5}\right)$. When they are far from boundary Γ, the solutions $u \in \mathbf{H}^p(S)$ with $p\ (\gg 1)$ are highly smooth. When they are close to Γ, the solutions $u \in \mathbf{H}^{1+\delta}(S)$ with $0 < \delta \ll 1$ are strongly singular. Such a solution singularity is even stronger than that in interior cracks and Motz's problem; see Chapters 1 and 6. The relaxed regularity, $u \in \mathbf{H}^p(S)$ with $p > 1$, is given in Lemma 14.2.1. The error estimates in Sections 14.2 and 14.3 and Chapters 2 and 6 are valid for the strongly singular boundary data.

To provide theoretical arguments, we first consider the simple case of a disk domain with radius a and the circular pseudo-boundaries with radius $R > a$ and $R \neq 1$. From Chapter 2, we have the following error bounds by the MFS,

$$\|u - u_N\|_{0,\Gamma} \leq C\left\{\frac{1}{N^{p-\frac{1}{2}}}\|u\|_{p,S} + \left(\frac{a}{R}\right)^{N-2n}\|u\|_{0,\Gamma}\right\},\ p > 1, \tag{14.4.8}$$

where C is a constant independent of n and N. Also we have from Chapter 2.

$$\text{Cond} \leq \frac{N|\ln R|}{2}\left(\frac{R}{a}\right)^{\frac{N}{2}}. \tag{14.4.9}$$

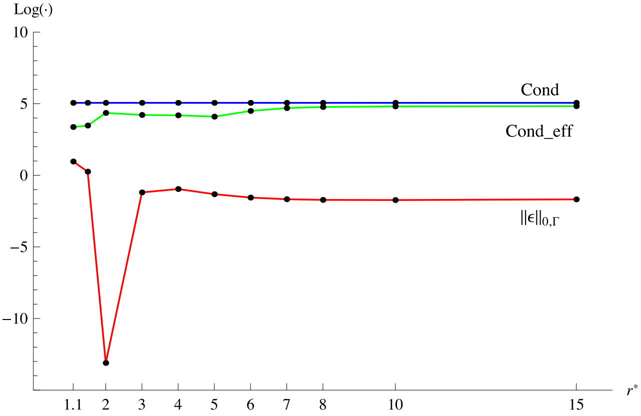

FIG. 14.5 – The curves of $\|\epsilon\|_{0,\Gamma}$, Cond and Cond_eff *via* r^* for $(\bar{\rho}_{\max}, \bar{\rho}_{\min}) = (6, 2)$.

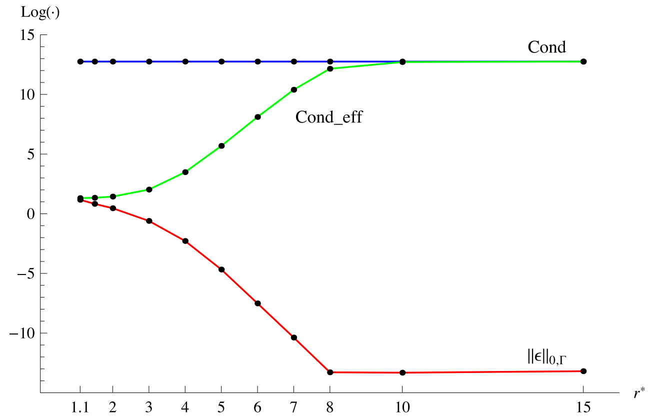

FIG. 14.6 – The curves of $\|\epsilon\|_{0,\Gamma}$, Cond and Cond_eff *via* r^* for $(\bar{\rho}_{\max}, \bar{\rho}_{\min}) = (8, 8)$.

Proposition 14.4.1. *Choose the disk domain with radius* a*, and use the circular pseudo-boundaries with radius* $R > a$ *and* $R \neq 1$*. For the highly smooth solution* $u \in \mathbf{H}^p(S)$ *with* $p \gg 1$*, the sensitivity index* $\kappa \approx \frac{1}{2}$ *for large* R*. For the strongly singular solution* $u \in \mathbf{H}^p(S)$ *with* $p > 1$ and $p \approx 1$*, the low convergence rate* $O\Big(\frac{1}{\sqrt{N}}\Big)$ *occurs. Also, the smaller* $R(> a)$ *is chosen, the smaller the sensitivity index is obtained.*

Proof. For $u \in \mathbf{H}^p(S)$ with $p \gg 1$, the dominant errors from (14.4.8) become

$$\|\epsilon\|_{0,\Gamma} = \|u - u_{\mathrm{N}}\|_{0,\Gamma} = O\bigg(\Big(\frac{a}{R}\Big)^N\bigg). \tag{14.4.10}$$

We obtain the sensitivity index $\kappa \approx \frac{1}{2}$ from (14.2.21), (14.4.9) and (14.4.10). Next for $u \in \mathbf{H}^p(S)$ with $p > 1$ and $p \approx 1$, the dominant errors from (14.4.8) become

$$\|\epsilon\|_{0,\Gamma} = O\bigg(\frac{1}{\sqrt{n}}\bigg) = O\bigg(\frac{1}{\sqrt{N}}\bigg), \tag{14.4.11}$$

which is irrelevant to R, indeed. Hence from (14.4.9), the smaller R is chosen, the smaller the Cond is obtained, and so is the sensitivity index. ■

The sensitivity index is defined in (14.2.21) from exponential rates of convergence/growth. For bounded N and n, the polynomial convergence rates of convergence/growth may be converted equivalently to the average exponential rates. Hence, the sensitivity index is also valid for low polynomial rates. The sensitivity index can be regarded as a criterion for comparing different methods and different techniques for wide application.

14.5 Concluding Remarks

1. The estimates of the Cond are derived in Theorem 14.2.1 for the MPS in the bounded simply-connected domains, and in Proposition 14.2.2 for the MFS with arbitrarily closed pseudo-boundaries. The stability analysis in this chapter and Chapter 15 is significant for two basic methods in applications. Both methods have the polynomial convergence rates and the exponential growth rates of the Cond.
2. The MFS-QR algorithm was proposed in Antunes [8], and characterizations are explored in Section 14.3.2. The new basis functions of the MFS-QR are found and given in (14.3.27) and (14.3.34); the MFS-QR is a special MPS. The coefficient relations of the two methods are provided in (14.3.33), which are verified in [251], numerically. The MFS-QR is not a variant of the MFS but a variant of the MPS.
3. Two basis boundary methods, the MPS and the MFS, are studied together in elliptic coordinates for solving Laplace's equation. From Tables 14.2 and 14.3 for highly smooth solutions, the numerical performance of the MFS is not much behind that of the MPS (*cf.* [178]). Moreover, the MFS-QR plays a role in bridging the MFS to the MPS. The MFS and the MPS can also be recognized as twins *via* the MFS-QR in the Trefftz family [169]. The comparisons in this chapter are more comprehensive than those in [178].
4. For the MFS, how to select pseudo-boundaries is an essential issue in computation in Chapter 6 (see [74]). To pursue better pseudo-boundaries, the sensitivity index is proposed in (14.2.21) from growth/convergence rates of stability *via* accuracy. The sensitivity index can be regarded as a criterion for comparing different methods and different techniques for wide applications.
5. For the five-pedal-flower-like domains in Figure 14.2, numerical comparisons are made in Section 14.4. The circular pseudo-boundaries are optimal for highly smooth solutions ($i.e.$, $u \in \mathbf{H}^p(S)$ with $p \gg 1$) but not for singular solutions ($i.e.$, $u \in \mathbf{H}^{1+\delta}(S)$ with $0 < \delta \ll 1$), where the pseudo-boundaries near boundary Γ may be better. Note that from Remark 14.4.1, a better pseudo-boundary may be different for different problems. For other boundary data and other shapes of S, better pseudo-boundaries should be re-evaluated based on the sensitivity index; see [253].
6. The comparisons for three numerical methods may be applied to other equations ($e.g.$, the Helmholtz equation) in 2D and 3D. The analysis on the MFS-QR is also valid for the Helmholtz equation in Antunes [9]; see Remark 9.4.1 in Chapter 9. The sensitivity index can be employed for other problems such as the Helmholtz equation and the mixed type of Dirichlet and Neumann boundary conditions. For the Tikhonov regularization (TR), the original sensitivity index κ^* may be used to select better regularization parameters; details are reported in Zhang *et al.* [259].

Chapter 15

Stability Analysis for Smooth Closed Pseudo-Boundaries

15.1 Introduction

Circulant matrices are often employed for stability analysis of the method of fundamental solutions (MFS); see Parts I and II. Bounds of the condition number (Cond) for circular/elliptic pseudo-boundaries are derived and the exponential growth rates are obtained. General pseudo-boundaries are suggested for more complicated solution domains in Chapters 6 and 14. Since the ill-conditioning is severe, the success in computation by the MFS mainly depends on stability. This chapter explores the stability analysis for the non-circular/non-elliptic pseudo-boundaries based on new techniques in Chapter 6 without using circulant matrices. The materials of this chapter are adapted from [252]. For non-circular/non-elliptic pseudo-boundaries, the error analysis of the MFS can be made by the Galerkin approaches as in the FEM and the BEM; details appear elsewhere.

Consider Laplace's equation with the Dirichlet boundary condition,

$$\Delta u = 0 \text{ in } S, \quad u = f \text{ on } \Gamma, \tag{15.1.1}$$

where S is a bounded simply-connected domain, and $\Gamma\,(=\partial S)$ its boundary. In this chapter, the source nodes are located on a smooth closed pseudo-boundary Γ_R outside S. Denote $P=(\rho,\theta)$ and source nodes $Q_j=(R_j,\phi_j)\in\Gamma_R$. Choose the fundamental solutions (FS),

$$\Phi_j(\rho,\theta)=\ln|\overline{PQ_j}|, \quad |\overline{PQ_j}|=\sqrt{R_j^2+\rho^2-2R_j\rho\,\cos(\theta-\phi_j)}. \tag{15.1.2}$$

We obtain a linear combination of FS as

$$u_N=\sum_{j=1}^{N} c_j\,\ln|\overline{PQ_j}|=\sum_{j=1}^{N} c_j\Phi_j(\rho,\theta), \tag{15.1.3}$$

where c_j are the coefficients. Let Γ be divided into small Γ_ℓ with the meshspacings $\triangle h_\ell$, *i.e.*, $\Gamma=\bigcup_{\ell=1}^{M}\Gamma_\ell$. We assume that the meshspacings $\triangle h_\ell$ are quasiuniform

DOI: 10.1051/978-2-7598-3171-5.c015
© Science Press, EDP Sciences, 2023

satisfying $\frac{\max_\ell|\triangle h_\ell|}{\min_\ell|\triangle h_\ell|} \le C$, where C is a constant independent of M. For simplicity, choose (ρ_ℓ, θ_ℓ) as the midpoint of $\mathbf{\Gamma}_\ell$. We obtain the collocation equations from the Dirichlet condition in (15.1.1),

$$\sqrt{\triangle h_\ell} \sum_{j=1}^{N} c_j \Phi_j(\rho_\ell, \theta_\ell) = \sqrt{\triangle h_\ell}\, f(\rho_\ell, \theta_\ell), \quad \ell = 1, 2, ..., M, \tag{15.1.4}$$

where $M \ge N$. The equation (15.1.4) leads to an overdetermined system, $\mathbf{Ax} = \mathbf{b}$, where matrix $\mathbf{A} \in \mathbf{R}^{M\times N}(M \ge N)$, and vectors $\mathbf{x} = \{c_1, c_2, ..., c_N\} \in \mathbf{R}^N$ and $\mathbf{b} \in \mathbf{R}^M$.

The stability analysis of the MFS was first studied in Kitagawa [125, 126], where both domains and pseudo-boundaries are circular, and the Dirichlet boundary conditions of Laplace's equation are considered. In Part I, the stability analysis is made for Laplace's equation. The circular pseudo-boundaries remain, but the non-circular domains are allowed. Moreover, the bounds of the Cond are derived for mixed boundary conditions in Chapter 4 (also see [163]), and for Neumann boundary conditions in Chapter 3. The stability analysis of circular pseudo-boundaries is explored for biharmonic equations in Chapter 10, the modified Helmholtz equations in [222], and the Helmholtz equations in Chapters 7–9. For elliptic pseudo-boundaries, the stability analysis is explored in Chapter 6 for Dirichlet boundary conditions of Laplace's equation. New proof techniques without circulant matrices are solicited. In this chapter, we consider arbitrary pseudo-boundaries (*i.e.*, non-circular/non-elliptic) and arbitrary domains and derive the bounds of the Cond. The non-circular/non-elliptic pseudo-boundaries are reported numerically in Chapter 14 and [38, 139, 252]; the strict stability analysis is imperative, which is the goal of this chapter.

15.2 Relations Between FS and PS

The MFS and the method of particular solutions (MPS) are classified into the Trefftz family (see [169]), and they are linked *via* the addition theorem. The analysis of the MFS can not be explored deeply without the MPS (see [73, 74, 151, 163, 167, 177, 254]); the MFS and the MPS are twins in the Trefftz family. The MPS is introduced as an auxiliary method, but the focus of this chapter is the MFS.

To explore the stability analysis for non-circular/non-elliptic boundaries in the MFS, we should solicit the elliptic coordinates (ρ, θ) defined in (III.3) in Part III. The addition theorem (Lemma III.1) in elliptic coordinates is essential in stability analysis. The particular solutions (PS) in elliptic coordinates are given from [180],

$$u(\rho, \theta) = \alpha_0 + \sum_{k=1}^{\infty} e^{-kR}(\alpha_k \cosh k\rho \cos k\theta + \beta_k \sinh k\rho \sin k\theta) := P_n + R_n,$$

where the PS of degree n and the residuals are given by

$$P_n = P_n(\rho, \theta) = \alpha_0 + \sum_{k=1}^{n} e^{-kR}(\alpha_k \cosh k\rho \cos k\theta + \beta_k \sinh k\rho \sin k\theta), \tag{15.2.1}$$

$$R_n = R_n(\rho, \theta) = \sum_{k=n+1}^{\infty} e^{-kR}(\alpha_k \cosh k\rho \cos k\theta + \beta_k \sinh k\rho \sin k\theta), \tag{15.2.2}$$

where $\{\alpha_k\}_{k=0}^{n}$ and $\{\beta_k\}_{k=1}^{n}$ are the expansion coefficients. Choose the source nodes $Q_j = (r_j, \phi_j)$ with $r_j > \rho(\phi_j)|_\Gamma$. From (III.7) in Part III, we have

$$\ln|\overline{PQ_j}| = r_j + \ln\left(\frac{\sigma}{2}\right) - 2\sum_{n=1}^{\infty}\frac{1}{n}e^{-nr_j}(\cosh n\rho \cos n\theta \cos n\phi_j + \sinh n\rho \sin n\theta \sin n\phi_j).$$

Then, the linear combination u_N in (15.1.3) can be denoted as one of P_n in (15.2.1):

$$u_N = P_n(\rho, \theta) = \alpha_0 + \sum_{k=1}^{n} e^{-kR}(\alpha_k \cosh k\rho \cos k\theta + \beta_k \sinh k\rho \sin k\theta),$$

where the coefficients

$$\begin{aligned} &\alpha_0 = \sum_{j=1}^{N} c_j\left\{r_j + \ln\left(\frac{\sigma}{2}\right)\right\}, \quad \alpha_m = -2\sum_{j=1}^{N} c_j \frac{1}{m} e^{-m(r_j - R)}\cos(m\phi_j), \\ &\beta_m = -2\sum_{j=1}^{N} c_j \frac{1}{m} e^{-m(r_j - R)}\sin(m\phi_j), \end{aligned} \tag{15.2.3}$$

where $2n+1 \le N$. Denote (15.2.3) as the linear algebraic equations,

$$\mathbf{y} = \mathbf{E}\mathbf{x}, \tag{15.2.4}$$

where vectors $\mathbf{x} = (c_1, ..., c_N)^T \in \mathbf{R}^N$ and $\mathbf{y} = (\alpha_0, \alpha_1, ..., \alpha_n, \beta_1, ..., \beta_n)^T \in \mathbf{R}^{2n+1}$, and matrix $\mathbf{E} \in \mathbf{R}^{(2n+1)\times N}$ has the entries,

$$\begin{aligned} &E_{1,j} = r_j + \ln\left(\frac{\sigma}{2}\right), \quad j = 1, 2, ..., N, \\ &E_{k+1,j} = -\frac{2}{k} e^{-k\left(r_j - R\right)}\cos\left(k\phi_j\right), \quad j = 1, 2, ..., N, \quad k = 1, 2, ..., n, \\ &E_{k+n+1,j} = -\frac{2}{k} e^{-k\left(r_j - R\right)}\sin\left(k\phi_j\right), \quad j = 1, 2, ..., N, \quad k = 1, 2, ..., n. \end{aligned}$$

We intend to establish the one-to-one correspondence between coefficients $\mathbf{y}$ and $\mathbf{x}$ in (15.2.4). Then let $N = 2n+1$. The matrix in (15.2.4) is denoted as

$$\mathbf{E} = \begin{pmatrix} r_1 + \ln\left(\frac{\sigma}{2}\right) & r_2 + \ln\left(\frac{\sigma}{2}\right) & \cdots & r_N + \ln\left(\frac{\sigma}{2}\right) \\ -2e^{-(r_1-R)}\cos(\phi_1) & -2e^{-(r_2-R)}\cos(\phi_2) & \cdots & -2e^{-(r_N-R)}\cos(\phi_N) \\ -e^{-2(r_1-R)}\cos(2\phi_1) & -e^{-2(r_2-R)}\cos(2\phi_2) & \cdots & -e^{-2(r_N-R)}\cos(2\phi_N) \\ \vdots & \vdots & \vdots & \vdots \\ -\frac{2}{n}e^{-n(r_1-R)}\cos(n\phi_1) & -\frac{2}{n}e^{-n(r_2-R)}\cos(n\phi_2) & \cdots & -\frac{2}{n}e^{-n(r_N-R)}\cos(n\phi_N) \\ -2e^{-(r_1-R)}\sin(\phi_1) & -2e^{-(r_2-R)}\sin(\phi_2) & \cdots & -2e^{-(r_N-R)}\sin(\phi_N) \\ -e^{-2(r_1-R)}\sin(2\phi_1) & -e^{-2(r_2-R)}\sin(2\phi_2) & \cdots & -e^{-2(r_N-R)}\sin(2\phi_N) \\ \vdots & \vdots & \vdots & \vdots \\ -\frac{2}{n}e^{-n(r_1-R)}\sin(n\phi_1) & -\frac{2}{n}e^{-n(r_2-R)}\sin(n\phi_2) & \cdots & -\frac{2}{n}e^{-n(r_N-R)}\sin(n\phi_N) \end{pmatrix}. \tag{15.2.5}$$

Assume that matrix $\mathbf{E}$ is nonsingular. From (15.2.4) we have $\mathbf{x} = \mathbf{E}^{-1}\mathbf{y}$, where the inverse matrix $\mathbf{E}^{-1} \in \mathbf{R}^{N\times N}$. In fact, the following $(2n+1)$ functions are the PS of Laplace's equation in elliptic coordinates [180, p.98],

$$\left\{ r + \ln\left(\frac{\sigma}{2}\right), e^{-(r-R)}\cos(\phi), ..., \frac{e^{-n(r-R)}}{n}\cos(n\phi), e^{-(r-R)}\sin(\phi), ..., \frac{e^{-n(r-R)}}{n}\sin(n\phi) \right\}, \tag{15.2.6}$$

where r and ϕ are two independent variables. When the source nodes (r_j, ϕ_j) are chosen suitably, matrix $\mathbf{E}$ is nonsingular (*i.e.*, there exists no degenerate scale), so that there exists the one-to-one correspondence between FS and PS.

Below, let us discuss the source nodes (R, ϕ_j) on ellipse at $\rho = R$. First, choose (R, ϕ_j) with $0 \le \phi_j < \phi_{j+1} < 2\pi$ non-uniformly. The matrix $\mathbf{E}$ in (15.2.5) is expressed by $\mathbf{E} = \mathbf{BG}$, where the diagonal matrix $\mathbf{B} \in \mathbf{R}^{N\times N} (N = 2n+1)$ is given by

$$\mathbf{B} = \mathrm{diag}\left\{ R + \ln\left(\frac{\sigma}{2}\right), -1, -\frac{1}{2}, ..., -\frac{1}{n}, -1, -\frac{1}{2}, ..., -\frac{1}{n} \right\},$$

and matrix $\mathbf{G} \in \mathbf{R}^{N\times N}$ by

$$\mathbf{G} = \begin{pmatrix} 1 & 1 & \cdots & 1 \\ 2\cos\phi_1 & 2\cos\phi_2 & \cdots & 2\cos\phi_N \\ \vdots & \vdots & \vdots & \vdots \\ 2\cos(n\phi_1) & 2\cos(n\phi_2) & \cdots & 2\cos(n\phi_N) \\ 2\sin\phi_1 & 2\sin\phi_2 & \cdots & 2\sin\phi_N \\ \vdots & \vdots & \vdots & \vdots \\ 2\sin(n\phi_1) & 2\sin(n\phi_2) & \cdots & 2\sin(n\phi_N) \end{pmatrix}. \tag{15.2.7}$$

Based on the interpolation of trigonometric functions in Atkinson [12, p.178], matrix $\mathbf{G}$ in (15.2.7) is nonsingular. When

$$R + \ln\left(\frac{\sigma}{2}\right) = \ln\left(\frac{a_R + b_R}{2}\right) \neq 0, \quad i.e., a_R + b_R \neq 2, \tag{15.2.8}$$

matrix $\mathbf{B}$ is nonsingular. Since the determinant $|\mathbf{E}| = |\mathbf{B}| \times |\mathbf{G}| \neq 0$, matrix $\mathbf{E}$ is nonsingular under (15.2.8).

Next, suppose that the source nodes (R, ϕ_j) are located uniformly as $\phi_j = jh$ with $h = \frac{2\pi}{N}$. Denote matrix $\mathbf{G}_1 \in \mathbf{R}^{N\times N}$ as

$$\mathbf{G}_1 = \begin{pmatrix} 1 & \cos\phi_1 & \cdots & \cos(n\phi_1) & \sin\phi_1 & \cdots & \sin(n\phi_1) \\ 1 & \cos\phi_2 & \cdots & \cos(n\phi_2) & \sin\phi_2 & \cdots & \sin(n\phi_2) \\ \vdots & \vdots & \vdots & \vdots & \vdots & \vdots & \vdots \\ 1 & \cos\phi_N & \cdots & \cos(n\phi_N) & \sin\phi_N & \cdots & \sin(n\phi_N) \end{pmatrix}.$$

We have $\mathbf{G}_1\mathbf{G} = N\mathbf{I}$ and $\mathbf{G}^{-1} = \frac{1}{N}\mathbf{G}_1$, where matrix $\mathbf{I} \in \mathbf{R}^{N\times N}$ is the identity matrix. Then we obtain $\mathbf{x} = \mathbf{E}^{-1}\mathbf{y} = (\mathbf{BG})^{-1}\mathbf{y} = \mathbf{G}^{-1}\mathbf{B}^{-1}\mathbf{y} = \frac{1}{N}\mathbf{G}_1\mathbf{B}^{-1}\mathbf{y}$ to give

$$c_j = \frac{1}{N}\left\{\frac{\alpha_0}{R + \ln\left(\frac{\sigma}{2}\right)} - \sum_{m=1}^{n} m[\alpha_m \cos(mjh) + \beta_m \sin(mjh)]\right\}, \quad j = 1, 2, ..., N. \quad (15.2.9)$$

The coefficient relations in (15.2.9) are exactly as those for the source nodes on ellipses in (6.3.25).

15.3 Bounds of Cond for Non-Elliptic Pseudo-Boundaries

Consider the source nodes $Q(r_j, \phi_j)$ on the non-elliptic pseudo-boundaries Γ_R *via* some equal-distribution (*e.g.*, *via* angle or arc-length). Let $M = N$, and then the collocation equations (15.1.4) lead to

$$\sqrt{\triangle h_\ell}\sum_{j=1}^{N} c_j \Phi_j(\rho_\ell, \theta_\ell) = \sqrt{\triangle h_\ell}\, f(\rho_\ell, \theta_\ell), \quad \ell = 1, 2, ..., N. \quad (15.3.1)$$

The equation (15.3.1) is denoted by the following square system,

$$\mathbf{Ax} = \mathbf{b}, \quad (15.3.2)$$

where matrix $\mathbf{A} \in \mathbf{R}^{N\times N}$, and vectors $\mathbf{x} = \{c_1, c_2, ..., c_N\}^T \in \mathbf{R}^N$ and $\mathbf{b} \in \mathbf{R}^N$. On the other hand, by using the PS in (15.2.1), we have

$$\begin{aligned} &\sqrt{\triangle h_\ell}\{P_n(\rho_\ell, \theta_\ell)\} \\ &= \sqrt{\triangle h_\ell}\left\{\alpha_0 + \sum_{k=1}^{n} e^{-kR}(\alpha_k \cosh(k\rho_\ell)\cos(k\theta_\ell) + \beta_k \sinh(k\rho_\ell)\sin(k\theta_\ell))\right\} \\ &= \sqrt{\triangle h_\ell}\, f(\rho_\ell, \theta_\ell), \quad (\rho_\ell, \theta_\ell) \in \Gamma. \end{aligned} \quad (15.3.3)$$

The equation (15.3.3) is denoted by

$$\mathbf{P}\mathbf{y} = \mathbf{b}, \tag{15.3.4}$$

where matrix $\mathbf{P} \in \mathbf{R}^{N\times N}$ and vector $\mathbf{y} = \{\alpha_0, \alpha_1, ..., \alpha_n, \beta_1, ..., \beta_n\}^T \in \mathbf{R}^N$. The equation (15.3.3) (or (15.3.4)) is called the method of particular solutions (MPS) in [169]. For $N = 2n+1$, we have from (15.2.4)

$$\mathbf{P}\mathbf{E}\mathbf{x} = \mathbf{b}, \tag{15.3.5}$$

where matrix $\mathbf{E} \in \mathbf{R}^{N\times N}$ in (15.2.5). Comparing (15.3.5) and (15.3.2), we have

$$\mathbf{A} = \mathbf{P}\mathbf{E}, \tag{15.3.6}$$

and then the determinants

$$|\mathbf{A}| = |\mathbf{P}| \times |\mathbf{E}|. \tag{15.3.7}$$

Suppose that no degenerate scale exists (*e.g.*, the condition (15.2.8) holds for elliptic pseudo-boundaries). We have $|\mathbf{E}| \neq 0$. Since there always exists a unique solution for the MPS, matrix $\mathbf{P}$ is nonsingular with $|\mathbf{P}| \neq 0$. We have $|\mathbf{A}| \neq 0$ from (15.3.7), and conclude the nonsingular matrix $\mathbf{A}$. By following the proof in Lemma 6.4.1, we obtain the following lemma.

Lemma 15.3.1. *For (15.3.6) there exists the bound,* $\sigma_{\min}(\mathbf{A}) \geq \sigma_{\min}(\mathbf{P}) \times \sigma_{\min}(\mathbf{E})$, *where* $\sigma_{\min}(\mathbf{P}) > 0$, *and* $\sigma_{\min}(\mathbf{E}) > 0$ *if no degenerate scale exists for* $\mathbf{\Gamma}_R$.

Since matrix $\mathbf{A}$ is not circulant as in [71], the approaches in Chapters 2 and 3 are invalid for stability analysis. We solicit the matrix relation $\mathbf{A} = \mathbf{P}\mathbf{E}$ in (15.3.6) for stability analysis, which is called the matrix splitting in Chapter 6. Below, we will seek lower bounds of the minimal singular values: $\sigma_{\min}(\mathbf{P})$ and $\sigma_{\min}(\mathbf{E})$. For the collocation equations (15.3.3), we have

$$\mathbf{y}^T\mathbf{P}^T\mathbf{P}\mathbf{y} = \widehat{\int_\Gamma} P_n^2 ds = \overline{\|P_n\|}_{0,\Gamma}^2,$$

where $\widehat{\int_\Gamma}$ is an integration approximation of $\int_\Gamma$. We assume that

$$\overline{\|P_n\|}_{0,\Gamma}^2 = \widehat{\int_\Gamma} P_n^2 ds \asymp \int_\Gamma P_n^2 ds = \|P_n\|_{0,\Gamma}^2, \tag{15.3.8}$$

where the notation, "$a \asymp b$", denotes that there exist two constants $c_0\,(>0)$ and C independent of n such that $c_0 b \leq a \leq Cb$ $(b > 0)$. Denote an inscribed ellipse $S_{r_{\min}}$ of S with $\rho = r_{\min}$ (*i.e.*, $S_{r_{\min}} \subset S$). We have the following lemma.

Lemma 15.3.2. *Let the asymptote (15.3.8) hold. For the discrete matrix* $\mathbf{P}$ *by the MPS from (15.3.3), there exists the lower bound,*

$$\sigma_{\min}(\mathbf{P}) \geq c_0 e^{-n(R-r_{\min})} \geq c_0 e^{-N(R-r_{\min})/2}, \tag{15.3.9}$$

where $c_0\,(>0)$ *is a constant independent of* $n\left(=\frac{N-1}{2}\right)$.

Proof. Since the particular solutions $u = P_n(\rho, \theta)$ satisfy Laplace's equation, there exist the bounds from [195, p.189],

$$\|u\|_{0,\Gamma} \geq c_0 \|u\|_{\frac{1}{2},S} \geq c_0 \|u\|_{\frac{1}{2},S_{r_{\min}}} \geq c_0 \|u\|_{0,\Gamma_{\min}}, \tag{15.3.10}$$

where $\Gamma_{\min} = \partial S_{r_{\min}}$. Based on the integrals in elliptic coordinates in [180], we obtain from (15.2.1), (15.3.10) and the orthogonality of trigonometric functions

$$\begin{aligned}
\mathbf{y}^T\mathbf{P}^T\mathbf{P}\mathbf{y} &= \overline{\|P_n\|_{0,\Gamma}^2} \geq c_0 \|P_n\|_{0,\Gamma}^2 \geq c_0 \|P_n\|_{0,\Gamma_{\min}}^2 \\
&= c_0 \int_0^{2\pi} \left\{ \alpha_0 + \sum_{k=1}^{n} e^{-kR} (\alpha_k \cosh k r_{\min} \cos k\theta + \beta_k \sinh k r_{\min} \sin k\theta) \right\}^2 \\
&\qquad \times \sigma \sqrt{\sinh^2 r_{\min} + \sin^2\theta}\, d\theta \\
&\geq c_0 \int_0^{2\pi} \left\{ \alpha_0 + \sum_{k=1}^{n} e^{-kR} (\alpha_k \cosh k r_{\min} \cos k\theta + \beta_k \sinh k r_{\min} \sin k\theta) \right\}^2 d\theta \\
&\geq c_0 \left\{ \alpha_0^2 + \sum_{k=1}^{n} e^{-2kR} (\alpha_k^2 \cosh^2 k r_{\min} + \beta_k^2 \sinh^2 k r_{\min}) \right\} \\
&\geq c_0 e^{-2n(R - r_{\min})} \left\{ \alpha_0^2 + \sum_{k=1}^{n} (\alpha_k^2 + \beta_k^2) \right\} \geq c_0 e^{-2n(R - r_{\min})} \mathbf{y}^T\mathbf{y}.
\end{aligned}$$

This implies

$$\sigma_{\min}(\mathbf{P}) = \sqrt{\min_{\mathbf{y} \neq 0} \frac{\mathbf{y}^T\mathbf{P}^T\mathbf{P}\mathbf{y}}{\mathbf{y}^T\mathbf{y}}} \geq c_0 e^{-n(R - r_{\min})} \geq c_0 e^{-N(R - r_{\min})/2},$$

where we have used $n = \frac{N-1}{2}$. This gives the desired result (15.3.9). ■

To drive the lower bound of $\sigma_{\min}(\mathbf{E})$ is more challenging. From (15.2.6), define two auxiliary functions,

$$Q_n(r, \phi) = \left(r + \ln\left(\frac{\sigma}{2}\right) \right) a_0 + \sum_{k=1}^{n} \frac{e^{-k(r-R)}}{k} \{ a_k \cos(k\phi) + b_k \sin(k\phi) \}, \tag{15.3.11}$$

$$Q_n^-(r, \phi) = \sum_{k=1}^{n} \frac{e^{-k(r-R)}}{k} \{ a_k \cos(k\phi) + b_k \sin(k\phi) \}, \tag{15.3.12}$$

where a_k and b_k are coefficients. The function $Q_n^-(r, \phi)$ is a part of $Q_n(r, \phi)$ by removing the first term $\left(r + \ln(\frac{\sigma}{2}) \right) a_0$. The functions (15.3.11) are harmonic to satisfy Laplace's equation [180, p.98]. Since $\sigma_{\min}(\mathbf{E}) = \sigma_{\min}(\mathbf{E}^T)$, we consider the transpose matrix $\mathbf{E}^T$. Let $Q_n(r, \phi)|_{\Gamma_R} = g(r, \phi)$, and establish the following collocation equations at source nodes (r_j, ϕ_j),

$$Q_n(r_j, \phi_j) = \left(r_j + \ln\left(\tfrac{\sigma}{2}\right)\right) a_0 + \sum_{k=1}^{n} \tfrac{e^{-k(r_j - R)}}{k} \{a_k \cos(k\phi_j) + b_k \sin(k\phi_j)\} = g(r_j, \phi_j),$$
$$j = 1, 2, ..., 2n+1. \tag{15.3.13}$$

The pseudo-collocation equations (15.3.13) are used for analysis, but not for real computation. Denote vector $\mathbf{z} = \{a_0, a_1, ..., a_n, b_1, ..., b_n\}^T$. We also denote (15.3.13) by linear algebraic systems,

$$\mathbf{E}^T \mathbf{z} = \mathbf{g}, \tag{15.3.14}$$

where matrix $\mathbf{E}$ is given in (15.2.5) and the known vector $\mathbf{g} \in \mathbf{R}^{2n+1}$. Similarly to (15.3.8), we also assume that

$$\widehat{\int_{\Gamma_R}} Q_n^2 \, ds \asymp \int_{\Gamma_R} Q_n^2 \, ds, \tag{15.3.15}$$

where $\widehat{\int}_{\Gamma_R}$ is an integration approximation of $\int_{\Gamma_R}$ by a quadrature rule. Note that the function $\left(r + \ln\left(\frac{\sigma}{2}\right)\right)$ is linearly independent of the other $2n$ functions in (15.2.6). For a general pseudo-boundary $\mathbf{\Gamma}_R$, when no degenerate scale exists, we conclude $\int_{\Gamma_R} \left(r + \ln\left(\frac{\sigma}{2}\right)\right)^2 d\ell > 0$ and $\int_{\Gamma_R} (Q_n^-(r, \phi))^2 d\ell > 0$. Otherwise, the singularity as $\sigma_{\min}(\mathbf{E}) = 0$ occurs from (15.3.7), and there must exist a degenerate scale. Moreover, similarly to [173] and [162, pp.119–121], we may assume

$$\begin{aligned}
\int_{\Gamma_R} Q_n^2(r, \phi) \, d\ell &\geq c_0 n^{-\mu} e^{-\nu n} \left\{ a_0^2 \int_{\Gamma_R} \left(r + \ln\left(\frac{\sigma}{2}\right)\right)^2 d\ell + \int_{\Gamma_R} (Q_n^-(r, \phi))^2 d\ell \right\} \\
&\geq c_0 n^{-\mu} e^{-\nu n} \left\{ a_0^2 + \int_{\Gamma_R} (Q_n^-(r, \phi))^2 d\ell \right\},
\end{aligned} \tag{15.3.16}$$

where two parameters $\mu \geq 0$ and $\nu \geq 0$. For an elliptic pseudo-boundary $\mathbf{\Gamma}_R$ with radius R, we have from (15.3.11) at $r_j \equiv R, \forall j$

$$\begin{aligned}
\int_{\Gamma_R} Q_n^2(r, \phi) \, d\ell &= \int_{\Gamma_R} \left\{ \left(R + \ln\left(\frac{\sigma}{2}\right)\right) a_0 + \sum_{k=1}^{n} \frac{1}{k} (a_k \cos(k\phi) + b_k \sin(k\phi)) \right\}^2 d\ell \\
&\geq c_0 \left\{ \int_0^{2\pi} \left\{ \ln\left(\frac{a_R + b_R}{2}\right) a_0 + \sum_{k=1}^{n} \frac{1}{k} (a_k \cos(k\phi) + b_k \sin(k\phi)) \right\}^2 d\phi \right\} \\
&= c_0 \left\{ 2\pi \left| \ln\left(\frac{a_R + b_R}{2}\right) \right|^2 a_0^2 + \pi \sum_{k=1}^{n} \frac{1}{k^2} (a_k^2 + b_k^2) \right\} \\
&\geq c_0 \left\{ a_0^2 + \int_{\Gamma_R} (Q_n^-(r, \phi))^2 d\ell \right\},
\end{aligned} \tag{15.3.17}$$

where we have used $a_R + b_R \neq 2$ from (15.2.8). The equation (15.3.17) indicates both $\mu = 0$ and $\nu = 0$ in (15.3.16).

Lemma 15.3.3. *Suppose that for* Γ_R*, no degenerate scale exists, and that there exist two parameters* $\mu \geq 0$ *and* $v \geq 0$ *such that the lower bound (15.3.16) holds. Also, assume that the equivalence (15.3.15) holds. Then for the source nodes* (r_j, ϕ_j)*, there exists the lower bound of the minimal singular value of matrix* $\mathbf{E}$ *in (15.2.5),*

$$\sigma_{\min}(\mathbf{E}) \geq c_0 \frac{e^{-\frac{v}{2}n}}{n^{\frac{1}{2}(1+\mu)}}, \tag{15.3.18}$$

where $c_0\,(>0)$ *is a constant independent of* $N\,(=2n+1)$*.*

Proof. We have from (15.3.14)

$$\begin{aligned}
\mathbf{z}^T\mathbf{E}\mathbf{E}^T\mathbf{z} &= \sum_{j=1}^{2n+1}\left\{\left(r_j + \ln\left(\frac{\sigma}{2}\right)\right)a_0 + \sum_{k=1}^{n}\frac{e^{-k(r_j-R)}}{k}(a_k\,\cos(k\phi_j) + b_k\,\sin(k\phi_j))\right\}^2 \\
&\geq \frac{1}{\max_j h_j}\sum_{j=1}^{2n+1} h_j\left\{\left(r_j + \ln\left(\frac{\sigma}{2}\right)\right)a_0 + \sum_{k=1}^{n}\frac{e^{-k(r_j-R)}}{k}(a_k\,\cos(k\phi_j) + b_k\,\sin(k\phi_j))\right\}^2 \\
&\geq c_0 N \widehat{\int_{\Gamma_R}} Q_n^2(r,\phi)\,d\ell,
\end{aligned} \tag{15.3.19}$$

where h_j are the meshspacings on Γ with $h_j \asymp \frac{1}{N}$, and $c_0\,(>0)$ is a constant independent of $N\,(=2n+1)$. Then from the assumption (15.3.15), there exists the lower bound,

$$\mathbf{z}^T\mathbf{E}\mathbf{E}^T\mathbf{z} \geq c_0 N \widehat{\int_{\Gamma_R}} Q_n^2(r,\phi)\,d\ell \geq c_0 N \int_{\Gamma_R} Q_n^2(r,\phi)\,d\ell. \tag{15.3.20}$$

Note that the factor $e^{-k(r_j-R)} \geq c_0$ with $r_j \leq R$ in (15.3.19). Denote by $\hat{\Gamma}_R$ the elliptic boundary with radius $r = R$ satisfying $r_j \leq R$. We have from (15.3.20), (15.3.16), and Lemma 15.3.4 given later

$$\begin{aligned}
\mathbf{z}^T\mathbf{E}\mathbf{E}^T\mathbf{z} &\geq c_0 N \int_{\Gamma_R} Q_n^2(r,\phi)\,d\ell \geq c_0 N n^{-\mu} e^{-vn}\left\{a_0^2 + \int_{\hat{\Gamma}_R}(Q_n^-(r,\phi))^2\,d\ell\right\} \\
&\geq c_0 N n^{-\mu} e^{-vn}\left\{a_0^2 + \int_0^{2\pi}\left\{\sum_{k=1}^{n}\frac{1}{k}(a_k\,\cos(k\phi) + b_k\,\sin(k\phi))\right\}^2 d\phi\right\} \\
&\geq c_0 N n^{-\mu} e^{-vn}\left\{a_0^2 + \sum_{k=1}^{n}\frac{1}{k^2}(a_k^2 + b_k^2)\right\} \\
&\geq c_0 N n^{-\mu} e^{-vn}\frac{1}{n^2}\left\{a_0^2 + \sum_{k=1}^{n}(a_k^2 + b_k^2)\right\} \geq c_0 \frac{e^{-vn}}{n^{(1+\mu)}}\mathbf{z}^T\mathbf{z}.
\end{aligned}$$

This gives

$$\sigma_{\min}(\mathbf{E}) = \sigma_{\min}(\mathbf{E}^T) = \sqrt{\min_{\mathbf{z}\neq 0} \frac{\mathbf{z}^T\mathbf{E}\mathbf{E}^T\mathbf{z}}{\mathbf{z}^T\mathbf{z}}} \geq c_0 \frac{e^{-\frac{\nu}{2}n}}{n^{\frac{1}{2}(1+\mu)}}.$$

■

To complete the proof of Lemma 15.3.3, we prove the following lemma.

Lemma 15.3.4. *Consider the source nodes $Q_j = (r_j, \phi_j)$. Denote the elliptic boundary $\hat{\Gamma}_R$ with radius $r = R$ satisfying $r_j \leq R$. For the functions $Q_n^-(r,\phi)$ in (15.3.12), there exists the lower bound, $\| Q_n^- \|_{0,\Gamma_R} \geq c_0 \| Q_n^- \|_{0,\hat{\Gamma}_R}$.*

Proof. The functions $Q_n^-(r,\phi)$ in (15.3.12) are the PS for exterior problems [180]. Denote the unbounded domain S_R^∞ with the interior boundary Γ_R, and the unbounded domain $\hat{S}_R^\infty$ with the interior ellipse boundary $\hat{\Gamma}_R$ at radius $r = R$ satisfying $r_j \leq R$. We have $\hat{S}_R^\infty \subset S_R^\infty$. The functions $Q_n^-(r,\phi)$ far from S may be simply expressed in polar coordinates as

$$Q_n^- = Q_n^-(r,\phi) = \sum_{k=1}^{n} \frac{1}{k}\left(\frac{R^\circ}{r^\circ}\right)^k \left\{a_k^\circ \cos(k\phi^\circ) + b_k^\circ \sin(k\phi^\circ)\right\} := H_n(r^\circ,\phi^\circ), \text{ as } r^\circ \gg R^\circ, \tag{15.3.21}$$

where (r°, ϕ°) are the polar coordinates with $r^\circ \asymp e^r$, constant $R^\circ \asymp e^R$, and $\{a_k^\circ, b_k^\circ\}$ are coefficients. Then for $H_n \, (= Q_n^-)$ missing the leading term, $\left(r + \ln\left(\frac{\sigma}{2}\right)\right) \asymp \ln r^\circ$, there exists the bound

$$|H_n(r^\circ,\phi^\circ)| \leq C\frac{1}{r^\circ}, \text{ as } r^\circ \to \infty. \tag{15.3.22}$$

Denote the operator $\nabla = \frac{\partial}{\partial x}\vec{i} + \frac{\partial}{\partial y}\vec{j}$. The weighted Sobolev norms are defined for the exterior domain S_R^∞ (see Sauter and Schwab [210, pp.82, 94]),

$$\|u(r^\circ)\|_{1,S_R^\infty} = \left\{\iint_{S_R^\infty} \left\{|\nabla u(r^\circ)|^2 + \frac{u^2(r^\circ)}{1+(r^\circ)^2}\right\} ds\right\}^{\frac{1}{2}},$$

$$|u(r^\circ)|_{1,S_R^\infty} = \left\{\iint_{S_R^\infty} |\nabla u(r^\circ)|^2 ds\right\}^{\frac{1}{2}}.$$

Under (15.3.22) and the Dirichlet condition $u(r^\circ)|_{\Gamma_R} = g^\circ$, there exists the equivalence from [210, p.95] and Amrouche *et al.* [7],

$$\|u(r^\circ)\|_{1,S_R^\infty} \asymp |u(r^\circ)|_{1,S_R^\infty}. \tag{15.3.23}$$

Below, for Q_n^- in (15.3.21), we will prove the bounded semi-norms on S_R^∞: $\| Q_n^- \|_{\frac{1}{2},S_R^\infty} \leq C$. Denote by $\Gamma_{r_{\text{hug}}}$ the circle with a huge radius $r_{\text{hug}} \gg R^\circ$. There exists the limit from (15.3.21)

$$\int_{\Gamma_{r_{\text{hug}}}} H_n \frac{\partial H_n}{\partial v}\, d\ell = \int_{\Gamma_{r_{\text{hug}}}} H_n(r^\circ, \phi^\circ) \frac{\partial}{\partial r^\circ} H_n(r^\circ, \phi^\circ)\, d\ell \tag{15.3.24}$$
$$= -\pi \sum_{k=1}^{n} \frac{1}{k} \left\{ \frac{R^\circ}{r_{\text{hug}}} \right\}^{2k} \{(a_k^\circ)^2 + (b_k^\circ)^2\} \to 0, \quad \text{as } r_{\text{hug}} \to \infty,$$

where v is the exterior normal of Γ_R. Since Q_n^- are harmonic functions, we have from (15.3.24) and the Green formula on an annular domain with the interior boundary Γ_R and the exterior boundary $\Gamma_{r_{\text{hug}}}$

$$\|\nabla Q_n^-\|^2_{0,S_R^\infty} = \int_{\Gamma_R} Q_n^- \frac{\partial Q_n^-}{\partial v}\, d\ell + \lim_{r_{\text{hug}} \to \infty} \int_{\Gamma_{r_{\text{hug}}}} H_n \frac{\partial H_n}{\partial r^\circ}\, d\ell = \int_{\Gamma_R} Q_n^- \frac{\partial Q_n^-}{\partial v}\, d\ell \le C. \tag{15.3.25}$$

From (15.3.23) and (15.3.25), there exist the bounds, $\|Q_n^-\|_{k,S_R^\infty} \le C, k = 0, 1$, to give

$$\|Q_n^-\|_{\frac{1}{2},S_R^\infty} \le \{\|Q_n^-\|_{0,S_R^\infty} \|Q_n^-\|_{1,S_R^\infty}\}^{\frac{1}{2}} \le C.$$

Similarly to (15.3.10) we have

$$\|Q_n^-\|_{0,\Gamma_R} \ge c_0 \|Q_n^-\|_{\frac{1}{2},S_R^\infty} \ge c_0 \|Q_n^-\|_{\frac{1}{2},\hat{S}_R^\infty} \ge c_0 \|Q_n^-\|_{0,\hat{\Gamma}_R}.$$

This completes the proof of Lemma 15.3.4. ■

Consider the source nodes (r_j, ϕ_j). Let $R = \max_j r_j$, and denote ellipse ℓ_R at $\rho = R$. Denote two semi-axes of ellipse ℓ_R at $\rho = R$ by $a_R = \sigma \cosh R$ and $b_R = \sigma \sinh R$; we have $e^R = (a_R + b_R)/\sigma$ from Remark 6.3.1 in Chapter 6. Similarly, for ellipse $\ell_{\min}$ with $\rho = r_{\min}$, denote $a_{\min} = \sigma \cosh r_{\min}$ and $b_{\min} = \sigma \sinh r_{\min}$. From Lemmas 15.3.1–15.3.3, we have the following key lemma.

Lemma 15.3.5. *Assume the asymptotes (15.3.8) and (15.3.15) hold. Suppose that for Γ_R, no degenerate scale exists, and that there exist two parameters $\mu \ge 0$ and $v \ge 0$ such that the bound (15.3.16) holds. For the source nodes $Q_j = (r_j, \phi_j)$, there exists the lower bound for matrix $\mathbf{A}$ from (15.3.1),*

$$\sigma_{\min}(\mathbf{A}) \ge \sigma_{\min}(\mathbf{P}) \times \sigma_{\min}(\mathbf{E}) \ge c_0 \frac{1}{N^{\frac{1}{2}(1+\mu)}} e^{-N\left(R - r_{\min} + \frac{v}{2}\right)/2}$$
$$= c_0 \frac{1}{N^{\frac{1}{2}(1+\mu)}} \left(\frac{a_{\min} + b_{\min}}{a_R + b_R} \times e^{-\frac{v}{2}} \right)^{\frac{N}{2}},$$

where $\mu \ge 0$ and $v \ge 0$.

We have $\sigma_{\max}(\mathbf{A}) \le C\sqrt{N}$ from (6.4.22), and give the following theorem.

Theorem 15.3.1. *Let the conditions in Lemma 15.3.5 hold. For a general pseudo-boundary* Γ_R*, there exists the bound,*

$$\mathrm{Cond}(\mathbf{A}) = \frac{\sigma_{\max}(\mathbf{A})}{\sigma_{\min}(\mathbf{A})} \le CN^{\left(1+\frac{\mu}{2}\right)} e^{N(R-r_{\min}+\frac{\nu}{2})/2} \le CN^{\left(1+\frac{\mu}{2}\right)} \left(\frac{a_R+b_R}{a_{\min}+b_{\min}} \times e^{\frac{\nu}{2}}\right)^{\frac{N}{2}}, \tag{15.3.26}$$

where $\mu \ge 0$ *and* $\nu \ge 0$.

The parameters μ and ν in (15.3.18) may be found numerically. From the computed results in [252, Section 4], the parameters $\mu = 0, 1$ and $\nu = 0$ are discovered, and the Cond estimates (15.3.26) may be simplified as

$$\mathrm{Cond}(\mathbf{A}) \le CN^{\left(1+\frac{\mu}{2}\right)} e^{N(R-r_{\min})/2} \le CN^{\left(1+\frac{\mu}{2}\right)} \left(\frac{a_R+b_R}{a_{\min}+b_{\min}}\right)^{\frac{N}{2}}. \tag{15.3.27}$$

Note that the estimates (15.3.27) are consistent with Theorem 6.4.2 for the elliptic pseudo-boundaries in Chapter 6.

The estimates in (15.3.26) involving semi-axes of two ellipses may not be convenient in application. Below, we provide a simplified estimate. Suppose that the domain boundary Γ is star-like, which can be denoted by a single-valued function $\rho = \rho(\theta)$, where (ρ, θ) are polar coordinates. The outside pseudo-boundary Γ_R can also be chosen as the other single-valued function $\bar{\rho} = \bar{\rho}(\theta)$ $(> \rho(\theta))$. Denote $\rho_{\min} \le \rho \le \rho_{\max}$ and $\bar{\rho}_{\min} \le \bar{\rho} \le \bar{\rho}_{\max}$. There exist bounds,

$$\beta_1 = \frac{a_R+b_R}{\bar{\rho}_{\max}+\bar{\rho}_{\min}} \ge 1, \quad \beta_2 = \frac{\rho_{\max}+\rho_{\min}}{a_{\min}+b_{\min}} \ge 1.$$

Theorem 15.3.2. *Let the conditions in Lemma 15.3.5 hold. Suppose that the domain boundary* Γ *and the pseudo-boundary* Γ_R *are star-like, denoted uniquely by* $(\rho(\theta), \theta)$ *and* $(\bar{\rho}(\theta), \theta)$ *with* $\rho(\theta) < \bar{\rho}(\theta)$ *in polar coordinates, respectively. Then there exists the simplified bound,*

$$\mathrm{Cond}(\mathbf{A}) \le CN^{\left(1+\frac{\mu}{2}\right)} \left(\frac{\bar{\rho}_{\max}+\bar{\rho}_{\min}}{\rho_{\max}+\rho_{\min}}\right)^{(1+\gamma)N/2}, \tag{15.3.28}$$

where $\rho_{\min} \le \rho \le \rho_{\max}$, $\bar{\rho}_{\min} \le \bar{\rho} \le \bar{\rho}_{\max}$ *and* $\gamma = \frac{\ln(\beta_1\beta_2)+\frac{\nu}{2}}{\ln\left(\frac{\bar{\rho}_{\max}+\bar{\rho}_{\min}}{\rho_{\max}+\rho_{\min}}\right)} \ge 0$. *Moreover, there exists* $0 < \delta \ll 1$ *such that*

$$\mathrm{Cond}(\mathbf{A}) \le C\left(\frac{a_R+b_R}{a_{\max}+b_{\min}}\right)^{(1+\gamma)N/2+\delta} = O\left(\left(\frac{\bar{\rho}_{\max}+\bar{\rho}_{\min}}{\rho_{\max}+\rho_{\min}}\right)^{\beta N}\right), \tag{15.3.29}$$

where $\beta = (1+\gamma)/2+\delta > \frac{1}{2}$.

Proof. We have from (15.3.26),

$$\begin{aligned}\mathrm{Cond}(\mathbf{A}) &\le CN^{\left(1+\frac{\mu}{2}\right)}\left(\frac{a_R+b_R}{a_{\min}+b_{\min}}\times e^{\frac{\nu}{2}}\right)^{\frac{N}{2}}\\ &= CN^{\left(1+\frac{\mu}{2}\right)}\left(\beta_1\beta_2 e^{\frac{\nu}{2}}\frac{\bar{\rho}_{\max}+\bar{\rho}_{\min}}{\rho_{\max}+\rho_{\min}}\right)^{\frac{N}{2}} = CN^{\left(1+\frac{\mu}{2}\right)}\left(\frac{\bar{\rho}_{\max}+\bar{\rho}_{\min}}{\rho_{\max}+\rho_{\min}}\right)^{(1+\gamma)N/2}.\end{aligned}$$

This is the first desired result (15.3.28), and then the second result (15.3.29) follows. ■

For (15.3.29), the power $\beta \in \left(\frac{1}{2}, 1\right]$ is found from the numerical experiments in [252]. For general pseudo-boundaries, the Cond also has an exponential growth rate, which is coincident with circular/elliptic pseudo-boundaries in Chapters 2–6.

The Cond estimates above may be extended to exterior problems. Denote by Γ the interior boundary of an exterior domain S^{∞}. The pseudo-boundary Γ_R is inside Γ. Also denote $\bar{\rho}_{\max} = \max\ \rho|_{\Gamma_R}$ and $\bar{\rho}_{\min} = \min\ \rho|_{\Gamma_R}$, and then $\bar{\rho}_{\max} + \bar{\rho}_{\min} < \rho_{\max} + \rho_{\min}$. The equation (15.3.29) is modified for exterior problems

$$\mathrm{Cond}(\mathbf{A}) = O\left(\left(\frac{\rho_{\max}+\rho_{\min}}{\bar{\rho}_{\max}+\bar{\rho}_{\min}}\right)^{\beta N}\right), \quad \beta > \frac{1}{2}. \tag{15.3.30}$$

Theorems 15.3.1 and 15.3.2 have been verified in [252] numerically. For singular solutions, numerical comparisons are also made for amoeba-like domains in [252] for different pseudo-boundaries *via* the sensitivity index.

Chapter 16

Singularity Problems from Source Functions; Removal Techniques

Consider the Dirichlet problem for Laplace's/Poisson's equation in a bounded simply-connected domain S. The source function $q\ \ln|\overline{PQ^*}|$ is a fundamental solution (FS), and it can be found in many physical problems. The singularity occurs when the boundary value data is affected by $q\ \ln|\overline{PQ^*}|$ as the source node Q^* is located near the boundary $\Gamma\,(=\partial S)$. So far, there is no comprehensive study on this kind of singularity. In this chapter, the solution singularity is explored and the reduced convergence rates are derived for the method of particular solutions (MPS) and the method of fundamental solutions (MFS). Classic domains, such as disks, ellipses, and polygons, are discussed for analysis and computation. For this new kind of solution singularity, the convergence rates of the MFS and the MPS are very low. The errors caused by numerical integration are critical to the solution's accuracy. A new analytic framework for the collocation Trefftz method (CTM) involving numerical integration is established in this chapter; this is an advanced development of previous chapters and [169]. Since the numerical solutions are poor in accuracy, removal techniques are essential in applications. New removal techniques are proposed for a node Q^* located near Γ. In this chapter, an additional FS, as $d_0\ \ln|\overline{PQ_0}|$, is added to the original FS in the traditional MFS, and the point charge $d_0\,(=q)$ and the source node Q_0 are unknowns to be sought by nonlinear solvers (such as the secant method). When the source node Q^* is located inside S but near Γ, both simple domains (such as disks, ellipses, and squares) and complicated domains (such as amoeba-like domains) are studied. The validity of the new removal techniques is supported by numerical experiments. The removal techniques proposed in this chapter may also be applied to solve source identification problems. A comprehensive study has been completed in this chapter for the solitary source function $q\ \ln|\overline{PQ^*}|$ as the source node Q^* is located near Γ. The materials of this chapter are adapted from [253].

DOI: 10.1051/978-2-7598-3171-5.c016
© Science Press, EDP Sciences, 2023

16.1 Introduction

For elliptic boundary value problems, singularities are caused by Case A: non-smooth solution domains, and case B: non-smooth data in the boundary conditions and the non-homogenous term. The singularities are studied systematically for non-smooth domains in Grisvard [91], and the singularity from corners and non-smooth boundary data is reported for Laplace's equation in Chapters 1 and 5, and Li *et al.* [168] and [169, Chapter 11]. The singularity can cause the reduced convergence rates of numerical solutions, and the removal techniques for corner singularity are explored in Li [146]. Consider a 2D bounded simply-connected domain S with boundary $\Gamma (= \partial S)$. In this chapter, we choose the Dirichlet boundary condition for Laplace's/Poisson's equation,

$$\Delta u(P) = 2\pi q \delta\Big(\big|\overline{PQ^*}\big|\Big) \text{ in } S, u = f \text{ on } \Gamma, \tag{16.1.1}$$

where $P \in S$, the source node $Q^* \notin \Gamma$, q is the point charge (or source) at Q^*, and $\delta(|\overline{PQ^*}|)$ is the Dirac-delta function at node Q^*. The Poisson equation is given by (16.1.1), when Q^* is located inside S (*i.e.*, inside Γ). When Q^* is located outside S, however, the equation (16.1.1) leads to the Laplace equation,

$$\Delta u(P) = 0 \text{ in } S, u = f \text{ on } \Gamma. \tag{16.1.2}$$

Denote the source function

$$u^* = u^*(P) = q \ln|\overline{PQ^*}|, \tag{16.1.3}$$

where the source node $Q^*(\notin \Gamma)$ is located near Γ. The source function (16.1.3) satisfies Laplace's/Poisson's equation (16.1.1). The Poisson equation (16.1.1) with $Q^* \in S$ is discussed in Section 16.7. The function $u^*(P)$ is a fundamental solution, which is also called the potential function in Morse and Feshbach [193] and Tikhonov and Samarskii [223], such as in heat transfer problems for the temperature field from the point heat source, potential problems for the flow potential from the point liquid source, and elastostatics problems for the electric potential from the point electric charge. From the source function, the Dirichlet boundary data in (16.1.1) are generated by (16.1.3) as $f = u^*|_\Gamma$. Then the singularity of solutions occurs due to Q^* near Γ, and the reduced convergence rates are incurred in numerical solutions. The function (16.1.3) was first employed by Chen *et al.* [38] to generate the Dirichlet boundary data and used for testing the MFS-QR in Antunes [8]. More numerical results are reported in Chapter 14 and Zhang *et al.* [251, 252]. This is a new kind of singularity problem different from those in [91, 146, 168, 169]. So far, there exists no comprehensive study on this new kind of singularity, which is the goal of this chapter.

The solution singularity of source functions is explored, and the reduced convergence rates by the MPS and the MFS are derived. Let δ denote the distance of Q^* from the boundary Γ. For polygonal domains, the low convergence rates as $O\Big(\frac{1}{\sqrt{\delta} n}\Big)$ and $O\Big(\frac{1}{\sqrt{\delta} N}\Big)$ are obtained, where $(2n+1)$ and N are the numbers of particular solutions (PS) and FS being used, respectively. However, for disk and elliptic domains, sharper convergence rates can be derived. For low convergence rates, the errors caused by numerical integration are critical to the solution's accuracy. A new analytic framework for the collocation Trefftz method (CTM) involving numerical integration is established in this chapter; this is an advanced development of the book [169]. Numerical experiments are carried out in [253] to verify the analysis made.

We choose the elliptic coordinates (ρ, θ) defined in (III.3). The PS in elliptic coordinates is given from [180],

$$u(\rho,\theta) = \alpha_0 + \sum_{k=1}^{\infty} e^{-k\rho_0}(\alpha_k \cosh k\rho \cos k\theta + \beta_k \sinh k\rho \sin k\theta) := P_n + R_n, \quad (16.1.4)$$

where ρ_0 is a parameter, and the PS of degree n and the residuals are given by

$$P_n = P_n(\rho,\theta) = \alpha_0 + \sum_{k=1}^{n} e^{-k\rho_0}(\alpha_k \cosh k\rho \cos k\theta + \beta_k \sinh k\rho \sin k\theta), \quad (16.1.5)$$

$$R_n = R_n(\rho,\theta) = \sum_{k=n+1}^{\infty} e^{-k\rho_0}(\alpha_k \cosh k\rho \cos k\theta + \beta_k \sinh k\rho \sin k\theta), \quad (16.1.6)$$

where $\{\alpha_k\}_{k=0}^n$ and $\{\beta_k\}_{k=1}^n$ are the expansion coefficients. Let $\mathbf{\Gamma}$ be divided into small $\mathbf{\Gamma}_\ell$ with the meshspacings $\triangle h_\ell$, *i.e.*, $\mathbf{\Gamma} = \bigcup_{\ell=1}^M \mathbf{\Gamma}_\ell$. For simplicity, choose (ρ_ℓ, θ_ℓ) as the midpoint of $\mathbf{\Gamma}_\ell$. By using the PS in (16.1.5), we have the collocation equations from the Dirichlet condition in (16.1.2),

$$\begin{aligned}&\sqrt{\triangle h_\ell}\{P_n(\rho_\ell,\theta_\ell)\}\\ &= \sqrt{\triangle h_\ell}\Big\{\alpha_0 + \sum_{k=1}^{n} e^{-k\rho_0}(\alpha_k \cosh(k\rho_\ell)\cos(k\theta_\ell) + \beta_k \sinh(k\rho_\ell)\sin(k\theta_\ell))\Big\} \quad (16.1.7)\\ &= \sqrt{\triangle h_\ell}\, f(\rho_\ell,\theta_\ell),\ (\rho_\ell,\theta_\ell) \in \mathbf{\Gamma}_\ell,\ \ell = 1, 2, \ldots, M.\end{aligned}$$

The equations (16.1.7) are denoted by $\mathbf{Py} = \mathbf{b}$, where matrix $\mathbf{P} \in \mathbf{R}^{M\times N}(M \geq N)$, and vectors $\mathbf{y}\,(\in \mathbf{R}^N) = \{\alpha_0, \alpha_1, \beta_1, \ldots, \alpha_n, \beta_n\}^T$ and $\mathbf{b}\,(\in \mathbf{R}^M)$ with $N = 2n+1$. The algorithms of (16.1.7) are called the method of particular solutions (MPS).

Let V_n be the set of the PS in (16.1.5). By the Trefftz method (TM) in [169], we seek $u_n \in V_n$ such that

$$I(u_n) = \min_{v\in V_n} I(v), \quad I(v) = \int_\Gamma (v-f)^2. \quad (16.1.8)$$

When the integral in (16.1.8) involves a numerical approximation, the TM reads: Seek $\hat{u}_n \in V_n$ such that

$$\widehat{I}(\hat{u}_n) = \min_{v\in V_n} \widehat{I}(v), \quad \widehat{I}(v) = \widehat{\int_\Gamma} (v-f)^2, \quad (16.1.9)$$

where $\widehat{\int}_\Gamma$ is a numerical approximation of $\int_\Gamma$. The collocation equations (16.1.7) are equivalent to (16.1.9) involving numerical integration.

In the MFS, the source nodes are located on a smooth closed pseudo-boundary Γ_R outside S. Let $P = (\rho, \theta)$ and source nodes $Q_j = (R_j, \phi_j) \in \Gamma_R$. Choose the FS,

$$\Phi_j(\rho, \theta) = \ln|\overline{PQ_j}|, \quad |\overline{PQ_j}| = \sqrt{R_j^2 + \rho^2 - 2R_j\rho\,\cos(\theta - \phi_j)}.$$

We use a linear combination of FS,

$$v_N = \sum_{j=1}^{N} c_j \ln|\overline{PQ_j}| = \sum_{j=1}^{N} c_j \Phi_j(\rho, \theta), \tag{16.1.10}$$

where c_j are the coefficients. We then obtain the collocation equations,

$$\sqrt{\triangle h_\ell} \sum_{j=1}^{N} c_j \Phi_j(\rho_\ell, \theta_\ell) = \sqrt{\triangle h_\ell}\, f(\rho_\ell, \theta_\ell), \quad \ell = 1, 2, \ldots, M, \tag{16.1.11}$$

where $M \geq N$. The equation (16.1.11) leads to an overdetermined system, $\mathbf{F}\mathbf{x} = \mathbf{b}$, where matrix $\mathbf{F} \in \mathbf{R}^{M \times N}(M \geq N)$, and vectors $\mathbf{x} = (c_1, c_2, \ldots, c_N)^T \in \mathbf{R}^N$ and $\mathbf{b} \in \mathbf{R}^N$.

This chapter is organized as follows. In the next section, an analytical framework for the CTM involving numerical integration is established. In Sections 16.3 and 16.4, the convergence rates are derived for the singularity solutions caused by the source function (16.1.3) in circular, elliptic, and polygonal domains. In Section 16.5, new removal techniques are developed, and in Section 16.6, numerical experiments are carried out to support the analysis and the removal techniques. In Section 16.7, the amoeba-like domains are discussed, and the removal techniques are linked to source identification problems. In the last section, a few concluding remarks are made.

16.2 Analytical Framework for CTM in [169]

First, we propose the analytical framework for the error bounds involving numerical integration in (16.1.9) by following the finite element method (FEM) in [68, 219]. Denote

$$(u, v) = \int_\Gamma \omega uv, \quad \|v\| = \|v\|_{0,\Gamma} = \left\{ \int_\Gamma \omega v^2 \right\}^{\frac{1}{2}}, \tag{16.2.1}$$

where the weight $\omega > 0$. There exists the inequality

$$(u, v) \leq \|u\| \|v\|. \tag{16.2.2}$$

Let V_n denote the set of functions (16.1.5). The solution $u_n \in V_n$ is expressed as

$$(u_n, v) = (f, v), \quad \forall v \in V_n, \; e.g., \quad \int_\Gamma \omega u_n v = \int_\Gamma \omega f v, \quad \forall v \in V_n. \tag{16.2.3}$$

Lemma 16.2.1. *There exists the bound,*

$$\|u - u_n\| \leq 2 \inf_{v \in V_n} \|u - v\|. \tag{16.2.4}$$

Proof. The exact solution u of (16.1.2) satisfies

$$(u, v) = (f, v), \quad \forall v \in L^2(\Gamma). \tag{16.2.5}$$

Since $V_n \subset L^2(\Gamma)$, the equation (16.2.5) leads to

$$(u, v) = (f, v), \quad \forall v \in V_n. \tag{16.2.6}$$

Then we have from (16.2.3) and (16.2.6)

$$(u - u_n, v) = 0, \quad \forall v \in V_n. \tag{16.2.7}$$

For $v, u_n \in V_n$, let $w_n = v - u_n \in V_n$. From (16.2.1), (16.2.2) and (16.2.7),

$$\|w_n\|^2 = (v - u_n, w_n) = (v - u, w_n) \leq \|u - v\| \|w_n\|, \tag{16.2.8}$$

to give $\|v - u_n\| \leq \|u - v\|$. By the triangle inequality, we have

$$\|u - u_n\| \leq \|u - v\| + \|v - u_n\| \leq 2\|u - v\|, \tag{16.2.9}$$

to give the desired result (16.2.4). ■

Next, consider numerical integration. The solution $\hat{u}_n \in V_n$ is expressed as

$$\overline{(\hat{u}_n, v)} = \overline{(f, v)}, \quad \forall v \in V_n, \quad e.g., \widehat{\int_\Gamma} \omega \hat{u}_n v = \widehat{\int_\Gamma} \omega f v, \quad \forall v \in V_n, \tag{16.2.10}$$

where $\overline{(u, v)} = \widehat{\int}_\Gamma \omega u v$, and $\widehat{\int}_\Gamma$ is a numerical approximation of $\int_\Gamma$ by some integration rules, such as the trapezoidal rule or the central rule.

Theorem 16.2.1. *There exists the bound,*

$$\|u - \hat{u}_n\| \leq 2 \inf_{v \in V_n} \|u - v\| + \sup_{w_n \in V_n} \frac{\left|\left(\int_\Gamma - \widehat{\int}_\Gamma\right) \omega \hat{u}_n w_n\right|}{\|w_n\|} + \sup_{w_n \in V_n} \frac{\left|\left(\int_\Gamma - \widehat{\int}_\Gamma\right) \omega f w_n\right|}{\|w_n\|}. \tag{16.2.11}$$

Proof. From (16.2.7) and (16.2.10), we have

$$\begin{aligned} (u - \hat{u}_n, v) &= (u, v) - (\hat{u}_n, v) = (f, v) - (\hat{u}_n, v) + \left\{\overline{(\hat{u}_n, v)} - \overline{(f, v)}\right\} \\ &= -\left(\int_\Gamma - \widehat{\int_\Gamma}\right) \omega \hat{u}_n v + \left(\int_\Gamma - \widehat{\int_\Gamma}\right) \omega f v, \quad \forall v \in V_n. \end{aligned} \tag{16.2.12}$$

For $w_n = v - \hat{u}_n \in V_n$, we have from (16.2.12) and (16.2.2)

$$\begin{aligned} \|w_n\|^2 &= (v - \hat{u}_n, w_n) = (v - u, w_n) + (u - \hat{u}_n, w_n) \\ &= (v - u, w_n) - \Big(\int_\Gamma - \widehat{\int_\Gamma}\Big)\omega \hat{u}_n w_n + \Big(\int_\Gamma - \widehat{\int_\Gamma}\Big)\omega f w_n \\ &\le \|u - v\|\|w_n\| + \left|\Big(\int_\Gamma - \widehat{\int_\Gamma}\Big)\omega \hat{u}_n w_n\right| + \left|\Big(\int_\Gamma - \widehat{\int_\Gamma}\Big)\omega f w_n\right|, \end{aligned} \tag{16.2.13}$$

to give

$$\|v - \hat{u}_n\| \le \|u - v\| + \frac{\left|\Big(\int_\Gamma - \widehat{\int}_\Gamma\Big)\omega \hat{u}_n w_n\right|}{\|w_n\|} + \frac{\left|\Big(\int_\Gamma - \widehat{\int}_\Gamma\Big)\omega f w_n\right|}{\|w_n\|}. \tag{16.2.14}$$

By the triangle inequality, we have

$$\begin{aligned} \|u - \hat{u}_n\| &\le \|u - v\| + \|v - \hat{u}_n\| \le 2\|u - v\| \\ &\quad + \sup_{w_n \in V_n} \frac{\left|\Big(\int_\Gamma - \widehat{\int}_\Gamma\Big)\omega \hat{u}_n w_n\right|}{\|w_n\|} + \sup_{w_n \in V_n} \frac{\left|\Big(\int_\Gamma - \widehat{\int}_\Gamma\Big)\omega f w_n\right|}{\|w_n\|}. \end{aligned} \tag{16.2.15}$$

This gives the desired result (16.2.11). ■

16.3 Error Bounds for Singular Solutions from (16.1.3)

In analysis and computation, for simplicity let the unit charge $q = 1$ in (16.1.3). In this section, the analysis is confined to the Laplace equation in (16.1.2) as Q^* outside Γ, and the analysis as Q^* inside Γ is similar. Also, we only explore the reduced convergence rates by the MPS and the MFS. The addition theorem in elliptic coordinates is also essential in error analysis. Choose the elliptic boundary with radius ρ and $Q^* = (r^*, \phi^*)$ with $r^* > \rho$. Then the function (III.7) is a harmonic solution of (16.1.2) with $q = 1$. In elliptic coordinates, the source function is expressed from (III.7) as

$$\begin{aligned} u = u^* &= \ln|\overline{PQ^*}| \\ &= r^* + \ln\Big(\frac{\sigma}{2}\Big) - 2\sum_{n=1}^{\infty} \frac{1}{n} e^{-nr^*}(\cosh n\rho \, \cos n\theta \, \cos n\phi^* + \sinh n\rho \, \sin n\theta \, \sin n\phi^*). \end{aligned} \tag{16.3.1}$$

Denote a specific harmonic function of order n of (16.1.5) by

$$\bar{u}_n = \bar{u}_n(\rho, \theta) = \bar{\alpha}_0 + \sum_{k=1}^{n} e^{-k\rho_0}(\bar{\alpha}_k \cosh k\rho \, \cos k\theta + \bar{\beta}_k \sinh k\rho \, \sin k\theta), \tag{16.3.2}$$

where the coefficients are given by

$$\bar{\alpha}_0 = r^* + \ln\Big(\frac{\sigma}{2}\Big), \; \bar{\alpha}_k = \frac{-2}{k} e^{-k(r^* - \rho_0)} \cos k\phi^*, \; \bar{\beta}_k = \frac{-2}{k} e^{-k(r^* - \rho_0)} \sin k\phi^*, \; k = 1, 2, \ldots, n.$$

We give the following lemma, whose proof is given in [253].

Lemma 16.3.1. *Let* Γ *be an elliptic boundary at* $\rho = a$. *For* $0 < \delta = r^* - a \ll 1$, *there exists the bound of the residual,*

$$\|R_n\|_{0,\Gamma} = \|u - \bar{u}_n\|_{0,\Gamma} \le C \frac{1}{n\sqrt{\delta}} e^{-n\delta}, \tag{16.3.3}$$

where C *is a bounded constant independent of* n.

For low convergence rates, the numerical integration errors are critical for better numerical solutions. Hence, we will solicit the analysis from Theorem 16.2.1. Let $Q^* = (r^*, \phi^*)$ with $r^* = \rho + \delta$. For the Dirichlet boundary condition $f = u|_\Gamma = u^*|_\Gamma$ from (16.3.1), we have

$$f = r^* + \ln\left(\frac{\sigma}{2}\right) - 2\sum_{n=1}^{\infty} \frac{1}{n} e^{-nr^*} (\cosh n\rho \, \cos n\theta \, \cos n\phi^* + \sinh n\rho \, \sin n\theta \, \sin n\phi^*), (\rho, \theta) \in \Gamma. \tag{16.3.4}$$

From (16.3.2), choose $w_n \in V_n$ as

$$w_n = \alpha_0 + \sum_{k=1}^{n} (\alpha_k \cos k\theta + \beta_k \sin k\theta), \tag{16.3.5}$$

where α_k and β_n are arbitrary coefficients. We give the following lemma, whose proof is given in [253].

Lemma 16.3.2. *For the elliptic boundary* Γ *at* ρ, *choose the function (16.3.1) with* $Q^* = (r^*, \phi^*)$ *at* $r^* = \rho + \delta$, *and use the trapezoidal rule with* $M \ge 2n + 1$. *For* $0 < \delta\,(= r^* - \rho) \ll 1$, *we have the following bound,*

$$\frac{\left|\left(\int_\Gamma - \widehat{\int}_\Gamma\right) \omega f w_n\right|}{\|w_n\|} \le C \frac{1}{n\sqrt{\delta}} e^{-(M-n)\delta}. \tag{16.3.6}$$

Theorem 16.3.1. *Let the conditions in Lemma 16.3.2 hold. There exists the error bound of the MPS,*

$$\|u - \hat{u}_n\|_{0,\Gamma} \le C \left\{ \frac{1}{n\sqrt{\delta}} e^{-n\delta} + \frac{1}{n\sqrt{\delta}} e^{-(M-n)\delta} \right\}. \tag{16.3.7}$$

Proof. First choose $\omega = \frac{1}{\tau(\theta)}$. We have

$$\left(\int_\Gamma - \widehat{\int_\Gamma}\right) \omega \hat{u}_n w_n = \left(\int_0^{2\pi} - \widehat{\int_0^{2\pi}}\right) \hat{u}_n w_n \, d\theta, \tag{16.3.8}$$

where $\hat{u}_n$ and w_n are the trigonometric polynomials of order n. Based on Basic Lemma A in Part I for the trapezoidal rule with $M \ge 2n + 1$, the second term on the right-hand side in (16.2.11) is the trivial zero because $\hat{u}_n w_n$ are the trigonometric polynomials of order $2n$. Choose $v = \bar{u}_n$, and then from Theorem 16.2.1 and Lemma 16.3.2, we have

$$\begin{aligned}\|u - \hat{u}_n\| &\leq 2 \inf_{v \in V_n} \|u - v\| + \sup_{w_n \in V_n} \frac{\left|\left(\int_\Gamma - \widehat{\int}_\Gamma\right)\omega f w_n\right|}{\|w_n\|} \qquad (16.3.9)\\ &\leq 2\|u - \bar{u}_n\| + O\left(\frac{1}{n\sqrt{\delta}}\, e^{-(M-n)\delta}\right) \leq 2\|R_n\| + O\left(\frac{1}{n\sqrt{\delta}}\, e^{-(M-n)\delta}\right).\end{aligned}$$

When $\omega = 1$, we have $\|v\| = \|v\|_{0,\Gamma}$. Hence, the norm $\|v\|$ with $\omega = \frac{1}{\tau(\theta)}$ is equivalent to $\|v\|_{0,\Gamma}$ since $\omega = \frac{1}{\tau(\theta)} = O(1)$ and $\tau(\theta) = O(1)$. From Lemma 16.3.1, we have

$$\|R_n\| \leq C\|R_n\|_{0,\Gamma} = O\left(\frac{1}{n\sqrt{\delta}}\, e^{-n\delta}\right). \qquad (16.3.10)$$

Therefore, we have from (16.3.9) and (16.3.10)

$$\|u - \hat{u}_n\| = O\left(\frac{1}{n\sqrt{\delta}}\, e^{-n\delta}\right) + O\left(\frac{1}{n\sqrt{\delta}}\, e^{-(M-n)\delta}\right). \qquad (16.3.11)$$

The desired result (16.3.7) follows from (16.3.11), based on the equivalence between $\|u - \hat{u}_n\|$ and $\|u - \hat{u}_n\|_{0,\Gamma}$. ■

Corollary 16.3.1. *Let the conditions in Lemma 16.3.2 hold. When $M = 2n+1$, there exists the error bound of the MPS,*

$$\|u - \hat{u}_n\|_{0,\Gamma} \leq C\left\{\frac{1}{n\sqrt{\delta}}\, e^{-n\delta} + \frac{1}{n\sqrt{\delta}}\, e^{-(n+1)\delta}\right\} = O\left(\frac{1}{n\sqrt{\delta}}\, e^{-n\delta}\right). \qquad (16.3.12)$$

Moreover, when $M = 4n$,

$$\|u - \hat{u}_n\|_{0,\Gamma} \leq C\left\{\frac{1}{n\sqrt{\delta}}\, e^{-n\delta} + \frac{1}{n\sqrt{\delta}}\, e^{-3n\delta}\right\} = O\left(\frac{1}{n\sqrt{\delta}}\, e^{-n\delta}\right). \qquad (16.3.13)$$

In (16.3.12), the numerical integration errors have the same order as the approximation errors (*i.e.*, $O(\|R_n\|_{0,\Gamma})$). Since the precision for singular solutions is critical, we choose $M = 4n$ in computation. From (16.3.13) the numerical integration errors are much smaller than the approximation errors. Such double collocation nodes (*i.e.*, $M \approx 2(2n+1)$) have often been used in the CTM (see [169]). Numerous numerical experiments have shown that the extra errors from numerical integration are insignificant. The error analysis involving numerical integration is also an advanced development of our previous MPS study in [169].

Remark 16.3.1. *Once the error bounds of the MPS are found, the error bounds by the MFS can be obtained from Chapters 6 and 14 (also see [74, 252]). Let $\hat{v}_N$ and $\hat{u}_n$ be the solutions from the MFS and the MPS, respectively. When N is large, for the elliptic pseudo-boundary at $\rho = R (> r_{\max})$, there exists the bound of the MFS,*

$$\|u-\hat{v}_N\|_{0,\Gamma} \le C\left\{e^{-(R-r_{\max})(N-2n)}\,e^{n(r_{\max}-r_{\min})}\|u\|_{0,\Gamma}+\|u-\hat{u}_n\|_{0,\Gamma}\right\}, \tag{16.3.14}$$

where $r_{\max} = \max \rho|_\Gamma$, $r_{\min} = \min \rho|_\Gamma$, *and* C *is a bounded constant independent of* $N\,(\geq 2n+1)$. *We may choose suitably large* N *such that the first term on the right-hand side in (16.3.14) may match the second term, to give* $\|u-\hat{v}_N\|_{0,\Gamma} = O(\|u-\hat{u}_n\|_{0,\Gamma})$. *Then both the MFS and the MPS reach the optimal convergence rates. Also by choosing* $M = 2N$ *in the MFS, the errors of numerical solutions are caused mainly by the approximation errors, but the numerical integration errors are less important.*

16.4 Singularity for Polygonal Domains and Arbitrary Domains

Besides circular and elliptic boundaries, other kinds of domain boundaries are investigated. First, we discuss the bounded simply-connected domains and polygonal domains. For the classic theory, the solutions $u \in C^2(S)$ of (16.1.2) must have second-order continuous derivatives. However, for the Sobolev theory, the solutions may be relaxed to $u \in \mathbf{H}^1(S)$, *i.e.*, the derivatives are integrable in S, where $\mathbf{H}^1(S)$ is the Sobolev space equipped with norms

$$\|u\|_{1,S} = \left\{\iint_S (u^2+u_x^2+u_y^2)\,ds\right\}^{\frac{1}{2}}, \quad |u|_{1,S} = \left\{\iint_S (u_x^2+u_y^2)\,ds\right\}^{\frac{1}{2}}. \tag{16.4.1}$$

We give the following lemma, whose proof is given in [253].

Lemma 16.4.1. *Consider the bounded simply-connected domain* S *with a smooth boundary* $\Gamma\,(=\partial S)$. *For the solution* $u = u^*(x,y) = \ln|\overline{PQ^*}|$ *with* $P \in \bar{S}$, *there exist the regularities,*

$$u \in \mathbf{H}^1(S) \text{ if } Q^* \notin \bar{S}, \tag{16.4.2}$$

$$u \notin \mathbf{H}^1(S) \text{ if } Q^* \in \Gamma. \tag{16.4.3}$$

The errors of the MPS are provided in Chapter 6 (also see [74, (3.13)]) as

$$\|u-u_n\|_{0,\Gamma} = O\left(\frac{1}{n^{p-\frac{1}{2}}}\|u\|_{p,S}\right), \quad p \geq 1, \tag{16.4.4}$$

$$\|u-u_n\|_{0,\Gamma} = O\left(\frac{1}{n^{p}}\|u\|_{p,\Gamma}\right), \quad p \geq \frac{1}{2}, \tag{16.4.5}$$

where $\|u\|_{p,S}$ are the Sobolev norms. Hence from (16.4.4) and (16.4.2), we have a very slow convergence rate for Q^* very near Γ,

$$\|u-u_n\|_{0,\Gamma} = O\left(\frac{1}{\sqrt{n}}\|u\|_{1,S}\right) = O\left(\frac{1}{\sqrt{n}}\right). \tag{16.4.6}$$

Next, we discuss a polygonal domain S. Suppose the node Q^* is near the edge $\overline{AB}$ of Γ with length a. For simplicity, the section $\overline{AB}$ is located on $[0,\ a]$ along the X axis and S above the X axis, and the node $Q^* = (x^*, -\delta)$ (or $Q^* = (x^*, \delta)$) is outside (or inside) S but near $\overline{AB}$, where δ is the minimal distance of Q^* to Γ; see Figure 16.1.

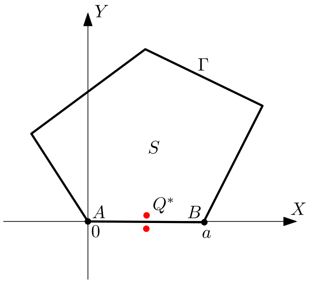

FIG. 16.1 – A polygonal domain with Q^*.

We give the following theorem, whose proof is given in [253].

Theorem 16.4.1. *Let polygon S be located as in Figure 16.1. Also choose the source function $u^*(x,y)$ in (16.1.3) with $q = 1$, where node $Q^* = (x,y) = (x^*, \pm\delta)$ with $0 < \delta \ll 1$. There exists the bound,*

$$\|u\|_{1,\Gamma} = O\left(\frac{1}{\sqrt{\delta}}\right). \tag{16.4.7}$$

16.5 Removal Techniques for Laplace's Equation

Consider the Laplace equation and the source function (16.1.3),

$$u^* = q\ \ln|\overline{PQ^*}|, \tag{16.5.1}$$

where the node $P \in \bar{S}$ and the source node Q^* is outside (or inside) but near Γ. The Dirichlet boundary function in (16.1.2) is generated by (16.5.1) as $f = u^*|_\Gamma$. From Sections 16.3 and 16.4, the convergence rates are low due to the singularity. In this section, we will explore new removal techniques for the MFS and the MPS to improve the solution accuracy.

16.5.1 For the Case of Q^* Outside Γ

Note that when Q^* is far from Γ (denoted as Q^*_{far}), the solution is highly smooth. Then we only consider the case when Q^* is near Γ. How can this type of singularity be removed? First, let us consider the case when Q^* is outside but near Γ (denoted as Q^*_{out}). When the node Q^*_{out} is known, we may choose the pseudo-boundary just passing over Q^*_{out} so that this singularity is eliminated completely. See numerical results in Chapter 14. The solution becomes highly smooth once the singularity is removed. Since node Q^*_{out} is very near Γ, the pseudo-boundary must also be located near Γ so that the convergence rates by the MFS are also low even for highly smooth solutions. From the analysis in Chapter 14 and [253], circular/elliptic pseudo-boundaries are optimal for highly smooth solutions. Another approach is to employ an additional source node Q_0 for FS. Then we have the new FS as

$$v_{N+1} = d_0 \ln|\overline{PQ_0}| + \sum_{i=1}^{N} c_i \ln|\overline{PQ_i}|, \tag{16.5.2}$$

where $Q_i\,(i = 1, 2, \ldots, N)$ are the original source nodes on circular/elliptic pseudo-boundaries. There are $(N+1)$ unknown coefficients d_0 and c_i; the numerical solutions can be easily obtained from Section 16.1. The high convergence rates can be restored, and the ill-conditioning will not worsen (see Proposition 16.5.3 below).

For the source function (16.5.1), suppose that the source node Q^* is unknown. By trial computation using (16.1.10) instead of (16.5.2), it is easy to find the location $P = (\bar{r}, \bar{\theta}) \in \Gamma$ with the largest errors from (16.5.1). For the circular boundary Γ, we denote

$$Q^*_{\text{out}} = \left(\bar{r} + \delta, \bar{\theta}\right), \quad 0 < \delta \ll 1, \tag{16.5.3}$$

where only δ is unknown. For the non-circular smooth boundaries Γ, we assume that node Q^* has a distance δ to P (*i.e.*, $|\overline{PQ^*_{\text{out}}}| = \delta$) along the exterior normal direction $\vec{n}$. Let ζ denote the angle of $\vec{n}$ from the X axis. Then we denote $Q^* = (x^*_{\text{out}}, y^*_{\text{out}})$, where

$$x^*_{\text{out}} = \bar{r}\,\cos\bar{\theta} + \delta\,\cos\zeta, \;\; y^*_{\text{out}} = \bar{r}\,\sin\bar{\theta} + \delta\,\sin\zeta. \tag{16.5.4}$$

By trial computation, the location of node Q^*_{out} is reduced to seek only δ, thus simplifying the nonlinear algorithm. The errors from (16.5.2) are given by

$$\|v_{N+1} - f\|_{0,\Gamma} = w(\delta; d_0; c_1, \ldots, c_N), \tag{16.5.5}$$

where the function w involves the unknowns: δ, d_0 and c_i. The number of unknowns is $N+2$. Let $\bar{V}^+_{N+2}$ denote the set of (16.5.5). The minimum of (16.5.5) will yield parameter δ, and coefficients d_0 and c_i:

$$\|v_{N+1} - f\|_{0,\Gamma} = \min_{v \in \bar{V}^+_{N+2}} \|v - f\|_{0,\Gamma}. \tag{16.5.6}$$

Equation (16.5.6) leads to a system of equations involving one nonlinear unknown parameter δ and $(N+1)$ linear unknown coefficients d_0 and c_i. To find all unknown source nodes Q_i, the nonlinear solutions are sought in [89, 189].

Since the nonlinear unknown is only one δ, we employ the iterative method to seek δ. Define by V_{N+1} the set of coefficients d_0 and $c_i\,(i = 1, 2, \ldots, N)$ in (16.5.2) only. Then the equation (16.5.6) is modified as

$$\|v_{N+1} - f\|_{0,\Gamma} = \min_{v \in V_{N+1}} \|v - f\|_{0,\Gamma}. \tag{16.5.7}$$

Since the equation (16.5.2) is linear for coefficients d_0 and c_i, the algorithms are also similar to those in Section 16.1. We may use the secant method. Let $w(\delta) = \|u - v_{N+1}\|_{0,\Gamma}$ denote the nonlinear function in (16.5.7). Suppose that two suitable initial values are given as $\delta^{(0)}$ and $\delta^{(1)}$. The approximate values of $\delta^{(\ell)}$ can be found by [12, p.65]:

$$\delta^{(\ell+1)} = \delta^{(\ell)} - w(\delta^{(\ell)}) \times \frac{\delta^{(\ell)} - \delta^{(\ell-1)}}{w(\delta^{(\ell)}) - w(\delta^{(\ell-1)})}, \quad \ell \geq 1. \tag{16.5.8}$$

A few steps by the secant method in (16.5.8) may reach a good approximation of δ; see the examples in Section 16.7.

16.5.2 For the Case of Q^* Inside Γ under the Image Node Existing

Consider Q^* inside Γ (*i.e.*, inside S) denoted by Q^*_{in}. Note that the function $\ln|\overline{PQ^*_{\text{in}}}|$ is not harmonic. For simple boundaries (*i.e.*, circles), an image node Q^*_{out} outside S can be found to respond to Q^*_{in} $(\in S)$ (see [45] and [223, p.354]). Then we may also choose (16.5.3) with $\ln|\overline{PQ^*_{\text{out}}}|$ outside S and apply the same removal techniques in Section 16.5.1. As for the arbitrary boundary Γ without image nodes, a remedy is provided in Section 16.7 to obtain the harmonic solutions.

First, consider the circular boundary Γ with radius a. Let $Q^*_{\text{in}} = (r_{\text{in}}, \phi^*)$ with $r_{\text{in}} < a$. We may find its image $Q^*_{\text{out}} = (r_{\text{out}}, \phi^*)$ by

$$r_{\text{out}} = \frac{a^2}{r_{\text{in}}} > a. \tag{16.5.9}$$

There exists the equality for $P \in \Gamma$ (the proof given below),

$$\frac{|\overline{PQ^*_{\text{in}}}|}{a} = \frac{|\overline{PQ^*_{\text{out}}}|}{r_{\text{out}}}. \tag{16.5.10}$$

Then we have

$$\ln\left(\frac{|\overline{PQ^*_{\text{in}}}|}{a}\right) = \ln\left(\frac{|\overline{PQ^*_{\text{out}}}|}{r_{\text{out}}}\right), \; \ln|\overline{PQ^*_{\text{in}}}| = \ln|\overline{PQ^*_{\text{out}}}| + \ln\left(\frac{a}{r_{\text{out}}}\right) = \ln|\overline{PQ^*_{\text{out}}}| + c,$$

where c is a constant. Although the function $\ln|\overline{PQ^*_{\text{in}}}|$ is not a harmonic solution, but $\ln|\overline{PQ^*_{\text{out}}}|$ is. Since the constant c is not needed in the MFS for the pseudo-boundary of $Q_i\,(i = 1, 2, \ldots, N)$ without degenerate scales, we may still set $Q_0 = Q^*_{\text{out}}$ as in (16.5.2), and use (16.5.3)–(16.5.6) as well as (16.5.7) and (16.5.8). Next, let us prove (16.5.10). We have for node $P(a, \theta) \in \Gamma$

$$\begin{aligned}|\overline{PQ^*_{\rm in}}| &= \sqrt{r^2_{\rm in} + a^2 - 2ar_{\rm in}\cos(\theta - \phi^*)}\\ &= a\sqrt{1 + \left(\frac{r_{\rm in}}{a}\right)^2 - 2\left(\frac{r_{\rm in}}{a}\right)\cos(\theta - \phi^*)},\end{aligned} \tag{16.5.11}$$

$$\begin{aligned}|\overline{PQ^*_{\rm out}}| &= \sqrt{r^2_{\rm out} + a^2 - 2ar_{\rm out}\cos(\theta - \phi^*)}\\ &= r_{\rm out}\sqrt{1 + \left(\frac{a}{r_{\rm out}}\right)^2 - 2\left(\frac{a}{r_{\rm out}}\right)\cos(\theta - \phi^*)}.\end{aligned} \tag{16.5.12}$$

By using (16.5.9) we have $\frac{a}{r_{\rm out}} = \frac{r_{\rm in}}{a}$. The equation (16.5.10) follows from (16.5.11) and (16.5.12).

Proposition 16.5.1. *Let the Dirichlet boundary conditions be generated from (16.5.1) with* $Q^*_{\rm in} = (r_{\rm in}, \phi^*)$ *inside* Γ. *For the circular boundary* Γ *with radius* a, *the image* $Q^*_{\rm out} = (r_{\rm out}, \phi^*)$ *from (16.5.9) is found, and the singularity can be eliminated completely by the removal techniques (16.5.3)–(16.5.6).*

Next, let us study the image node for the elliptic boundary Γ at ρ. We give the following proposition, whose proof is given in [253].

Proposition 16.5.2. *For an elliptic boundary* Γ *at* ρ, *denote* $Q^*_{\rm in} = (r^*, \phi^*) = (\rho - \delta, \phi^*)$ *and* $Q^*_{\rm out} = (\rho + \delta, \phi^*)$ *with* $\delta \ll \rho$ *in elliptic coordinates. Then*

$$\ln|\overline{PQ^*_{\rm in}}| = \ln|\overline{PQ^*_{\rm out}}| + \bar{u}(\rho, \theta), \quad P \in \Gamma, \tag{16.5.13}$$

where the harmonic function $\bar{u}(\rho, \theta)$ *is expressed in elliptic coordinates as (16.1.4)*

$$\bar{u}(\rho, \theta) = \bar{\alpha}_0 + \sum_{n=1}^{\infty} e^{-n\rho_0}(\bar{\alpha}_n \cosh n\rho \cos n\theta + \bar{\beta}_n \sinh n\rho \sin n\theta), \tag{16.5.14}$$

where the coefficients have $\bar{\alpha}_0 = -\delta$, $|\bar{\alpha}_n| = O(\delta)$, *and* $|\bar{\beta}_n| = O(\delta)$ *(or* $|\bar{\alpha}_n| \approx 0$, $|\bar{\beta}_n| \approx 0$*).*

For the FS in (16.5.2), we obtain the collocation equations on Γ,

$$\sqrt{\triangle h_\ell}\left\{d_0 \ln|\overline{PQ_0}| + \sum_{j=1}^{N} c_j \Phi_j(\rho_\ell, \theta_\ell)\right\} = \sqrt{\triangle h_\ell}\, f(\rho_\ell, \theta_\ell),\ \ \ell = 1, 2, \ldots, M, \tag{16.5.15}$$

where $M \geq N + 1$. Let $\mathbf{y} = \{d_0, c_1, \ldots, c_N\}^T$. The equation (16.5.15) leads to an overdetermined system,

$$\mathbf{F}^+\mathbf{y} = \mathbf{b}, \tag{16.5.16}$$

where matrix $\mathbf{F}^+ \in \mathbf{R}^{M\times(N+1)}$ $(M \geq N + 1)$, and vectors $\mathbf{y} \in \mathbf{R}^{N+1}$ and $\mathbf{b} \in \mathbf{R}^M$. When the minimum (16.5.6) is applied, the δ can be found by the secant method. Then matrix $\mathbf{F}^+$ in (16.5.16) is known. For matrix $\mathbf{F}^+$ given, the condition number and the effective condition number are also denoted by Cond and Cond_eff in Part I (also see [162]). Note that one more source node Q_0 near Γ is added to the original source nodes $Q_i\,(i=1,2,\ldots,N)$ on pseudo-boundaries in the traditional MFS. For stability of (16.5.16), we have the following proposition, whose proof is given in [253].

Proposition 16.5.3. *Consider the disk domains and use circular pseudo-boundaries. Suppose that the collocation equations (16.5.15) from (16.5.2) are used, where one source node Q_0 near Γ is added in the traditional FS. The stability of the MFS will not worsen.*

16.6 Numerical Experiments

Numerical verification for the reduced convergence rates is given in [253]. We have carried out the removal techniques for classic domains, such as the unit disk, ellipses, and squares, and give numerical results in [253]. Below, we only report those for elliptic domains. Consider an elliptic solution domain S, whose boundary Γ is defined by $\left(\frac{x}{a}\right)^2+\left(\frac{y}{b}\right)^2=1$ with $a=2$ and $b=0.5$ (see Figure 16.2). We have $\sigma=\sqrt{a^2-b^2}=\sqrt{3.75}$, and $\sinh\rho_0=\frac{0.5}{\sigma}=\frac{0.5}{\sqrt{3.75}}=0.2582$. Choose the generating function

$$g=\cos(x)e^y+\ln|\overline{PQ^*_{\text{out}}}|-\ln|\overline{PQ^*_{\text{in}}}|, \tag{16.6.1}$$

to produce the Dirichlet boundary data as $f=g|_\Gamma$. Denote Case I: $Q^*_{\text{out}}=(r^*,\phi^*)=\left(\rho_0+0.1,\frac{\pi}{2}\right)$ and $Q^*_{\text{in}}=\left(\rho_0-0.1,\frac{\pi}{2}\right)$, and Case II: $Q^*_{\text{out}}=(\rho_0+0.01,0)$ and $Q^*_{\text{in}}=(\rho_0-0.01,0)$. The MPS by using (16.1.5) is chosen, and the results are given in Table 16.1. From Table 16.1, we find for two cases,

$$\|\epsilon\|_{0,\Gamma}=O(0.65^n),\quad \text{Cond}=6.68. \tag{16.6.2}$$

The convergence rates may reach those obtained for the smooth function $u=\cos(x)e^y$ only. The singularity can be removed; this also verifies Proposition 16.5.2.

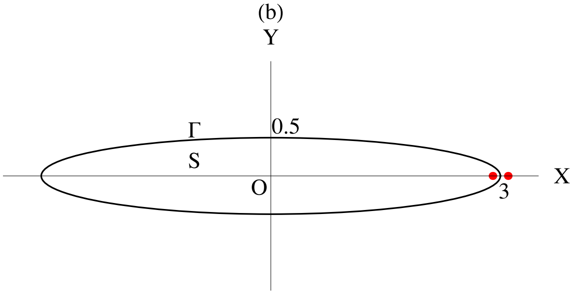

FIG. 16.2 – Elliptic boundaries, with two source nodes Q^*_{in} and Q^*_{out}.

Next, choose the generating function

$$g_1 = \cos(x)e^y + \ln|\overline{PQ^*_{\text{out}}}|, \tag{16.6.3}$$

where $Q^*_{\text{out}} = (\rho^*, \phi^*) = (\rho + 0.01, 0)$ in elliptic coordinates. By adding the same FS: $\ln|\overline{PQ_0}|$, the admissible functions in the MPS are given by

$$u_{n+1}(\rho, \theta) = \alpha_0 + \sum_{k=1}^{n} e^{-k\rho_0}(\alpha_k \cosh k\rho \cos k\theta + \beta_k \sinh k\rho \sin k\theta) + d_0 \ln|\overline{PQ_0}|, \tag{16.6.4}$$

where (ρ, θ) are the elliptic coordinates with $\rho_0 = 0.2554$, $Q_0 = (\rho_0 + \delta, 0)$, d_0 and α_k, β_k are unknown coefficients, but δ is unknown to be sought by the secant method (16.5.8). The iteration results are given in Table 16.2 to restore the accuracy to that of Table 16.1.

Third, choose the generating function

$$g_2 = \cos(x)e^y + \ln|\overline{PQ^*_{\text{in}}}|, \tag{16.6.5}$$

where $Q^*_{\text{in}} = (\rho_0 - 0.01, 0)$. For the MFS, the admissible functions

$$v_{N+1}((\rho, \theta) = d_0 \ln|\overline{PQ_0}| + \sum_{i=1}^{N} c_i \ln|\overline{PQ_i}|, \tag{16.6.6}$$

TAB. 16.1 – The errors and the condition numbers for elliptic Γ in two cases by the MPS by using (16.1.5), where $\epsilon = u - u_n$, and the generating function (16.6.1) is chosen.

Cases	n	M	$\Vert\epsilon\Vert_{\infty,\Gamma}$	$\Vert\epsilon\Vert_{0,\Gamma}$	Cond	Cond_eff	$\Vert\mathbf{x}\Vert$	$\sigma_{\min}$
Case I $Q^*_{\text{out}} = (\rho_0 + 0.1, \frac{\pi}{2})$ $Q^*_{\text{in}} = (\rho_0 - 0.1, \frac{\pi}{2})$	8	32	5.31(−3)	6.41(−3)	6.67	3.35	1.63	4.47(−1)
	16	64	1.26(−4)	1.50(−4)	6.68	3.35	1.63	4.47(−1)
	24	96	3.37(−6)	3.96(−6)	6.68	3.35	1.63	4.47(−1)
	32	128	9.74(−8)	1.13(−7)	6.68	3.35	1.63	4.47(−1)
	40	160	2.97(−9)	3.43(−9)	6.68	3.35	1.63	4.47(−1)
	48	192	9.35(−11)	1.08(−10)	6.68	3.35	1.63	4.47(−1)
	56	224	3.01(−12)	3.47(−12)	6.68	3.35	1.63	4.47(−1)
	64	256	1.03(−13)	1.14(−13)	6.68	3.35	1.63	4.47(−1)
	72	288	7.11(−15)	9.08(−15)	6.68	3.35	1.63	4.47(−1)
Case II $Q^*_{\text{out}} = (\rho_0 + 0.01, 0)$ $Q^*_{\text{in}} = (\rho_0 - 0.01, 0)$	8	32	6.85(−4)	4.42(−4)	6.67	2.52	1.96	4.47(−1)
	16	64	1.18(−5)	7.46(−6)	6.68	2.52	1.96	4.47(−1)
	24	96	2.01(−7)	1.26(−7)	6.68	2.52	1.96	4.47(−1)
	32	128	3.40(−9)	2.13(−9)	6.68	2.53	1.96	4.47(−1)
	40	160	5.78(−11)	3.62(−11)	6.68	2.53	1.96	4.47(−1)
	48	192	1.05(−12)	6.18(−13)	6.68	2.53	1.96	4.47(−1)
	56	224	9.56(−14)	2.96(−14)	6.68	2.53	1.96	4.47(−1)
	64	256	8.89(−14)	1.20(−14)	6.68	2.53	1.96	4.47(−1)

where $Q_0 = (\rho_0 + 0.01, 0)$ is still outside Γ and the source nodes $Q_i = \big(\rho_0 + 0.5, i\frac{2\pi}{N}\big)$. There exists no overlap between Q_0 and $Q_i\,(i \geq 1)$ due to $\delta \ll 1$. Note that d_0 and c_i are the unknown coefficients, but δ is unknown to be sought by the secant method (16.5.8). The results are given in Table 16.3 by $N = 48$ and $d_0 = 1.000000033497895$, to restore the high accuracy as $O(10^{-13})$. The terminal value $\delta = 0.01$ in Table 16.3 supports Proposition 16.5.2 again.

16.7 Applications to Amoeba-Like Domains

16.7.1 Numerical Results

The accuracy of numerical solutions can be greatly improved by using the removal techniques in Section 16.5. Here we choose the amoeba-like domains for example. Consider the amoeba-like domain with a boundary $\Gamma\,(= \partial S)$ defined by (see Figure 16.3)

$$r(\theta) = e^{\sin\theta} \sin^2(2\theta) + e^{\cos\theta} \cos^2(2\theta), \quad 0 \leq \theta < 2\pi. \tag{16.7.1}$$

Consider the source function (16.1.3) with $q = 1$. We choose small $\delta = 0.01, 0.001$ and the MFS. Since the circular pseudo-boundaries are optimal for highly smooth solutions, we only employ them in this section (see Figure 16.3). The numerical results of the MFS are provided in Table 16.4. For the singular source functions $\ln|\overline{PQ^*_{\text{out}}}|$ and $\ln|\overline{PQ^*_{\text{in}}}|$, we can see from Table 16.4 at $\delta = \pm 0.001$,

$$\|\epsilon\|_{\infty,\Gamma} = O(N^{-0.13}), \quad \|\epsilon\|_{0,\Gamma} = O(N^{-0.54}), \quad \text{Cond} = O(1.51^N), \quad \text{Cond\_eff} = O(1.15^N). \tag{16.7.2}$$

The errors in (16.7.2) coincide with the estimate $\|\epsilon\|_{0,\Gamma} = O\Big(\frac{1}{\sqrt{N}}\Big)$ from (16.4.6). For the highly smooth source function, $\ln|\overline{PQ^*_{\text{far}}}|$ with $Q^*_{\text{far}} = (5, 0)$, we can see

$$\|\epsilon\|_{\infty,\Gamma} = O(0.75^N), \|\epsilon\|_{0,\Gamma} = O(0.74^N), \ \text{Cond} = O(1.51^N), \ \text{Cond\_eff} = O(1.49^N). \tag{16.7.3}$$

Denote the maximal and the minimal distances by $r_{\max} = \max r|_\Gamma$ and $r_{\min} = \min r|_\Gamma$, respectively, to the center (x_o, y_o) in Figure 16.3. For the interior Dirichlet problem of Laplace's equation, there exist the estimates in Chapter 2 (also see [151, 163])

$$\|u - v_N\|_{0,\Gamma} \leq C\left\{\left(\frac{r_{\max}}{R}\right)^{N-2n}\left(\frac{r_{\max}}{r_{\min}}\right)^{n}\|u\|_{0,\Gamma} + \|u - u_n\|_{0,\Gamma}\right\}, \tag{16.7.4}$$

$$\text{Cond} = O\left(N^{v}\left(\frac{R}{r_{\min}}\right)^{\frac{N}{2}}\right), \tag{16.7.5}$$

TAB. 16.2 – The errors and the condition numbers for elliptic Γ by the secant method to seek δ with the MPS by using (16.6.4), where $\epsilon = u - u_{n+1}$, $n = 24$ and $M = 4n$, and the generating function (16.6.3) with $Q^*_{\text{out}} = (\rho + 0.01, 0)$ is chosen.

(ρ^*, ϕ^*)	k	$\delta^{(k)}$	$\\|\epsilon\\|_{\infty,\Gamma}$	$\\|\epsilon\\|_{0,\Gamma}$	Cond	Cond_eff	$\\|\mathbf{x}\\|$	$\sigma_{\min}$
Initial value	0	0.0020000000000000	4.80(−1)	7.23(−2)	2.61(1)	1.24(1)	2.55	1.46(−1)
Initial value	1	0.0040000000000000	3.02(−1)	4.60(−2)	3.19(1)	1.62(1)	2.39	1.19(−1)
$(\rho_0 + 0.01, 0)$	2	0.0075020621637934	9.99(−2)	1.59(−2)	4.07(1)	2.22(1)	2.24	9.25(−2)
	3	0.0093475118189717	2.38(−2)	3.84(−3)	4.53(1)	2.51(1)	2.21	8.31(−2)
	4	0.0099366703360650	2.25(−3)	3.65(−4)	4.67(1)	2.59(1)	2.21	8.04(−2)
	5	0.0099984517589414	5.48(−5)	8.89(−6)	4.69(1)	2.60(1)	2.21	8.02(−2)
	6	0.0099999963575769	1.29(−7)	2.09(−8)	4.69(1)	2.60(1)	2.21	8.02(−2)
	7	0.0099999999997913	7.42(−12)	1.20(−12)	4.69(1)	2.60(1)	2.21	8.02(−2)
	8	0.0100000000000010	1.69(−14)	1.13(−14)	4.69(1)	2.60(1)	2.21	8.02(−2)

TAB. 16.3 – The errors and the condition numbers for elliptic Γ by the secant method to seek δ with the MFS by using (16.6.6) with $\rho = \rho_0 + 0.5$, where $\epsilon = u - v_{N+1}$, $N = 48$ and $M = 2N$, and the generating function (16.6.5) with $Q^*_{\text{in}} = (\rho_0 - 0.01, 0)$ is chosen.

(ρ^*, ϕ^*)	k	$\delta^{(k)}$	$\\|\epsilon\\|_{\infty,\Gamma}$	$\\|\epsilon\\|_{0,\Gamma}$	Cond	Cond_eff	$\\|\mathbf{x}\\|$	$\sigma_{\min}$
Initial value	0	0.0020000000000000	3.14(−1)	3.71(−2)	1.44(12)	6.80(2)	4.67(8)	1.45(−11)
Initial value	1	0.0040000000000000	1.87(−1)	2.33(−2)	1.45(12)	9.29(2)	3.43(8)	1.44(−11)
$(\rho_0 - 0.01, 0)$	2	0.0073846878349284	6.59(−2)	8.29(−3)	1.45(12)	2.15(3)	1.49(8)	1.43(−11)
	3	0.0092541995429041	1.68(−2)	2.16(−3)	1.46(12)	7.55(3)	4.26(7)	1.43(−11)
	4	0.0099145734662091	1.85(−3)	2.41(−4)	1.46(12)	6.59(4)	4.89(6)	1.43(−11)
	5	0.0099972807588805	5.86(−5)	7.64(−6)	1.46(12)	2.07(6)	1.56(5)	1.42(−11)
	6	0.0099999900974100	2.13(−7)	2.78(−8)	1.46(12)	5.68(8)	5.67(2)	1.42(−11)
	7	0.0099999999989540	2.26(−11)	2.95(−12)	1.46(12)	2.39(11)	1.35	1.42(−11)
	8	0.0100000000000036	6.57(−14)	5.34(−14)	1.46(12)	2.40(11)	1.34	1.42(−11)

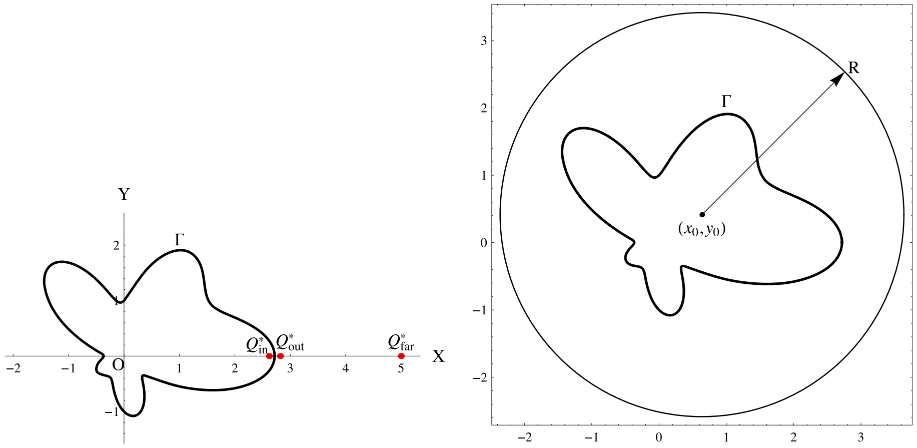

FIG. 16.3 – The boundary Γ of the amoeba-like domain defined by (16.7.1), accompanied by three source nodes Q^*_{in}, Q^*_{out} and $Q^*_{\text{far}} = (5, 0)$ in (16.1.3) (Left side), and the circular pseudo-boundaries with radius R and center at $(x_o, y_o) = (0.6386, 0.4145)$ (Right side).

where constant $\nu\,(\geq 1)$. From the values $r_{\max} = 2.3291$, $r_{\min} = 0.8067$ and $R = 3$, we have the dominant part of (16.7.4)

$$T_N = O\left(\left(\frac{r_{\max}}{R}\right)^N\right) = O\left(\left(\frac{2.3291}{3}\right)^N\right) = O(0.777^N), \tag{16.7.6}$$

to coincide with (16.7.3) for the highly smooth function (16.1.3) at Q^*_{far}. Moreover, we have from (16.7.5)

$$\text{Cond} = O\left(N^\nu \left(\frac{R}{r_{\min}}\right)^{\frac{N}{2}}\right) = O\left(N^\nu \times \left(\frac{3}{0.8067}\right)^{\frac{N}{2}}\right) = O(N^\nu \times 1.928^N). \tag{16.7.7}$$

The numerical bounds of the Cond in (16.7.2) and (16.7.3) are also consistent with (16.7.7).

Choose the generating functions,

$$g_1(P) = \ln|\overline{PQ^*}| + \ln|\overline{PQ^*_{\text{far}}}|, \quad Q^* = Q^*_{\text{out}} \text{ (or } Q^* = Q^*_{\text{in}}), \quad Q^*_{\text{far}} = (5, 0). \tag{16.7.8}$$

By adding $\ln|\overline{PQ_0}|$, the admissible functions are given by

$$v_{N+1}(r, \theta) = d_0 \ln|\overline{PQ_0}| + \sum_{i=1}^{N} c_i \ln|\overline{PQ_i}|, \tag{16.7.9}$$

where $Q_0 = (x, y) = (e \pm \delta, 0)$ with $\delta > 0$, and d_0 and c_i are unknown coefficients. The parameter δ is sought by the secant method, and the results are listed in Table 16.5. Both Q^*_{out} and Q^*_{in} are found to be the Q_0 in (16.7.9) correctly after a few

TAB. 16.4 – The errors and the condition numbers for the amoeba-like Γ by the MFS using (16.1.10) with circular pseudo-boundaries with radius $R = 3$, where $\epsilon = u - v_N$, $Q^*_{\text{in}} = (e - \delta, 0)$, $Q^*_{\text{out}} = (x^*, y^*) = (\delta, 0)$ with $\delta = 0.01, 0.001$, and $Q^*_{\text{far}} = (5, 0)$.

Generating functions	n	M	$\Vert\epsilon\Vert_{\infty,\Gamma}$	$\Vert\epsilon\Vert_{0,\Gamma}$	Cond	Cond_eff	$\Vert\mathbf{x}\Vert$	$\sigma_{\min}$
$\ln\vert PQ^*_{\text{in}}\vert$ $Q^*_{\text{in}} = (e - 0.01, 0)$	8	16	2.97	2.65	1.52(2)	7.50	1.06(1)	7.29(−2)
	32	64	1.96	8.70(−1)	4.43(6)	9.93(2)	8.60(2)	5.04(−6)
	48	96	2.07	8.71(−1)	2.12(9)	2.14(3)	1.50(5)	1.29(−8)
	64	128	1.43	4.78(−1)	3.99(12)	1.41(5)	3.62(6)	7.93(−12)
	80	160	1.44	5.35(−1)	1.40(15)	4.30(5)	3.72(8)	2.51(−14)
$\ln\vert PQ^*_{\text{in}}\vert$ $Q^*_{\text{in}} = (e - 0.001, 0)$	8	16	5.16	4.72	1.52(2)	6.55	1.65(1)	7.29(−2)
	32	64	4.20	1.95	4.43(6)	6.35(2)	1.58(3)	5.04(−6)
	48	96	4.58	1.94	2.12(9)	1.22(3)	2.96(5)	1.29(−8)
	64	128	3.70	1.32	3.99(12)	2.67(4)	2.11(7)	7.93(−12)
	80	160	3.79	1.36	1.40(15)	1.26(5)	1.37(9)	2.51(−14)
$\ln\vert PQ^*_{\text{out}}\vert$ $Q^*_{\text{out}} = (e + 0.01, 0)$	8	16	3.00	2.67	1.52(2)	7.48	1.07(1)	7.29(−2)
	32	64	1.98	8.81(−1)	4.43(6)	9.93(2)	8.61(2)	5.04(−6)
	48	96	2.09	8.78(−1)	2.12(9)	2.13(3)	1.50(5)	1.29(−8)
	64	128	1.47	5.02(−1)	3.99(12)	7.41(4)	6.92(6)	7.93(−12)
	80	160	1.45	5.38(−1)	1.40(15)	3.15(5)	5.08(8)	2.51(−14)
$\ln\vert PQ^*_{\text{out}}\vert$ $Q^*_{\text{out}} = (e + 0.001, 0)$	8	16	5.17	4.72	1.52(2)	6.55	1.65(1)	7.29(−2)
	32	64	4.20	1.95	4.43(6)	6.35(2)	1.58(3)	5.04(−6)
	48	96	4.58	1.94	2.12(9)	1.22(3)	2.96(5)	1.29(−8)
	64	128	3.71	1.32	3.99(12)	2.63(4)	2.14(7)	7.93(−12)
	80	160	3.79	1.36	1.40(15)	1.25(5)	1.39(9)	2.51(−14)
$\ln\vert PQ^*_{\text{far}}\vert$ $Q^*_{\text{far}} = (5, 0)$	8	16	3.46(−2)	3.04(−2)	1.52(2)	1.11(2)	6.63(−1)	7.29(−2)
	32	64	4.45(−6)	2.66(−6)	4.43(6)	3.22(6)	3.34(−1)	5.04(−6)
	48	96	4.37(−8)	2.74(−8)	2.12(9)	1.51(9)	2.78(−1)	1.29(−8)
	64	128	6.57(−9)	3.48(−9)	3.99(12)	1.37(12)	5.01(−1)	7.93(−12)
	80	160	2.88(−11)	1.48(−11)	1.40(15)	3.14(14)	6.87(−1)	2.51(−14)

iterations, and the constant $d_0 = 1$ is obtained. The high accuracy as $O(10^{-13})$ has been achieved in Table 16.5. Proposition 16.5.3 is also valid for the amoeba-like domains based on (16.7.5). Hence, the stability remains the same when an additional source node Q_0 near Γ is added in (16.7.9). This guarantees the validity of the secant method; see Table 16.5.

16.7.2 Removal Techniques Linked to Source Identification Problems

Let us link the removal techniques to source identification problems. Define the source identification problem as **Problem A**. Consider

$$\Delta u(P) = qc^*\delta\Big(|\overline{PQ^*}|\Big) \text{ in } S, \ \ u|_\Gamma = f = f_s + \{q\ln|\overline{PQ^*}|\}|_\Gamma, \tag{16.7.10}$$

where the constant $c^* = 2\pi$, the source node $Q^* \notin \Gamma$ and f_s is a smooth function. We prove that the source function (16.1.3) satisfies the Poisson equation in (16.7.10) (*i.e.*, (16.1.1)) as $Q^* = Q^*_{\text{in}} (\in S)$. The Dirac-delta function $\delta(|\overline{PQ^*}|)$ is defined by $\delta(|\overline{PQ^*}|) = 0$ at node $P \neq Q^*$, $\delta(|\overline{PQ^*}|) = \infty$ at $P = Q^*$, and $\iint_{R^2} \delta(|\overline{PQ^*}|)\, ds_P = 1$. First, we have $\Delta u(P) = 0$ at $P \neq Q^*_{\text{in}}$ but $\Delta u(P) = \infty$ at $P = Q^*_{\text{in}}$. The latter is proved by contradiction: assume that $\Delta u(P)|_{P=Q^*_{\text{in}}} \leq \bar{c}_0$, where $\bar{c}_0\ (> 0)$ is a bounded positive constant. For point $M_0 \in S$, we have from [146, (1.69)]

$$u(M_0) = -\frac{1}{2\pi}\left\{\int_\Gamma \left(\ln|\overline{PM_0}|\frac{\partial u}{\partial \nu} - u\frac{\partial}{\partial \nu}(\ln|\overline{PM_0}|)\right) d\ell_P - \iint_S (\ln|\overline{PM_0}|)\Delta u(P)\, ds_P\right\}. \tag{16.7.11}$$

Let $M_0 = Q^*_{\text{in}}$ and $u(P) = \ln|\overline{PM_0}|$. Let $K_\varepsilon\,(\subset S)$ denote a disk with radius $\varepsilon\ (\leq \delta \ll 1)$ and center at M_0. We have from (16.7.11)

$$\begin{aligned} u(M_0) &= \frac{1}{2\pi}\iint_S \ln|\overline{PM_0}|\Delta u(P)\, ds_P = \frac{1}{2\pi}\iint_{K_\varepsilon} \ln|\overline{PM_0}|\Delta u(P)\, ds_P \\ &= -\frac{1}{2\pi}\iint_{K_\varepsilon} \Big|\ln|\overline{PM_0}|\Big|\Delta u(P)\, ds_P \geq -\frac{\bar{c}_0}{2\pi}\iint_{K_\varepsilon}\Big|\ln|\overline{PM_0}|\Big|\, ds_P = -\,\bar{c}_1, \end{aligned} \tag{16.7.12}$$

where $\bar{c}_1$ is also a positive constant. However, we have $u(M_0) = \ln|\overline{PM_0}| = -\infty$ at $P = M_0$, thus to violate (16.7.12). This contradiction confirms that $\Delta u(P)|_{P=Q^*_{\text{in}}} = \infty$. Next, we have the constant in (16.7.10)

$$c^* = \frac{1}{q}\iint_{R^2} \Delta u^* = \frac{1}{q}\iint_{K_\varepsilon} \Delta u^* = \frac{1}{q}\int_{\partial K_\varepsilon} \frac{\partial u^*}{\partial \nu} = \int_0^{2\pi} \frac{1}{\varepsilon}\varepsilon\, d\theta = 2\pi, \tag{16.7.13}$$

to give the Poisson equation in (16.1.1), which is also consistent with Chen *et al.* [45, (6)]. Suppose that the Dirichlet boundary data f is given and that the source pattern function as $\ln|\overline{PQ_0}|$ is also known. The goal is to seek the source location Q^* and the charge q. Such a goal can be fulfilled by the numerical solutions (16.7.9), Tab. 16.5 – The errors and the condition numbers for the amoeba-like Γ by the secant method to seek δ with the MFS using (16.7.9) with the circular pseudo-boundary at $R = 3$, where $\epsilon = u - v_{N+1}$, $N = 120$ and $M = 240$, and the generating function (16.7.8) is chosen.

(x^*, y^*)	k	$\delta^{(k)}$	$\|\epsilon\|_{\infty,\Gamma}$	$\|\epsilon\|_{0,\Gamma}$	Cond	Cond_eff	$\|\mathbf{x}\|$	$\sigma_{\min}$
Initial value	0	0.0020000000000000	4.06(−1)	7.40(−2)	1.36(17)	7.77(5)	6.15(9)	1.83(−15)
Initial value	1	0.0040000000000000	2.61(−1)	5.01(−2)	1.35(17)	1.26(6)	3.73(9)	1.86(−15)
$Q^*_{\text{out}} = (e + 0.01, 0)$	2	0.0081890930240614	5.86(−2)	1.26(−2)	1.38(17)	5.70(6)	8.27(8)	1.86(−15)
	3	0.0095967733892493	1.19(−2)	2.66(−3)	1.34(17)	2.84(7)	1.70(8)	1.81(−15)
	4	0.0099728432387588	7.82(−4)	1.77(−4)	1.31(17)	4.27(8)	1.11(7)	1.84(−15)
	5	0.0099996706749956	9.48(−6)	2.15(−6)	1.44(17)	3.58(10)	1.34(5)	1.82(−15)
	6	0.0100000001588578	4.57(−9)	1.03(−9)	1.33(17)	7.38(13)	6.49(1)	1.82(−15)
	7	0.0100000003178390	9.13(−9)	2.06(−9)	1.31(17)	3.67(13)	1.30(2)	1.83(−15)
	8	0.0099999999986632	3.83(−11)	8.58(−12)	1.36(17)	3.29(15)	1.46	1.82(−15)
	9	0.0099999999973286	7.66(−11)	1.72(−11)	1.42(17)	2.73(15)	1.72	1.87(−15)
	10	0.0099999999999895	2.75(−13)	8.97(−14)	1.38(17)	3.71(15)	1.29	1.83(−15)
Initial value	0	−0.0010000000000000	3.95(−1)	7.29(−2)	1.40(17)	2.04(5)	2.33(10)	1.84(−15)
Initial value	1	−0.0020000000000000	3.38(−1)	6.14(−2)	1.36(17)	2.40(5)	1.98(10)	1.83(−15)
$Q^*_{\text{in}} = (e - 0.01, 0)$	2	−0.0073265125798887	1.07(−1)	2.57(−2)	1.34(17)	1.14(6)	4.07(9)	1.87(−15)
	3	−0.0111588864695238	7.24(−2)	1.90(−2)	1.43(17)	1.52(6)	3.07(9)	1.86(−15)
	4	−0.0219966747236658	8.58(−1)	2.52(−1)	1.37(17)	9.70(4)	6.58(10)	1.37(−15)
	5	−0.0102772757895882	1.64(−2)	4.19(−3)	1.46(17)	7.39(6)	6.31(8)	1.87(−15)
	6	−0.0100790744154180	4.58(−3)	1.16(−3)	1.45(17)	2.70(7)	1.73(8)	1.87(−15)
	7	−0.0100032400494495	1.86(−4)	4.70(−5)	1.45(17)	6.89(8)	6.98(6)	1.81(−15)
	8	−0.0100000359453106	2.06(−6)	5.21(−7)	1.48(17)	6.13(10)	7.72(4)	1.84(−15)
	9	−0.0100000000294661	1.69(−9)	4.27(−10)	1.47(17)	7.49(13)	6.32(1)	1.84(−15)
	10	−0.0100000000000482	3.21(−12)	8.43(−13)	1.47(17)	3.91(15)	1.21	1.84(−15)

Tab. 16.5 – (continued).

(x^*, y^*)	k	$\delta^{(k)}$	$\Vert\epsilon\Vert_{\infty,\Gamma}$	$\Vert\epsilon\Vert_{0,\Gamma}$	Cond	Cond_eff	$\Vert\mathbf{x}\Vert$	$\sigma_{\min}$
Initial value	0	−0.0002000000000000	3.41(−1)	5.53(−2)	1.35(17)	5.71(5)	8.38(9)	1.85(−15)
Initial value	1	−0.0004000000000000	2.27(−1)	3.68(−2)	1.33(17)	8.60(5)	5.50(9)	1.87(−15)
$Q^*_{\text{in}} = (e - 0.001, 0)$	2	−0.0007969303367521	6.65(−2)	1.08(−2)	1.38(17)	2.97(6)	1.61(9)	1.85(−15)
	3	−0.0009619928643445	1.19(−2)	1.94(−3)	1.36(17)	1.68(7)	2.90(8)	1.81(−15)
	4	−0.0009981337549312	5.86(−4)	9.53(−5)	1.32(17)	3.42(8)	1.40(7)	1.84(−15)
	5	−0.0010000028779164	9.06(−7)	1.47(−7)	1.35(17)	2.24(11)	2.16(4)	1.82(−15)
	6	−0.0010000057706843	1.82(−6)	2.95(−7)	1.36(17)	1.09(11)	4.36(4)	1.86(−15)
	7	−0.0010000000001013	3.38(−11)	5.59(−12)	1.41(17)	3.50(15)	1.38	1.82(−15)
	8	−0.0009999999999920	1.78(−12)	5.74(−13)	1.40(17)	3.96(15)	1.22	1.83(−15)
	9	−0.0009999999999796	5.52(−12)	9.56(−13)	1.33(17)	3.74(15)	1.29	1.83(−15)
	10	−0.0010000000000108	4.03(−12)	7.04(−13)	1.38(17)	3.80(15)	1.26	1.85(−15)

which have high accuracy by removal techniques. In this section, the numerical solutions for node $Q_0\,(=Q^*_{\text{out}}, Q^*_{\text{in}})$ also solve the source identification problem A.

Next, consider $Q_0\,(=Q^*_{\text{in}})\in S$, the equation (16.7.9) leads to

$$v_{N+1}(P)=v_{N+1}(\rho,\theta)=d_0\,\ln|\overline{PQ^*_{\text{in}}}|+\sum_{i=1}^{N}c_i\,\ln|\overline{PQ_i}|, \tag{16.7.14}$$

where $Q^*_{\text{in}}\in S$ and $P=(\rho,\theta)\in S$. Define the pseudo identification problem for $Q^*_{\text{in}}\in S$ only: **Problem B.** Consider the Dirichlet problem of Laplace's equation,

$$\Delta u(P)=0 \text{ in } S,\ \ u|_\Gamma=f=f_s+\left\{q\,\ln|\overline{PQ^*_{\text{in}}}|\right\}\Big|_\Gamma. \tag{16.7.15}$$

The goal is to discover the singular part $q\,\ln|\overline{PQ^*_{\text{in}}}|$ of function f as if there were a source node $Q^*_{\text{in}}\,(\in S)$. For circular, elliptic, and polygonal boundaries, the harmonic numerical solutions may be obtained by using the image source node Q^*_{out} outside Γ.

Let us consider the pseudo identification problem B for the amoeba-like domain. There is a dilemma that the numerical solutions (16.7.14) are not harmonic functions in S. Below, let us find the harmonic solutions. Note that the functions (16.7.14) are harmonic except at $P=Q^*_{\text{in}}$. From [223, p.327], it is possible to find a harmonic function $v^*_{N+1}(P)$ in the entire domain S.

Let $u=u^*+v$, where both u^* and v are harmonic functions satisfying

$$\Delta u^*(P)=0 \text{ in } S,\quad u^*|_\Gamma=f^*=\left\{q\,\ln|\overline{PQ^*_{\text{in}}}|\right\}\Big|_\Gamma, \tag{16.7.16}$$

$$\Delta v(P)=0 \text{ in } S,\quad v|_\Gamma=f_s. \tag{16.7.17}$$

Since the source pattern function as $w(P)=d_0\,\ln|\overline{PQ^*_{\text{in}}}|$ is known, we obtain the harmonic function in S from (16.7.11)

$$u^*(P)=-\frac{1}{2\pi}\int_\Gamma\left\{\frac{\partial w(Q)}{\partial\nu_Q}\ln|\overline{PQ}|-w(Q)\frac{\partial}{\partial\nu_Q}(\ln|\overline{PQ}|)\right\}d\ell_Q. \tag{16.7.18}$$

The harmonic function v in (16.7.17) is given in the second term on the right-hand side of (16.7.9),

$$v_N(P)=\sum_{i=1}^{N}c_i\,\ln|\overline{PQ_i}|. \tag{16.7.19}$$

Then the approximate harmonic functions $\tilde{u}(P)$ at $P\in S$ for the source identification problem B are found as

$$\tilde{u}(P)=u^*(P)+\sum_{i=1}^{N}c_i\,\ln|\overline{PQ_i}|. \tag{16.7.20}$$

For the circular boundary Γ with radius a, the harmonic solution $u^*(P)$ can be found simply based on the Poisson integral. Denote $P=(\rho,\theta)\in S$ and $Q=(a,\phi)\in\Gamma$. We have from [223, p.345]

$$u^*(P)=u^*(\rho,\theta)=\frac{1}{2\pi}\int_0^{2\pi}w(\phi)\left\{\frac{a^2-\rho^2}{a^2+\rho^2-2a\rho\,\cos(\theta-\phi)}\right\}d\phi, \tag{16.7.21}$$

where $w(\phi)=w(P)=\{d_0\,\ln|\overline{PQ^*_{\rm in}}|\}|_\Gamma$. The equation (16.7.21) is an integral representation involving closed functions, which is desirable in physical problems (see [193, p.791]). The harmonic functions are also found as (16.7.20) but with (16.7.21). Note that in (16.7.18) and (16.7.21), the integrals are nearly singular because node $Q^*_{\rm in}$ is near Γ. The techniques in Gu *et al.* [92, 93] may be used to provide the correct harmonic solutions. Hence, the above dilemma has been clarified.

Remark 16.7.1. *Let us compare the singularity of source functions with that of interior crack problems (e.g., Motz's problem in Chapter 1 and [151, 169]). From the singular solution* $u=O\left(r^{\frac{1}{2}}\right)$ *for Motz's problem, we have* $u\in\mathbf{H}^{1-\delta}(\Gamma)$ *with* $0<\delta\ll 1$, *and the slow convergence rates as* $\|u-u_n\|_{0,\Gamma}=O\left(\frac{1}{n^{1-\delta}}\right)$ *occur by the MPS. For the singularity caused from* $q\ln|\overline{PQ_0}|$ *as* Q_0 *near* Γ, *the solution* $u\in\mathbf{H}^{\beta}(\Gamma)$ *with* $\beta\geq\frac{1}{2}$ *may happen, and the slowest convergence rate* $\|u-u_n\|_{0,\Gamma}=O\left(\frac{1}{\sqrt{n}}\right)$ *may be incurred (also see (16.4.6)). Hence, the removal techniques in this chapter are imperative to reach satisfactory solutions in practical applications.*

Remark 16.7.2. *For the pseudo identification problem B, we may choose a few* $L\,(\geq 1)$ *unknown nodes* $Q^{(k)}_{\rm out}=\left(x^{(k)}_{\rm out},y^{(k)}_{\rm out}\right)$ *outside* Γ, *and employ* $(N+L)$ *fundamental solutions,*

$$v_{N+L}=\sum_{k=1}^{L}d_k\,\ln\left|\overline{PQ^{(k)}_{\rm out}}\right|+\sum_{i=1}^{N}c_i\,\ln|\overline{PQ_i}|. \tag{16.7.22}$$

By solving the nonlinear system of $Q^{(k)}_{\rm out}$, *the singularity may be removed, and the harmonic solutions can be obtained. The nonlinear equations for source nodes* $Q^{(k)}_{\rm out}$ *can be solved by the MATLAB routines* **lsqnonlin** *and* **fsolve** *as in [38, 89].*

Remark 16.7.3. *The removal techniques in this chapter can be applied to different types of logarithmic singularity*

$$u^*=u^*(P)=q\left(\ln|\overline{PQ^*}|\right)^{\beta},\quad \beta>0, \tag{16.7.23}$$

and strong singularity as node Q^* *near boundary* Γ,

$$u^*=u^*(P)=q\frac{1}{|\overline{PQ^*}|^{\beta}},\quad \beta>0. \tag{16.7.24}$$

Details are given in [253]. In Mathon and Johnston [189], all locations of Q_i *are unknown. Since the number of* Q_i *is not small in applications, some complexities of large-scale nonlinear solvers (such as suitable initial values) may be encountered. In (16.7.22), we choose a few nonlinear parameters, and the troubles of nonlinear problems may be bypassed or easily handled. The numerical examples in Section 16.7 are encouraging and promising. The algorithms and the removal techniques in this chapter may grant new vitality to the MFS for further devolvement and wide application. There remains a question: how can we know the patterns of singular functions as in (16.7.23) and (16.7.24)? The more singularity properties we know, the more efficient the removal techniques will be. Before the removal techniques proposed in Section 16.5, we have explored in-depth the singularity properties of the source function (16.5.1) in Sections 16.3 and 16.4. For the problems to be solved, the singularity pattern should first be discovered, and then the algorithms and the removal techniques in this chapter can be applied.*

16.8 Concluding Remarks

To close this chapter, let us address its novelties.

1. The analytical framework for the errors involving numerical integration of the MPS is provided in Section 16.2, which is important to the reduced convergence rates from the singularity caused by the source function (16.1.3). This is an advanced development of analysis for the CTM in the book [169].
2. For the source function (16.1.3) when Q^* is near boundary Γ, the solutions have $u \in \mathbf{H}^1(S)$ for arbitrary domains from Lemma 16.4.1. The singularity from (16.1.3) may be stronger than that of the interior crack (see Remark 16.7.1). For polygonal domains, the solutions have $u\,(\in \mathbf{H}^1(\Gamma)) = O\Big(\frac{1}{\sqrt{\delta}}\Big)$ from Theorem 16.4.1, where $\delta\,(\ll 1)$ is the distance of Q^* to boundary Γ. For circular and elliptic domains, the sharper convergence rates $O\Big(\frac{1}{n\sqrt{\delta}}\,e^{-n\delta}\Big)$ of the MPS are obtained in Section 16.3.
3. The removal techniques are proposed in Section 16.5, where an additional source node Q_0 is added to the original source nodes in the traditional MFS. The source location Q_0 and the charge d_0 are unknown, which can be sought by the secant method. The stability by using v_{N+1} in (16.5.2) remains the same as the MFS; see Proposition 16.5.3. This is also an advanced development of the MFS.
4. When $Q_0\,(= Q^*_{\text{in}}) \in S$, the image source node Q^*_{out} outside Γ may be solicited not only to provide the harmonic solutions in S but also to identify the source node $Q^*_{\text{in}}\,(\in S)$ by image reflection. For elliptic domains, Proposition 16.5.2 is new (*cf.* [223, p.354])) for image concepts and numerical methods.
5. In Section 16.7, the amoeba-like domains are discussed. The source identification Problem A and the pseudo source identification Problem B are proposed. For Problem B, the harmonic solutions in S are provided in (16.7.20) and (16.7.21). Note that the source identification Problems A and B are different from those in Karageorghis *et al.* [119, p.319].

6. The source function (16.1.3) (*i.e.*, the FS) is essential to physics, mathematics, and computation [104, 169, 193, 210, 223]. When the source node Q^* is near boundary Γ, there occurs the new singularity problem differently from those in [91, 146, 168, 169]. A comprehensive study has been made for the solution singularity, the reduced convergence rates of the MPS and the MFS, and the removal techniques. Hence, the analysis and algorithms in this chapter are important for both theory and computation in partial differential equations (PDE).
7. In Remark 16.7.3, the removal techniques are extended to different types of logarithmic singularity and strong singularity as node Q^* near boundary Γ. The $(N+1)$ linear coefficients and a few nonlinear parameters are chosen in the MFS algorithms, thus greatly degrading the troubles encountered in large-scale nonlinear solvers. The new study in this chapter may grant new vitality to the MFS for further devolvements and wide applications.

Chapter 17

Source Nodes on Pseudo Radial-Lines

Consider Laplace's equation in a bounded simply-connected domain S in 2D. In the standard method of fundamental solutions (MFS), the source nodes are located on a closed contour outside the domain boundary $\Gamma\,(=\partial S)$, called pseudo-boundaries. For circular/elliptic pseudo-boundaries and the pseudo-boundaries near boundary Γ, the analysis and the computation have been studied in previous chapters. New locations of source nodes are studied along pseudo radial-lines outside Γ in this chapter. First, choose the source nodes located on one pseudo radial-line. We prove that the MFS using one pseudo radial-line of source nodes is divergent. Then we propose two pseudo radial-lines, where the source nodes as (R_i, ϕ_1^*) and (R_i, ϕ_2^*) are chosen, and two different angles ϕ_1^* and ϕ_2^* are fixed. The error analysis is provided with adaptive error estimates in [256], which involve the numerical coefficients that have been obtained. Numerical results are encouraging and promising. Since the success of the MFS mainly depends on stability, we derive the lower and the upper bounds of condition number (Cond) for disk domains in [257]. Both lower and upper bounds are intriguing in stability study for the MFS. Numerical experiments are carried out to verify the stability analysis made. The new algorithms using two pseudo radial-lines in this chapter may become a competent boundary method in the MFS family. The materials of this chapter are adapted from [256, 257].

17.1 Introduction

Consider Laplace's equation with the Dirichlet boundary condition,

$$\Delta u = 0 \text{ in } S, \quad u = f \text{ on } \Gamma, \tag{17.1.1}$$

where S is a bounded simply-connected domain and $\Gamma\,(=\partial S)$ its smooth boundary. Let $P = (\rho, \theta)$ and the source nodes $Q_j = (R_j, \phi_j)$ outside S. Choose the fundamental solutions (FS),

$$\Phi_j(\rho, \theta) = \ln|\overline{PQ_j}|, \quad |\overline{PQ_j}| = \sqrt{R_j^2 + \rho^2 - 2R_j\rho\,\cos(\theta - \phi_j)}. \tag{17.1.2}$$

DOI: 10.1051/978-2-7598-3171-5.c017
© Science Press, EDP Sciences, 2023

We obtain a linear combination of FS as

$$u_N = \sum_{j=1}^{N} c_j \ln|\overline{PQ_j}| = \sum_{j=1}^{N} c_j \Phi_j(\rho,\theta), \tag{17.1.3}$$

where c_j are unknown coefficients. Let Γ be divided into small Γ_ℓ with the meshspacings $\triangle h_\ell$, *i.e.*, $\Gamma = \bigcup_{\ell=1}^{M} \Gamma_\ell$. We assume that the meshspacings $\triangle h_\ell$ are quasiuniform satisfying $\frac{\max_\ell |\triangle h_\ell|}{\min_\ell |\triangle h_\ell|} \le C$, where C is a constant independent of M. For simplicity, choose (ρ_ℓ, θ_ℓ) as the midpoint of Γ_ℓ. We obtain the collocation equations from the Dirichlet boundary condition in (17.1.1),

$$\sqrt{\triangle h_\ell} \sum_{j=1}^{N} c_j \Phi_j(\rho_\ell, \theta_\ell) = \sqrt{\triangle h_\ell}\, f(\rho_\ell, \theta_\ell), \quad \ell = 1, 2, ..., M, \tag{17.1.4}$$

where $M \ge N$. The equation (17.1.4) leads to an overdetermined system $\mathbf{Ax} = \mathbf{b}$, where matrix $\mathbf{A} \in \mathbf{R}^{M\times N}(M \ge N)$, and vectors $\mathbf{x} = (c_1, c_2, ..., c_N)^T \in \mathbf{R}^N$ and $\mathbf{b} \in \mathbf{R}^M$.

In the standard MFS, the source nodes are located on a closed contour outside the domain boundary $\Gamma\,(= \partial S)$, called pseudo-boundaries. Error and stability analysis is made for circular/elliptic pseudo-boundaries in the previous chapters. We study the new locations of source nodes along pseudo radial-lines outside Γ. Denote the source nodes by (R_i, ϕ^*) in polar coordinates, where $R_i > \rho_{\max} = \max \rho|_\Gamma$ but angle ϕ^* is fixed. Hence the source nodes are located on one radial-line at $\phi = \phi^*$. The algorithms of the MFS using one pseudo radial-line are divergent. Then two pseudo radial-lines are proposed, where the source nodes as (R_i, ϕ_1^*) and (R_i, ϕ_2^*) are chosen, and two different angles ϕ_1^* and ϕ_2^* are fixed. Error analysis is made with adaptive error estimates in [256], which involve the numerical coefficients that have been obtained. Numerical results are encouraging and promising. Since the success of the MFS mainly depends on stability, we further study two pseudo radial-lines of source nodes but focus on stability analysis in this chapter. Both the lower and upper bounds of Cond are derived for disk domains. Denote two pseudo radial-lines of source nodes by

$$\begin{aligned} &Q_j^- = \big(R_j, \phi_1^*\big), \quad Q_j^+ = \big(R_j, \phi_2^*\big), \quad j = 0, 1, 2, ..., n, \\ &\phi_1^* < \phi_2^*, \quad \rho_{\max} < R_0 < R_1 < \cdots < R_n = R_{\max}. \end{aligned} \tag{17.1.5}$$

The source nodes in (17.1.5) are located along two different radial-lines at $\phi = \phi_1^*$ and $\phi = \phi_2^*$. Consider two types of FS in (17.1.3) as

$$\textbf{Basic Case}: u_N = \sum_{j=0}^{n} c_j \Phi_j^-(\rho,\theta) + \sum_{j=1}^{n} c_j^* \Phi_j^+(\rho,\theta), \tag{17.1.6}$$

$$\textbf{Variant Case}: u_N = \sum_{j=0}^{n} c_j \Phi_j^-(\rho,\theta) + \sum_{j=0}^{n} c_j^* \Phi_j^+(\rho,\theta), \tag{17.1.7}$$

where $N = 2n+1, 2n+2$, c_j and c_j^* are unknown coefficients, and

$$\Phi_j^-(\rho,\theta) = \ln|\overline{PQ_j^-}| = \ln\sqrt{R_j^2 + \rho^2 - 2R_j\rho\,\cos(\theta - \phi_1^*)}, \tag{17.1.8}$$

$$\Phi_j^+(\rho,\theta) = \ln|\overline{PQ_j^+}| = \ln\sqrt{R_j^2 + \rho^2 - 2R_j\rho\,\cos(\theta - \phi_2^*)}. \tag{17.1.9}$$

For these two pseudo radial-lines, we study in detail two kinds of locations of source nodes in [256], Case I: uniform $R_i \in [R_0, R_{\max}]$ and Case II: uniform $x_i = \frac{\rho_{\max}}{R_i} \in [a, b]$, where $0<a<b<1$. Numerical experiments for Cases I and II are carried out in [256] to seek better parameters $R_0, R_{\max}$ and (ϕ_1^*, ϕ_2^*). Case II is superior to Case I due to better stability and better numerical performance, so we prefer Case II. Based on the numerical experiments in [256], large $R_{\max} = 10000$ in Case II may render better numerical performance. Since the angles as $\phi_2^* - \phi_1^* = \frac{\pi}{4n}$ and $\phi_2^* - \phi_1^* = \frac{\pi}{6} - \frac{\pi}{4n}$ are also beneficial, they are chosen for analysis and computation in this chapter.

Since the success of the MFS mainly depends on stability, numerical stability is imperative and challenging. Since the discrete matrices consist of the Vandermonde matrix whose ill-conditioning is notorious, the lower bound of Cond is an important topic (see [84–86, 199, 229] and [99, Chapter 21]). Both the lower and upper bounds of Cond are first derived for disk domains. Let $\rho_{\max} < R_0 \le R_i \le R_{\max}$, where $\rho_{\max} = \max \rho|_\Gamma$. The following lower bounds are derived in Theorem 17.3.1 for Basic Case in (17.1.6),

$$\text{Cond}(\mathbf{A}) \ge \frac{2^{2n-2}}{\pi} \times \left(\frac{R_0}{\rho_{\max}}\right)^{n-1}, \quad N = 2n+1. \tag{17.1.10}$$

For Variant Case in (17.1.7), the lower bounds are derived in [257], which are smaller than those in (17.1.10).

In Case II, the nodes $x_i = \frac{\rho_{\max}}{R_i}$ are located on $[a, b]$ uniformly, where $a = \frac{\rho_{\max}}{R_{\max}} = O\left(\frac{1}{n}\right)$ and $b = \frac{\rho_{\max}}{R_0} < 1$. The upper bound estimates are derived for Variant Case in Case II and given in (17.3.28) as

$$\text{Cond}(\mathbf{A}) \le C(\ln R_{\max}) N^{1.5+\gamma+\beta} \times 2^{\frac{3}{2}N} \times \left(\frac{R_0}{\rho_{\max}}\right)^{\frac{N}{2}}, \tag{17.1.11}$$

where $\beta \ge 0$ and $\gamma = 0, 1$ are for $\phi_2^* - \phi_1^* = \frac{\pi}{4n}$ and $\frac{\pi}{6} - \frac{\pi}{4n}$, respectively and C is a bounded constant independent of N. Comparing (17.1.11) with (17.1.10), there occurs an additional exponential rate $O(\sqrt{2}^N)$ of Cond for $N \gg 1$.

The exponential growth of Cond is confirmed from (17.1.10) and (17.1.11), which is the same as that in the standard MFS but lower than the super-exponential growth of the boundary knot method (BKM) in Section 7.5. Both lower and upper bound estimates of Cond in this chapter are intriguing in the stability study for the MFS in the previous chapters. All numerical Cond is coincident with the lower and upper bound estimates.

Remark 17.1.1. *Error analysis is the other important criterion for numerical algorithms. We derive the error bounds in [256]. Suppose the solution* $u \in \mathbf{H}^p(\Gamma)$ *with* $p > 1$. *Choose Variant Case (17.1.7) and use the source nodes in (17.1.5). There exists the error bound,*

$$\|u - u_N\|_{0,\Gamma} \leq C\left\{\frac{\|u\|_{p,\Gamma}}{N^p} + \frac{\|\mathbf{x}\|}{\sqrt{N}}\left(\frac{\rho_{\max}}{R_0}\right)^{\frac{N}{2}}\right\}, \tag{17.1.12}$$

where C *is a constant independent of* N. *Moreover, there also exists the bound,*

$$\|u - u_N\|_{0,\Gamma} \leq C\left\{\sum_{k=n+1}^{\infty}(|a_k| + |b_k|) + \frac{1}{N}\sum_{j=0}^{n}(|c_j| + |c_j^*|)x_j^{n+1}\right\}, \tag{17.1.13}$$

where $N = 2n+2$ *and* $x_j = \frac{\rho_{\max}}{R_j}$, c_j *and* c_j^* *are the numerical coefficients in (17.1.7), and* a_k *and* b_k *the expansion coefficients in (17.2.1) below. The error bounds (17.1.12) and (17.1.13) are valid for all kinds of* (R_i, ϕ_1^*) and (R_i, ϕ_2^*), *and they can be applied to non-disk domains. The error bounds (17.1.12) and (17.1.13) involve the coefficients* c_j *and* c_j^*, *which are known only after the numerical computation has been completed. They are called adaptive errors (AE). The error bounds (17.1.13) are useful in the application as the effective condition number (see [162]). Suppose that the solution is nonsingular as* $u \in \mathbf{H}^p(\Gamma)$ *with* $p \geq 2$. *Hence, we may employ the second term on the right-hand side in (17.1.13) as the AE,*

$$AE := \frac{1}{N}\left\{\sum_{j=0}^{n}(|c_j| + |c_j^*|)x_j^{n+1}\right\}, \quad x_j = \frac{\rho_{\max}}{R_j}. \tag{17.1.14}$$

The equation (17.1.14) with $c_0^* = 0$ *is valid for Basic Case in (17.1.6). Numerical verification for the adaptive errors is given in [256].*

This chapter is organized as follows. In the next section, we prove that the algorithms of one pseudo radial-line diverge. Then two pseudo radial-lines are essential. In Section 17.3, the lower and upper bounds of Cond are provided for two pseudo radial-lines. In Section 17.4, numerical experiments are carried out to verify the analysis made. In the last section, a few remarks are made.

17.2 Pseudo Radial-Lines

17.2.1 One Pseudo Radial-Line

The particular solutions (PS) of (17.1.1) are given by

$$u(\rho,\theta) = a_0 + \sum_{k=1}^{\infty}\left(\frac{\rho}{\rho_{\max}}\right)^k (a_k \cos k\theta + b_k \sin k\theta) := P_n + R_n, \tag{17.2.1}$$

where $\rho_{\max} = \max\, \rho|_\Gamma$, and the PS of degree n and the residuals are given by

$$P_n = P_n(\rho, \theta) = a_0 + \sum_{k=1}^{n} \left(\frac{\rho}{\rho_{\max}}\right)^k (a_k \cos k\theta + b_k \sin k\theta), \tag{17.2.2}$$

$$R_n = R_n(\rho, \theta) = \sum_{k=n+1}^{\infty} \left(\frac{\rho}{\rho_{\max}}\right)^k (a_k \cos k\theta + b_k \sin k\theta), \tag{17.2.3}$$

where a_k and b_k are the expansion coefficients. Let $P(\rho, \theta) \in \bar{S}$ and the source nodes $Q(R, \phi)$ with $R > \rho_{\max}$. From Lemma I.3 in Part I, we have

$$\ln|\overline{PQ}| = \ln\sqrt{R^2 + \rho^2 - 2R\rho\, \cos(\theta - \phi)} = \ln R - \sum_{k=1}^{\infty} \frac{1}{k}\left(\frac{\rho}{R}\right)^k \cos k(\theta - \phi), \;\; \rho < R. \tag{17.2.4}$$

First, we employ one pseudo radial-line, and choose the source nodes, $Q_j^* = (R_j, \phi^*)$, $\rho_{\max} < R_1 < R_2 < \cdots < R_N$, where the angle $\phi^* \in [0, 2\pi)$ is unchanged. From (17.2.4) we have

$$\ln|\overline{PQ_j^*}| = \ln\sqrt{R_j^2 + \rho^2 - 2R_j\rho\, \cos(\theta - \phi^*)} = \ln R_j - \sum_{k=1}^{\infty} \frac{1}{k}\left(\frac{\rho}{R_j}\right)^k \cos k(\theta - \phi^*).$$

Then, a linear combination u_N^* in (17.1.3) can be denoted as one of P_n in (17.2.2),

$$u_N^* \approx P_n^*(\rho, \theta) = a_0^* + \sum_{k=1}^{n} \left(\frac{\rho}{\rho_{\max}}\right)^k (a_k^* \cos k\theta + b_k^* \sin k\theta), \tag{17.2.5}$$

where the coefficients

$$\begin{aligned} a_0^* &= \sum_{j=1}^{N} c_j \ln R_j, \quad a_k^* = -\sum_{j=1}^{N} c_j \frac{1}{k}\left(\frac{\rho_{\max}}{R_j}\right)^k \cos(k\phi^*), \\ b_k^* &= -\sum_{j=1}^{N} c_j \frac{1}{k}\left(\frac{\rho_{\max}}{R_j}\right)^k \sin(k\phi^*), \end{aligned} \tag{17.2.6}$$

where $N \geq 2n + 1$. The equations (17.2.6) are denoted by a linear algebraic equation,

$$\mathbf{y} = \mathbf{E}\mathbf{x}, \tag{17.2.7}$$

where vectors $\mathbf{x} = (c_1, c_2, ..., c_N)^T \in \mathbf{R}^N$ and $\mathbf{y} = (a_0^*, a_1^*, ..., a_n^*, b_1^*, ..., b_n^*)^T \in \mathbf{R}^{2n+1}$, and matrix $\mathbf{E} \in \mathbf{R}^{(2n+1)\times N}$ has the entries,

$$\begin{aligned} &\mathbf{E}_{1,j} = \ln R_j, \quad j = 1, 2, ..., N, \\ &\mathbf{E}_{k+1,j} = -\frac{1}{k}\left(\frac{\rho_{\max}}{R_j}\right)^k \cos(k\phi^*), \quad j = 1, 2, ..., N, \quad k = 1, 2, ..., n, \\ &\mathbf{E}_{k+n+1,j} = -\frac{1}{k}\left(\frac{\rho_{\max}}{R_j}\right)^k \sin(k\phi^*), \quad j = 1, 2, ..., N, \quad k = 1, 2, ..., n. \end{aligned}$$

We intend to establish the one-to-one correspondence between the vectors $\mathbf{y}$ and $\mathbf{x}$ in (17.2.7). Let $N = 2n+1$. The matrix in (17.2.7) is denoted by

$$\mathbf{E} = \begin{pmatrix} \ln R_1 & \ln R_2 & \cdots & \ln R_N \\ -\frac{\rho_{\max}}{R_1}\cos(\phi^*) & -\frac{\rho_{\max}}{R_2}\cos(\phi^*) & \cdots & -\frac{\rho_{\max}}{R_N}\cos(\phi^*) \\ -\frac{1}{2}\left(\frac{\rho_{\max}}{R_1}\right)^2\cos(2\phi^*) & -\frac{1}{2}\left(\frac{\rho_{\max}}{R_2}\right)^2\cos(2\phi^*) & \cdots & -\frac{1}{2}\left(\frac{\rho_{\max}}{R_N}\right)^2\cos(2\phi^*) \\ \vdots & \vdots & \vdots & \vdots \\ -\frac{1}{n}\left(\frac{\rho_{\max}}{R_1}\right)^n\cos(n\phi^*) & -\frac{1}{n}\left(\frac{\rho_{\max}}{R_2}\right)^n\cos(n\phi^*) & \cdots & -\frac{1}{n}\left(\frac{\rho_{\max}}{R_N}\right)^n\cos(n\phi^*) \\ -\frac{\rho_{\max}}{R_1}\sin(\phi^*) & -\frac{\rho_{\max}}{R_2}\sin(\phi^*) & \cdots & -\frac{\rho_{\max}}{R_N}\sin(\phi^*) \\ -\frac{1}{2}\left(\frac{\rho_{\max}}{R_1}\right)^2\sin(2\phi^*) & -\frac{1}{2}\left(\frac{\rho_{\max}}{R_2}\right)^2\sin(2\phi^*) & \cdots & -\frac{1}{2}\left(\frac{\rho_{\max}}{R_N}\right)^2\sin(2\phi^*) \\ \vdots & \vdots & \vdots & \vdots \\ -\frac{1}{n}\left(\frac{\rho_{\max}}{R_1}\right)^n\sin(n\phi^*) & -\frac{1}{n}\left(\frac{\rho_{\max}}{R_2}\right)^n\sin(n\phi^*) & \cdots & -\frac{1}{n}\left(\frac{\rho_{\max}}{R_N}\right)^n\sin(n\phi^*) \end{pmatrix}. \tag{17.2.8}$$

Suppose that matrix $\mathbf{E}$ is nonsingular. From (17.2.7) we have $\mathbf{x} = \mathbf{E}^{-1}\mathbf{y}$, where the inverse matrix $\mathbf{E}^{-1} \in \mathbf{R}^{N\times N}$. The particular solutions in (17.2.5) can be approximated by the FS in (17.1.3). Otherwise, the solutions from the MFS are divergent.

Proposition 17.2.1. *For the source nodes* $Q_j = (R_j, 0)$ *with* $\rho_{\max} < R_1 < R_2 < \cdots < R_N$, *matrix* $\mathbf{E}$ *in (17.2.8) is singular. Then the solutions from the MFS in (17.1.3) are divergent.*

Proof. First, let $N = 2n+1$. We have from (17.2.8)

$$\mathbf{E} = \begin{pmatrix} \ln R_1 & \ln R_2 & \cdots & \ln R_N \\ -\frac{\rho_{\max}}{R_1} & -\frac{\rho_{\max}}{R_2} & \cdots & -\frac{\rho_{\max}}{R_N} \\ -\frac{1}{2}\left(\frac{\rho_{\max}}{R_1}\right)^2 & -\frac{1}{2}\left(\frac{\rho_{\max}}{R_2}\right)^2 & \cdots & -\frac{1}{2}\left(\frac{\rho_{\max}}{R_N}\right)^2 \\ \vdots & \vdots & \vdots & \vdots \\ -\frac{1}{n}\left(\frac{\rho_{\max}}{R_1}\right)^n & -\frac{1}{n}\left(\frac{\rho_{\max}}{R_2}\right)^n & \cdots & -\frac{1}{n}\left(\frac{\rho_{\max}}{R_N}\right)^n \\ 0 & 0 & \cdots & 0 \\ 0 & 0 & \cdots & 0 \\ \vdots & \vdots & \vdots & \vdots \\ 0 & 0 & \cdots & 0 \end{pmatrix}. \tag{17.2.9}$$

The coefficients b_k^* in front of terms $\left(\frac{\rho}{\rho_{\max}}\right)^k \sin k\theta$ in (17.2.5) are all zeros. Next, for $N > 2n+1$, the coefficients b_k^* in (17.2.5) are also all zeros. When one coefficient $b_k \neq 0$, the solutions from the MFS are divergent. ■

In the numerical examples of [45, 48], only the solution, $u(x, y) = u(x, -y)$, was chosen so that all trivial coefficients $b_k = 0, \forall k$, and convergence of numerical solutions still showed up (see [45, (24)]).

Proposition 17.2.2. *For the source nodes $Q_j = (R_j, \phi^*)$ with $\rho_{\max} < R_1 < R_2 < \cdots < R_N$, matrix $\mathbf{E}$ in (17.2.8) is also singular. Then the solutions from the MFS in (17.1.3) are divergent for general harmonic functions.*

Proof. Denote the diagonal matrix $\mathbf{D}\,(\in \mathbf{R}^{(2n+1)\times(2n+1)})$ by

$$\mathbf{D} = -\mathrm{diag}\left\{-1, \cos\phi^*, \frac{1}{2}\cos 2\phi^*, \ldots, \frac{1}{n}\cos n\phi^*, \sin\phi^*, \frac{1}{2}\sin 2\phi^*, \ldots, \frac{1}{n}\sin n\phi^*\right\}. \quad (17.2.10)$$

We have $\mathbf{E} = \mathbf{D}\mathbf{E}^*$, where matrix $\mathbf{E}^*\,(\in \mathbf{R}^{(2n+1)\times N})$ is given by

$$\mathbf{E}^* = \begin{pmatrix} \ln R_1 & \ln R_2 & \cdots & \ln R_N \\ \frac{\rho_{\max}}{R_1} & \frac{\rho_{\max}}{R_2} & \cdots & \frac{\rho_{\max}}{R_N} \\ \left(\frac{\rho_{\max}}{R_1}\right)^2 & \left(\frac{\rho_{\max}}{R_2}\right)^2 & \cdots & \left(\frac{\rho_{\max}}{R_N}\right)^2 \\ \vdots & \vdots & \vdots & \vdots \\ \left(\frac{\rho_{\max}}{R_1}\right)^n & \left(\frac{\rho_{\max}}{R_2}\right)^n & \cdots & \left(\frac{\rho_{\max}}{R_N}\right)^n \\ \frac{\rho_{\max}}{R_1} & \frac{\rho_{\max}}{R_2} & \cdots & \frac{\rho_{\max}}{R_N} \\ \left(\frac{\rho_{\max}}{R_1}\right)^2 & \left(\frac{\rho_{\max}}{R_2}\right)^2 & \cdots & \left(\frac{\rho_{\max}}{R_N}\right)^2 \\ \vdots & \vdots & \vdots & \vdots \\ \left(\frac{\rho_{\max}}{R_1}\right)^n & \left(\frac{\rho_{\max}}{R_2}\right)^n & \cdots & \left(\frac{\rho_{\max}}{R_N}\right)^n \end{pmatrix}. \quad (17.2.11)$$

First, let $N = 2n+1$. Since the kth row of matrix $\mathbf{E}^*$ is identical to the other $(n+k)$th row at $k \in [2, n+1]$, matrix $\mathbf{E}^*$ is singular and so is matrix $\mathbf{E}$. The harmonic functions P_n in (17.2.2) can not be approximated by the u_N^* in (17.1.3), so the divergence statement in Proposition 17.2.2 is confirmed. Next, consider $N > 2n+1$. Denote a sub-matrix of (17.2.11) by

$$\mathbf{E}_1^*\,(\in \mathbf{R}^{n\times N}) = \begin{pmatrix} \frac{\rho_{\max}}{R_1} & \frac{\rho_{\max}}{R_2} & \cdots & \frac{\rho_{\max}}{R_N} \\ \left(\frac{\rho_{\max}}{R_1}\right)^2 & \left(\frac{\rho_{\max}}{R_2}\right)^2 & \cdots & \left(\frac{\rho_{\max}}{R_N}\right)^2 \\ \vdots & \vdots & \vdots & \vdots \\ \left(\frac{\rho_{\max}}{R_1}\right)^n & \left(\frac{\rho_{\max}}{R_2}\right)^n & \cdots & \left(\frac{\rho_{\max}}{R_N}\right)^n \end{pmatrix}, \quad (17.2.12)$$

and denote sub-diagonal matrices from matrix $\mathbf{D}$ in (17.2.10) by

$$\mathbf{D}_1\,(\in \mathbf{R}^{n\times n}) = -\text{diag}\left\{\cos\phi^*, \frac{1}{2}\cos 2\phi^*, ..., \frac{1}{n}\cos n\phi^*\right\}, \tag{17.2.13}$$

$$\mathbf{D}_2\,(\in \mathbf{R}^{n\times n}) = -\text{diag}\left\{\sin\phi^*, \frac{1}{2}\sin 2\phi^*, ..., \frac{1}{n}\sin n\phi^*\right\}. \tag{17.2.14}$$

Moreover, also denote two sub-vectors of $\mathbf{y}$ by $\mathbf{y}_1 = (a_1^*, ..., a_n^*)^T \in \mathbf{R}^n$ and $\mathbf{y}_2 = (b_1^*, ..., b_n^*)^T \in \mathbf{R}^n$. From (17.2.7) and (17.2.8), we have $\mathbf{y}_1 = \mathbf{D}_1\mathbf{E}_1^*\mathbf{x}$ and $\mathbf{y}_2 = \mathbf{D}_2\mathbf{E}_1^*\mathbf{x}$ to give a compulsory relation between two sub-vectors $\mathbf{y}_1$ and $\mathbf{y}_2$,

$$\mathbf{y}_2 = \mathbf{D}_2\mathbf{D}_1^{-1}\mathbf{y}_1, \tag{17.2.15}$$

where the diagonal matrix $\mathbf{D}_2\mathbf{D}_1^{-1} = \text{diag}\{\tan\phi^*, \tan 2\phi^*, ..., \tan n\phi^*\}$. For any harmonic polynomial (17.2.2) of order n without the coefficient relations (17.2.15), the solutions from the MFS in (17.1.3) diverge. This completes the proof of Proposition 17.2.2. ■

17.2.2 Two Pseudo Radial-Lines

To guarantee the convergence of numerical solutions, we propose two pseudo radial-lines of source nodes as follows,

$$\begin{aligned} &Q_j = (R_j, 0), \quad Q_j^* = (R_j, \phi^*), \quad j = 0, 1, 2, ..., n, \\ &\rho_{\max} < R_0 < R_1 < \cdots < R_n = R_{\max}, \end{aligned} \tag{17.2.16}$$

where $\rho_{\max} = \max\, \rho|_\Gamma$. The FS in (17.1.3) are expressed in two cases:

$$\textbf{Basic Case}: u_N = \sum_{j=0}^{n} c_j\Phi_j(\rho,\theta) + \sum_{j=1}^{n} c_j^*\Phi_j^*(\rho,\theta), \tag{17.2.17}$$

$$\textbf{Variant Case}: u_N = \sum_{j=0}^{n} c_j\Phi_j(\rho,\theta) + \sum_{j=0}^{n} c_j^*\Phi_j^*(\rho,\theta), \tag{17.2.18}$$

where $N = 2n+1$ or $N = 2n+2$, c_j and c_j^* are unknown coefficients, and

$$\Phi_j(\rho,\theta) = \ln|\overline{PQ_j}| = \ln\sqrt{R_j^2 + \rho^2 - 2R_j\rho\,\cos\theta}, \tag{17.2.19}$$

$$\Phi_j^*(\rho,\theta) = \ln|\overline{PQ_j^*}| = \ln\sqrt{R_j^2 + \rho^2 - 2R_j\rho\,\cos(\theta-\phi^*)}. \tag{17.2.20}$$

The source nodes in (17.2.16) are located along two radial-lines at $\phi = 0$ and $\phi = \phi^*(>0)$. We first choose a small angle $\phi^* = \frac{\pi}{4n}$, and then choose a big angle $\phi^* = \frac{\pi}{6} - \frac{\pi}{4n}$. We call (17.2.17) Basic Case algorithm with $N = 2n+1$ since the one-to-one correspondence remains between vectors $\mathbf{y}$ and $\mathbf{x}$ in (17.2.7). Moreover, we call (17.2.18) Variant Case algorithm with $N = 2n+2$.

17.3 Stability Analysis

17.3.1 Lower Bound Estimates of Cond for Basic Case

For lower bound estimates of Cond, we choose the FS in Basic Case (17.1.6). For the FS in Variant Case (17.1.7), the lower bound estimates of Cond are given in Remark 17.3.1 below. Consider a small angle $\phi_2^* - \phi_1^* = \phi^* = \frac{\pi}{4n}$. For disk domains, the Cond remains the same if the X-axis rotates with an angle ϕ_1^* in the counterclockwise direction. Without loss of generality, we simply choose $(\phi_1^*, \phi_2^*) = (0, \phi^*) = \left(0, \frac{\pi}{4n}\right)$. The FS in (17.1.8) and (17.1.9) lead to

$$\ln|\overline{PQ_j^-}| = \ln\sqrt{R_j^2 + \rho^2 - 2R_j\rho\,\cos\theta} = \ln R_j - \sum_{k=1}^{\infty} \frac{1}{k}\left(\frac{\rho}{R_j}\right)^k \cos k\theta,$$

$$\ln|\overline{PQ_j^+}| = \ln\sqrt{R_j^2 + \rho^2 - 2R_j\rho\,\cos(\theta - \phi^*)} = \ln R_j - \sum_{k=1}^{\infty} \frac{1}{k}\left(\frac{\rho}{R_j}\right)^k \cos k(\theta - \phi^*).$$

From (17.2.4), the linear combination u_N in Basic Case (17.1.6) can be used to approximate one of P_n in (17.2.2),

$$u_N^+ \approx P_n^+(\rho, \theta) = a_0^+ + \sum_{k=1}^{n} \left(\frac{\rho}{\rho_{\max}}\right)^k (a_k^+ \cos k\theta + b_k^+ \sin k\theta), \tag{17.3.1}$$

where the coefficients

$$\begin{aligned} a_0^+ &= c_0 \ln R_0 + \sum_{j=1}^{n} (c_j + c_j^*) \ln R_j, \quad a_k^+ = -\frac{c_0}{k}\left(\frac{\rho_{\max}}{R_0}\right)^k - \sum_{j=1}^{n} \frac{1}{k}\left(\frac{\rho_{\max}}{R_j}\right)^k \{c_j + c_j^* \cos(k\phi^*)\}, \\ b_k^+ &= -\sum_{j=1}^{n} c_j^* \frac{1}{k}\left(\frac{\rho_{\max}}{R_j}\right)^k \sin(k\phi^*). \end{aligned} \tag{17.3.2}$$

Denote (17.3.2) by the linear algebraic equations,

$$\mathbf{y} = \mathbf{E}\mathbf{x}, \tag{17.3.3}$$

where vectors $\mathbf{x} = \{c_0, c_1, ..., c_n, c_1^*, ..., c_n^*\}^T$, $\mathbf{y} = \{a_0^+, a_1^+, ..., a_n^+, b_1^+, ..., b_n^+\}^T \in \mathbf{R}^{2n+1}$. There exists the one-to-one correspondence between vectors $\mathbf{x}$ and $\mathbf{y}$. The matrix $\mathbf{E} \in \mathbf{R}^{(2n+1)\times(2n+1)}$ is denoted by

$$\mathbf{E} = \begin{pmatrix} \mathbf{E}_{11} & \mathbf{E}_{12} \\ \mathbf{O} & \mathbf{E}_{22} \end{pmatrix}, \tag{17.3.4}$$

where the sub-matrices

$$\mathbf{E}_{11}\ (\in \mathbf{R}^{(n+1)\times(n+1)}) = \begin{pmatrix} \ln R_0 & \ln R_1 & \cdots & \ln R_n \\ -\frac{\rho_{\max}}{R_0} & -\frac{\rho_{\max}}{R_1} & \cdots & -\frac{\rho_{\max}}{R_n} \\ \frac{-1}{2}\left(\frac{\rho_{\max}}{R_0}\right)^2 & \frac{-1}{2}\left(\frac{\rho_{\max}}{R_1}\right)^2 & \cdots & \frac{-1}{2}\left(\frac{\rho_{\max}}{R_n}\right)^2 \\ \vdots & \vdots & \vdots & \vdots \\ \frac{-1}{n}\left(\frac{\rho_{\max}}{R_0}\right)^n & \frac{-1}{n}\left(\frac{\rho_{\max}}{R_1}\right)^n & \cdots & \frac{-1}{n}\left(\frac{\rho_{\max}}{R_n}\right)^n \end{pmatrix},$$

$$\mathbf{E}_{22}\ (\in \mathbf{R}^{n\times n}) = \begin{pmatrix} -\frac{\rho_{\max}}{R_1}\sin\phi^* & \cdots & -\frac{\rho_{\max}}{R_n}\sin\phi^* \\ \frac{-1}{2}\left(\frac{\rho_{\max}}{R_1}\right)^2\sin 2\phi^* & \cdots & \frac{-1}{2}\left(\frac{\rho_{\max}}{R_n}\right)^2\sin 2\phi^* \\ \vdots & \vdots & \vdots \\ \frac{-1}{n}\left(\frac{\rho_{\max}}{R_1}\right)^n\sin n\phi^* & \cdots & \frac{-1}{n}\left(\frac{\rho_{\max}}{R_n}\right)^n\sin n\phi^* \end{pmatrix},$$

$$\mathbf{E}_{12}\ (\in \mathbf{R}^{(n+1)\times n}) = \begin{pmatrix} \ln R_1 & \cdots & \ln R_n \\ -\frac{\rho_{\max}}{R_1}\cos\phi^* & \cdots & -\frac{\rho_{\max}}{R_n}\cos\phi^* \\ \frac{-1}{2}\left(\frac{\rho_{\max}}{R_1}\right)^2\cos 2\phi^* & \cdots & \frac{-1}{2}\left(\frac{\rho_{\max}}{R_n}\right)^2\cos 2\phi^* \\ \vdots & \vdots & \vdots \\ \frac{-1}{n}\left(\frac{\rho_{\max}}{R_1}\right)^n\cos n\phi^* & \cdots & \frac{-1}{n}\left(\frac{\rho_{\max}}{R_n}\right)^n\cos n\phi^* \end{pmatrix},$$

and the null matrix $\mathbf{O} \in \mathbf{R}^{n\times(n+1)}$. We have from (17.3.4) and [71, p.21]

$$\mathrm{Det}(\mathbf{E}) = \mathrm{Det}(\mathbf{E}_{11}) \times \mathrm{Det}(\mathbf{E}_{22}) \neq 0. \tag{17.3.5}$$

Hence for source nodes $Q_j = (R_j, 0)$ and $Q_j^* = (R_j, \phi^*)$ in (17.2.16), matrix $\mathbf{E}$ in (17.3.4) is nonsingular.

By using Basic Case (17.1.6), the collocation equations (17.1.4) are modified by

$$\sqrt{\triangle h_\ell}\left\{\sum_{j=0}^{n} c_j \mathbf{\Phi}_j^-(\rho_\ell,\theta_\ell) + \sum_{j=1}^{n} c_j^* \mathbf{\Phi}_j^+(\rho_\ell,\theta_\ell)\right\} = \sqrt{\triangle h_\ell}\, f(\rho_\ell,\theta_\ell), \quad \ell = 1,2,...,N, \tag{17.3.6}$$

where $N = 2n+1$. The equation (17.3.6) is denoted by the following square system,

$$\mathbf{A}\mathbf{x} = \mathbf{b}, \tag{17.3.7}$$

where matrix $\mathbf{A} \in \mathbf{R}^{N\times N}$, and vectors $\mathbf{x} = (c_0, c_1, ..., c_n, c_1^*, ..., c_n^*)^T \in \mathbf{R}^N$ and $\mathbf{b} \in \mathbf{R}^N$. On the other hand, by using PS in (17.2.2) we have

$$\begin{aligned} \sqrt{\triangle h_\ell}\{P_n(\rho_\ell, \theta_\ell)\} &= \sqrt{\triangle h_\ell}\left\{ a_0^+ + \sum_{k=1}^{n} \left(\frac{\rho_\ell}{\rho_{\max}}\right)^k (a_k^+ \cos k\theta_\ell + b_k^+ \sin k\theta_\ell)\right\} \\ &= \sqrt{\triangle h_\ell}\, f(\rho_\ell, \theta_\ell), \quad \ell = 1, 2, ..., N. \end{aligned} \tag{17.3.8}$$

The equation (17.3.8) is denoted by

$$\mathbf{P}\mathbf{y} = \mathbf{b}, \tag{17.3.9}$$

where matrix $\mathbf{P} \in \mathbf{R}^{N\times N}$ and vectors $\mathbf{y} = (a_0^+, a_1^+, ..., a_n^+, b_1^+, ..., b_n^+)^T \in \mathbf{R}^N$ and $\mathbf{b} \in \mathbf{R}^N$. The algorithms using (17.3.8) (or (17.3.9)) are called the method of particular solutions (MPS) in [169]. Let $N = 2n+1$. We have from (17.3.9) and (17.3.3)

$$\mathbf{PEx} = \mathbf{b}, \tag{17.3.10}$$

where matrix $\mathbf{E} \in \mathbf{R}^{N\times N}$. Comparing (17.3.10) and (17.3.7), we have

$$\mathbf{A} = \mathbf{PE}. \tag{17.3.11}$$

First, we focus on evaluating the lower bounds of Cond($\mathbf{E}$). Denote the Vandermonde matrix $\mathbf{V}_n \in \mathbf{R}^{n\times n}$ by

$$\mathbf{V}_n = \begin{pmatrix} 1 & 1 & \cdots & 1 \\ x_1 & x_2 & \cdots & x_n \\ \vdots & \vdots & \vdots & \vdots \\ x_1^{n-1} & x_2^{n-1} & \cdots & x_n^{n-1} \end{pmatrix}, \quad \mathbf{V}_n^T = \begin{pmatrix} 1 & x_1 & \cdots & x_1^{n-1} \\ 1 & x_2 & \cdots & x_2^{n-1} \\ \vdots & \vdots & \vdots & \vdots \\ 1 & x_n & \cdots & x_n^{n-1} \end{pmatrix}, \tag{17.3.12}$$

where x_i are distinct, and $\mathbf{V}_n^T$ the transposed Vandermonde matrix. In our study, $x_i = \frac{\rho_{\max}}{R_i}$, $\rho_{\max} = \max \rho|_\Gamma$, and $\rho_{\max} < R_0 < R_1 < \cdots < R_n = R_{\max}$. There exist the bounds,

$$0 < a = \frac{\rho_{\max}}{R_{\max}} = \frac{\rho_{\max}}{R_n} \le x_i \le \frac{\rho_{\max}}{R_0} = b < 1. \tag{17.3.13}$$

From Tyrtyshnikov [229, Section 3], we have the following lemma, whose proof is given in [257].

Lemma 17.3.1. *Denote the diagonal matrix* $\mathbf{\Lambda}_n = \mathrm{diag}\{q_1, q_2, \ldots, q_n\} \in \mathbf{R}^{n\times n}$ *with* $q_i \neq 0, i = 1, 2, ..., n$, *and the Vandermonde matrix* $\mathbf{V}_n$ *in (17.3.12) with distinct* x_i *satisfying (17.3.13). There exists the lower bound of condition number*

$$\mathrm{Cond}(\mathbf{V}_n \mathbf{\Lambda}_n) \ge \frac{2^{2n-3}}{b^{n-1}}. \tag{17.3.14}$$

Based on (17.3.11) and Lemma 17.3.1, we give the following theorem, whose proof is given in [257].

Theorem 17.3.1. *For the source nodes $Q_j = (R_j, 0)$ and $Q_j^* = (R_j, \phi^*)$ in (17.2.16) with $\phi^* = \frac{\pi}{4n}$ by Basic Case (17.1.6), where $0 < a \le x_i = \frac{\rho_{\max}}{R_i} \le \frac{\rho_{\max}}{R_0} = b < 1$, there exists the lower bound for disk domains,*

$$\text{Cond}(\mathbf{A}) \ge \frac{2^{2n-2}}{\pi} \times \left(\frac{R_0}{\rho_{\max}}\right)^{n-1} = \frac{2^{N-3}}{\pi} \times \left(\frac{R_0}{\rho_{\max}}\right)^{\frac{N-3}{2}}, \quad n \ge 2, \tag{17.3.15}$$

where $N = 2n+1$.

Remark 17.3.1. *The lower bound estimates of Cond in Theorem 17.3.1 are confined to Basic Case with a small angle $\phi^* = \frac{\pi}{4n}$. We can derive the lower bounds in general cases. Variant Case in (17.1.7) is more useful because even N is often chosen in application. We derive lower bounds of Cond for Variant Case in [257] as*

$$\text{Cond}(\mathbf{F}) \ge \sqrt{\frac{16}{17}}\frac{2^{2n-4}}{\pi} \times \left(\frac{R_0}{\rho_{\max}}\right)^{n-2} = \sqrt{\frac{16}{17}}\frac{2^{N-6}}{\pi} \times \left(\frac{R_0}{\rho_{\max}}\right)^{\frac{N-6}{2}}, \quad n \ge 3, \tag{17.3.16}$$

where $N = 2n+2$ and matrix $\mathbf{F}$ is given in (17.3.18) below. When $\frac{\rho_{\max}}{R_0} = 2$, the lower bounds in (17.3.16) are smaller than those in (17.3.15) with a factor approximate to $\frac{1}{8}$. Since lower bounds in Basic Case are supported by numerical examples in Section 17.4 and [256], they are more important in application.

17.3.2 Upper Bound Estimates of Cond for Variant Case by Case II

In application, Variant Case (17.1.7) with even N is more useful than Basic Case (17.1.6) with odd N. The upper bounds of Cond are derived only for Variant Case (17.1.7) under Case II in this section. Then the collocation equations are given by

$$\sqrt{\triangle h_\ell} \sum_{j=0}^{n} \left\{ c_j \mathbf{\Phi}_j^-(\rho_\ell, \theta_\ell) + c_j^* \mathbf{\Phi}_j^+(\rho_\ell, \theta_\ell) \right\} = \sqrt{\triangle h_\ell}\, f(\rho_\ell, \theta_\ell), \quad \ell = 1, 2, ..., M, \tag{17.3.17}$$

where $N = 2n+2$ and $M \ge N$, and $\mathbf{\Phi}_j^+(\rho,\theta)$ and $\mathbf{\Phi}_j^-(\rho,\theta)$ are also given in (17.1.8) and (17.1.9). The equation (17.3.17) is denoted by an overdetermined system,

$$\mathbf{F}\mathbf{x} = \mathbf{b}, \tag{17.3.18}$$

where matrix $\mathbf{F} \in \mathbf{R}^{M\times N}$, and vectors $\mathbf{x} = (c_0, c_1, ..., c_n, c_0^*, c_1^*, ..., c_n^*)^T \in \mathbf{R}^N$ and $\mathbf{b} \in \mathbf{R}^M$. From the addition theorem (17.2.4), the linear combination u_N in (17.1.7) can be used to approximate one of P_n in (17.2.2):

$$u_N^+ \approx P_n^+(\rho,\theta) = a_0^+ + \sum_{k=1}^{n} \left(\frac{\rho}{\rho_{\max}}\right)^k (a_k^+ \cos k\theta + b_k^+ \sin k\theta), \tag{17.3.19}$$

where the coefficients

$$\begin{aligned} a_0^{+} &= \sum_{j=0}^{n}(c_j + c_j^*)\ln R_j, \quad a_k^{+} = -\sum_{j=0}^{n}\frac{1}{k}\left(\frac{\rho_{\max}}{R_j}\right)^k \{c_j + c_j^* \cos(k\phi^*)\}, \\ b_k^{+} &= -\sum_{j=0}^{n} c_j^* \frac{1}{k}\left(\frac{\rho_{\max}}{R_j}\right)^k \sin(k\phi^*). \end{aligned} \tag{17.3.20}$$

Denote (17.3.20) by the linear algebraic equations,

$$\mathbf{y} = \mathbf{E}^{+}\mathbf{x}, \tag{17.3.21}$$

where vectors $\mathbf{x} = \{c_0, c_1, ..., c_n, c_0^*, c_1^*, ..., c_n^*\}^T$, $\mathbf{y} = \{a_0^{+}, a_1^{+}, ..., a_n^{+}, b_1^{+}, ..., b_n^{+}\}^T \in \mathbf{R}^{2n+1}$, and matrix $\mathbf{E}^{+} \in \mathbf{R}^{(2n+1)\times(2n+2)}$ is denoted by

$$\mathbf{E}^{+} = \begin{pmatrix} \mathbf{E}_{11}^{+} & \mathbf{E}_{12}^{+} \\ \mathbf{O}^{+} & \mathbf{E}_{22}^{+} \end{pmatrix}, \tag{17.3.22}$$

where the null matrix $\mathbf{O}^{+} \in \mathbf{R}^{n\times(n+1)}$, and the sub-matrices $\mathbf{E}_{11}^{+}, \mathbf{E}_{12}^{+} \in \mathbf{R}^{(n+1)\times(n+1)}$ and $\mathbf{E}_{22}^{+} \in \mathbf{R}^{n\times(n+1)}$ are given by

$$\mathbf{E}_{11}^{+} = \begin{pmatrix} \ln R_0 & \ln R_1 & \cdots & \ln R_n \\ -\frac{\rho_{\max}}{R_0} & -\frac{\rho_{\max}}{R_1} & \cdots & -\frac{\rho_{\max}}{R_n} \\ \frac{-1}{2}\left(\frac{\rho_{\max}}{R_0}\right)^2 & \frac{-1}{2}\left(\frac{\rho_{\max}}{R_1}\right)^2 & \cdots & \frac{-1}{2}\left(\frac{\rho_{\max}}{R_n}\right)^2 \\ \vdots & \vdots & \vdots & \vdots \\ \frac{-1}{n}\left(\frac{\rho_{\max}}{R_0}\right)^n & \frac{-1}{n}\left(\frac{\rho_{\max}}{R_1}\right)^n & \cdots & \frac{-1}{n}\left(\frac{\rho_{\max}}{R_n}\right)^n \end{pmatrix},$$

$$\mathbf{E}_{12}^{+} = \begin{pmatrix} \ln R_0 & \ln R_1 & \cdots & \ln R_n \\ -\frac{\rho_{\max}}{R_0}\cos\phi^* & -\frac{\rho_{\max}}{R_1}\cos\phi^* & \cdots & -\frac{\rho_{\max}}{R_n}\cos\phi^* \\ \frac{-1}{2}\left(\frac{\rho_{\max}}{R_0}\right)^2\cos 2\phi^* & \frac{-1}{2}\left(\frac{\rho_{\max}}{R_1}\right)^2\cos 2\phi^* & \cdots & \frac{-1}{2}\left(\frac{\rho_{\max}}{R_n}\right)^2\cos 2\phi^* \\ \vdots & \vdots & \vdots & \vdots \\ \frac{-1}{n}\left(\frac{\rho_{\max}}{R_0}\right)^n\cos n\phi^* & \frac{-1}{n}\left(\frac{\rho_{\max}}{R_1}\right)^n\cos n\phi^* & \cdots & \frac{-1}{n}\left(\frac{\rho_{\max}}{R_n}\right)^n\cos n\phi^* \end{pmatrix},$$

$$\mathbf{E}_{22}^{+} = \begin{pmatrix} -\frac{\rho_{\max}}{R_0}\sin\phi^* & -\frac{\rho_{\max}}{R_1}\sin\phi^* & \cdots & -\frac{\rho_{\max}}{R_n}\sin\phi^* \\ \frac{-1}{2}\left(\frac{\rho_{\max}}{R_0}\right)^2\sin 2\phi^* & \frac{-1}{2}\left(\frac{\rho_{\max}}{R_1}\right)^2\sin 2\phi^* & \cdots & \frac{-1}{2}\left(\frac{\rho_{\max}}{R_n}\right)^2\sin 2\phi^* \\ \vdots & \vdots & \vdots & \vdots \\ \frac{-1}{n}\left(\frac{\rho_{\max}}{R_0}\right)^n\sin n\phi^* & \frac{-1}{n}\left(\frac{\rho_{\max}}{R_1}\right)^n\sin n\phi^* & \cdots & \frac{-1}{n}\left(\frac{\rho_{\max}}{R_n}\right)^n\sin n\phi^* \end{pmatrix}.$$

On the other hand, by using PS in (17.2.2) we have

$$\begin{aligned}\sqrt{\triangle h_\ell}\{P_n(\rho_\ell,\theta_\ell)\} &= \sqrt{\triangle h_\ell}\left\{ a_0^+ + \sum_{k=1}^{n}\left(\frac{\rho_\ell}{\rho_{\max}}\right)^k (a_k^+ \cos k\theta_\ell + b_k^+ \sin k\theta_\ell)\right\}\\ &= \sqrt{\triangle h_\ell}\, f(\rho_\ell,\theta_\ell), \quad \ell = 1,2,...,M. \end{aligned} \tag{17.3.23}$$

The equation (17.3.23) is also denoted by an overdetermined system,

$$\mathbf{Gy} = \mathbf{b}, \tag{17.3.24}$$

where matrix $\mathbf{G} \in \mathbf{R}^{M\times(N-1)}$ and vector $\mathbf{y} = (a_0^+, a_1^+, ..., a_n^+, b_1^+, ..., b_n^+)^T \in \mathbf{R}^{N-1}$, where $M \geq N$ and $N = 2n+2$. The algorithms using (17.3.23) (or (17.3.24)) are also called the MPS. We have from (17.3.24) and (17.3.21),

$$\mathbf{GE}^+\mathbf{x} = \mathbf{b}, \tag{17.3.25}$$

where matrix $\mathbf{E}^+ \in \mathbf{R}^{(N-1)\times N}$. Comparing (17.3.25) and (17.3.18), we have

$$\mathbf{Fx} = \mathbf{GE}^+\mathbf{x}. \tag{17.3.26}$$

From (17.3.26) we have the bound,

$$\text{Cond}(\mathbf{F}) \leq \text{Cond}(\mathbf{G})\text{Cond}(\mathbf{E}^+). \tag{17.3.27}$$

By (17.3.27), the upper bounds of Cond can be derived. We have the following bounds, whose proof is given in [257].

Theorem 17.3.2. *For the source nodes $Q_j^- = (R_j, 0)$ and $Q_j^+ = (R_j, \phi^*)$ in (17.2.16), the uniform locations for $x_i = \frac{\rho_{\max}}{R_i} \in [a,b]$ in Case II are chosen, where $b = \frac{\rho_{\max}}{R_0} < 1$ and $a = \frac{\rho_{\max}}{R_{\max}} = O(\frac{1}{n})$. Then for Variant Case (17.1.7), there exists the upper bound for disk domains,*

$$\begin{aligned}\text{Cond}(\mathbf{F}) &\leq C(\ln R_{\max})(n+1)^{1.5+\gamma+\beta} \times 2^{3(n+1)} \times \left(\frac{R_0}{\rho_{\max}}\right)^{(n+1)}\\ &\leq C(\ln R_{\max})N^{1.5+\gamma+\beta} \times 2^{\frac{3}{2}N} \times \left(\frac{R_0}{\rho_{\max}}\right)^{\frac{N}{2}}, \end{aligned} \tag{17.3.28}$$

where $N = 2n+2$, C is a bounded constant independent of n, constant $\beta \geq 0$ and $\gamma = 0$ is for $\phi^* = \frac{\pi}{4n}$ and $\gamma = 1$ for $\phi^* = \frac{\pi}{6} - \frac{\pi}{4n}$. Besides, parameter $\gamma = 1$ is also for the angles: $\phi^* = \frac{p}{q}\pi - \frac{\pi}{4n}$, where two positive integers p and q with $p \leq \frac{1}{2}q$ are independent of n.

To close this section, let us provide the upper bound estimates of Cond for non-circular boundaries Γ. Denote Γ by a single-valued function $\rho(\theta)$ with $\theta \in [0, 2\pi)$. For two pseudo radial-lines along angles ϕ_1^* and ϕ_2^*, denote $r_{\max} = \max\{\rho(\phi_1^*), \rho(\phi_2^*)\}$. The algorithms (17.1.5)–(17.1.8) remain the same only if $\rho_{\max}$ is replaced by $r_{\max}$, and so do the bounds (17.3.28), to give

$$\mathrm{Cond}(\mathbf{E}^+) \le C(\ln R_{\max}) N^{1.5+\gamma+\beta} \times 2^{\frac{3}{2}N} \left(\frac{R_0}{r_{\max}}\right)^{\frac{N}{2}}. \tag{17.3.29}$$

We can also prove

$$\mathrm{Cond}(\mathbf{G}) \le C\left(\frac{\rho_{\max}}{\rho_{\min}}\right)^{n} \le C\left(\frac{\rho_{\max}}{\rho_{\min}}\right)^{\frac{N}{2}}, \tag{17.3.30}$$

where $N = 2n+2$, and $\rho_{\max} = \max\, \rho|_\Gamma$ and $\rho_{\min} = \min\, \rho|_\Gamma$. Then we obtain the upper bound estimates from (17.3.29) and (17.3.30),

$$\begin{aligned} \mathrm{Cond}(\mathbf{F}) &\le \mathrm{Cond}(\mathbf{G})\mathrm{Cond}(\mathbf{E}^+) \\ &\le C(\ln R_{\max}) N^{1.5+\gamma+\beta} \times 2^{\frac{3}{2}N} \left(\frac{R_0}{r_{\max}}\right)^{\frac{N}{2}} \left(\frac{\rho_{\max}}{\rho_{\min}}\right)^{\frac{N}{2}}. \end{aligned} \tag{17.3.31}$$

When $r_{\max} = \rho_{\max}$, the equation (17.3.31) leads to (17.3.28),

$$\mathrm{Cond}(\mathbf{F}) \le C(\ln R_{\max}) N^{1.5+\gamma+\beta} \times 2^{\frac{3}{2}N} \left(\frac{R_0}{\rho_{\min}}\right)^{\frac{N}{2}}. \tag{17.3.32}$$

17.4 Numerical Experiments

17.4.1 Disk Domains

For Case I with uniform $R_i \in [R_0, R_{\max}]$, numerical experiments are provided in [256]. Since the upper bounds of Cond are derived only for Case II with uniform $x_i = \frac{\rho_{\max}}{R_i} \in [a, b]$, numerical experiments are carried out for Case II in this section. First, consider the unit disk domain with $\rho_{\max} = 1$. In computation, choose the following uniform distribution of source nodes in Case II,

$$b = \frac{\rho_{\max}}{R_0} < 1, \quad a = \frac{\rho_{\max}}{R_n} = \frac{\rho_{\max}}{R_{\max}}, \quad \rho_{\max} < R_0 < R_1 < \cdots < R_n = R_{\max}, \tag{17.4.1}$$

$$x_i = b + i\frac{a-b}{n}, \quad R_i = \frac{\rho_{\max}}{x_i}, \quad i = 0, 1, ..., n. \tag{17.4.2}$$

The equations (17.4.1) and (17.4.2) are simplified by

$$\frac{1}{R_i} = \frac{1}{R_0} - \frac{i}{n}\left(\frac{1}{R_0} - \frac{1}{R_{\max}}\right), \quad i = 0, 1, ..., n. \tag{17.4.3}$$

The source nodes (R_i, ϕ_1^*) and (R_i, ϕ_2^*) are located on two radial-lines at $\phi = \phi_1^*, \phi_2^*$. The sensitivity index κ in Part III is used to select better parameters $R_0, R_{\max}$ and (ϕ_1^*, ϕ_2^*). From [256], $R_0 = 2$ and $R_{\max} = 25, 10000$ are suggested, and both $\phi_2^* - \phi_1^* = \frac{\pi}{4n}$ and $\phi_2^* - \phi_1^* = \frac{\pi}{6} - \frac{\pi}{4n}$ are beneficial for better numerical performance.

Denote the lower bound (17.3.15) by

$$\text{Lower} := \frac{2^{2n-2}}{\pi} \times \left(\frac{R_0}{\rho_{\max}}\right)^{n-1}. \tag{17.4.4}$$

Also denote the key part of upper bound (17.3.28) with $\beta = 0$ and $C = 1$ by

$$\text{Upper} := (\ln R_{\max}) N^{\gamma+1.5} \times 2^{\frac{3}{2}N} \times \left(\frac{R_0}{\rho_{\max}}\right)^{\frac{N}{2}}, \tag{17.4.5}$$

where $\gamma = 0$ and $\gamma = 1$ are for $\phi_2^* - \phi_1^* = \frac{\pi}{4n}$ and $\phi_2^* - \phi_1^* = \frac{\pi}{6} - \frac{\pi}{4n}$, respectively. The parameter $\beta = 0$ is supported by the numerical testing in [257]. Although Lower in (17.4.4) and Upper in (17.4.5) are derived from Basic and Variant Cases, respectively, they are used for both Basic and Variant Cases in computation.

The exact solution $u(x, y) = \cos(y)e^x$ is used for the unit disk domain. We choose the FS in Basic Case (17.1.6) and Variant Case (17.1.7) and give the results in Tables 17.1 and 17.2, where the lower and the upper bound estimates of Cond are computed from (17.4.4) and (17.4.5), respectively. From Table 17.1 at $R_0 = 2, R_{\max} = 25$ and $(\phi_1^*, \phi_2^*) = (0, \phi^*) = \big(0, \frac{\pi}{4n}\big)$, we can find from $N = 5, 17$

$$\|\epsilon\|_{\infty,\Gamma} = O(0.468^N), \quad \|\epsilon\|_{0,\Gamma} = O(0.475^N), \tag{17.4.6}$$

$$\text{Cond} = O\big(3.19^N\big), \quad \text{Cond\_eff} = O\big(1.82^N\big), \quad \kappa = 1.56, \tag{17.4.7}$$

where $\epsilon = u - u_N$. From Table 17.2 at $R_0 = 2$ and $R_{\max} = 10000$ at $(\phi_1^*, \phi_2^*) = \big(\frac{\pi}{2} - \frac{\pi}{8n}, \frac{\pi}{2} + \frac{\pi}{8n}\big)$, we can find from $N = 6, 18$

$$\|\epsilon\|_{\infty,\Gamma} = O\big(0.589^N\big), \quad \|\epsilon\|_{0,\Gamma} = O(0.585^N),$$

$$\text{Cond} = O\big(2.49^N\big), \quad \text{Cond\_eff} = O\big(1.37^N\big), \quad \kappa = 1.70.$$

Small errors as $O(10^{-9})$ are obtained by double precision in Table 17.1; they are good enough for scientific/engineering problems. The curves for errors and Cond are drawn *via* n in Figures 17.1 and 17.2 from Tables 17.1 and 17.2. We can see that all numerical Cond are within the lower and the upper bound estimates. In Figures 17.1 and 17.2, the Y-axis is scaled by logarithm, and the curves of Lower and Upper in (17.4.4) and (17.3.28) are straight-lines approximately. This confirms that the Cond grows exponentially; the same as the standard MFS in previous chapters (also see [74, 163, 252]). Since the estimates of Cond are derived *via* matrix $\mathbf{E}$ (or $\mathbf{E}^+$), the numerical Cond is closer to Cond($\mathbf{E}$) (or Cond($\mathbf{E}^+$)) in Figures 17.1 and 17.2. All Cond($\mathbf{E}$) (or Cond($\mathbf{E}^+$)) are within Lower and Upper. Moreover, the effective condition number (Cond_eff) is much smaller than Cond because it will play a key role in numerical partial differential equations (PDE) (see [162]).

For one-radial-line of source nodes $Q_j = (R_j, \phi^*)$, we also choose uniform distribution for $x_i = \frac{\rho_{\max}}{R_i} \in [R_1, R_{\max}]$ as

TAB. 17.1 – The errors and the condition numbers by using Basic Case (17.1.6) for Case II (17.4.3) with $\rho_{\max}=1$, $R_0=2$, $R_{\max}=25$, $(\phi_1^*,\phi_2^*)=\big(0,\frac{\pi}{4n}\big)$, $N=2n+1$ and $M=40$, where matrix $\mathbf{E}$ in (17.3.4), and Lower and Upper from (17.4.4) and (17.3.28), respectively.

n	N	$\|\epsilon\|_{\infty,\Gamma}$	$\|\epsilon\|_{0,\Gamma}$	Cond	Cond_eff	$\|\mathbf{x}\|$	$\sigma_{\min}$	Cond($\mathbf{E}$)	Lower	Upper
2	5	9.74(−2)	1.19(−1)	3.09(3)	8.44(1)	9.46	1.01(−2)	2.27(3)	2.55	3.69(4)
4	9	5.41(−3)	7.96(−3)	2.37(5)	9.02(2)	5.81(1)	1.55(−4)	2.23(5)	1.63(2)	2.28(7)
6	13	1.23(−4)	2.02(−4)	2.59(7)	1.13(4)	4.48(2)	1.60(−6)	3.77(7)	1.04(4)	1.01(10)
8	17	1.07(−5)	1.56(−5)	3.40(9)	1.10(5)	5.40(3)	1.36(−8)	8.21(9)	6.68(5)	3.88(12)
10	21	3.41(−7)	5.59(−7)	4.56(11)	9.14(6)	8.03(3)	1.10(−10)	1.88(12)	4.27(7)	1.36(15)
12	25	3.50(−8)	4.62(−8)	6.96(13)	5.06(7)	2.05(5)	7.79(−13)	4.37(14)	2.73(9)	4.53(17)
14	29	3.86(−9)	2.87(−9)	1.93(16)	3.80(9)	4.03(5)	5.29(−15)	1.02(17)	1.75(11)	1.45(20)
16	33	2.25(−9)	1.45(−9)	5.50(16)	5.13(9)	2.81(5)	5.61(−15)	2.35(19)	1.12(13)	4.50(22)

TAB. 17.2 – The errors and the condition numbers by the MFS using Variant Case (17.1.7) for Case II (17.4.3) at $(\phi_1^*,\phi_2^*)=\big(\frac{\pi}{2}-\frac{\pi}{8n},\frac{\pi}{2}+\frac{\pi}{8n}\big)$ with $\rho_{\max}=1$, $R_0=2$, $R_{\max}=10000$, $N=2n+2$ and $M=40$, where matrix $\mathbf{E}^+$ in (17.3.22), and Lower and Upper from (17.4.4) and (17.3.28), respectively.

n	N	$\|\epsilon\|_{\infty,\Gamma}$	$\|\epsilon\|_{0,\Gamma}$	Cond	Cond_eff	$\|\mathbf{x}\|$	$\sigma_{\min}$	Cond($\mathbf{E}^+$)	Lower	Upper
2	6	3.61(−1)	4.58(−1)	5.76(6)	5.78(1)	9.65(3)	1.45(−5)	9.55(2)	2.55	5.54(5)
4	10	2.38(−2)	3.27(−2)	2.48(8)	2.78(1)	8.39(5)	3.47(−7)	2.05(5)	1.63(2)	3.05(8)
6	14	7.63(−3)	1.10(−2)	9.28(9)	3.35(2)	2.53(6)	9.58(−9)	3.91(7)	1.04(4)	1.30(11)
8	18	6.25(−4)	7.43(−4)	3.28(11)	2.59(3)	1.12(7)	2.80(−10)	7.37(9)	6.68(5)	4.83(13)
10	22	5.44(−5)	7.85(−5)	1.18(13)	1.24(4)	8.17(7)	8.00(−12)	1.37(12)	4.27(7)	1.67(16)
12	26	1.11(−5)	1.51(−5)	5.72(14)	3.31(5)	1.44(8)	1.70(−13)	2.15(14)	2.73(9)	5.50(18)
14	30	3.65(−5)	1.91(−5)	5.18(16)	2.23(6)	4.57(8)	7.95(−15)	1.90(16)	1.75(11)	1.74(21)
16	34	1.84(−5)	9.26(−6)	1.10(17)	4.99(6)	1.76(8)	9.22(−15)	3.10(18)	1.12(13)	5.39(23)

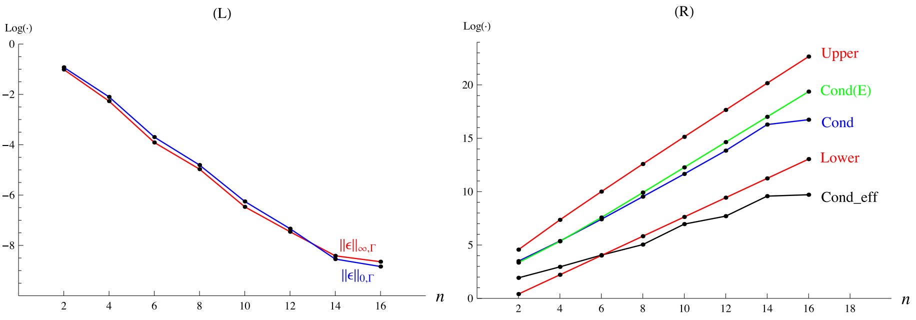

FIG. 17.1 – The curves *via* n are drawn based on Table 17.1 for $\|\epsilon\|_{\infty,\Gamma}$ and $\|\epsilon\|_{0,\Gamma}$ (L) and for Cond, Cond($\mathbf{E}$), Cond_eff, Lower and Upper (R).

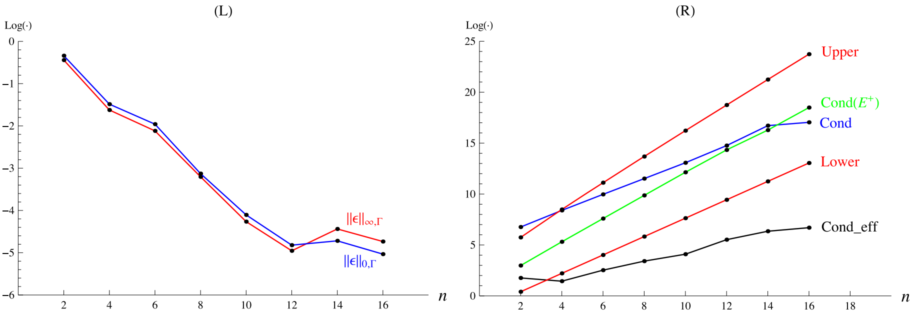

FIG. 17.2 – The curves *via* n are drawn based on Table 17.2 for $\|\epsilon\|_{\infty,\Gamma}$ and $\|\epsilon\|_{0,\Gamma}$ (L) and for Cond, Cond($\mathbf{E}^+$), Cond_eff, Lower and Upper (R).

$$\frac{1}{R_j} = \frac{1}{R_1} - \frac{j-1}{N-1}\left(\frac{1}{R_1} - \frac{1}{R_{\max}}\right), \quad j = 1, ..., N. \tag{17.4.8}$$

For one pseudo radial-line, Tables 17.3 and 17.4 show a failure for general solutions, thus verifying Propositions 17.2.1 and 17.2.2. The algorithm is still convergent for specific solutions. For the solution $u(x, y) = \cos(y)e^x$, the Fourier expansions have trivial coefficients $b_k^* = 0, k = 1, 2, ...,$ so the one-line algorithms at $\phi^* = 0$ also give convergent solutions as shown in Table 17.4. However, for the other solution $u(x, y) = \cos(x)e^y$, the one-line algorithms diverge as shown in Table 17.3; this verifies Proposition 17.2.1 again. Note that the solutions $\cos(x)e^y$ and $\cos(y)e^x$ are identical if x is changed by y. Convergence and divergence are switched if $\phi^* = 0$ is replaced by $\phi^* = \frac{\pi}{2}$; see Tables 17.3 and 17.4. When $\phi^* = \frac{\pi}{4}$, the one-line algorithms diverge for both kinds of solutions; this verifies Proposition 17.2.2 again. Both analysis and computation confirm that the two-line algorithms are essential.

We investigate the effects of $R_0 \in [1.1, 100]$ at $(\phi_1^*, \phi_2^*) = \left(0, \frac{\pi}{6} - \frac{\pi}{4n}\right)$ and $R_{\max} = 10000$, and the curves *via* R_0 are drawn at $N = 18$ and $n = 8$ in Figure 17.3

Tab. 17.3 – (Failure except for $\phi^* = \frac{\pi}{2}$) The errors and the condition numbers by the MFS using $Q_j = (R_j, \phi^*)$ in (17.4.8) with $\rho_{\max} = 1$, $R_1 = 2$, $R_{\max} = 25$ and $M = 40$, where the solution $u(x, y) = \cos(x)e^y$ is used.

ϕ^*	N	$\\|\epsilon\\|_{\infty,\Gamma}$	$\\|\epsilon\\|_{0,\Gamma}$	Cond	Cond_eff	$\\|\mathbf{x}\\|$	$\sigma_{\min}$
$\phi^* = 0$	5	1.71	2.00	2.07(1)	2.43(1)	3.14(−1)	1.06
	9	1.19	1.80	7.04(3)	8.40	2.64(2)	3.65(−3)
	17	1.18	1.80	1.88(8)	3.16(2)	1.49(5)	1.72(−7)
	25	1.18	1.80	3.60(12)	7.86(4)	9.71(6)	1.06(−11)
	33	1.33	1.82	1.02(17)	6.00(1)	3.20(14)	4.22(−16)
$\phi^* = \frac{\pi}{4}$	5	1.30	1.58	2.07(1)	2.45	3.12	1.06
	9	1.11	1.55	7.04(3)	2.10(1)	1.06(2)	3.65(−3)
	17	1.10	1.55	1.88(8)	1.71(3)	2.74(4)	1.72(−7)
	25	1.10	1.55	3.60(12)	5.16(4)	1.48(7)	1.06(−11)
	33	2.83	2.12	7.33(16)	6.32	2.17(15)	5.89(−16)
$\phi^* = \frac{\pi}{2}$	5	4.78(−1)	6.75(−1)	2.07(1)	1.64	4.66	1.06
	9	1.38(−2)	2.22(−2)	7.04(3)	7.61(1)	2.92(1)	3.65(−3)
	17	2.89(−5)	4.44(−5)	1.88(8)	1.51(4)	3.11(3)	1.72(−7)
	25	6.71(−8)	1.10(−7)	3.60(12)	6.47(6)	1.18(5)	1.06(−11)
	33	1.39(−9)	1.13(−9)	6.56(16)	6.40(10)	1.92(5)	6.59(−16)

Tab. 17.4 – (Failure except for $\phi^* = 0$) The errors and the condition numbers by the MFS using $Q_j = (R_j, 0)$ in (17.4.8) with $\rho_{\max} = 1$, $R_1 = 2$, $R_{\max} = 25$ and $M = 40$, where the solution $u(x, y) = \cos(y)e^x$ is used.

ϕ^*	N	$\\|\epsilon\\|_{\infty,\Gamma}$	$\\|\epsilon\\|_{0,\Gamma}$	Cond	Cond_eff	$\\|\mathbf{x}\\|$	$\sigma_{\min}$
$\phi^* = 0$	5	4.78(−1)	6.75(−1)	2.07(1)	1.64	4.66	1.06
	9	1.38(−2)	2.22(−2)	7.04(3)	7.61(1)	2.92(1)	3.65(−3)
	17	2.89(−5)	4.44(−5)	1.88(8)	1.51(4)	3.11(3)	1.72(−7)
	25	6.71(−8)	1.10(−7)	3.60(12)	6.47(6)	1.18(5)	1.06(−11)
	33	1.09(−9)	8.58(−10)	1.02(17)	3.23(10)	5.94(5)	4.22(−16)
$\phi^* = \frac{\pi}{4}$	5	1.30	1.58	2.07(1)	2.45	3.12	1.06
	9	1.11	1.55	7.04(3)	2.10(1)	1.06(2)	3.65(−3)
	17	1.10	1.55	1.88(8)	1.71(3)	2.74(4)	1.72(−7)
	25	1.10	1.55	3.60(12)	7.87(4)	9.69(6)	1.06(−11)
	33	3.01	2.14	7.33(16)	6.32	2.17(15)	5.89(−16)
$\phi^* = \frac{\pi}{2}$	5	1.71	2.00	2.07(1)	2.43(1)	3.14(−1)	1.06
	9	1.19	1.80	7.04(3)	8.40	2.64(2)	3.65(−3)
	17	1.18	1.80	1.88(8)	3.16(2)	1.49(5)	1.72(−7)
	25	1.18	1.80	3.60(12)	1.04(5)	7.32(6)	1.06(−11)
	33	2.35	2.29	6.56(16)	6.49	1.89(15)	6.59(−16)

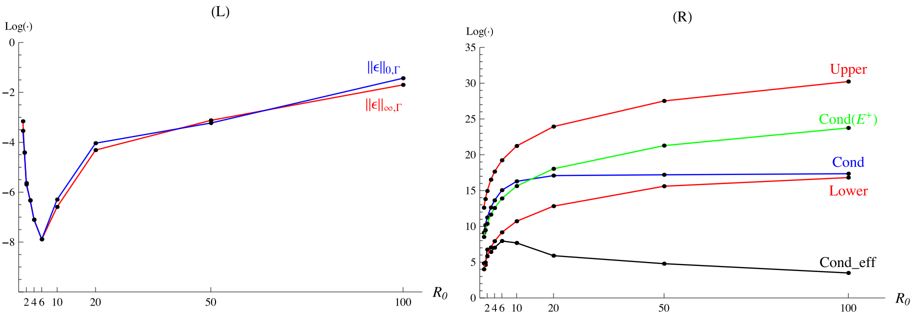

FIG. 17.3 – When $N = 18$ and $n = 8$, the curves *via* R_0 are drawn for $\|\epsilon\|_{\infty,\Gamma}$ and $\|\epsilon\|_{0,\Gamma}$ (L) and for Cond, Cond($\mathbf{E}^+$), Cond_eff, Lower and Upper (R).

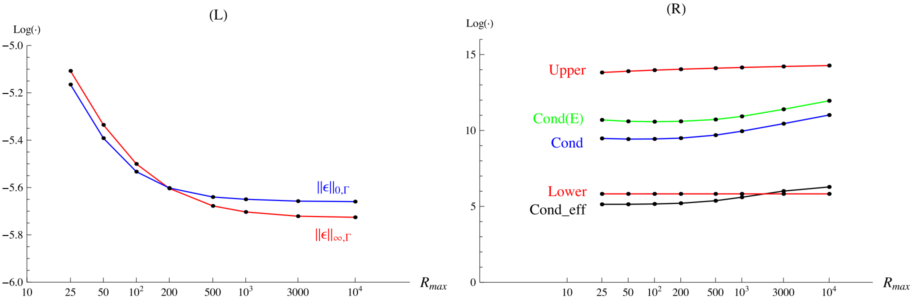

FIG. 17.4 – When $N = 17$ and $n = 8$, the curves *via* $R_{\max}$ are drawn for $\|\epsilon\|_{\infty,\Gamma}$ and $\|\epsilon\|_{0,\Gamma}$ (L) and for Cond, Cond($\mathbf{E}$), Cond_eff, Lower and Upper (R).

for errors, Cond, Lower, and Upper. Also we choose $R_0 = 2$ and $(\phi_1^*, \phi_2^*) = \left(0, \frac{\pi}{6} - \frac{\pi}{4n}\right)$ but change $R_{\max} \in [25, 10000]$. For $N = 18$ and $n = 8$, the curves *via* $R_{\max}$ are drawn in Figure 17.4 for errors, Cond, Lower, and Upper. Detailed tables are given in [257]. All numerical Cond also coincide with their theoretical estimates.

17.4.2 Non-Disk Domains

Consider the peanut-like domain, where the domain boundary $\Gamma\,(=\partial S)$ is defined by $(x, y) = (r(\theta)\cos\theta, r(\theta)\sin\theta)$, where

$$r(\theta) = \sqrt{\cos(2\theta) + \sqrt{2 - \sin^2(2\theta)}}, \quad 0 \le \theta \le 2\pi. \tag{17.4.9}$$

For (17.4.9), we have $a^* = r(0) = \sqrt{1 + \sqrt{2}} = 1.5538$ and $b^* = r\left(\frac{\pi}{2}\right) = 0.6436$. The solutions are given by $u(x, y) = \cos(y)e^x$ and the source function in Chapter 16

$$u^* = u(x^*, y^*) = \ln|\overline{PQ^*}|, \tag{17.4.10}$$

where node $Q^* = Q^*_{\text{far}}$ is outside and far from Γ as $Q^* = Q^*_{\text{far}} = (x^*, y^*) = (0, 3)$. Then the solution (17.4.10) is also highly smooth. Denote Γ by a single-valued function $\rho(\theta)$ with $\theta \in [0, 2\pi)$. For two pseudo radial-lines along angles ϕ_1^* and ϕ_2^*, denote $r_{\max} = \max\{\rho(\phi_1^*), \rho(\phi_2^*)\}$. The algorithms with (17.2.16) remain the same when $\rho_{\max}$ is replaced by $r_{\max}$. We use Basic Case (17.1.6) and Variant Case (17.1.7) and give the results in Tables 17.5 and 17.6. From Table 17.5 for the solution $u(x, y) = \cos(y)\, e^x$, we can see

$$\begin{aligned}
&\phi^* = \frac{\pi}{4n} \text{ at } R_{\max} = 100: \ \|\epsilon\|_{0,\Gamma} = O(0.500^N), \quad \text{Cond} = O(3.22^N), \quad \kappa = 1.69,\\
&\phi^* = \frac{\pi}{6} - \frac{\pi}{4n} \text{ at } R_{\max} = 100: \ \|\epsilon\|_{0,\Gamma} = O(0.460^N), \quad \text{Cond} = O(2.92^N), \quad \kappa = 1.38,\\
&\phi^* = \frac{\pi}{4n} \text{ at } R_{\max} = 10000: \ \|\epsilon\|_{0,\Gamma} = O(0.497^N), \quad \text{Cond} = O(2.79^N), \quad \kappa = 1.47,\\
&\phi^* = \frac{\pi}{6} - \frac{\pi}{4n} \text{ at } R_{\max} = 10000: \ \|\epsilon\|_{0,\Gamma} = O(0.456^N), \quad \text{Cond} = O(2.48^N), \quad \kappa = 1.16.
\end{aligned} \tag{17.4.11}$$

The best results are found in (17.4.11) as $\|\epsilon\|_{0,\Gamma} = O(0.456^N)$, $\text{Cond} = O(2.48^N)$ and $\kappa = 1.16$. From Table 17.6 for the source solution (17.4.10) with $Q^* = Q^*_{\text{far}}$, we can see

$$R_{\max} = 100: \ \|\epsilon\|_{0,\Gamma} = O(0.428^N), \ \text{Cond} = O(1.80^N), \ \kappa = 0.69, \tag{17.4.12}$$

$$R_{\max} = 10000: \ \|\epsilon\|_{0,\Gamma} = O(0.427^N), \ \text{Cond} = O(1.71^N), \ \kappa = 0.63. \tag{17.4.13}$$

Excellent numerical solutions are found as $\|\epsilon\|_{0,\Gamma} = O(0.427^N), \text{Cond} = O(1.71^N)$ and $\kappa = 0.63$ in (17.4.13) at $R_{\max} = 10000$. The very small errors as $O(10^{-11})$ can be achieved in Table 17.6. The locations of source nodes used in Table 17.6 are illustrated in Figure 17.5. When $R_{\max} = 10000$, the curves *via* N are drawn in Figure 17.6 from Table 17.6 for errors, Cond, Cond_eff, Lower, and Upper. The numerical Cond are consistent with the upper bound estimates for non-disk domains in (17.3.31) and (17.3.32). Also, the numerical Cond are all beyond Lower in (17.4.4).

Remark 17.4.1. *Let us compare the numerical performance between the pseudo radial-lines in this chapter and the pseudo-boundaries in previous chapters. For smooth solutions and the solution domain* S *near disks/ellipses, circular/elliptic pseudo-boundaries are optimal. For disk domains in Section 17.4.1, when circular pseudo-boundaries are chosen, smaller errors with* $O(10^{-11})$ *than those in Tables 17.1 and 17.2 can be obtained from the numerical results in [256]. For peanut-like domains, when elliptic pseudo-boundaries are chosen, the errors with* $O(10^{-13})$ *and the sensitivity index* $\alpha = 0.807$ *are obtained from the numerical results in [256] to offer better numerical performance. For complicated* Γ *and singular solutions, however, pseudo-boundary* Γ_R *near* Γ *are beneficial as shown in Chapters 14–16. Since there are various types (i.e., shapes) of* Γ_R*, seeking better types of* Γ_R *is non-trivial. By contrast, two radial-lines are defined only by four parameters* $(R_0, R_{\max}, \phi_1^*, \phi_2^*)$*. Better source nodes in Cases I and II can be found easily by the*

Tab. 17.5 – The errors and the condition numbers for Γ defined by (17.4.9) by the MFS using Basic Case (17.1.6) in Case II (17.4.3), where $r_{\max} = \rho_{\max} = a^* = 1.5538$, $\rho_{\min} = b^* = 0.6436$, $R_0 = 3$ and $M = 40$, and the exact solution with $u(x, y) = \cos(y)e^x$ and $(\phi_1^*, \phi_2^*) = (0, \phi^*)$ is chosen, and Lower from (17.4.4), and Upper from (17.3.32) with $\beta = 0$ and $C = 1$.

ϕ^*, $R_{\max}$	N	$\Vert\epsilon\Vert_{\infty,\Gamma}$	$\Vert\epsilon\Vert_{0,\Gamma}$	Cond	Cond_eff	$\Vert\mathbf{x}\Vert$	$\sigma_{\min}$	Lower	Upper
$\frac{\pi}{4n}$, 100	5	4.19(−2)	5.31(−2)	2.02(4)	1.76(2)	2.91(1)	2.21(−3)	2.46	4.37(5)
	9	1.31(−3)	1.74(−3)	1.60(6)	1.13(3)	3.14(2)	3.19(−5)	1.47(2)	1.47(9)
	17	9.59(−6)	1.31(−5)	2.49(10)	6.16(5)	7.25(3)	2.53(−9)	5.22(5)	7.37(15)
	25	1.60(−7)	1.03(−7)	4.87(15)	1.17(9)	6.42(5)	1.50(−14)	1.86(9)	2.54(22)
	33	2.01(−6)	1.08(−6)	6.23(16)	5.47(9)	2.94(5)	7.02(−15)	6.60(12)	7.45(28)
$\frac{\pi}{6} - \frac{\pi}{4n}$, 100	5	4.19(−2)	5.31(−2)	5.46(4)	4.75(2)	2.91(1)	8.18(−4)	2.46	2.19(6)
	9	1.30(−3)	1.74(−3)	1.24(6)	8.78(2)	3.13(2)	4.11(−5)	1.47(2)	1.32(10)
	17	5.86(−6)	4.74(−6)	2.11(10)	5.45(5)	6.95(3)	2.99(−9)	5.22(5)	1.25(17)
	25	1.12(−7)	7.24(−8)	4.61(15)	1.34(9)	5.31(5)	1.59(−14)	1.86(9)	6.35(23)
	33	1.15(−7)	7.68(−8)	6.40(16)	7.66(9)	1.86(5)	7.94(−15)	6.60(12)	2.46(30)
$\frac{\pi}{4n}$, 10000	5	3.66(−2)	5.34(−2)	3.69(6)	1.15(4)	4.29(1)	2.28(−5)	2.46	8.74(5)
	9	1.45(−3)	2.02(−3)	2.38(8)	8.38(4)	3.65(2)	3.69(−7)	1.47(2)	2.94(9)
	17	9.08(−6)	1.22(−5)	8.27(11)	7.50(6)	1.30(4)	1.16(−10)	5.22(5)	1.47(16)
	25	5.08(−8)	3.39(−8)	9.50(15)	2.75(9)	3.76(5)	1.09(−14)	1.86(9)	5.08(22)
	33	1.48(−7)	6.55(−8)	9.82(16)	7.59(9)	1.63(5)	9.16(−15)	6.60(12)	1.49(29)
$\frac{\pi}{6} - \frac{\pi}{4n}$, 10000	5	3.65(−2)	5.34(−2)	1.00(7)	3.68(4)	3.65(1)	8.41(−6)	2.46	4.37(6)
	9	1.45(−3)	2.02(−3)	1.81(8)	4.03(4)	5.75(2)	4.87(−7)	1.47(2)	2.64(10)
	17	5.20(−6)	4.27(−6)	5.45(11)	4.65(5)	1.38(5)	1.76(−10)	5.22(5)	2.51(17)
	25	5.28(−8)	3.44(−8)	7.03(15)	2.03(9)	3.77(5)	1.48(−14)	1.86(9)	1.27(24)
	33	1.14(−7)	4.56(−8)	7.60(16)	8.72(9)	1.27(5)	1.02(−14)	6.60(12)	4.92(30)

TAB. 17.6 – The errors and the condition numbers for Γ defined by (17.4.9) by the MFS using Variant Case (17.1.7) in Case II (17.4.3) with $\rho_{\max} = a^* = 1.5538$, $r_{\max} = b^* = 0.6436$, $R_0 = 1$ and $M = 40$, and the source function (17.4.10) with $Q^* = Q^*_{\text{far}}$ and $(\phi^*_1, \phi^*_2) = \left(\frac{\pi}{2} - \frac{\pi}{8n}, \frac{\pi}{2} + \frac{\pi}{8n}\right)$ is chosen, where Lower from (17.4.4) with replacing $\rho_{\max}$ by $r_{\max}$, and Upper from (17.3.31) with $r_{\max} = \rho_{\min}, \beta = 0$ and $C = 1$.

$R_{\max}$	N	$\|\epsilon\|_{\infty,\Gamma}$	$\|\epsilon\|_{0,\Gamma}$	Cond	Cond_eff	$\|\mathbf{x}\|$	$\sigma_{\min}$	Lower	Upper
100	6	1.76(−2)	2.75(−2)	7.19(3)	1.99(3)	6.25(−1)	5.81(−3)	1.98	1.83(6)
	10	5.02(−4)	7.02(−4)	7.45(4)	2.09(4)	5.89(−1)	5.86(−4)	7.64(1)	3.54(9)
	14	2.89(−6)	4.22(−6)	7.07(5)	1.58(5)	7.04(−1)	6.51(−5)	2.95(3)	5.29(12)
	18	7.47(−7)	1.03(−6)	8.32(6)	1.75(6)	7.09(−1)	5.82(−6)	1.14(5)	6.94(15)
	22	2.85(−8)	3.43(−8)	1.53(8)	3.45(7)	6.30(−1)	3.32(−7)	4.40(6)	8.45(18)
	26	5.78(−10)	5.60(−10)	2.57(10)	4.86(9)	7.17(−1)	2.07(−9)	1.70(8)	9.77(21)
	30	1.07(−9)	7.45(−10)	6.98(13)	1.05(13)	8.64(−1)	7.98(−13)	6.57(9)	1.09(25)
	34	1.15(−10)	7.10(−11)	2.57(16)	4.06(14)	6.92(−1)	2.57(−14)	2.54(11)	1.19(28)
10000	6	1.72(−2)	2.71(−2)	1.41(6)	1.97(5)	6.24(−1)	5.88(−5)	1.98	3.66(6)
	10	5.42(−4)	7.59(−4)	1.38(7)	2.02(6)	5.88(−1)	6.08(−6)	7.64(1)	7.09(9)
	14	3.92(−7)	5.83(−7)	1.16(8)	1.43(7)	6.91(−1)	7.32(−7)	2.95(3)	1.06(13)
	18	7.21(−7)	1.00(−6)	9.06(8)	1.06(8)	7.17(−1)	9.54(−8)	1.14(5)	1.39(16)
	22	3.50(−8)	4.27(−8)	6.59(9)	8.56(8)	6.33(−1)	1.33(−8)	4.40(6)	1.69(19)
	26	4.24(−11)	5.07(−11)	1.57(11)	1.83(10)	6.91(−1)	5.71(−10)	1.70(8)	1.95(22)
	30	9.34(−10)	6.65(−10)	9.79(13)	9.20(12)	8.45(−1)	9.29(−13)	6.57(9)	2.18(25)
	34	2.19(−10)	1.31(−10)	3.28(16)	2.45(14)	7.19(−1)	4.11(−14)	2.54(11)	2.37(28)

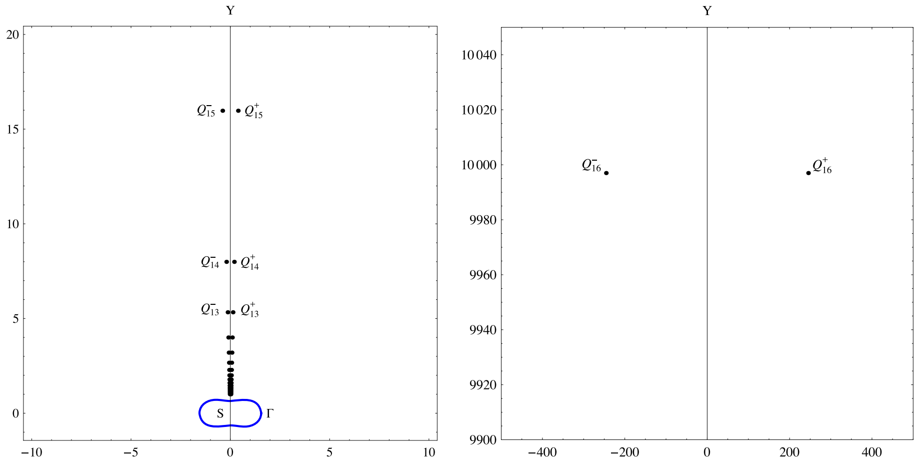

FIG. 17.5 – The locations of source nodes with $\left(\frac{\pi}{2}-\frac{\pi}{8n},\frac{\pi}{2}+\frac{\pi}{8n}\right)$ of Variant Case II at $R_0 = 1$ and $R_{\max} = 10000$ at $n = 16$ and $N = 34$ in Table 17.6.

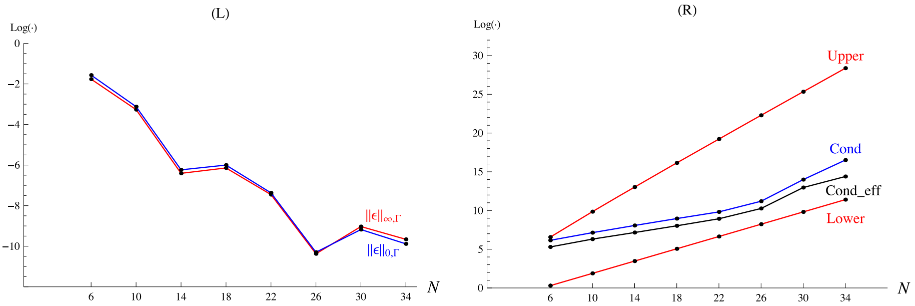

FIG. 17.6 – The curves *via* N are drawn based on Table 17.6 at $R_{\max} = 10000$ for $\|\epsilon\|_{\infty,\Gamma}$ and $\|\epsilon\|_{0,\Gamma}$ (L) and for Cond, Cond_eff, Lower, and Upper (R).

sensitivity index. See [256]. This is an advantage of the new algorithms in this chapter. Next, the non-circular/non-elliptic pseudo-boundaries may suffer from degenerate scales that are unknown. By contrast, no degenerate scales exist for pseudo radial-lines based on (17.3.28) and (17.3.31). This is the other remarkable advantage of the new algorithms in this chapter.

17.5 Concluding Remarks

Let us address the novelties of this chapter.

1. Two pseudo radial-lines of source nodes are studied for the MFS, and new algorithms are proposed in this chapter. Numerical experiments are provided in

[256] for seeking better parameters R_0, $R_{\max}$ and (ϕ_1^*, ϕ_2^*) for Cases I and II. Error analysis is provided in Remark 17.1.1 but stability analysis is explored, which is more essential and challenging for the MFS.

2. Since the discrete matrices consist of the Vandermonde matrix whose ill-conditioning is notorious, the lower bounds of Cond are an important topic (see [85, 86, 199, 229] and [99, Chapter 21]). For disk domains, the lower bound estimates of Cond are given in Theorem 17.3.1. Moreover, the upper bound estimates of Cond are given in (17.3.28).
3. Compared upper bounds to lower bounds, there occurs an additional exponential factor $O(\sqrt{2}^N)$. Both the lower and upper bounds of Cond provide a complete knowledge of the stability of the new algorithms in this chapter; they are intriguing in stability analysis for the MFS in previous chapters. All numerical Cond agree with the theoretical estimates.
4. The algorithms of two pseudo radial-lines are applied to disk domains and peanut-like domains in Section 17.4, and small errors can be obtained for smooth solutions. The upper bounds of Cond for non-disk domains are also supported by numerical condition numbers. Numerical results from the new algorithms of the MFS are encouraging and promising, which may satisfy the requirements of scientific/engineering problems. Since the new algorithms using pseudo radial-lines are supported by theory and computation in this chapter, they may become a new competent boundary method in the MFS family.

Epilogue

The more freedom you have,
the more gains you can get.

To evaluate the numerical methods, several important criteria are as follows (see Section 6.5): (1) accuracy, (2) stability, (3) bypassing the spurious eigenvalues and the degenerate scales, (4) wide applications, (5) complexity and CPU time, and (6) simple algorithms and easy programming. Accuracy and stability are the most important criteria. High accuracy and good stability can not succeed for one method simultaneously. See "*the trade-off principle*" in Wendland [243, p.208]. For the MFS, the analysis in this book is devoted to the first three criteria. The polynomial convergence rates can be achieved, while the condition numbers grow exponentially. For the BKM in Section 7.5, a super-exponential growth of Cond occurs. For Helmholtz equations in the unbounded domain with interior boundaries, the modified MFS is proposed to eliminate all spurious eigenvalues (see Chapters 8 and 9).

For the six criteria, the MFS owns high scores except stability, which is related to the locations of source nodes. For the interior Dirichlet problems (IDP) in 3D, the source nodes are located on a larger pseudo-surface S_R. The spheres S_R (or the circles in 2D) are most simple and effective in computation and analysis. The source nodes are located on S_R, based on the abscissas of quadrature rules, and simple grids of coordinate lines of the source nodes are chosen, called "*the grid-like*" source nodes. The advantages of such choices may reach the polynomial convergence rates based on the error analysis and the numerical examples in the entire book.

In most engineering problems, the relative errors as $O(10^{-5})$ are satisfactory. For double-precision with 16 working decimal digits, if the ill-conditioning consumes 10 decimal working digits, the correct numerical solutions can be obtained by the MFS. The algorithms of the MFS are simple and efficient by using the grid-like source nodes (see Chapter 13); users only need to know the quadrature rules. It is due to the modest human effort needed that the MFS has become an attractive and competitive method for scientific/engineering computing.

The sensitivity index may find more applications. Since the ill-conditioning is severe in the MFS, the sensitivity index κ in (III.2) becomes a useful tool to find better source nodes. As a consequence, the sensitivity index can also be used to remove the degenerate scales automatically. For circular pseudo-boundaries with radius R, the best R can be found by the smallest κ. For elliptic pseudo-boundaries with two semi-axes a_R and b_R, the best $(a_R + b_R)$ can be found by the smallest κ. When the degenerate scales happen at $R = 1$ in circular pseudo-boundaries and at $a_R + b_R = 2$ in elliptic pseudo-boundaries, the Cond is extremely large. Hence the sensitivity index κ must be very large. The degenerate scales are removed automatically in better pseudo-boundaries with a smaller sensitivity index. This is particularly advantageous for the non-circular/non-elliptic pseudo-boundaries because the degenerate scales are unknown in advance.

The truncated singular value decomposition (TSVD) and the Tikhonov regularization (TR) may be employed to reduce the severe ill-conditioning of the MFS (see Li *et al.* [161]). Consider the linear algebraic equations $\mathbf{Ax} = \mathbf{b}$, where matrix $\mathbf{A} \in \mathbf{R}^{m\times n}$ $(m \geq n)$ is nearly singular. We choose the TR

$$\min_{\mathbf{x}\in\mathbf{R}^n}\{\|\mathbf{Ax}-\mathbf{b}\|^2 + \lambda^2\|\mathbf{x}\|^2\}. \tag{E1}$$

The regularization parameter λ is involved in (E1), and its better (or optimal) choices are essential in both theory and computation. The sensitivity index may be applied to the TR to find the optimal regularization parameter. The most important criterion is to reduce condition numbers (Cond). The optimal regularization parameter for the TR is derived in [259] as $\lambda = (\sigma_{\max}\sigma_{\min})^{\frac{1}{2}}$ to give the minimal condition number,

$$\text{Cond}_\lambda(\mathbf{A}) \approx \frac{1}{2}\sqrt{\text{Cond}(\mathbf{A})},$$

where $\sigma_{\max}$ and $\sigma_{\min}$ (> 0) are the maximal and the minimal singular values of matrix $\mathbf{A}$, respectively. Based on the sensitivity index, the parameter of the best numerical performance can be found by

$$\min_\lambda\left\{-\frac{\log(\text{Cond}_\lambda)}{\log(\|\mathbf{Ax}_\lambda-\mathbf{b}\|)}\right\}, \text{ or } \min_\lambda\left\{-\frac{\log(\|\mathbf{x}_\lambda\|)}{\log(\|\mathbf{Ax}_\lambda-\mathbf{b}\|)}\right\}, \tag{E2}$$

where small errors $x(\lambda) = \|\mathbf{Ax}_\lambda - \mathbf{b}\| = o(1)$ are obtained from (E1), and Cond_λ and $\|\mathbf{x}_\lambda\|$ denote the severe ill-conditioning. New algorithms (E2) for seeking the parameter λ are simpler than the L-curve techniques in Hansen [96] and the generalized cross validation (GCV). Details are reported in Zhang *et al.* [259].

From this book, good source nodes can be found to reach high accuracy and to control ill-conditioning. Therefore, the pseudo-boundaries and the pseudo radial-lines are not as pessimistic as one thought before. Contrarily,

the more freedom you have, the more gains you can get.

The pseudo-boundaries and the pseudo radial-lines have become an attractive characteristic of the MFS. The analysis of errors and stability with numerical computations in this book has provided a solid theoretical basis of the MFS to make it an effective numerical method for PDEs. This book is essential to the MFS.

In the BEM, the source node Q (imaged as a "soul") is confined on the boundary $\Gamma\,(=\partial S)$. In the MFS, the Q is released from Γ. After the seventeen chapters have been elaborated on, we are concerned with how far the source nodes can go from the solution domain S. The source nodes can go too far to imagine. In Chapter 17, consider the unit disk S, and one pair of source nodes may go to $10^4 \sim 10^6$ as far as from S.[1] The average radius of the earth is 6.371(3) km, and the average distance between the earth and the Sun is 1.496(8) km. The ratio $\frac{1.496(8)}{6.371(3)} = 2.348(4)$. The far pair of source nodes could even reach the Sun if the S were our earth; surprising! This reminds us of a playful, powerful monkey (called Sun-Wu-Kong), a Chinese legend.

To close this book, let us cite a quotation:

"*What you must do*?" said Monkey,
"*Should you lure the monster from its hiding place,*
but be certain it is a fight you can survive."

The Journey to the West,
Wu Cheng En 1505–1580 (or 1500–1582).

---

[1] In fact, we have tested the far pair of source nodes at the distance $R_{\max} = 10^4, 10^5$ and 10^6, but only reported the results of those at $R_{\max} = 10^4$ due to better numerical performance in Zhang *et al.* [256]. See Figure 17.5.

References

[1] Abramowitz M., Stegun I.A. (1965) *Handbook of mathematical functions with formulas, graphs, and mathematical tables.* Dover, New York.

[2] Adams R.A. (1975) *Sobolev spaces.* Academic Press, New York.

[3] Alves C.J.S., Antunes P.R.S. (2005) The method of fundamental solutions applied to the calculation of eigenfrequencies and eigenmodes of 2D simply connected shapes, *CMC* **2(4)**, 251–265.

[4] Alves C.J.S., Chen C.S. (2005) A new method of fundamental solutions applied to nonhomogeneous elliptic problems, *Adv. Comput. Math.* **23**, 125–142.

[5] Alves C.J.S., Leitao V.M.A. (2006) Crack analysis using an enriched MFS domain decomposition techniques, *Eng. Anal. Bound. Elem.* **30**, 160–166.

[6] Alves C.J.S., Valtchev S.S. (2006) Comparison between meshfree and boundary element methods applied to BVPs in domains with corners, *Proceedings of III European conference on computational mechanics* (C.A. Motasoares *et al.*, Ed.). Springer, Dordrecht, pp. 521–521.

[7] Amrouche C., Girault V., Giroire J. (1997) Dirichlet and Neumann exterior problems for the n-dimensional Laplace operator an approach in weighted Sobolev spaces, *J. Math. Pures Appl.* **76**, 55–81.

[8] Antunes P.R.S. (2018) Reducing the ill conditioning in the method of fundamental solutions, *Adv. Comput. Math.* **44**, 351–365.

[9] Antunes P.R.S. (2018) A numerical algorithm to reduce ill-conditioning in meshless methods for the Helmholtz equation, *Numer. Algorithms* **79**, 879–897.

[10] Antunes P.R.S. (2011) Numerical calculation of eigensolutions of 3D shapes using the method of fundamental solutions, *Numer. Meth. PDE* **27**, 1525–1550.

[11] Atkinson K. (1982) Numerical integration on the sphere, *J. Austral. Math. Soc. (Series B)* **23**, 332–347.

[12] Atkinson K.E. (1989) *An introduction to numerical analysis*, 2nd edn. John Wiley & Sons, New York.

[13] Atkinson K.E. (1997) *The numerical solution of integral equations of the second kind.* Cambridge University Press.

[14] Atkinson K., Han W. (2012) *Spherical harmonics and approximations on the unit sphere: An introduction.* Springer, Berlin.

[15] Babuška I., Aziz A.K. (1972) Survey lectures on the mathematical foundations on the finite element method, *The mathematical foundations of the finite element method with applications to partial differential equations* (A.K. Aziz, Ed.). Academic Press, New York.

[16] Babuška I., Szabo B.A., Katz I.N. (1981) The p-version of the finite element method, *SIAM J. Numer. Anal.* **18**, 515–545.

[17] Balakrishnan K., Ramachandran P.A. (1999) A particular solution Trefftz method for non-linear Poisson problems in heat and mass transfer, *J. Comput. Phy.* **150**, 239–267.

[18] Balakrishnan K., Ramachandran P.A. (2001) Osculatory interpolation in the method of fundamental solution for nonlinear Poisson problems, *J. Comput. Phy.* **172**, 1–18.

[19] Baricz A., Masirevic D.J., Pogany T.K., Szasz R. (2015) On an identity for zeros of Bessel functions, *J. Math. Anal. Appl.* **422**, 27–36.

[20] Barnett A.H., Betcke T. (2008) Stability and convergence of the method of fundamental solutions for Helmholtz problems on analytic domains, *J. Comput. Phy.* **227(14)**, 7003–7026.

[21] Beentjes C.H.L. (2015) *Quadrature on a spherical surface*, Research notes. Mathematical Institute, University of Oxford, Oxford, UK.

[22] Betcke T., Trefethen L.N. (2005) Reviving the method of particular solutions, *SIAM Rev.* **47 (3)**, 469–491.

[23] Bergman S. (1961) *Integral operators in the theory of linear partial differential equations.* Springer-Verlag, Berlin.

[24] Berntsson F., Eldén L. (2001) Numerical solution of a Cauchy problem for the Laplace equation, *Inverse Probl.* **17**, 839–853.

[25] Bin-Mohsin B.A. (2013) *The method of fundamental solutions for Helmholtz-type problems*, Doctoral dissertation. The University of Leeds, Department of Applied Mathematics.

[26] Bogomolny A. (1985) Fundamental solutions method for elliptic boundary value problems, *SIAM J. Numer. Anal.* **22**, 644–669.

[27] Brebbia C.A., Telles J.C.F., Wrobel L.C. (1984) *Boundary element techniques: Theory and applications in engineering.* Springer-Verlag, Berlin.

[28] Brenner S.C., Scott L.R. (1994) *The mathematical theory of finite element methods.* Springer-Verlag, New York.

[29] Buffa A., Hiptmair R. (2005) Regularized combined field integral equations, *Numer. Math.* **100**, 1–19.

[30] Burton A.J., Miller G.F. (1971) The application of integral equation methods to the numerical solution of some exterior boundary-value problems, *Proc. Roy. Soc. Lond. A* **323**, 201–210.

[31] Calderon A.P. (1958) Uniqueness in the Cauchy problems for partial differential equations, *American J. Math.* **80**, 16–36.

[32] Campbell S.L., Meyer C.D. (1979/1991) *Generalized inverses of linear transformations.* Pitman/Dover, New York.

[33] Canuto C., Hussaini M.Y., Quarteroni A., Zang T.A. (2006) *Spectral methods, fundamentals in single domains.* Springer, New York.

[34] Chen I.L. (2006) Using the method of fundamental solutions in conjunction with the degenerate kernels in cylindrical acoustic problems, *J. Chin. Inst. Eng.* **29**, 445–457.

[35] Chen I.L., Chen J.T., Liang M.T. (2001) Analytical study and numerical experiments for radiation and scattering problems using the CHIEF methods, *J. Sound Vib.* **248**, 809–828.

[36] Chen C.S., Cho H.A., Golberg M.A. (2006) Some comments on the ill-conditioning of the method of fundamental solutions, *Eng. Anal. Bound. Elem.* **30**, 405–410.

[37] Chen C.S., Hon Y.C., Schaback R.A. (2007) *Scientific computing with radial basis functions*, preprint. Department of Mathematics, University of Southern Mississippi, Hattiesburg, MS39406, USA.

[38] Chen C.S., Karageorghis A., Li Y. (2016) On choosing the location of the sources in the MFS, *Numer. Algorithms* **72**, 107–130.

[39] Chen C.S., Karageorghis A., Smyrlis Y.S. (2008) *The method of fundamental solutions – A meshless method.* Dynamic Publishers, Inc. USA.

[40] Chen J.T., Chen K.H. (1998) Analytical study and numerical experiments for Laplace equation with overspecified boundary conditions, *Appl. Math. Model.* **22**, 703–725.

[41] Chen J.T., Chen I.L., Lee Y.T. (2005) Eigensolutions of multiply connected membranes using the method of fundamental solutions, *Eng. Anal. Bound. Elem.* **29**, 166–174.

[42] Chen J.T., Han H., Kuo S.R., Kao S.K. (2014) Regularization methods for ill-conditioned system of the integral equation of the first kind with the logarithmic kernel, *Inverse Probl. Sci. Eng.* **22**, 1176–1195.

[43] Chen J.T., Lee Y.T., Chou K.H. (2010) Revisit of two classical elasticity problems by using the null-fields integration equations, *J. Mechanics* **26(3)**, 393–401.

[44] Chen J.T., Lee J.W., Leu S.Y. (2011) Analytical investigation for true and spurious eigensolutions of multiply-connected membranes containing elliptical boundaries using the dual BIEM, *Int. J. Solids Struct.* **48**, 729–744.

[45] Chen J.T., Lee Y.T, Yu S.R., Shieh S.C. (2009) Equivalence between Trefftz method and method of fundamental solution for annular Green's function using the addition theorem and image concept, *Eng. Anal. Bound. Elem.* **33**, 678–688.

[46] Chen J.T., Lin J.H., Kuo S.R., Chyuan S.W. (2001) Boundary element analysis for the Helmholtz eigenvalue problems with a multiply connected problem, *Proc. Roy. Soc. Lond. A* **457**, 2521–2546.

[47] Chen J.T., Liu L.W., Hong H.K. (2003) Spurious and true eigensolutions of Helmholtz BIEs and BEMs for a multiply connected problem, *Proc. R. Soc. Lond. A* **459**, 1891–1924.

[48] Chen J.T., Shieh H.C., Tsai J.J., Lee T.W. (2010) A study on the method of fundamental solutions using an image concept, *Appl. Math. Model.* **34**, 4253–4266.

[49] Chen J.T., Wu C.S., Lee Y.T., Chen K.H. (2007) On the equivalence of the Trefftz method and method of fundamental solutions for Laplace and biharmonic equations, *Comput. Math. Appl.* **53**, 851–879.

[50] Chen L.C. (1999) *Very high accurate solutions of Motz's problem by the conformal transformation method*, Master thesis. Department of Applied Mathematics, National Sun Yet-sen University, Kaohsiung.

[51] Chen G., Zhou J. (1992) *Boundary element methods.* Academic Press, Chapter 9, New York.

[52] Chen W., Fu Z.J., Chen C.S. (2014) *Recent advances in radial basis function collocation method.* Springer, New York.

[53] Chen W., Hon Y.C. (2003) Numerical investigation on convergence of boundary knot method in the analysis of homogeneous Helmholtz, modified Helmholtz, and convection-diffusion problems, *Comput. Meth. Appl. Mech. Eng.* **192**, 1859–1875.

[54] Chen W., Tanaka M. (2002) A meshless, integration-free, and boundary-only RBF technique, *Comput. Math. Appl.* **43**, 379–391.

[55] Chen Y. (1994) *Galerkin methods for solving singular layer integral equations in three dimensions*, Doctoral dissertation. University of Iowa.

[56] Cheng A.H.-D., Cabral J.J.S.P. (2005) Direct solution of ill-posed boundary value problems by radial basis function collocation method, *Inter. J. Numer. Meth. Eng.* **64**, 45–64.

[57] Cheng A.H.-D., Chen C.S., Karageorghis A. (2021) *Method of fundamental solutions-concepts and applications*, Monograph. University of Mississippi, University, MS 38677, USA.

[58] Cheng A.H.-D., Hong Y. (2020) An overview of the method of fundamental solutions-Solvability, uniqueness, convergence and stability, *Eng. Anal. Bound. Elem.* **120**, 118–152.

[59] Cheng J., Hon Y.C., Wei T., Yamamoto M. (2001) Numerical computation of a Cauchy problem for Laplace's equation, *ZAMM-J. Appl. Math. Mech.* **81**, 665–674.

[60] Chi Y.T. (2009) *The method of fundamental solution for Laplace's equation in 3D*, Master thesis. Department of Applied Mathematics, National Sun Yat-sen University, Kaohsiung, Taiwan.

[61] Chiba F., Ushijima T. (2009) Exponential decay of errors of a fundamental solution method applied to a reduced wave problem in the exterior region of a disc, *J. Comp. Appl. Math.* **231**, 869–885.

[62] Chien W.Z. (1989) *Variational and finite element methods* (in Chinese). East Asia Publishing, Taipei.

[63] Cho H.A., Golberg M.A, Muleshkov A.S., Li X. (2004) Trefftz methods for time-dependent partial differential equations, *CMC* **1**, 1–37.

[64] Christiansen S. (1976) On Kupradze's functional equations for plane harmonic problems, *Function theoretic methods in differential equations* (R.P. Gilbert, R.J. Weinacht, Eds). Pitman, London, Research Notes in Mathematics, Vol. 8, pp. 205–243.

[65] Christiansen S. (1982) On the two methods for elimination of non-unigue solutions of an integral equation with logarithmic kernel, *Appl. Anal.* **13**, 1–18.

[66] Christiansen S., Meister E. (1981) Condition number of matrices derived from two classes of integral equations, *Math. Meth. Appl. Sci.* **3**, 364–392.

[67] Ciarlet P.G. (1978) *The finite element method for elliptic problems.* North-Holland.

[68] Ciarlet P.G. (1991) Basic error estimates for elliptic problems, *Handbook of numerical analysis II: Finite element methods (part I)* (P.G. Ciarlet, T.L. Lions, Eds). North-Holland.

[69] Comodi M.I., Mathon R. (1991) A boundary approximation method for fourth order problem, *Math. Models Meth. Appl. Sci.* **1**, 437–445.

[70] Courant R., Hilbert D. (1953) *Methods of mathematical physics, I.* Wiley-Interscience Publishers, New York.

[71] Davis P.J. (1979) *Circulant matrices.* John Wiley & Sones, New York.

[72] Davis P.J., Rabinowitz P. (1984) *Methods of numerical integration: Second edition.* Academic Press, Inc., Orlando, Florida.

[73] Dou F., Li Z.C., Chen C.S., Tian Z. (2018) Analysis on the method of fundamental solutions for biharmonic equations, *Appl. Math. Comput.* **339**, 346–366.

[74] Dou F., Zhang L.P., Li Z.C., Chen C.S. (2020) Source nodes on elliptic pseudo-boundaries in the method of fundamental solutions for Laplace's equation; selection of pseudo-boundaries, *J. Comput. Appl. Math.* **377**, 112861.

[75] Drombosky T.W., Meyer A.L., Ling L. (2009) Applicability of the method of fundamental solutions, *Eng. Anal. Bound. Elem.* **33**, 637–643.

[76] Dwight H.B. (1961) *Tables of integrals and other mathematical data*, 4th edn. The MacMillan Company, New York, p. 197.

[77] Engleder S., Steinbach O. (2007) Modified boundary integration formulations for the Helmholtz equation, *J. Math. Anal. Appl.* **331**, 396–407.

[78] Eisenstat S.C. (1974) On the rate of convergence of the Bergman-Vekua method for the numerical solution of elliptic boundary value problems, *SIAM J. Numer. Anal.* **11**, 654–680.

[79] Elbert A. (2001) Some recent results on zeros of Bessel functions and othogonal polynomials, *J. Comput. Appl. Math.* **133**, 65–83.

[80] Fairweather G., Karageorghis A. (1998) The method of fundamental solutions for elliptic boundary value problems, *Adv. Comput. Math.* **9**, 69–95.

[81] Fairweather G., Karageorghis A., Martin P.A. (2003) The method of fundamental solutions for scattering and radiation problems, *Eng. Anal. Bound. Elem.* **27**, 759–769.

[82] Fornberg B., Piret C. (2007) A stable algorithm for flat radial basis functions on a sphere, *SIAM J. Sci. Comput.* **30**, 60–80.

[83] de Freitas J.A.T. (1998) Formulation of elastostatic hybrid-Trefftz stress elements, *Comput. Meth. Appl. Mech. Eng.* **153**, 127–151.

[84] Gautschi W. (1962) On inverse of Vandermonde and confluent Vandermonde matrices, *Numer. Math.* **4**, 117–123.

[85] Gautschi W. (1990) How (un)stable are Vandermonde systems? *Asymptotic and computational analysis* (R. Wong, Ed.). Lecture Notes in Pure and Applied Mathematics. Marcel Dekker, New York, Vol. 124, pp. 193–210.

[86] Gautschi W., Inglese G. (1988) Lower bounds for the condition number of Vandermonde matrices, *Numer. Math.* **52**, 241–250.

[87] Golberg M.A., Chen C.S. (1998) The method of fundamental solutions for potential, Helmholtz and diffusion problems, *Boundary integral methods: Numerical and mathematical aspects* (M.A. Golberg, Ed.). WIT Press, pp. 103–176.

[88] Golub G.H., van Loan C.F. (1996) *Matrix and computation*, 4th edn. John Hopkins University Press, Baltimore and London.

[89] Grabski J.K., Karageorghis A. (2019) Moving pseudo-boundary method of fundamental solutions for nonlinear potential problems, *Eng. Anal. Bound. Elem.* **105**, 78–86.

[90] Gradshteyn I.S., Ryzhik I.M. (1980) *Tables of integrals, series and products.* Academic Press, New York.

[91] Grisvard P. (1985) *Elliptic problems in nonsmooth domains*, Pitman Advanced Publishing Program. Boston and London, pp. 328–338.

[92] Gu Y., Gao H., Chen W., Zhang C. (2016) A general algorithm for evaluation nearly singular integrals in anisotropic three-dimensional boundary element analysis, *Comput. Meth. Appl. Mech. Eng.* **308**, 483–498.

[93] Gu Y., Gao H., Chen W., Wang H., Zhang C. (2017) A general algorithm for evaluating nearly strong-singular (and beyond) integrals in three-dimensional boundary element analysis, *Comput. Mech.* **59**, 779–793.

[94] Hadamard J. (1923) *Lectures on Cauchy problem in linear partial differential equations.* Yale University Press, New Haven.

[95] Hansen P.C. (1990) Truncated singular value decomposition solutions to discrete ill-posed problems with ill-determined numerical rank, *SIAM J. Sci. Stat. Comput.* **11**, 503–518.

[96] Hansen P.C. (1998) *Rank-deficient and discrete ill-posed problems: Numerical aspects of linear inversion.* SIAM, Philadelphia.

[97] Henrot A. (2003) Minimization problems for eigenvalues of the Laplacian, *J. Evol. Equ.* **3**, 443–461.

[98] Hetnarski R.B., Ignaczak J. (2011) *The mathematical theory of elasticity*, 2nd edn. CRC Press, Boca Raton, FL, USA.

[99] Higham N.J. (1996) *Accuracy and stability of numerical algorithms.* SIAM, Philadelphia.

[100] Hon Y.C., Chen W. (2003) Boundary knot method for 2D and 3D Helmholtz and convection-diffusion problems under complicated geometry, *Inter. Numer. Meth. Eng.* **56**, 1931–1948.

[101] Hon Y.C., Schaback R. (2013) Solving the 3D Laplace equation by meshless collocation via harmonic kernels, *Adv. Comput. Math.* **38**, 1–19.

[102] Hon Y.C., Wei T. (2003) A meshless scheme for solving inverse problems of Laplace equation, *Recent development in theories and numerics.* World Scientific Publishing, River Edge, NJ, pp. 291–300.

[103] Hrycak T., Schmutzhard S. (2016) A Nicholson-type integral for the cross-product of the Bessel functions, *J. Math. Anal. Appl.* **436**, 168–178.

[104] Hsiao G.C., Wendland W.L. (2008) *Boundary integral equations.* Springer, Berlin, pp. 189–194.

[105] Huang H.T., Li Z.C., Yan N. (2004) New error estimates of Adini's elements for Poisson's equations, *Appl. Numer. Math.* **50**, 49–74.

[106] Huang J., Huang H.T., Li Z.C., Wei Y. (2011) Stability analysis via condition number and effective condition number for the first kind boundary integral equations by advanced quadrature methods, a comparison, *Eng. Anal. Bound. Elem.* **35**, 667–677.

[107] Huang J., Lu T., Li Z.C. (2009) Mechanical quadrature methods and their splitting extrapolations for boundary integral equations of first kind on open contours, *Appl. Numer. Math.* **59**, 2908–2922.

[108] Jin B., Zheng Y., Marin L. (2006) The method of fundamental solutions for some inverse boundary value problems associated with the steady-state anisotropic heat conduction, *Inter. J. Numer. Meth. Eng.* **65**, 1865–1891.

[109] Jirousek J. (1978) Basic for development of large finite elements locally satisfying all field equations, *Comput. Meth. Appl. Mech. Eng.* **14**, 65–92.

[110] Jirousek J., Venkatesh A. (1992) Hybrid Trefftz plane elasticity element with p-method capabilities, *Inter. J. Numer. Meth. Eng.* **35**, 1443–1472.

[111] Jirousek J., Wroblewski A. (1996) T-elements: State of the art and future trends, *Arch. Comput. Meth. Eng.* **3**, 323–434.

[112] John F. (1982) *Partial differential equations*, 4th edn, Chapter 3. Springer-Verlag, New York.

[113] Johnston R.L., Mathon R. (1979) The computation of electric-dipole fields in conducting media, *Inter. J. Numer. Meth. Eng.* **14**, 1739–1760.

[114] Karageorghis A. (1992) Modified methods of fundamental solutions for harmonic and biharmonic problems with boundary singularities, *Numer. Meth. PDE* **8**, 1–19.

[115] Karageorghis A. (2001) The method of fundamental solutions for the calculation of the eigenvalues of the Helmholtz equation, *Appl. Math. Letters* **14**, 837–842.

[116] Karageorghis A., Fairweather G. (1987) The method of fundamental solutions for numerical solutions of the biharmonic equation, *J. Comput. Phy.* **69**, 434–459.

[117] Karageorghis A., Fairweather G. (1988) The Almansi method of fundamental solutions for solving biharmonic problems, *Inter. J. Numer. Meth. Eng.* **26**, 1665–1682.

[118] Karageorghis A., Fairweather G. (1987) The method of fundamental solutions for the numerical solution of biharmonic equation, *J. Comput. Phy.* **69**, 434–459.

[119] Karageorighis A., Lesnic D., Marin L. (2011) A survey of applications of the MFS to inverse problems, *Inverse Probl. Sci. Eng.* **19**, 309–336.

[120] Katsurada M. (1989) A mathematical study of the charge simulation method II, *J. Fac. Sci. Univ. Tokyo Sect. IA Math.* **36**, 135–162.

[121] Katsurada M. (1990) Asymptotic error analysis of the charge simulation method in a Jordan region with analytic boundary, *J. Fac. Sci. Univ. Tokyo Sect. IA Math.* **37**, 635–657.

[122] Katsurada M. (1994) Charge simulation method using exterior mapping functions, *Japan J. Indust. Appl. Math.* **11**, 47–61.

[123] Katsurada M., Okamoto H. (1996) The collocation points of the fundamental solution method for the potential problem, *Comput. Math. Appl.* **31**, 123–137.

[124] Kirsch A. (1996) *An introduction to the mathematical theory of inverse problems.* Springer-Verlag, New York.

[125] Kitagawa T. (1988) On the numerical stability of the method of fundamental solutions applied to the Dirichlet problem, *Japan J. Appl. Math.* **5**, 123–133.

[126] Kitagawa T. (1991) Asymoptic stability of the fundamental solution methods, *J. Comput. Appl. Math.* **38**, 263–269.

[127] Klibanov M.V., Santosa F. (1991) A computational quasi-reversibility method for Cauchy problems for Laplace's equation, *SIAM J. Appl. Math.* **51**, 1653–1673.

[128] Kolodziej J.A., Zielinski A.P. (2009) *Boundary collocation techniques and their application in engineering.* WIT Press, Southampton, Boston.

[129] Kondapalli P.S., Shippy D.J., Fairweather G. (1992) The method of fundamental solutions for transmission and scattering of elastic waves, *Comput. Meth. Appl. Mech. Eng.* **96**, 255–269.

[130] Kress R. (2014) *Linear integral equations*, 3rd edn. Springer-Verlag, New York.

[131] Kupradze V.D. (1963) Potential methods the theory of elasticity, *Progress in solid mechanics, vol. 3* (I.N. Sneddon, R. Hill, Eds). Amsterdam, North-Holland.

[132] Kupradze V.D., Aleksidze M.A. (1964) The method of functional equations for the approximate solution of certain boundary value problems, *USSR Comput. Math. Math. Phy.* **4**, 82–126.

[133] Kythe P.K. (1996) *Fundamental solutions for differential operators and applications.* Birkhauser, Boston, USA.

[134] Lebedev V.I. (1976) Quadrature on a sphere, *USSR Comput. Math. Math. Phy.* **16**, 10–24.

[135] Lee J.W., Chen J.T., Nien C.F. (2019) Indirect boundary element method combining extra fundamental solutions for solving exterior acoustic problems with fictitious frequencies, *J. Acoust. Soc. Am.* **145**, 3116–3132.

[136] Lee M.G., Li Z.C., Huang H.T., Chiang J.Y. (2013) Conservative schemes and degenerate scale problems of null-field method for Dirichlet problems of Laplace's equation, *Eng. Anal. Bound. Elem.* **37**, 95–106.

[137] Lee M.G., Li Z.C., Zhang L.P., Huang H.T., Chiang J.Y. (2014) Algorithm singularity of the null-field method for Dirichlet problems of Laplace's equation in annular and circular domains, *Eng. Anal. Bound. Elem.* **41**, 160–172.

[138] Lee M.G., Young L.J., Li Z.C., Chu P.C. (2010) Combined Trefttz method of particular and fundamental solutions for corner and crack singularity of linear elastostatics, *Eng. Anal. Bound. Elem.* **34**, 632–654.

[139] Li M., Chen C.S., Karageorghis A. (2013) The MFS for the solutions of harmonic boundary value problems with non-harmonic boundary conditions, *Comput. Math. Appl.* **66**, 2400–2423.

[140] Li X. (2004) Convergence of the method of fundamental solutions for solving the boundary value problems of modified Helmholtz equation, *Appl. Math. Comput.* **159**, 113–125.

[141] Li X. (2005) On convergence of the method of fundamental solutions for solving the Dirichlet problem of Poisson's equation, *Adv. Comput. Math.* **23**, 265–277.

[142] Li X. (2006) On solving boundary value problems of modified Helmholtz equation by plane wave functions, *J. Comput. Appl. Math.* **195**, 66–82.

[143] Li X. (2008) Convergence of the method of fundamental solutions for Poisson's equation on the unit sphere, *Adv. Comput. Math.* **28**, 269–282.

[144] Li Z.C. (1989) A nonconforming combination for solving elliptic problems with interfaces, *J. Comput. Phy.* **80(2)**, 288–313.

[145] Li Z.C. (1990) *Numerical methods for elliptic equations with singularities: Boundary methods and nonconforming combinations*. World Scientific, Singapore.

[146] Li Z.C. (1998) *Combined methods for elliptic equations with singularities, interfaces and infinities*. Kluwer Academic Publishers, Dordrecht, Boston.

[147] Li Z.C. (1998) Boundary penalty finite element methods for blending surfaces, I. basic theory, *J. Comput. Math.* **16**, 457–480.

[148] Li Z.C. (2007) Error analysis of the Trefftz method for solving Laplace's eigenvalue problems, *J. Comput. Appl. Math.* **200**, 231–254.

[149] Li Z.C. (2008) Combinations of method of fundamental solutions for Laplace's equation with singularities, *Eng. Anal. Bound. Elem.* **32**, 856–869.

[150] Li Z.C. (2008) The fundamental solutions for Laplace's equation with mixed boundary condition, as Chapter 2, *The method of fundamental solutions – A meshless method* (C.S. Chen, A. Karageorghis and Y.S. Smyrlis, Eds). Dynamic Publishers, Inc., USA, pp. 29–49.

[151] Li Z.C. (2009) The method of fundamental solutions for annular shaped domains, *J. Comput. Appl. Math.* **228**, 355–372.

[152] Li Z.C. (2012) *Analysis of method of fundamental solution for biharmonic equations*, Technical report.

[153] Li Z.C. (2012) Error analysis for hybrid Trefftz methods coupling traction conditions in linear elastostatics, *Number. Meth. PDE* **28**, 861–887.

[154] Li Z.C., Chiang J.Y., Huang H.T., Lee M.G. (2016) The interior field method for Laplace's equation in circular domains with circular holes, *Eng. Anal. Bound. Elem.* **67**, 173–185.

[155] Li Z.C., Chien C.S., Huang H.T. (2007) Effective condition number for finite difference method, *J. Comput. Appl. Math.* **198**, 208–235.

[156] Li Z.C., Chu P.C., Young L.J., Lee M.G. (2010) Models of corner and crack singularity of linear elastostatics and their numerical solutions, *Eng. Anal. Bound. Elem.* **34**, 533–548.

[157] Li Z.C., Huang H.T. (2008) Effective condition number for numerical partial differential equations, *Numer. Linear Algebra Appl.* **15**, 575–594.

[158] Li Z.C., Huang H.T., Chen J.T., Wei Y. (2010) Effective condition number and its applications, *Computing* **89**, 87–112.

[159] Li Z.C., Huang H.T., Lee M.G., Chiang J.Y. (2013) Error analysis of the method of fundamental solutions for linear elastostatics, *J. Comput. Appl. Math.* **251**, 133–153.

[160] Li Z.C., Huang H.T., Liaw C.P., Lee M.G. (2012) The null-field method of Dirichlet problems of Laplace's equation on circular domains with circular holes, *Eng. Anal. Bound. Elem.* **36**, 477–491.

[161] Li Z.C., Huang H.T., Wei Y. (2011) Ill-conditioning of the truncation singular value decomposition and the Tikhonov regularization and their application to numerical partial differential equations, *Numer. Linear Algebra Appl.* **18**, 205–221.

[162] Li Z.C., Huang H.T., Wei Y., Cheng A.H.-D. (2015) *Effective condition number for numerical partial differential equations*, 2nd edn. Science Press, Beijing.

[163] Li Z.C., Huang J., Huang H.T. (2010) Stability analysis of method of fundamental solutions for mixed boundary value problems of Laplace's equation, *Computing* **88**, 1–29.

[164] Li Z.C., Lee M.G., Chen J.T. (2011) New series expansions of fundamental solutions of linear elastostatics in 2D, *Computing* **92**, 199–224.

[165] Li Z.C., Lee M.G., Chiang J.Y. (2012) The collocation Trefftz methods for the Stokes equations with singularity, *Number. Meth. PDE* **29(2)**, 361–395.

[166] Li Z.C., Lee M.G., Chiang J.Y., Liu Y.P. (2011) The Trefftz method using fundamental solutions for biharmonic equations, *J. Comput. Appl. Math.* **235**, 4350–4367.

[167] Li Z.C., Lee M.G., Huang H.T., Chiang J.Y. (2017) Neumann problems of 2D Laplace's equation by method of fundamental solutions, *Appl. Numer. Math.* **119**, 126–145.

[168] Li Z.C., Lu T.T., Hu H.Y., Cheng A.H.-D. (2005) Particular solutions of Laplace's equations on polygons and new models involving mild singularities, *Eng. Anal. Bound. Elem.* **29**, 59–75.

[169] Li Z.C., Lu T.T., Hu H.Y., Cheng A.H.-D. (2008) *Trefftz and collocation methods.* MIT, Southampton.

[170] Li Z.C., Lu T.T., Huang H.T., Cheng A.H.-D. (2007) *Trefftz, collocation and other boundary methods – A comparison*, *Numer. Meth. PDE* **23**, 93–144.

[171] Li Z.C., Lu T.T., Huang H.T., Cheng A.H.-D. (2009) Error analysis of Trefftz method for Laplace's equations and its applications, *Comput. Model. Eng. Sci.* **52**, 39–81.

[172] Li Z.C., Lu T.T., Tsai H.S., Cheng A.H.-D. (2006) The Trefftz method for solving eigenvalue problems, *Eng. Anal. Bound. Elem.* **39**, 292–308.

[173] Li Z.C., Lu T.T., Wei Y. (2009) Effective condition number of Trefftz methods for biharmonic equations with crack singularities, *Numer. Linear Algebral Appl.* **16**, 145–171.

[174] Li Z.C., Lu T.T., Xie G.Q. (2012) The method of fundamental solutions and its combinations for exterior problems, *Eng. Anal. Bound. Elem.* **36**, 394–403.

[175] Li Z.C., Mathon R. (1990) Boundary methods for elliptic problems on unbounded domains, *J. Comput. Phy.* **89(2)**, 414–431.

[176] Li Z.C., Mathon R., Sermer P. (1987) Boundary methods for solving elliptic problems with singularities and interfaces, *SIAM J. Numer. Anal.* **24**, 487–498.

[177] Li Z.C., Wei Y., Chen Y., Huang H.T. (2019) The method of fundamental solutions for the Helmholtz equation, *Appl. Numer. Math.* **135**, 510–536.

[178] Li Z.C., Young L.J., Huang H.T., Liu Y.P., Cheng A.H.-D. (2010) Comparisons of fundamental solutions and particular solutions for Trefftz methods, *Eng. Anal. Bound. Elem.* **34**, 248–258.

[179] Li Z.C., Zhang L.P., Lee M.G. (2016) Interior field methods for Neumann problems of Laplace's equation in elliptic domains, comparisons with degenerate scales, *Eng. Anal. Bound. Elem.* **71**, 190–202.

[180] Li Z.C., Zhang L.P., Wei Y., Lee M.G., Chiang J.Y. (2015) Boundary methods for Dirichlet problems of Laplace's equation in elliptic domains with elliptic holes, *Eng. Anal. Bound. Elem.* **61**, 92–103.

[181] Li Z.C., Zhang L.P., Wei Y., Huang H.T. (2018) *Analysis for the Helmholtz equation by method of fundamental solutions using Hankel functions*, Technical report.

[182] van Loan C.F. (1976) Generalizing the singular value decomposition, *SIAM J. Numer. Anal.* **13**, 76–83.

[183] Lohofer G. (1998) Inequalities for the associated Legendre functions, *J. Approx. Theory* **95**, 178–193.

[184] Liu C.S. (2007) A modified Trefftz method for two-dimensional Laplace equation considering the domain's characteristic length, *Comput. Model. Eng. Sci.* **21(1)**, 53–65.

[185] Lu T.T., Hu H.Y., Li Z.C. (2004) Highly accurate solutions of Motz's and the cracked beam problems, *Eng. Anal. Bound. Elem.* **28**, 1387–1403.

[186] MacRobert T.M. (1967) *Spherical harmonics*, 3rd edn. Pergamon Press, Oxford, England, U.K.

[187] Marin L. (2009) An iterative MFS algorithm for Cauchy problem associated with the Laplace equation, *Comput. Model. Eng. Sci.* **48**, 121–152.

[188] Marin L. (2011) Relaxation procedures for an iterative MFS algorithm for two-dimensional steady-state isotropic heat conduction Cauchy problems, *Eng. Anal. Bound. Elem.* **35**, 415–429.

[189] Mathon R., Johnston R.L. (1977) The approximate solution of elliptic boundary-value problems by fundamental solutions, *SIAM J. Numer. Anal.* **14**, 638–650.

[190] McLean W. (1986) A spectral Galerkin method for a boundary integral equation, *Math. Comput.* **47**, 597–607.

[191] Mey G.D. (1978) Integral equations for potential problems with the source function not located on the boundary, *Comput. Struct.* **8**, 113–115.

[192] Mogilevskaya S.G., Linkov A.M. (1998) Complex fundamental solutions and complex variables boundary element method in elasticity, *Comput. Mech.* **22**, 88–92.

[193] Morse P.M., Feshbach H. (1953) *Methods of theoretical physics.* McGraw-Hill Book Company Inc., New York.

[194] Nennig B., Perrey-Debain E., Chazot J.-D. (2011) The method of fundamental solutions for acoustic wave scattering by a single and a periodic array of poroelastic scatterers, *Eng. Anal. Bound. Elem.* **35**, 1019–1028.

[195] Oden J.T., Reddy J.N. (1976) *An introduction to the mathematical theory of finite elements.* John Wiley & Sons, New York.

[196] Ogata H., Chiba F., Ushijima T. (2011) A new theoretical error estimate of the method of fundamental solutions applied to reduced wave problems in the exterior region a disk, *J. Comput. Appl. Math.* **235**, 3395–3412.

[197] Ohe T., Ohnaka K. (2004) Uniqueness and convergence of numerical solution of the Cauchy problem for the Laplace equation by a charge simulation method, *Japan J. Indust. Appl. Math.* **21**, 339–359.

[198] Olver F.W.J., Lozier D.W., Boisvert R.F., Clark C.W. (2010) *NIST handbook of mathematical functions.* Cambridge University Press, Cambridge, New York.

[199] Pan V.Y. (2016) How bad are Vandermonde matrices? *SIAM J. Matrix Anal. Appl.* **37(2)**, 676–694.

[200] Park Y., Kim J., Jung J., Lee E., Min C. (2018) An efficient MILU preconditioning for solving the 2D Poisson equation with Neumann boundary condition, *J. Comput. Phy.* **356**, 115–126.

[201] Plagianakos V.P., Nousis N.K., Vrahatis M.N. (2001) Locating and computing in parallel all the simple roots of special functions using PVM, *J. Comput. Appl. Math.* **133**, 545–554.

[202] Porzrikidis C. (1992) *Boundary integral and singularity methods for linearized viscous flow.* Cambridge University Press, New York.

[203] Qin Q.H. (2000) *The Trefftz finite and boundary element method.* WIT Press, Southampton, Boston.

[204] Quarteroni A., Valli A. (1994) *Numerical approximation of partial differential equations.* Springer-Verlag, Berlin.

[205] Ramachandran P.A. (2002) Method of fundamental solutions: Singular value decomposition analysis, *Commun. Numer. Meth. Eng.* **18**, 789–801.

[206] Reinhardt H.J., Han H., Hao D.N. (1999) Stability and regularization of a discrete approximation to the Cauchy problems of Laplace's equation, *SIAM J. Numer. Anal.* **36**, 890–905.

[207] Reutskiy S.Y. (2006) The method of fundamental solutions for Helmholtz eigenvalue problems in simply and multiply connected domains, *Eng. Anal. Bound. Elem.* **30**, 150–159.

[208] Saavedra I., Power H. (2003) Multipole fast algorithm for the least-squares approach of the method of fundamental solutions for three-dimensional harmonic problems, *Numer. Meth. PDE* **19**, 828–845.

[209] Sadd M.H. (2009) *Elasticity: Theory, applications, and numerics*, 2nd edn. Academic Press, Burlington, MA, USA.

[210] Sauter S.A., Schwab C. (2011) *Boundary element methods.* Springer, London.

[211] Schaback R. (June 11–13, 2007) *Adaptive numerical solution of MFS systems*, a plenary talk at the First Inter. Workshop on the Method of Fundamental Solutions (MFS2007), Ayia Napa, Cyprus.

[212] Schaback R. (2009) Adaptive numerical solution of MFS systems, as Chapter 1, *The method of fundamental solutions – A meshless method* (C.S. Chen, A. Karageorghis, Y.S. Smyrlis, Eds). Dynamic Publishers, Inc., USA, pp. 1–27.

[213] Schaback R. (2009) Solving the Laplace equation by meshless collocation using harmonic kernels, *Adv. Comput. Math.* **31**, 457–470.

[214] Shigeta T., Young D.L. (2009) Method of fundamental solutions with optimal regularization techniques for the Cauchy problem of the Laplace equation with singular points, *J. Comput. Phy.* **228**, 1903–1915.

[215] Smyrlis Y.S. (2006) The method of fundamental solutions: A weighted least squares approach, *BIT Numer. Math.* **46**, 163–194.

[216] Smyrlis Y.S. (2009) Applicability and applications of the method of fundamental solutions, *Math. Comput.* **78(267)**, 1399–1434.

[217] Smyrlis Y.S., Karageorghis A. (2004) A linear least-squares MFS for certain elliptic problems, *Numer. Algorithms* **35**, 29–44.

[218] Smyrlis Y.S., Karageorghis A. (2004) Numerical analysis of the MFS for certain harmonic problems, *ESAIM: Math. Model. Numer. Anal.* **38**, 495–517.

[219] Strang G., Fix G.J. (1973) *An analysis of the finite element method.* Prentice-Hall, Englewood Cliffs, New Jersey.

[220] Stroud A.H. (1971) *Approximate calculation of multiple integrals.* Prentice-Hall, New Jersey.

[221] Thompson R.C. (1972) Principal submatrices IX: Interlacing inequalities for singular values of submatrices, *Linear Algebra Appl.* **6**, 1–12.

[222] Tian Z., Li Z.C., Huang H.T., Chen C.S. (2017) The method of fundamental solutions for the modified Helmholtz equation, *Appl. Math. Comput.* **305**, 262–281.

[223] Tikhonov A.N., Samarskii A.A. (1963) *Equations of mathematical physics* (D.M. Brink, Trans.). Pergamon Press, Oxford.

[224] Trefftz E. (1926) Ein Gegenstuck zum Ritz'schen Verfahren, *Proc. 2nd Int. Cong. Appl. Mech., Zurch*, 131–137.

[225] Tsai C.C., Lin P.H. (2013) On the exponential convergence of method of fundamental solutions, *Special issue of method of fundamental solutions* (C.S. Chen, J.T. Chen, D.L. Young, Eds), in *Inter. J. Comput. Meth.* **10**, No. 02, 1341007. World Scientific, Singapore.

[226] Tsai C.C., Young D.L. (2013) Using the method of fundamental solutions for obtaining exponentially convergent Helmholtz eigensolutions, *CMES* **94(2)**, 175–205.

[227] Tsai C.C., Young D.L., Chen C.W., Fan C.M. (2006) The method of fundamental solutions for eigenproblems in domains with and without interior holes, *Proc. R. Soc. Lond. A* **462**, 1443–1466.

[228] Tsangaris T., Smyrlis Y.S., Karageorghis A. (2006) Numerical analysis of the method of fundamental solution for harmonic problems in annular domains, *Numer. Meth. PDE* **22**, 507–539.

[229] Tyrtyshnikov E.E. (1994) How bad are Hankel matrices? *Numer. Math.* **67**, 261–269.

[230] Ushijima T., Chiba F. (2003) A fundamental solution method for the reduced wave problem in a domain exterior to a disc, *J. Comput. Appl. Math.* **152**, 545–557.

[231] Ushijima T., Chiba F. (2003) Error estimates for a fundamental solution method applied to reduced wave problems in a domain exterior to a disc, *J. Comput. Appl. Math.* **159**, 137–148.

[232] Ushijima T., Chiba F. (2009) Exponential decay of errors of a fundamental solution method applied to a reduced wave problem in the exterior region of a disc, *J. Comput. Appl. Math.* **231**, 869–885.

[233] Vekua I.N. (1967) *New methods for solving elliptic equations (North-Holland series in applied mathematics & mechanics).* North-Holland, Amsterdam.

[234] Verde M.F., Macmillan N.A., Rotello C.M. (2006) Measures of sensitivity based on a single hit rate and false alarm rate: The accuracy, precision, and robustness of d', A_z, and A', *Percept. Psychophy.* **68(4)**, 643–654.

[235] Wang F.Z., Chen W., Jiang X. (2010) Investigation of regularized techniques for boundary knot method, *Int. J. Numer. Methods Biomed. Eng.* **26**, 1868–1877.

[236] Wang F.Z., Ling L., Chen W. (2009) Effective condition number for boundary knot method, *CMC* **12**, 57–70.

[237] Wang H., Qin Q.H. (2019) *Methods of fundamental solutions in solid mechanics.* Elsevier, Amsterdam.

[238] Wang Y., Rudy Y. (2006) Application of the method of fundamental solutions to potential-based inverse electrocardiography, *Ann. Biomed. Eng.* **34**, 1272–1288.

[239] Watson G.N. (1980) *A treatise on the theory of Bessel functions.* Cambridge University Press.

[240] Wei T., Hon Y.C., Ling L. (2007) Method of fundamental solutions with regularization techniques for Cauchy problems of elliptic operators, *Eng. Anal. Bound. Elem.* **31**, 373–385.

[241] Wei T., Zhou D.Y. (2010) Convergence analysis of the Cauchy problem of Laplace's equation by a regularized method of fundamental solutions, *Adv. Comput. Math.* **33**, 491–510.

[242] Wei Y., Lu T.T., Huang H.T., Li Z.C. (2012) Effective condition number for weighted linear least squares problems and applications to the Trefftz method, *Eng. Anal. Bound. Elem.* **36**, 53–62.

[243] Wendland H. (2004) *Scattered data approximation.* Cambridge University Press, Cambridge.

[244] Young D.L., Jane S.J., Fan C.M., Murugesan K., Tsai C.C. (2006) The method of fundamental solutions for 2D and 3D Stokes problems, *J. Comput. Phy.* **211**, 1–8.

[245] Young D.L., Tsai C.C., Chen C.W., Fan C.M. (2008) The method of fundamental solutions and condition number analysis for inverse problems of Laplace equation, *Comp. Math. Appl.* **55**, 1189–1200.

[246] Yu D.H. (2002) *Natural boundary integral method and its applications.* Science Press/Kluwer Academic Publishers, Beijing/New York.

[247] Zhang J.Y., Wang F.Z. (2012) Boundary knot method: An overview and some novel approaches, *Comput. Model. Eng. Sci.* **88(2)**, 141–152.

[248] Zhang L.P. (2009) *The method of fundamental solutions and effective condition number*, Thesis of undergraduates. School of Information Science and Engineering, LanZhou University, China.

[249] Zhang L.P., Li Z.C., Chen Z., Huang H.T. (2020) The Laplace equation in three dimensions by the method of fundamental solutions and the method of particular solutions, *Appl. Numer. Math.* **154**, 47–69.

[250] Zhang L.P., Li Z.C., Huang H.T., Chen Z. (2020) Super-exponential growth rates of condition number in the boundary knot method for the Helmholtz equation, *Appl. Math. Letters* **105**, 106333.

[251] Zhang L.P., Li Z.C., Huang H.T., Lee M.G. (2021) Comparisons of method of fundamental solutions, method of particular solutions and the MFS-QR; stability analysis, *Eng. Anal. Bound. Elem.* **123**, 182–199.

[252] Zhang L.P., Li Z.C., Lee M.G., Huang H.T. (2022) Stability analysis of the method of fundamental solutions with smooth closed pseudo-boundaries for Laplace's equation; better pseudo-boundaries, *Numer. Algorithms* **89**, 1183–1222.

[253] Zhang L.P., Li Z.C., Huang H.T., Lee M.G. (2021) Singularity problems from source functions as source nodes located near boundaries; numerical methods and removal techniques, *Eng. Anal. Bound. Elem.* **130**, 300–321.

[254] Zhang L.P., Li Z.C., Huang H.T., Wei Y. (2019) The modified method of fundamental solutions for exterior problems of the Helmholtz equation; spurious eigenvalues and their removals, *Appl. Numer. Math.* **145**, 236–260.

[255] Zhang L.P., Li Z.C., Wei Y., Chiang J.Y. (2013) Cauchy problems of Laplace's equation by methods of fundamental solutions and particular solutions, *Eng. Anal. Bound. Elem.* **37**, 765–780.

[256] Zhang L.P., Li Z.C., Huang H.T., Lee M.G. (2022) New locations of source nodes for method of fundamental solutions solving Laplace's equation; pseudo radial-lines, *Eng. Anal. Bound. Elem.* **136**, 93–115.

[257] Zhang L.P., Li Z.C., Lee M.G., Huang H.T. (2023) Lower and upper bounds of condition number for Vandermonde-wise matrices and method of fundamental solutions using pseudo radial-lines, *Numer. Linear Algebra Appl.* **30**(2), e2466.

[258] Zhang L.P., Li Z.C., Wei Y., Huang H.T. (2022) Spurious eigenvalues-free algorithms of the method of fundamental solutions for solving the Helmholtz equation in bounded multiply connected domains, *Numer. Algorithms* **91**, 895–932. (https://doi.org/10.1007/s11075-022-01286-y).

[259] Zhang L.P., Li Z.C., Wei Y., Huang H.T. (2023) New regularization techniques for ill-conditioning problems and their applications; choices of regularization parameters, *Eng. Anal. Bound. Elem.* **152**, 347–361.

[260] Zhou D., Wei T. (2008) The method of fundamental solutions for solving a Cauchy problem of Laplace's equation in a multi-connected domain, *Inverse Probl. Sci. Eng.* **16**, 389–411.

Glossary of Symbols

2D: two dimensions.

3D: three dimensions.

AE: adaptive error.

BAM: boundary approximation method.

BIE: boundary integral equation.

BIEM: boundary integral equation method.

BKM: boundary knot method.

CPU: central processing unit.

CTM: collocation Trefftz method.

EDP: exterior Dirichlet problem.

FDM: finite difference method.

FEM: finite element method.

FS: fundamental solutions.

FVM: finite volume method.

HTM: hybrid Trefftz method.

HP-TM: hybrid plus penalty Trefftz method.

IDP: interior Dirichlet problem.

IFM: interior field method.

LBB: Ladyzhenskaya-Babuska-Brezzi.

LSM: least-squares method

MFS: method of fundamental solutions.

MFS-QR: algorithms of Antunes [8].

MPS: method of particular solutions.

NFM: null field method.

ODE: ordinary differential equation.

PDE: partial differential equation.

PS: particular solutions.

RBF: radial basis function.

SHF: spherical harmonic functions.

SM: spectral method.

SPS: singular particular solutions.

SVD: singular value decomposition.

TM: Trefftz method.

TSVD: truncated singular value decomposition.

TR: Tikhonov regularization.

C, c_0: the positive bounded constant.

w, w_j: the weight constant.

P_c: the penalty constant.

$\mathbf{C}$: the set of complex numbers.

$\mathbf{R}$: the set of real numbers.

S: the solution domain.

$S_a = S_1 \backslash S_2$: the annual domain with $S_2 \subset S_1$.

S_∞: the unbounded solution domain.

S_{in}: a disk inside of S.

$S_\rho = \{(\rho, \theta, \phi) | \rho = \text{const}, 0 \le \theta < \pi, 0 \le \phi < 2\pi\}$: a sphere with radius ρ.

$U = \{(\rho, \theta, \phi) | \rho = 1, 0 \le \theta < \pi, 0 \le \phi < 2\pi\}$: a unit sphere.

$\mathbf{\Gamma}$: the exterior boundary of the solution domain.

$\mathbf{\Gamma}_0$: the interface boundary.

$\mathbf{\Gamma}_D$: the exterior boundary with Dirichlet boundary condition.

$\mathbf{\Gamma}_N$: the exterior boundary with Neumann boundary condition.

$\mathbf{\Gamma}_R$: the exterior boundary with Robin (mixed) boundary condition.

$\mathbf{\Gamma}_{\text{in}}$: the interior boundary.

Γ_{out}: the exterior boundary.

Γ_ρ: a circule with radius ρ.

$T : X \to Y$; T: maps X into Y.

$\mathbf{Ax} = \mathbf{b}$: the linear algebraic system, where $\mathbf{A} \in \mathbf{R}^{n\times n}$ may be symmetric and positive definite matrix, $\mathbf{x} \in \mathbf{R}^n$ and $\mathbf{b} \in \mathbf{R}^n$ are unknown and known vectors, respectively.

$\mathbf{Fx} = \mathbf{b}$: the overdetermined system, where $\mathbf{F} \in \mathbf{R}^{m\times n}$ $(m \geq n)$ is the stiffness matrix, $\mathbf{x} \in \mathbf{R}^n$ and $\mathbf{b} \in \mathbf{R}^m$ are the unknown and the known vectors, respectively.

$\mathbf{F} = \mathbf{U\Sigma V}^T$: the singular value decomposition, where $\mathbf{U} = \{\mathbf{u}_1, \mathbf{u}_2, ..., \mathbf{u}_m\} \in \mathbf{R}^{m\times m}$ and $\mathbf{V} = \{\mathbf{v}_1, \mathbf{v}_2, ..., \mathbf{v}_n\} \in \mathbf{R}^{n\times n}$ are orthogonal matrices, and $\mathbf{\Sigma} = \text{diag}(\sigma_1, \sigma_2, ..., \sigma_n) \in \mathbf{R}^{m\times n}$ is a diagonal matrix with the singular values $\sigma_i \geq 0$.

$\mathbf{G} = \mathbf{QR}$: the QR decomposition of matrix $\mathbf{G} \in \mathbf{R}^{m\times n}$, where $\mathbf{Q} \in \mathbf{R}^{m\times m}$ and $\mathbf{R} \in \mathbf{R}^{m\times n}$ are the orthogonal and the upper-triangular matrices, respectively.

$\text{Cond} = \frac{\sigma_{\max}}{\sigma_{\min}}$: the traditional condition number in the 2-norm, where $\sigma_{\max}$ and $\sigma_{\min}$ are the maximal and the minimal singular values, respectively.

$\widehat{\text{Cond}} = \frac{\sigma_{\max}}{\sigma_{\min-\text{next}}}$: the modified condition number.

$\text{Cond\_eff} = \frac{\|\mathbf{b}\|}{\sigma_{\min}\|\mathbf{x}\|}$: effective condition number in the 2-norm.

$\kappa = -\frac{\ln b}{\ln a}$: the sensitivity index with $\|\epsilon\|_{0,\Gamma} = O(a^N)$ $(a<1)$ and $\text{Cond} = O(b^N)$ $(b \geq 1)$.

$a \asymp b$: there exist two positive constants c_0 and C such that $c_0 b \leq a \leq Cb$.

$T_N(g) = h\sum_{k=0}^{N-1} g(kh) = \Sigma_N(g)$: the trapezoidal rule with $h = \frac{2\pi}{N}$ for $\displaystyle\int_0^{2\pi} g(x)\,dx$.

$\triangle_N(g) = T_N(g) - \displaystyle\int_0^{2\pi} g(x)\,dx$.

$\widehat{\int}, \widehat{\int\int}$: the numerical approximation of $\int, \int\int$.

$\text{circulant}(a_1, a_2, ..., a_N)$: the circulant matrix $\begin{pmatrix} a_1 & a_2 & \cdots & a_N \\ a_N & a_1 & \cdots & a_{N-1} \\ \vdots & \vdots & \ddots & \vdots \\ a_2 & a_3 & \cdots & a_1 \end{pmatrix}$.

$\text{diag}(a_1, a_2, ..., a_N)$: the diagonal matrix $\begin{pmatrix} a_1 & 0 & \cdots & 0 \\ 0 & a_2 & \cdots & 0 \\ \vdots & \vdots & \ddots & \vdots \\ 0 & 0 & \cdots & a_N \end{pmatrix}$.

the Vandermonde matrix $\mathbf{V}_n = \begin{pmatrix} 1 & 1 & \cdots & 1 \\ x_1 & x_2 & \cdots & x_n \\ \vdots & \vdots & \vdots & \vdots \\ x_1^{n-1} & x_2^{n-1} & \cdots & x_n^{n-1} \end{pmatrix}$, where x_i are distinct.

$\triangle D_i = D_i - \tilde{D}_i$.

$\triangle h_\ell$: the meshspacing of small section $\mathbf{\Gamma}_\ell$.

$\nabla = \left(\dfrac{\partial}{\partial x}, \dfrac{\partial}{\partial y}\right)$: the gradient operator.

$\Delta = \dfrac{\partial^2}{\partial x^2} + \dfrac{\partial^2}{\partial y^2}$: the Laplace operator in two dimensions.

$\Delta = \dfrac{\partial^2}{\partial x^2} + \dfrac{\partial^2}{\partial y^2} + \dfrac{\partial^2}{\partial z^2}$: the Laplace operator in three dimensions.

$\Delta u = f$: the Poison equation.

$\Delta u = 0$: the Laplace equation.

$\Delta u + \lambda u = 0$: the Laplace eigenvalue equation.

$u_\nu = \frac{\partial u}{\partial \nu}$: the normal derivative of u on boundary $\mathbf{\Gamma}$.

D^α: the partial differential operator of order $|\alpha|$.

$\|u\|_{0,S} = \left\{\iint_S u^2\, d\mathbf{x}\right\}^{\frac{1}{2}}$.

$\|u\|_{\frac{1}{2},\Gamma} = \left\{\|u\|_{0,\Gamma}^2 + \int_\Gamma\int_\Gamma \frac{(u(P)-u(Q))^2}{|\overline{PQ}|^2}\, d\ell(Q)\, d\ell(P)\right\}^{\frac{1}{2}}$.

$\|u\|_{-\frac{1}{2},\Gamma} = \sup\limits_v \frac{\left|\int_\Gamma uv d\ell\right|}{\|v\|_{\frac{1}{2},\Gamma}}$.

$|u|_{p,S} = \left\{\sum\limits_{|\alpha|=p} \iint_S |D^\alpha u|^2\, d\mathbf{x}\right\}^{\frac{1}{2}}$.

$\|u\|_{p,S} = \left\{\sum\limits_{|\alpha|\,\leq\, p} \iint_S |D^\alpha u|^2\, d\mathbf{x}\right\}^{\frac{1}{2}}$.

$\|u\|_B = \left\{\|u\|_{0,\Gamma_D}^2 + w^2 \|\frac{\partial u}{\partial \nu} + \alpha u\|_{0,\Gamma_R}^2\right\}^{\frac{1}{2}}$: the boundary norm.

$C^p(S)$: the space of p-times continuously differentiable functions on S.

$C^\infty[0,\, 2\pi]$: the space of smooth functions on $[0, 2\pi]$.

$\mathbf{L}^2(S) = \left\{u \middle| \|u\|_{0,S} = \left\{\iint_S u^2\, d\mathbf{x}\right\}^{\frac{1}{2}} < \infty\right\}$.

$\mathbf{H}^p(S) = \{u \in \mathbf{L}^2(S) \big| D^\alpha u \in \mathbf{L}^2(S), 0 \leq |\alpha| \leq p\}$.

$\mathbf{H}^p(S)/\mathbf{P}_0(S)$: the quotient space, where $\mathbf{H}^p(S)$ are the Sobolev space and $\mathbf{P}_0(S)$ is a constant space.

$\Gamma(x) = \int_0^\infty t^{x-1}e^{-t}dt, x > 0$: the Gamma function.

$I_j(x) = \sum_{k=0}^{\infty} \frac{1}{\Gamma(k+1)\Gamma(k+j+1)} \left(\frac{x}{2}\right)^{2k+j} = \frac{(\frac{x}{2})^j}{\Gamma(j+\frac{1}{2})\Gamma(\frac{1}{2})} \int_{-1}^{1} (1-t^2)^{j-\frac{1}{2}} \cosh(xt)\, dt$: the Bessel functions for purely imaginary argument.

$J_\mu(r) = \sum_{i=0}^{\infty} \frac{(-1)^i}{\Gamma(i+1)\Gamma(i+\mu+1)} \left(\frac{r}{2}\right)^{2i+\mu}$: the Bessel functions of the first kind.

$Y_\mu(r) = \frac{J_\mu(r)\cos(\mu\pi) - J_{-\mu}(r)}{\sin(\mu\pi)}$: the Neumann functions of the first kind.

$H_n^{(1)}(z) = J_n(z) + \mathbf{i}\, Y_n(z)$: the Hankel function of the first kind of order n, where $\mathbf{i} = \sqrt{-1}$, and $J_n(z)$ and $Y_n(z)$ are the Bessel and the Neumann functions of order n, respectively.

$M_\mu(x) = |H_\mu^{(1)}(x)| = \sqrt{J_\mu^2(x) + Y_\mu^2(x)} = \left\{ \frac{8}{\pi^2} \int_0^\infty \mathcal{K}_0(2x \sinh(t))\cosh(2\mu t)\, dt \right\}^{\frac{1}{2}}$, $\mu \geq 0$, $x > 0$: the modular of Hankel function.

$\mathcal{K}_n(x) = \frac{\Gamma(n+\frac{1}{2})2^n}{x^n\Gamma(\frac{1}{2})} \int_0^\infty \frac{\cos(xu)}{(u^2+1)^{n+\frac{1}{2}}}\, du = \frac{1}{2}\int_{-\infty}^{\infty} e^{-x\cosh(\eta) - n\eta}\, d\eta$: the Bessel function of the third kind of order $n \geq 1$.

$\mathcal{K}_0(x) = \int_0^\infty e^{-x \cosh\eta}\, d\eta, x > 0$: the Bessel function of the third kind of order zero.

$P_n(x) = \frac{1}{2^n n!} \frac{d^n}{dx^n} [(x^2-1)^n]$: the Legendre polynomial.

$P_n^{(m)}(x) = (1-x^2)^{\frac{m}{2}} \frac{d^m}{dx^m} [P_n(x)]$, $0 \leq m \leq n$, $P_n^{(0)}(x) = P_n(x)$.

$Y_n(\theta,\phi) = A_n P_n(\cos\theta) + \sum_{m=1}^{n} P_n^{(m)}(\cos\theta)\{A_{n,m}\cos(m\phi) + B_{n,m}\sin(m\phi)\}$: the spherical harmonic functions, where A_n, $A_{n,m}$ and $B_{n,m}$ are real coefficients.

$\hat{P}_n(x) = \left\{\frac{2n+1}{2}\right\}^{\frac{1}{2}} P_n(x)$, $\hat{P}_n^{(m)}(x) = \left\{\frac{2n+1}{2}\frac{(n-m)!}{(n+m)!}\right\}^{\frac{1}{2}} P_n^{(m)}(x)$: the normalized Legendre polynomials.

Index

2π-periodic function, 21, 314
k-order piecewise Lagrange polynomial, 86
$\mathbf{L}^2$ norm, 32
1-norm, 145
2-norm, 240, 296
3D exterior problem, 93
3D Helmholtz equation, 302, 332
3D problem, 13, 301, 302, 330, 332

A
Abscissas, 13, 309, 323
Accuracy, 12, 39, 45, 66, 93, 119, 128, 149, 181, 327, 335, 339
Adaptive errors (AE), 404
Addition theorem, 22, 103, 131, 217, 255, 256, 271, 277, 311, 332, 337
Additional FS, 375
Admissible function, 5, 86, 242, 307, 389
Airy function, 173
Almansi FS, 216
Amoeba-like domain, 120, 375, 390
Annular domain, 15, 70, 197, 371
Annular domain problem, 61
Arbitrary pseudo-boundary, 339
Auxiliary function, 367
Auxiliary problem, 31, 57
Auxiliary solution, 80

B
Ball domain, 354
Basic Case, 402, 408, 409
Basis function, 348, 349, 351
Bessel differential equation, 204
Bessel function, 127, 128, 192, 324
Bessel functions of the third kind, 173
Bias derivative, 86
BIE of the first kind, 165
Biharmonic equation, 2, 215, 242
Boundary element method (BEM), 9, 120, 210
Boundary energy, 253
Boundary error, 6, 96, 121, 145, 152, 179, 243, 269
Boundary integral equation (BIE), 13, 97
Boundary integral equation method (BIEM), 13, 165
Boundary knot method (BKM), 39, 149, 192
Boundary norm, 55, 63, 67, 70, 198
Boundary point method, 2

C
Cartesian coordinates, 101, 336, 340
Cauchy boundary, 289
Cauchy condition, 282, 287
Cauchy data, 282
Cauchy problem, 281
Cauchy-Kowalevski Theorem, 285
Cauchy–Navier equation, 2, 126, 248, 249
Central rule, 4, 20, 62, 253
Charge nodes, 3, 20, 254
Charge simulation method, 2
Chebyshev polynomial, 84
Chebyshev rule, 323
Circle, 2, 3, 19, 27, 42, 67, 136, 156, 201, 254, 283, 370
Circulant, 180
Circulant block matrix, 202, 240
Circulant matrix, 16, 19, 33, 39, 41, 46, 147, 202, 231, 234, 240, 361
Circular domain, 210, 228, 229, 339
Circular hole, 119
Circular interior boundary, 179
Circular pseudo-boundary, 39, 100, 181, 336, 339, 355, 388
Clamped boundary condition, 215, 242
Classic domain, 375, 388
Closed pseudo-boundary, 342, 361, 378, 401

Collocation equations, 5, 21, 32, 71, 102, 130, 146, 158, 228, 284, 342, 349, 355, 362, 368, 402, 410
Collocation nodes, 32, 45, 146, 179, 292
Collocation Trefftz method (CTM), 5, 21, 43, 253, 375
Combination of FS and RBF, 90
Combination of MFS and MPS, 95
Combination of TM with PS and FS, 95
Combined method, 12, 77, 90
Complex fundamental solution, 157, 192
Complex MFS using the Hankel function, 214
Complex solution, 159, 181, 193, 212
Complicated domain, 375
Computer storage, 12
Condition number (Cond), 37, 180, 243, 296, 307
Conjecture, 128
Conjugate, 158, 193
Consistent condition, 41, 42
Constant space, 44
Continuity extension, 29, 322
Corner singularity, 44, 77, 376
Corner singularity problem, 77, 78
Coupling technique, 12, 77
CPU time, 12
Crack problem, 91
Crack singularity, 77, 91
Cross-product, 205
CTM using FS, 264
Cylindrical coordinates, 324
Cylindrical harmonic function, 324
Cylindrical pseudo-surface, 328
Cylindrical source nodes, 328

D
D-D conditions, 205
D-N conditions, 205
Decimal digit, 182
Degeneracy, 161, 195
Degenerate scale, 13, 31, 106, 119, 347, 368
Determinant, 237, 366
Diagonal matrix, 203, 230, 347, 364, 407
Dirac-delta function, 376, 394
Dirichlet boundary condition, 3, 5, 19, 61, 90, 128, 254, 340, 361, 387, 402
Dirichlet problem, 70, 151, 197
Dirichlet–Laplace eigenvalue problem, 195, 204, 210
Discrete matrix, 59, 114, 124, 210, 366, 403
Discrete norm, 53, 309
Discrete singularity method, 2
Disk, 3, 19, 375
Disk domain, 32, 128, 359, 388, 415
Displacement condition, 247, 252, 269
Displacement-traction condition, 252
Double precision, 182, 297, 325, 345, 416
Double-layer potential, 156, 165

E
Effective condition number (Cond_eff), 2, 16, 39, 149, 243, 296, 325, 387
Eigenfunction, 204
Eigenvalue problem, 140
Eigenvalue, 16, 33, 35, 46, 147, 163, 195, 204, 230, 236
Eigenvector, 33
Elastostatics problem, 247, 376
Electric potential, 376
Ellipse, 101, 340, 344, 375
Elliptic coordinates, 101, 336, 340, 348, 377
Elliptic domain, 113, 117, 339
Elliptic hole, 119
Elliptic pseudo-boundary, 39, 100, 336, 339, 382
Embedding theorem, 64, 68, 227, 265
Energy, 4, 42, 61, 67, 79, 95, 283
Equal-distribution, 365
Error analysis, 11, 39, 70, 103, 131, 159, 193, 254, 290, 313, 380
Error bound, 66, 71, 107
Error function, 72
Euclidean distance, 309
Euclidean norm, 243
Explicit basis function, 351
Exterior boundary, 73, 371
Exterior Dirichlet problem (EDP), 155, 333
Exterior normal, 3, 42, 61, 79
Exterior normal derivative, 95
Exterior problem, 13, 91
Exterior source nodes, 197, 211

F
Fictitious boundary, 100
Fictitious resonance frequency, 162
Finite difference method (FDM), 12, 77, 87
Finite element method (FEM), 12, 77, 86, 119, 378
Finite volume method (FVM), 12
Five-pedal-flower-like domain, 339, 354
Flat radial basis function, 354
Fourier coefficient, 25, 63, 107, 135, 256, 273
Fourier expansion, 25, 256, 273
Fourier matrix, 180, 202, 229
Fourier series, 25, 107, 135, 175, 273
Full rank, 37
Fundamental collocation method, 2
Fundamental solution (FS), 3, 20, 42, 70, 95, 102, 129, 146, 250, 283, 310, 361, 378
Fundamental solution method, 2

G
Gamma function, 129
Gap, 160, 168, 195, 204
Gauss–Chebyshev rule, 327
Gauss–Green formula, 249
Gauss–Jacobi rule, 324
Gauss–Legendre rule, 309, 314, 325, 327
Gaussian integration, 324
Gaussian nodes, 5, 21, 43, 284
Gaussian rule, 4, 20, 43, 62, 158, 193, 253, 315
Gaussian rule of six nodes, 6
Geometric series, 22
Green formula, 80, 288, 371
Grid-like, 13, 301

H
Hadamard product, 348
Hankel function, 127, 128, 157, 173, 192
Harmonic, 20
Harmonic function, 13, 65, 249, 254, 371, 380, 387, 397
Harmonic kernel, 350
Harmonic polynomial, 11, 24, 45, 55, 63, 78, 217, 254, 255, 257
Harmonic solution, 262, 286, 355
Harmonic vector, 249
Heat transfer problem, 376
Helmholtz equation, 128, 149, 157, 192, 201, 332
Holmgrens theorem, 285
HTM using FS, 252, 266
HTM using PS, 252
Hybrid combination of TM (H-TM), 79
Hybrid plus penalty combination of MFS and FEM, 86
Hybrid plus penalty coupling, 86
Hybrid plus penalty TM (HP-TM), 82
Hybrid Trefftz method (HTM), 252

I
Identity matrix, 365
Ill-conditioning, 2, 39, 149, 336, 339, 345, 403
Ill-posed Cauchy problem, 300
Ill-posedness, 287, 300
Image node, 387
Imaginary, 21
Indirect TM combination, 84
Infinity norm, 309
Inner product, 55
Instability, 2, 7, 110, 149, 295, 300, 345
Interface problem, 15, 61
Interior boundary, 73, 371
Interior boundary conditions, 66
Interior crack problem, 398
Interior Dirichlet problem (IDP), 192, 332
Interior ellipse boundary, 370
Interior field method (IFM), 119
Interior Neumann problem, 44
Interior pseudo-boundary, 213
Interior source nodes, 198, 211
Interpolation polynomial, 267
Inverse inequality, 58, 67, 78, 288, 290
Inverse problem, 287
Inverse property, 146
Iterative method, 385

J
Jacobi-trapezoidal-Legendre rule, 325

K
Kansa method, 90
Katsurada approaches, 191, 128
Korn inequality, 248
Kronecker delta, 248

L
Lagrange multiplier, 84, 252
Lagrange multiplier TM combination, 84
Laplace equation, 3, 19, 42, 61, 101, 254, 340, 361, 376, 401
Laurent series, 285
LBB condition, 84, 266
Leading coefficient, 7
Leading eigenvalue, 33
Least-squares MFS, 5
Least-squares problem, 353
Least-squares solution, 283
Legendre polynomial, 303
Legendre polynomial of order n, 310
Linear algebraic equation, 363, 405
Linear combination, 4, 70, 158, 215, 251, 342
Linear elastostatics, 77, 126, 248
Linear strain tensor, 247
Lipschitz boundary, 30
Lipschitz-continuous, 193
Local polar coordinates, 211
Local refinements, 7
Logarithmic function, 356
Logarithmic singularity, 398
Long strip-shaped domain, 100
Long-narrow domain, 13, 39
Low frequency, 131
Lower bound, 369, 409, 411, 416

M
Matrix splitting, 366
Matrix splitting techniques, 114
Maximal eigenvalue, 50, 291, 307
Maximal singular value, 296, 309
Meshless method, 192
Meshspacings, 4, 21, 43, 193, 253, 341, 402

Method of fundamental solutions (MFS), 97, 252, 254, 339, 378
Method of particular solution (MPS), 252, 254, 305, 339, 341, 366, 377, 411
MFS using Bessel functions, 129
MFS-QR, 12, 210, 214, 335, 339, 349
Minimal eigenvalue, 50, 291, 307
Minimal singular value, 296, 309, 369
Minimum principle, 252
Minimum property, 55
Mixed boundary condition, 3, 61, 128, 242
Mixed boundary problem, 15, 61
Modified condition number, 43, 49
Modified fundamental solutions, 198
Modified Hankel function, 191, 214
Modified MFS, 13, 156, 165
Modular, 173
Motz problem, 5, 79, 121, 398
Multiply-connected, 39, 191, 210

N
N-D conditions, 205
N-N conditions, 205
Negative norm, 31, 57, 84
Neumann boundary condition, 5, 42, 128
Neumann function, 127, 128, 157, 192
Nicholson integral, 173
Non-circular boundary, 414
Non-circular domain, 339
Non-circular pseudo-boundary, 100, 186, 361
Non-disk domain, 420
Non-elliptic domain, 113, 339
Non-elliptic pseudo-boundary, 361, 365
Non-homogenous, 376
Non-smooth data, 376
Non-smooth solution domain, 376
Non-uniformly, 364
Nonlinear, 375
Nonsingular, 17, 38, 50, 114, 229, 292, 350, 364, 410
Normal matrix, 240
Normal vector, 249
Normalized Legendre polynomial, 305
Null field method (NFM), 119, 339
Null matrix, 410
Numerical integration, 379

O
Original FS, 375
Orthogonal, 350
Orthogonality, 23, 132, 226, 303, 367
Orthogonality property, 55
Orthogonalization, 353
Over-specified boundary condition, 282, 286
Overdetermined system, 43, 52, 159, 193, 294, 342, 387, 402, 414

P
Parameter mapping, 330
Parametric equation, 181
Partial differential equations (PDE), 11, 13, 86, 97, 126, 244, 284, 400, 416
Particular solution (PS), 70, 93, 105, 132, 159, 194, 197, 217, 251, 333, 340, 377, 404
Peanut-like domain, 13, 420
Penalty combination of MFS and FDM, 88
Periodical boundary condition, 33
Periodical function, 35, 255
Permutation transformation, 203, 230
Perturbation error, 287
Perturbations, 296
Piecewise admissible function, 78, 88, 90
Piecewise bilinear function, 88
Piecewise fundamental solution, 67
Piecewise harmonic polynomial, 68
Piecewise liner function, 88
Piecewise particular solution, 95
Piecewise polynomial of order p, 252
Plane stress problem, 251
Poisson equation, 376
Poisson ratio, 250
Polar coordinates, 70, 370
Polygon, 375
Polygonal domain, 30, 376, 383
Positive definite, 291
Positive definite, 50
Potential function, 376
Precision, 314
Preconditioning, 12
Pseudo-boundary, 100, 355, 401
Pseudo-circular boundary, 31
Pseudo-collocation equations, 368
Pseudo-sphere, 326
Pseudo-surface, 13
Pseudo identification problem, 397
Pseudo radial-line, 13, 335, 401, 402, 408

Q
QR decomposition, 254, 297, 348, 349
Quadrature rule, 4, 13, 43, 62, 84, 89, 253
Quasiuniform, 86, 361, 402
Quotient space, 44, 58, 248

R
Radial basis functions (RBF), 77, 90
Radial basis functions method (RBFM), 12
Radial direction, 62
Random noise data, 287
RBF-QR, 354

Rectangular domain, 286
Rectangular pseudo-boundary, 122
Regularization, 2, 295
Relative error, 296
Removal technique, 335, 375, 384, 398
Residual, 63, 105, 132, 159, 194, 200, 217, 341, 377, 381, 405
Rigid motion, 248
Ring domain, 201, 204, 210
Robin boundary condition, 3, 61
Robin problem, 81
Rotation, 248
Rounding error, 7

S
Schwarz inequality, 28, 50, 110, 137, 177, 225, 292
Secant method, 375, 386
Semi-axes, 101, 340
Semi-disk, 78
Semi-norm, 306, 370
Sensitivity index, 336, 339, 346, 359
Series expansion, 72, 103, 217, 336
Significant digit, 345
Similar matrix, 230, 350
Simple domain, 375
Simplified MFS-QR, 352
Simply supported boundary condition, 242
Simply-connected, 3, 19, 39, 61, 101, 128, 192, 283, 332, 340, 361, 383
Single-layer potential, 156, 165
Single-valued function, 344, 372, 414
Singular boundary method, 192
Singular function, 66
Singular particular solution (SPS), 5, 77, 78
Singular value, 43, 53, 294
Singular value decomposition (SVD), 2, 43, 254, 297
Singularity, 5, 77, 368, 375, 387
Singularity problem, 9, 77, 335, 376
Smooth closed pseudo-boundary, 361
Sobolev imbedded theorem, 29
Sobolev interpolation theory, 58
Sobolev norm, 24, 55, 159, 194, 248, 256, 305, 383
Sobolev space, 44, 287, 383
Sobolev theory, 383
Sommerfeld radiation condition, 157, 333
Source function, 12, 376, 384, 420
Source function method, 2
Source identification problem, 394
Source nodes, 3, 20, 32, 42, 61, 70, 146, 179, 254, 261, 283, 314, 365, 405
Spectral method (SM), 119
Spectral radius, 240
Spherical Bessel function, 332
Spherical coordinates, 302
Spherical harmonic function (SHF), 303, 332, 301, 354
Spherical surface, 306
Spurious eigenvalue, 13, 119, 127, 140, 160, 162, 183, 191, 198, 210, 334
Square domain, 242
Stability, 11, 44, 93, 114, 119, 163, 210, 244, 270, 307, 339, 343, 388, 401
Stability analysis, 12, 15, 32, 45, 113, 125, 146, 179, 201, 228, 335, 409
Standard MFS, 157, 159
Star-like domain, 120
Starfish-like domain, 354
Stiffness matrix, 41, 58
Stirling formula, 143, 169, 174
Stress tensor, 248
Strong singularity, 356, 398
Sturm-Liouville problem, 204
Sub-annular domain, 75
Sub-matrix, 407, 413
Sub-vector, 408
Super-exponential, 39, 150
Super-linear, 152
Superfluous boundary, 100
Superfluous eigenvalue, 191
Superposition method, 2
Symmetric, 16, 33, 46, 50, 180, 291, 307

T
Taylor series, 286
Temperature field, 376
Tikhonov regularization (TR), 2, 12, 428
Traction, 250
Traction condition, 252, 269
Traction vector, 249
Trade-off principle, 120, 427
Traditional MFS, 375
Translation, 248
Transpose matrix, 367
Transposed Vandermonde matrix, 411
Trapezoidal rule, 20, 21, 136, 158, 193, 223, 255, 309, 314, 315, 324
Trefftz method (TM), 4, 20, 67, 102, 158, 193, 283, 377
Triangle inequality, 64, 68, 379
Triangular elements, 86
Trigonometric function, 23, 34
Truncated singular value decomposition (TSVD), 2, 12, 38, 428

U
Unbounded domain, 39, 77, 91, 157, 370
Uniform collocation nodes, 7

Uniform distribution, 347, 415, 416
Uniform partition, 326
Uniformly, 3, 17, 20, 32, 42, 113, 219, 254, 292, 350, 403
Unitary, 229
Unlimited working digits, 12
Upper bound, 414, 416, 421
Upper-triangular matrix, 348
Upper triangular elements, 88

V
Vandermonde matrix, 403, 411
Variant Case, 408, 412

W
Weight, 4, 21, 62, 67, 95, 253, 305, 308, 309, 378
Well-known condition, 146
Well-posed Cauchy problem, 300
Working digits, 12, 183, 270, 345